AFTERSHOCK VULNERABILITY ASSESSMENT OF DAMAGED REINFORCED CONCRETE BUILDINGS IN CALIFORNIA

A Thesis
Presented to
The Academic Faculty

by

Jong-Su Jeon

In Partial Fulfillment
of the Requirements for the Degree
Doctor of Philosophy in the
School of Civil and Environmental Engineering

Georgia Institute of Technology
August, 2013

AFTERSHOCK VULNERABILITY ASSESSMENT OF DAMAGED REINFORCED CONCRETE BUILDINGS IN CALIFORNIA

Approved by:

Dr. Reginald DesRoches, Advisor
School of Civil and Environmental Engineering
Georgia Institute of Technology

Dr. Ioannis Brilakis, Co-advisor
Department of Engineering
University of Cambridge

Dr. Laura N. Lowes
Department of Civil and Environmental Engineering
University of Washington, Seattle

Dr. Zhigang Peng
School of Earth and Atmospheric Sciences
Georgia Institute of Technology

Dr. Yang Wang
School of Civil and Environmental Engineering
Georgia Institute of Technology

Date Approved: [June 7, 2013]

I would like to dedicate this research to my wife Min Jung and my son Inhae.

ACKNOWLEDGEMENTS

I would like to express deep gratitude and sincere thanks to my co-advisor, Dr. Reginald DesRoches and Dr. Ioannis Brilakis, whose invaluable advice, encouragement, and guidance made the successful completion of this research possible. I am also thankful to my thesis committee Dr. Laura Lowes, Dr. Zhigang Peng, and Dr. Yang Wang, for their valuable suggestions and contributions. Additionally, I thank Professor Joseph M. Bracci of Texas A&M University, who shared the experimental results for the shake-table test.

I have been very fortunate to be surrounded by very talented and friendly fellow graduate students. I would like to give my special thanks to my former and current officemates, Mr. Timothy Wright, Dr. Abdollah Safieezadeh, Dr. Karthik Ramanathan, Mr. Pablo Vega Behar, and Ms. Laura Schultz for all the encouragement and support over the last four years. Special thanks are extended to the research team members of Dr. Stephanie Paal and Mr. Cal Bearman writing research papers and sharing their research results so that I integrate their outputs into my research.

I am thankful to my mother Gapyeon Im, my father Junggyu Jeon, my sisters Youngok Jeon, Heeok Jeon, Junghee Jeon, and my brother Jongsang Jeon for their unconditional love, encouragement, and support, without which I would not be here today. No words can explain how grateful I am and how fortunate I feel.

I would like to express by deepest and most heartfelt gratitude to my wife Min Jung and my son Inhae. This experience has required a lot of personal sacrifice from Min Jung, including financial, physical, and emotional. It was more than I had right to ask but

something she was willing to give. To her and him I not only give my thanks but also my love.

Also, I would like to thank the agency which funded my graduate studies and this work. The material presented in this research is based upon work supported by the National Science Foundation under Grant Numbers CMMI-1000700. Any opinions, findings and conclusions or recommendations expressed in this material are those of the author(s) and do not necessarily reflect the views of the National Science Foundation.

TABLE OF CONTENTS

LIST OF TABLES

LIST OF FIGURES

SUMMARY

Although the knowledge and technology of seismic analysis and seismic risk assessment tools have rapidly advanced in the past several decades, current seismic design codes and damage estimation methods ignore the effect of successive earthquakes on structures. In light of recent strong seismic events, mainshock-damaged structures are shown to be more vulnerable to severe damage and collapse during subsequent events. The increase in vulnerability during aftershocks results in the likelihood of increased damage and loss-of-life and property.

After a major earthquake, structural engineers must assess whether mainshock-damaged buildings can be re-occupied or not, with due consideration to the threat of aftershocks. The outcome of this post-earthquake inspection is utilized to quantifiably judge the current status of structures (so-called *building tagging*). This tagging criterion is closely related to the evaluation of the residual capacity of damaged buildings as well as the computation of the probability of being in a damage state after an aftershock (aftershock fragility). The increased vulnerability estimation associated with the additional damage plays a significant role in assessing potential losses to facilitate crucial decision making such as emergency response mobilization, inspection priority, recovery strategy, and re-occupancy decision. The main objective of this research is to develop a probabilistic framework for accounting for these increased vulnerabilities in terms of the extent of damage associated with mainshock ground motions. Aftershock fragility curves are developed accounting for both the uncertainty from the seismic hazard and the uncertainty from the structural capacity. This proposed approach also allows for the

inherent variability, such as modeling characteristics associated with the design codes, present in non-ductile and ductile reinforced concrete frames found in California.

CHAPTER 1

INTRODUCTION

1.1 Problem Description and Motivation

Although the knowledge and technology of seismic analysis and seismic risk assessment tools have rapidly advanced in the past several decades, current seismic design codes and damage estimation methods neglect the effect of multiple earthquakes on structures. However, in light of recent strong seismic events (the 1994 Northridge earthquake, USA, Hauksson and Jones 1995; the 1999 Kocaeli earthquake, Turkey, USGS 2000; the 2010 Haiti earthquake, DesRoches et al. 2011; the 2010 Darfield and 2011 Christchurch earthquakes, New Zealand, Smyrou et al. 2011; the 1997 Umbria-Marche earthquake, Italy, Decanni et al. 2000; the 2012 Emilia earthquake, Italy, Decanini et al. 2012), all of which were followed by many aftershocks, damaged structures are shown to be more vulnerable to severe damage and collapse. The increased vulnerability from aftershocks significantly threatens the safety of occupants in these structures. In addition, a mainshock-damaged structure may be incapable of resisting the excitation of a strong aftershock, not only increasing the risk of major damage or building collapse but also causing the additional loss of life and property. Moreover, because of this potential for larger aftershock ground motions, even buildings that have suffered minimal damage during the mainshock may have some likelihood of being damaged as a result of the occurrence of an aftershock. Mainshock-damaged buildings are even more susceptible to accumulated damage associated with aftershocks because their reduced structural

capacity exacerbates the threshold of the ground motion intensity needed to cause further damage (Yeo and Cornell 2005).

USGS (2000) reported that the 1999 Kocaeli earthquake with a mainshock of moment magnitude (M_w) 7.4 on August 17 had an aftershock of M_w 5.9 on September 13, which is the largest magnitude aftershock at that time. This aftershock killed 7 people, injured at least 239 people, and caused dozens of buildings to collapse in three cities near the epicenter. Figure 1.1 shows a building in Gölcük before and after it collapsed during an M_w 5.9 aftershock on September 13. The building was slightly damaged by the mainshock (inundation of the first story), and was fully collapsed by the smaller aftershock. Another documented example is the M_w 6.0 Emilia, Italy earthquake on May 20 2012, which had two large aftershocks of M_w greater than 5.0 within 60 hours.

(a) After mainshock of M_w 7.4 (Aug. 17) (b) After aftershock of M_w 5.9 (Sep. 13)

Figure 1.1 Damage progression before and after the Kocaeli aftershock (USGS 2000)

Decanini et al. (2012) have reported that the damage of the Town hall in Sant'Agostino observed on the afternoon of May 21 is more pronounced than media

reports; thus, the 20th afternoon aftershock has increased the collapse. Figure 1.2 shows the Town hall damaged by the aftershock. The aftershock sequences caused 16 deaths, 350 injuries, and approximately 14,000 homeless (reported on May 29) whereas the mainshock caused seven deaths, 50 injuries, and 4,500 homeless (reported on May 21). These historical evidences again emphasize the direct implications of aftershocks on the increased vulnerability of buildings.

Figure 1.2 Building damage after the Emilia earthquake (Decanin et al. 2012)

Decanini et al. (2000) informed that the 1997 Umbria-Marche earthquake with a mainshock of M_w 5.7 on September 26 with two large aftershocks; the second event of M_w 6.0 took place approximately nine hours after the mainshock and the third event of M_w 5.7 occurred on October 14. The earthquakes appeared somewhat anomalous in that the aftershock is equally strong and even stronger than the first event. This sequences caused many considerable consequences; the death toll approximately stands at ten, some 150 people were injured, the damage was estimated at 3.5 billion dollars, about 26000 houses (about one third available in the area) were unsafe, and more than 1300 buildings

are collapsed or seriously damaged. These earthquake sequences alert people to the potential occurrence of equally strong or even stronger aftershocks.

As alluded to earlier, in spite of increased interest in the damage accumulation associated with multiple earthquakes (mainshock-aftershock sequences), most of current seismic performance evaluation and seismic risk assessment tools deal with risk associated with a mainshock event only. These classical tools disregard the additional damage associated with aftershocks. This limitation is associated with large computation burdens, lack of additional damage data through post-earthquake inspection associated with aftershock events with low frequency but high consequence, and many parameters that are related to the cumulative damage potential and make the analysis complicated such as structural period elongation, aftershock ground motion intensities, and maximum and residual structural responses following a mainshocks. Nevertheless, recent advances in knowledge of analytical tool and enhancement of computer performance have alleviated the above difficulties.

In order to overcome the existing limitations above in post-earthquake inspection, performance evaluation, and risk assessment in an aftershock environment, a collaborative research project has been conducted by faculty and graduate students at the Georgia Institute of Technology and the University of Washington and funded by the National Science Foundation (NSF). The overarching goal is to develop and validate an automated framework for assessing the damage state and evaluate the seismic risk assessment of reinforced concrete (RC) buildings. Very briefly, the project includes three parts, as illustrated in Figure 1.3; machine-vision based structural element and damage detection for rapid post-earthquake inspection (Zhu 2012, German 2013), damage

characterization associated with component (member) response based on the extensive investigation of available experimental data in the literature (Bearman 2012), and the development of aftershock fragility assessment framework for building systems (this research). Adjacent research parts are interconnected in order to establish a link between observed damage state and member performance state and to link the member response corresponding to drift ratio and initial damage state as a result of mainshocks for generating characterized aftershock fragility curves. As the last portion of this project, this research will propose the framework for the aftershock vulnerability assessment of RC buildings by utilizing the results obtained from the preceding work.

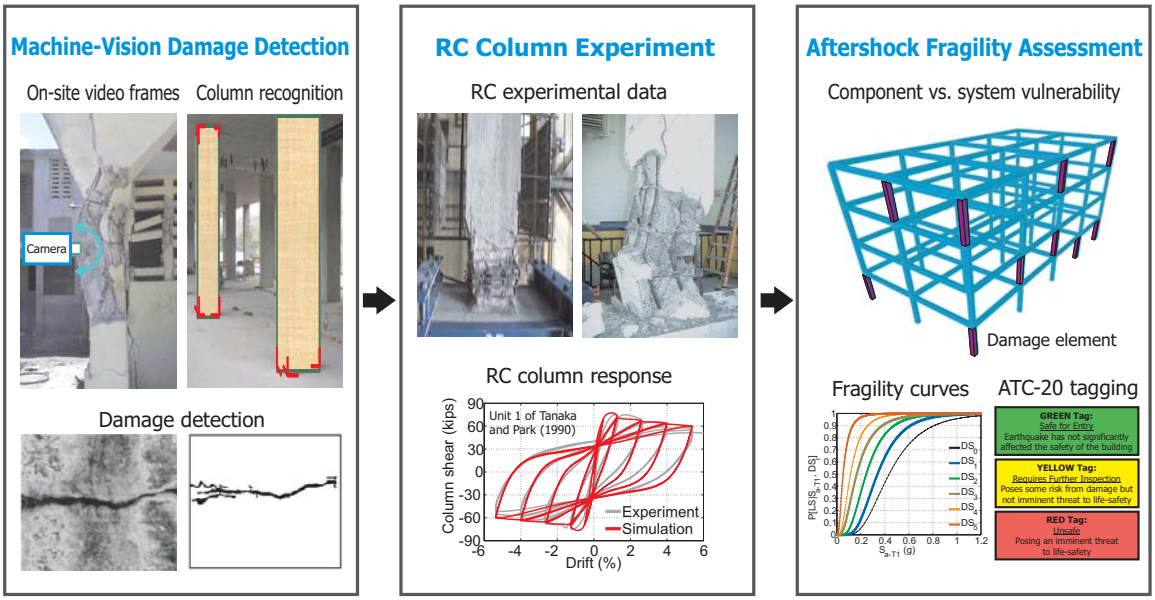

Figure 1.3 Research project overview

After a major earthquake, structural engineers must assess whether mainshock-damaged buildings can be re-occupied or not, with due consideration to the threat of aftershocks. The outcome of this post-earthquake inspection is utilized to quantifiably

judge the current status of structures (so-called *building tagging*). This building tagging criterion is closely related to the evaluation of the residual capacity of damaged buildings (but survived) as well as the computation of the probability of being in a damage state after an aftershock (aftershock fragility). The aftershock fragility, the most common emerging tool in seismic risk assessment, is specifically a conditional probability that determines the likelihood that a damaged structure will meet or exceed a specified level of damage (limit state), given an aftershock intensity measure and a mainshock-damaged condition, with the aftershock ground motions hazard at the site of interest. As proved in mainshock fragility curves by Ranf et al. (2007), employing these aftershock fragility curves to help streamline reconnaissance efforts can effectively reduce the duration of the functional assessment stage of recovery. Furthermore, the outcome of these aftershock fragility curves plays a significant role in assessing potential losses to facilitate crucial decision making such as emergency response mobilization, inspection priority, and re-occupancy decision. Moreover, in the case of the successive occurrences of multiple earthquakes in a short time period, the repair time is not enough to assess the residual capacity of structures by a post-earthquake reconnaissance team.

As shown, aftershock fragility curves can serve many important roles. However, if they are to be effectively used in the activities, it is imperative that reliable aftershock fragility curves are available. Structural engineers or other decision makers must have confidence in the results before they will use it. After all, this research aims at developing the aftershock fragility curves for non-ductile and ductile RC frames typical to California, the highest seismic region in the United States. The aftershock fragility curves are generated using detailed analytical frame models and back-to-back nonlinear time history

analyses. Additionally, the procedure should simulate the extent of existing damage linked with post-earthquake inspection or experimental data to investigate the damage accumulation and associated increased vulnerability of the structures due to aftershock events.

1.2 Research Objective

The importance of aftershock consideration for conducting probabilistic seismic risk assessment is identified in the previous section. The ultimate objective of this research is to develop a framework for the aftershock fragility assessment of typical RC building frames that can estimate their increased vulnerabilities related to aftershocks and the associated economic loss and repair cost. Prior to computing the aftershock fragility relation, the visible damage estimation of softened structures after mainshocks must be conducted to link these damage states with engineering demand parameters on the basis of damage progression observed in existing experimental column tests. Accordingly, these identified member-level damage information is employed in order to characterize initial damage states associated with mainshocks employed in the aftershock fragility assessment framework. The specific activities that will be completed as part of this research are as follows:

1. Identify the most common RC building types in compliance with older and modern design codes in California.
2. Develop the analytical modeling technique for RC components which can capture potential failure modes. The accurate and detailed analytical models enable

reliable probabilistic assessment that can identify the structural response and damage progression with visual damage descriptions.

3. Simulate damaging earthquakes (mainshocks) that can represent the damage conditions of the frames. The different drift levels associated with the seismic response of RC members are utilized to generate mainshock ground motions by which the members experience the damage conditions corresponding to these drifts.
4. Perform mainshock-aftershock analyses for each mainshock-aftershock-frame pair to monitor the engineering demand parameter: incremental dynamic analysis–nonlinear time history analysis and cyclic nonlinear pushover analysis–nonlinear time history analysis. For aftershock analyses, the NTHA approach is employed to account for realistic ground motions that may happen at site of interest.
5. Develop and compare probabilistic aftershock demand models and aftershock fragility curves with different initial damage states. The analytical results can quantitatively and efficiently estimate the increased vulnerability of damaged frames.

1.3 Dissertation Outline

The dissertation is organized into seven chapters with the following contents:

Chapter 2 summarizes existing research on mainshock-aftershock responses of structures, classical and aftershock fragility curves, and analytical modeling techniques.

Chapter 3 describes extensive details about the modeling strategies for critical components of RC building frames such as flexure and shear behavior of columns and ductile and non-ductile beam-column joints. Model validations are performed for experimental data available in literature.

Chapter 4 provides building design information and associated analytical frame model. The deterministic responses are presented to provide insight into the response of frame components.

Chapter 5 lays out the framework for the generation of aftershock fragility curves for RC building frames. Details are provided regarding the multi-phase framework: construction of stochastic frame models accounting for material uncertainties, selection of mainshock and aftershock ground motion suites, characterization of initial damage states, formulation of probabilistic aftershock demand models, definition of capacity model, and computation of aftershock fragility function.

Chapter 6 presents the applicability of the proposed framework described in Chapter 5 to different building types and analytical frame model models. For each analytical frame model, aftershock fragility curves are compared for different mainshock-damaged conditions associated with initial damage states. Subsequently, the aftershock fragility curves are compared for various analytical frame models and building types.

Chapter 7 presents the conclusions from the present research, along with providing impacts of the work and suggestions for future research.

CHAPTER 2

REVIEW AND ASSESSMENT OF THE STATE OF THE ART

This chapter summarizes and critically appraises the impact of aftershocks on structures, previous studies in the development of aftershock fragilities of structures, and the primary concept and analytical techniques of typical (mainshock) fragility functions and analytical modeling techniques that are prerequisite conditions for computing the fragility curves for aftershocks.

2.1 Significance of Aftershocks

In spite of increased interest in the effect of multiple earthquakes (mainshock-aftershock sequences), very few studies have investigated the seismic performance of structures under multiple earthquakes. The subsequent paragraphs present a review of some studies addressing incremental damage on structures as a result of aftershock ground motions.

A pioneering analytical study of nonlinear single-degree-of-freedom (SDOF) systems under repeated ground motions was conducted by Mahin (1980). To assess the effect of the accumulation of damage, the author performed mainshock-aftershock analyses for elasto-perfectly plastic SDOF models using the 1972 Managua earthquake, which had two large aftershocks. The mainshock with the peak ground acceleration (PGA) of 0.351g induced significant inelastic deformations in the system. The first aftershock (PGA = 0.120g) had relatively little effect while the second aftershock (PGA = 0.277g) caused large inelastic deformations, more than doubling displacement ductility. Similarly, energy dissipations were increased. The author proved that aftershocks can substantially

increase structural damage and the accumulation of damage led to collapse during aftershocks.

Aschheim and Black (1999) proposed the hysteretic pinching model of SDOF oscillators for concrete and masonry wall buildings to assess the effect of prior earthquake damage on their peak displacement responses. Their work was conducted as a part of the ATC-43 project of the Applied Technology Council. The SDOF model accounted for the strength of the oscillator, period of vibration, and extent of prior damage. The ground motions used in the study were 18 pairs of repeated ground motions containing varied frequency content, duration, and the presence or absence of near-field forward directivity effects. However, their work is limited because prior damage was represented as only a reduction in initial stiffness under the assumption that residual displacements are negligible. This assumption may underestimate overall deformations in real situations, especially for weakened structures due to strong mainshocks.

Amadio et al. (2003) investigated the dependence of damage accumulation associated with repeated seismic actions. Their work was motivated by the considerable damage to historical architecture caused by the 1997 Umbria-Marche earthquake in Italy (Decanini et al. 2000). The authors analyzed a series of SDOF systems with different hysteretic models and a multi-degree-of-freedom (MDOF) system for a 3-story, 2-bay steel moment-resisting frame subjected to repeated ground motions. Their analytical results indicated that multiple earthquakes can imply a considerable accumulation of damage and a significant reduction in the q-factor which accounts for the inelastic energy dissipation of the structure. However, as the authors themselves acknowledged, their

work cannot be examined exhaustively since they accounted for only one natural and two artificial ground motions.

Lee and Foutch (2000) proposed a systematic evaluation approach that allows the design professional to estimate the performance of damaged SMRFs subjected to sets of Los Angeles (LA) ground motions (developed as a part of the SAC project) representing different hazard levels. The authors utilized back-to-back identical accelerograms for mainshock-aftershock analysis to compute the confidence level that a building will meet the given performance. This identical mainshock-aftershock event, however, is highly unlikely to happen. To alleviate the conservative occurrence, Li and Ellingwood (2007) employed the approach of Sunasaka and Kiremidjian (1993) to generate aftershock ground motion ensembles that might lead to additional damage by scaling a set of LA ground motions by a factor obtained from the aftershock hazard near Eureka, California. The authors considered two cases for assembling mainshock-aftershock sequences: identical and randomized mainshock-aftershock sequences. For both cases, aftershock ensembles were scaled. Their study indicated that the former case leads to larger peak story drift demand in MDOF systems as compared to the latter case. This finding may be attributed to the same frequency contents of mainshock and aftershock earthquakes.

Hazigiorgiou and Liolios (2010) performed an extensive parametric study on the inelastic behavior of eight low- and mid-rise RC planar frames under 45 strong repeated ground motions consisting of five real and 40 artificial sequences. The authors indicated that multiple earthquakes gave rise to an increased displacement demand associated with a significant damage accumulation, and they claimed that traditional seismic design procedures should be reevaluated. Faisal et al. (2013) subsequently examined the

influence of repeated earthquakes on the maximum story ductility demands of three-dimensional RC frames. After selecting 20 far-field ground motions, the authors assembled single, double, and triple events as input ground motions. Double and triple events increased 1.4 and 1.3 times maximum story ductility demand when compared to single events.

Ruiz-García and Negrete-Manriquez (2011) evaluated the impact of 14 as-recorded mainshock-aftershock sequences (far-field and near-fault) on peak and residual drift demands in three steel moment-resisting frames. The authors found that the frequency characteristics of the mainshock-aftershock sequences, such as the predominant period of ground motion and the bandwidth, are weakly correlated through statistical observation. Additionally, the authors demonstrated that the effect of aftershocks during performance-based assessment of existing structures should be accounted for using as-recorded mainshock-aftershock sequences instead of artificial sequences. However, the lack of as-recorded sequences that can lead to initial and additional damage may have a limitation in performing the probabilistic seismic risk assessment of structures through numerous analyses.

The studies reviewed above have demonstrated that mainshock-aftershock sequences can increase maximum and permanent deformation demands on structures. This result can be deduced from using sufficiently larger aftershock ground motions that can cause additional damage on structures. Additionally, due to the lack of as-recorded successive earthquakes inducing damage accumulation, artificial mainshock-aftershock sequences randomly paired have been widely used for the evaluation of residual capacity and increased demand of damaged structures.

2.2 Existing Mainshock and Aftershock Fragility Assessment

This section provides the extension of mainshock (classical) fragility formulation into aftershock fragility through an in-depth review of seismic risk assessment framework for mainshocks.

2.2.1 Review of fragility assessment for mainshock

The seismic risk assessment framework developed for mainshocks can be expressed by the total probability theorem (Ellingwood et al. 2007), as presented in equation (2.1):

$$P[Loss > c] = \sum_{im}\sum_{LS}\sum_{ds} P[Loss > c \mid DS = ds]P[DS = ds \mid LS]P[LS \mid IM = im]P[IM = im] \tag{2.1}$$

where IM denotes the intensity measure of earthquake ground motions, im is the realization of the intensity measure, $P[LS|IM = im]$ is the probability of reaching a structural limit state (LS) conditioned on a given level of $IM = im$, $P[DS = ds|LS]$ is the probability of damage state (DS) conditioned on limit state (LS), and $P[Loss > c|DS = ds]$ is the probability that the loss exceeds c conditioned on a given level of $DS = ds$.

As shown in equation (2.1), loss assessment requires an integrated approach for dealing with seismic hazard ($P[IM = im]$), structural response ($P[LS|IM = im]$), the relation between structural response and damage ($P[DS = ds|LS]$), and the link between damage and economic loss ($P[Loss > c|DS = ds]$). The term $P[LS|IM = im]$ is referred to as the fragility, which is the conditional probability of reaching a structural limit state LS, which may range from loss of function to incipient collapse, given the occurrence of a particular level of intensity im. Such a margin can be utilized to evaluate structural

deficiencies identified during an inspection or condition assessment and can provide a measure to assess if the observed deficiencies might be expected to affect the system risk significantly (Wen et al. 2004).

Seismic vulnerability assessment procedures can be classified into three approaches based on post-earthquake surveys, expert opinion (ATC 1985), and analytical simulations. The observation-based procedures (Gulkan and Sozen 1999, Yucemen et al., 2004, Rossetto and Elnashai 2003, Shinozuka et al., 2000) can incorporate the damage data collected in historic events into fragility functions. However, these empirical fragilities have some limitations such as the lack of sufficient damage data, discrepancies in the damage assessments following a seismic event, variation in the ground motion intensities at the damage sites dependent on the earthquake source. The ATC-13 report (ATC 1985) introduced the expert opinion to develop fragility curves for civil infrastructure subjected to seismic demand to alleviate the limited observational data from the San Fernando earthquake. However, the reliability of the fragilities is questionable in that the fragilities are subjective and the associated degree of conservatism is unknown (Rossetto and Elnashai 2003). Due to the drawbacks of observation- and expert-based approaches, recent approaches have relied on analytical simulations through which the relation between structural responses and ground motion intensities is established.

When performing the simulation-based fragility assessment, the widely used analytical techniques are nonlinear time history analysis (NTHA) (Celik and Ellingwood 2008, Jeong et al. 2012, Singhal and Kiremidjian 1996, Mosalam et al. 1997, Kwon and Elnashai 2006) and incremental dynamic analysis (IDA) (Kirçil and Polat 2006, Haselton

et al. 2011, Liel et al. 2011, Barkhordary and Tariverdilo 2011) developed by Vamvatsikos and Cornell (2002). Both approaches are more reliable yet computationally intensive techniques than nonlinear static pushover (NSP) approach. Although the fragility approaches by the researchers differed slightly, the fundamental concepts were the same.

NTHA provides the flexibility to account for analytical models with hysteretic material characteristics and geometric nonlinearities and requires numerous ground motions with various levels of their intensities to establish a relationship between the intensities and their associated seismic responses. The method is referred to as a *cloud* approach (Baker and Cornell 2006) that enables probabilistic seismic demand analysis (PSDA). This method has a great advantage of being compatible with a closed form solution and it can reduce the computational expense of the estimation compared to NTHA. However, it includes the pre-assumption about the probability distribution of the demand model.

On the other hand, IDA is a promising analysis technique that provides comprehensive seismic design and capacity prediction capability through a series of NTHAs under a multiply scaled suite of ground motions. Unlike NTLHA, IDA can be referred to as a *stripe* approach (Baker and Cornell 2006) where ground motions are incrementally scaled and analysis is performed at different hazard levels. The stripe approach can offer the transition of the structural response from elastic to inelastic behavior, finally leading to global dynamic instability and the accurate and reliable estimates of the global collapse capacity of the structure. However, this approach requires more structural analyses than the cloud approach (NTHA) where the responses are

demanded at different levels of intensities. Additionally, the assumption about scaling ground motions, namely no change in the frequency content of ground motions, can produce unrealistic ground motion records that may not be representative of the seismic hazard in the region.

Because the extensive investigation on the development of fragility curves for mainshocks is beyond the scope of this research, this section addressed only the primary concept of the fragility function and analytical techniques which will be employed in the generation of fragility curves for aftershocks.

2.2.2 Existing fragility assessment for aftershock

Although seismic fragility assessment for mainshocks has been fully developed by researchers, studies on probabilistic seismic risk assessment of structures subjected to multiple earthquakes are as yet scarce. These limited studies (Li and Ellingwood 2007, Bazzuro et al. 2006, Maffaei et al. 2008, Luco et al. 2004, Ryu et al. 2011, Uma et al. 2011) were performed using the formulation of fragility functions for mainshocks and analysis techniques mentioned in the previous section. A few studies on the probabilistic risk assessments for aftershocks are reviewed below.

Li and Ellingwood (2007) developed a demand model accounting for the seismic responses of a SMRF building during aftershocks with different aftershock magnitudes and performed the comparison of the demand models with different ground motion suites: mainshocks, replicated mainshock-aftershock sequences, and randomly paired mainshock-aftershock sequences. The authors indicated that the amplitude and frequency content of the aftershocks have a significant impact on the structural damage patterns

through the comparison of replication and randomization cases in that, under the randomization case, the damage pattern changed as a result of the aftershocks unlike the replication case. Additionally, the authors found the probability for which the aftershock causes large additional damage is small if the initial damage by the mainshock is small. However, the probability of reaching a damage state was computed using a suite of aftershock ground motions developed with different aftershock magnitudes regardless of the extent of damage developed by the mainshock.

Bazzurro et al. (2006) proposed a parameterized pushover load analysis approach to develop the aftershock fragility curves of steel frames for capacity limit states ranging from the onset of damage to building collapse directly related to post-earthquake building occupancy status called *tagging*. The output of this method can be derived using an initial NSP for a mainshock and the later subsequent NSPs for aftershocks. This method exploited the knowledge of the nonlinear static behavior of a specific building under incremental lateral loads to estimate its nonlinear dynamic response expected for different levels of ground motion intensities. The authors entered the NSP curve for each damage state into the SPO2IDA tool (Vamvatsikos and Cornell 2006) for inferring dynamic response and then developed aftershock collapse fragility curves for identifying the building condition after earthquakes. Maffei et al. (2008) subsequently identified potential difficulties that structural engineers would encounter in using the procedure described in the work of Bazzurro et al. (2006). This method is much less computationally intensive, and thus provides the structural engineers with the rapid assessment of building vulnerability to collapse. However, this method did not account for the effect of cyclical degradation (stiffness and strength degradation), which may

increase the seismic demand, in that NSP are performed up to a roof drift associated with a damage state, and then followed by unloading to zero base shear.

Following the previous studies, Luco et al. (2004) computed the residual capacity of a mainshock-damaged structure to compare static and dynamic analysis techniques. They found that the static analysis approach (Bazzuro et al. 2006) underestimated the median residual capacity compared to the dynamic analysis technique (back-to-back NTHAs for randomized mainshock-aftershock sequences) for the structure severely damaged after a mainshock, which experienced large inelastic deformation associated with the degradation in strength and stiffness. Based on the results of the back-to-back dynamic analyses, the authors proposed a calibrated static approach to determine the reliable residual capacity of the damaged building. However, the calibration cannot be performed without the results of back-to-back NTHAs. Therefore, a more refined static approach without additional efforts is needed.

More recently, Ryu et al. (2011) proposed a methodology for developing collapse fragilities for mainshock-damaged buildings. For this purpose, a sequence of IDAs for mainshock and aftershock ground motions was utilized to establish the collapse fragility functions for a SDOF system representing a typical New Zealand 5-story RC moment frame building. The mainshock-damaged condition of the SDOF system was realized using IDA. The proposed approach can include uncertainty in mainshock responses for a given post-mainshock damage state and uncertainty in limit states, and it helps structural engineers to assess whether a damaged building can continue to be occupied after a mainshock. As a companion study of Ryu et al. (2011), Uma et al. (2011) compared aftershock fragility curves of New Zealand and US RC buildings employing the approach

of Ryu et al. (2011). For this purpose, SDOF systems including the effect of cyclic deterioration were considered, and a set of damage state thresholds are employed under the assumption of lognormal distribution of the fragility curves. More recently, Raghunandan et al. (2012) computed the damage transition probabilities from a specific damage state in a first event to the damage state in a second event along with the aftershock fragility function of a SDOF system for a New Zealand RC building by using the relation obtained from Ryu et al. (2011). However, these SDOF models will not yield accurate results, and this approximation suffers from the inability to capture damage localized in different components of a structure, primarily the joints and columns.

For the generation of the aftershock fragility functions of buildings, the recent studies (Luco et al. 2004, Ryu et al. 2012, Uma et al. 2011) employed the stripe approach (IDA) to compute the fragility curves with initial damage states associated with mainshocks while Li and Ellingwood (2007) utilized the cloud method (NTHA) to develop the curves with a magnitude of aftershock ground motions. This research will utilize the cloud approach for aftershock analyses, which can involve realistic ground motions and can readily draw the probability of being in a damage state from the closed form, along with the consideration of existing damage conditions induced by mainshocks.

2.3 Modeling Critical Components in RC Frames

2.3.1 Shear-dominated column model

RC columns designed or constructed prior to 1970's are highly prevalent in the United States and around the world. Flexure-dominated columns experience comparable inelastic large deformations, retain shear and axial load capacities large deformations, and fail

during large lateral loads by rebar fracture and buckling, concrete crushing, and/or lateral instability. However, shear-dominated columns fail in shear and exhibit dramatic strength and stiffness degrading behavior until axial collapse occurs because of their inadequate reinforcement details. Once this shear failure is triggered before or after flexural yielding, their shear and deformation capacities are gradually lost. Existing column's shear failure models are presented with commentary on their advantages and disadvantages.

Early attempts to describe the shear failure model of columns are found in the work of Otani and Sozen (1972), Spacone et al. (1996), Zeris and Mahin (1991). To capture the occurrence of shear failure, they modified nonlinear flexure elements such lumped plasticity or fiber section elements through a post-processing without explicitly accounting for shear behavior. Although the post-processing can capture the detection of column's shear failure, it cannot estimate appropriate inelastic shear deformations and degrading behavior.

Continuum finite elements have been developed to capture the degrading behavior after shear failure (Kaneko et al. 2001, Ozbolt et al. 2001, Shing and Spencer 2001). Although these models can accurately address shear deformations in frame, they require significant computation effort for modeling larger structures under seismic excitations.

Alternatively, the most popular technique for simulating the shear response of existing columns is the addition of a shear spring in series with flexure elements (Pincheira et al. 1999, Lee and Elnashai 2001, Sezen and Chowdhury 2009), as shown in Figure 2.1. The above researchers employed the modified compression field theory (Vecchio and Collins 1986, hereafter MCFT) to define the backbone curve of the shear spring. To incorporate nonlinear behavior in shear, Pincheira et al. (1999) added a zero-

length shear spring that can account for the strength and stiffness degradation with increasing deformation amplitude. Although their model yielded satisfactory results and properly includes the effects of strength decay, they used a small fictitious positive stiffness on the descending branch of the backbone to circumvent the convergence issue within the existing solution algorithm, resulting in a force unbalance at each increment whenever strength degradation occurs. Additionally, the procedure can be very computationally intensive and may not predict the dynamic characteristics of a softening structure. Lee and Elnashai (2001) also utilized the MCFT to establish the backbone curve of a spring and developed hysteretic rules including the variation of column axial loads. Although their shear model can capture the hysteretic response of columns with a relatively flat yield plateau, it did not address the post-peak degrading slope of the backbone curve. Sezen and Chowdhury (2009) developed the hysteretic model including the flexure-shear-axial interaction based on the backbone curve obtained from the MCFT, and also employed the bond-slip model developed by Sezen and Moehle (2003). Although their model provided reasonable strength degrading behavior, the overall response was not predicted well in many cycles mainly because the sum of experimental component displacements did not match the total experimental displacement. Furthermore, the MCFT only predicts the backbone curve of shear model up to the point of maximum strength, and therefore requires additional assumptions for defining the shear strength degradation.

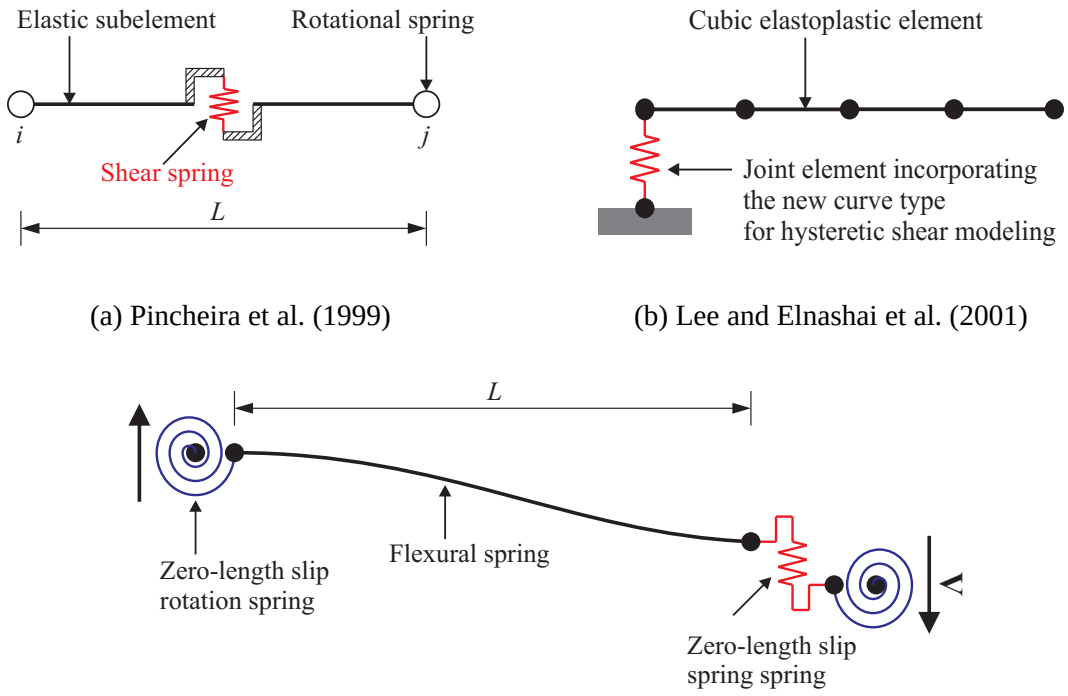

(a) Pincheira et al. (1999)

(b) Lee and Elnashai et al. (2001)

(c) Sezen and Chowdury (2009)

Figure 2.1 Column shear models employing the MCFT

A few shear strength models (Watanabe and Ichinose 1992, Aschheim and Moehle 1992, Sezen 2002) are useful for estimating the column shear strength as a function of deformations. However, they do not provide a reliable estimate of the drift capacity at shear failure (Elwood and Moehle 2005). Current design philosophy (ATC 1996 and ASCE 2000) reported that drift capacity models are an essential contributor for displacement-based design for existing building structures. A limited number of drift capacity models are reviewed for columns experiencing flexural yielding prior to shear failure. Pujol et al. (1999) proposed a drift capacity model for shear-dominated columns, which established a conservative estimate of the maximum drift ratio through the statistical evaluation of an experimental database of 92 columns with both circular and rectangular cross sections. However, the database includes columns with transverse

reinforcement ratios exceeding 0.01, which is used in ductile frames. To provide a better estimate of drift capacity at shear failure, Elwood and Moehle (2005) proposed an empirical drift capacity model by using a database of 50 flexure-shear-critical RC columns with configurations representative of those used in pre-1970s building construction.

Using the drift capacity model of Elwood and Moehle (2005), Elwood (2004) developed a new material model (limit state material) that can identify a shear failure associated with column shear and column's total deformation. Figure 2.2 illustrates a shear spring in series with a nonlinear beam-column element. Flexural deformation is concentrated in the beam-column element, and shear deformation is delivered by the shear spring. To define the constitutive relationship for the shear spring, the hysteretic uniaxial material with strength degradation (called limit state material) was utilized available in OpenSees (McKenna et al. 2010). The limit state material has a predefined trilinear backbone curve and five parameters to define pinching and stiffness degradation. The limit state material traces the behavior of the beam-column element and changes the backbone of the material model to include strength degradation once the response of the beam-column element exceeds a predefined limit state surface (limit curve). Analytical predictions of a three-column frame show a good correlation with experimental results from shake table tests by Elwood and Moehle (2003). However, a significant change in the structure once a limit curve is reached enables the limit state material to be particularly sensitive to any variability in the limit curve. Additionally, a limited number of comparison studies with experimental results make it difficult to accurately model the limit curve.

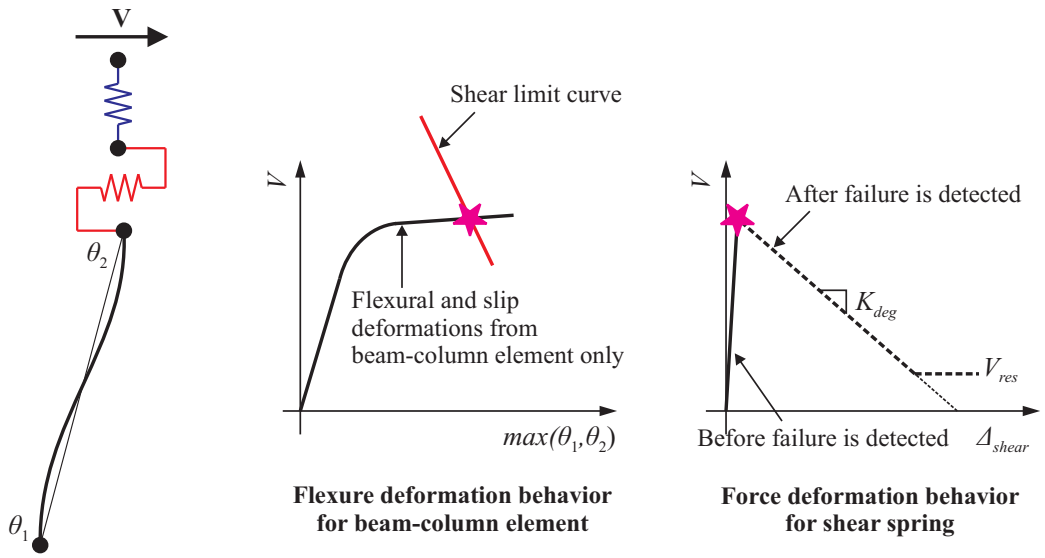

Figure 2.2 Limit state material used to model shear failure (Elwood 2004)

LeBorgne (2012) extended the model of Elwood (2004) to estimate the lateral strength degrading behavior of RC columns prone to shear failure. Figure 2.3 shows the analytical model of flexure-shear-critical columns developed by LeBorgne (2012). LeBorgne (2012) developed a rotation-based shear failure model while Elwood (2004) proposed a drift-based shear failure model. The shear model triggers shear failure once either a shear capacity or a plastic hinge rotation capacity is reached. The shear model can account for cyclic shear damage up to complete loss of lateral strength and stiffness. Once shear failure is detected, a zero-length shear spring with a trilinear backbone curve linked in series with beam-column elements modifies its constitutive properties to consider pinching and strength and stiffness degradation. The constitutive properties were determined through linear regressions for pinching parameters extracted from experimental data. The author compared analytical predictions and experimental results for shear-dominated columns. Although the shear model offers very effective and

accurate results, the direct use of this shear model in the current version of OpenSees (McKenna et al. 2010) is not possible and instead, two dynamic link libraries are required to use the shear model (LeBorgne 2012). Furthermore, its applicability to full frames has not been addressed for dynamic analysis, and dynamic instability remains questionable.

A review of previous research on the shear behavior of older columns indicates that a reliable column shear failure model should be accurate, computationally efficient and compatible with existing software programs in order to conduct numerous nonlinear dynamic analyses. However, none of the column shear models reviewed above meets all three of those requirements. Due to its computational efficiency and compatibility with OpenSees (McKenna et al. 2010), the column shear model, developed by Elwood (2004), will be used in this research.

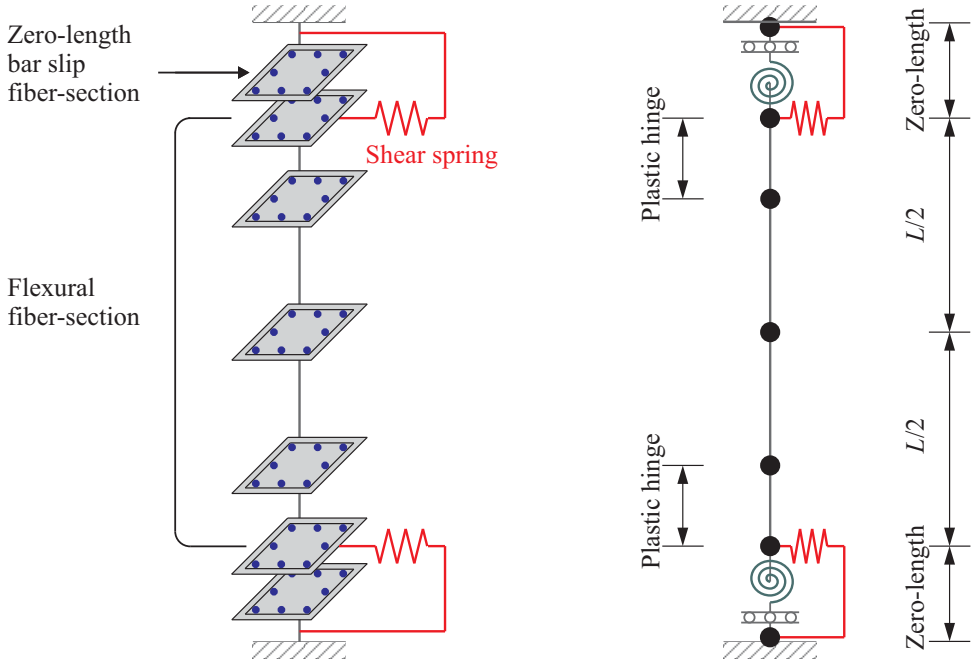

Figure 2.3 Analytical model developed by LeBorgne (2012)

2.3.2 Beam-column joint model

A joint shear model that can account for the cyclic strength and stiffness deterioration is critically important to this research. This section reviews existing joint shear strength models and monotonic or hysteretic joint shear models.

2.3.2.1 Joint shear strength model

Hwang and Lee (1999, 2000) developed a softened strut-and-tie model to predict RC joint shear strength for both interior and exterior beam-column joints. The softened strut-and-tie model is based on the strut-and-tie concept and derived to satisfy equilibrium, compatibility, and constitutive relationship for cracked reinforced concrete. Although the analytical predictions for joint shear strength are well-correlated with experimental results for 63 exterior and interior beam-column joints, the proposed approach became more complicated by introducing these principles of mechanics in contrast to the simplicity of the strut-tie-model. The database includes specimens with governing failure modes of beam flexural failures, joint shear failures with and without beam yielding and regardless of joint transverse reinforcement.

Attaalla (2004) suggested an analytical equation to estimate joint shear strength for interior and exterior beam-column joints. The proposed equation reflects most significant parameters that influence the joint behavior (such as axial forces in the beam and column, horizontal and vertical joint reinforcement ratios, and geometry), and it accounts for the compression-softening phenomenon associated with cracked reinforced concrete. For the model validation, 69 exterior and 61 interior beam-column joints are

used, all of which are specimens experiencing joint shear failures with or without beam yielding.

Shiohara (2004) proposed a mathematical model to determine the joint shear strength of interior, exterior, and knee beam-column joints. The quadruple flexural resistance within a joint panel played an important role in defining joint shear failures. Joint shear strength was calculated from force equilibrium in four rigid segments within the joint panel. However, the model validation based on experimental results was not provided.

Park and Mosalam (2012b) proposed a strut-and-tie model to predict the joint shear strength of exterior beam-column joints without transverse reinforcement which experienced joint shear failures with and without beam yielding. The proposed joint shear strength model accounted for joint aspect ratio and beam reinforcement ratio. Although their model can predict the joint shear strength for non-ductile exterior and corner joints well, their proposed formulation cannot be applied to interior or roof joints. In order to overcome the limitation of the applicability to other joint types, Park and Mosalam (2013) modified the joint shear strength model proposed by Park and Mosalam (2012) by multiplying the formulation for exterior joints by the shear strength ratio, which is the ratio of joint shear strength coefficient for other three types of joints (interior, roof, and knee joints) to the exterior joint shear strength coefficient. Although analytical predictions provide reasonable results through the comparison of those and experiments, actual joint strength coefficient ratio based experimental observation is different.

Kim and LaFave (2009) proposed the statistical joint shear strength model by using a Bayesian method based on 136 and 18 experimental beam-column

subassemblages with and without joint transverse reinforcement, respectively, which are specimens experiencing joint shear failures. For ductile joints, they constructed the joint shear strength model by performing a step-wise removal process to extract key parameters among ten parameters (spacing ratio, ratio of recommended to provided amount of joint transverse reinforcement, ratios of beam depth to column depth and beam width to column width, joint transverse reinforcement index, beam reinforcement index, joint eccentricity, in-plane and out-of-plane geometry, concrete compressive strength). Additionally, for non-ductile joints (without joint transverse reinforcement), a probabilistic joint strength model was established by modifying that for ductile joints because none of the included parameters in the proposed equation for ductile cases should be taken as zero. The ductile joint shear strength model provides reliable estimates while the non-ductile joint shear strength model should be improved because of the limited size of non-ductile joint in the database.

Hassan (2011) suggested an empirical bond strength model to evaluate the joint shear strength for exterior and corner joints with the short embedment length of beam bottom reinforcement. The bond strength equation includes axial load, beam bar diameter, cover to bar diameter, cover to bar diameter ratio, and the presence of transverse beams to improve existing bond strength models. Using the proposed equation and equilibrium, the equivalent joint shear strength associated with bond failure was derived and compared with 21 experimental results. The mean and coefficient of variation of the ratio of experimental and calculated joint shear strength coefficient are 0.94 and 0.14, respectively. The proposed equation is only applicable for the case of pullout failure before rebar yielding.

2.3.2.2 Modeling joint shear behavior

Alath and Kunnath (1995) modeled the joint shear deformation with a rotational spring model with degrading hysteresis. The joint panel was represented by introducing four rigid links, as illustrated in Figure 2.4(a). The backbone curve of the joint shear stress-strain relationship was determined empirically, while the cyclic response was captured using a hysteretic model calibrated by experimental cyclic response. The model was validated through the comparison of experimental and analytical response of a non-ductile interior beam-column joint subassemblage.

Youssef and Ghobarah (2001) proposed a joint element in which two diagonal translational springs linking the opposite corners of the panel zone simulate the joint shear deformation, as shown in Figure 2.4(b). The backbone curve of the joint was defined using the MCFT. To account for the effect of bar-slip within the joint and concrete crushing at the joint perimeter, three translational springs at each joint face were used. The analytical model was validated using the experimental results of ductile and non-ductile exterior beam-column joints. The model requires a large number of translational springs and a separate constitutive relationship for each spring, which may not be available and restrict its applicability.

Lowes and Altoontash (2003) proposed a four-node 12-DOF joint element that consists of eight zero-length bar slip springs, four interface shear springs, and a panel that deforms only in shear, as illustrated in Figure 2.4(c). Because of limited research on the bond-slip data of full-scale frames or beam-column joint subassemblages, back the monotonic and cyclic response of the bar stress-slip relationship were developed from experimental studies of anchorage-zone specimens and based on the assumption that

bond stress within the joint is constant or piecewise constant. To define the backbone curve of the shear panel, the MCFT was utilized. The cyclic response of the panel zone was modeled by a highly pinched hysteresis relationship, deduced from the experimental results of Stevens et al. (1991). A relatively stiff elastic load-deformation response was assumed for the interface-shear elements.

Mitra and Lowes (2007) subsequently evaluated the model developed earlier by Lowes and Altoontash (2003) by comparing the simulated response with the experimental response of beam-column joint subassemblages. The experimental data used for the model validation included interior specimens with at least a minimal amount of joint transverse reinforcement. Therefore, the model may not capture the hysteretic response for joints with little or no joint transverse reinforcement. Mitra and Lowes (2007) demonstrated that in joints with low amounts of transverse reinforcement, shear is transferred primarily through a compression strut, a mechanism, which is stronger and stiffer than predicted by the MCFT.

Altoontash (2004) simplified the model proposed by Lowes and Altoontash (2003) by introducing a model consisting of four zero-length bar-slip rotational springs located at beam- and column-joint interfaces and a zero-length joint rotational spring at an internal node. Figure 2.4(d) represents an idealization of the model. The constitutive relationship of the shear panel follows the model of Lowes and Altoontash (2003). To alleviate the limitation of the MCTF for joints with no transverse reinforcement, the calibration of constitutive parameters was still required. Altoontash (2004) modified the beam or column fiber sections to represent the bar pull-out mechanisms based on the assumption that the development length is adequate to prevent complete pullout.

However, this assumption is not necessarily true for joints with discontinuous beam bottom reinforcement. The validation was performed for interior beam-column joint subassemblages tested by Walker (2001) and a 0.7 scale two-story RC frame tested by Tsai et al. (2001).

Figure 2.4(e) illustrates an idealization of the joint model developed by Shin and LaFave (2004). The joint model consists of four rigid elements located along the edges of the panel zone connected via hinges and three nonlinear rotational springs embedded in one of the four hinges. These rotational springs are used to simulate the inelastic behavior of joint core under shear loading. To describe the nonlinear response associated with bar-slip and the plastic hinge in the beams, supplementary rotational springs are placed between the beam ends and the joint. The MCFT was utilized to determine the moment curvature relationship of the three nonlinear springs attached in parallel to capture the joint shear behavior and the bond-slip rotational springs were calibrated following the model of Morita and Kaku (1984). The analytical predictions were compared with the experimental results of ductile RC interior beam-column joint subassemblages.

The aforementioned joint models (Youssef and Ghobarah 2001, Lowes and Altoontash 2003, Mitra and Lowes 2007, Altoontash 2004, Shin and LaFave 2004) were developed employing the MCFT to define the backbone curve of a joint panel. However, the review of the previous models demonstrates that the MCFT approach is not appropriate to predict the shear strength for non-ductile joints with insufficient joint transverse reinforcement. Additionally, LaFave and Shin (2005) demonstrated that the MCFT may underestimate the joint shear strength for such joints. Therefore, the MCFT

can provide the reasonable estimate of joint shear strength for ductile joints while the application of the MCFT to non-ductile joints requires additional modifications.

Celik and Ellingwood (2008) developed a non-ductile joint model based on the experimental determination of joint panel shear stress-strain relationship, with inclusion of the bond stress of insufficient beam bottom reinforcement anchorage. Following the model of Alath and Kunnath (1995), the joint model was constructed. The backbone curve of the joint is a quad-linear curve consisting of four key points: concrete cracking, member yielding, ultimate, and residual conditions. Thus, this proposed approach is limited to the case when shear failure occurs after beam yielding. Ordinates on the backbone curve of the joint were computed through moment-curvature analyses for members adjacent to the joint. Then, the joint shear strength was adopted as the smallest of experimental and analytical values. Furthermore, the damage pinching parameters of the joint were not addressed, and therefore their model underestimates the joint shear and overall deformation for the case of joints experiencing a highly pinched hysteresis.

Sharma et al. (2011) proposed a principal tensile stress-shear deformation relationship to simulate the shear behavior for non-ductile exterior joints with different reinforcement details. As presented in Figure 2.4(f), the joint panel consists of one joint rotational spring in the beam region and two joint shear springs in the column portion. The beam and columns were modeled as lumped plasticity elements. Using the principal tensile stresses proposed by Priestley (1997), the authors assumed separate principal tensile stress-shear deformations for exterior joints with beam bottom reinforcement bent-in and straight with short embedment, respectively. In particular, the latter was intended to simulate the bond failure associated with the pullout action of discontinuous beam

bottom reinforcement. The model validation was performed for non-ductile exterior beam-column joint assemblages with different types of beam bottom reinforcement. However, their model can only be applied to exterior beam-column joints.

Anderson et al. (2008) proposed a monotonic and cyclic shear stress-strain model for joints without transverse reinforcement tested by Walker (2001) and Alire (2002). The model replicated cyclic degradation in strength and stiffness and energy dissipation of the unloading and reloading branches. The model can provide accurately the hysteretic response of the joint for various displacement histories, joint shear stress demands, and concrete compressive strength. Because the model was developed without using existing software programs, the proposed approach is not suitable for modeling large structures.

From the literature review above, the mechanics-based or empirical-based joint model is limited to a specific joint type (interior or exterior as well as non-ductile or ductile). Therefore, a unified joint shear model that can be simply and properly applied to various joint types is required when creating the analytical frame model.

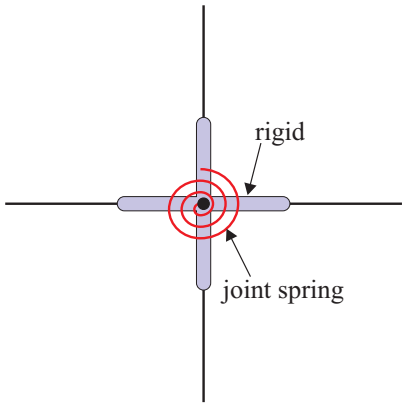

(a) Alath and Kunnath (1995)

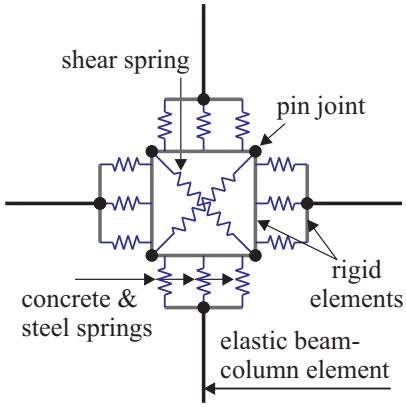

(b) Youssef and Ghobarah (2001)

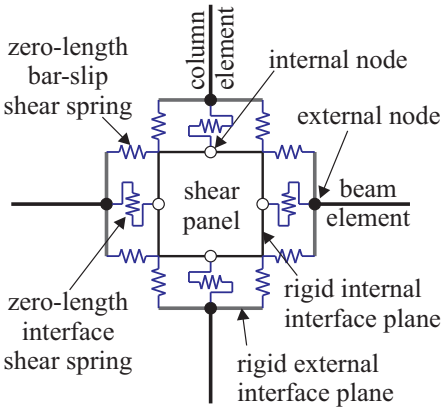

(c) Lowes and Altoontash (2003)

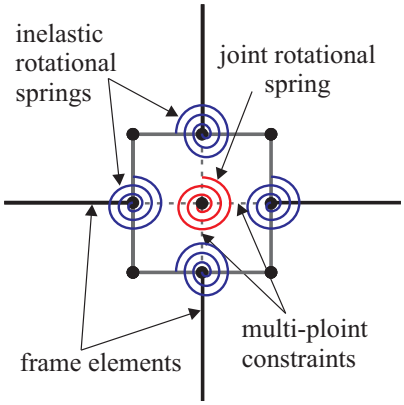

(d) Altoontash (2004)

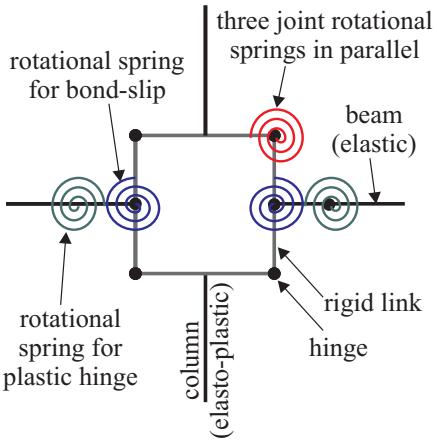

(e) Shin and LaFave (2004)

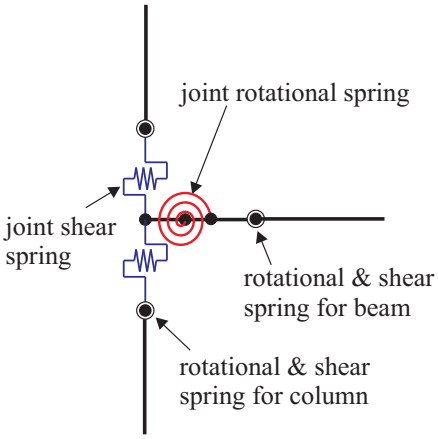

(f) Sharma et al. (2011)

Figure 2.4 Existing beam-column joint models

2.4 Summary

This chapter first reviewed literature addressing the effect of aftershocks on structures in terms of their increased demand and vulnerability under multiple earthquakes. Following the analytical study of Mahin (1980), several studies demonstrated that aftershocks might imply a considerable accumulation of damage and that a thorough understanding of the impact of aftershock can be achieved through numerous mainshock-aftershock sequences. To investigate additional damage after aftershocks, aftershock ground motions should produce additional damage. Although as-recorded (real) mainshock-aftershock sequences can reflect real seismic responses, they cannot significantly increase peak and permanent drift demands in some cases. These insufficient as-recorded data have led researchers to employ artificial mainshock-aftershock sequences when performing the seismic risk assessment of structures. Among the artificial sequences, mainshock-aftershock sequences randomly assembled provided more accurate estimates compared to identical sequences. For these reasons, randomly paired mainshock-aftershock sequences will serve as input motions for the development of aftershock fragility curves.

More recently, efforts to achieve a probabilistic risk assessment for aftershocks have been performed by few researchers. Aftershock fragility curves can be developed by thoroughly understanding the fundamental concept and simulation techniques for mainshock (typical) fragility functions. Most existing aftershock fragility curves given a mainshock response have been generated only by the stripe approach (IDA) for SDOF systems. However, the stripe method can have limitations such as computational expense and the use of unrealistic aftershock ground motions, and the SDOF models cannot provide accurate results as well as localized failure modes. Therefore, this research will

employ a cloud method for MDOF models that is comparable with a closed form of aftershock fragility function and that reflects feasible ground motions.

The appropriate prediction of the analytical models is an essential prerequisite for the reliable estimate of seismic performance and risk assessment of RC frames. For this purpose, existing analytical modeling techniques for frame's critical components such as shear-dominated columns and beam-column joints are finally reviewed, and their merits and shortcomings are discussed. For shear-dominated columns, the column shear model developed by Elwood (2004) will be employed by sufficiently validating the model for numerous specimens. Additionally, for beam-column joints, a unified joint model will be proposed by modifying the joint shear model developed by Anderson et al. (2008), so it can be applied to all different types of joints. These models will be incorporated in the finite element models of RC frames in subsequent aftershock fragility analyses.

CHAPTER 3

ANALYTICAL MODELING TECHNIQUE OF RC FRAME COMPONENTS

The earliest seismic provisions in the United States were introduced following the 1906 San Francisco earthquake (Popov 1994). This provision is intended to account for the effect of earthquakes and wind force using a lateral pressure of 1.4 kPa. Following the 1933 Long Beach earthquake, the concept of seismic lateral forces proportional to mass was incorporated into practice. Since 1933, the building code provisions have been considerably evolved to incorporate improvements in earthquake engineering and seismic risk assessment, especially in response to experiences during major earthquakes in California such as the 1971 San Fernando, the 1989 Loma Prieta, and the 1994 Northridge earthquakes. In order to improve the seismic resistance and to ensure ductile failure, these seismic design codes had accounted for minimum lateral design force requirements as well as the detailing requirements. For example, Table 3.1 shows the evolution of design philosophies for columns (Sezen 2002). This change in the seismic code requirements can result in the distinct difference in the structural capacities of non-ductile and ductile structures. Table 3.2 summarizes the design attributes of non-ductile and ductile RC components, and Figure 3.1 illustrates the reinforcing details of the two frames. The ductile frames are designed to have sufficient deformation capacities and energy dissipation capabilities of components while the non-ductile frames can infer unpredictable partial damage and collapse associated with little or no consideration of seismic resistance. These insufficient reinforcement details can cause shear failure or lap-

splice failure in columns, joint shear failure or bond failure due to discontinuous beam bottom reinforcement in joints, premature column failure owing to the design concept of weak column-strong beam. Figure 3.2 shows types of possible brittle failures in the non-ductile frames. Therefore, a thorough understanding of design attributes based on the time of building design or construction are required for the establishment of analytical models for critical components. These analytical models should capture the inelastic behavior of these components to reduce the (epistemic) uncertainties in seismic risk assessment. Furthermore, all analytical models are implemented in an open source, object-oriented software framework, OpenSees (McKenna et al. 2010).

This chapter presents the analytical modeling techniques for critical RC components such as the flexure and shear behavior in columns and the joint shear behaviors of non-ductile and ductile beam-column joints. Furthermore, the analytical models are validated through the comparison with experimental results available in the literature.

Table 3.1 Column dimension and detailing requirements in US building codes (Sezen 2002)

	1961 UBC (ICBO 1961)	ACI 318-71 (1971)	ACI 318-02 (2002)
Minimum width (b_c)	254 mm	NA	254 mm or $0.4d_c$
Minimum depth (d_c)	305 mm	NA	305 mm
ρ (longitudinal)	$0.01 \le \rho \le 0.08$	$0.01 \le \rho \le 0.06$	$0.01 \le \rho \le 0.06$
Tie spacing in the middle	• Smallest of $16\phi_b$, $48\phi_{b\text{-}tie}$, and minimum dimension	• Smallest of $16\phi_b$, $48\phi_{b\text{-}tie}$, minimum dimension • Smallest of 254 mm and $d_c/2$ for ductile columns	• Smallest of 152 mm and $6\phi_b$
Tie spacing in the end	NA	• Smallest of $16\phi_b$, $48\phi_{b\text{-}tie}$, minimum dimension • $d_c/4$ for ductile columns	• Smallest of 102 mm and $b_c/2$
Hooks	NA	135º hook	135º hook
Failure mode	brittle	brittle and ductile	ductile

Table 3.2 Design attributes of non-ductile and ductile RC frame components

	Non-ductile component	Ductile component
Beam	• May have discontinuous bottom longitudinal reinforcement in joints and no top reinforcement in the middle • Relatively wide transverse reinforcement with 90º hooks	• Continuous bottom longitudinal reinforcement in joints, sufficient development length • Shear capacity design, transverse reinforcement with 135º hooks
Column	• Weak column-strong beam: soft story failure mode, column hinging • Short lap-splice in longitudinal reinforcement • Widely spaced transverse reinforcement with 90º hooks	• Strong column-weak beam • Adequate lap-splice in longitudinal reinforcement • Shear capacity design, closely spaced transverse reinforcement with 135º hooks
Beam-column joint	• No or little transverse reinforcement • Inadequate anchorage length of bottom beam reinforcement	• Sufficient transverse reinforcement • Continuous bottom beam Reinforcement
Slab-column connection	• Flexure	• Continuous slab bottom reinforcement • No flat slab

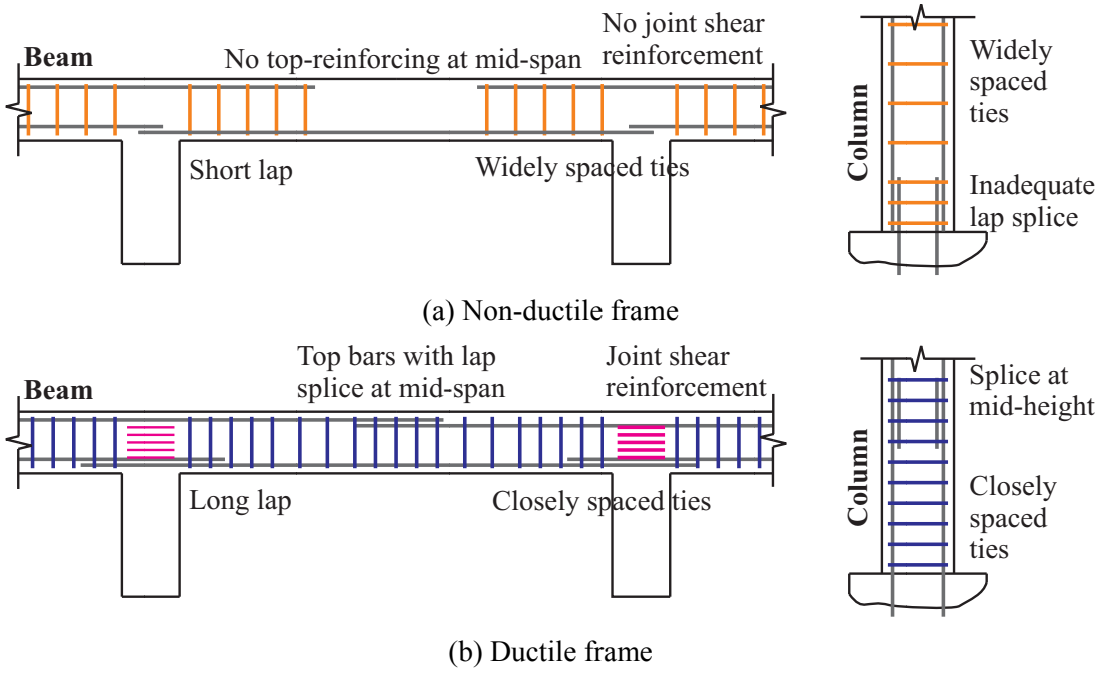

Figure 3.1 Reinforcing details of non-ductile and ductile RC frames

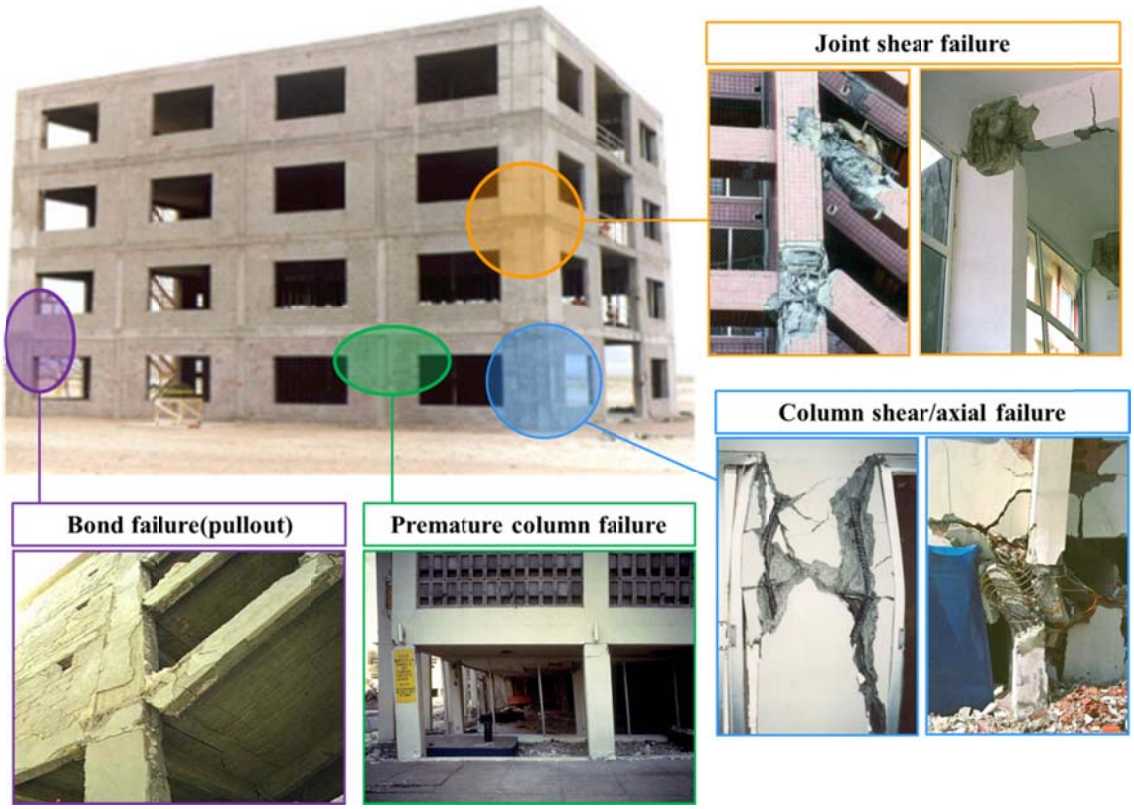

Figure 3.2 Potential failure modes in non-ductile RC frames

3.1 Modeling Flexure Behavior of Columns and Beams

3.1.1 Analytical model

Figure 3.3 illustrates the analytical models of columns and beams dominated by flexure. The columns are modeled as an elastic element in the middle and two fiber section beam-column elements in the plastic hinge region(s) while the beams are modeled as a beamWithHinges element (Scott and Fenves 2006) that is composed of three parts: two plastic hinge zones (fiber section) at the ends of the element and a linear elastic region (effective stiffness) in the middle of the element. Different elements are utilized for the columns and the beams to capture a stable inelastic behavior in columns and reduce computational time under static or dynamic analysis when analyzing large building structures.

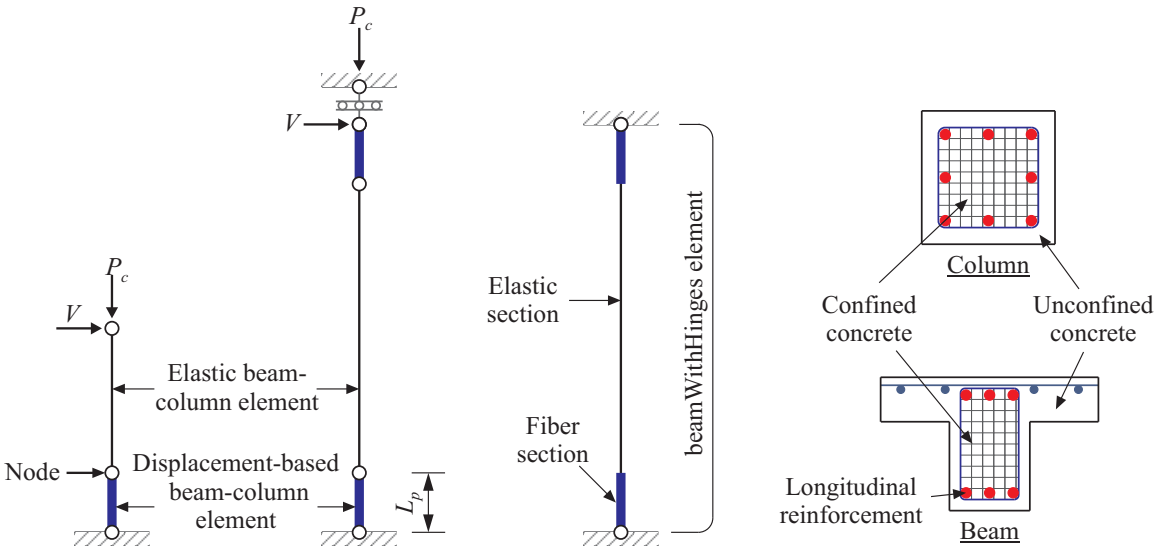

Figure 3.3 Analytical flexure models of columns and beams

For both components, the plastic hinge length L_p is assumed to be the corresponding section depth. All fiber sections used in columns and beams consist of unconfined (cover) and confined (core) concrete properties assigned to the fibers together with a precise location of the longitudinal reinforcement. Both unconfined and confined concrete can be modeled using Concrete02 to account for their tensile behavior. The model of Mander et al. (1988) includes the enhanced compressive strength and ductility of the core concrete associated with the confinement factor. Additionally, the longitudinal reinforcement is represented using Steel02 based on the Giuffré-Menegotto-Pinto model (Menegotto and Pinto 1983) to include isotropic strain hardening. Additionally, the effective width of the slab can be calculated following the recommendation of ACI318-02 (2002).

The effective stiffness of elastic materials in columns and beams are calculated by the recommendation in ASCE/SEI 41 (Elwood et al. 2007), as shown in Figure 3.4. For columns with axial load factor (defined as the axial load, P_c on a column divided by its cross-sectional area, A_g and concrete compressive strength, f_c, ALF = $P_c/A_g f_c$) ≤ 0.1, the modification factor is 0.3 while for columns with ALF ≥ 0.5, the factor 0.7. Otherwise, the factor is computed by linear interpolation between 0.3 and 0.7. For all beams, the factor is 0.3. This work has recommended that the lower bound stiffness modification factor be taken equal to 0.3 to reduce the risk of underestimating shear forces in columns sharing lateral load with other components, and that by inference it can be applicable to beams.

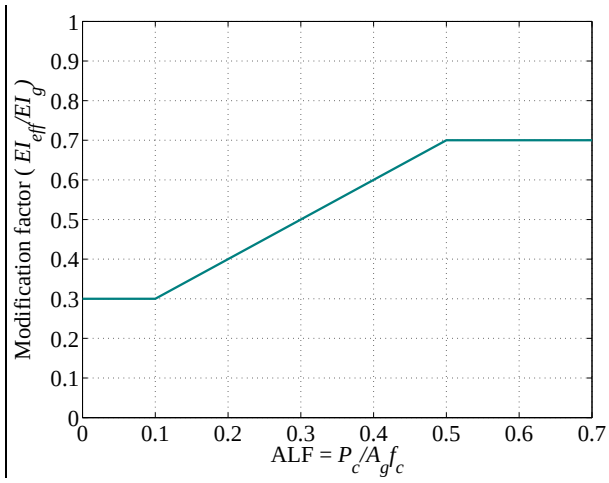

Figure 3.4 Effective stiffness determination of Elwood et al. (2007)

3.1.2 Validation of analytical model

For the validation of the analytical models, six specimens experiencing the ductile behavior are selected, which are available in the literature (Unit 4 of Ang et al. (1981), NC-4 of Azizinamini et al. (1988), Unit 6 of Saatcioglu and Ozcebe (1989), Unit 1 of Tanaka and Park (1990), BG-3 of Saatcioglu and Grira (1999), and Unit 9 of Park and Paulay (1990)). The experimental data are obtained from the PEER structural performance database (Berry et al. 2004). A detailed description of specimen configuration and loading method can be found in the references. Figure 3.5 shows the comparison of the experimental and analytical shear force-drift results for columns with flexure-dominated behavior. In general, the overall behavior shows excellent correlation with regard to strength, stiffness, and energy dissipation. Table 3.3 indicates the maximum column shear forces obtained from experiment and analysis. It is indicated that the maximum shear forces from analyses show a good agreement with the experimental measurements (less than 5% difference). Therefore, the analytical models can accurately provide the inelastic behavior of columns dominated by flexure.

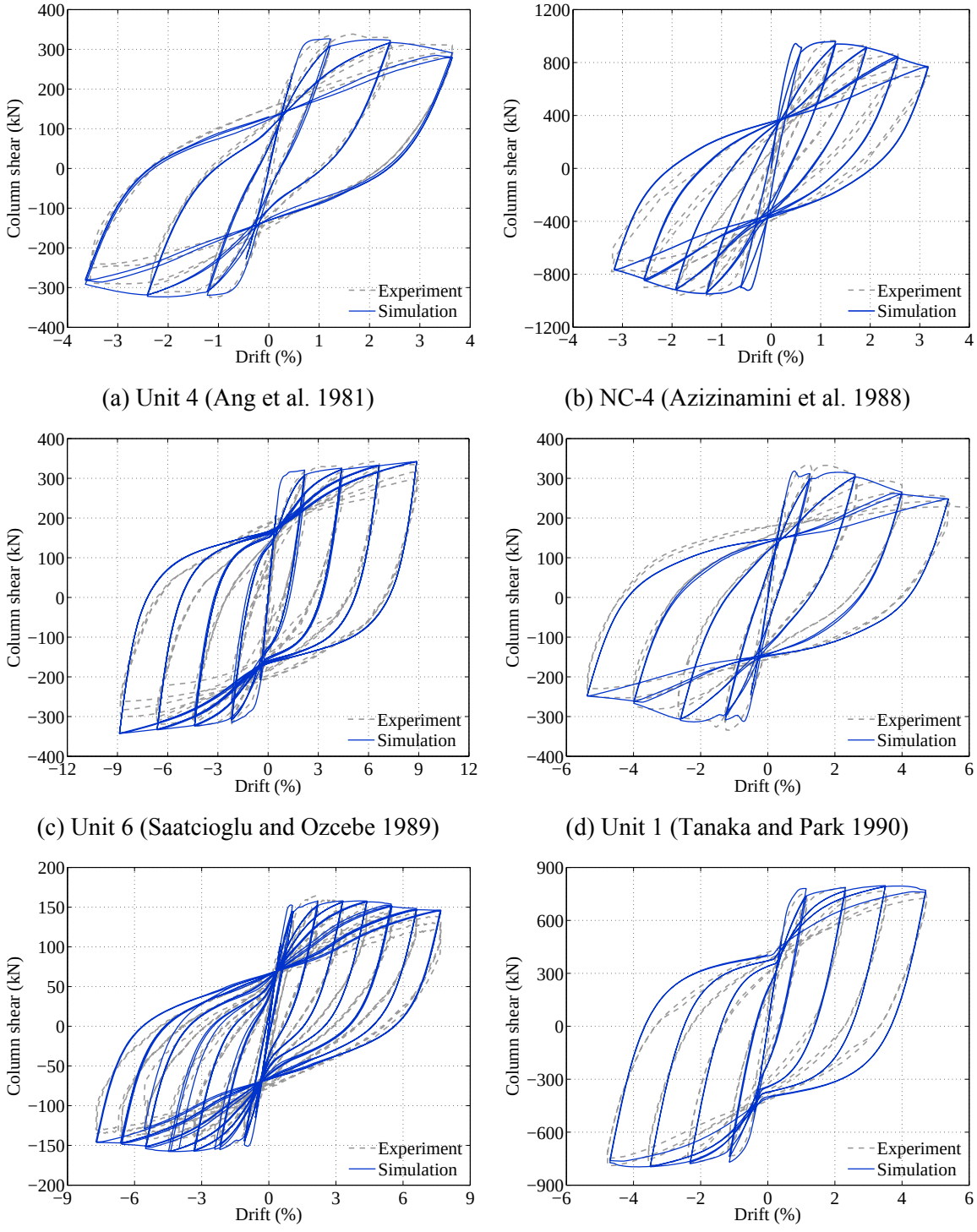

(a) Unit 4 (Ang et al. 1981)

(b) NC-4 (Azizinamini et al. 1988)

(c) Unit 6 (Saatcioglu and Ozcebe 1989)

(d) Unit 1 (Tanaka and Park 1990)

(e) BG-3 (Saatcioglu and Grira 1999)

(f) Unit 9 (Park and Paulay 1990)

Figure 3.5 Comparison between experimental and analytical force-drift hysteresis loops for flexure-critical columns

Table 3.3 Comparison of experimental and analytical maximum shear force for flexure-critical columns

Specimens	Maximum shear force (kN)		Difference (%)
	Experiment	Analysis	
Unit 4 (Ang et al. 1981)	338	326	-3.6
NC-4 (Azizinamini et al. 1988)	966	960	-0.7
Unit 6 (Saatcioglu and Ozcebe 1989)	343	342	-0.1
Unit 1 (Tanaka and Park 1990)	334	318	-4.6
BG-3 (Saatcioglu and Grira 1999)	164	158	-3.9
Unit 9 (Park and Paulay 1990)	786	797	+1.4

3.2 Modeling Shear Behavior of Columns

3.2.1 Analytical model

Flexure-shear-critical columns are modeled as two fiber section beam-column elements, an elastic element, two zero-length bar-slip fiber section elements associated with the effect of bond slip at the end of columns, and a shear spring, as implemented in Figure 3.6. The fiber section beam-column elements and an elastic element are modeled in the same way as the flexure dominant columns. To account for the bar slip at the end of a column, the constitutive law of the longitudinal reinforcement is modified from a stress-strain relationship to a stress-slip relation to employ the zero-length element. The slip-strain relationship is presented by Sezen (2002):

$$slip = \frac{\varepsilon_y f_y \phi_b}{8u_e}, \quad u_e = 0.9\sqrt{f_c}, \quad SF_{slip} = \frac{slip}{\varepsilon_y} \tag{3.1}$$

where ε_y is the longitudinal reinforcement yield strain, f_y the longitudinal reinforcement yield stress (MPa), d_b the diameter of longitudinal reinforcement (mm), f_c the concrete compressive strength (MPa), u_e the elastic bond stress (MPa), and SF_{slip} the scale factor. By multiplying the strains of steel and concrete by the scale factor (SF_{slip}), modified

concrete and steel stress-slip relationship is employed in the zero-length fiber section element.

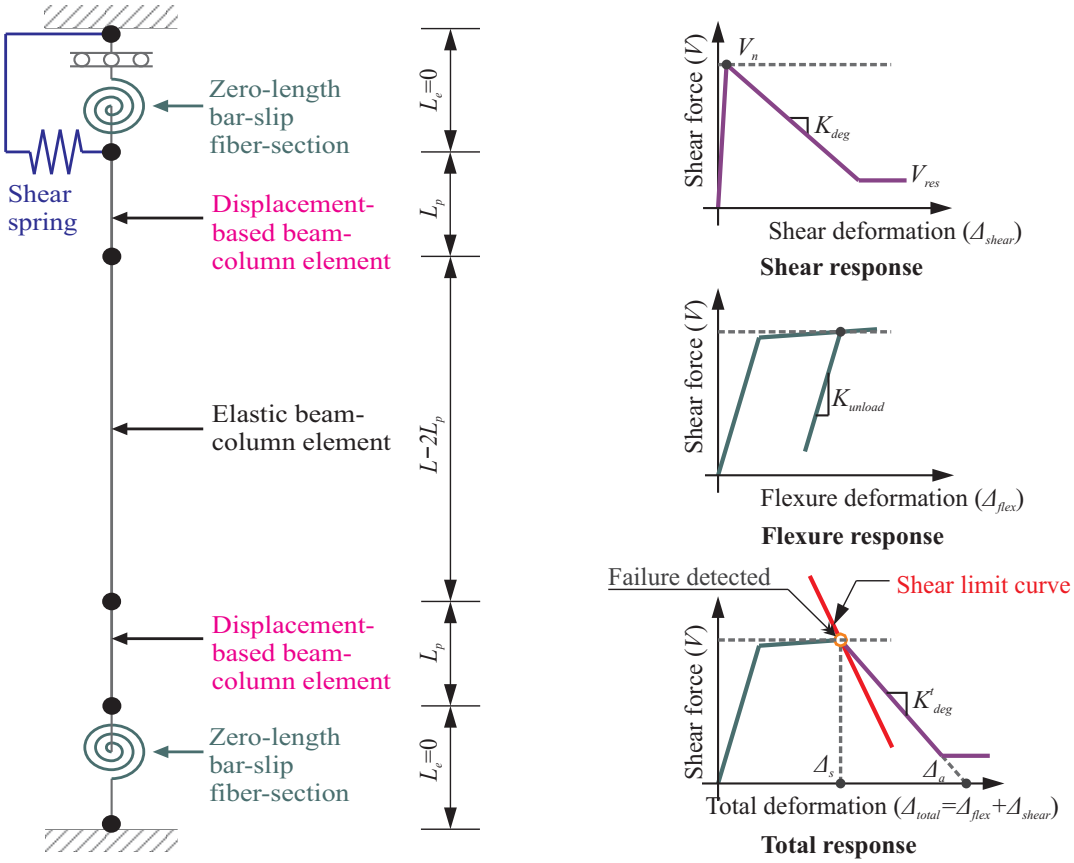

Figure 3.6 Modeling flexure-shear-critical column

To describe the shear behavior in the columns, the limit state material developed by Elwood (2004) is employed. Once the column's total response exceeds a predetermined shear failure surface (so-called *limit shear curve*), its shear response follows the constitutive law of the limit shear curve to include pinching and strength and stiffness degradation. The limit shear curve consists of the column shear capacity (V_n), the degrading slope (K_{deg}), and residual shear strength (V_{res}), as indicated in Figure 3.6.

After shear failure is detected, the degrading slope of the total response (K^t_{deg}) can be computed in equation (3.2) (Elwood 2004):

$$K^t_{\deg} = \frac{V_n}{\Delta_a - \Delta_s} \tag{3.2}$$

where Δ_a the displacement calculated under the axial load at the time of shear failure, and Δ_s the displacement at the onset of shear failure. If K^t_{deg} is determined, the degrading flexibility of the shear spring ($1/K_{\deg}$) can be calculated by subtracting the flexural flexibility ($1/K_{unload}$) from $1/K^t_{deg}$. Additionally, Δ_a can be obtained from equation (3.3) (Elwood 2004):

$$\frac{\Delta_a}{L} = \frac{4}{100} \frac{1+\tan^2\theta}{\tan\theta + P(s/A_v f_{yt} d_{cc} \tan\theta)} \tag{3.3}$$

where L is the length of column, d_{cc} the depth of column core from centerline to centerline of transverse reinforcement, s the spacing of transverse reinforcement, A_v the area of transverse reinforcement, f_{yt} the yield strength of transverse reinforcement, P the axial load on the column, and θ the critical crack angle from horizontal (assumed to be 65°). A detailed description of the limit state material (limit shear curve) can be found in Elwood (2004).

3.2.2 Validation of analytical model

As mentioned in Chapter 2, Elwood (2004) did not address the validity of the column shear model under reversed cyclic pushover loadings. To overcome this drawback, this research performs the validation of the shear model of Elwood (2004) by comparing

analytical and experimental results for shear-dominated columns available in the literature.

The shear failure model in the current version of OpenSees can be triggered only when a drift at the initiation of shear failure is above 0.01. Therefore, to model some shear-dominated columns detected below a drift of 0.01, the source code can be modified using a smaller value than 0.01. Furthermore, the shear force at shear failure (shear strength, V_n) can be determined from the equation of ACI318-02 (2002) or ASCE 41-06 (Elwood et al. 2007). However, if the shear strength calculated from these equations is larger than the plastic shear force or smaller than the yielding shear force obtained from a flexure analysis (without a shear spring), the overall behavior would not appropriately capture the drop in load-carrying capacity associated with a shear failure for flexure-shear-critical columns. The shear spring remains elastic and the simulated results would be the same as a model without a shear spring. Therefore, this research utilizes a shear force obtained from the flexure analysis (without a shear spring model) near the experimental shear strength to capture the shear behavior. The equation for the shear force at shear failure (V_n) in the source code can be also modified because there is no variation in axial force on a column under monotonic and reversed cyclic static pushover loadings. Moreover, for simplicity, the unloading stiffness is assumed to be the stiffness modification factor of 0.5 described in the previous section, in the model validation.

To verify the analytical model for the flexure-shear-critical columns, a database of 42 flexure-shear-critical specimens are collected from PEER database or other experimental work available in the literature and are simulated in OpenSees (McKenna et al. 2010). Table 3.4 depicts the collected database for these columns, which does not

include specimens experiencing the shear failure before flexure yielding in order to ensure the applicability of the model of Elwood (2004). Figure 3.7 shows the comparison of experimental and analytical hysteretic responses for six specimens in order to examine the accuracy of the shear model with different configurations of column tests: double curvature (DC), cantilever (C), and double ended columns (DE). A detailed description of test configuration, material properties, and loading conditions can be found in the references. The comparison plots for all 42 specimens can be found in Appendix A. Although the hysteretic rules of the shear model result in slightly higher stiffness and strength than experimental results for some cases, the analytical shear model can appropriately capture the degrading slope and cyclic deterioration regardless of the configuration of column specimens. Moreover, Table 3.5 presents the maximum column shear forces from experiment and analysis for these six specimens. It is demonstrated that the maximum shear force from analysis shows a good agreement with the experimental measurements (less than 5% difference). Therefore, the shear model can adequately predict the overall strength and stiffness of the response.

Table 3.4 Collected shear-dominated column database

Reference	Specimen	Test type	f_c (MPa)	f_{yt} (MPa)	b_c (mm)	h_c (mm)	d_c (mm)	s (mm)	L (mm)	ρ_w	P (kN)	$V_{n,exp}$ (kN)
Sezen (2002)	Specimen 1	DC	21.1	476	457	457	392	305	2946	0.0017	667	315
	Specimen 4	DC	21.8	476	457	457	392	305	2946	0.0017	667	295
Lynn et al. (1996)	3CLH18	DC	25.6	400	457	457	393	457	2946	0.0007	503	277
	3SLH18	DC	25.6	400	457	457	393	457	2946	0.0007	503	270
	2SLH18	DC	33.1	400	457	457	397	457	2946	0.0007	503	229
	2CMH18	DC	25.5	400	457	457	397	457	2946	0.0007	1512	305
	3CMH18	DC	27.6	400	457	457	393	457	2946	0.0007	1512	328
	3CMD12	DC	27.6	400	457	457	393	305	2946	0.0017	1512	355
	3SMD12	DC	25.5	400	457	457	393	305	2946	0.0017	1512	365
Ohue et al. (1985)	2D16RS	DC	32.2	316	200	200	175	50	800	0.0057	183	98
	4D13RS	DC	29.9	316	200	200	175	50	800	0.0057	183	110
Esaki (1996)	H-2-1/5	DC	23.0	364	200	200	175	50	800	0.0052	184	108
	HT-2-1/5	DC	20.2	364	200	200	175	75	800	0.0052	162	106
	H-2-1/3	DC	23.0	364	200	200	175	40	800	0.0065	307	118
	HT-2-1/3	DC	20.2	364	200	200	175	60	800	0.0065	269	116
Nagasaka (1982)	HPRC19-32	DC	21.0	344	200	200	180	20	600	0.0141	294	113
Ono et al. (1989)	CA025C	DC	26.3	426	200	200	170	70	600	0.0081	265	130
	CA060C	DC	26.3	426	200	200	170	70	600	0.0081	635	137
Mostafaei et al. (2009)	No. 5	DC	28.5	410	300	300	260	50	750	0.0043	540	322
Ousalem et al. (2002)	No. 4	DC	13.5	384	300	300	260	75	900	0.0028	365	170
	No. 8	DC	18.0	384	300	300	260	75	900	0.0028	486	204
	No. 12	DC	18.0	384	300	300	260	75	900	0.0028	324	220
Ousalem et al. (2003)	No. 14	DC	26.1	410	300	300	260	50	900	0.0043	540	300
	No. 15	DC	26.1	410	300	300	260	50	900	0.0086	540	356
	No. 16	DC	26.1	410	300	300	260	50	600	0.0043	540	339
Saatcioglu and Ozcebe (1989)	U1	C	26.1	470	350	350	305	150	1000	0.0030	0	276
	U2	C	30.2	470	350	350	305	150	1000	0.0030	600	279
	U3	C	34.8	470	350	350	305	75	1000	0.0060	600	271
Ikeda (1968)	43-H-3	DE	19.6	563	200	200	173	100	500	0.0028	78	152
	44-H-4	DE	19.6	563	200	200	173	100	500	0.0028	78	142
	45-H-5	DE	19.6	563	200	200	173	100	500	0.0028	157	164
	46-H-6	DE	19.6	563	200	200	173	100	500	0.0028	157	158
	62-L-4	DE	19.6	477	200	200	173	100	500	0.0028	78	115
	63-L-5	DE	19.6	477	200	200	173	100	500	0.0028	157	137
	64-L-6	DE	19.6	477	200	200	173	100	500	0.0028	157	139
Kokusho (1964)	81-$_1$C$_{32}$	DE	21.5	332	200	200	170	100	500	0.0033	157	178
	372-$_2$C$_{12}$	DE	19.9	353	200	200	170	100	500	0.0033	157	143
	373-$_2$C$_{22}$	DE	20.4	353	200	200	170	100	500	0.0033	157	177
Takeda and Yoshioka (1970)	115-085A56	DE	20.6	342	300	300	248	56	700	0.0084	494	560
	118-085A80	DE	20.6	342	300	300	248	56	700	0.0084	706	563
	139-12AA56	DE	19.6	371	300	300	248	40	450	0.0118	494	758
	140-12AA80	DE	19.6	371	300	300	248	40	450	0.0118	706	754

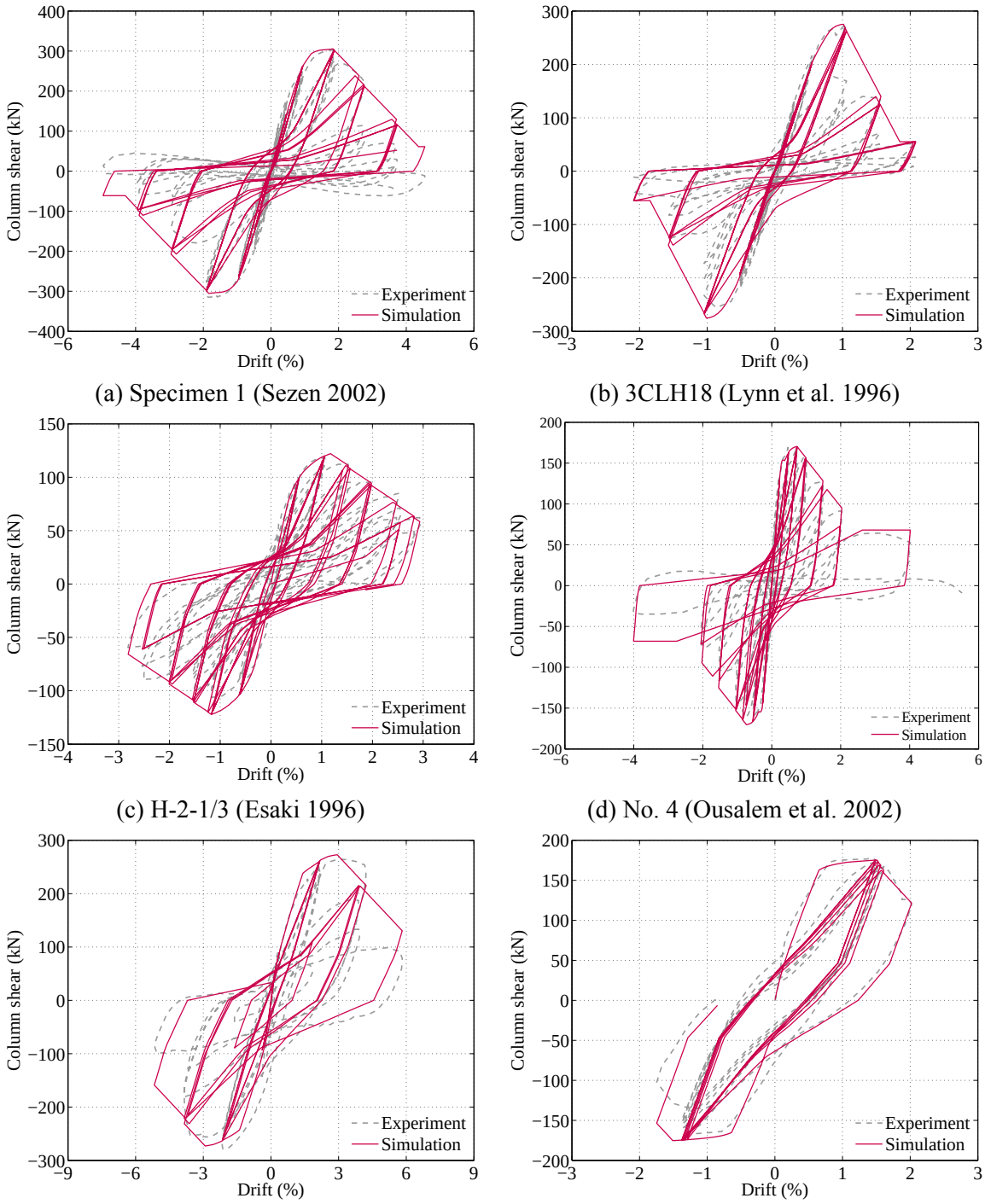

(a) Specimen 1 (Sezen 2002)

(b) 3CLH18 (Lynn et al. 1996)

(c) H-2-1/3 (Esaki 1996)

(d) No. 4 (Ousalem et al. 2002)

(e) U2 (Saatcioglu and Ozcebe 1989)

(f) 81-$_1$C$_{32}$ (Kokusho 1964)

Figure 3.7 Comparison between experimental and analytical force-drift hysteresis loops for flexure-shear-critical columns

Table 3.5 Comparison of experimental and analytical maximum shear force for flexure-shear-critical columns

Specimens	Maximum shear force (kN)		Difference (%)
	Experiment	Analysis	
Specimen 1 (Sezen 2002)	315	306	-2.9
3CLH18 (Lynn et al. 1996)	277	275	-0.6
H-2-1/3 (Esaki 1996)	118	122	+3.3
No. 4 (Ousalem et al. 2002)	170	170	+0.3
U2 (Saatcioglu and Ozcebe 1989)	279	273	-2.0
81-$_1C_{32}$ (Kokusho 1964)	178	175	-1.5

3.3 Modeling Non-Ductile Beam-Column Joints

Beam-column joints can be classified into two groups following the recommendation of ASCE41-06 (Elwood et al. 2007); a joint is ductile if hoops are spaced at less than the half of column depth within the joint, and otherwise, a joint is non-ductile.

The main deficiencies in older RC buildings are inelastic mechanisms that are not suitable for ductile response and inadequate detailing of yielding components, including beam column joints. The specific joint details and resulting deficiencies vary depending on the local construction practices. The most common deficiencies are lack of joint transverse reinforcement and insufficient anchorage of beam bottom longitudinal reinforcement in joints. Figure 3.8 shows typical reinforcing details in non-ductile beam-column joints that can be found in the work of Moiser (2000) and Kunnath et al. (1995) for older RC buildings in California and the Central and Southern United States, respectively. Non-ductile joints with the design details in Figures 3.8(a) and 3.8(c) and those in Figures 3.8(b) and (c) may undergo significant joint shear and bond failure, respectively, during more severe earthquakes. Therefore, the analytical model should predict these potential failure modes associated with the reinforcing details in joints.

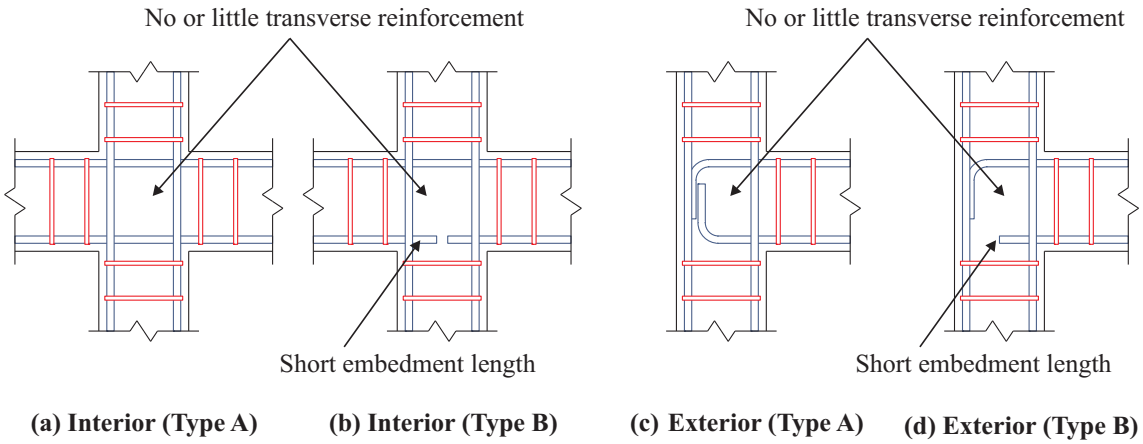

Figure 3.8 Typical reinforcing details in non-ductile beam-column joints

3.3.1 Joint shear failure model

To describe the shear behavior of beam-column joints, this research employs the joint model developed by Alath and Kunnath (1995). The joint panel can be represented as four rigid offsets with one zero-length rotational spring, as depicted in Figure 3.9. Other parts of beam-column joint subassemblages are modeled in the same manner as columns and beams.

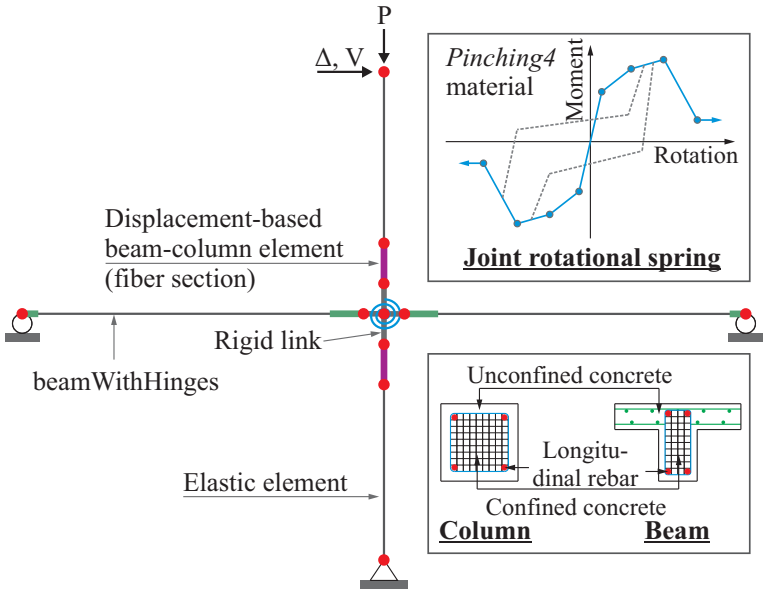

Figure 3.9 Analytical model of a beam-column joint subassemblage

Anderson et al. (2008) proposed the backbone curve of the joint shear stress-strain relationship for non-ductile interior joints based on the experimental work of Walker (2001) and Alire (2002), which is a quad-linear curve and can be simply implemented to other specimens. This research employs the model of Anderson et al. (2008) up to the third point on the curve, but modifies the fourth point based on experimental observations. Figure 3.10 shows the modified backbone curve of the joint shear stress-strain relationship. The first and second points are fixed, and the ordinates on the third and fourth points ($v_{j,max}$ and $v_{j,res}$) can be determined from experimental joint shear strength. Residual joint stress ($v_{j,4}$) is defined as 20% of joint shear strength ($v_{j,3}$) in order to alleviate convergence issues. Thus, the unknowns are the abscissas on the third and four points ($\gamma_{j,max}$ and $\gamma_{j,res}$), which are also determined from experimental observations.

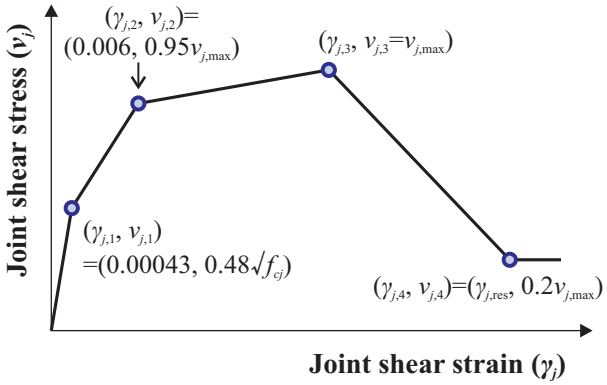

Figure 3.10 Proposed backbone curve of joint shear stress-strain relationship

Once the backbone curve of the joint shear stress-strain relationship is determined, the equivalent joint rotational moment-rotation relationship can be computed from the from the structure geometry and force equilibriums (Figure 3.11):

$$M_j = \frac{v_j A_j}{(1-b_j/L_b)/jd_b - \alpha/L_c}, \quad \theta_j = \gamma_j \tag{3.4}$$

where M_j is the joint rotational moment, v_j the joint shear stress, h_c the depth of the column, b_j the effective width of the joint panel calculated from ACI 352R-02 (2002), A_j the joint area ($A_j = h_c \cdot b_j$), L_b the total length of the left and right beams, L_c the total length of the top and bottom columns, j the internal moment arm factor (assumed to be 0.875 in this study), d_b the effective depth of the beam, α a constant equal to 2 for the top floor joints and 1 for the others, θ_j the joint rotation, and γ_j the joint shear strain. Since the joint rotation is the angle change between the two adjacent edges of the panel zone, the joint rotation equals the joint shear strain. A detailed derivation of the equation can be found in work of Celik and Ellingwood (2007).

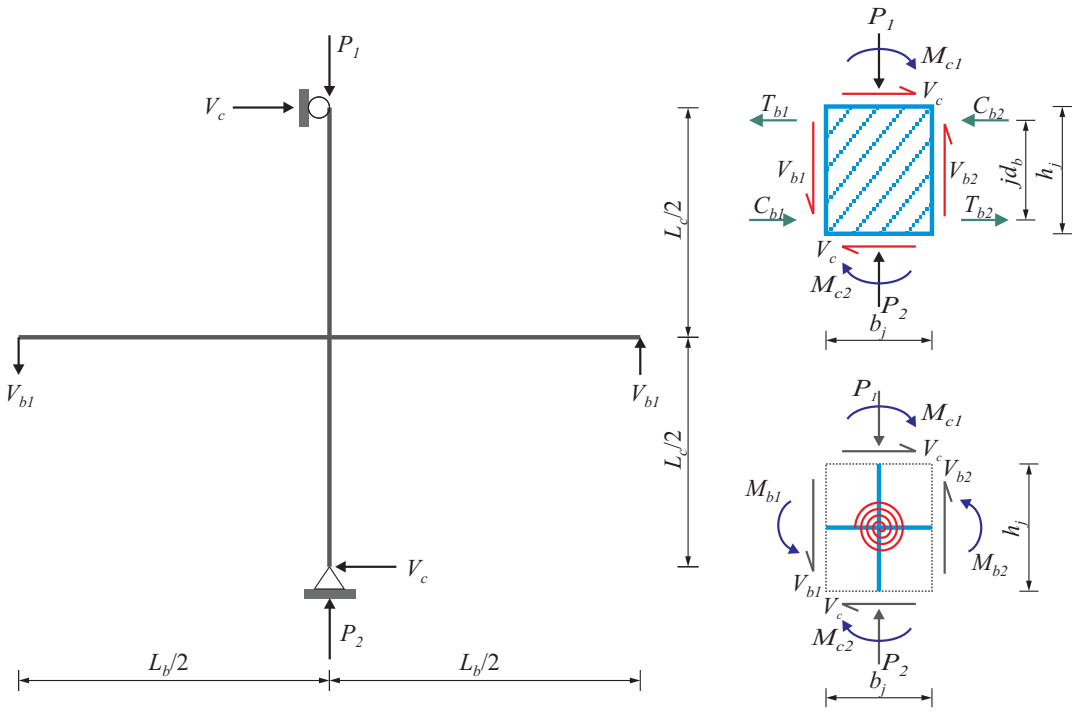

(a) Geometry of subassemblage (b) Force equilibrium of joint panel

Figure 3.11 Structural geometry and force equilibrium around a joint

The joint rotational spring is modeled using the *Pinching4* material developed by Lowes and Altoontash (2003) available in OpenSees (McKenna et al. 2010). As shown in Figure 3.12, the material model can be defined as a response backbone, an unload-reload path, and three damage rules: unloading stiffness degradation, strength degradation, and reloading strength degradation. A detailed formulation for damage index can be found in the work of Lowes and Altoontash (2003).

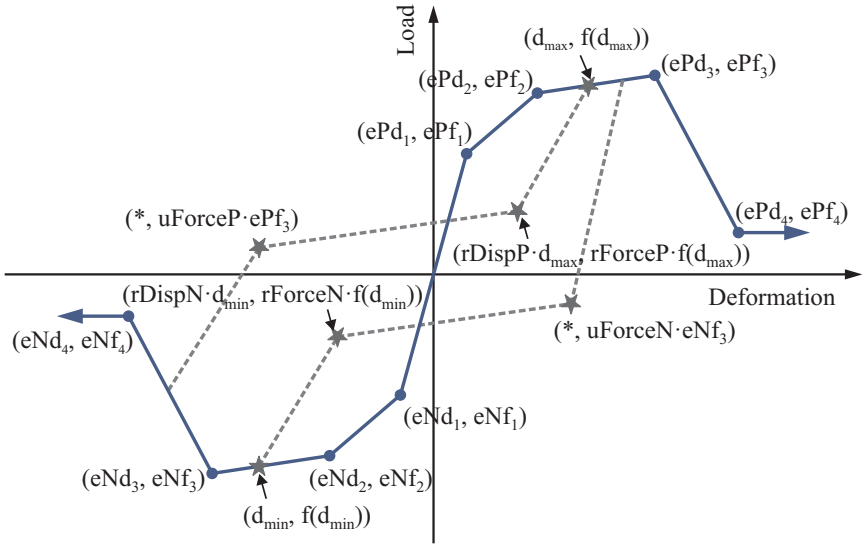

Figure 3.12 Constitutive model proposed by Lowes and Altoontash (2003)

3.3.2 Empirical joint bond failure model

Beam-column joints with short embedment length of beam bottom reinforcement within joints may undergo unpredictable brittle failure under more severe earthquakes, that is, premature bond pullout failure at less than 50% of the actual joint shear capacity directly related to the embedded length, as shown in Figure 3.13. In order to account for the reduced shear strength associated with the insufficient embedment length, this research utilizes the empirical bond strength model of Hassan (2011), which was developed

through the experimental observations of 21 specimens with no beam yielding. The bond strength model includes influential parameters such as column axial load (P), beam reinforcement diameter (ϕ_b), ratio of cover to reinforcement diameter (c/ϕ_b), presence of transverse beams, as expressed in equation (3.5):

$$\tau_{\max} = 1.1\left(\frac{P}{f_c A_g}\right)^{1/4} \sqrt{f_c}\,\Psi_s \Omega \frac{c}{\phi_b} \tag{3.5}$$

where $\tau_{\max}$ is the concrete average bond stress capacity of discontinuous beam bottom reinforcement, the reinforcement factor, Ψ_s is the reinforcement factor; $\Psi_s = 1$ for $\phi_b \geq 19$ mm and $\Psi_s = 1.25$ for $\phi_b \leq 19$ mm), and Ω is the transverse beam confinement factor; Ω = 1 for exterior joints with no transverse beam; Ω = 1.12 for exterior joints with one transverse beam; Ω = 1.20 for exterior joints with two transverse beams. c/ϕ_b is the minimum of bottom and side concrete cover-to-rebar diameter ratio measuring cover to rebar centroid, which is less than 2.5.

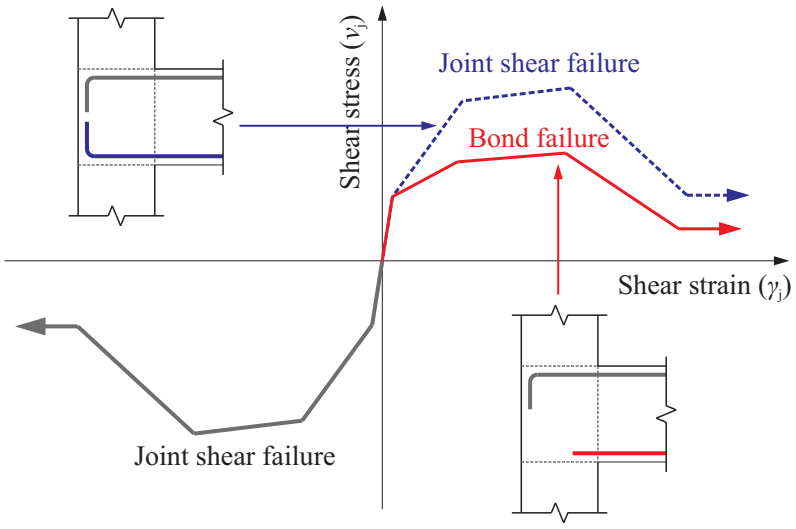

Figure 3.13 Backbone curve of joint shear failure model and bond failure model

Using the structure geometry and force equilibriums, as illustrated in Figure 3.14, the equivalent shear strength associated with insufficient embedment length can be calculated in equation (3.6):

$$v_{j,\max} = \frac{T_s}{A_j}\left[1 - \frac{(1+0.5h_c/l_b)jd_b}{L_c}\right] \tag{3.6}$$

where

$$T_s = n_b l_{sp} \pi \phi_b \tau_{\max} \tag{3.7}$$

and T_s is the tension force in beam longitudinal reinforcement corresponding to pullout failure, n_b the number of beam longitudinal reinforcement, l_{bsp} the embedment length within a joint, ϕ_b the diameter of the reinforcement, and l_b the beam length measured from the face of column to the face of column to the end of beam for subassemblages or the mid-span of beam for frames.

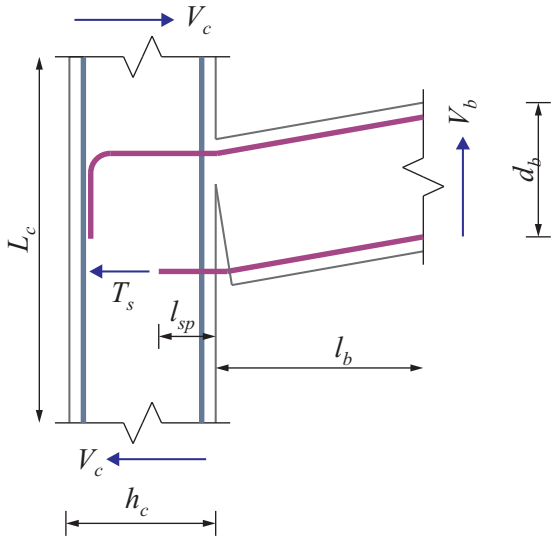

Figure 3.14 Equilibrium for bond failure model

Figure 3.15 shows the comparison of experimental and predicted equivalent joint shear strength (Hassan 2011). The mean and COV of the predicted-to-experimental shear strength ratio are 1.099 and 0.161, respectively. These values indicate that the empirical bond strength model provides reasonable estimates for joints with insufficient anchorage. In this research, the reduced equivalent joint shear strength is converted into the equivalent joint rotational moment using equation (3.4) to utilize the Pinching4 material in OpenSees (McKenna et al. 2010).

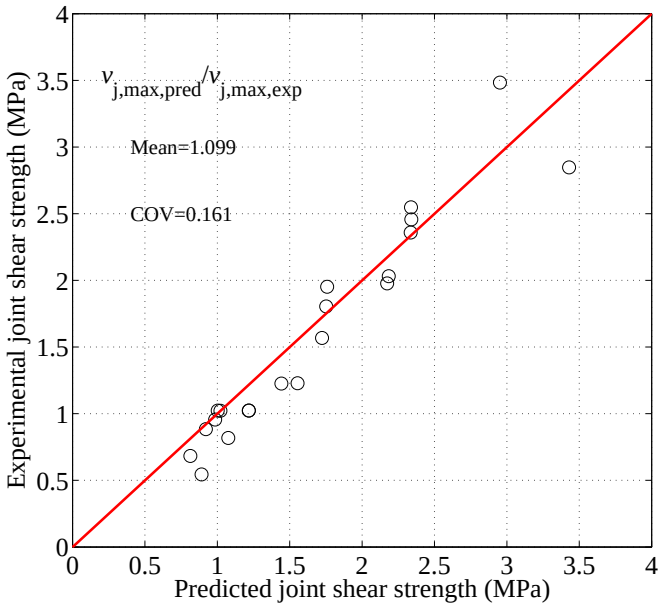

Figure 3.15 Comparison of experimental and predicted joint shear strength (Hassan 2011)

Experimental studies have suggested that bond slip causes additional rotation at the end of beams. However, Leon (1989) demonstrated that the boundary conditions of the subassemblages different from those of the indeterminate frame lead to a large amount of the slip in the experiment. For the intermediate frame, such slip would not likely occur. Additionally, Hoffman et al. (1992) mentioned that bond slip is very small

and usually is difficult to visually detect during the testing of indeterminate frames. Thus, the additional rotation as a result of the bond slip can be reduced in the analysis for RC frames. For this reason, this research did not account for the supplementary rotation introduced by the bond slip at the end of beams.

3.3.3 Validation of analytical model for subassemblages

To examine the validity of the joint shear and bond failure model for non-ductile beam-column joints, a database of 28 exterior and 35 interior beam-column joint subassemblages are gathered from experimental work available in the literature and are analyzed in OpenSees (McKenna et al. 2010). The database includes two failure modes: joint shear failure (a total of 57 specimens) and joint bond failure (a total of 6 specimens), and consists of specimens without and with transverse beams orthogonal to joints. Additionally, it is composed of specimens exhibiting joint shear failure before and after member (beam or column) yielding and joint bond failure.

The validation is performed based on experimental results to extract the parameters of backbone and hysteretic rules (Pinching4 material) so that those parameters can be adequately employed in modeling RC frames. Figure 3.16, Figure 3.17, and Figure 3.18 depict the comparison of experimental and analytical results for three groups: six exterior joints with joint shear failure, five exterior joints with joint bond failure, and six interior joints with joint shear failure, respectively. From these figures, it can be seen that the analytical results are well-correlated with experimental results with regard to strength, stiffness, and energy dissipation. In some specimens, the analytical model overestimates initial stiffness. This may be attributed to bond slip in members adjacent to a joint, which

is not taken into account in this research. It is, however, qualitatively clear that the comparison improves at higher deformation levels. Additionally, Table 3.6 summarizes the maximum lateral forces obtained from experiment and simulation for 17 specimens. From the table, good agreement is observed between the analytical predictions and the experimental results within a reasonable margin of 10 %. The joint bond failure model has a relatively large difference in maximum joint shear strength because the joint shear strength is calculated using the bond strength model of Hassan (2011). All of 63 comparison plots can be found in Figure A.2, Figure A.3, and Figure A.4 (Appendix A).

Table 3.7 and Table 3.8 present the modeling parameters of the Pinching4 material for non-ductile exterior and interior beam-column joints, respectively, which are extracted from the model validation described above. These values are examined separately for exterior and interior joints. The mean value of these parameters will be utilized when simulating structures in a probabilistic risk assessment.

Table 3.6 Comparison of experimental and analytical maximum lateral force for non-ductile beam-column joint subassemblages

Joint type	Failure mode	Specimens	Maximum lateral force (kN)		Difference (%)
			Experiment	Analysis	
Exterior	Joint shear failure	Unit 5 (Clyde et al. 2000)	267	266	-0.4
		T1 (Ghobarah and Said 2002)	115	117	+1.9
		JO (Ilki et al. 2011)	68	69	+1.7
		B0 (Karayannis et al. 2008)	58	63	+7.7
		Unit 6 (Pantelides et al. 2002)	198	196	-1.3
		F1 (Tsonos and Papanikolaou 2003)	68	64	+1.8
Exterior	Joint bond failure	Exterior (Aycardi et al. 1994)	2.5 (-5.7)§	2.6 (-5.3)	+4.0 (-6.9)
		T-BS3 (El-Amoury 2004)	61 (-95)	60 (-87)	-0.9 (-8.4)
		Unit 1 (Pantelides et al. 2002)	91 (-194)	99 (-195)	+8.1 (+0.4)
		Unit 2 (Pantelides et al. 2002)	126 (-188)	127 (-192)	+0.4 (+2.1)
		SP-1 (Sasmal et al. 2011)	48 (-86)	49 (-82)	+2.2 (-5.4)
Interior	Joint shear failure	PEER09 (Alire 2002)	416	390	-6.1
		OH (Goto and Joh 1996)	132	132	+0.4
		AL1 (Li et al. 2009)	53	52	-1.8
		JE-1 (Ohwada 1977)	22	22	-0.9
		RC (Ota et al. 2000)	318	301	-5.3
		PEER22 (Walker 2001)	359	350	-2.7

§ A value in paparenthesis indicates the maximum lateral force in the negative direction.

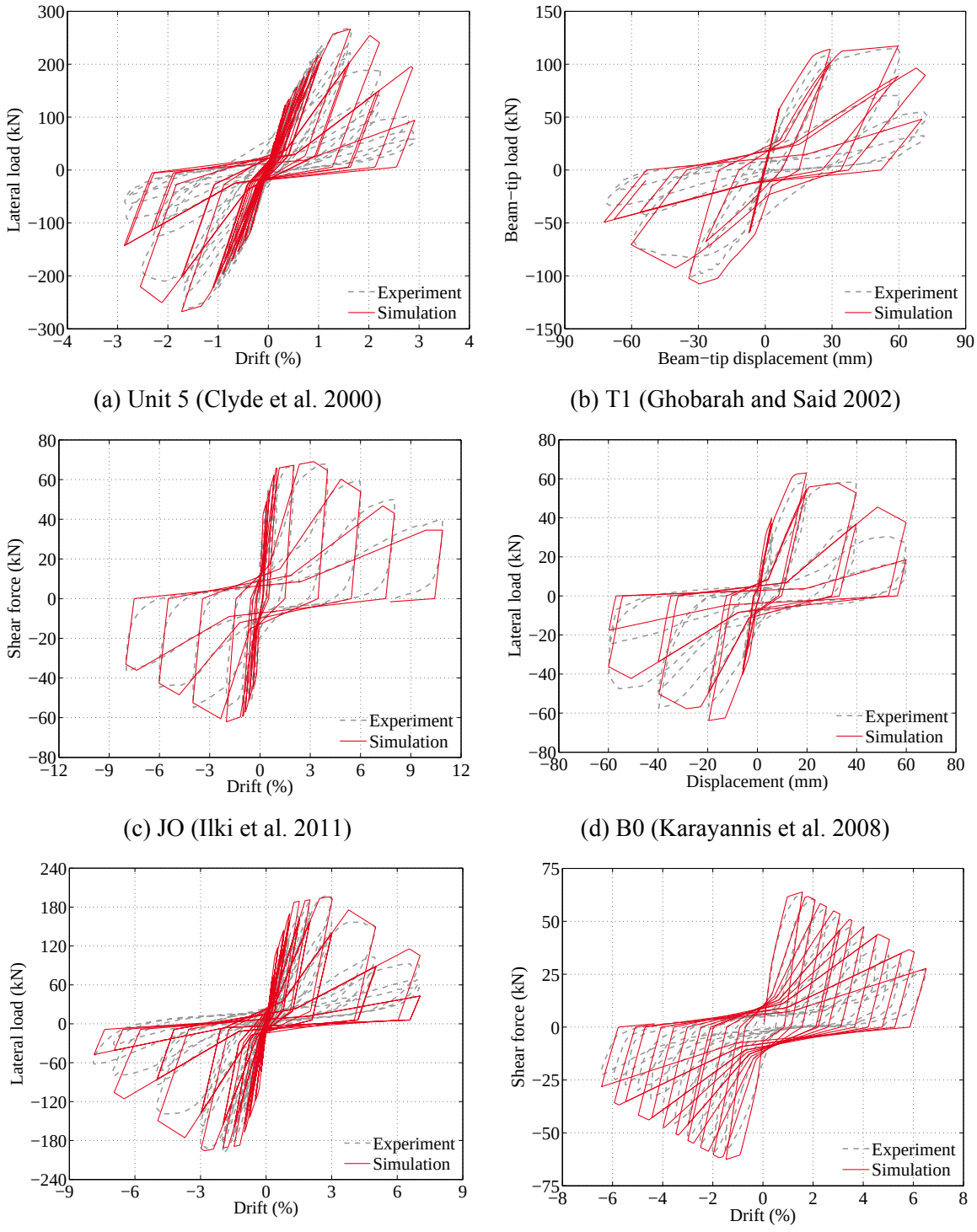

(a) Unit 5 (Clyde et al. 2000)

(b) T1 (Ghobarah and Said 2002)

(c) JO (Ilki et al. 2011)

(d) B0 (Karayannis et al. 2008)

(c) Unit 6 (Pantelides et al. 2002)

(f) F1 (Tsonos and Papanikolaou 2003)

Figure 3.16 Comparison between hysteretic responses of experiment and analysis for non-ductile exterior joints with joint shear failure

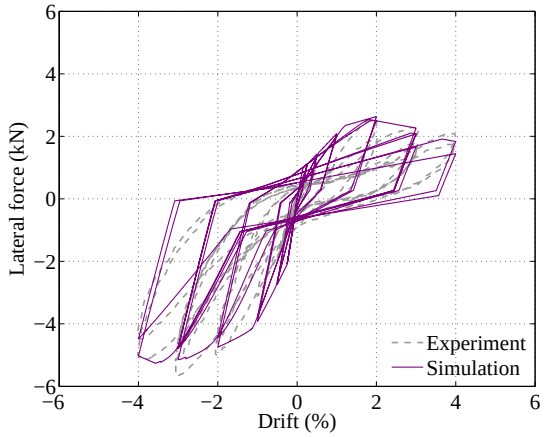

(a) Exterior (Aycardi et al. 1994)

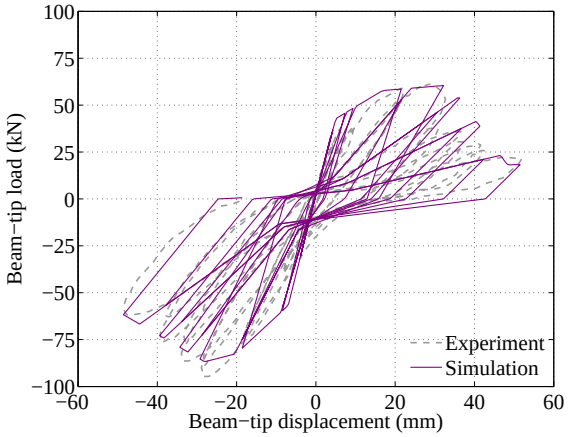

(b) T-BS3 (El-Amoury 2004)

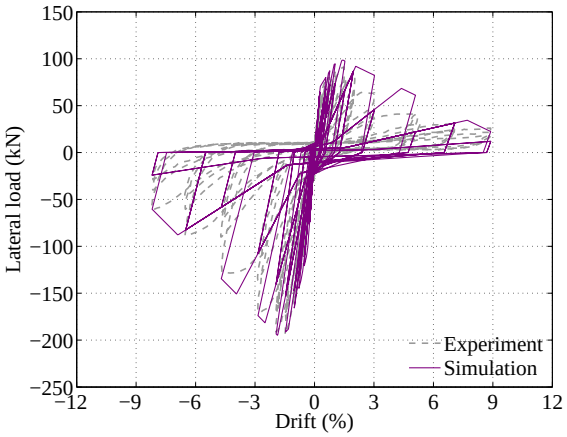

(c) Unit 1 (Pantelides et al. 2002)

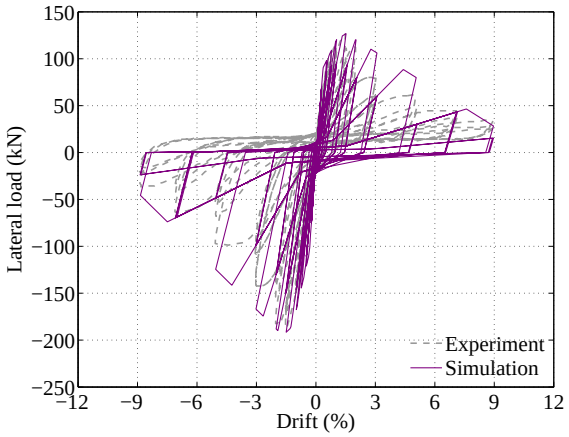

(d) Unit 2 (Pantelides et al. 2002)

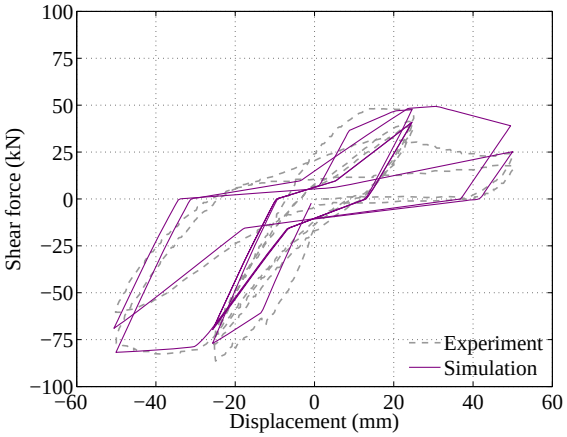

(e) SP-1 (Sasmal et al. 2011)

Figure 3.17 Comparison between hysteretic responses of experiment and analysis for non-ductile exterior joints with joint bond failure

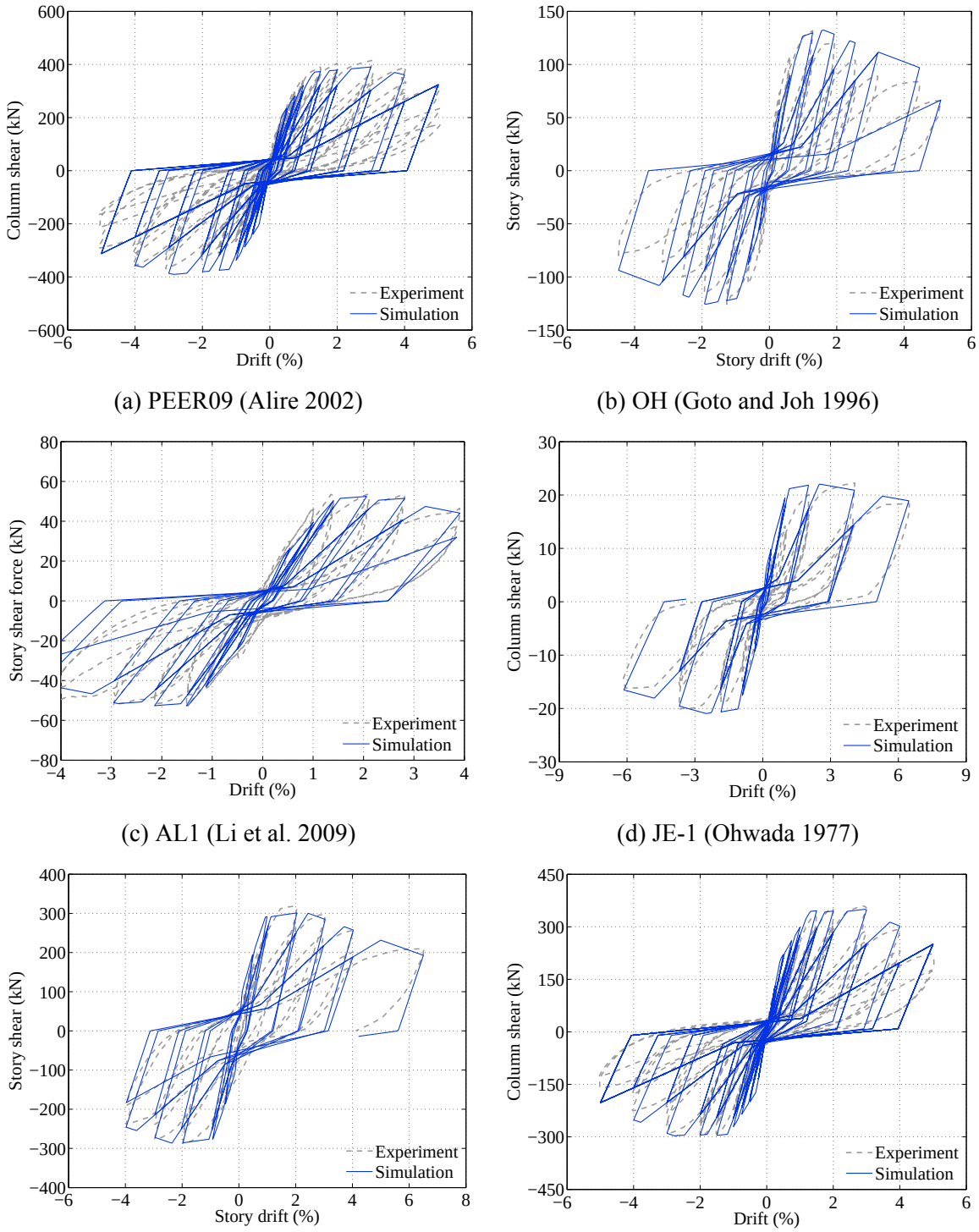

(a) PEER09 (Alire 2002)

(b) OH (Goto and Joh 1996)

(c) AL1 (Li et al. 2009)

(d) JE-1 (Ohwada 1977)

(e) RC (Ota et al. 2000)

(f) PEER22 (Walker 2001)

Figure 3.18 Comparison between hysteretic responses of experiment and analysis for non-ductile interior joints

Table 3.7 Modeling parameters of Pinching4 material for non-ductile exterior joints

Reference	Speci-men	Failure mode§	Joint shear strain ($\times 10^{-3}$)		Pinching damage parameters†								
					rDisp		*rForce*		*uForce*		α_{K1}	α_{D1}	α_{F1}
			$\gamma_{j,3}$	$\gamma_{j,4}$	Pos	Neg	Pos	Neg	Pos	Neg			
Clyde et al. (2000)	Unit 2	J	12	40	0.20	0.20	0.20	0.20	-0.15	-0.15	0.50	0.60	0.00
	Unit 4	J	10	40	0.20	0.20	0.15	0.15	-0.10	-0.10	0.80	0.50	0.00
	Unit 5	J	10	30	0.20	0.20	0.15	0.15	-0.10	-0.10	0.80	1.00	0.00
	Unit 6	J	12	40	0.20	0.20	0.20	0.20	-0.15	-0.15	0.50	0.60	0.00
Ghobarah and Said (2002)	T1	BJ	20	54	0.15	0.15	0.25	0.25	0.00	0.00	1.05	0.40	0.05
Ilki et al. (2011)	JO‡	J	20	116	0.25	0.25	0.25	0.25	0.00	0.00	0.90	0.25	0.00
	JOP	J	20	116	0.20	0.15	0.25	0.25	0.00	0.00	0.90	0.20	0.00
Karayannis et al. (2008)	A0	BJ	20	89	0.20	0.20	0.15	0.15	0.00	0.00	1.00	0.30	0.05
	B0	BJ	20	84	0.25	0.15	0.15	0.20	0.00	0.00	0.80	0.40	0.45
	C0	BJ	20	84	0.25	0.30	0.15	0.15	0.00	0.00	0.90	0.30	0.20
Liu (2006)	RC-1	BJ	10	91	0.15	0.15	0.15	0.15	0.00	0.00	1.05	0.40	0.05
Pantelides et al. (2002)	Unit 3	J	20	89	0.20	0.20	0.20	0.10	0.00	0.00	1.00	0.50	0.05
	Unit 4	J	20	60	0.20	0.20	0.20	0.10	0.00	0.00	1.00	0.40	0.10
	Unit 5	J	20	80	0.20	0.20	0.20	0.10	-0.15	-0.10	1.00	0.40	0.05
	Unit 6	J	20	89	0.20	0.20	0.20	0.10	-0.15	-0.10	1.00	0.40	0.05
Tsonos and Papanikolaou (2003)	F1	J	10	90	0.15	0.15	0.25	0.25	0.00	0.00	0.90	0.20	0.10
	F2	BJ	20	89	0.20	0.20	0.20	0.20	0.00	0.00	0.90	0.10	0.05
	L1	J	15	84	0.25	0.25	0.20	0.20	0.00	0.00	0.90	0.20	0.00
Tsonos (2007)	G1	J	20	140	0.20	0.20	0.10	0.15	0.00	0.00	0.95	0.25	0.05
Wong (2005)	BS-L	J	20	66	0.15	0.15	0.20	0.20	-0.20	-0.20	1.20	0.50	0.00
	BS-OL	J	20	89	0.15	0.15	0.20	0.20	-0.20	-0.20	1.20	0.20	0.00
	BS-U	J	15	89	0.20	0.20	0.20	0.20	-0.20	-0.20	1.20	0.20	0.10
	JA-NN03	BJ	20	66	0.20	0.20	0.20	0.20	-0.20	-0.20	1.20	0.30	0.10
Aycardi et al. (1994)	Exterior‡	J, A	20	100	0.10	0.10	0.20	0.20	-0.05	-0.05	0.80	0.20	0.10
El-Amoury (2004)	T-SB3	J, A	10	44	0.20	0.20	0.20	0.20	0.00	0.00	1.05	0.20	0.00
Pantelides et al. (2002)	Unit 1	J, A	10	80	0.20	0.20	0.15	0.15	0.00	0.00	1.05	0.60	0.00
	Unit 2	J, A	10	80	0.20	0.20	0.15	0.15	0.00	0.00	1.05	0.60	0.00
Sasmal et al. (2011)	SP-1	J, A	15	66	0.20	0.20	0.20	0.20	0.00	0.00	0.70	0.40	0.00
Mean			***16***	***77***	***0.19***	***0.19***	***0.19***	***0.18***	***-0.06***	***-0.06***	***0.94***	***0.38***	***0.06***
COV			0.32	0.31	0.18	0.20	0.19	0.26	1.37	1.40	0.19	0.49	1.63

§ J, BJ, CJ, and A refer to joint shear failure without member yielding, joint shear failure after beam yielding, and joint shear failure after column yielding, bond failure associated with short embedment length, respectively.

† *rDisp*, *rForce*, and *uForce* are the ratio of maximum deformation at which reloading begins, ratio of envelope force corresponding to maximum deformation at which reloading begins, and ratio of monotonic strength developed upon loading, respectively. α_{Ki}, α_{Di}, and α_{Fi} are coefficients for unloading stiffness degradation, reloading stiffness degradation, and strength degradation, respectively. For all specimens, [α_{K2}, α_{K3}, α_{K4}, α_{K5}] = [0.00, 0.10, 0.00, 0.95], [α_{D2} α_{D3} α_{D4} α_{D5}] = [0.00, 0.15, 0.00, 0.95], [α_{F2} α_{F3} α_{F4} α_{F5}] = [0.0, 0.32, 0.10, 0.25].

‡ Specimen with two transverse beams

Table 3.8 Modeling parameters of Pinching4 material for non-ductile interior joints

Reference	Speci-men	Failure mode§	Joint shear strain ($\times 10^{-3}$)		Pinching damage parameters†								
					rDisp		*rForce*		*uForce*		α_{K1}	α_{D1}	α_{F1}
			$\gamma_{j,3}$	$\gamma_{j,4}$	Pos	Neg	Pos	Neg	Pos	Neg			
Alire (2002)	PEER0995	BJ	20	89	0.15	0.15	0.15	0.15	0.00	0.00	0.90	0.40	0.00
	PEER1595	BJ	20	100	0.15	0.15	0.15	0.15	0.00	0.00	0.80	0.40	0.10
	PEER4150	J	20	100	0.15	0.15	0.15	0.15	0.00	0.00	0.90	0.40	0.40
Aycardi et al. (1994)	Interior‡	BJ, A	20	100	0.15	0.15	0.20	0.25	0.00	0.00	1.00	0.20	0.00
Hakuto et al. (2000)	O4	BJ	20	89	0.25	0.25	0.15	0.15	0.00	0.00	1.00	0.30	0.00
	O5	BJ	20	89	0.25	0.25	0.10	0.10	0.00	0.00	1.00	0.40	0.10
Goto and Joh (1996)	J-OH	J	15	102	0.30	0.30	0.20	0.20	0.00	0.00	0.90	0.40	0.05
Lee et al. (2010)	JI0	J	15	89	0.25	0.25	0.25	0.25	0.00	0.00	1.00	0.40	0.10
Li et al. (2002)	A1	J	20	89	0.27	0.27	0.15	0.15	0.00	0.00	1.00	0.40	0.30
	M1	BJ	20	89	0.25	0.25	0.10	0.10	0.00	0.00	1.00	1.00	0.00
Li et al. (2009)	AS1‡	J	20	94	0.20	0.20	0.25	0.25	0.00	0.00	1.00	0.30	0.00
	AL1‡	J	20	107	0.20	0.20	0.15	0.15	0.00	0.00	1.00	0.30	0.35
	AS2‡	J	20	100	0.20	0.20	0.20	0.20	0.00	0.00	1.00	0.35	0.05
	AL2‡	J	20	107	0.15	0.15	0.20	0.20	0.00	0.00	1.00	0.25	0.00
Ohwada (1970)	NO1	J	10	72	0.30	0.30	0.18	0.18	0.00	0.00	1.00	0.35	0.05
Ohwada (1973)	P2	J	20	140	0.30	0.30	0.20	0.20	0.00	0.00	1.00	0.35	0.05
Ohwada (1977)	JO-1	J	20	140	0.30	0.30	0.20	0.20	0.00	0.00	1.00	0.40	0.05
	JE-1	J	20	260	0.30	0.35	0.20	0.20	0.00	0.00	0.95	0.40	0.05
Ota et al. (2004)	RC	BJ	20	107	0.20	0.20	0.25	0.30	0.00	0.00	0.95	0.30	0.05
Owada (1984)	LJO-6‡	CJ	15	89	0.20	0.20	0.25	0.20	0.00	0.00	1.00	0.35	0.05
	LJXY-6‡	CJ	15	275	0.20	0.20	0.20	0.20	0.00	0.00	0.90	0.35	0.05
	LJXY-7‡	CJ	15	275	0.20	0.20	0.20	0.20	0.00	0.00	0.90	0.35	0.05
	LJXY-8‡	CJ	20	116	0.20	0.20	0.20	0.20	0.00	0.00	0.95	0.35	0.05
Owada (2000)	JO-5	J	20	157	0.25	0.25	0.20	0.20	0.00	0.00	0.90	0.30	0.10
	JXY-3‡	CJ	20	212	0.30	0.20	0.15	0.15	0.00	0.00	0.90	0.30	0.10
Pimanmas & Chaimahawan (2010)	J0	J	15	89	0.25	0.25	0.15	0.15	0.00	0.00	1.00	0.30	0.00
Walker (2001)	PEER14	BJ	20	89	0.15	0.15	0.15	0.15	0.00	0.00	0.75	0.40	0.10
	CD1514	BJ	20	100	0.13	0.13	0.25	0.25	0.00	0.00	1.00	0.10	0.00
	CD3014	BJ	20	100	0.13	0.13	0.25	0.25	0.00	0.00	1.20	0.10	1.00
	PADH14	BJ	20	100	0.13	0.13	0.25	0.25	0.00	0.00	1.20	0.10	1.00
	PEER22	BJ	20	89	0.20	0.20	0.15	0.15	0.00	0.00	1.00	0.40	0.20
	CD3022	BJ	20	100	0.10	0.10	0.15	0.15	0.00	0.00	1.20	0.10	0.60
	PADH22	BJ	20	89	0.13	0.13	0.25	0.25	0.00	0.00	1.20	0.10	1.00
Wang and Hsu (2009)	Ko-JI1	J	15	73	0.20	0.20	0.30	0.30	0.00	0.00	1.00	0.40	0.30
	Ho-JI1	J	20	89	0.20	0.20	0.20	0.20	0.00	0.00	1.00	0.20	0.10
Mean			***19***	***117***	***0.21***	***0.21***	***0.19***	***0.19***	***0.00***	***0.00***	***0.99***	***0.33***	***0.18***
COV			0.14	0.46	0.29	0.29	0.25	0.26	0.00	0.00	0.10	0.47	1.57

†, §, and ‡ are the same as non-ductile exterior joints

3.3.4 Validation of analytical model for a scale model frame

In order to investigate the applicability of the analytical models mentioned in the previous sections to a full frame model, this research selects a one-third scale model frame tested by Bracci et al. (1992) that can represent the most common RC building designed for only gravity loads without seismic provisions in accordance with ACI 318-89 (1989). Figure 3.19 illustrates the geometry of the model frame used in the experimental work of Bracci et al. (1992). This non-ductile RC frame has inadequate column shear capacity due to a lack of confinement and poor reinforcement details, lap splice of column reinforcement in its potential plastic hinge regions, and weak joints due to limited shear capacity associated with little or no joint transverse reinforcement and inadequate anchorage of bottom beam reinforcement. Further details on the material properties and reinforcement details can be found in the reference.

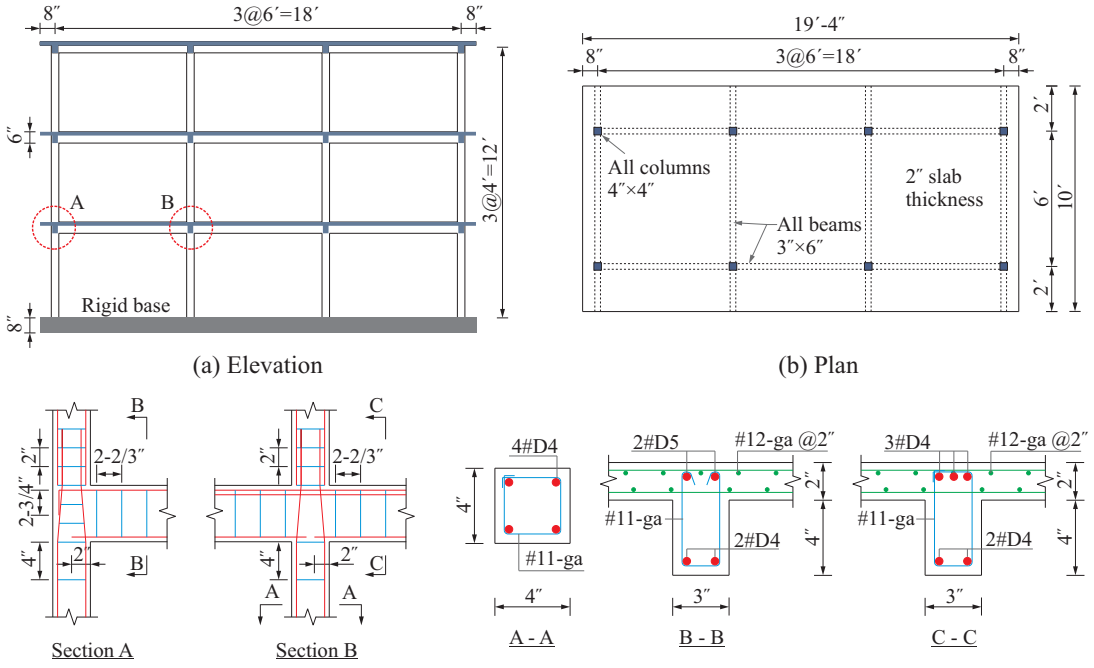

Figure 3.19 Geometry and reinforcement details of the structure (Bracci et al. 1992)

Following the analytical modeling approach mentioned in the previous sections, the analytical model of the scale model frame is built in OpenSees (McKenna et al. 2010). The exterior and interior joint shear strength is determined from the companion exterior and interior subassemblages tested by Aycardi et al. (1994). In addition, the reduced joint shear strength as a result of insufficient anchorage in a joint is calculated using the bond strength model of Hassan (2011). The calibration is performed controlling the pinching damage parameters to obtain its appropriate responses. Moreover, the shear behavior of columns is not accounted for in the model validation because the companion columns conducted by Aycardi et al. (1994) seems to be dominated by flexure response. For dynamic analysis, lumped mass at every connection is employed based on the load combination 1.05D (dead load) and 0.25L (live load), and the 2% Rayleigh damping in the first two modes is used. An eigenvalue analysis revealed a fundamental period of approximately 0.67 seconds. This is a very dominant mode in that it activates 87 percent of its mass. Furthermore, the input motion is the 1952 Taft earthquake, N21E component scaled to 0.2g, as presented in Figure 3.20 (Bracci et al. 1992).

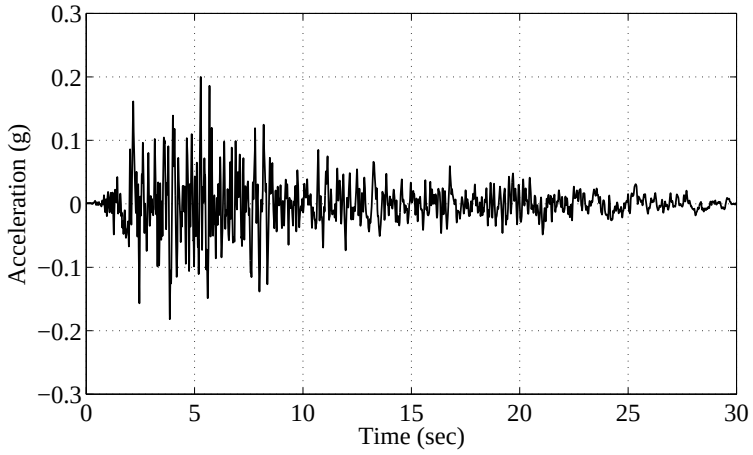

Figure 3.20 Input motion (1952 Taft earthquake scaled to 0.2g)

Figures 3.21 and Figure 3.22 depict the comparison of story displacement and story shear force time history responses of the Bracci et al. (1992) experiment with those of the simulation, respectively. Table 3.9 shows the comparison of maximum story displacement and maximum shear force for each story obtained from experiment and analysis. The maximum third story (roof) displacement for analysis shows a good agreement with the experimental measurement less than 3% difference while the maximum first story displacement has a considerable difference. This significant difference may be attributed to the application of the same joint shear strength to joints at different floor levels. However, all the story displacement time histories appropriately capture the response period. Additionally, the amplitude decays after a peak value of the story displacement response near 5 seconds, as shown in Figure 3.21. However, the amplitude increases between 18 and 23 seconds. It is attributable to the deterioration in unloading and reloading strength and stiffness during this time period. The analytical model accurately captures the strength and stiffness degradation of the experimental structure. Although the analytical results slightly underestimate the story shear forces (particularly, 10% difference in maximum base shear), as presented in Figure 3.22, the overall shear force response accurately predicted the actual response.

Table 3.9 Comparison of maximum responses from experiment and analysis

Story	Maximum story displacement (mm)			Maximum story shear force (kN)		
	Experiment	Analysis	Diff. (%)	Experiment	Analysis	Diff. (%)
Third	34	34	+ 2.3	25	29	14.7
Second	29	26	-11.7	41	37	-11.0
First	16	12	-29.9	55	50	- 9.0

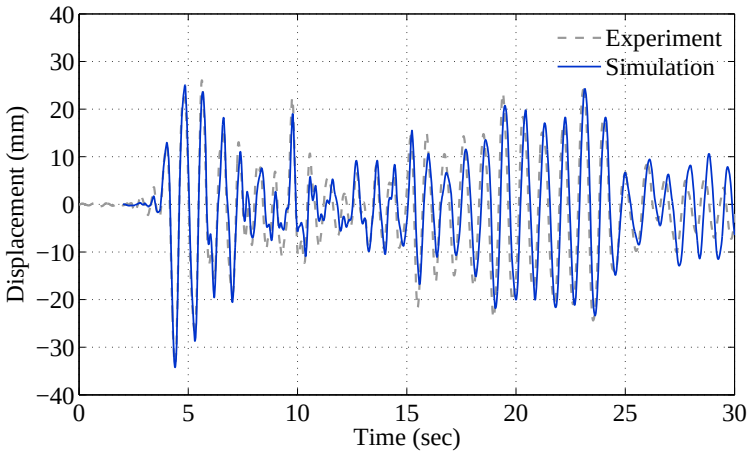

(a) 4th floor

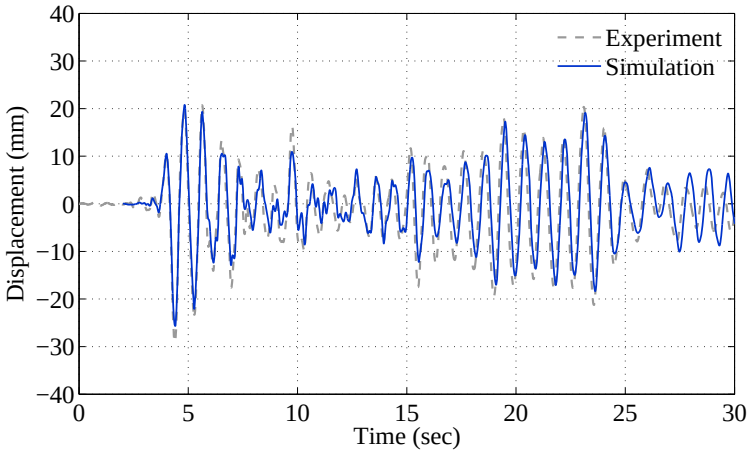

(b) 3rd floor

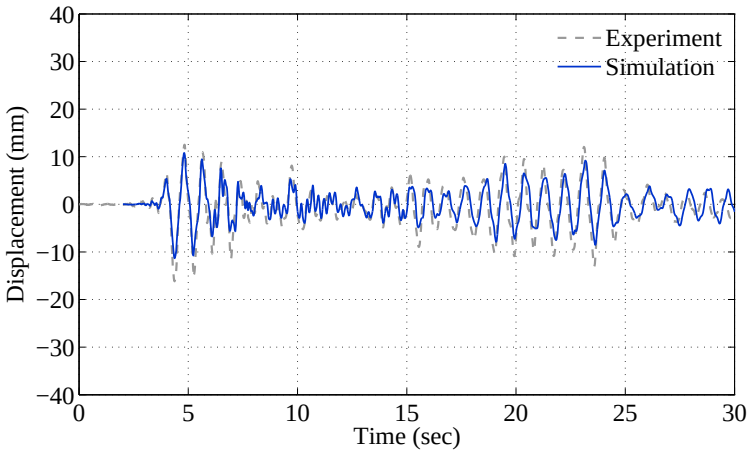

(c) 2nd floor

Figure 3.21 Comparison of floor displacement time histories of experiment and analysis

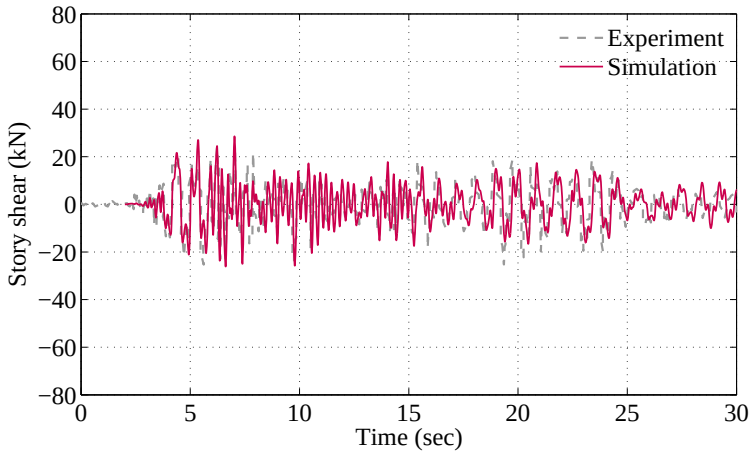

(a) 3rd story

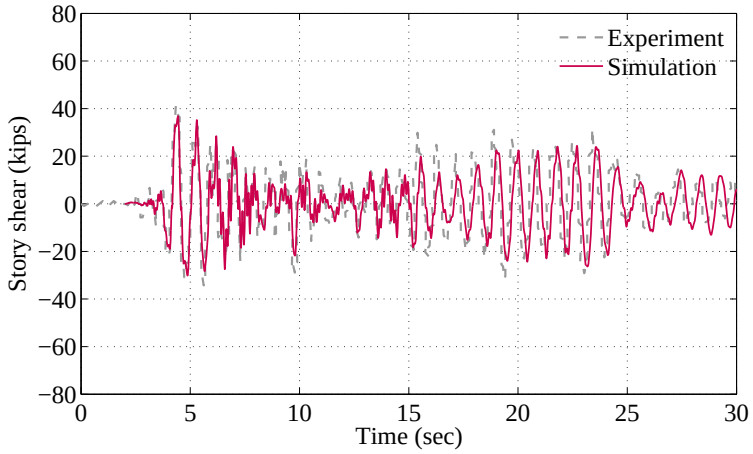

(b) 2nd story

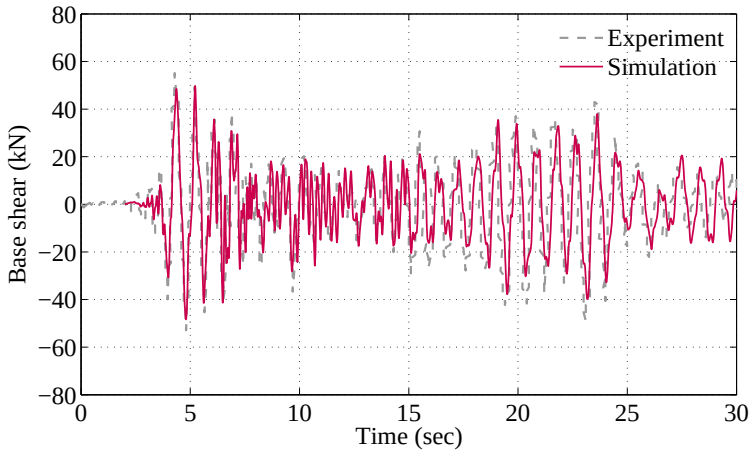

(c) 1st story

Figure 3.22 Comparison of story shear force time histories of experiment and analysis

3.4 Modeling Ductile Beam-Column Joints

For ductile RC frames, beam-column joints are often modeled with rigid joint zones. However, Shin and LaFave (2004) argued that the joint regions are not rigid, but experience significant shear deformations that can contribute greatly to global deformation. Therefore, the analytical model must predict the inelastic behavior of ductile beam-column joints. As mentioned before, this research defines a beam-column joint with joint transverse reinforcement spaced at less than the half of column depth as a ductile joint, as illustrated in Figure 3.23.

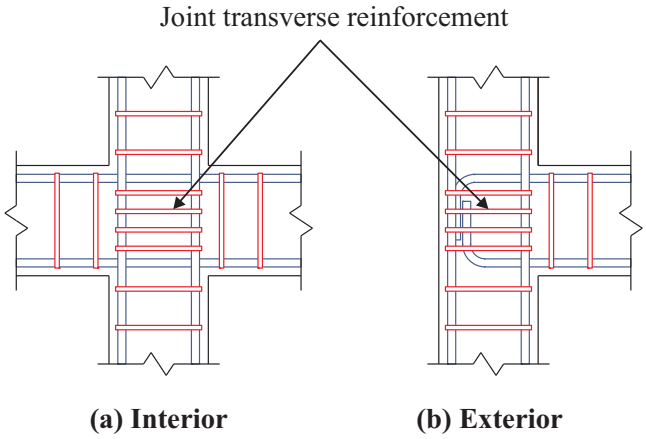

Figure 3.23 Typical reinforcing details in ductile beam-column joints

Analytical modeling procedures follow the same as those for non-ductile beam-column joints except for joint bond failure. To investigate the propriety of the analytical joint shear model for ductile beam-column joints, a database of 44 exterior and 89 interior beam-column joint subassemblages are collected from experimental work available in the literature and are simulated in OpenSees (McKenna et al. 2010). The

database includes specimens experiencing joint shear failure before and after beam yielding, specimens without and with transverse beams orthogonal to joints.

The validation is performed based on experimental results, especially experimental joint shear strength, in order to extract the modeling parameters of the Pinching4 material that can be adequately used for analyzing RC frames. Figure 3.24 and Figure 3.25 present the comparison of experimental and analytical results for exterior and interior beam-column joints, respectively. From these figures, it is indicated that the analytical results match well with experimental results in terms of strength, stiffness, and energy dissipation. In some specimens, the analytical model overestimates initial stiffness which may be attributed to bond slip, which is not included in this study. It is, however, qualitatively clear that the prediction improves at higher deformation levels. Additionally, Table 3.10 indicates the maximum lateral forces from experiment and simulation for 12 specimens. It is indicated that the maximum shear forces from analyses shows a good agreement with the experimental results (less than 5% difference). All of 133 comparison plots can be found in Figure A.5 and Figure A.6 (see Appendix A).

Table 3.11 and Table 3.12 show the modeling parameters of the Pinching4 material for ductile exterior and interior beam-column joints, respectively, which are extracted from the model validation described above. These values are examined separately for exterior and interior joints. Like the case of non-ductile beam-column joins, the mean value of these parameters will be used for analyzing ductile RC frames in a probabilistic risk assessment.

Table 3.10 Comparison of experimental and analytical maximum lateral force for ductile beam-column joint subassemblages

Joint type	Failure mode	Specimens	Maximum lateral force (kN)		Difference (%)
			Experiment	Analysis	
Exterior	Joint shear failure	1B (Ehsani and Wight 1985)	147	155	+5.1
		B3 (Fujii and Morita 1991)	64	64	-0.1
		NO12 (Kaku and Asakusa 1991)	43	43	-0.2
		RC-2 (Nishiyama et al. 1989)	71	71	+0.3
		S6 (Tsonos et al. 1992)	58	56	-3.7
		JA-NY15 (Wong 2005)	88	91	+3.3
Interior	Joint shear failure	SP1 (Inoue et al. 1990)	326	328	+0.6
		J-6 (Oka and Shiohara 1992)	266	262	-1.4
		NO1 (Takamori et al. 2006)	1308	1291	-1.3
		S1 (Teng and Zhou 2003)	117	114	-2.4
		NO08 (Teraoka 1997)	268	259	-3.4
		NO3 (Yoshino et al. 1997)	49	51	+2.3

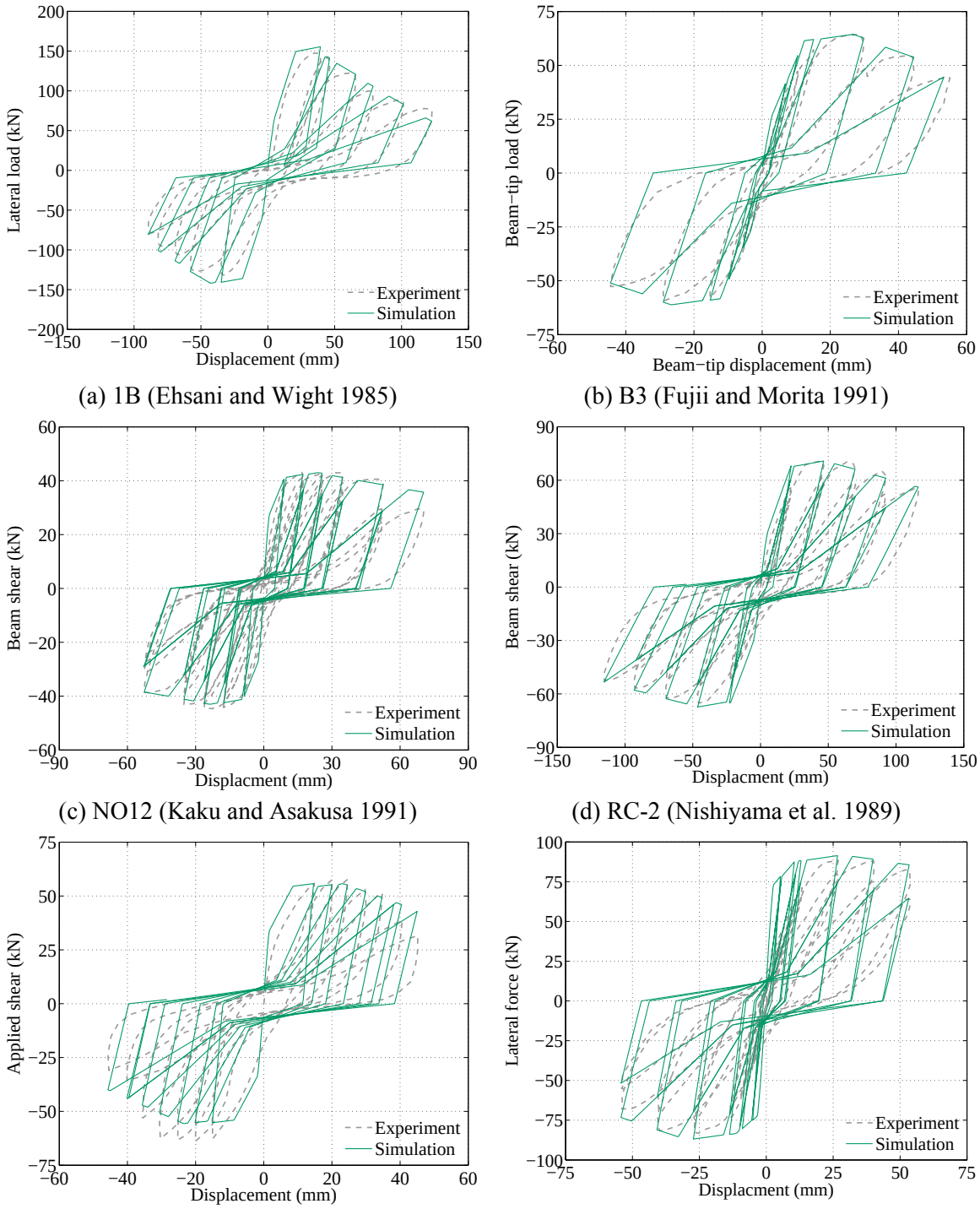

(a) 1B (Ehsani and Wight 1985)

(b) B3 (Fujii and Morita 1991)

(c) NO12 (Kaku and Asakusa 1991)

(d) RC-2 (Nishiyama et al. 1989)

(c) S6 (Tsonos et al. 1992)

(f) JA-NY15 (Wong 2005)

Figure 3.24 Comparison between hysteretic responses of experiment and analysis for ductile exterior joints

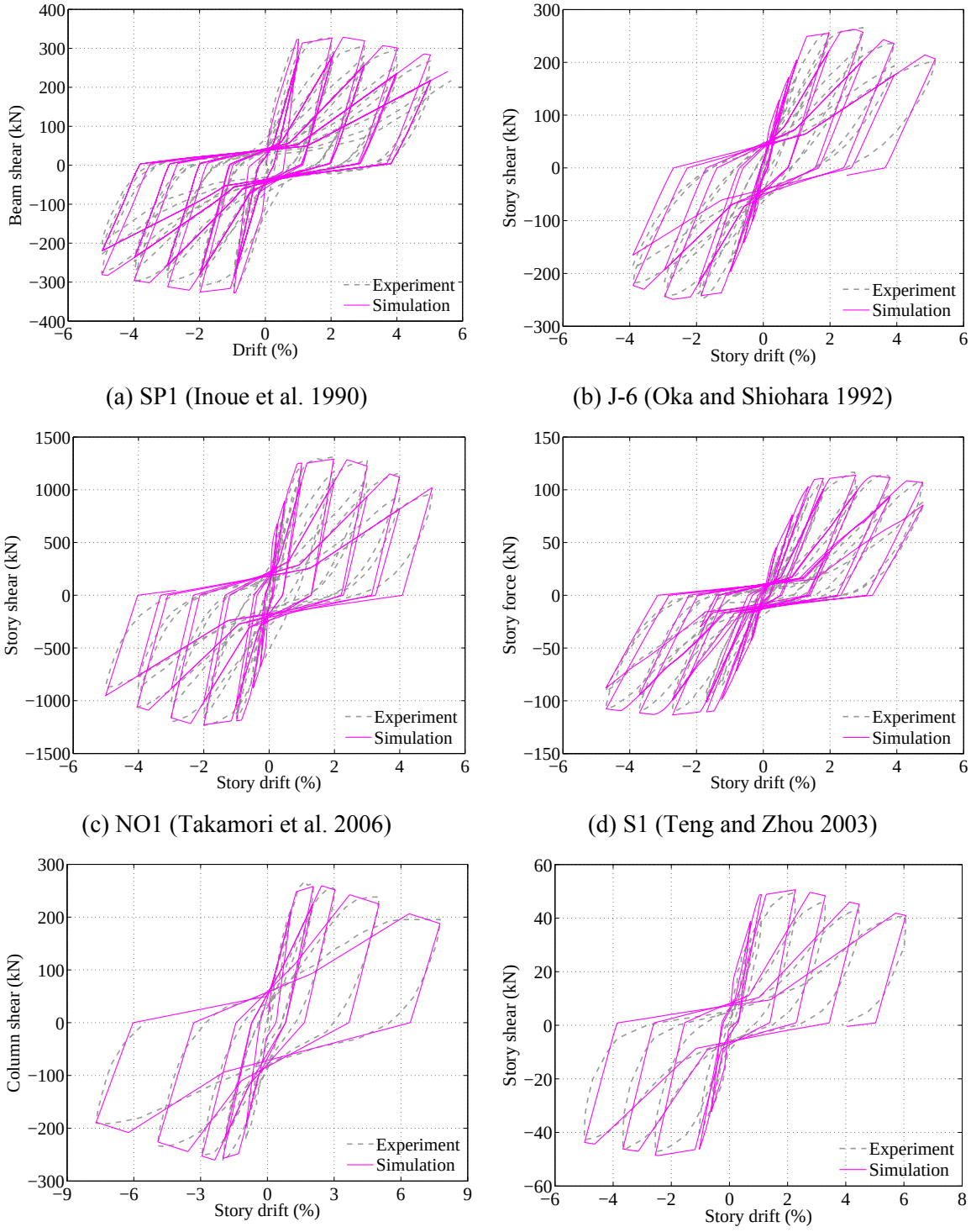

(a) SP1 (Inoue et al. 1990)

(b) J-6 (Oka and Shiohara 1992)

(c) NO1 (Takamori et al. 2006)

(d) S1 (Teng and Zhou 2003)

(e) NO08 (Teraoka 1997)

(f) NO3 (Yoshino et al. 1997)

Figure 3.25 Comparison between hysteretic responses of experiment and analysis for ductile interior joints

Table 3.11 Modeling parameters of Pinching4 material for ductile exterior joints

Reference	Speci-men	Failure mode§	Joint shear strain ($\times 10^{-3}$)		Pinching damage parameters†								
					rDisp		*rForce*		*uForce*		α_{K1}	α_{D1}	α_{F1}
			$\gamma_{j,3}$	$\gamma_{j,4}$	Pos	Neg	Pos	Neg	Pos	Neg			
Chen and Chen (1999)	JC	BJ	20	180	0.25	0.25	0.20	0.20	0.00	0.00	1.00	0.25	0.05
Ehsani and	HL11	J	20	157	0.20	0.20	0.15	0.20	0.00	0.00	1.05	0.25	0.05
Alameddine (1991)	LL11	J	20	212	0.30	0.30	0.20	0.20	0.00	0.00	1.05	0.10	0.05
	LL14	BJ	20	212	0.30	0.30	0.20	0.20	0.00	0.00	1.05	0.10	0.05
	LH14	BJ	20	212	0.35	0.35	0.15	0.15	0.00	0.00	1.05	0.15	0.05
Ehsani et al. (1987)	NO4	BJ	20	140	0.25	0.30	0.25	0.15	0.00	0.00	0.95	0.25	0.05
	NO5	BJ	20	107	0.20	0.20	0.35	0.35	0.00	0.00	1.00	0.00	0.05
Ehsani and Wight	1B	J	20	94	0.25	0.25	0.20	0.20	-0.20	-0.20	1.00	0.20	0.15
(1985)	2B	J	20	94	0.25	0.25	0.23	0.23	-0.20	-0.20	1.20	0.10	0.20
	3B	BJ	20	94	0.25	0.25	0.20	0.20	-0.20	-0.20	1.20	0.10	0.05
	5B	J	20	140	0.25	0.25	0.25	0.30	0.00	0.00	0.95	0.10	0.05
	6B	BJ	20	140	0.25	0.25	0.40	0.30	0.00	0.00	0.95	0.00	0.05
Fujii and Morita	B1	J	20	140	0.25	0.25	0.15	0.25	0.00	0.00	0.95	0.25	0.05
(1991)	B2	J	20	140	0.25	0.25	0.15	0.25	0.00	0.00	0.95	0.25	0.05
	B3	J	20	116	0.25	0.25	0.20	0.25	0.00	0.00	0.95	0.35	0.05
	B4	J	20	140	0.25	0.20	0.20	0.25	0.00	0.00	0.95	0.35	0.05
Ishida et al. (1996)	A-0	J	20	180	0.20	0.15	0.20	0.25	0.00	0.00	1.00	0.35	0.05
	A-0-F	BJ	20	140	0.20	0.15	0.15	0.15	0.00	0.00	1.00	0.35	0.05
Joh et al. (1989)	LO-NO	J	20	157	0.25	0.25	0.15	0.15	0.00	0.00	1.00	0.25	0.05
	HH-NO	J	20	157	0.25	0.25	0.20	0.20	0.00	0.00	1.00	0.25	0.05
	LO-N96	J	20	157	0.25	0.25	0.15	0.15	0.00	0.00	1.00	0.25	0.05
	HH-N96	J	20	157	0.25	0.25	0.20	0.20	0.00	0.00	1.00	0.25	0.05
Joh et al. (1992)	NRC-J5	J	20	340	0.25	0.25	0.25	0.25	0.00	0.00	0.95	0.25	0.05
	NRC-J10	BJ	20	157	0.25	0.25	0.10	0.15	0.00	0.00	1.00	0.35	0.05
	NRC-J13	BJ	20	212	0.25	0.25	0.15	0.20	0.00	0.00	0.95	0.25	0.05
Kaku and Asakusa	NO03	BJ	20	980	0.30	0.30	0.15	0.15	0.00	0.00	1.00	0.25	0.05
(1991)	NO05	BJ	20	180	0.25	0.25	0.20	0.20	0.00	0.00	1.00	0.30	0.05
	NO06	BJ	20	260	0.30	0.30	0.10	0.15	0.00	0.00	1.00	0.25	0.05
	NO09	BJ	25	245	0.30	0.30	0.15	0.15	0.00	0.00	1.00	0.25	0.05
	NO11	BJ	25	245	0.30	0.30	0.20	0.20	0.00	0.00	1.00	0.25	0.05
	NO12	BJ	20	260	0.30	0.30	0.10	0.15	0.00	0.00	1.00	0.25	0.05
Kanada et al. (1984)	U41L	BJ	15	131	0.25	0.25	0.10	0.15	0.00	0.00	1.00	0.35	0.05
Lee and Lee (2000)	EJ+0.0	J	20	180	0.30	0.30	0.15	0.20	0.00	0.00	1.00	0.35	0.05
	EJ+0.1	J	20	80	0.30	0.30	0.15	0.20	0.00	0.00	1.00	0.60	0.05
Nishiyama et al.(1989)	RC-2	BJ	20	180	0.25	0.30	0.15	0.20	0.00	0.00	1.00	0.30	0.05
Takeuchi et al. (2003)	O-5	J	15	95	0.20	0.20	0.20	0.20	0.00	0.00	1.00	0.30	0.05
Tsonos (2007)	A1	BJ	20	140	0.25	0.25	0.45	0.30	0.00	0.00	0.95	0.20	0.05
Tsonos et al. (1992)	S1	BJ	20	340	0.25	0.25	0.35	0.35	0.00	0.00	0.95	0.10	0.05
	S2	BJ	20	127	0.25	0.25	0.20	0.20	0.00	0.00	0.95	0.20	0.05
	S6	J	20	100	0.25	0.25	0.20	0.20	0.00	0.00	0.95	0.15	0.05
	S6'	BJ	20	100	0.25	0.25	0.20	0.20	0.00	0.00	0.95	0.15	0.05
	F2	J	20	100	0.25	0.25	0.20	0.20	0.00	0.00	1.00	0.15	0.05
Wong (2005)	JA-NY03	BJ	20	180	0.20	0.20	0.10	0.15	0.00	0.00	1.00	0.30	0.05
	JA-NY15	BJ	20	260	0.25	0.25	0.20	0.20	0.00	0.00	1.00	0.30	0.05
Mean			***20***	***185***	***0.26***	***0.25***	***0.20***	***0.21***	***-0.01***	***-0.01***	***1.00***	***0.24***	***0.06***
COV			0.08	0.74	0.13	0.16	0.38	0.25	-3.74	-3.74	0.05	0.46	0.48

†, §, and ‡ are the same as non-ductile exterior joints

Table 3.12 Modeling parameters of Pinching4 material for ductile interior joints

Reference	Speci-men	Failure mode[§]	Joint shear strain ($\times 10^{-3}$)		Pinching damage parameters†								
					rDisp		*rForce*		*uForce*		α_{K1}	α_{D1}	α_{F1}
			$\gamma_{j,3}$	$\gamma_{j,4}$	Pos	Neg	Pos	Neg	Pos	Neg			
Durrani and Wight (1985)	X1	BJ	20	140	0.25	0.25	0.35	0.40	0.00	0.00	0.90	0.10	0.00
	X2	BJ	20	212	0.30	0.30	0.35	0.35	0.00	0.00	0.90	0.10	0.00
	X3	BJ	20	260	0.35	0.25	0.35	0.20	0.00	0.00	0.90	0.05	0.00
Endoh et al. (1991)	HLC	BJ	20	260	0.20	0.25	0.25	0.30	0.00	0.00	0.90	0.30	0.00
	LA1	J	20	260	0.20	0.25	0.30	0.30	0.00	0.00	0.90	0.30	0.00
Fujii and Morita (1991)	A1	J	20	140	0.30	0.25	0.25	0.28	0.00	0.00	0.85	0.25	0.05
	A3	J	20	157	0.30	0.30	0.25	0.28	0.00	0.00	0.90	0.30	0.05
	A4	J	20	157	0.25	0.25	0.25	0.32	0.00	0.00	0.85	0.20	0.05
Goto and Joh (1996)	HH	J	15	131	0.25	0.25	0.15	0.20	0.00	0.00	0.90	0.40	0.05
Goto and Joh (2003)	LM-60	BJ	20	260	0.20	0.20	0.25	0.25	0.00	0.00	0.90	0.30	0.05
	LM-125	BJ	20	260	0.20	0.20	0.25	0.25	0.00	0.00	0.95	0.30	0.05
	HM-60	BJ	20	260	0.25	0.25	0.20	0.20	0.00	0.00	0.90	0.30	0.05
	HM-125	BJ	20	260	0.20	0.20	0.25	0.25	0.00	0.00	0.95	0.30	0.05
	HH-125	BJ	20	260	0.20	0.20	0.25	0.25	0.00	0.00	0.95	0.20	0.05
Hiramatsu et al. (1995)	S1	BJ	20	260	0.25	0.25	0.30	0.30	0.00	0.00	0.95	0.35	0.05
Inoue et al. (1990)	SP1[‡]	BJ	20	212	0.20	0.20	0.20	0.20	0.00	0.00	0.95	0.25	0.10
	SP2	BJ	20	180	0.20	0.20	0.40	0.25	0.00	0.00	0.95	0.30	0.05
Ishida et al. (2001)	CN	BJ	20	260	0.20	0.25	0.22	0.20	0.00	0.00	1.00	0.30	0.05
	ES[‡]	BJ	20	260	0.20	0.20	0.20	0.20	0.00	0.00	1.00	0.30	0.05
Jinno et al. (1991)	NO1	BJ	20	260	0.25	0.20	0.15	0.20	0.00	0.00	0.90	0.40	0.05
	NO2	J	20	260	0.20	0.20	0.20	0.25	0.00	0.00	0.90	0.40	0.05
	NO3	BJ	20	180	0.20	0.20	0.25	0.35	0.00	0.00	0.95	0.40	0.05
	NO4	BJ	20	180	0.15	0.15	0.25	0.40	0.00	0.00	0.90	0.35	0.05
	NO5	BJ	20	180	0.15	0.15	0.30	0.35	0.00	0.00	0.95	0.40	0.05
	NO6	BJ	20	180	0.15	0.15	0.30	0.35	0.00	0.00	0.95	0.40	0.05
	NO7	BJ	20	180	0.15	0.15	0.30	0.40	0.00	0.00	0.95	0.40	0.05
	NO8	BJ	20	180	0.15	0.15	0.30	0.40	0.00	0.00	0.95	0.40	0.05
Joh et al. (1991a)	JXO-B1	BJ	20	140	0.25	0.30	0.20	0.20	0.00	0.00	0.95	0.25	0.05
	JXO-B5	BJ	20	157	0.25	0.25	0.25	0.20	0.00	0.00	0.90	0.25	0.05
Joh et al. (1991b)	JXO-8MH	BJ	20	140	0.20	0.20	0.15	0.15	0.00	0.00	0.95	0.25	0.05
Kaku et al. (1993)	J31A	BJ	20	116	0.15	0.15	0.25	0.40	0.00	0.00	0.95	0.40	0.05
Kamimura et al. (2004)	NN.1	BJ	20	260	0.40	0.40	0.15	0.20	0.00	0.00	0.95	0.20	0.05
Kashiwazaki et al. (1992)	MKJ-1	BJ	20	260	0.15	0.15	0.13	0.20	0.00	0.00	1.00	0.10	0.05
Kitayama et al. (1991)	J1[‡]	BJ	20	260	0.30	0.30	0.20	0.25	0.00	0.00	0.85	0.45	0.05
Kitayama et al. (2000)	PB1	BJ	20	260	0.25	0.25	0.20	0.20	0.00	0.00	0.95	0.20	0.05
	PNB2	BJ	20	180	0.25	0.25	0.20	0.20	0.00	0.00	0.95	0.25	0.05
	PNB3	BJ	20	180	0.25	0.25	0.20	0.20	0.00	0.00	0.95	0.30	0.05
Kurose et al. (1991)	J1	BJ	30	130	0.35	0.35	0.25	0.35	0.00	0.00	0.85	0.45	0.05
Kusuhara et al. (2004)	JE-0	BJ	20	140	0.30	0.30	0.15	0.15	0.00	0.00	0.95	0.50	0.05
	JE-55	BJ	20	140	0.25	0.30	0.15	0.15	0.00	0.00	0.95	0.30	0.05
Lee et al. (2009)	J1	J	20	180	0.25	0.30	0.25	0.15	0.00	0.00	0.95	0.25	0.05
Matsumoto et al. (2010)	B-0	BJ	20	157	0.20	0.20	0.25	0.25	0.00	0.00	0.95	0.25	0.05
	B-5	BJ	20	260	0.15	0.10	0.25	0.25	0.00	0.00	0.95	0.25	0.05
	J-0	J	20	140	0.25	0.23	0.35	0.35	0.00	0.00	0.95	0.32	0.05
	J-5	J	20	140	0.25	0.23	0.35	0.35	0.00	0.00	0.95	0.25	0.05
Morita et al. (2004)	M1	J	20	212	0.30	0.30	0.15	0.20	0.00	0.00	0.95	0.20	0.05
	M6	J	20	212	0.25	0.25	0.15	0.20	0.00	0.00	0.95	0.20	0.05

Table 3.12 Modeling parameters of Pinching4 material for ductile interior joints (continued)

Reference	Speci-men	Failure mode§	Joint shear strain ($\times 10^{-3}$)		Pinching damage parameters†								
					rDisp		*rForce*		*uForce*		α_{K1}	α_{D1}	α_{F1}
			$\gamma_{j,3}$	$\gamma_{j,4}$	Pos	Neg	Pos	Neg	Pos	Neg			
Noguchi and Kashiwazaki (1992)	OKJ-1	BJ	25	105	0.30	0.25	0.35	0.35	0.00	0.00	0.85	0.25	0.00
	OKJ-4	BJ	25	123	0.20	0.20	0.40	0.40	0.00	0.00	0.95	0.25	0.00
	OKJ-5	J	25	135	0.25	0.25	0.35	0.40	0.00	0.00	0.95	0.35	0.00
	OKJ-6	J	25	105	0.30	0.30	0.35	0.35	0.00	0.00	0.90	0.25	0.00
Ohwada (1970)	No. 2	J	20	260	0.25	0.35	0.20	0.20	0.00	0.00	0.95	0.20	0.05
Ohwada (1977)	JO-2	J	20	260	0.30	0.30	0.20	0.20	0.00	0.00	0.95	0.45	0.05
Oka and Shiohara (1992)	J-1	BJ	20	116	0.30	0.25	0.25	0.28	0.00	0.00	0.95	0.35	0.00
	J-6	J	20	116	0.25	0.25	0.30	0.30	0.00	0.00	0.95	0.35	0.00
	J-8	BJ	15	119	0.25	0.25	0.30	0.28	0.00	0.00	0.95	0.35	0.00
	J-10	J	20	116	0.20	0.20	0.20	0.25	0.00	0.00	0.90	0.35	0.00
Ozaki et al. (2010)	NO1	BJ	20	180	0.20	0.25	0.15	0.15	0.00	0.00	0.95	0.25	0.05
	NO2	BJ	20	157	0.20	0.25	0.15	0.15	0.00	0.00	0.95	0.25	0.05
Raffaelle and Wight (1992)	SP1	BJ	20	260	0.35	0.35	0.20	0.20	0.00	0.00	0.95	0.20	0.05
	SP2	BJ	20	260	0.35	0.35	0.20	0.20	0.00	0.00	0.95	0.25	0.05
	SP3	BJ	20	260	0.25	0.25	0.25	0.25	0.00	0.00	0.95	0.15	0.05
	SP4	BJ	20	260	0.30	0.30	0.15	0.15	0.00	0.00	0.95	0.25	0.05
Shin and LaFave (2004)	SL1‡	BJ	20	260	0.40	0.40	0.15	0.15	0.00	0.00	0.95	0.15	0.05
	SL2‡	BJ	20	260	0.35	0.35	0.15	0.15	0.00	0.00	0.95	0.25	0.05
	SL4‡	BJ	20	260	0.30	0.30	0.15	0.15	0.00	0.00	0.90	0.20	0.05
Shinjo et al. (2009)	B-1	BJ	20	89	0.15	0.15	0.40	0.40	0.00	0.00	0.95	0.30	0.05
	J-1	J	20	76	0.15	0.15	0.35	0.40	0.00	0.00	0.95	0.35	0.05
	BJ-1	J	20	80	0.15	0.15	0.40	0.40	0.00	0.00	0.95	0.35	0.05
Takamori et al. (2006)	NO1	BJ	20	127	0.25	0.25	0.25	0.25	0.00	0.00	0.95	0.25	0.05
	NO2	BJ	20	116	0.25	0.25	0.25	0.25	0.00	0.00	0.95	0.25	0.05
	NO3	BJ	20	127	0.25	0.25	0.25	0.25	0.00	0.00	0.95	0.25	0.05
Teng and Zhou (2003)	S1	BJ	20	260	0.40	0.40	0.15	0.15	0.00	0.00	0.95	0.25	0.07
	S2	BJ	20	260	0.40	0.40	0.15	0.20	0.00	0.00	0.95	0.25	0.05
	S5	BJ	20	260	0.30	0.30	0.15	0.15	0.00	0.00	0.95	0.25	0.05
Teraoka (1997)	NO01	J	15	131	0.25	0.25	0.30	0.30	0.00	0.00	0.90	0.30	0.05
	NO04‡	J	15	131	0.25	0.25	0.35	0.40	0.00	0.00	0.90	0.30	0.05
	NO07‡	BJ	15	145	0.30	0.30	0.45	0.45	0.00	0.00	0.90	0.20	0.00
	NO08‡	BJ	15	164	0.30	0.30	0.45	0.45	0.00	0.00	0.90	0.35	0.00
	NO09‡	J	15	131	0.25	0.25	0.30	0.40	0.00	0.00	0.90	0.35	0.05
	NO10‡	J	15	131	0.25	0.25	0.40	0.40	0.00	0.00	0.90	0.35	0.05
	NO35‡	BJ	15	131	0.25	0.25	0.25	0.20	0.00	0.00	1.00	0.40	0.05
	NO36‡	BJ	15	131	0.25	0.25	0.25	0.20	0.00	0.00	1.00	0.40	0.05
Yashito et al. (1996)	No. 1	BJ	20	180	0.25	0.25	0.25	0.25	0.00	0.00	1.00	0.25	0.05
	No. 3	BJ	20	157	0.25	0.25	0.25	0.25	0.00	0.00	1.00	0.35	0.05
	No. 4	J	20	157	0.25	0.25	0.30	0.35	0.00	0.00	1.00	0.30	0.05
Yoshino et al. (1997)	NO1	BJ	20	260	0.20	0.20	0.15	0.20	0.00	0.00	0.90	0.35	0.05
	NO3	BJ	20	212	0.25	0.25	0.20	0.22	0.00	0.00	0.90	0.35	0.05
Zaid et al. (1999)	S3	BJ	20	140	0.30	0.35	0.20	0.20	0.00	0.00	0.85	0.30	0.05
Mean			***20***	***187***	***0.25***	***0.25***	***0.25***	***0.26***	***0.00***	***0.00***	***0.93***	***0.29***	***0.04***
COV			0.11	0.32	0.25	0.25	0.32	0.33	0.00	0.00	0.04	0.29	0.46

†, §, and ‡ are the same as non-ductile exterior joints

3.5 Summary

This chapter presents the analytical modeling techniques for RC frame's critical components associated with the design codes, particularly their reinforcing details. Analytical models of RC frame's primary components that can account for shear in the columns and shear or bond in the joints of RC frames are employed, modified, and developed, following a review of existing models. For shear-dominated columns, the shear model developed by Elwood (2004) is employed. To resolve the drawback of the model, this research proves the applicability of the model to experimental columns subjected to reversed cyclic pushover loadings. The shear model is validated using the results from experimental shear-dominated columns available in the literature. For beam-column joint models, the model from Anderson et al. (2008) is utilized with modifications to the degrading slope in order to construct the backbone curve of the joint shear stress-strain relationship. Since this model was developed for non-ductile interior joints, this research shows the applicability of the model to other joint types such as non-ductile exterior joints, ductile exterior and interior joints by comparing experimental results with analytical predictions. Additionally, reduced joint shear strength associated with bond slip is accounted for by using the bond strength model developed by Hassan (2011) for non-ductile joints with discontinuous beam bottom reinforcement. Finally, hysteric rules including the effect of cyclic deterioration are extracted in comparison to experimental results in order to apply them to the frame model. Application of the proposed column shear model and beam-column joint model for seismic demand analyses of RC frames demonstrates the importance of capturing the shear behavior of the components accurately in assessing their seismic performance.

CHAPTER 4

DESCRIPTION, MODELING, AND RESPONSE OF RC BUILDINGS

The seismic risk assessment of a building inventory in a region requires the selection of sample buildings that are representative of design and construction practices in that region as well as accurate finite element models for numerical simulations of these buildings. The sample buildings selected in the research are the most common types of non-ductile and ductile RC buildings designed or constructed in California. Based on building information in accordance with the design codes and analytical modeling techniques mentioned in Chapter 3, high fidelity analytical frame models accounting for geometric and material nonlinearities are utilized in this research in order to achieve reliable fragility assessments. The ability to capture the inelastic behavior of critical components is dictated by the fidelity and robustness of the model. The evaluation of seismic performance for these frames is finally conducted using the NSP and the NTHA in terms of local and global demands.

4.1 Description of Typical RC Building Frames in California

Liel (2008) and Haselton (2006) proposed a series of building frames in terms of building height, lateral force resisting system, and design requirements to perform the seismic risk analysis for non-ductile RC frames (ordinary moment frames, OMF) and ductile RC frames (special moment frame, SMF), respectively. The building frames are representative of common older and modern building types in California. The researchers accounted for important key design parameters that can considerably affect seismic

performance such as the plastic rotation capacity of members, strength and stiffness of members, and deformation capacity of system. Among many design variables was the ratio of tributary areas for gravity and lateral loads, as illustrated in Figure 4.1. Perimeter frames have lateral force resisting frames on the exterior of the building and a flat-slab floor system while space frames have moment-resisting frames along every column line.

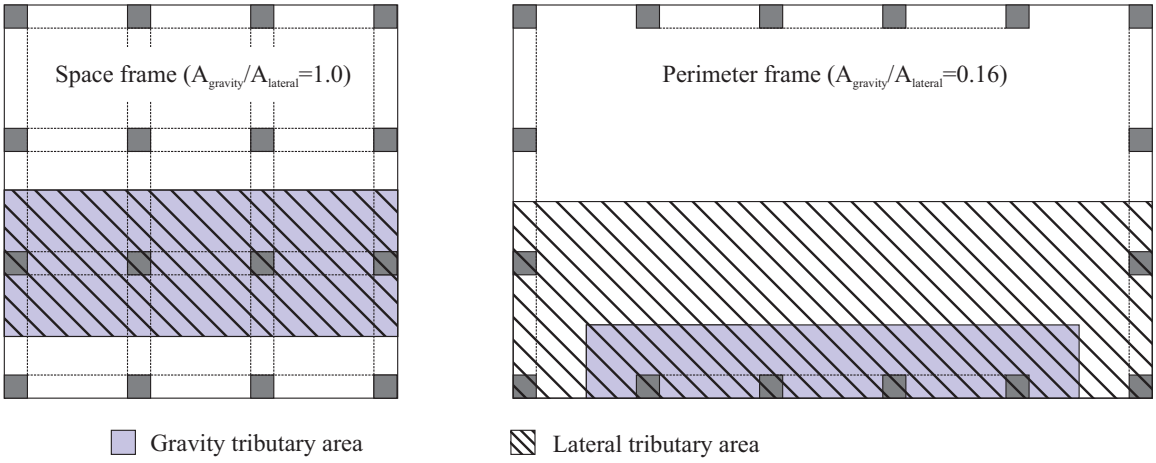

Figure 4.1 Ratio of gravity to lateral tributary areas for a space and perimeter frame systems (Haselton 2006)

4.1.1 Non-ductile RC frames

Liel (2008) identified a set of archetypes to evaluate the seismic risk assessment of older RC frame structures. This author presented a set of 26 archetypical non-ductile RC frames that can be representative of typical office buildings in California. Each non-ductile frame was designed according to the requirements of the 1967 Uniform Building Code (UBC), which represents the state of seismic design in California between 1950 and 1975 (ICBO 1967). The 1967 UBC equivalent lateral load procedure for seismic design was used to determine the required design base shear for seismic zone 3, the highest

seismic zone at the time, which included most of California. In addition, the same material strengths were used in designing all the frames: 27.6 MPa concrete and 414 MPa steel for both longitudinal and transverse reinforcement. All members were designed to be 15% stronger than the minimum requirement in the code. Other modeling assumptions are similar to those by Haselton (2006) which will be explained in the next section. Table 4.1 presents typical building footprint sizes for the various buildings in the analysis. All frames have 7.62 m bay spacing.

Table 4.1 Representative building geometries for non-ductile frames (Liel 2008)

Building story	Story height (first, upper)	Plan dimensions
2~4 story	4.572 m, 3.962 m	38.100 m × 53.340 m
8~12 story	4.572 m, .3.962 m	38.100 m × 38.100 m

4.1.2 Ductile RC frames

Haselton (2006) presented the class of RC ductile frames designed by current building code provisions of the 2003 IBC (ICC 2003), ASCE 7-02 (ASCE 2002), and ACI 318-02 (ACI 2002) to ensure the ductile behavior which prevents or delays unpredictable failure or even sudden collapse under seismic events. Each ductile frame was designed for a high seismic site in California (soil class S_d, S_{ms} = 1.5g, and S_{m1} = 0.9g) corresponding to NEHRP soil category D. The maximum considered earthquake (MCE) used in building code design (ICC 2003) is depicted in Figure 4.2. The general design assumptions used in the design process for the ductile frames are indicated in Table 4.2. Practicing engineers reviewed all relevant design assumptions to ensure consistency with common design practice. The author also assumed that the governing failure mode is side-sway collapse Based on the design assumptions, the author developed a matrix of 30 archetypical designs for six building heights (1~20 stories), two bay widths (6.096 m and 9.144 m),

perimeter and space frames, and three foundation fixities. Moreover, Table 4.3 indicates typical building footprint sizes for various buildings used in the work of Haselton (2006). Further details on the design information can be found in the reference.

Table 4.2 Design assumptions of the archetype ductile frames (Haselton 2006)

Design parameter	Design assumption
Beam stiffness	$0.5EI_g$
Column stiffness	0.7 EI_g for all axial load levels
Slab consideration	Slab not included in stiffness/strength design
Joint stiffness	Elastic joint stiffness
Conservatism applied in element flexural and shear strength design	1.15 of required strength
Conservatism applied in joint strength design	1.0 of required strength
Conservatism applied in strong-column weak-beam design	Expected ratio of 1.3 (instead of 1.2)

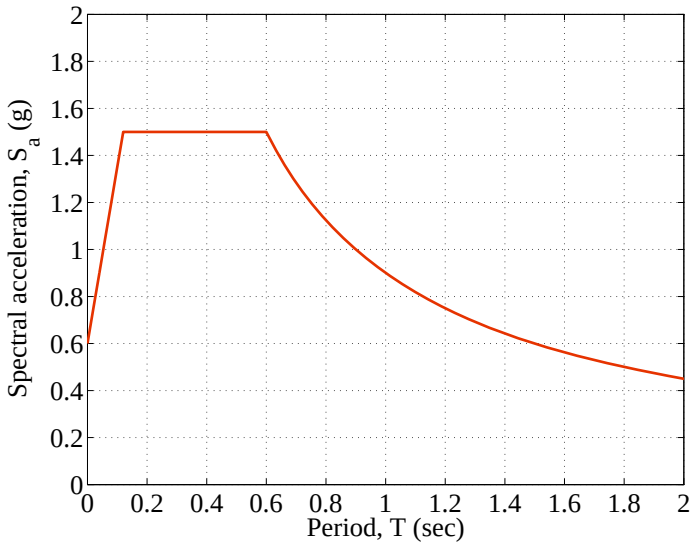

Figure 4.2 MCE ground motion spectrum at the Los Angeles site

Table 4.3 Representative building geometries for ductile frames (Haselton 2006)

Building story	Story height (first, upper)	Plan dimensions
1~4 story	4.572 m, 3.962 m	36.576 m × 54.864 m
8~20 story	4.572 m, .3.962 m	36.576 m × 36.576 m

4.1.3 Selection of analyzed RC frames

In this research, 4-story and 8-story RC frames representative of low- and mid-rise buildings are chosen in a series of non-ductile and ductile RC frames. Non-ductile RC frames used in this research include space and perimeter frame system because the former is more typical of office buildings and the latter was constructed in the form of flat-slab gravity systems that can be found in industrial facilities. On the contrary, for ductile frames, perimeter frame systems are selected because they are typical of ductile RC frame structures that are mainly found in office buildings and industrial facilities. Additionally, space frames are not taken into account because they would be expected to respond in a more ductile fashion to earthquake loading. Table 4.4 lists RC frames to be analyzed. Figure 4.3 and Figure 4.4 provide the primary design features for an example of non-ductile and ductile RC frames selected in this research, respectively. Figure B.1 through Figure B.6 in Appendix B show design information for all frames selected in this research. Table 4.5 also summarizes the material properties of six RC frames. Each RC frame will be modeled to various analytical frame models (i.e., joint rigid offset model, joint shear or bond model, column shear model, joint and column shear model) using the associated design information in the figures in order to assess the influence of modeling assumptions and governing failure modes on seismic performance, particularly deformation demand. The frame models will be discussed in the next section.

Table 4.4 List of RC frames

Type	Frame ID	No. of stories	System	Design ID number	Reference
Non-ductile	OMF-4S	4	Space	ID3004	Liel (2008)
frame	OMF-4P	4	Perimeter	ID3003	
	OMF-8S	8	Space	ID3016	
	OMF-8P	8	Perimeter	ID3015	
Ductile	SMF-4P	4	Perimeter	ID1003	Haselton (2006)
frame	SMF-8P	8	Perimeter	ID1011	

Table 4.5 Material properties with different frame types

Type	Frame ID	Concrete compressive strength (MPa)			Steel yield strength (MPa)	
		1st story column	Other columns	Beam	Nominal	Expected
Non-ductile	OMF-4S	27.6	27.6	27.6	414 MPa	462 MPa
frame	OMF-4P	27.6	27.6	27.6	414 MPa	462 MPa
	OMF-8S	27.6	27.6	27.6	414 MPa	462 MPa
	OMF-8P	27.6	27.6	27.6	414 MPa	462 MPa
Ductile	SMF-4P	48.3	34.5	34.5	414 MPa	462 MPa
frame	SMF-8P	41.4	34.5	34.5	414 MPa	462 MPa

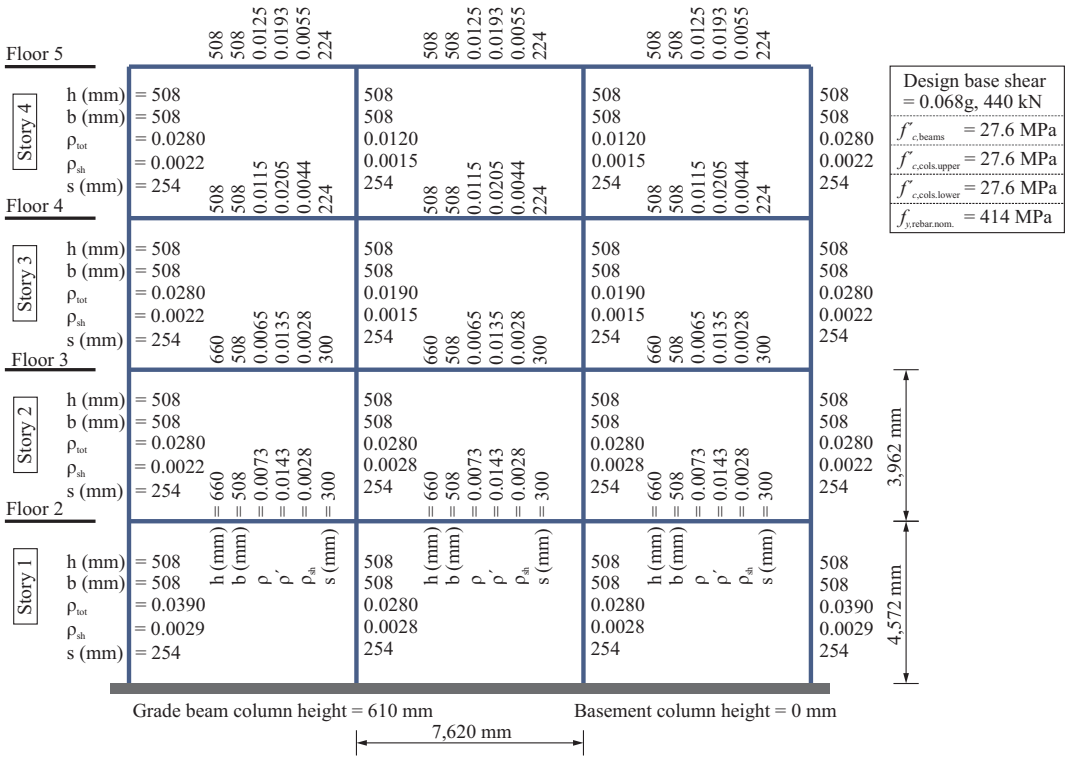

Figure 4.3 Design information of 4-story non-ductile space frame (OMF-4S) (Liel 2008)

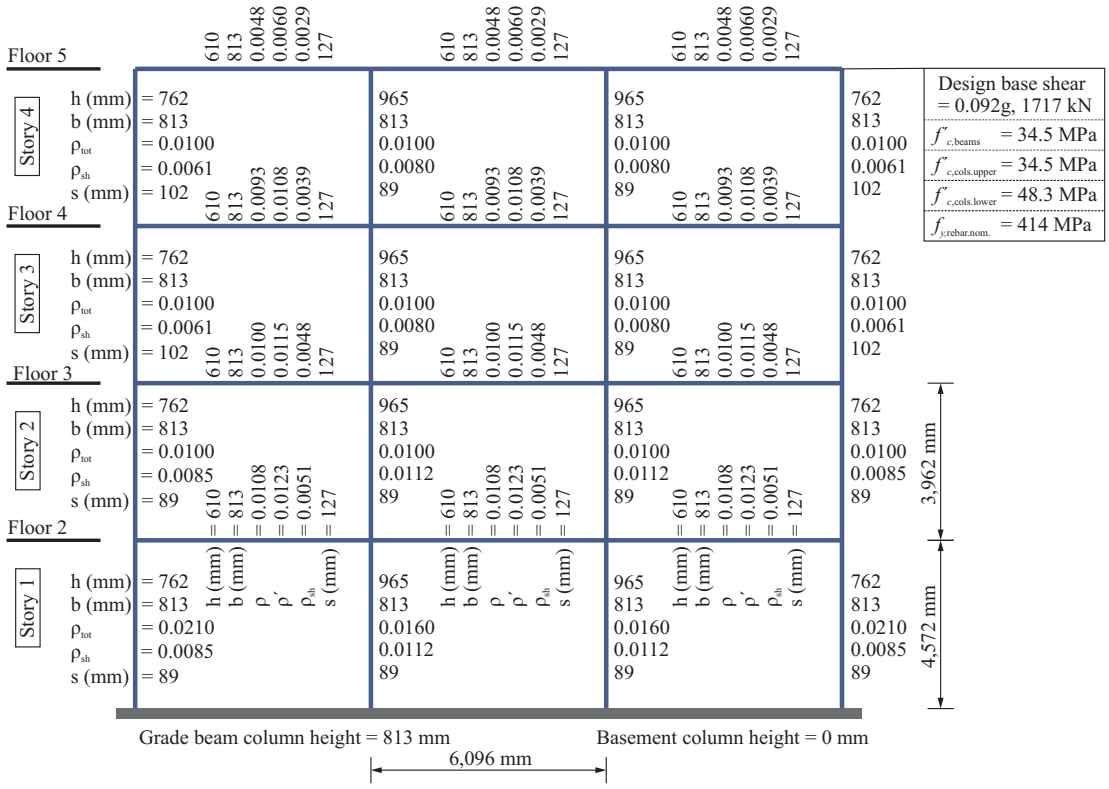

Figure 4.4 Design information of 4-story ductile perimeter frame (SMF-4P) (Haselton 2006)

4.2 Analytical Frame Model

4.2.1 Overall modeling technique

The analytical models used by Liel (2008) and Haselton (2006) were developed using lumped plasticity elements for columns and beams. Each column or beam consists of one elastic element and a nonlinear zero-length rotational spring at the end of the member. The rotational spring includes monotonic and cyclic inelastic behavior without explicitly modeling extra components. This approach can capture the accurate global response of columns, but it cannot account for the shear behavior in columns and the effect of axial-flexure interaction in columns. Additionally, this approach cannot determine where inelastic action will occur in multi-story frames. Therefore, this research employs the fiber section beam-column elements that can capture structural member response such as

the interaction of axial force with bending moment, the hardening or softening behavior of materials, and the effect of transverse confinement in RC columns and beams. Moreover, for shear-dominated columns, the addition of a shear spring series with flexure elements can provide the stiffness and strength degradation for shear-dominated columns.

To investigate the seismic performance and increased vulnerability of RC frames selected in the previous section with different governing failure modes, analytical frame models are suggested and are analyzed with different modeling techniques, as listed in Table 4.6. For non-ductile frames, each frame model with joint shear model (XXX-XX-JS) is selected as a baseline frame model in this research. For the 4-story space frame (OMF-4S), five different analytical frame models are chosen in order to identify the effect of joint shear (JS), joint bond (JB), column shear (CS), and coupled joint and column shear (JCS) models on frames. For other frames, three analytical frame models are selected: joint shear (JS), column shear (CS), and coupled joint and shear (JCS) models. For ductile frames, each perimeter frame is created for two failure modes, such as joint rigid offset and joint shear failure models, in order to take the inelastic behavior of joints into consideration.

Table 4.6 Analytical frame model with different modeling techniques

Type	System	No. of stories	Frame model	Modeling technique
Non-ductile	Space	4	OMF-4S-RO	Joint rigid offset
			OMF-4S-JS	Joint shear failure
			OMF-4S-JB	Joint bond failure
			OMF-4S-CS	Column shear failure
			OMF-4S-JCS	Joint and column shear failure
	Space	8	OMF-8S-JS	Joint shear failure
			OMF-8S-JC	Column shear failure
			OMF-8S-JCS	Joint and column shear failure
	Perimeter	4	OMF-4P-JS	Joint shear failure
			OMF-4P-JC	Column shear failure
			OMF-4P-JCS	Joint and column shear failure
	Perimeter	8	OMF-8P-JS	Joint shear failure
			OMF-8P-CS	Column shear failure
			OMF-8P-JCS	Joint and column shear failure
Ductile	Perimeter	4	SMF-4P-RO	Joint rigid offset
			SMF-4P-JS	Joint shear failure
	Perimeter	8	SMF-8P-RO	Joint rigid offset
			SMF-8P-JS	Joint shear failure

Figure 4.5 illustrates the overall analytical frame model including the modeling techniques for RC frame's components. All components are modeled in the same manner as described in Chapter 3. All frames have a slab thickness of 203 mm and the effective width of the slab calculated from the provision of ACI318-02 (2002). Based on tributary areas, gravity loads are assigned to distributed loads on beams and all mass is lumped at beam-column connections. Figure 4.1 depicts the determination of the gravity and lateral tributary areas for space and perimeter frames. For the space frame, an interior moment frame resists the gravity loads and lateral loads. Unlike these space frames, the perimeter frame resists lateral loads and interior columns carries only gravity loads. In this system, P-Delta effects are accounted for using a combination of gravity loads on the perimeter frame and gravity loads on a fictitious (leaning) column. Additionally, the gravity loads on the leaning column can be calculated by subtracting the gravity load portion on

internal columns from the lateral tributary area (half of the plan view of the frame) and all the mass corresponding to the lateral tributary area is assigned only to the perimeter frame. The floor dead load and mass was determined based on the load combination 1.05D (D = 175psf) + 0.25L (L = 25psf). For the perimeter frame system, the truss elements connecting the perimeter frame to the leaning column behave only axially and have a span length equal to the half of the beam span length. The elastic column element has the moment of inertia and cross-sectional area approximately two orders of magnitude greater than the internal columns to account for the effect of all the gravity columns. Zero-length elements connect the columns to the truss elements, behave as rotational springs, and have an extremely small stiffness value so that the leaning column does not carry any moment. The base of the leaning column is modeled as a pin.

A remarkable finding from the frame design is that columns designed in non-ductile frames were expected to yield before failing in shear because they have taller story heights, as Liel (2008) herself acknowledged. In general, sudden brittle failures (shear failure prior to yielding) have typically been observed in short columns. Thus, the column shear model developed by Elwood (2004) can be utilized to describe the flexure-shear behavior. As mentioned in Chapter 3, employing the shear strength equation of the ACI or ASCE provisions cannot appropriately ensure the flexure behavior prior to detecting shear failure (brittle failure before reaching the flexure yielding). Additionally, the shear strength formulation developed by Elwood (2004) in the source code is very difficult to suitably predict a shear force at shear failure. To alleviate this inappropriate implementation, this research performs an NSP for each column flexure model (without a shear spring) to find shear force at yielding condition. The initiation of shear failure is

assumed to lie between shear forces at yielding and maximum condition for the column model without a shear spring. The degrading slope of total response (K^{t}_{deg}) can be calculated from the onset of shear failure and axial limit drift in equation (3.3). Then, the final shear behavior of the column with a shear spring is identified through static and reversed cyclic pushover analyses.

A crucial modeling technique is the determination of joint shear strength for non-ductile and ductile beam-column joints. In Chapter 3, the validation of analytical models is performed by employing experimental joint shear strength on the backbone curves. However, these experimental observations cannot be utilized when creating full frame models. Thus, a reliable estimation for joint shear strength is required to build analytical frame models. To determine the shear strength for beam-column joints, this research proposes the probabilistic joint shear strength model for non-ductile and ductile joints through the statistical method based on experimental observations. All other modeling parameters are represented using their median values obtained from the validation work in Chapter 3. The detailed description on the joint shear strength will be discussed in the next sections. Furthermore, for the bond failure model in Table 4.6, the embedment length within a joint is assumed to be 152 mm following the minimum requirement of ACI 315-63 (ACI 1963), which is used to calculate reduced joint shear strength associated with inadequate anchorage.

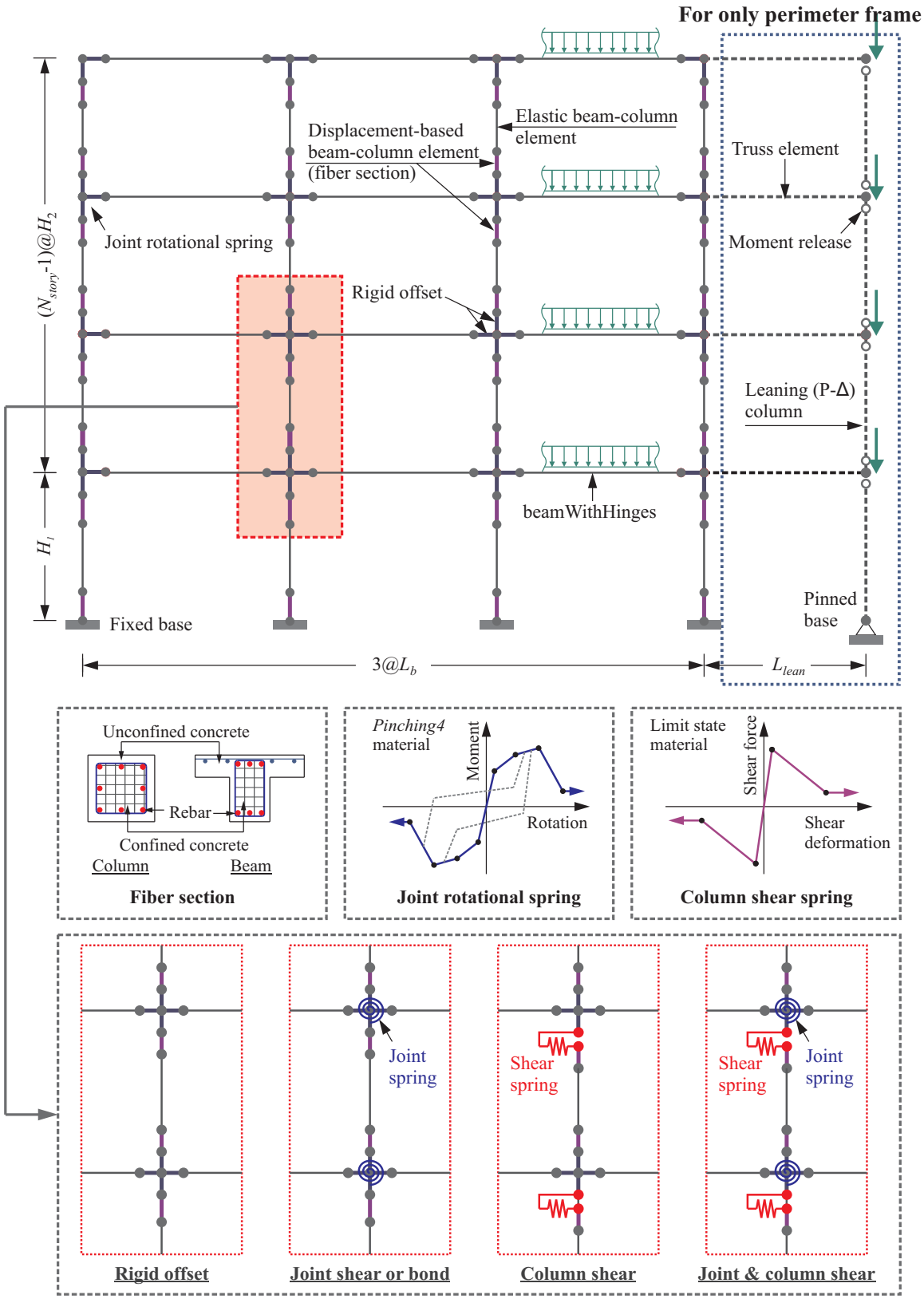

Figure 4.5 Overall analytical frame model

4.2.2 Proposed joint shear strength model

Kim and LaFave (2009) proposed the statistical joint shear strength model by using a Bayesian method based on 136 and 18 experimental ductile and non-ductile subassemblages, respectively. Additionally, the authors constructed the joint shear strength model by performing a step-wise removal process to extract key parameters among ten parameters (spacing ratio, ratio of recommended to provided amount of joint transverse reinforcement, ratios of beam depth to column depth and beam width to column width, joint transverse reinforcement index, beam reinforcement index, joint eccentricity, in-plane and out-of-plane geometry, concrete compressive strength). The basic formulation with ten parameters can be expressed in equation (4.1):

$$v_{j,\max} = \beta_0 \left(\frac{s_{pro}}{s_{req}}\right)^{\beta_1} \left(\frac{A_{sh,pro}}{A_{sh,req}}\right)^{\beta_2} \left(\frac{b_b}{b_c}\right)^{\beta_3} \left(\frac{h_b}{h_c}\right)^{\beta_4} \left(1-\frac{e}{b_c}\right)^{\beta_5} JI^{\beta_6} BI^{\beta_7} JP^{\beta_8} TB^{\beta_9} f_{cj}^{\ \beta_{10}} \tag{4.1}$$

where s_{pro}/s_{req} and $A_{sh,pro}/A_{sh,req}$ are the ratio of the spacing and cross-sectional area of joint transverse reinforcement provided to that required in ACI 352R-02 (2002), respectively; b_b/b_c and h_b/h_c are the ratio of beam width to column width and beam depth to column depth, respectively; e is the joint eccentricity between beams and columns; JI is the joint transverse reinforcement index which is defined as the product of the volumetric joint transverse reinforcement ratio (ρ_j) and the joint transverse reinforcement yield stress (f_{yj}) divided by the joint concrete compressive strength (f_{cj}); BI is the beam reinforcement index which is defined as the product of the beam longitudinal reinforcement ratio (ρ_j) and the beam longitudinal reinforcement yield stress (f_{yb}) divided by the beam concrete compressive strength (f_{cb}); JP is a parameter for describing in-plane

geometry (1 for interior, 0.75 for exterior, and 0.5 for knee joints); *TB* is the joint confinement factor (1.0 for subassemblages with 0 or 1 transverse beams and 1.2 for subassemblages with 2 transverse beams); and β_i (i = 1,…,10) is a coefficient.

A remarkable feature in equation (4.1) is that the formulation does not account for the effect of column axial load on joint shear strength. In fact, there is no consensus within the research community as to the effect of axial load (Mitra 2007). It has been argued that axial load enhances the joint shear capacity by confining the joint core (Kitayama et al. 1987) and by equilibrating part of an inclined compressive strut that forms in the joint associated with joint shear action (Paulay 1989, Park and Mosalam 2012). However, it has also been concluded that column axial load influences the deformation but not the joint shear strength (Meinheit and Jirsa 1977, Fujii and Morita 1991, Kitayama et al. 1991, Bonacci and Pantazopoulou 1993). Because of this ambiguous conclusion, the impact of the column axial force on joint shear strength is not accounted for in this research. Moreover, the effect of column longitudinal reinforcement is not included following the work of Kim and LaFave (2009).

With the basic predictor variables proposed by Kim and LaFave (2009), a multiple linear regression that is employed to represent the relationship between a response (dependent) variable and several predictor (independent) variables in a log-transformed space is performed to establish a non-ductile or ductile joint shear strength model. To determine significant key parameters among possible predictor variables, step-wise regressions are performed until a satisfactory model is found. Moreover, to identify key predictor variables in the joint shear strength model, an analysis of variance (ANOVA) test is performed in a log-transformed space. In the ANOVA test, the *F*-

statistic tests the claim that there is no significant relationship between predictor variables and single response variable (null hypothesis) while the *t*-statistic tests the claim that there is no relationship between an individual predictor variable and a response variable (null hypothesis). If a *p*-value is less than a particular significance level, it is customary to reject the null hypothesis. For the *F*-statistic, at the *p*-value less than the significant level, at least one of coefficients (β_i) in the model is significant whereas for the *t*-statistic, at the p-value less than the significant level, the predictor variable is significant. Therefore, stepwise linear regressions are performed until the model satisfies the condition that the *p*-value for all predictor variables in the *t*-statistic is less than the significance level. Conventionally, a reasonable significant level is 0.05 or less. This research uses a 0.05 significance level to determine influencing predictor variables.

Before accepting the output from the multiple linear regression analysis, it is essential to identify whether a linear regression model is appropriate as well as to examine whether the variance of the error terms is constant (Neter et al. 1996). These tasks can be achieved by examining a scatter-plot of the residuals against fitted values and against a predictor variable with the horizontal zero line. If the residuals fall within a horizontal band centered around zero in the plots, the model displays no systematic tendencies (e.g., curvilinear, non-constant variance) to overestimate or underestimate the value of the independent variables. Moreover, a normal probability plot is constructed in order to investigate the normality of the distribution of the residuals. If the points in the plot lie approximately on a straight line, the distribution of the residuals can be regarded as normal. These examinations provide the appropriateness of the linear regression model.

4.2.2.1 Non-ductile beam-column joint

The database collected by Kim and LaFave (2009) is not enough for non-ductile beam-column joints to appropriately estimate their joint shear strength. Therefore, in order to propose a reliable joint shear strength model for non-ductile beam-column joints, this research collects data from 265 existing experimental tests exhibiting joint shear failure with or without member yielding. The database consists of 155 and 13 exterior subassemblages with 0/1 and 2 transverse beams, respectively, and 66 and 27 interior subassemblages with 0/1 and 2 transverse beams, respectively, as shown in Table 4.7. However, the database does not include the joint eccentricity and knee joints for non-ductile joints because of lack of experimental data. Table C.1 in Appendix C provides a detailed description of the database.

Table 4.7 Number of experimental non-ductile joint database

Joint type	Number of transverse beams			Summation
	0	1	2	
Exterior	125	30	13	168
Interior	63	3	27	93
Total				**261**

This research utilizes basic predictor (exploratory or independent) variables suggested by Kim and LaFave (2009) to develop the joint shear strength model. For non-ductile joints, variables related to joint transverse reinforcement (s_{pro}/s_{req}, $A_{sh,pro}/A_{sh,req}$, JI) are removed from the basic predictor variables. Figure 4.6 depicts the plots of joint shear strength against predictor variables for the database. Table 4.8 summarizes the minimum, maximum, mean, standard deviation (SD), and coefficient of variation (COV) for experimental joint shear strength and each predictor variable in the database.

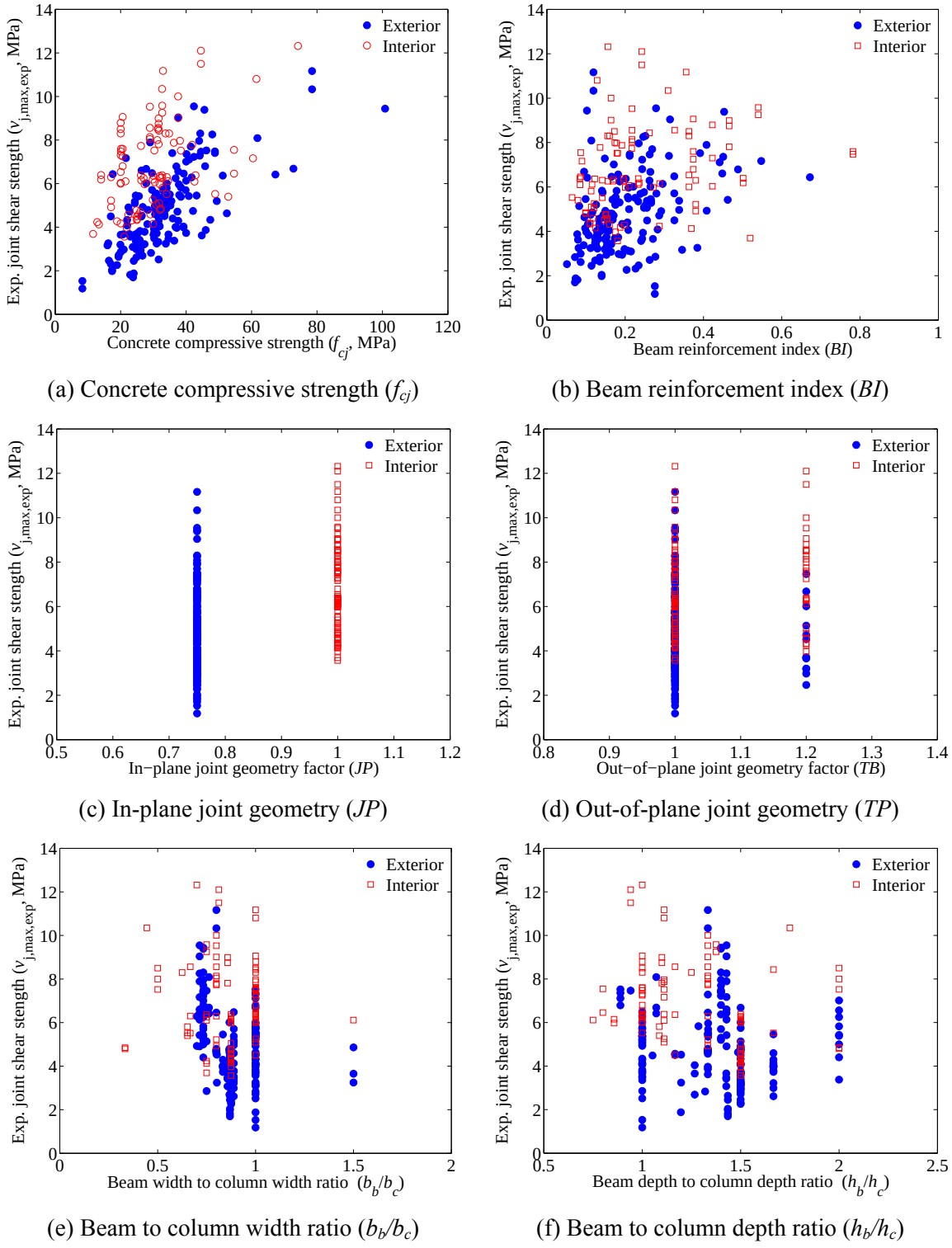

(a) Concrete compressive strength (f_{cj})

(b) Beam reinforcement index (*BI*)

(c) In-plane joint geometry (*JP*)

(d) Out-of-plane joint geometry (*TP*)

(e) Beam to column width ratio (b_b/b_c)

(f) Beam to column depth ratio (h_b/h_c)

Figure 4.6 Experimental joint shear strength vs. predictor variables for non-ductile joints

Table 4.8 Range of predictor variables for non-ductile beam-column joint database

	$v_{j,max,exp}$ (MPa)	f_{cj} (MPa)	*BI*	*JP*	*TB*	h_b/h_c	b_b/b_c
Minimum	1.18	8.30	0.05	0.75	1.00	0.75	0.33
Maximum	12.32	100.80	0.78	1.00	1.20	2.00	1.50
Mean	5.56	31.94	0.22	0.84	1.03	1.33	0.87
SD	2.10	11.83	0.12	0.12	0.07	0.28	0.15
COV	0.40	0.38	0.67	0.16	0.07	0.21	0.17

With six basic predictor variables, a stepwise multiple linear regression analysis in a log-transformed space is performed in order to propose a non-ductile joint shear strength model, as expressed in equation (4.2):

$$v_{\max}(MPa) = 0.586(TB)^{0.774}(BI)^{0.495}(JP)^{1.250}(f_{cj})^{0.941} \tag{4.2}$$

To examine significant predictor variables affecting the joint shear strength model in equation (4.2), and ANOVA test is also performed in a log-transformed space. Table 4.9 shows the intercept, coefficients, *p*-value corresponding to each coefficient in the *t*-statistic, *p*-value in the *F*-statistic, and the square root of the mean variance of residuals (RMSE). Thus, it is indicated that the first four variables are significant predictor variables in the model in that all the *p*-values in *F*-statistic and in *t*-statistic approach to zero. From this statistical observation, two variables such as h_b/h_c and b_b/b_c are insignificant predictor variables. Moreover, R^2 and adjusted R^2 are 0.858 and 0.859, respectively.

Joint shear strengths computed from equation (4.2) in the database are compared with experimental joint shear strengths, as shown in Figure 4.7. The mean value and coefficient of variation (COV) of predicted-to-experimental joint shear strength ratio are

1.011 and 0.148, respectively. It is indicated that the proposed joint shear strength model for non-ductile joints provides reasonable predictions.

Table 4.9 Stepwise linear regression for non-ductile joint strength model

Predictor variables	Coefficient	*t*-statistic	*p*-value
$\ln(f_{cj})$	0.941	31.873	**0.000**
$\ln(BI)$	0.495	24.210	**0.000**
$\ln(JP)$	1.250	17.457	**0.000**
$\ln(TB)$	0.774	5.155	**0.000**
$\ln(h_b/h_c)$	0.034	0.724	0.470
$\ln(b_b/b_c)$	-0.009	-0.171	0.865
Intercept = -0.534	RMSE = 0.152	F = 386.921, p-value = 3.242×10^{-107}	

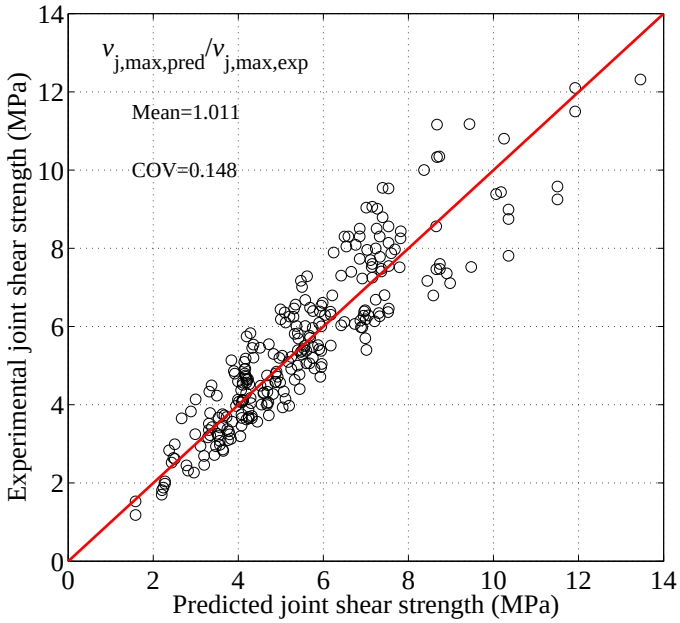

Figure 4.7 Comparison of experimental and predicted joint shear strength for non-ductile joints

To look through the aptness of the multiple linear regression model, the scatter-plots of the residuals against the fitted values and against the predictor variable are described. Figure 4.8(a) depicts the residual plot against the fitted values ($\ln(v_{j,max,pred})$) while Figure 4.8(b) through Figure 4.8(e) contain the residual plot against four significant

predictor variables such as ln(f_{cj}), ln(BI), ln(JP), ln(TB), respectively. Since the scatter-plots do not exhibit any systematic pattern, the multiple linear model is appropriate. Additionally, a normal probability plot in Figure 4.8(f) appears approximately linear (although slight divergence in the tails of the plot is witnessed), and thus the distribution of the residuals can be referred to as normal. Therefore, these examinations prove the aptness of the non-ductile joint strength model in equation (4.2). In conclusion, the non-ductile joint shear strength model obtained from the structure geometry and material properties can be utilized for constructing the backbone curves of non-ductile beam-column joints in RC frames.

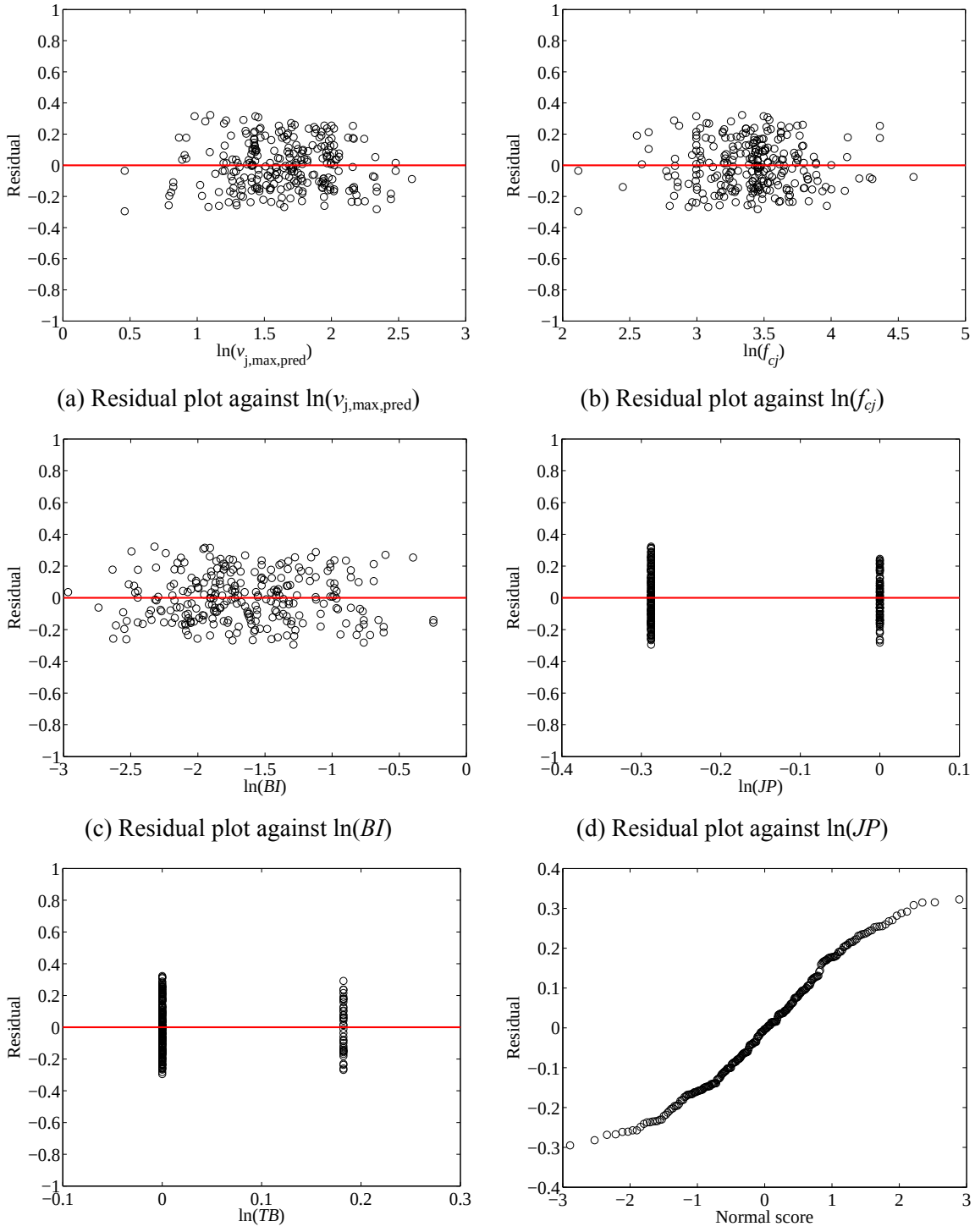

(a) Residual plot against ln($v_{j,max,pred}$)

(b) Residual plot against ln(f_{cj})

(c) Residual plot against ln(*BI*)

(d) Residual plot against ln(*JP*)

(e) Residual plot against ln(*TB*)

(f) Normal probability plot of residuals

Figure 4.8 Diagnostic residual plots for non-ductile joint database

4.2.2.2 Ductile beam-column joint

Using the same procedure as for non-ductile beam-column joints, a ductile joint shear strength model is proposed based on experimental investigations with a wide range of design parameters. For this purpose, this research collects data from 454 existing experimental tests exhibiting joint shear failure with or without beam yielding. The database consists of 158 and 14 exterior subassemblages with 0/1 and 2 transverse beams, respectively, and 231 and 51 interior subassemblages with 0/1 and 2 transverse beams, respectively, as presented in Table 4.10. The database collected in this research is more abundant than that of Kim and LaFave (2009) except for knee joints. The database does not include knee joints for ductile joints. Table C.2 provides a detailed description of the database. Unlike non-ductile beam-column joints, a total of ten parameters are used to develop a ductile joint shear strength model. Figure 4.9 shows the plot of joint shear strength against ten predictor variables. Table 4.11 summarizes the minimum, maximum, mean, SD, and COV for experimental joint shear strength and each predictor variable.

Table 4.10 Number of experimental ductile joint database

Joint type	Number of transverse beams			Summation
	0	1	2	
Exterior	144	14	14	172
Interior	204	27	51	282
Total				**454**

Table 4.11 Range of experimental ductile beam-column joint database

	$v_{j,max,exp}$ (MPa)	f_{cj} (MPa)	*JI*	*BI*	*JP*	*TB*	h_b/h_c	$1-e/b_c$	b_b/b_c	s ratio	A_{sh} ratio
Min.	2.92	13.44	0.01	0.07	0.75	1.00	0.80	0.69	0.39	0.25	0.03
Max.	24.65	182.0	0.44	0.68	1.00	1.20	2.00	1.00	1.00	1.87	4.30
Mean	8.72	42.76	0.08	0.24	0.91	1.03	1.12	0.98	0.74	0.84	0.54
SD	3.88	23.59	0.06	0.12	0.12	0.07	0.19	0.06	0.13	0.37	0.40
COV	0.50	0.68	0.84	0.56	0.12	0.07	0.19	0.06	0.17	0.49	0.31

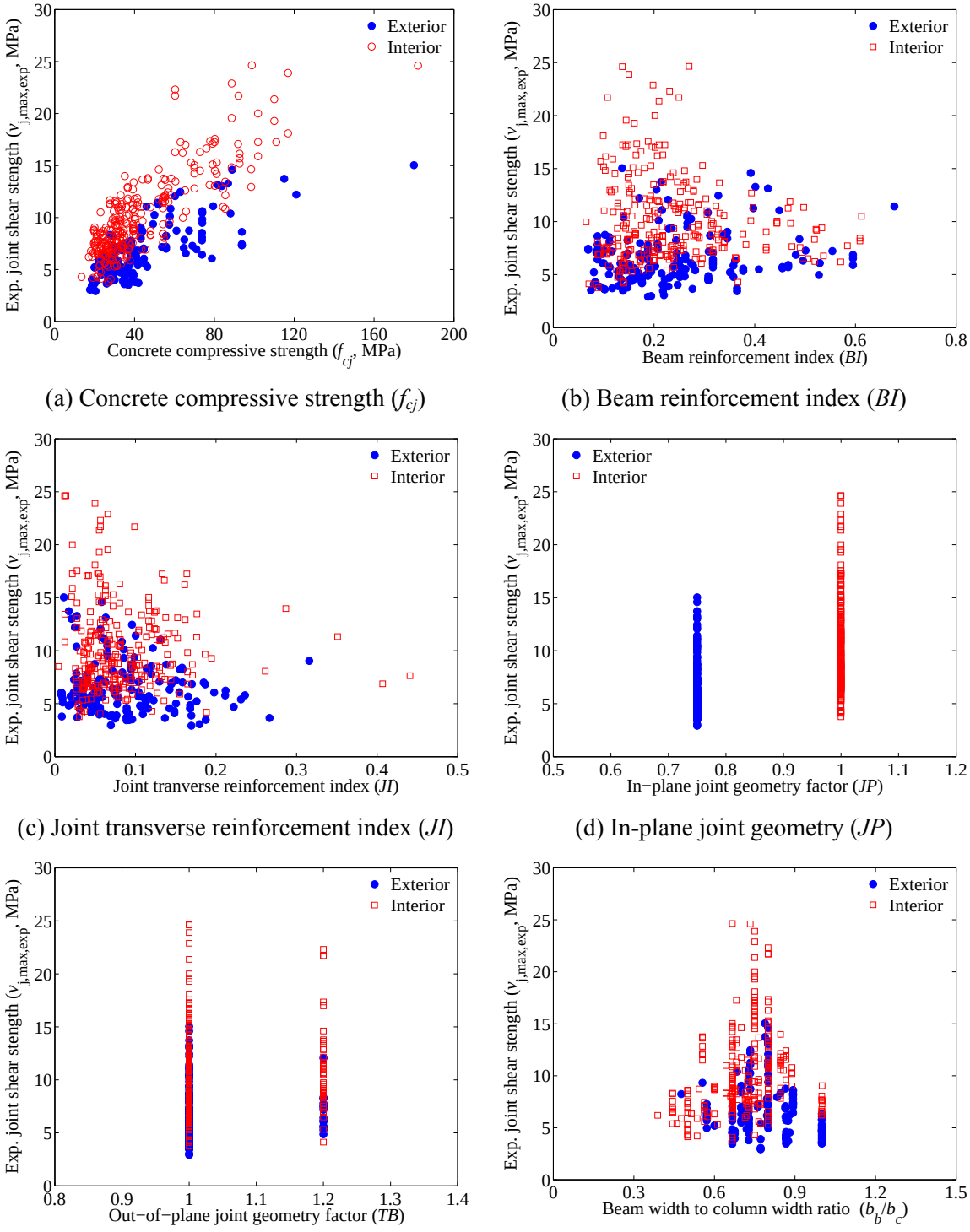

(a) Concrete compressive strength (f_{cj})

(b) Beam reinforcement index (*BI*)

(c) Joint transverse reinforcement index (*JI*)

(d) In-plane joint geometry (*JP*)

(e) Out-of-plane joint geometry (*TP*)

(f) Beam to column width ratio (b_b/b_c)

Figure 4.9 Experimental joint shear strength vs. predictor variables for ductile joints

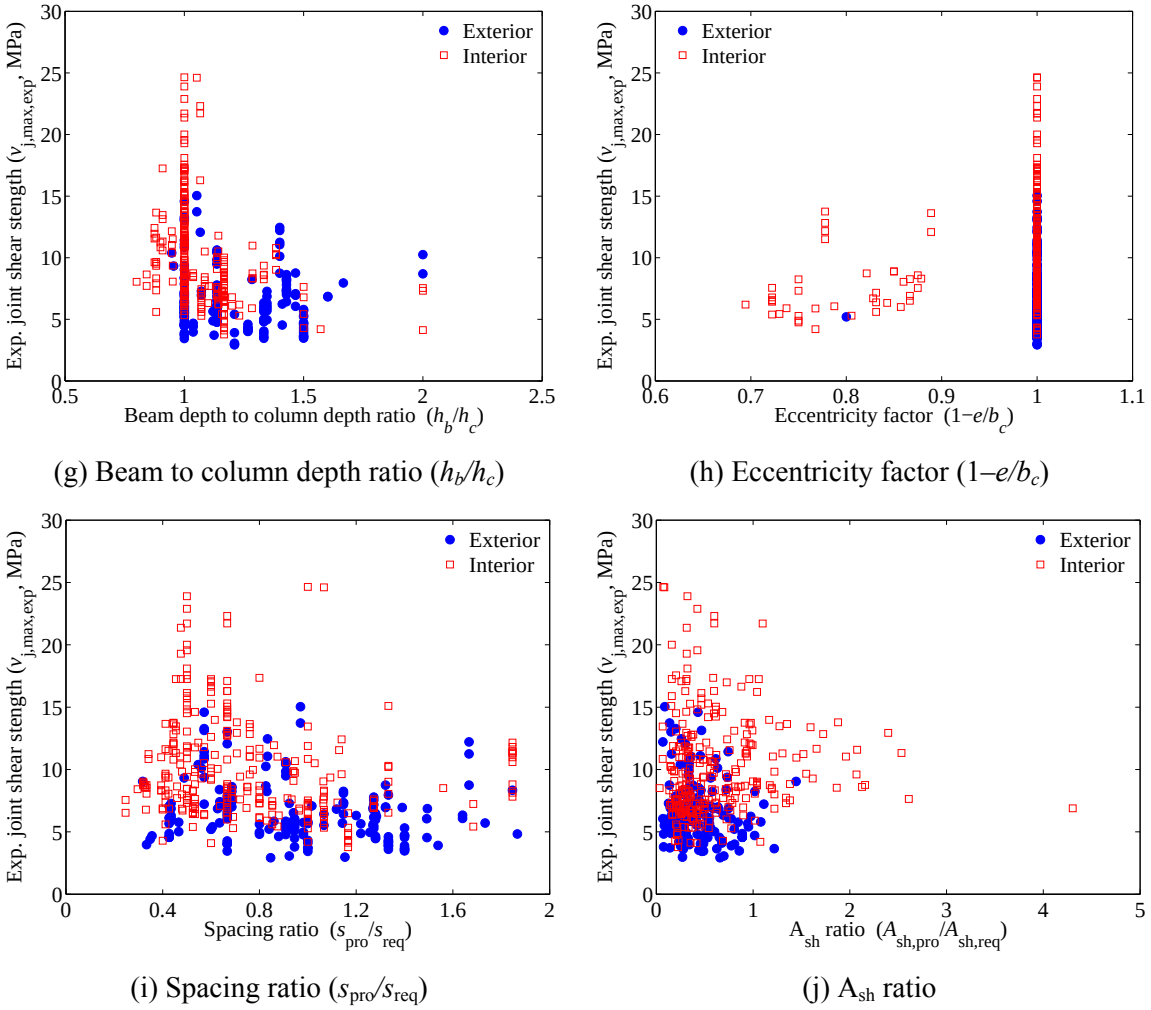

(g) Beam to column depth ratio (h_b/h_c)

(h) Eccentricity factor ($1–e/b_c$)

(i) Spacing ratio (s_{pro}/s_{req})

(j) A_{sh} ratio

Figure 4.9 Experimental joint shear strength vs. predictor variables for ductile joints (continued)

Given ten predictor variables employed in the work of Kim and LaFave (2009), a stepwise multiple linear regression analysis in a log-transformed space is carried out in order to construct a ductile joint shear strength model, as presented in equation (4.3):

$$v_{\max}(MPa) = 1.113(JI)^{0.078}\left(1-\frac{e}{b_c}\right)^{0.280}\left(\frac{b_b}{b_c}\right)^{0.125}(TB)^{1.103}(BI)^{0.342}(JP)^{1.509}(f_{cj})^{0.796} \tag{4.3}$$

To identify influential predictor variables establishing the joint shear strength model in equation (4.3), an ANOVA test is also performed in a log-transformed space.

Table 4.12 shows the intercept, coefficients, *p*-value corresponding to each coefficient in the *t*-statistic, *p*-value in the *F*-statistic, and RMSE. Therefore, it can be concluded that the first five variables and the seventh and eighth variables are significant predictor variables in the model in that all the *p*-values in *F*-statistic and in *t*-statistic are less than a significance level of 0.05. From this statistical observation, three variables such as h_b/h_c, s_{pro}/s_{req}, and $A_{sh,pro}/A_{sh,req}$ are insignificant predictor variables. For the final model, R^2 and adjusted R^2 are 0.913 and 0.912, respectively.

Table 4.12 Stepwise linear regression for ductile joint strength model

Predictor variables	Coefficient	*t*-statistic	*p*-value
$\ln(f_{cj})$	0.796	55.692	**0.000**
$\ln(JI)$	0.078	8.413	**0.000**
$\ln(BI)$	0.342	25.390	**0.000**
$\ln(JP)$	1.509	33.966	**0.000**
$\ln(TB)$	1.103	11.759	**0.000**
$\ln(h_b/h_c)$	0.088	1.930	0.054
$\ln(1-e/b_c)$	0.280	2.611	**0.009**
$\ln(b_b/b_c)$	0.125	2.860	**0.004**
$\ln(s_{pro}/s_{req})$	-0.009	-0.527	0.598
$\ln(A_{sh,pro}/A_{sh,req})$	-0.014	-0.629	0.530
Intercept = 0.108	RMSE = 0.123	F = 668.622, p-value = 5.937×10^{-107}	

Joint shear strength calculated from equation (4.3) is compared with experimental joint shear strength, as shown in Figure 4.10. The mean value and COV of predicted-to-experimental joint shear strength ratio are 1.007 and 0.122, respectively. It can be indicated that the proposed joint shear strength model for ductile joints offers appropriate estimates.

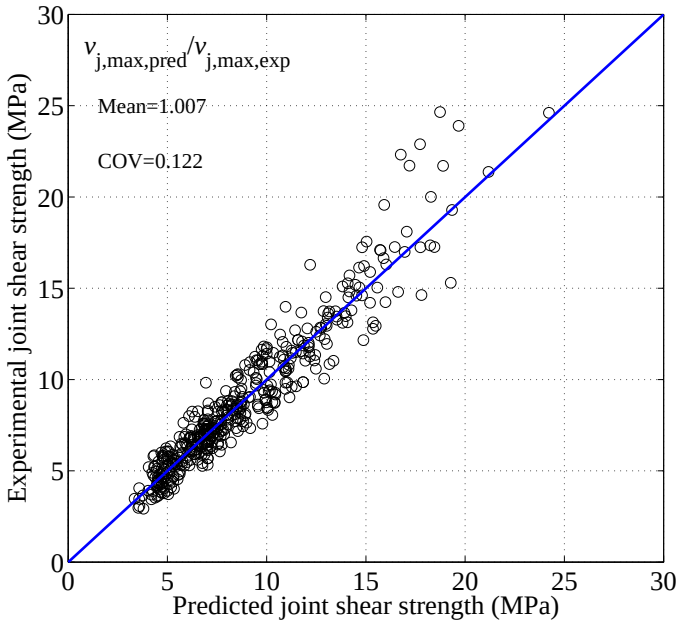

Figure 4.10 Comparison of experimental and predicted joint shear strength for ductile joints

To confirm the appropriateness of the multiple linear regression model, the scatter-plots of the residuals against the fitted values and against the predictor variable are investigated. Figure 4.11(a) presents the residual plot against the fitted values ($\ln(v_{j,max,pred})$) whereas Figures 4.11(b) through Figure 4.11(h) show the residual plot against four significant predictor variables such as $\ln(f_{cj})$, $\ln(JI)$, $\ln(BI)$, $\ln(JP)$, $\ln(TB)$, $\ln(1-e/b_c)$, $\ln(b_b/b_c)$, respectively. Moreover, a normal probability plot constructed in Figure 4.11(i) indicates that the distribution of the residuals can be referred to as normal in that the pattern is approximately linear. Therefore, these investigations prove the appropriateness of the ductile joint strength model in equation (4.3). As a result, the ductile joint shear strength model computed from the structure geometry and material properties can be employed for creating the backbone curves of ductile beam-column joints in RC frames.

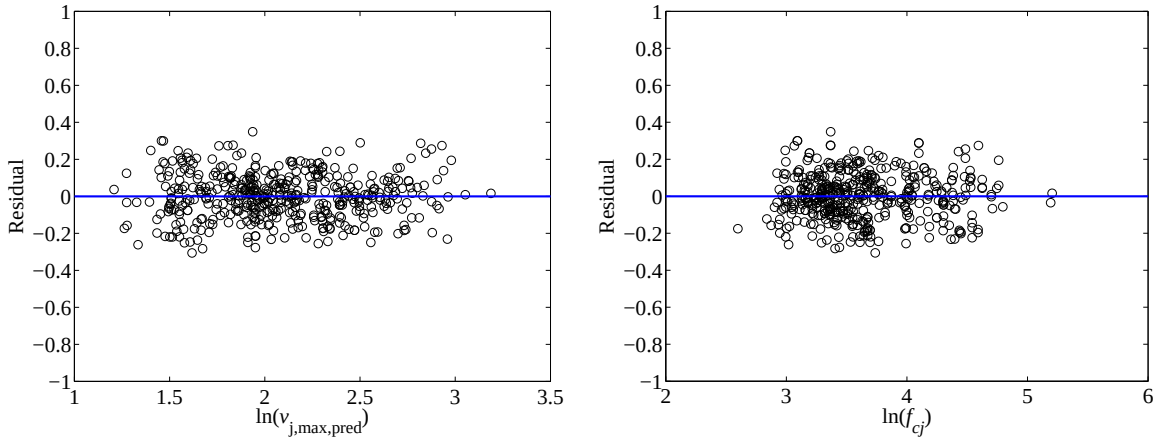

(a) Residual plot against ln($v_{j,max,pred}$)

(b) Residual plot against ln(f_{cj})

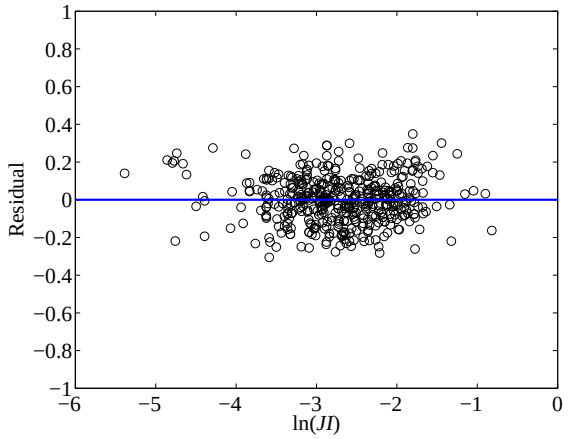

(c) Residual plot against ln(*JI*)

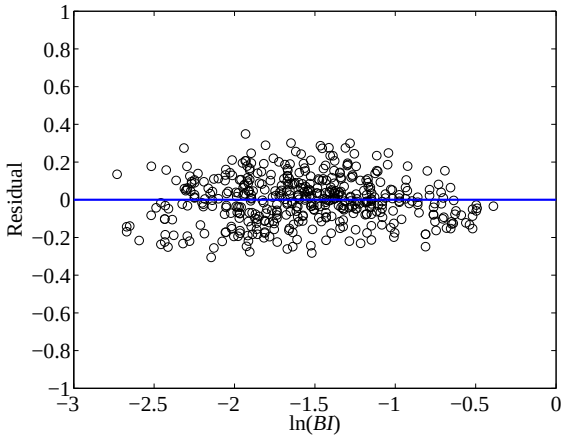

(d) Residual plot against ln(*BI*)

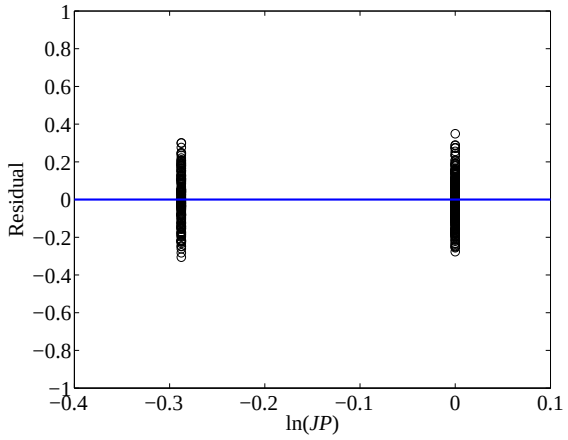

(e) Residual plot against ln(*JP*)

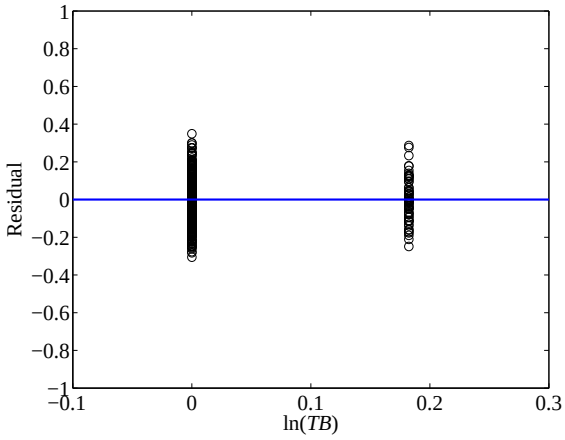

(f) Residual plot against ln(*TB*)

Figure 4.11 Diagnostic residual plots for ductile joint database

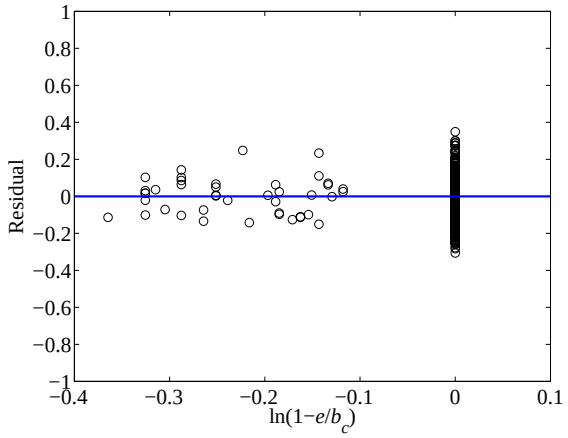

(g) Residual plot against ln(1–e/b_c)

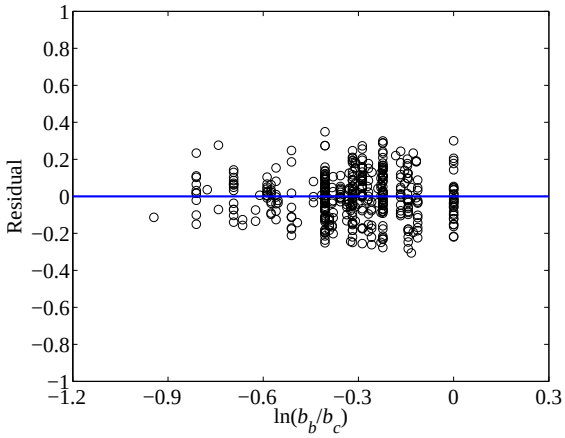

(h) Residual plot against ln(b_b/b_c)

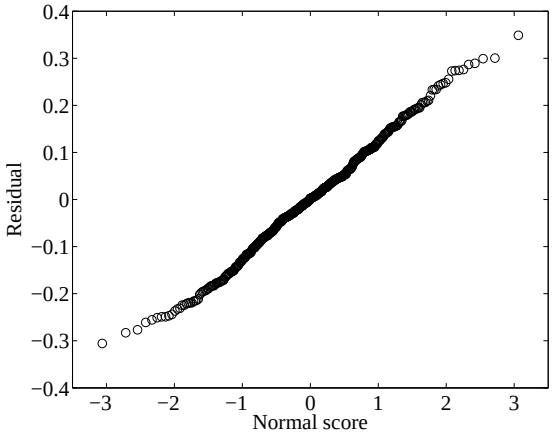

(i) Normal probability plot of residuals

Figure 4.11 Diagnostic residual plots for ductile joint database (continued)

4.2.3 Model limitations

The inelastic analytical frame models represent an idealization of real structures including their structure geometry, material properties, and reinforcing details with some simplifying assumptions. The model assumptions are presented below.

(1) Bond slip associated with members adjacent to a joint, particularly joints with discontinuous beam bottom reinforcement, is neglected. Although the analytical predictions slightly overestimate the initial stiffness related to the effect of bond

slip, as shown in the model validation, the effect of bond slip can be reduced in real structures (indeterminate frames).

(2) Bond slip at the column-footing or column-beam connections is neglected, unlike the model validation for shear-dominated columns. However, in the frame model, column longitudinal reinforcement is assumed to be adequately embedded in well-compacted concrete so that its yield strength can be developed reliably without associated deformations, such as slip or pullout.

(3) Lap-splices at the bottom of columns are ignored. Some shear-dominated columns involved in the model validation have insufficient lap-splice length at the bottom of the columns. From the model validation in Chapter 3, it can be indicated that even column models without the lap-splice model can appropriately capture the overall inelastic behavior of such columns.

(4) The effect of gravity columns in perimeter frame systems is not considered.

(5) Foundation and floor diaphragms are assumed to be rigid (i.e., no flexibility).

4.3 Seismic Response of RC Frames

The evaluation of seismic demand is performed through NSP and NTHA. The monotonic NSP is conducted to identify the drift capacity (roof and interstory), lateral strength (base shear), and potential failure mechanisms of frames. On the other hand, NTHA is carried out to investigate the maximum and residual drift capacities (interstory) and hysteretic behavior of members. All material properties are used following the work of Liel (2008) and Haselton (2006).

4.3.1 Pushover analysis

Monotonic nonlinear pushover analyses (NSP) are performed in order to examine the global load-deformation relationship for the analytical frame models. All NSPs are carried out using the lateral load pattern recommended in ASCE 7-05 (2005):

$$C_x = \frac{w_x h_x^k}{\sum_{i=1}^{n} w_i h_i^k} \tag{4.4}$$

where C_x is the normalized load at floor level x, w_i and w_x are the proportion of the total effective seismic weight of the structure (W) located or assigned to level i and x, respectively; h_i and h_x are the height from the base to level i and x; and k is an exponent related to the structure period. k is equal to 1 for structures with a period of 0.5 sec or less; k is equal to 2 for structures with a period of 2.5 sec or more; and for structures with a period between 0.5 and 2.0, k can be determined by linear interpolation between 1 and 2.

The NTHAs are performed for all RC frames listed in Table 4.6. In this research, failure is defined as when there is a 20% reduction in the maximum base shear. However, SMF-4P-RO does not reach a failure point (20% reduction in the maximum base shear). In this case, the failure point is defined at a roof drift of 4.5%. Additionally, one plot shows the pushover results with different modeling variables. Table 4.13 summarizes the maximum base shear, roof and interstory drifts at the maximum base shear and at failure, and story level at which maximum interstory drift occurs, for all analytical frame models. The story level of the maximum interstory drift can offer insight into the global failure mechanism in a frame. Moreover, it can be indicated from the table that most analytical frame models would be expected to fail in the second story, unlike those without joint

modeling. This finding is attributed to the relatively larger difference between joint shear capacities in the second and third floor calculated from equation (4.2) or equation (4.3). The pushover analysis results for a non-ductile frame (OMF-4S) and a ductile frame (SMF-8P) are discussed below.

Table 4.13 Summary of pushover analysis results

Frame model	At maximum base shear				At failure			
	Base shear (kN)	Roof drift (%)	Maximum story		Base shear (kN)	Roof drift (%)	Maximum story	
			Drift (%)	Failure			Drift (%)	Failure
OMF-4S-RO	1423	1.44	1.82	1st	1138	3.72	8.49	1st
OMF-4S-JS	989	1.89	2.45	2nd	791	3.62	4.95	2nd
OMF-4S-JB	942	2.00	2.65	2nd	753	3.40	4.71	2nd
OMF-4S-CS	1394	1.29	1.54	1st	791	1.61	2.64	1st
OMF-4S-JCS	987	1.96	2.64	2nd	790	3.03	4.85	2nd
OMF-8S-JS	1419	1.73	2.36	5th	1128	2.99	4.30	4th
OMF-8S-CS	1630	1.58	2.16	3rd	1304	4.37	7.33	2nd
OMF-8S-JCS	1418	1.73	2.36	5th	1134	2.29	3.16	5th
OMF-4P-JS	1667	1.72	2.05	2nd	1332	3.37	4.09	3rd
OMF-4P-CS	2231	1.39	1.62	2nd	1784	2.88	3.60	2nd
OMF-4P-JCS	1662	1.72	2.05	2nd	1329	3.34	4.05	3rd
OMF-8P-JS	2163	1.37	1.85	4th	1726	2.59	4.17	4th
OMF-8P-CS	NA	NA	NA	NA	NA	NA	NA	NA
OMF-8P-JCS	NA	NA	NA	NA	NA	NA	NA	NA
SMF-4P-RO	2947	1.14	1.58	2nd	2739	4.50	6.88	2nd
SMF-4P-JS	2875	1.35	1.80	2nd	2297	4.34	6.66	2nd
SMF-8P-RO	2180	0.57	0.96	2nd	1743	2.22	4.67	2nd
SMF-8P-JS	2122	0.84	1.21	2nd	1696	2.18	4.26	2nd

§ NA means not applicable.

4.3.1.1 Non-ductile 4-story space frame (OMF-4S)

Figure 4.12(a) presents the comparison of base shear-roof drift relationships with five different modeling variables for the OMF-4S frame: rigid offset model, joint shear model, bond failure model, column shear model, and joint and column shear model. OMF-4S-RO (joint rigid offset) model has the greatest initial stiffness, the highest maximum base shear, and lower roof drift at maximum base shear because the model behaves in a ductile

manner. OMF-4S-CS (column shear) model has the same pushover curve as the joint rigid offset model until a roof drift of around 2%, but lower maximum base shear than the joint rigid offset model because the column shear failure is initiated prior to reaching their maximum shear force. After reaching the maximum base shear, the pushover curve is suddenly dropped because of the dramatic loss of lateral capacity in the first story columns. OMF-4S-JS (joint shear), OMF-4S-JB (joint bond), and OMF-4S-JCS (joint and column shear) models had lower initial stiffness and lower maximum base shear (about 30% reduction) than frame models without a joint model as a result of the spread of inelastic action into the joints. Because of the reduced joint shear strength associated with bond slip in the exterior joints, OMF-4S-JB model shows a reduction of 5% in the maximum base shear in comparison to the frame models with joint shear failure. OMF-4S-JCS model follows the same pushover curve as OMF-4S-JS model until a roof drift of around 3%, and then the pushover curve abruptly decreases due to the dramatic loss of lateral resistance in all the second story columns. The column shear failure occurs at a higher drift than for OMF-4S-CS model. It can be explained that the column shear failure is delayed due to the reduced column shear force associated with the concentration of inelastic behavior in the joints. Figure 4.12(b) shows the comparison of the maximum interstory drift distributions along the frame height at maximum base shear and at failure with five different modeling variables. OMF-4S-RO and OMF-4S-CS models have the first story failure mechanism while others have the second story failure mechanism. This is attributable to a relatively large difference between joint shear capacities in the second and third floor.

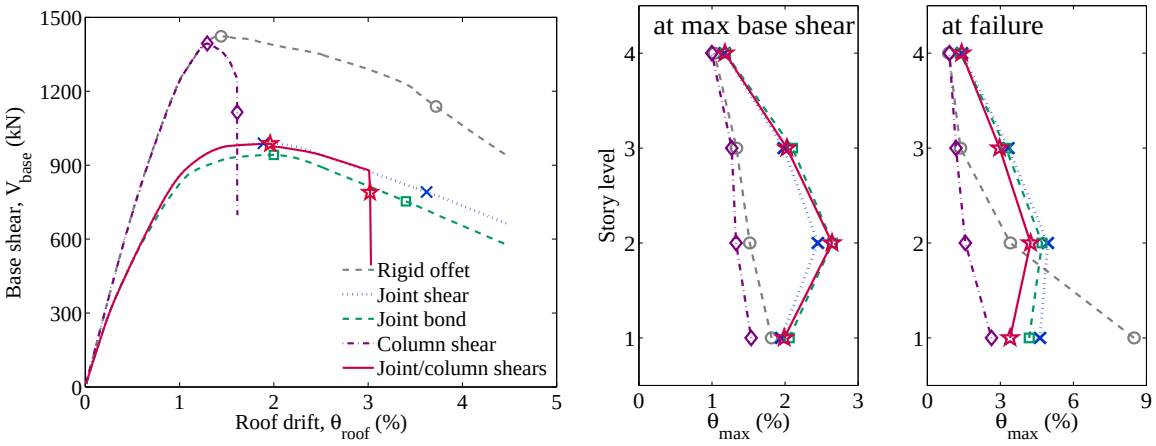

(a) Base shear-roof drift relationship (b) Interstory drift distribution

Figure 4.12 Pushover analysis results for non-ductile 4-story space frame (OMF-4S)

4.3.1.2 Ductile 8-story perimeter frame (SMF-8P)

Figure 4.13(a) show the comparison of base shear-roof drift curves with and without joint shear for the SMF-8P frame. The analytical frame model with joint (JS) has lower initial stiffness, lower higher maximum base shear, and less ductile at higher levels of roof drift than the joint rigid offset model (RO) due to the spread of inelastic action into the joints. Both frame models keeps falling sharply (due to P-Δ effect) after reaching the maximum base shear. The joint shear model brings about the relatively small reduction in the maximum base shear, but the significant increase in the post-cracking stiffness (from cracking to maximum), resulting in the considerable deformation demand. Additionally, due to the pinching effect of the joints, the joint shear model would have much smaller energy dissipation capacity than the rigid offset model when performing the cyclic pushover analysis. Figure 4.13(b) presents the comparison of the maximum interstory drift distributions along the story level at maximum base shear and at failure with and

without joint shear for the SMF-8P frame. All the frame models would be expected to have the second story failure mechanism.

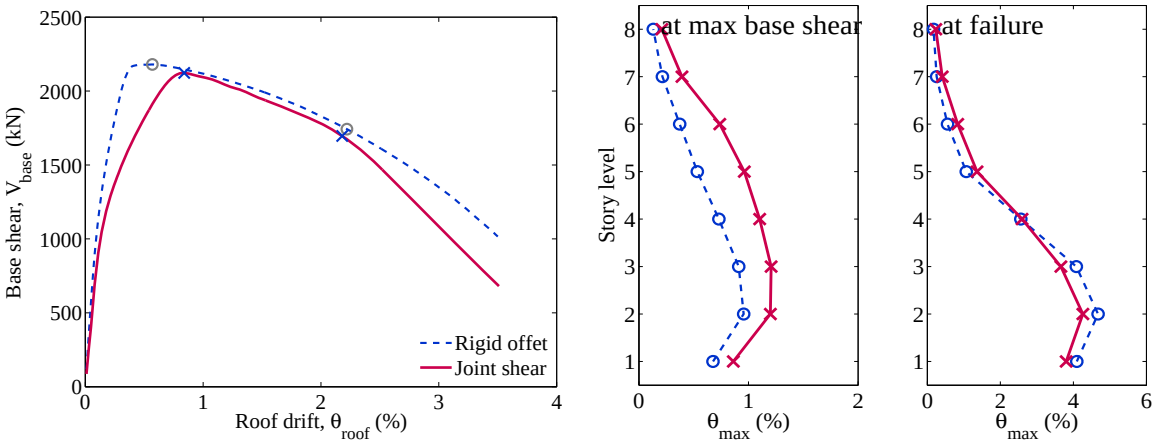

(a) Base shear-roof drift relationship (b) Interstory drift distribution

Figure 4.13 Pushover analysis results for ductile 8-story perimeter frame (SMF-8P)

4.3.2 Nonlinear time history analysis

In order to investigate the seismic response of analytical frame models under a seismic excitation with different modeling techniques, NTHAs are performed for a non-ductile frame (OMF-4S) and a ductile frame (SMF-4P). The seismic response is illustrated using a single ground motion from a suite of ground motions developed by Baker et al. (2011) which will be explained in Chapter 5. The selected ground motion has a moment magnitude of 6.53, a hypocentral distance of 29.5 km, and a duration of 39.3 sec. The ground motion also has a peak ground acceleration (PGA) of 0.375g and its five percent damaped response spectrum is presented in Figure 4.14.

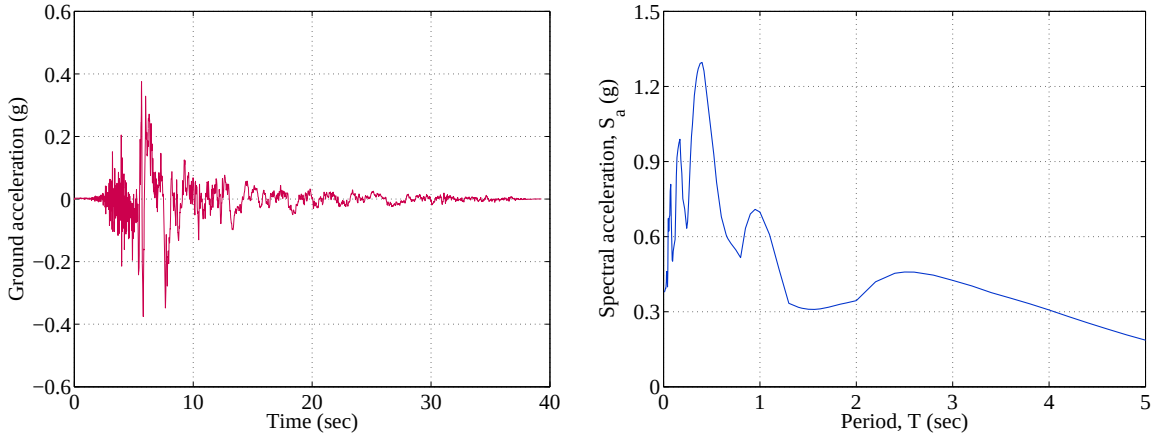

(a) Ground acceleration time history (d) Spectral acceleration (5% damping)

Figure 4.14 Ground motion used for illustration of seismic responses

4.3.2.1 Non-ductile 4-story space frame (OMF-4S)

Figure 4.15 shows the comparison of interstory drift time histories with different modeling techniques for the OMF-4S frame. Table 4.14 summarizes the maximum response parameters with regard to interstory drifts and column shear forces for different analytical frame models. It can be indicated that the maximum interstory drift occurs in the first story level for the analytical frame models without joint modeling such as OMF-4S-RO and OMF-4S-CS models, but it takes place in the second story level for the analytical frame models with joint modeling. In particular, OMF-4S-JCS model has the largest value of a maximum interstory drift of 4.3% as well as a residual interstory drift of 1.7% in the second story as a result of the effect of coupling the inelastic responses of joints and columns. This larger residual drift demand might have the potential for more damage to the frame under a subsequent ground motion (aftershock). Moreover, a remarkable finding is the reduction in the column shear force for frame models with joint

shear or bond modeling when compared to those without joint modeling. It may be attributed to the concentration of inelastic action in joints.

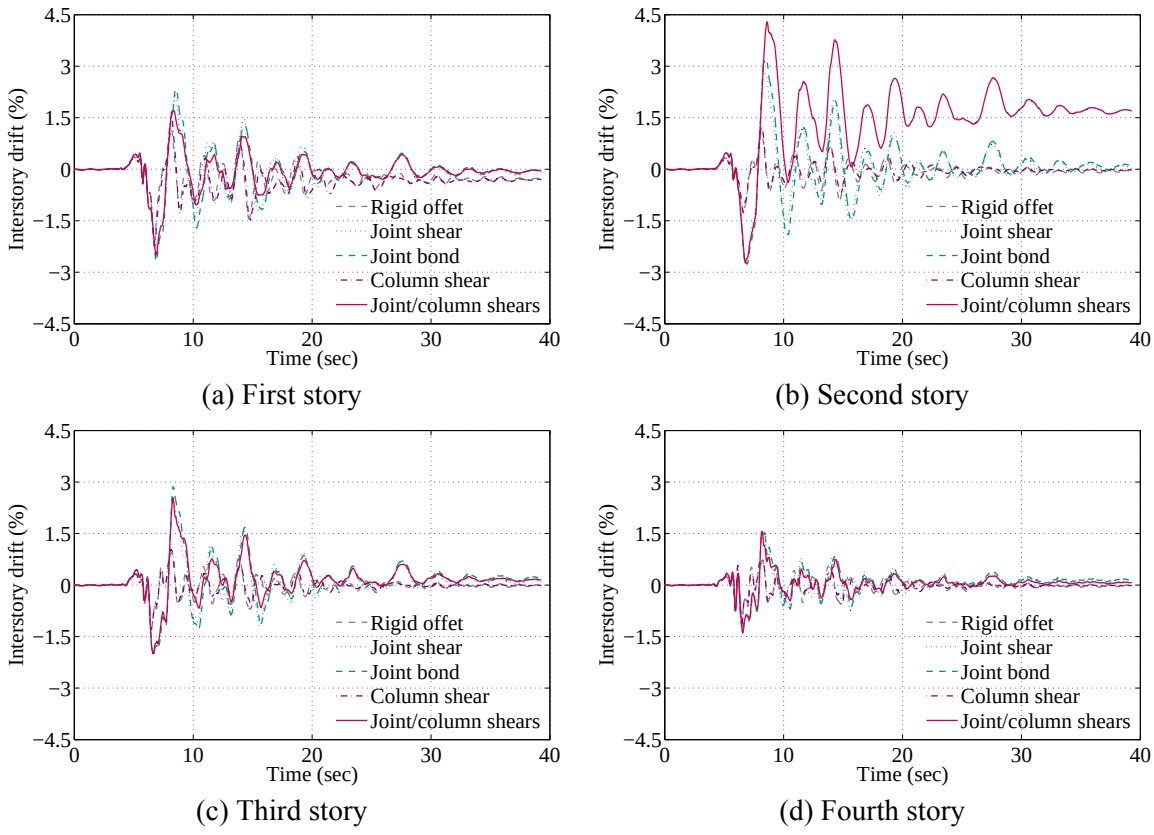

Figure 4.15 Comparison of interstory drift time histories for OMF-4S frame

Table 4.14 Maximum seismic response parameters for OMF-4S frame

Frame model	Story	Interstory drift (%)		Maximum story shear (kN)	
		Maximum	Residual	Exterior	Interior
OMF-4S-RO (rigid offset)	1st	**2.14**	0.30	445	375
	2nd	1.26	0.07	284	481
	3rd	1.29	0.02	274	330
	4th	1.18	0.02	274	241
OMF-4S-JS (joint shear)	1st	2.56	0.10	310	329
	2nd	**2.90**	0.01	199	321
	3rd	2.60	0.08	190	252
	4th	1.44	0.07	219	211
OMF-4S-JB (joint bond)	1st	2.68	0.07	299	325
	2nd	**3.18**	0.08	198	337
	3rd	2.87	0.19	192	255
	4th	1.53	0.15	219	206
OMF-4S-CS (column shear)	1st	**2.24**	0.30	417	371
	2nd	1.27	0.02	283	475
	3rd	1.30	0.01	275	328
	4th	1.18	0.02	240	238
OMF-4S-JCS (joint and column Shear)	1st	2.50	0.05	300	327
	2nd	**4.29**	**1.70**	199	300
	3rd	2.54	0.15	200	251
	4th	1.57	0.07	214	207

To examine the inelastic response of columns, the second column shear force-total drift relationships in the first story for four different analytical frame models are depicted in Figure 4.16: with joint rigid offset (RO), joint shear (JS), joint bond (JB), and column shear (CS). The OMF-4S-JCS model is not exhibited in this figure because more severe damage is observed in the second story. In Figure 4.16(b) and Figure 4.16(c), the shear force-drift hysteresis for the analytical frame models including joint shear or bond (OMF-4S-JS and OMF-4S-JB) are almost identical, but OMF-4S-JB model has larger drift demand. These frame models have more energy dissipation capacity than OMF-4S-RO model in Figure 4.16(a) and a 12% reduction of maximum shear force as a result of redistribution of internal forces adjacent to the joints when compared to those without

joint modeling. In Figure 4.16(d), the initial and degraded column stiffness is observed after shear failure. Prior to shear failure, the overall response follows the flexural hysteretic behavior of the fiber beam-column element since the response is almost identical to OMF-4S-RO model. After detecting shear failure, the shear deformations dominate the overall response of the column and the pinched hysteretic response of the shear spring model leads to the additional stiffness and strength degradation, as presented in Figure 4.17. This figure shows the overall, shear, and flexure hysteretic responses in the first story columns for the analytical frame model including the column shear model (OMF-4S-CS). It can be shown that the fourth column experiences only flexural behavior while others suffer shear failure. While the estimated flexure and overall drifts are similar for the interior and exterior columns, the observed shear drifts for the interior columns are greater than those for the exterior column; maximum shear drifts for the interior and exterior column are 0.7% and 1.04%, respectively. The larger shear drifts might cause a greater loss of shear strength for the interior columns since the shear response significantly affects the overall response after the initiation of shear failure.

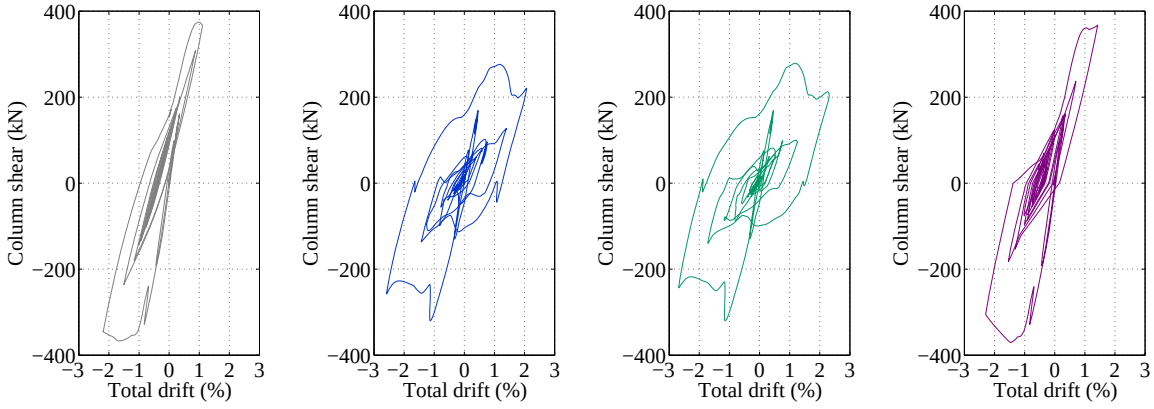

(a) OMF-4S-RO (b) OMF-4S-JS (c) OMF-4S-JB (d) OMF-4S-CS

Figure 4.16 Column shear force-story drift hysteresis in the first story for OMF-4S frame

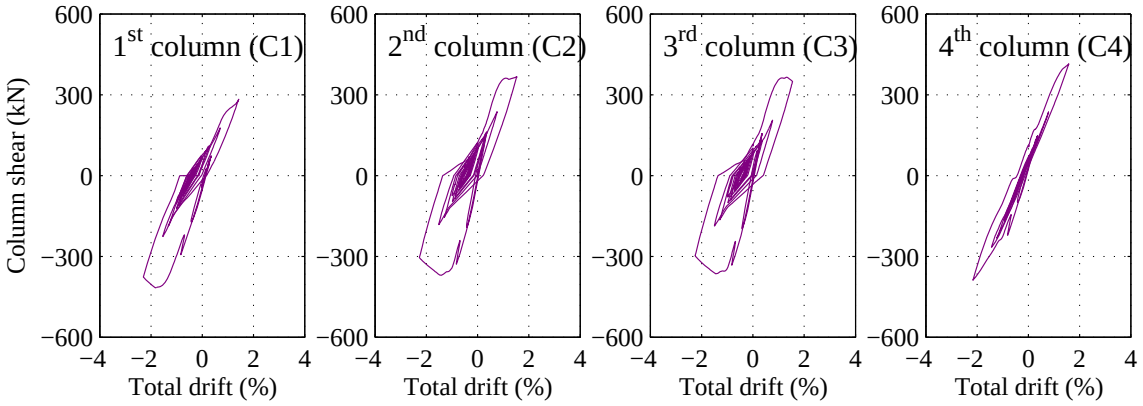

(a) Total response

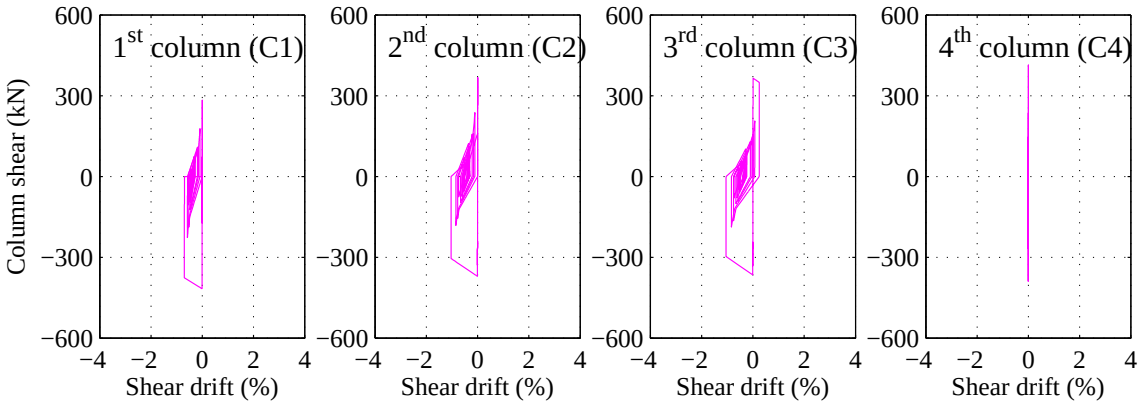

(b) Shear response

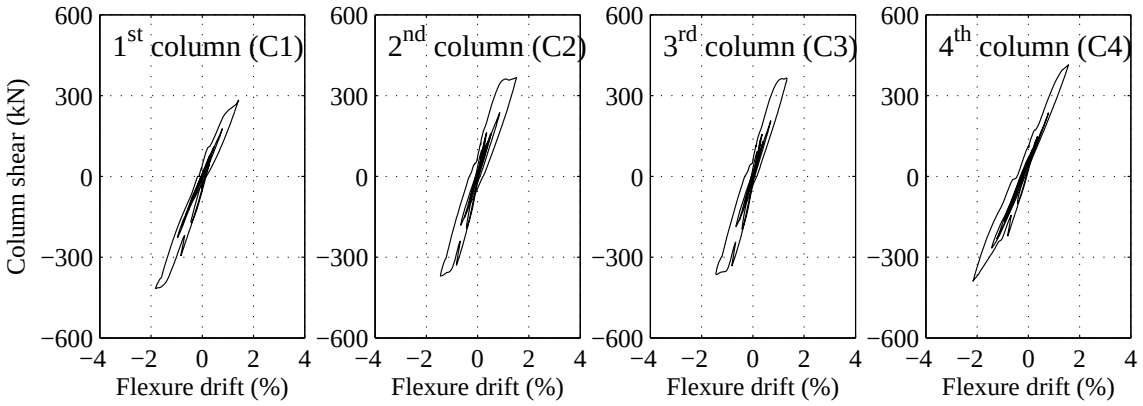

(c) Flexure response

Figure 4.17 Overall, shear, and flexure responses in the first story for OMF-4S-CS model

Comparison of the joint moment-rotation response for the analytical model frames with joint modeling is undertaken to investigate the effect of joint behavior on the failure model of the frame. Figure 4.18 depicts the joint rotational moment-rotation hysteresis for exterior and interior beam-column joints in the second floor with different analytical frame models: OMF-4S-JS, OMF-4S-JB, and OMF-4S-JCS models. The hysteresis for the interior joint in OMF-4S-JS model in Figure 4.18(a) is almost identical to that in OMF-4S-JB model in Figure 4.18(b), but its maximum rotation demand decreases by approximately 7%. Both interior joints have reached their maximum joint shear strength and have experienced the degrading behavior. However, it can be indicated from Figure 4.18(c) that the interior joint for OMF-4S-JCS model has less rotation demand when compared to that for OMF-4S-JS model and does not attain the maximum joint shear strength. This observation can be explained that the rotation demand dose not reach the rotation corresponding to its joint shear capacity due to the degrading shear behavior in the interior column. On the other hand, the exterior joint for OMF-4S-JS model in Figure 4.18(d) is almost the same hysteresis as that for OMF-4S-JCS model in Figure 4.18(f). Unlike these two models, the exterior joint hysteresis for OMF-4S-JB model exhibits inelastic joint behavior in the first quadrant as a result of the reduced joint shear strength due to the short embedment length of 152 mm. Furthermore, all the three models have similar maximum rotation demand in the third quadrant.

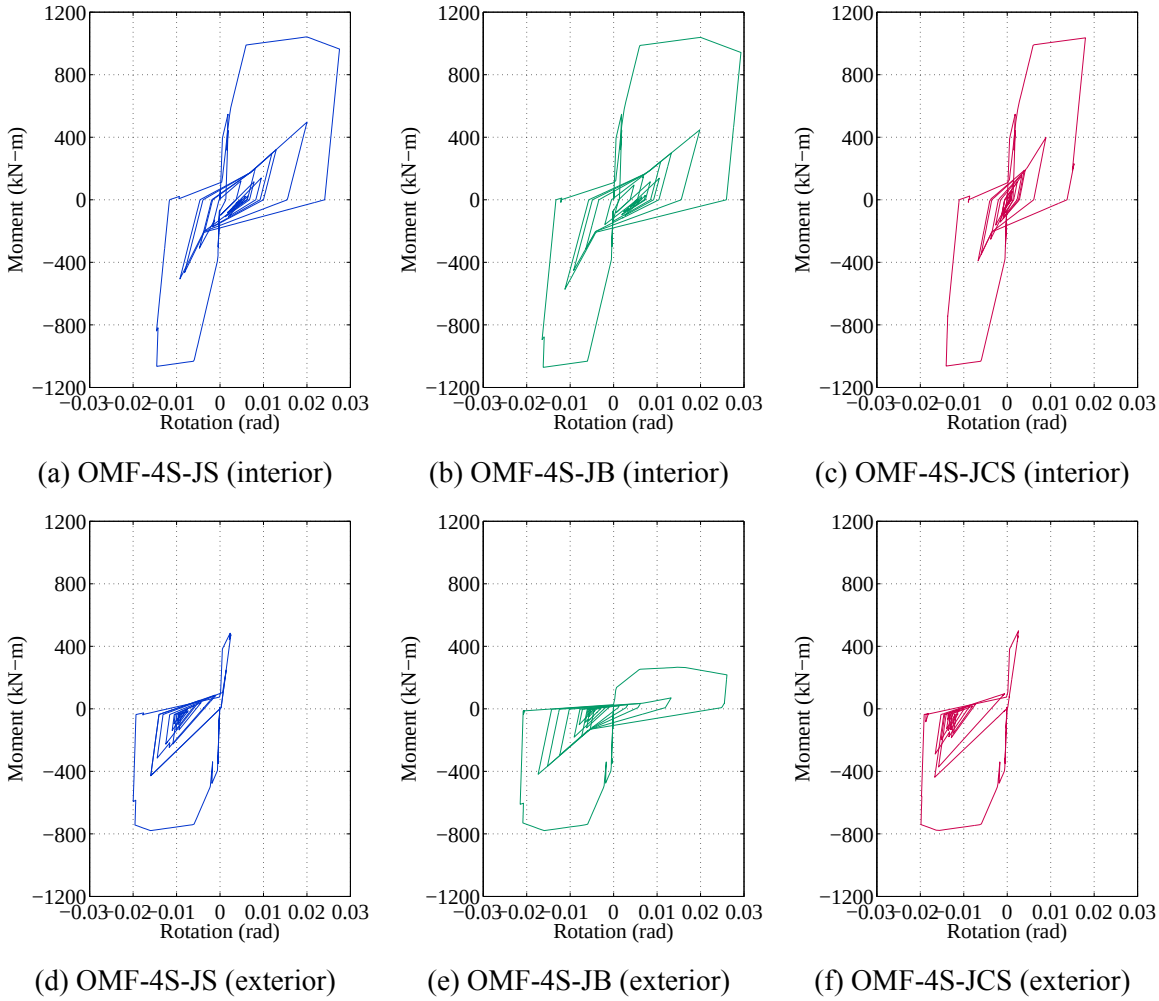

(a) OMF-4S-JS (interior) (b) OMF-4S-JB (interior) (c) OMF-4S-JCS (interior)

(d) OMF-4S-JS (exterior) (e) OMF-4S-JB (exterior) (f) OMF-4S-JCS (exterior)

Figure 4.18 Joint rotational moment-rotation relationship in the second floor for OMF-4S frame

4.3.2.2 Ductile 8-story perimeter frame (SMF-8P)

Figure 4.19 presents the comparison of interstory drift time histories with and without joint shear modeling for the SMF-8P frame. The response period is slightly elongated due to joint shear, and the increase in drift associated with the effect of joint shear is obvious. In particular, differences in the drift response with and without shear become significant after 7 sec at which time the maximum responses are experienced in all columns. Additionally, lower story columns experience a considerable residual drift after the

maximum responses as a result of the effect of joint shear. It indicates that columns are subjected to higher drift demands due to joint shear (approximately 25% higher in the second story), hence more damage would be expected to occur. Table 4.15 indicates the maximum response parameters in terms of interstory drifts and column shear forces for the analytical frame models without and with joint shear. It can be indicated that the maximum interstory drift occurs in the second story level for both analytical frame models. As is the case of the OMF-4S frame, it can be found from the table that there is a reduction in the column shear force for the analytical frame model with joint shear when compared to that without joint shear. It may be attributed to the spread of inelastic action into joints.

Table 4.15 Maximum seismic response parameters for SMF-8P frame

Frame model	Story	Interstory drift (%)		Maximum story shear (kN)	
		Maximum	Residual	Exterior	Interior
SMF-8P-RO (rigid offset)	1st	3.16	0.08	873	1109
	2nd	**3.48**	0.03	529	1167
	3rd	2.66	0.10	517	790
	4th	1.47	0.11	375	672
	5th	0.67	0.05	319	567
	6th	0.45	0.01	397	539
	7th	0.36	0.01	297	494
	8th	0.20	0.00	174	313
SMF-8P-JS (joint shear)	1st	4.99	1.85	699	974
	2nd	**5.28**	**2.05**	564	873
	3rd	3.59	1.51	413	781
	4th	1.91	0.70	340	693
	5th	0.91	0.22	379	560
	6th	0.72	0.08	316	461
	7th	0.45	0.04	259	335
	8th	0.25	0.03	171	278

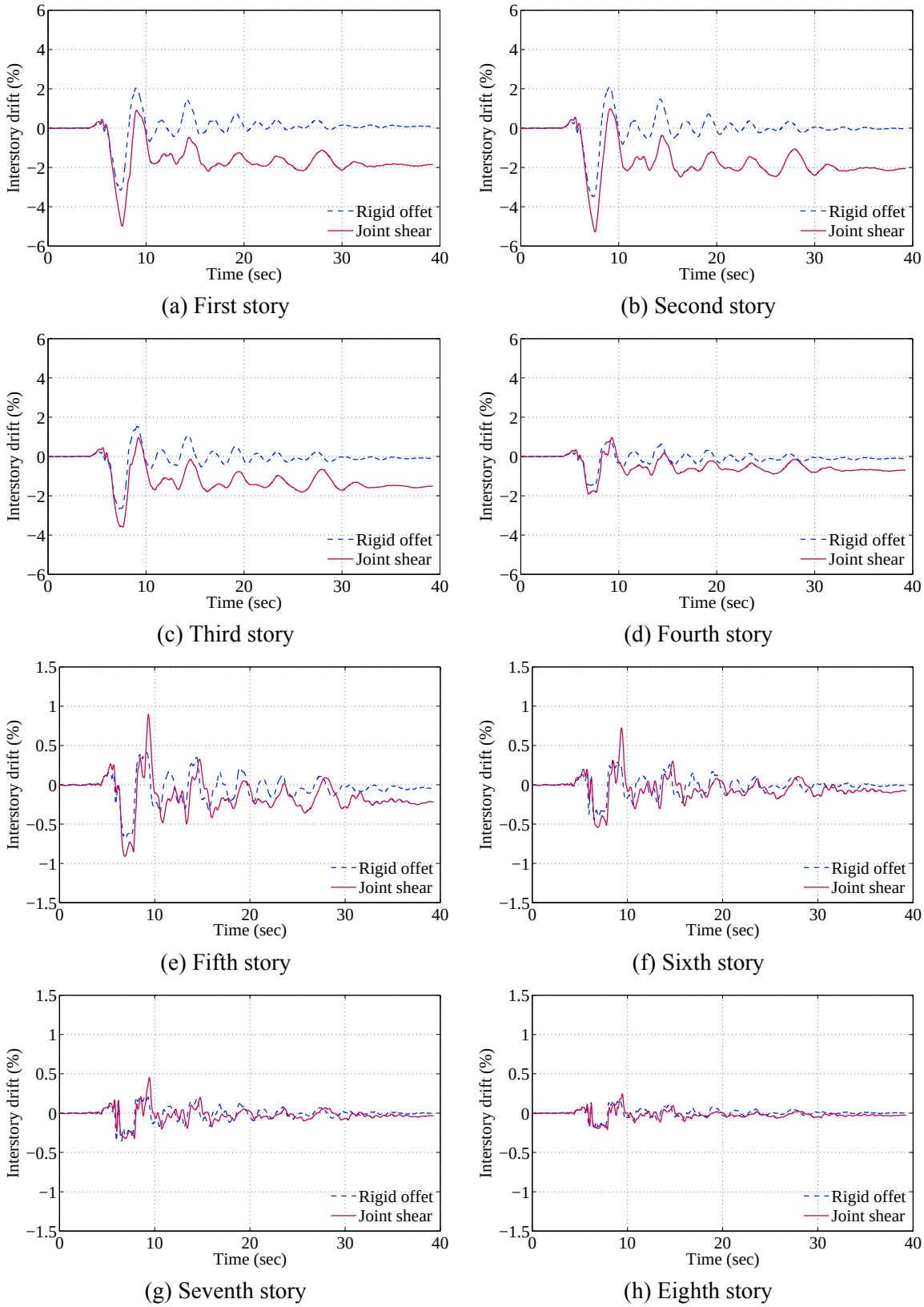

Figure 4.19 Comparison of interstory drift time histories for SMF-8P frame

To investigate the influence of joint shear on columns, the column shear-drift responses in the second story for the analytical frame models with and without joint shear are depicted in Figure 4.20. The drift demand dramatically increases (52% higher) and the maximum column shear force decreases (14% lower) as a result of the effect of joint shear. Additionally, joint shear results in the considerable permanent deformation and pinched hysteresis that might significantly affect the seismic response of the frame subjected to a repeated ground motion. Figure 4.21 shows the rotational moment-rotation relationship for interior and exterior joints in the frame model. It can be indicated that the interior and exterior joints experience the maximum joint strength and pronounced pinched hysteresis.

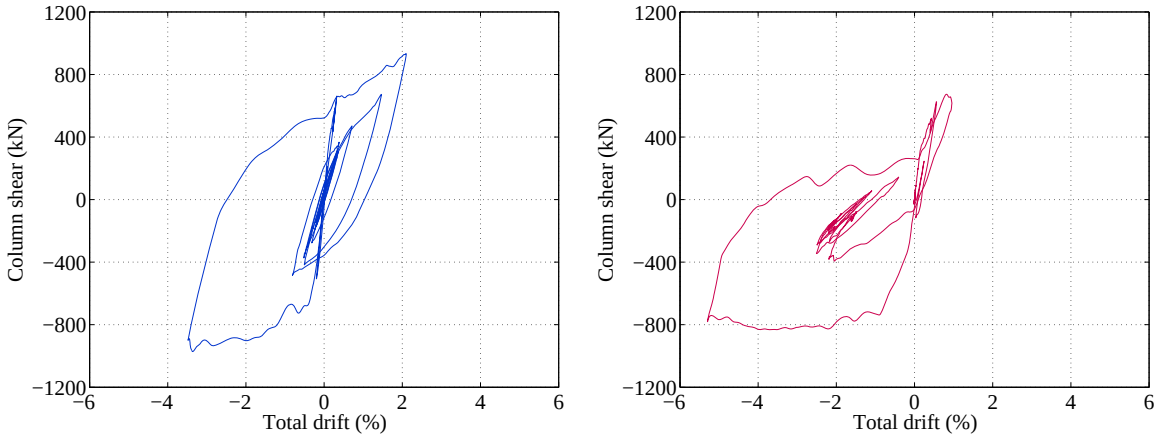

(a) SMF-8P-RO (b) SMF-8P-JS

Figure 4.20 Column shear force-story drift hysteresis in the second story for SMF-8P frame

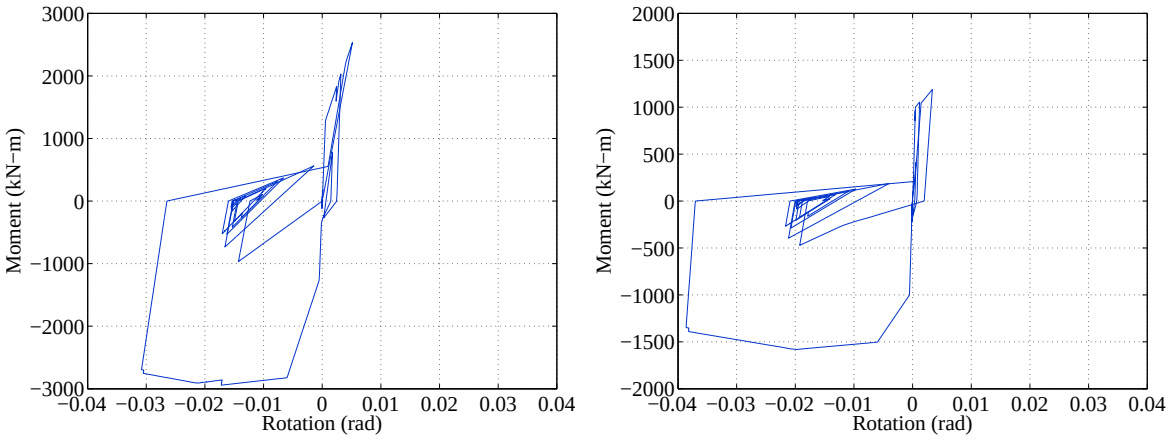

(a) Interior joint (b) Exterior joint

Figure 4.21 Joint rotational moment-rotation relationship in the second floor for SMF-8P-JS model

4.4 Summary

This chapter presents the selection of non-ductile and ductile RC frames designed by Liel (2008) and Haselton (2006) in accordance with the design code provisions, respectively. Those frames are typical of office buildings and industrial facilities in California and two different lateral load resisting systems: space frames and perimeter frames. This research selects the most typical RC frames amongst those designed by the authors. In order to investigate the collapse mechanism of these frames with different analytical modeling techniques, this research regards joint shear, joint bond, and column shear failure as modeling variables. The analytical frame models are created in OpenSees (McKenna et al. 2010) with incorporation of the analytical modeling approach presented in Chapter 3. The perimeter frame system is modeled by adding the leaning columns to account for P-Δ effect. For the shear model developed by Elwood (2004), the behavior of older columns should ensure their flexure yielding since they have taller height. Additionally, the joint model developed by Anderson et al. (2008) presented in the model validation has the

limitation that this model is developed based on experimental joint shear strength. Thus, the joint shear strength model for non-ductile and ductile beam-column joints is proposed in order to ensure the applicability of this joint model to analytical frame models. Each joint strength model is obtained though the statistical method based on collected experimental results available in the literature. Finally, the seismic performance for these analytical frame models is evaluated through the pushover analysis and nonlinear time history analysis. The analytical models with joint shear increase the drift demand and reduce the maximum shear force and initial stiffness as a result of the spread of inelastic action into joints. The analytical frame model with joint shear and column shear is the most vulnerable in that it has a sudden drop of lateral load resistance in pushover analysis and the largest maximum and residual deformation in both analyses.

CHAPTER 5

FRAMEWORK FOR DEVELOPMENT OF AFTERSHOCK FRAGILITY CURVES

This chapter outlines the framework which is selected in the development of analytical aftershock fragility curves for RC frames in order to account for the damage accumulation and increased vulnerability for those frames. The framework adopted here is composed of independent modules linked by pinch point variables such as intensity measures (IM) and engineering demand parameters (EDPs). Most existing aftershock fragility curves are developed using a stipe approach (incremental dynamic analysis (IDA)) for aftershock analyses while this research generate the aftershock fragility curves employing a cloud approach (nonlinear time history analysis (NTHA)) for aftershock analyses in order to account for realistic aftershock ground motions that can representative of the specific region. Figure 5.1 illustrates a schematic of the framework and its essential components such as the suite of mainshock and aftershock ground motions, probabilistic analytical frame models, characterization of initial damage states associated with mainshock ground motions, mainshock-aftershock analyses, probabilistic aftershock demand models (PADMs), capacity limit states, and aftershock fragility formulation.

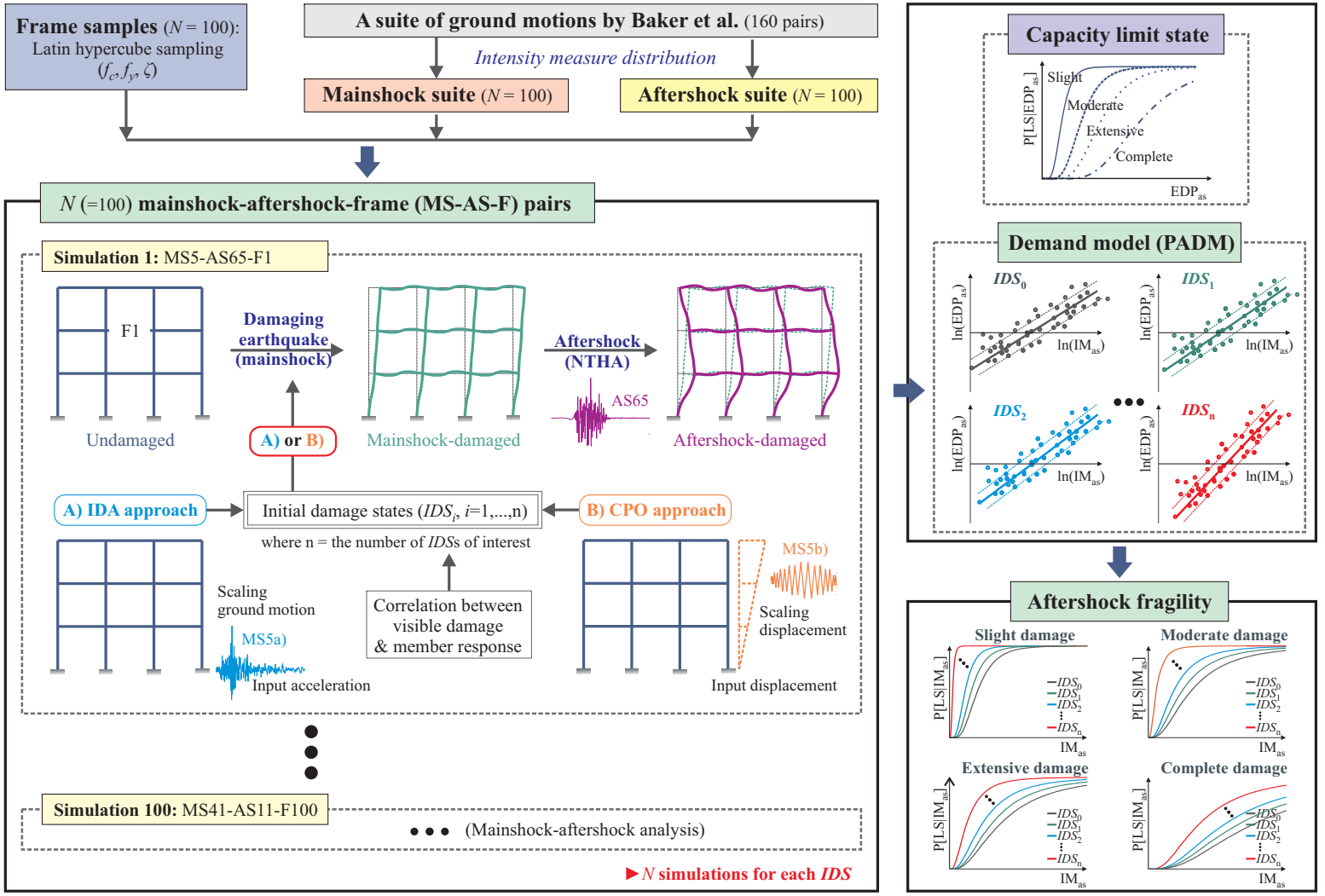

Figure 5.1 Graphical representation of aftershock fragility framework

5.1 Aftershock Fragility Formulation

5.1.1 Classical fragility function

As mentioned in Chapter 2, (typical) seismic fragility is explicitly expressed as a conditional probability that gives the likelihood that a structure will reach or exceed a specified level of damage for a given ground intensity measure (IM). To derive the fragility function, a probabilistic seismic demand model (PSDM) that relates the seismic median demand to the IM is employed using NTHA. The relationship between the demand and IM can be expressed in the power form (Cornell et al. 2002, Ellingwood et al. 2007), as given in equation (5.1):

$$S_D = a \cdot IM^b \tag{5.1}$$

where S_D is the median value of the demand as a function of an IM, parameters a and b can be computed by a linear regression analysis of $\ln(S_D)$ on $\ln(IM)$ obtained from simulations. The dispersion ($\beta_{D|IM}$) accounting for the uncertainty in the relation is estimated based on equation (5.2):

$$\beta_{D|IM} = \sqrt{\frac{\sum \left[\ln(d_i) - \ln(a \cdot IM^b)\right]^2}{N-2}} \tag{5.2}$$

where N is the number of simulations. Finally, the PSDM, probability that the D exceeds d conditioned on the IM can be computed as in equation (5.3):

$$P[D \geq d \mid IM] = 1 - \Phi\left[\frac{\ln(d) - \ln(S_D)}{\beta_{D|IM}}\right] \tag{5.3}$$

Similarly, the probability that the structural capacity (C) is less than d can be written as in equation (5.4):

$$P[C < d \mid IM] = \Phi\left[\frac{\ln(d) - \ln(S_C)}{\beta_C}\right] \tag{5.4}$$

where S_C and β_C are the median value and dispersion of the structural capacity associated with the limit state. With the formulation of the seismic demand and structural capacity, the fragility function can be represented as in equation (5.5):

$$P[D > C \mid IM] = \Phi\left[\frac{\ln(S_D / S_C)}{\sqrt{\beta_{D|IM}^2 + \beta_C^2}}\right] \tag{5.5}$$

5.1.2 Aftershock fragility function

Unlike classical fragility, aftershock fragility is a conditional probability that determines the likelihood that a damaged structure will meet or exceed a specified level of damage, given an aftershock intensity measure (IM_{as}) and an initial damage state (IDS) associated with the mainshock in order to reflect the increased vulnerability of structures. This aftershock fragility function can be estimated by developing a probability distribution for the aftershock demand conditioned on the IM_{as}. Modifying the power function of a classical demand model proposed by Cornell et al. (2002), an aftershock demand model can be computed as in equation (5.6):

$$S_{D,as} = a \cdot IM_{as}^{\ b} \tag{5.6}$$

where $S_{D,as}$ is the median value of the aftershock demand model as a function of the IM_{as}, and a and b are constants estimated using a regression analysis for the aftershock demand model in the log-transformed space (so-called *PADM*). The dispersion ($\beta_{D|IMas}$) is estimated using equation (5.7):

$$\beta_{D|IMas} = \sqrt{\frac{\sum\left[\ln(d_i) - \ln(a \cdot IM_{as}{}^{b})\right]^2}{N-2}} \tag{5.7}$$

With the addition of the initial damage state as a result of mainshocks, the aftershock fragility curves can be obtained as in equation (5.8):

$$P[D > C \mid IM_{as}, IDS] = \Phi\left[\frac{\ln(S_{D,as} / S_C)}{\sqrt{\beta_{D|IMas}^2 + \beta_C^2}}\right] \tag{5.8}$$

The following is a brief summary of the basic procedure for computing the aftershock fragility curves, as shown Figure 5.1:

1. Generate N statistical samples of a subject frame. These samples can be generated by sampling on significant modeling parameters. Thus, N nominally identical but statistically significant frame samples are generated through Latin hypercube sampling (LHS) (McKay et al. 1979).
2. Assemble a suite of N ground motions that can be applicable to the area of interest.
3. Generate N mainshock damaging earthquakes that can simulate the mainshock-damaged conditions of structures corresponding to predefined IDSs. Two approaches to describe the damaging earthquakes are suggested in this research;

(1) NTHA within IDA and (2) cyclic pushover analysis approach (CPO). This research focuses mainly on the former.

4. Randomly assemble *N* frame-mainshock-aftershock pairs, and then perform back-to-back nonlinear time history analyses for each frame-mainshock-aftershock pair. Alternatively, the mainshock analysis can be replaced by CPO. Key seismic responses are monitored along with the IM_{as}. In this research, maximum interstory drift is chosen as the seismic demand in the development of fragility curves.
5. Generate a PADM, a linear regression of the aftershock demand-intensity measure pairs in the log-transformed space.
6. Develop an aftershock fragility curves with various initial damage states using equation (5.8).

5.2 Stochastic Analytical Frame Models

Uncertainty in the demand placed on RC frames can be categorized into two groups, specifically aleatoric and epistemic. Alreatoric uncertainty is related to inherent randomness in the occurrence of seismic events and is essentially irreducible. The limited historical data leads to statistical error in the estimates of the aleatoric uncertainty. In contrast, epistemic uncertainty associated with a lack of knowledge and assumptions in modeling techniques can generally be reduced with additional information and more comprehensive analysis (Ellingwood and Wen 2005). The uncertainty related to the recorded ground motions in the suite is conventionally referred to as aleatory in nature associated with the inherent randomness in the seismological mechanisms. Uncertainty in structural and material properties is account for in this research.

Uncertainties in modeling parameters such as concrete compressive strength (f_c), steel yield strength (f_y), structural damping (ξ) are included in this research. These parameters that can affect the member or system capacity are inherently random, and the randomness can be modeled by random variable based on experimental results (Wen et al. 2004). The concrete compressive strength and steel yield strength are assumed to be described by normal and lognormal probability distributions, respectively (Healy et al. 1980, MacGregor et al. 1983, Bartlett and MacGregor 1996). Additionally, the properties of construction material such as concrete and steel evolve over time. The mean value (μ) of concrete strength is defined following the work of Liel (2008) and Haselton (2006): 27.6 MPa for non-ductile frames and 34.5~48.3 MPa for ductile frames. The coefficient of variation (COV) for the concrete compressive strength is assumed following the work of Healy et al. (1980). The COV is determined in accordance with concrete strength and concrete quality dependent on placement and field curing. The mean value of the steel yield strength is the expected value of 462 MPa for both non-ductile and ductile frames (Liel 2008, Haselton 2006), and its COV is also assumed to be 0.08 following the work of Healy et al. (1980). Furthermore, the impact of damping is very important in dynamic analysis. The damping ratio is assumed to be described by a lognormal probability distribution (Healy et al. 1980, Celik and Ellingwood 2010). The mean value and COV of damping ratio are considered those used in the RC frames designed by Liel (2008) and Haselton (2006). Table 5.1 summarizes the probability distributions for each of the above parameters.

To capture the uncertainty in the modeling parameters listed in Table 5.1, statistically significant yet nominally identical frame models are developed by sampling

across the range of these parameters using Latin hypercube sampling (LHS) technique (Mckay et al. 1979). The LHS provides a more efficient sampling scheme to cover the probability space of the random variables when compared to pure random sampling using naïve Monte Carlo simulation (Celik and Ellingwood 2010). Each independent analytical frame model is then randomly paired with one (for classical fragilities) or two (for aftershock fragilities) of ground motions identified in the next section.

Table 5.1 Structural modeling uncertainties

Random variables	Mean	COV	Distribution	References	Frame
Concrete Strength (f_c)	27.6 MPa	0.176	Normal	Healy et al. (1980)	Non-ductile
	34.5 MPa	0.151			Ductile
	41.4 MPa	0.136			Ductile
	48.3 MPa	0.126			Ductile
Steel yield Strength (f_y)	462 MPa	0.080	Lognormal	Healy et al. (1980)	Both
Damping ratio (ξ)	0.065	0.600	Lognormal	Haselton (2007)	Ductile
	0.050	0.600		Liel (2008)	Non-ductile

5.3 A Suite of Ground Motions

Assembling a suite of ground motions that can appropriately represent the seismic hazard is crucial to developing fragility curves applicable to RC frames spread over a wide geographic area. The suite of ground motions must contain a wide range of IMs expected in the area interest based on seismic hazard analysis. For this purpose, this research selects a suite of ground motions developed by Baker et al. (2011) that can be utilized to analyze a variety of structures potentially located in active seismic regions such as California. The suite includes 120 pairs of broad-band ground motions with the distribution of response spectra associated with moderately large earthquakes at small distances and 40 pairs of ground motions with strong velocity pulses expected at sites

experiencing near-fault directivity. The suite of ground motions consists of four sets: Set 1A (broad-band, magnitude (M_w) = 7, distance to rupture (R_{rup}) = 10 km, soil site), Set 1B (broad-band, M_w = 6, R_{rup} = 25 km, soil site), Set 2 (broad-band, M_w = 7, R_{rup} =10 km, rock site), and Set 3 (pulse-like, near-fault). Each set is composed of 40 pairs of ground motions. Figure 5.2 illustrates the response spectra in logarithmic scale for each set in the ground motions developed by Baker et al. (2011). A detailed description of the suite can be found in the reference.

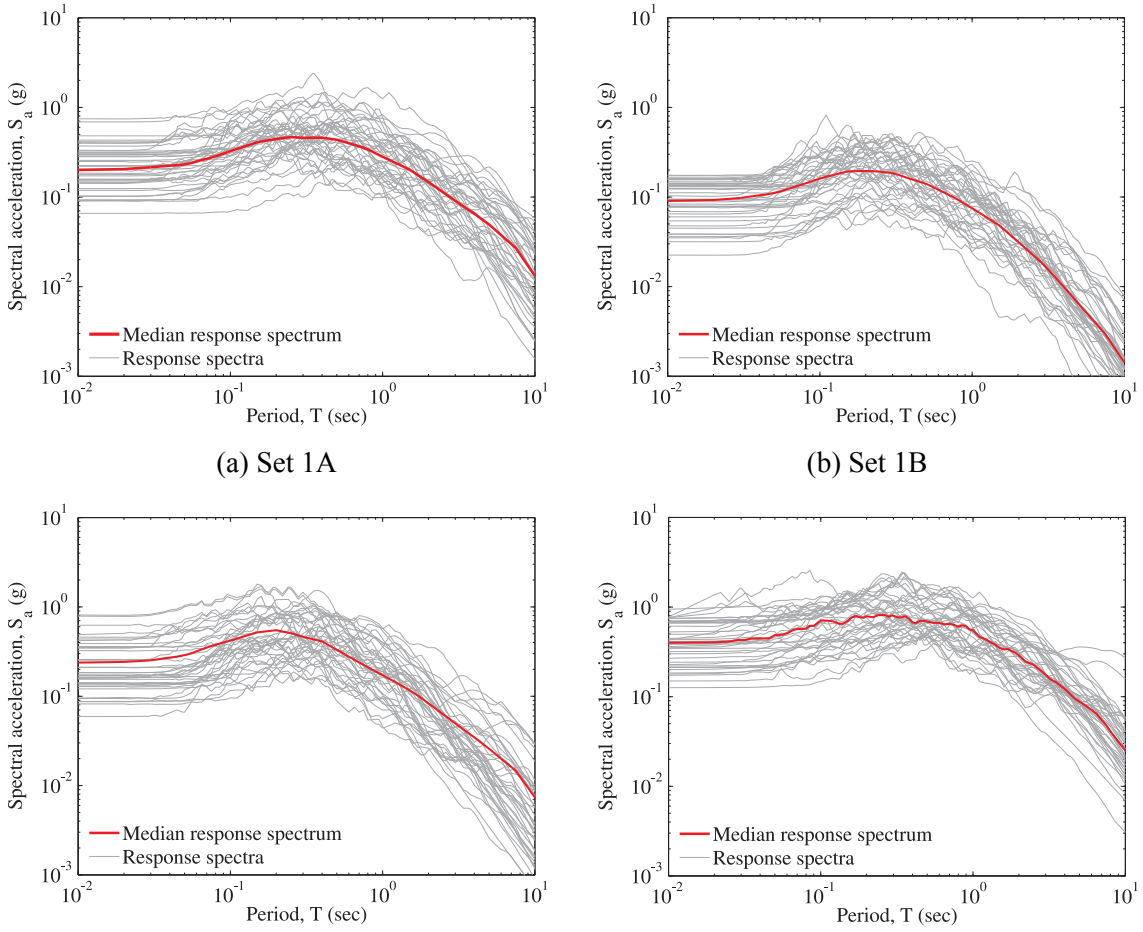

(a) Set 1A (b) Set 1B

(c) Set 2 (d) Set 3

Figure 5.2 Response spectra for each set in the Baker suite

In this research, 100 ground motions that can represent the original ground motion suite are re-assembled in order to reduce the time-consumption of the runs. For this purpose, an optimal IM is defined in the classical PSDM analyses with an assumption that an optimal IM for the PADM follows that for the classical PSDM. If an inappropriate IM is selected from the classical PSDM, the resulting PADM might be worse because mainshock-damaged structures have a variety of residual deformation that can significantly influence maximum response in aftershock analyses. Mainshock ground motions are extracted using the probability distribution of the defined IM, and then a suite of aftershock ground motions is obtained using the IM.

5.3.1 Optimal intensity measure in classical PSDM

The choice of an optimal IM to correlate with structural damage is very important. The optimal IM can provide the accuracy of the demand model in estimating seismic demand as well as the reasonable estimate of vulnerability of structures in case of the dependence of the uncertainty associated with the demand model on an IM. Shafieezadeh et al. (2012) probed into the properties of an optimal IM: efficiency, practicality, proficiency, and sufficiency. Efficiency is commonly used to establish the superiority of an IM. An efficient IM not only reduces the amount of variability in the demand parameter for a given IM, but also keeps it constant over the entire range of the selected IM. An efficient IM is commonly referred to a lower value of the dispersion ($\beta_{D|IM}$). Sufficiency is the property where an IM is independent of earthquake characteristics such as magnitude (M_w) and distance (R). It can be quantified by the *p*-value which is a measure of the probability that the points in a scatter-plot of residuals against a variable lie on a straight

line. By definition, *p*-value is the probability of rejecting the null hypothesis which is the independence of IM from M_w or R. If the *p*-value obtained from a linear regression of the residuals ($\varepsilon_{d|IM}$) from the PSDM against M_w or R is greater than the significance level (here, 5%), Mw or R is not statistically significant, and thus an IM is sufficient. Additionally, practicality is a measure of the dependence of the demand on the IM and its good indicator is the slope (*b*). A higher value of *b* indicates that the IM is more practical. Finally, proficiency is a composite measure of efficiency and practicality. It is obtained by substituting equation (5.1) into equation (5.3) and then by rearranging terms in the formulation as below:

$$P[D \geq d \mid IM] = \Phi\left[\frac{\ln(IM) - \frac{\ln(d) - \ln a}{b}}{\zeta}\right] \tag{5.9}$$

where

$$\zeta = \frac{\beta_{D|IM}}{b} \tag{5.10}$$

where ζ is the modified dispersion and a measure of proficiency. A lower value of ζ indicates a more proficient IM. Additionally, the coefficient of determination (R^2) not only proves the power law assumption of the PSDM, but also strengthens the characteristic of efficiency and proficiency. Therefore, an optimal IM would be determined by smaller values of $\beta_{D|IM}$ and ζ, larger values of *b* and R^2 and larger *p*-value than the significance level. A detailed description of these properties can be found in Shafieezadeh et al. (2012).

These properties will be utilized to determine the most optimal IM for the RC frames selected in this research. This research focuses on determining an optimal IM among structure-independent IMs in order to employ the identical suite of mainshock and aftershock ground motions to all types of building structures with the design variables such as non-ductile and ductile frames, space and perimeter frames, frame heights. For this purpose, 160 ground motion (randomly selected from two horizontal components)-frame pairs are analyzed for OMF-4S-JS model and then classical PSDM are constructed in terms of structure-independent IMs and maximum interstory drift (θ_{max}). The candidate IMs are peak ground acceleration (PGA), peak ground velocity (PGV), peak ground deformation (PGD), Arias intensity (I_a), cumulative absolute velocity (CAV), and spectral acceleration at period 1.0 sec ($S_{a\text{-}1s}$). Table 5.2 presents the comparison of the characteristic properties for the six IMs. In terms of efficiency and proficiency, PGV is the most optimal IM. CAV is the most practical IM followed by $S_{a\text{-}1s}$ and PGV. Therefore, it can be concluded that PGV is the most optimal IM in terms of the above properties. Figure 5.3 presents a sample PSDM for maximum interstory drift using PGA and PGV as the IM. Moreover, sufficiency is achieved by investigating the *p*-values for the candidate IMs with respect to M_w and R. Based on the significance level (0.05), PGV and $S_{a\text{-}1s}$ is all sufficient. $S_{a\text{-}1s}$ is the most sufficient with respect to M_w while PGV is the most sufficient with respect to R. Figure 5.4 shows the linear regression on the residuals for θ_{max} with respect to M_w and R. The plots clearly display that the best fit lines are almost horizontal thereby demonstrating the sufficiency. Therefore, PGV will be a means to provide the suite of mainshock and aftershock ground motions as well as to develop the aftershock fragility curves for the RC frames.

Table 5.2 Comparison of characteristic property measures for various IMs

IM	Efficiency, Practicality, Proficiency				Sufficiency (p-value)	
	$\beta_{D\|IM}$	b	ζ	R^2	M_w	R (km)
PGA (g)	0.637	0.989	0.655	0.615	0.000	0.438
PGV (m/s)	**0.316**	0.991	**0.319**	**0.906**	0.103	**0.844**
PGD (m)	0.511	0.686	0.745	0.753	0.000	0.000
I_a (m/s)	0.503	0.637	0.799	0.761	0.470	0.019
CAV (m/s)	0.598	**1.205**	0.497	0.662	0.000	0.000
$S_{a\text{-}1s}$ (g)	**0.397**	0.993	0.400	0.050	**0.543**	0.147

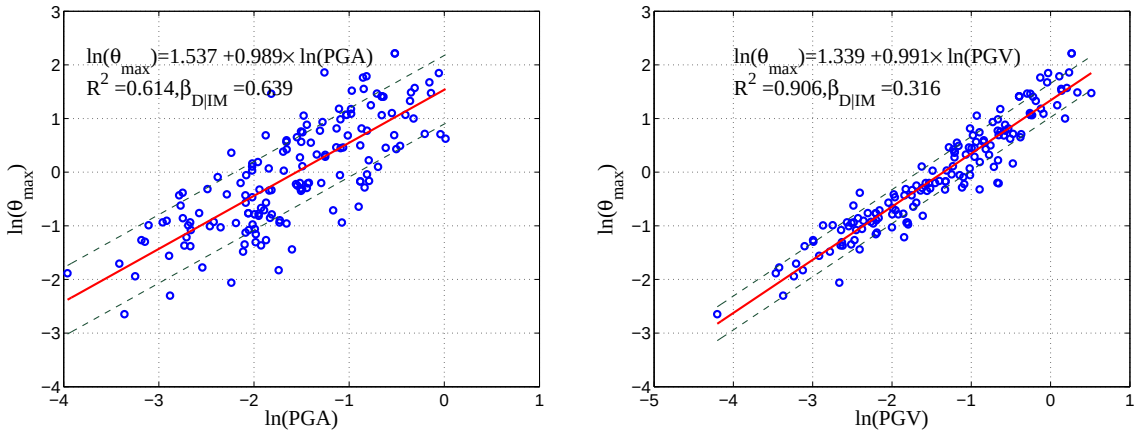

(a) PGA (b) PGV

Figure 5.3 Classical PSDMs for IMs: PGA and PGV

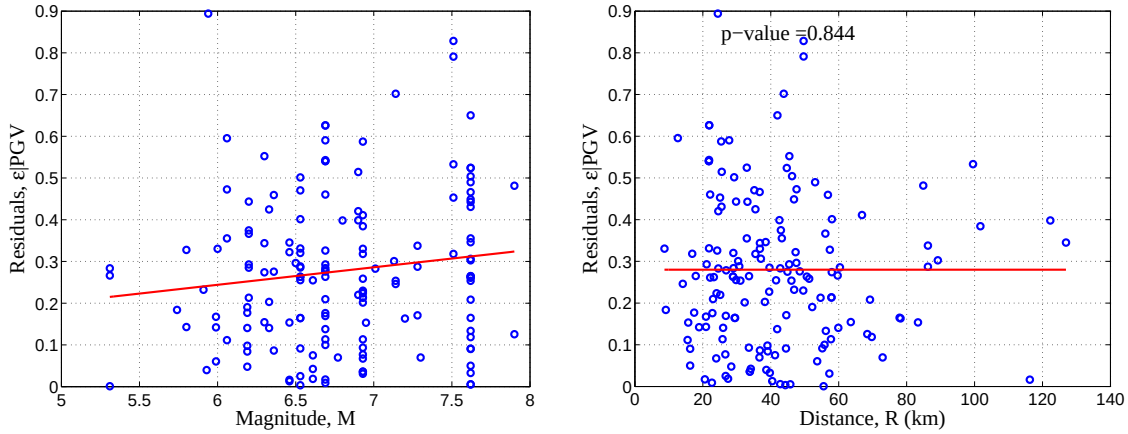

(a) Magnitude (M_w) (b) Distance (R)

Figure 5.4 Sufficiency of PGV with respect to magnitude and distance

5.3.2 Selection of mainshock and aftershock ground motion suite

PGV enables an appropriate suite of mainshock and aftershock ground motions. This assembled suite can reduce the time-consumption of the runs, but represent the original ground motion suite. For the suite of mainshock ground motions, 25 ground motions for each set will be re-assembled in this research. To obtain the suite of 100 mainshock ground motions used for simulating the finite element frame models, the distribution of PGV for each set is assumed to be lognormal, as presented in Figure 5.5, and the LHS technique is also exploited to extract the random samples of PGVs. Finally, ground motions with PGV values chosen are close to those sampled from the distribution. In these figures, λ_{PGV} and ζ_{PGV} are the parameters of the lognormal distribution, which means that these parameters are, respectively, the mean and standard deviation of ln(PGV). These selected ground motions are gradually scaled until a member experiences the IDSs corresponding to maximum interstory drifts.

The choice of aftershock ground motions are considered in company with PADMs and aftershock fragility curves. Therefore, selecting the suite of aftershock ground motions will be discussed in detail in Section 5.6 after explaining how to develop the PADMs and aftershock fragility curves.

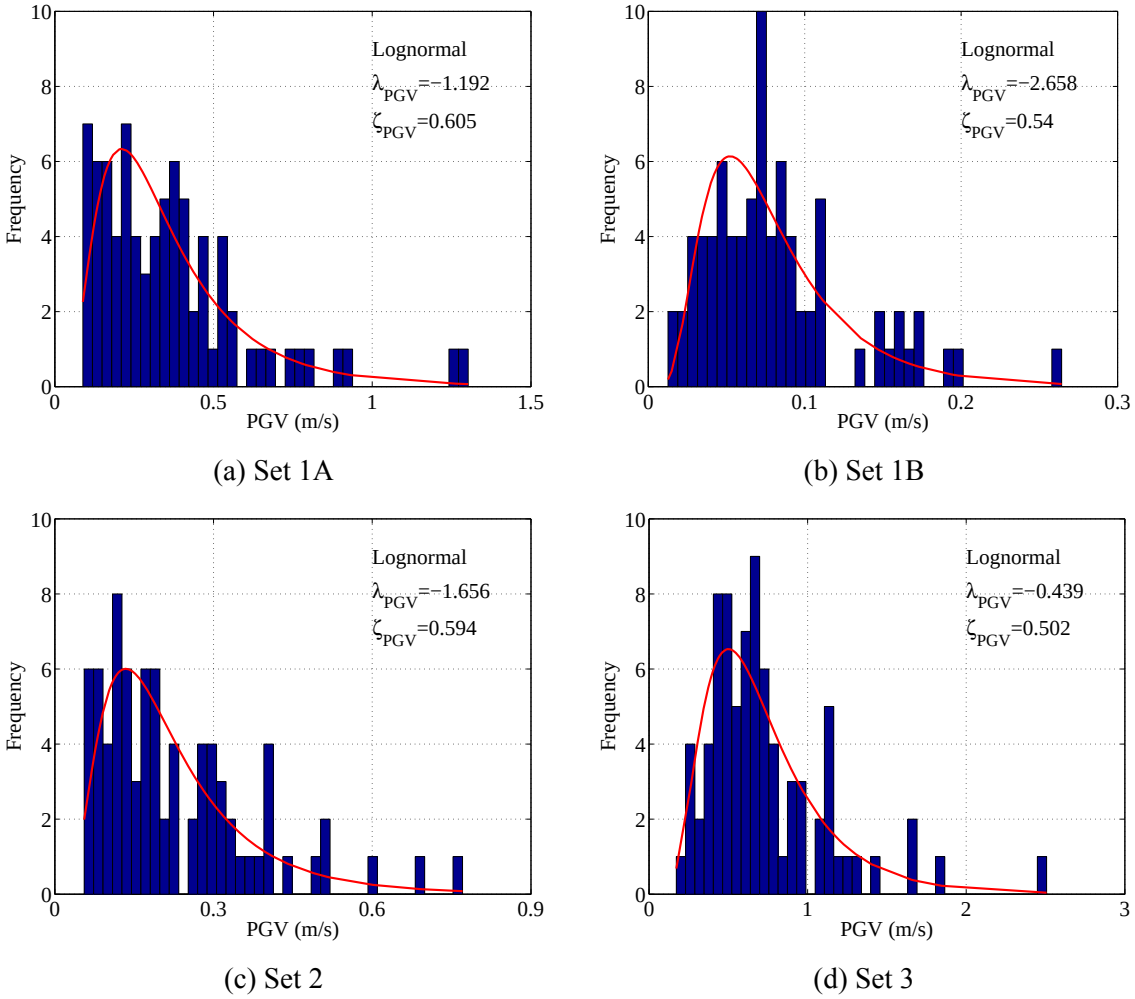

Figure 5.5 Probability density function (PDF) of PGV

5.4 Mainshock-Aftershock Analysis

5.4.1 Characterization of initial damage states

As defined in the formulation of aftershock fragility function, evaluating the aftershock risk assessment of structures necessitates the investigation of the extent of damage caused by mainshocks. This assessment can be achieved by establishing the relationship between observed damage patterns and response mechanisms for RC frame members. To identify the characteristics of the damage patterns associated with the specific response mechanisms and how these damage patterns evolve due to earthquakes, Bearman (2012)

investigated a database of RC column tests (Sezen 2002, Bae 2005) and test images (Eberhard et al. 2010, Sedra et al. 2010, PEER 2011). FEMA 306 (1998) asserted that information about the performance characteristics of a building frame can be derived from the estimation of drift demand that mainshocks (damaging earthquakes) placed on it. The effort is consistent with the report of FEMA 306 (1998), and thus, from this observation, the author established the relationship between the maximum drift and visible damage for flexure- and shear-dominated RC columns. Additionally, the author accounted for the effect of axial load on columns to identify the associated drift capacity with each stage of the damage progression. In each stage, a value of drift capacity for a column under low axial load was specified as well as that under high axial load. The critical axial load factor (ALF = P_c/f_cA_g) was identified as 0.5 such that any ALF equal to or above this value was regarded as high (HAL), and any value below this value was referred to as a low axial load (LAL).

Figure 5.6(a) and Figure 5.6(b) illustrate the damage progression of flexure-dominated columns under low and high axial load, respectively, tested by Bae (2005). In the testing, several photos were obtained and associated with certain points on the lateral load-drift hysteresis of each specimen. This information helps to postulate the correlation between visible damage and the existing state of the column. As shown in figures, the column under low axial load is less drift capacity than that under low axial load. Based on this information, Bearman (2012) proposed the typical damage progression with respect to visually perceived damage and associated maximum drift capacity, as indicated in Table 5.3. In addition to flexure-dominated columns, the damage progression of shear-dominated columns under low and high axial load tested by Sezen (2002) are depicted in

Figure 5.7(a) and Figure 5.7(b), respectively. In the same manner as flexure-dominated columns, Bearman (2012) also suggested the typical damage progression in terms of visible damage description and associated maximum drift capacity, as shown in Table 5.4.

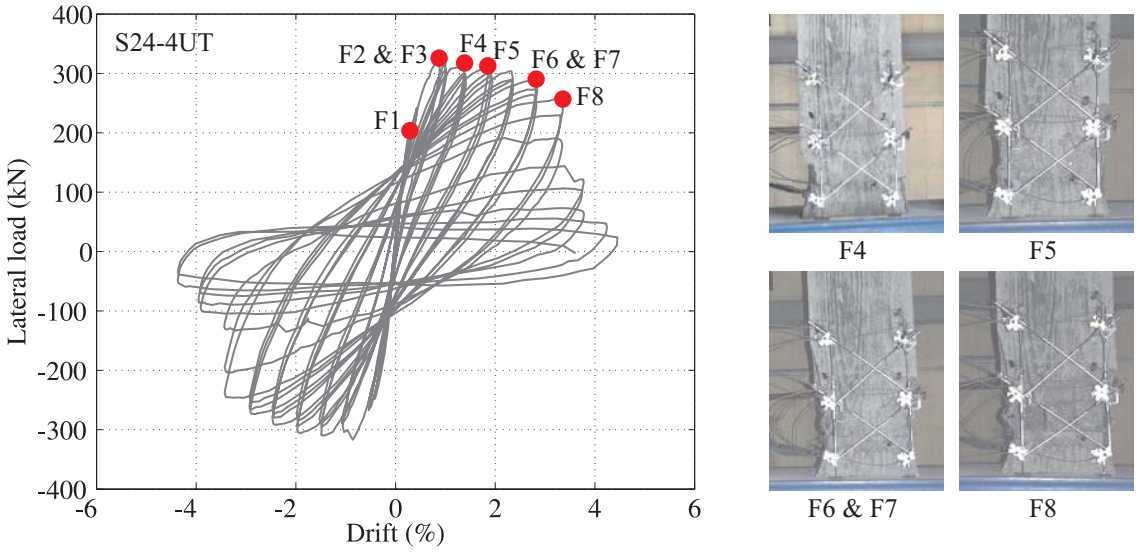

F4: Initial concrete spalling, F5: Concrete spalling exposing longitudinal steel,
F6 & F7: Longitudinal bar buckling and crushing of core concrete, F8: Longitudinal bar fracture

(a) Under low axial load (ALF = 0.20)

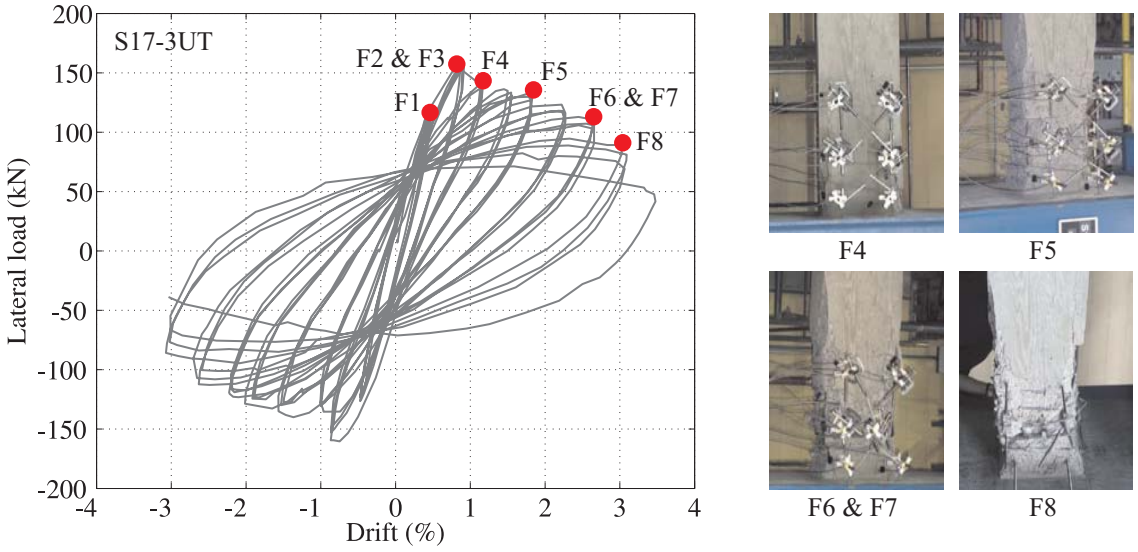

F4: Concrete spalling on flexural and side faces, F5: Concrete spalling exposing longitudinal steel,
F6 & F7: Longitudinal bar buckling and crushing of core concrete, F8: Longitudinal bar fracture

(b) Under high axial load (ALF = 0.50)

Figure 5.6 Damage progression of flexure-dominated columns (Bae 2005)

Table 5.3 Summary of damage progression for flexure-dominated columns (Bearman 2012)

Damage state	Damage description	Drift (%)	
		LAL	HAL
F1: Flexural cracking	• Top and bottom 1/3 of column • Perpendicular to column axis • Span width of column • Uniformly spaced • Initially hairline cracks (≤ 0.1 mm) • Prior to spalling ≈ 2.5 mm (HAL) and 5.0 mm (LAL) at maximum displacement	0.30	0.50
F2: Longitudinal cracking	• Top and bottom 1/3 of column • Parallel to column axis • Prior to spalling ≈ 4 mm	1.00	0.75
F3: Shear cracking	• Top and bottom 1/3 of column • At 35 to 65° angle from the horizontal • Initially hairline cracks (≤ 0.1 mm) • Prior to spalling ≈ 5 mm (HAL) and 10 mm (LAL) at maximum displacement	1.00	0.75
F4: Initial concrete spalling	• Initially occur at top and bottom ¼ of ends • Complete spalling ≈ b_c from ends	1.50	0.75
F5: Concrete spalling and exposing longitudinal rebar	• Initially exposed at $b_c/2$ from ends • Exposed length ≈ b_c	2.00	1.00
F6: Longitudinal rebar buckling	• Initially occur at ≈ $b_c/2$ from ends • Total buckling length ≈ $b_c/2$	4.50	3.00
F7: Crushing of core concrete	• Same location as bar buckling	4.50	3.00
F8: Longitudinal rebar fracture	• Same location as bar buckling	6.00	3.50
F9: Loss of lateral load-carrying capacity		4.00	2.00
F10: Loss of axial load-carrying capacity		6.00	4.50

§ b_c = column width, LAL = low axial load, and HAL = high axial load

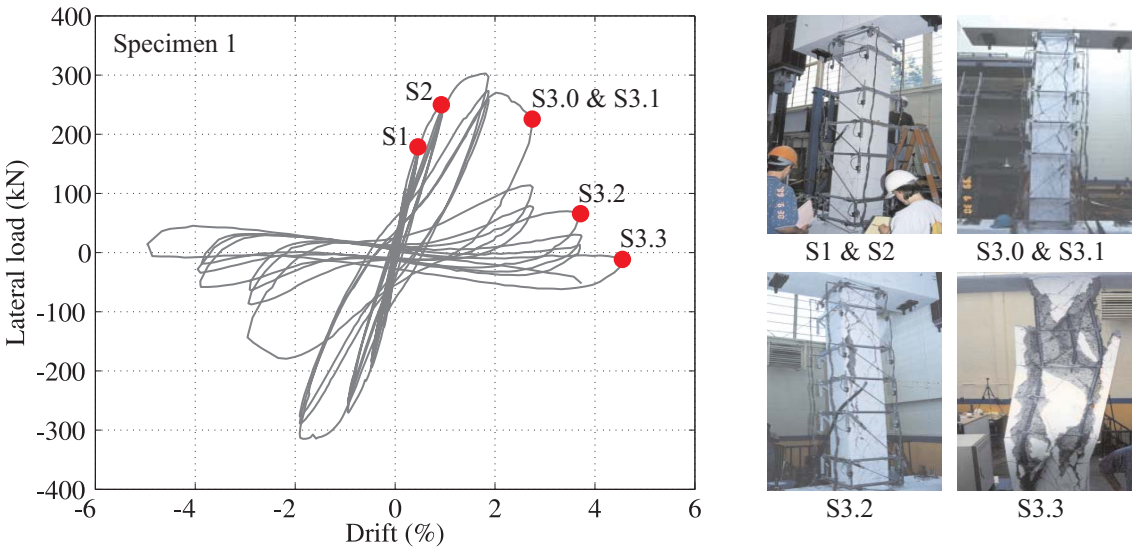

S1 & S2: Flexural and shear craking, S3.0 & S3.1: Widening and localization of shear cracking, S3.2: Concrete spalling on side faces, S3.3: Longitudinal bar buckling

(a) Under low axial load (ALF = 0.15)

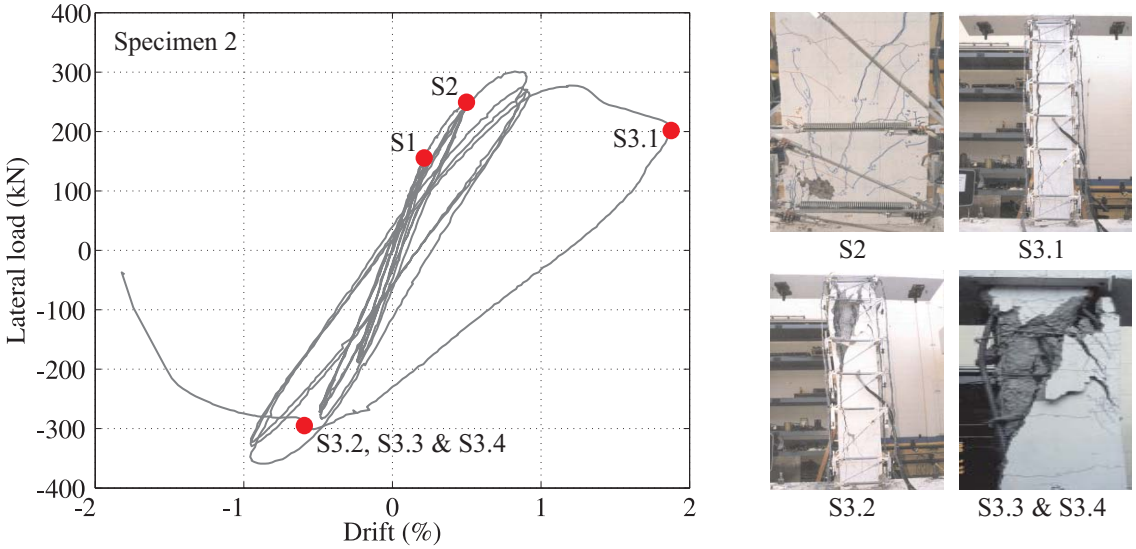

S2: Shear craking, S3.1: Widening and localization of longitudinal cracking on side face, S3.2: Concrete spalling on side face, S3.3 & S3.4: Longitudinal bar buckling and core crushing after loss of load carrying capacity

(b) Under high axial load (ALF = 0.60)

Figure 5.7 Damage progression of shear-dominated columns (Sezen 2002)

Table 5.4 Summary of damage progression for shear-dominated columns (Bearman 2012)

Damage state	Damage description	Drift (%)	
		LAL	HAL
S1: Flexural and longitudinal cracking	• Same as flexure-dominated columns (HAL) for F1 and F2 except as noted • Flexural cracks prior to S3 ≈ 1.3 mm • Longitudinal cracks prior to S3 ≈ 2.5 mm	0.25	0.25
S2: Shear cracking	• Same as flexure-dominated columns (HAL) for F3 except as noted • May occur at any height	0.50	0.50
S3.0: Widening and localization of shear cracks	• May occur at any height • At 35 to 65° angle from the horizontal • Prior to spalling ≈ 7.6 mm (HAL) and 12.7 mm (LAL) at residual condition	2.00	1.75
S3.1: Longitudinal cracking on side faces	• May run the entire height of column • Meet localized shear cracks near edge • Prior to spalling ≈ 2.5 mm at residual condition	2.50	1.75
S3.2: Concrete spalling on side faces	• Possible spall shape: triangle where shear and longitudinal cracks meet, parallelogram encompassing primary shear crack • Edges of spall are at 35 to 65° angle from the horizontal • May occur at any height	2.50	1.75
S3.3: Longitudinal rebar buckling	• May occur at any height	2.50	1.75
S3.4: Crushing of core concrete	• Typically occur with bar buckling • May occur at any height	2.50	1.75
S3.5: Loss of lateral load-carrying capacity		2.50	1.75
S3.6: Loss of axial load-carrying capacity		4.50	1.75

§ LAL = low axial load and HAL = high axial load

Using the maximum drifts associated with the onset of damage states presented in Table 5.3 and Table 5.4, initial damage states (IDSs) as a result of mainshocks are defined, as presented in Table 5.5 through 5.8 for shear- and flexure-dominated columns under low and axial load. As indicated in tables, the number of damage states is reduced

and the description of initial damage states is rearranged in accordance with the associated maximum drifts. For the definition of the finial initial damage state, visible damage states is linked with unobservable damage states such as loss of lateral and axial load-carrying capacity (F9 and F10 for flexure-dominated columns and S3.5 and S3.6 for shear-dominated columns). For example, in the case of flexure-dominated columns, IDS_5 (under low axial load) or IDS_4 (under high axial load) are established as one damage state for F6, F7, and F9 because the experimental data demonstrate that the loss of lateral load-carrying capacity (F9) is associated with longitudinal rebar buckling (F6) and core crushing (F7). Additionally, IDS_6 (under low axial load) or IDS_5 (under high axial load) are combined as a damage state for F8 and F10 because the experimental data indicate that the loss of axial load-carrying capacity (F10) is attributed to longitudinal rebar fracture (F8). Moreover, for shear-dominated columns, an unobservable initial damage state indicating longitudinal rebar yielding is added because of the large difference of maximum drift between previous (0.5%) and following damage state (2.0% for low axial load case or 1.75% for high axial load case). The experimental data indicate that longitudinal rebar yielding was generally observed at a drift of 1.0%.

The initial damage states for flexure- and shear-dominated columns are incorporated to simulate the mainshock-damaged condition of ductile and non-ductile RC frames, respectively. This condition is accomplished by generating damaging earthquakes (i.e., the effect of mainshock) by which a member experiences an initial damage state predefined). Furthermore, the axial load factor for the analytical frames selected in this research remains below 0.5, and therefore, this research adopts the initial damage states for flexure- and shear-dominated columns under low axial load (Table 5.5 and Table 5.7)

to characterize the mainshock-damaged condition of the frames. Additionally, IDS_6, which is regarded as the structural collapse, is not account for because this research focuses on structures that survived after mainshock events.

Table 5.5 Initial damage states for flexure-dominated columns under low axial load (ALF < 0.5)

IDS	Damage state	Maximum drift (%)
IDS_1	Flexural cracking (F1)	0.30
IDS_2	Longitudinal and shear cracking (F2, F3)	1.00
IDS_3	Initial concrete spalling (F4)	1.50
IDS_4	Concrete spalling and exposing longitudinal rebar (F5)	2.00
IDS_5	Longitudinal rebar buckling, crushing of core concrete, loss of lateral load-carrying capacity (F6, F7, F9)	4.50
IDS_6	Longitudinal rebar fracture, and axial load-carrying capacity (F8, F10)	6.00

Table 5.6 Initial damage states for flexure-dominated columns under high axial load (ALF ≥ 0.5)

IDS	Damage state	Maximum drift (%)
IDS_1	Flexural cracking (F1)	0.50
IDS_2	Longitudinal and shear cracking, initial concrete spalling (F2, F3, F4)	0.75
IDS_3	Concrete spalling and exposing longitudinal rebar (F5)	1.00
IDS_4	Longitudinal rebar buckling, crushing of core concrete, loss of lateral load-carrying capacity (F6, F7, F9)	3.00
IDS_5	Longitudinal rebar fracture, loss of axial load-carrying capacity (F8, F10)	3.50

Table 5.7 Initial damage states for shear-dominated columns under low axial load (ALF < 0.5)

IDS	Damage state	Maximum drift (%)
IDS_1	Flexural and longitudinal cracking (S1)	0.25
IDS_2	Shear cracking (S2)	0.50
IDS_3	Relatively widened shear cracking (reinforcement yielding)	1.00
IDS_4	Widening and localization of shear cracks (S3.0)	2.00
IDS_5	Longitudinal cracking on side faces, concrete spalling on side faces, crushing of core concrete, and loss of lateral load-carrying capacity (S3.1, S3.2, S3.3, S3.4, S3.5)	2.50
IDS_6	Loss of axial load-carrying capacity (S3.6)	4.50

Table 5.8 Initial damage states for shear-dominated columns under high axial load (ALF ≥ 0.5)

IDS	Damage state	Maximum drift (%)
IDS_1	Flexural and longitudinal cracking (S1)	0.25
IDS_2	Shear cracking (S2)	0.50
IDS_3	Relatively widened shear cracking (reinforcement yielding)	1.00
IDS_4	Widening and localization of shear cracks, longitudinal cracking on side faces, concrete spalling on side faces, crushing of core concrete, and loss of lateral and axial load-carrying capacity (S3.0, S3.1, S3.2, S3.3, S3.4, S3.5, S3.6)	1.75

5.4.2 Simulating damaging earthquakes

In order to quantify the influence of damaging earthquakes on the response of RC frames, two approaches may be taken; the first simulates the damage caused by the damaging earthquake (modeling a mainshock-damaged structure), and the second generated the damaging earthquakes (simulating a damaging ground motion). FEMA 307 (1998) adopted the first approach by modifying the force-deformation relationship of a SDOF oscillator. However, this approach cannot capture the localized damage of element levels associated with the limitation of SDOF models. Therefore, this research proposes approaches that can generate the effect of mainshocks (damaging earthquakes) on the global and local responses of RC frames, as a part of the above second approach. Two approaches are suggested employing the definition of initial damage states mentioned in the previous section in this research; (1) IDA approach and (2) CPO (hypothetical mainshocks) approach in Figure 5.8 and Figure 5.9, respectively. Both approaches enable the simulation of the damaging earthquakes to cause the specified initial damage states. The estimation of these damage states can be quantitatively obtained by monitoring the interstory drift of the frames. As presented in the figures, the main difference between two the former is whether ground motions or imposed deformations is scaled to obtain

the damaging earthquakes. The first approach is capable of capturing the dynamic characteristics, thereby resulting in a range of residual deformations, by adopting real ground motions as mainshocks. However, the IDA approach requires many efforts to obtain damaging earthquakes so that a RC frame attains the initial damage state. On the other hand, the second approach can be easily applied and much less computationally intensive by applying hypothetical ground motions rather than real ground motions for the mainshock analysis. The CPO approach requires the assumptions of a pushover load pattern and constant residual deformation. The pushover lateral load pattern is followed by ASCE 7-05 (2005), and the input drift history is adopted as the general wave form used in the experimental tests. The roof drift gradually increases up to a maximum interstory drift level and then deceases to the assumed residual drift that is defined as the drift at zero base shear. The residual deformation can be assumed to the mean or median value of residual deformations obtained from the approach or a value calculated from the equation of Bearman (2012) who proposed the relationship between maximum and residual drift for columns.

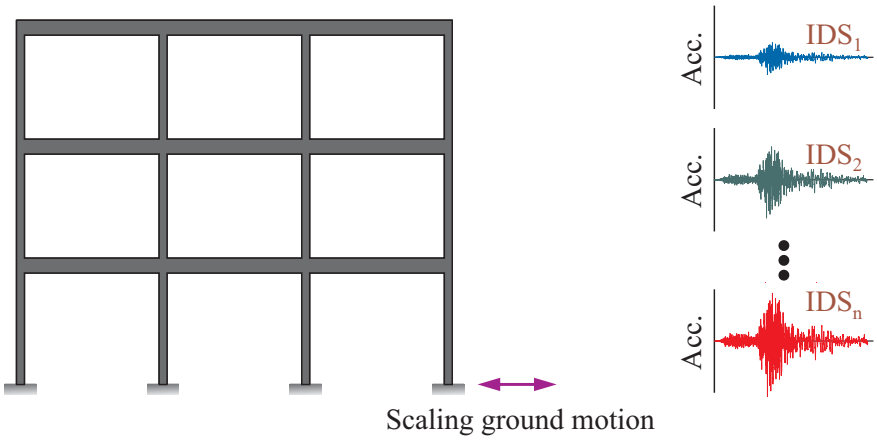

Figure 5.8 Damaging earthquakes (IDA)

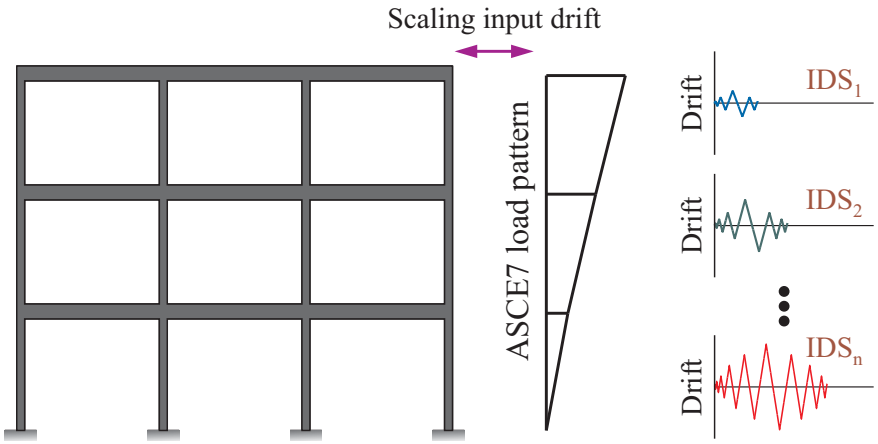

Figure 5.9 Damaging earthquakes (CPO)

5.4.3 Mainshock-aftershock analysis

Ground motions or input drifts obtained from IDA or CPO approach play a role in a suite of mainshocks with different initial damage states for mainshock-aftershock analyses. While mainshock analysis is performed by one of the two approaches, aftershock analysis is accomplished by conducting nonlinear time history analysis (NTHA). Each mainshock ground motion or input drift (hypothetical mainshock) is randomly paired with an aftershock ground motion in addition to a stochastic analytical frame model. For each mainshock-aftershock-frame, back-to-back nonlinear time history analysis is performed to monitor key seismic responses (here, interstory drifts) and aftershock intensity measures (here, PGV). Figure 5.10 illustrates a mainshock-aftershock sequence (IDA) for each initial damage state (IDS). In general, a mainshock can be classified as an earthquake with the highest magnitude or intensity while foreshocks and aftershocks are quakes that occur before and after a larger one in the same location. As shown in the figure, a seismic event that is followed by a larger earthquake in the same area can be classified as a foreshock-mainshock sequence. When the first earthquake is larger than

the subsequent events, it can be classified as a mainshock-aftershock sequence. However, in this research, first and second earthquakes are referred to as mainshock and aftershock ground motions, regardless of their relative magnitudes or intensities. For each back-to-back dynamic analysis, a frame will be subjected to an identical aftershock ground motion following different mainshocks to investigate how the extent of damage associated with mainshocks affects the seismic response of the frame under a future aftershock ground motion. Moreover, to stabilize the response after mainshock analysis, extra ground acceleration whose magnitudes are zero over the time period of 10 sec is added between mainshock and aftershock ground motions. Furthermore, both positive and negative factors of aftershock ground motions (or their progress direction) are applied to mainshock-damaged frames because aftershock maximum responses depend on the polarity of aftershock ground motions (Ryu et al. 2011), as shown in Figure 5.11. The figure indicates that the maximum drift for negative factor in aftershock analysis is approximately 1.4 times as high as that for positive factor. If this polarity is not accounted for in aftershock analysis, more severely damaged frames might have less seismic demand than less damaged ones. Therefore, this factor should be taken into account when performing aftershock fragility assessment.

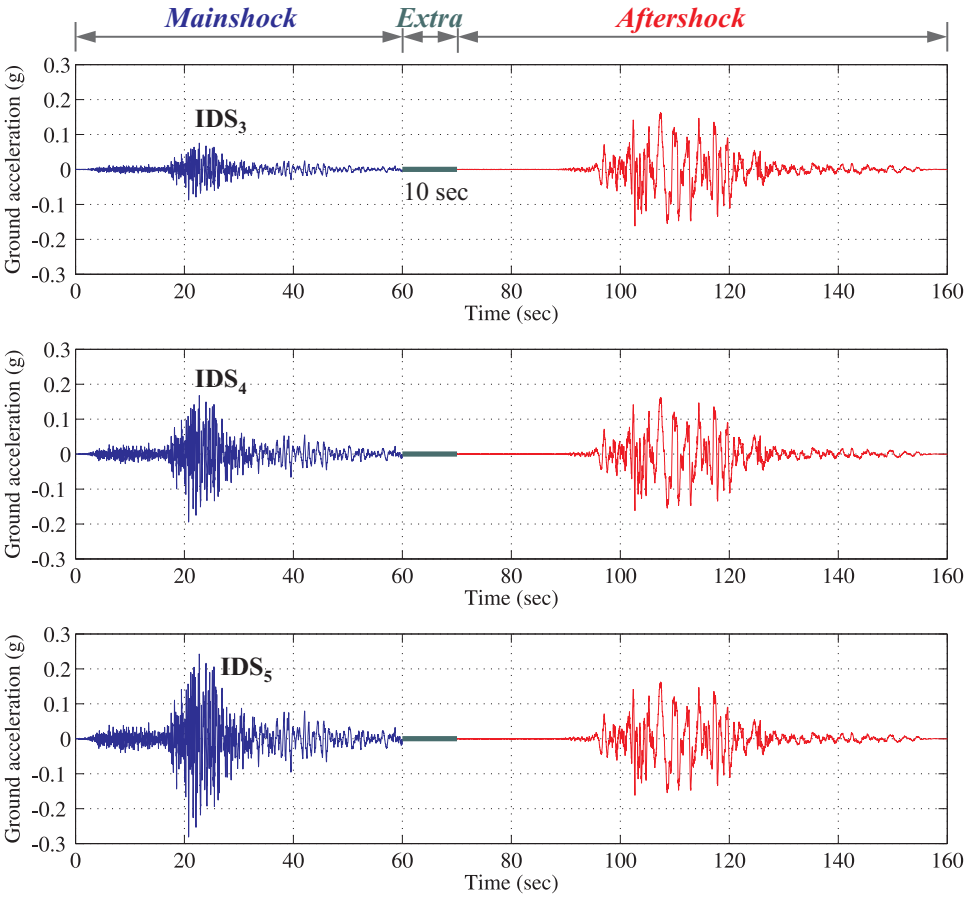

Figure 5.10 Mainshock-aftershock sequences with various mainshocks corresponding to IDSs

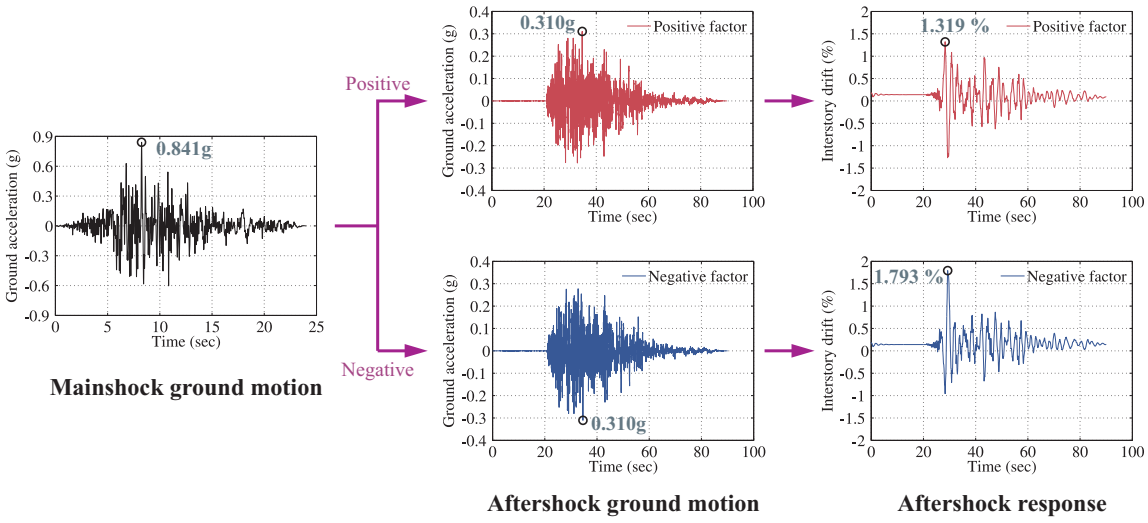

Figure 5.11 Aftershock responses accounting for the polarity of an aftershock ground motion

5.5 Development of Aftershock Fragility Curves

Aftershock fragility curves can be achieved by using PADMs with the addition of capacity limit states predetermined. This section describes the PADMs, capacity limit states, and aftershock fragility curves.

5.5.1 Probabilistic aftershock demand models (PADMs)

Global response (interstory drift) is selected as an EDP in this research because of limited data of localized damage description for joint or column shear failure. Interstory responses are monitored in mainshock-aftershock analyses. As mentioned in Section 5.1, given the assumed lognormal distribution of aftershock seismic demand, a linear regression of the demand-aftershock intensity measure pairs in the log-transformed space (PADM), determines the median, the dispersion ($\beta_{D|IMas}$), slope, intercept, and coefficient of determination (R^2), as illustrated in Figure 5.12. In this research, this PADM relates the aftershock IM (i.e., peak ground velocity (PGV_{as})) to the EDP (i.e., the maximum interstory drift ($\theta_{max,as}$)). The PADM is computed for each initial damage state i (i = 1,…,n) presented in Table 5.5 and Table 5.7 for ductile and non-ductile RC frames, respectively, where n is the number of initial damage states of interest.

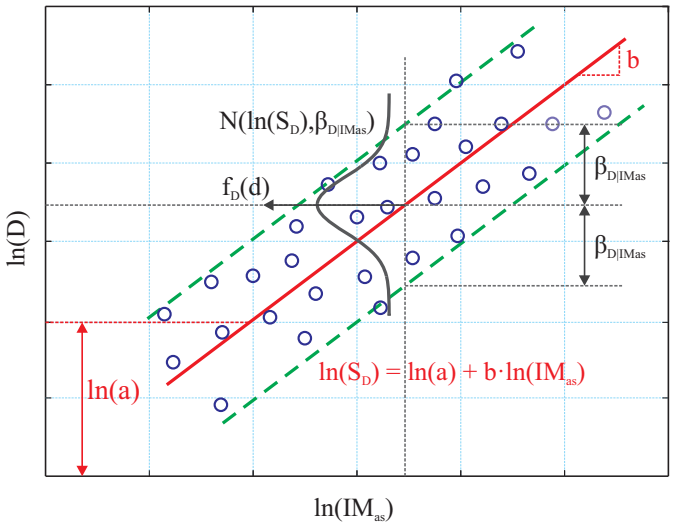

Figure 5.12 Probabilistic aftershock demand model (PADM)

5.5.2 Capacity limit state

HAZUS-MH (FEMA 2003) has provided the qualitative damage descriptions with four limit states (slight, moderate, extensive, and complete), as presented in Table 5.9. These damage descriptions can be integrated with quantitative engineering demand parameters seismic events (so-called damage-EDP relationship). To establish this damage state-drift relationship, the work of Bearman (2012) is employed in the same manner as the characterization of initial damage states. By linking seismic demands (drift) with damage descriptions, four limit states can be determined for non-ductile and ductile RC frames, as indicated in Table 5.10. Under the assumption that a limit state follows a lognormal distribution, these drifts obtained from the damage estimation are adopted as the median values (S_C) of capacity limit states. Additionally, the dispersion (β_C) of all limit states is assumed to be 0.30 in this research. Those two parameters will be utilized to develop aftershock fragility curves. Although different analytical frame models have different limit states, the same limit states are used in this research to compare and identify the

probability of being in a damage state and the median value of aftershock fragility curves under an identical condition.

Table 5.9 Description of HAZUS-MH (FEMA 2003)

Limit state	Damage description
Slight	• Flexural or shear type hairline cracks in some beams and columns near joints or within joints
Moderate	• Most beams and columns exhibit hairline cracks. • Some of ductile frame components have reached yield capacity indicated by larger flexural cracks and some concrete spalling. • Non-ductile frames components may exhibit larger shear cracks and spalling.
Extensive	• Some ductile frame components have reached their ultimate capacity indicated by large flexural cracks, spalled concrete and rebar buckling. • Non-ductile frame components may have suffered shear failures or bond failures at reinforcement splices, or broken ties or rebar buckling in columns which may result in partial collapse.
Complete	• Structure is collapsed or in imminent danger of collapse associated with the brittle failure of non-ductile frame or loss of frame stability.

Table 5.10 Capacity limit state model for maximum interstory drift (%)

	Slight		Moderate		Extensive		Complete	
Frame type	S_C	β_C	S_C	β_C	S_C	β_C	S_C	β_C
Non-ductile	0.4	0.3	0.9	0.3	2.5	0.3	4.5	0.3
Ductile	0.5	0.3	1.0	0.3	4.5	0.3	6.0	0.3

5.5.3 Aftershock fragility curves

With the aftershock probabilistic seismic demand models described in Section 5.5.1 and the limit state models determined in Section 5.5.2, it is necessary and possible to develop the aftershock fragility curves with different initial damage states (IDSs) for non-ductile and ductile RC frames. This is achieved in closed form using equation (5.8), where $S_{D,as}$ and S_C are is the median value of the aftershock demand and chosen limit states. Substituting equation (5.6) into equation (5.8) and rearranging the formulation, equation (5.8) can be expressed as equation (5.11):

$$P[LS \mid IM_{as}, IDS] = \Phi\left[\frac{\ln(IM_{as}) - \ln(\lambda_{as})}{\beta_{as}}\right] \tag{5.11}$$

where

$$\lambda_{as} = \exp\left[\frac{\ln(S_C) - \ln(a)}{b}\right] \tag{5.12}$$

and

$$\beta_{as} = \frac{\sqrt{\beta_{D|IMas}^2 + \beta_C^2}}{b} \tag{5.13}$$

where λ_{as} is defined as the median value of the aftershock intensity measure for the selected capacity limit state (LS) (slight, moderate, extensive, complete), so-called the median value of the aftershock fragility curve, a and b are the regression coefficients of the PADM, and β_{as} is the dispersion of the aftershock fragility curve.

Figure 5.13 illustrates the aftershock fragility curves with different capacity limit states for undamaged and damaged RC frames using equation 5.11, equation 5.12, and equation 5.13.

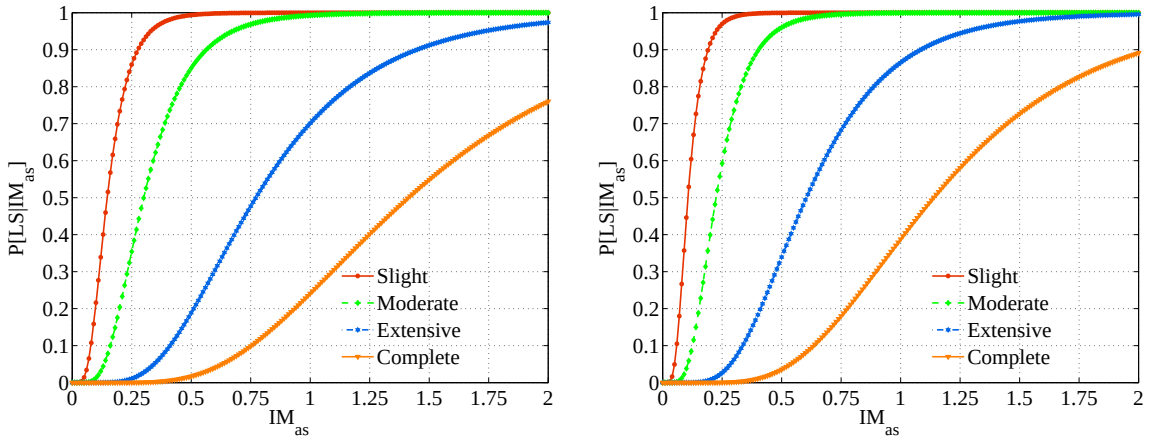

(a) Undamaged frame (IDS_0) (b) Damaged frame (IDS_4)

Figure 5.13 Illustrations of aftershock fragility curves

5.6 Impact of an Aftershock Ground Motion Suite Selection

As mentioned in Section 5.3.2, aftershock ground motions are carefully selected together with PADMs and aftershock fragility curves. To examine the impact of aftershock ground motions on structural responses, for simplicity, an analytical frame model without the variability of material uncertainties is subjected to one mainshock ground motion and different aftershock ground motions (a total of 360 simulations) with two different initial damage states: undamaged (IDS_0) and damaged (IDS_5) conditions. Then, the PADMs are developed, as shown in Figure 5.14(a). It can be indicated that, in the case of the damaged condition (IDS_5), the single linear regression model for the entire range of data in a log-transformed space does not provide an appropriate fit of the data. The plotted

values for IDS_5 are almost constant in the range of lower PGV_{as} (smaller magnitude aftershocks) because the final response depends mainly on large magnitude mainshocks compared to aftershocks (no or little aftershock effects). As illustrated in Figure 5.14(b), the linear regression fit for the mainshock-damaged structures (IDS_5) results in crossover fragility curves that slightly or moderately damaged structures associated with mainshocks may have higher probabilities of being in a certain damage state at the higher IM_{as} than severely damaged structures.

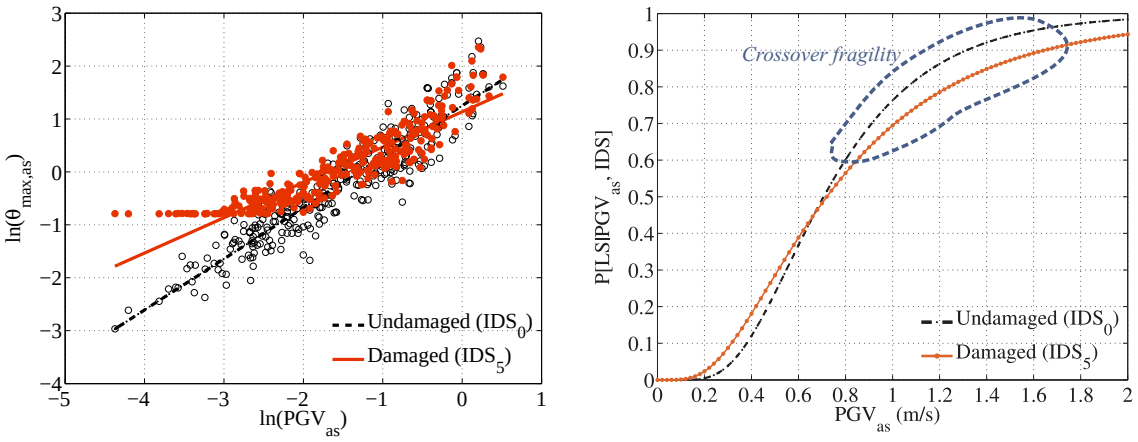

(a) Linear PADMs (b) Crossover fragility

Figure 5.14 Inappropriate PADMs and crossover fragility

To capture the scatter-plot in the whole range of IM_{as} and avoid the crossover fragility curves, a bilinear model of PADM can be employed by minimizing the residuals between actual and fitted values (Ramamoorthy et al. 2006, Shafieezadeh 2011). The bilinear model can offer better results with regard to the reduction in the dispersion and increase in the determination of coefficient. However, most fragility curves have been developed employing the linear demand model for a practical use. For this purpose,

Ramamoorthy et al. (2006) proposed a continuous fragility curve over the entire range of intensity measures by using a nonlinear least square regression. However, the coefficients of the demand model (modified single linear regression) such as the intercept and the slope extracted from the continuous fragility curve might be different from those from the single linear regression. Thus, the continuous fragility curve might lose the inherent trend in the scatter-plot of demand against intensity measure.

The bilinear model obtained from the data in Figure 5.15(a) can consist of an almost a relatively lower sloped line for the first branch and a sloped line for the second branch in that the first branch can is the best fit line for data with no or little aftershock effect. Figure 5.15(b) presents the resulting aftershock fragility curves with the bilinear model. It can be demonstrated that the contribution of the first branch is small while that of the second brand governs the fragility function in the whole range of aftershock intensity measures. Therefore, to preserve the inherent properties of the linear best fit for practical applications, this research excludes aftershock ground motions with smaller magnitudes that cannot affect the aftershock responses. Since the aftershock ground motions should result in additional damage to structures, ground motions with PGV values less than 0.140 m/s are removed. Then, an aftershock ground motion suite can be re-assembled from the remaining ground motions (210 out of 320 ground motions). As is done in the selection of mainshock ground motions, an aftershock ground motion suite (a total of 100) is assembled from the distribution of PGV for the remainder by using the LHS technique (Mckay et al. 1979). Figure 5.16 depicts the response spectra for a suite of aftershock ground motions obtained through the above procedure for all analyzed RC frame models. The suite of aftershock ground motions developed for a frame might not

be appropriate for other frame type. However, it can be argued that an identical suite of aftershock ground motions can be utilized for different frame type because the most influential component that affects aftershock demand is the variability of the ground motion (Ellingwood et al. 2007, Kwon and Elnashai 2006). This assumption will be proved through the resulting aftershock fragility curves for different analytical frame models in Chapter 6.

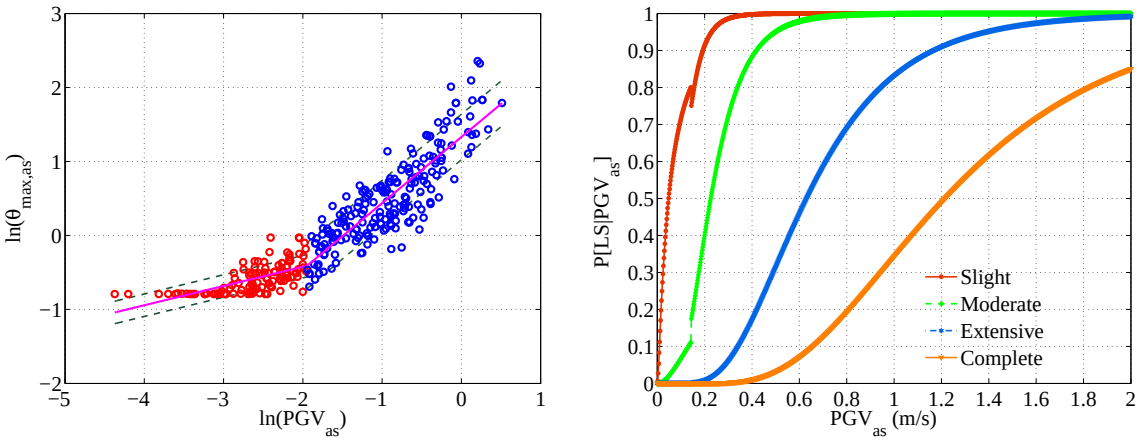

(a) Bilinear PADM (b) Resulting aftershock fragility curves

Figure 5.15 Illustrations of aftershock fragility curves with a bilinear PADM model

With the appropriate selection of mainshock and aftershock ground motion suites, the PADMs and aftershock fragility curves with different IDSs are generated for the stochastic finite element models, as shown in Figure 5.17. These results explain the increased vulnerability of damaged members that experience the cyclic strength and stiffness deterioration under mainshock-damaged conditions. The resulting aftershock fragility curves cannot exhibit crossover fragilities, thereby indicating that more severely damaged structures as a result of mainshocks have higher probabilities of being in a

damage state over the entire range of intensity measures. Furthermore, if the number of ground motions is relatively small, it is recommended that the bilinear model of a PADM be utilized for developing aftershock fragility curves.

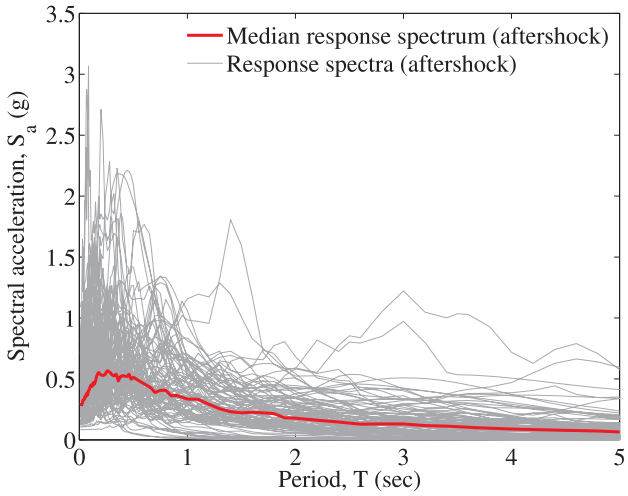

Figure 5.16 A suite of aftershock ground motions

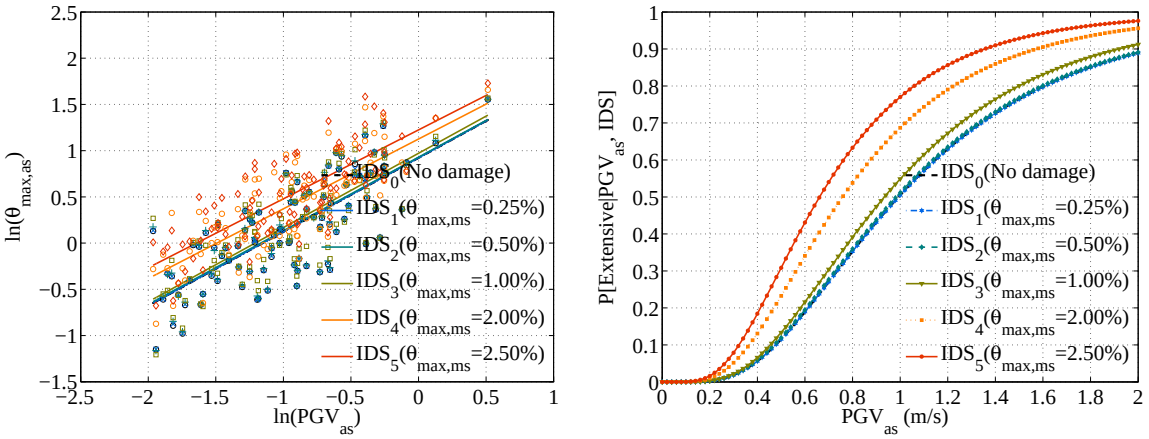

(a) PADM (b) Aftershock fragility (extensive)

Figure 5.17 Illustrations of appropriate PADMs and aftershock fragility curves

5.7 Summary

This chapter describes the analytical procedure for the development of aftershock fragility curves for RC frames. Unlike existing aftershock fragility assessment (stripe approach (IDA)), the framework is developed using a cloud method (NTHA) for aftershock analysis to account for realistic ground motions that can occur at the site of interest. This procedure consists of creating the stochastic analytical models accounting for modeling uncertainties, selecting a suite of mainshock and aftershock ground motions, simulating damaging earthquakes associated with the characterization of initial damage states, performing mainshock-aftershock analyses, computing PADMs, and generating aftershock fragility curves. Particularly, the mainshock-damaged condition of structures can be accomplished by correlating visible damage with member response based on the observation of existing experimental column tests and by generating mainshock ground motions through IDA or CPO approach. Furthermore, the aftershock fragility function is developed by modifying the classical fragility function and by assuming the lognormal distribution of aftershock demand and capacity limit state. An important finding is that ground motions with smaller aftershock intensity do not significantly affect the final responses for mainshock-damaged structures. Therefore, aftershock ground motions that can cause the additional damage to structures should be selected. Although the suite of aftershock ground motions is developed for a frame model, this suite will provide reasonable results for other structure types because the most influential component that affects the seismic demand is the variability of the ground motion. This assumption will be proved through the resulting aftershock fragility curves for different analytical frame models in Chapter 6.

CHAPTER 6

AFTERSHOCK FRAGILITY ASSESSMENT OF RC FRAMES

This chapter presents the application of the proposed framework for aftershock fragility assessment described in Chapter 5 to different types of RC frames mentioned in Chapter 4 in order to develop quantitative evaluation tools for their accumulated damage and increased vulnerability associated with aftershock ground motions. These estimations of additional damage plays a significant role in assessing potential losses to facilitate crucial decision making such as emergency response mobilization, inspection priority, recovery strategy, and re-occupancy decision. Aftershock fragility curves that relate the probability of meeting or exceeding a particular limit state given an imposed aftershock intensity demand will be a means to quantify the increased vulnerability of structures in the post-mainshock probabilistic risk assessment.

Following the aftershock assessment framework mentioned in the previous chapter, this research develops and compares probabilistic aftershock demand models (PADMs) and aftershock fragility curves for the most common RC building frames in California with different building types, building heights, and analytical frame models associated with potential failure mechanism. Additionally, this research generates the PADMs and aftershock fragility curves with different mainshock-damaged conditions of the RC frames associated with initial damage states (IDSs) and compares the probability of being in a certain damage state or median value of fragility curves to investigate how the extent of initial damage due to mainshock ground motions affects the additional damage due to aftershock ground motions.

6.1 Choice of RC Frames for Aftershock Fragility Assessment

To reduce computational efforts in aftershock fragility assessment, this research selects analytical frame models from those chosen in Chapter 4, listed in Table 6.1. For all frame models, the joint shear model is selected as the baseline frame model to investigate the difference in the median values of the resulting aftershock fragility curves for different RC frames. In the case of non-ductile RC frames, the OMF-4S frame has five different analytical frame models accounting for their potential failure modes: joint rigid offset, joint shear or joint bond, column shear, and both concurrent joint and column shear. The OMF-8S frame has three different analytical frame models with the joint shear model, column shear, and joint and shear model. Additionally, this research does not include the effect of column shear in non-ductile perimeter frames with four stories and eight stories (OMF-4P and OMF-8P frames) because a lot of simulations for these frames would fail even in nonlinear time history analyses under the undamaged condition of these frame models with column shear, as illustrated in Figure 6.1 which shows the scatter-plot of maximum interstory against intensity measure in a log-transformed space for undamaged OMF-4P frames with column shear model. Their vulnerability is associated with their inherent characteristic such as P-Δ effects. To account for the large number of collapsed simulations, a binary regression model (will be explained in the next section) is introduced because the linear regression model in equation 5.1 or equation 5.6 does not include this behavior (Ellingwood et al. 2010). Additionally, to utilize the linear regression model, the aftershock ground motion suite developed in Chapter 5 should be reselected for these frames. In this process, because reselected aftershock ground motions can cause the increased seismic demand for more fragile frame model (concurrent joint

and column shear model is the most fragile), the reselection should be carefully conducted. Therefore, this research will not consider these analytical frame models without allowing additional efforts. In the case of ductile RC frames, this research takes account of two analytical frame models with and without joint shear in the fragility generation to examine the difference in the aftershock demands for frames with and without joint shear.

Table 6.1 Analytical frame models for aftershock fragility assessment

Frame	Type	No. of stories	Frame model	Modeling description
Non-ductile	Space	4	OMF-4S-RO	Joint rigid offset
			OMF-4S-JS	Joint shear
			OMF-4S-JB	Joint bond
			OMF-4S-CS	Column shear
			OMF-4S-JCS	Joint and column shear
		8	OMF-8S-JS	Joint shear
			OMF-8S-CS	Column shear
			OMF-8S-JCS	Joint and column shear
	Perimeter	4	OMF-4P-JS	Joint shear
		8	OMF-8P-JS	Joint shear
Ductile	Perimeter	4	SMF-4P-RO	Joint rigid offset
			SMF-4P-JS	Joint shear
	Perimeter	8	SMF-8P-RO	Joint rigid offset
			SMF-8P-JS	Joint shear

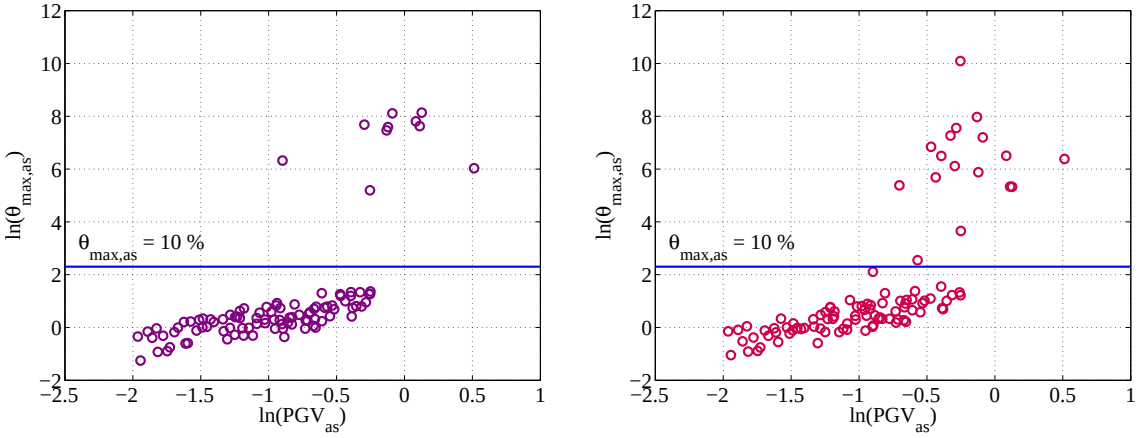

(a) Column shear model (b) Joint and column shear model

Figure 6.1 PADMs for undamaged OMF-4P frame with column shear

6.2 Accounting for Collapsed Simulations

The seismic demand model requires the consideration of collapsed simulations that have unrealistically large demand values or the convergence issue in the numerical algorithms since the plot of maximum drift and intensity measure data for ground motions that result in a dynamic instability on the frame model cannot be accounted for in the linear regression model presented in equation (5.1) or equation (5.6). To include the collapsed simulations, Ellingwood et al. (2010) and Baker and Cornell (2006) recommended the usage of a binary regression analysis (logistic regression). It can be achieved by combing the possibilities of collapse or no collapse using the total probability theorem. In other words, $P[D \geq d \,|IM = im_1]$ can be explicitly expressed as the probability of collapse given im_1 (logistic regression) plus the probability of non-collapse given im_1 (linear regression), where im_1 is a specific intensity measure. A detailed description can be found in the work of Baker and Cornell (2006).

Ellingwood et al. (2010) performed fragility analyses for steel frames with partially restrained beam-column connections, and their simulation results showed that two out of 40 ground motions (5%) caused the collapse of structures. The authors mentioned that a small portion of collapsed simulations significantly affects the binary regression. As a result, following the recommendation of Ellingwood et al. (2010), this research removes the collapsed simulations leading to dynamic instability from the demand-intensity measure pairs obtained from the simulations. Table 6.2 shows the number of collapsed simulations and number of simulations used in the generation of PADMs and aftershock fragility curves for the frame models listed in Table 6.1. To compare the fragility results with different modeling techniques for each frame, the

number of simulations included in the fragility assessment is unified for each frame. It can be indicated that the portion of collapsed simulations for all frame models lies within around 5%.

Table 6.2 Number of collapsed simulations

Frame	Type	No. of stories	Frame model	No. of collapses	No. of simulations used for aftershock fragilities
Non-ductile	Space	4	OMF-4S-RO	0	96
			OMF-4S-JS	0	
			OMF-4S-JB	1	
			OMF-4S-CS	3	
			OMF-4S-JCS	4	
		8	OMF-8S-JS	1	97
			OMF-8S-CS	2	
			OMF-8S-JCS	3	
	Perimeter	4	OMF-4P-JS	6	94
		8	OMF-8P-JS	4	96
Ductile	Perimeter	4	SMF-4P-RO	0	99
			SMF-4P-JS	1	
	Perimeter	8	SMF-8P-RO	0	99
			SMF-8P-JS	1	

6.3 Probabilistic Aftershock Demand Models

Mainshock-aftershock analyses (back-to-back nonlinear time history analyses) are performed for 100 mainshock-aftershock-frame pairs under the suite of mainshock and aftershock ground motions discussed in Chapter 5 in order to monitor key responses (here, maximum interstory drifts). Then, probabilistic aftershock demand models (PADMs) are generated for analytical frame models listed in Table 6.1, in terms of initial damage states representing different mainshock-damaged conditions. The aftershock demand model equations are presented in tabular form for the transformed state space.

Because of the very nature of the model formats, specific discussion of the aftershock demand models is difficult. Comparison of analytical frame models and frame

types are best performed using aftershock fragility curves. Therefore, in this section, the aftershock demand models are presented without an associated description. Furthermore, as mentioned in Chapter 5, the IDA approach is primarily utilized to simulate mainshock ground motions needed in the generation of the aftershock demand models in order to account for the dynamic characteristics in mainshock analyses.

6.3.1 Non-ductile RC frames

6.3.1.1 Non-ductile 4-story space frame (OMF-4S frame)

Figure 6.2 shows the PADMs with different modeling techniques for the OMF-4S frame: OMF-4S-RO (joint rigid offset), OMF-4S-JS (joint shear), OMF-4S-JB (joint bond), OMF-4S-CS (column shear), and OMF-4S-JCS (joint and column shear). The initial damage states chosen in this research are six different damage states corresponding to maximum interstory drift: no initial damage (IDS_0), 0.25% (IDS_1), 0.50% (IDS_2), 1.0% (IDS_3), 2.0% (IDS_4), and 2.5% (IDS_5). As indicated in Figure 6.2(a) and Figure 6.2(b), the PADMs are almost identical from IDS_0 to IDS_2 because most structural components remain elastic under these mainshock ground motions. These PADMs do not affect the resulting aftershock fragility curves. On the other hand, the difference between IDS_3 and IDS_4 is significant because of the inelastic behavior (i.e., cyclic strength and strength deterioration) of components due to mainshocks. Therefore, for other frame models, PADMs with IDS_0, IDS_3, IDS_4, and IDS_5 are developed in this research. Table 6.3 presents the aftershock demand models with different IDSs for each analytical frame model of the OMF-4S frame.

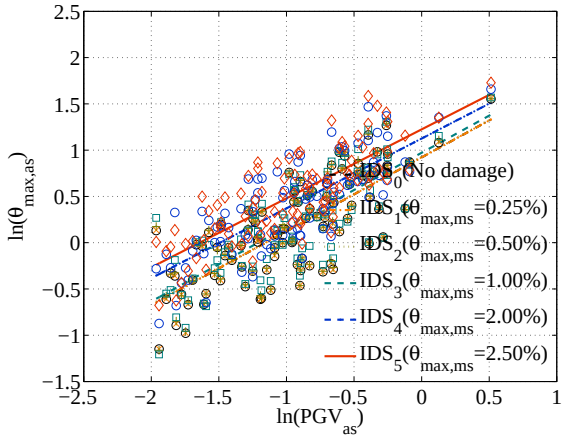

(a) OMF-4S-RO (joint rigid offset)

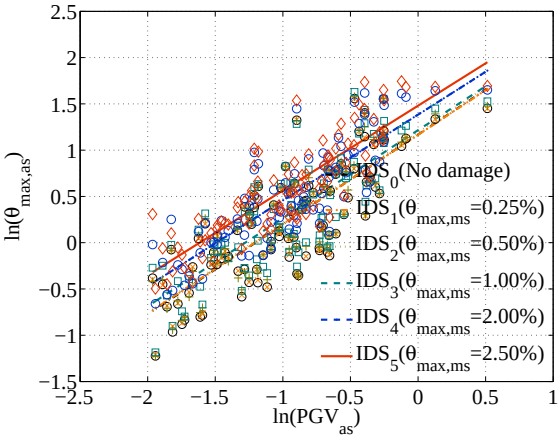

(b) OMF-4S-JS (joint shear)

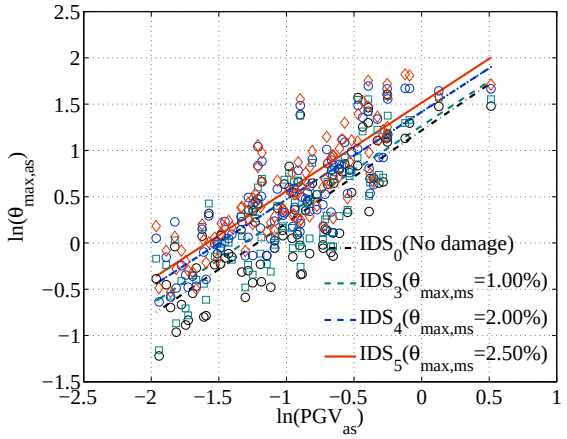

(c) OMF-4S-JB (joint bond)

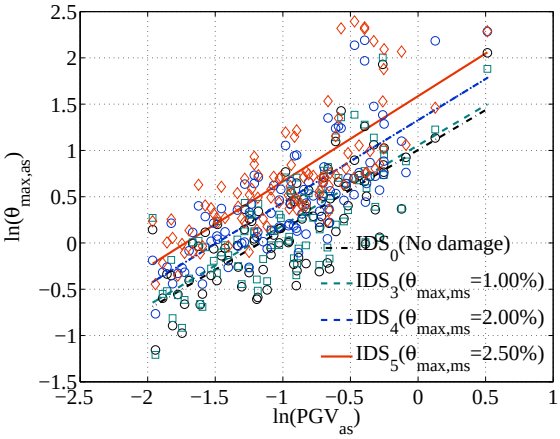

(d) OMF-4S-CS (column shear)

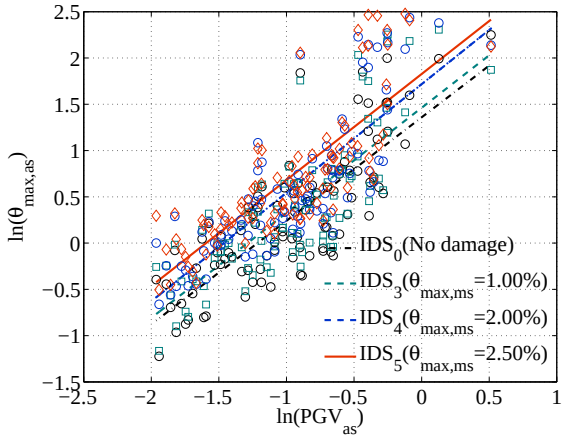

(e) OMF-4S-JCS (joint and column shear)

Figure 6.2 PADMs with different IDSs for analytical frame models of OMF-4S frame

Table 6.3 PADMs with different IDSs for analytical frame models of OMF-4S frame

Frame model	IDS	PADM	R^2	$\beta_{D\|PGVas}$
OMF-4S-RO	IDS_0	$\ln(\theta_{max,as}) = 0.921 + 0.799 \times \ln(PGV_{as})$	0.590	0.345
(rigid offset)	IDS_1	$\ln(\theta_{max,as}) = 0.922 + 0.799 \times \ln(PGV_{as})$	0.590	0.345
	IDS_2	$\ln(\theta_{max,as}) = 0.929 + 0.796 \times \ln(PGV_{as})$	0.587	0.346
	IDS_3	$\ln(\theta_{max,as}) = 0.971 + 0.803 \times \ln(PGV_{as})$	0.603	0.338
	IDS_4	$\ln(\theta_{max,as}) = 1.126 + 0.755 \times \ln(PGV_{as})$	0.618	0.307
	IDS_5	$\ln(\theta_{max,as}) = 1.224 + 0.746 \times \ln(PGV_{as})$	0.639	0.290
OMF-4S-JS	IDS_0	$\ln(\theta_{max,as}) = 1.168 + 0.971 \times \ln(PGV_{as})$	0.648	0.371
(joint shear)	IDS_1	$\ln(\theta_{max,as}) = 1.166 + 0.966 \times \ln(PGV_{as})$	0.648	0.369
	IDS_2	$\ln(\theta_{max,as}) = 1.191 + 0.975 \times \ln(PGV_{as})$	0.657	0.365
	IDS_3	$\ln(\theta_{max,as}) = 1.216 + 0.951 \times \ln(PGV_{as})$	0.667	0.348
	IDS_4	$\ln(\theta_{max,as}) = 1.383 + 0.927 \times \ln(PGV_{as})$	0.722	0.298
	IDS_5	$\ln(\theta_{max,as}) = 1.480 + 0.916 \times \ln(PGV_{as})$	0.735	0.285
OMF-4S-JB	IDS_0	$\ln(\theta_{max,as}) = 1.216 + 0.971 \times \ln(PGV_{as})$	0.652	0.379
(joint bond)	IDS_3	$\ln(\theta_{max,as}) = 1.266 + 0.951 \times \ln(PGV_{as})$	0.664	0.355
	IDS_4	$\ln(\theta_{max,as}) = 1.416 + 0.927 \times \ln(PGV_{as})$	0.710	0.313
	IDS_5	$\ln(\theta_{max,as}) = 1.515 + 0.916 \times \ln(PGV_{as})$	0.738	0.294
OMF-4S-CS	IDS_0	$\ln(\theta_{max,as}) = 1.005 + 0.862 \times \ln(PGV_{as})$	0.580	0.381
(column shear)	IDS_3	$\ln(\theta_{max,as}) = 1.055 + 0.866 \times \ln(PGV_{as})$	0.590	0.374
	IDS_4	$\ln(\theta_{max,as}) = 1.327 + 0.891 \times \ln(PGV_{as})$	0.584	0.390
	IDS_5	$\ln(\theta_{max,as}) = 1.586 + 0.922 \times \ln(PGV_{as})$	0.577	0.409
OMF-4S-JCS	IDS_0	$\ln(\theta_{max,as}) = 1.359 + 1.118 \times \ln(PGV_{as})$	0.648	0.428
(joint and	IDS_3	$\ln(\theta_{max,as}) = 1.462 + 1.135 \times \ln(PGV_{as})$	0.638	0.443
column shear)	IDS_4	$\ln(\theta_{max,as}) = 1.717 + 1.173 \times \ln(PGV_{as})$	0.664	0.433
	IDS_5	$\ln(\theta_{max,as}) = 1.827 + 1.146 \times \ln(PGV_{as})$	0.659	0.427

6.3.1.2 Non-ductile 8-story space frame (OMF-8S frame)

Figure 6.3 presents the PADMs with different modeling techniques for the OMF-8S frame: OMF-8S-JS (joint shear), OMF-8S-CS (column shear), and OMF-8S-JCS (joint and column shear), summarized in Table 6.4.

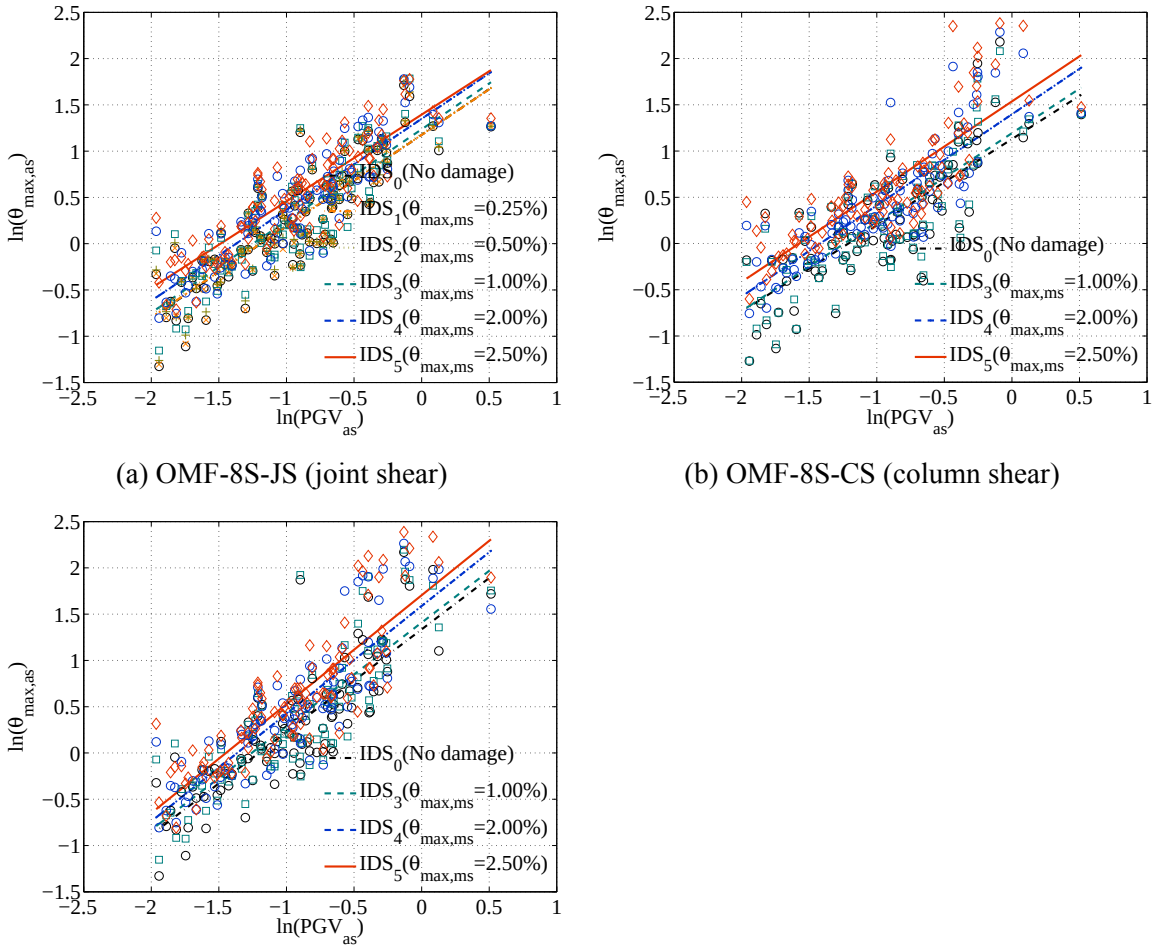

(a) OMF-8S-JS (joint shear)

(b) OMF-8S-CS (column shear)

(c) OMF-8S-JCS (joint and column shear)

Figure 6.3 PADMs with different IDSs for analytical frame models of OMF-8S frame

Table 6.4 PADMs with different IDSs for analytical frame models of OMF-8S frame

Frame model	IDS	PADM	R^2	$\beta_{D\|PGVas}$
OMF-8S-JS	IDS_0	$\ln(\theta_{max,as}) = 1.176 + 0.989 \times \ln(PGV_{as})$	0.736	0.312
(joint shear)	IDS_1	$\ln(\theta_{max,as}) = 1.176 + 0.986 \times \ln(PGV_{as})$	0.735	0.313
	IDS_2	$\ln(\theta_{max,as}) = 1.186 + 0.978 \times \ln(PGV_{as})$	0.735	0.310
	IDS_3	$\ln(\theta_{max,as}) = 1.236 + 0.991 \times \ln(PGV_{as})$	0.729	0.319
	IDS_4	$\ln(\theta_{max,as}) = 1.350 + 0.983 \times \ln(PGV_{as})$	0.768	0.285
	IDS_5	$\ln(\theta_{max,as}) = 1.394 + 0.937 \times \ln(PGV_{as})$	0.764	0.275
OMF-8S-CS	IDS_0	$\ln(\theta_{max,as}) = 1.129 + 0.933 \times \ln(PGV_{as})$	0.606	0.396
(column shear)	IDS_3	$\ln(\theta_{max,as}) = 1.193 + 0.962 \times \ln(PGV_{as})$	0.638	0.382
	IDS_4	$\ln(\theta_{max,as}) = 1.397 + 0.985 \times \ln(PGV_{as})$	0.687	0.350
	IDS_5	$\ln(\theta_{max,as}) = 1.536 + 0.975 \times \ln(PGV_{as})$	0.669	0.361
OMF-8S-JCS	IDS_0	$\ln(\theta_{max,as}) = 1.168 + 1.110 \times \ln(PGV_{as})$	0.709	0.375
(joint and	IDS_3	$\ln(\theta_{max,as}) = 1.216 + 1.120 \times \ln(PGV_{as})$	0.700	0.387
column shear)	IDS_4	$\ln(\theta_{max,as}) = 1.383 + 1.163 \times \ln(PGV_{as})$	0.739	0.365
	IDS_5	$\ln(\theta_{max,as}) = 1.480 + 1.177 \times \ln(PGV_{as})$	0.737	0.371

6.3.1.3 Non-ductile 4- and 8-story perimeter frames (OMF-4P and OMF-8P frames)

Figure 6.4(a) and Figure 6.4(b) show the PADMs for the OMF-4S frame and the OMF-8S frame with joint shear, respectively, presented in Table 6.5.

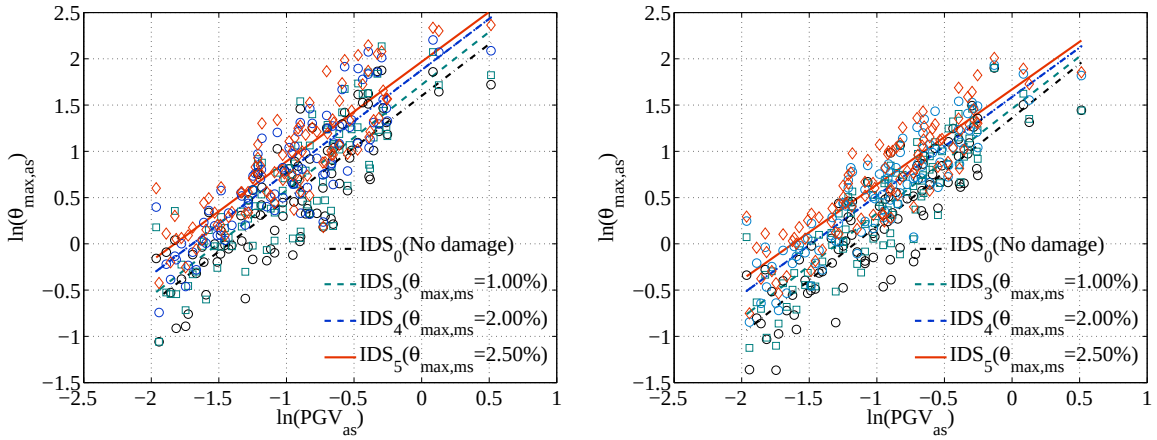

(a) OMF-4P-JS (joint shear) (b) OMF-8P-JS (joint shear)

Figure 6.4 PADMs with different IDSs for OMF-4P and OMF-8P frames (joint shear)

Table 6.5 PADMs with different IDSs for OMF-4P and OMF-8P frames (joint shear)

Frame model	IDS	PADM	R^2	$\beta_{D\|PGVas}$
OMF-4P-JS	IDS_0	$\ln(\theta_{max,as}) = 1.599 + 1.121 \times \ln(PGV_{as})$	0.709	0.369
(joint shear)	IDS_3	$\ln(\theta_{max,as}) = 1.720 + 1.141 \times \ln(PGV_{as})$	0.718	0.368
	IDS_4	$\ln(\theta_{max,as}) = 1.879 + 1.108 \times \ln(PGV_{as})$	0.769	0.312
	IDS_5	$\ln(\theta_{max,as}) = 1.968 + 1.077 \times \ln(PGV_{as})$	0.759	0.312
OMF-8P-JS	IDS_0	$\ln(\theta_{max,as}) = 1.361 + 1.169 \times \ln(PGV_{as})$	0.768	0.335
(joint shear)	IDS_3	$\ln(\theta_{max,as}) = 1.460 + 1.131 \times \ln(PGV_{as})$	0.792	0.302
	IDS_4	$\ln(\theta_{max,as}) = 1.587 + 1.068 \times \ln(PGV_{as})$	0.807	0.272
	IDS_5	$\ln(\theta_{max,as}) = 1.670 + 1.029 \times \ln(PGV_{as})$	0.794	0.273

6.3.2 Ductile RC frames

For ductile RC perimeter frames, the initial damage states chosen in this research are six different damage states corresponding to maximum interstory drift: no initial damage (IDS_0), 0.30% (IDS_1), 1.0% (IDS_2), 1.5% (IDS_3), 2.0% (IDS_4), and 4.5% (IDS_5). As described in the previous section, IDS_0 through IDS_2 is expected to remain almost elastic behavior in mainshock analyses, and therefore four damage states are selected in this research: IDS_0, IDS_3, IDS_4, and IDS_5.

6.3.2.1 Ductile 4-story perimeter frame (SMF-4P frame)

Figure 6.5(a) and Figure 6.5(b) presents the PADMs for the SMF-4P frame with and without joint shear, respectively, indicated in Table 6.6.

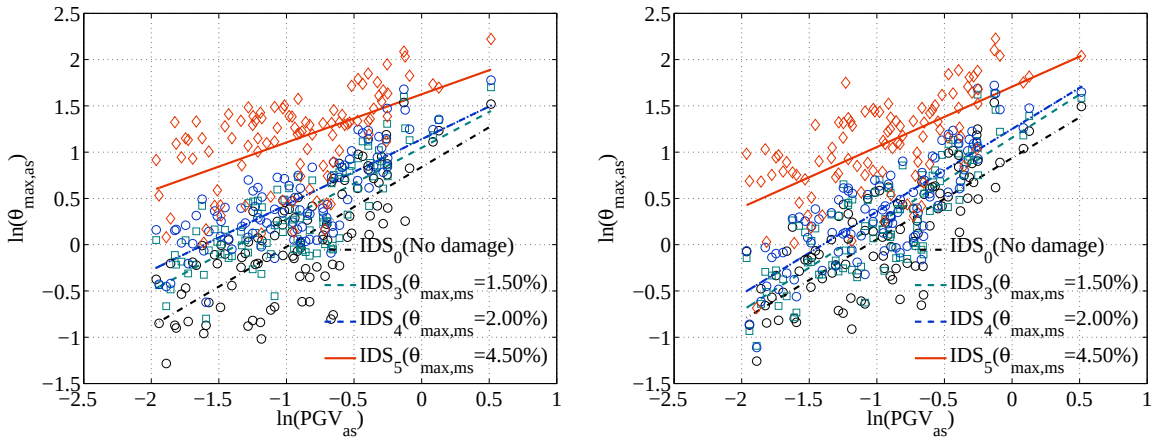

(a) SMF-4P-RO (rigid offset) (b) SMF-4P-JS (joint shear)

Figure 6.5 PADMs with different IDSs for analytical frame models of SMF-4P frame

Table 6.6 PADMs with different IDSs for analytical frame models of SMF-4P frame

Frame model	IDS	PADM	R^2	$\beta_{D\|PGVas}$
SMF-4P-RO	IDS_0	$\ln(\theta_{max,as}) = 0.839 + 0.861 \times \ln(PGV_{as})$	0.568	0.399
(rigid offset)	IDS_3	$\ln(\theta_{max,as}) = 1.048 + 0.773 \times \ln(PGV_{as})$	0.642	0.307
	IDS_4	$\ln(\theta_{max,as}) = 1.140 + 0.708 \times \ln(PGV_{as})$	0.617	0.296
	IDS_5	$\ln(\theta_{max,as}) = 1.625 + 0.521 \times \ln(PGV_{as})$	0.319	0.405
SMF-4P-JS	IDS_0	$\ln(\theta_{max,as}) = 0.936 + 0.879 \times \ln(PGV_{as})$	0.608	0.375
(joint shear)	IDS_3	$\ln(\theta_{max,as}) = 1.156 + 0.936 \times \ln(PGV_{as})$	0.690	0.333
	IDS_4	$\ln(\theta_{max,as}) = 1.250 + 0.892 \times \ln(PGV_{as})$	0.683	0.323
	IDS_5	$\ln(\theta_{max,as}) = 1.707 + 0.652 \times \ln(PGV_{as})$	0.438	0.393

6.3.2.2 Ductile 8-story perimeter frame (SMF-8P frame)

Figure 6.6(a) and Figure 6.6(b) illustrate the PADMs for the SMF-8P frame with and without joint shear, respectively, summarized in Table 6.7.

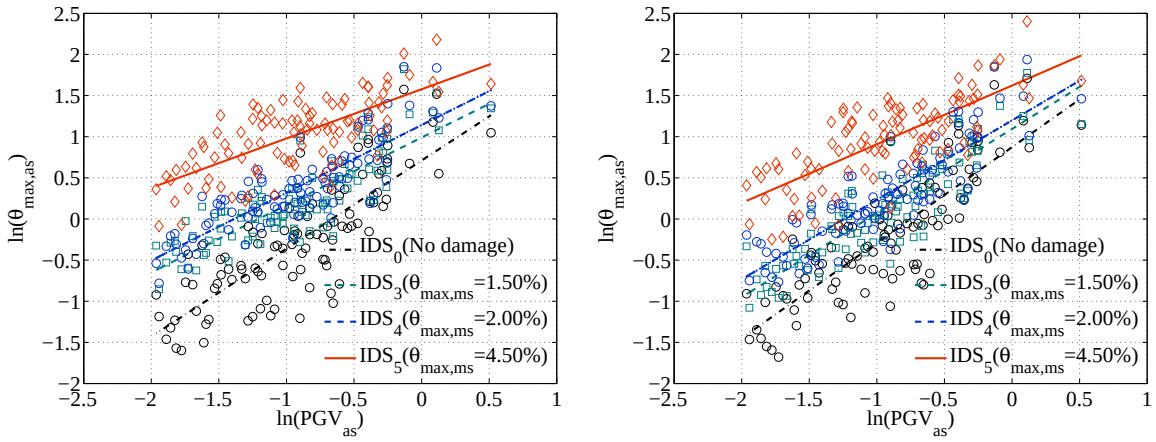

(a) SMF-8P-RO (rigid offset) (b) SMF-8P-JS (joint shear)

Figure 6.6 PADMs with different IDSs for analytical frame models of SMF-8P frame

Table 6.7 PADMs with different IDSs for analytical frame models of SMF-8P frame

Frame model	IDS	PADM	R^2	$\beta_{D\|PGVas}$
SMF-8P-RO	IDS_0	$\ln(\theta_{max,as}) = 0.711 + 1.071 \times \ln(PGV_{as})$	0.658	0.413
(rigid offset)	IDS_3	$\ln(\theta_{max,as}) = 0.990 + 0.820 \times \ln(PGV_{as})$	0.700	0.287
	IDS_4	$\ln(\theta_{max,as}) = 1.142 + 0.823 \times \ln(PGV_{as})$	0.721	0.274
	IDS_5	$\ln(\theta_{max,as}) = 1.578 + 0.599 \times \ln(PGV_{as})$	0.510	0.315
SMF-8P-JS	IDS_0	$\ln(\theta_{max,as}) = 0.873 + 1.162 \times \ln(PGV_{as})$	0.706	0.402
(joint shear)	IDS_3	$\ln(\theta_{max,as}) = 1.095 + 1.023 \times \ln(PGV_{as})$	0.762	0.306
	IDS_4	$\ln(\theta_{max,as}) = 1.198 + 0.966 \times \ln(PGV_{as})$	0.748	0.300
	IDS_5	$\ln(\theta_{max,as}) = 1.622 + 0.714 \times \ln(PGV_{as})$	0.567	0.334

6.4 Aftershock Fragility Curves

Using the probabilistic aftershock demand models (PADMs) obtained in Section 6.4.1 in addition to the capacity limit states indicated in Section 5.5.2, the aftershock fragility curves are generated for non-ductile and ductile RC frames under their different mainshock-damage conditions. The aftershock fragility functions can be easily computed in a close form, presented in equation (5.11) through equation (5.13). The aftershock fragility curves developed in this research can provide not only the increased vulnerability associated with damage accumulation under mainshock-aftershock sequences but also insight into their relative vulnerability of RC frames with different modeling techniques corresponding to the design codes. This task can be easily achieved by evaluating the relative change in the median values of the aftershock fragility curves indicated in equation (5.12). A positive change indicates a less vulnerable structure while a negative change indicates a more vulnerable structure. Figure 6.7 presents an illustration of the relative change in the median values. For all RC frames, the joint shear model is selected as the reference frame model.

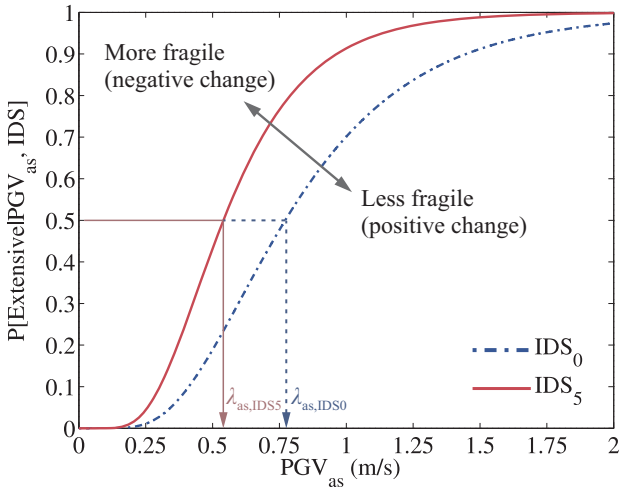

Figure 6.7 Illustration of relative change in median values

Table 6.8 and Table 6.9 present the median values (λ_{as}) and dispersions (ζ_{as}) of the resulting aftershock fragility curves for non-ductile and ductile RC frame models, respectively, in terms of the limit states, initial damage states, modeling characteristics, and frame types). Their relative vulnerability can be expressed as the difference in the median values while the shape of the curves can be governed by the dispersions. As the dispersion increases, the slope of the curves decreases. In the tables, the dispersion of the curves, for all limit damage state in each row, is the identical, because the same dispersion in all the capacity models assumed in Section 5.5.2. The impact of initial damage states, modeling characteristics, and simulation methods for damaging earthquakes on the aftershock fragility curves will be discussed in the subsequent sections.

Table 6.8 Aftershock fragilities for non-ductile RC analytical frame models

Frame model	IDS	Median values (λ_{as})				Dispersion (ζ_{as})
		Slight	Moderate	Extensive	Complete	
OMF-4S-RO (rigid offset)	IDS_0	0.100	0.277	0.994	2.073	0.572
	IDS_1	0.100	0.276	0.993	2.073	0.573
	IDS_2	0.098	0.272	0.984	2.059	0.575
	IDS_3	0.095	0.262	0.934	1.941	0.562
	IDS_4	0.067	0.196	0.758	1.652	0.569
	IDS_5	0.057	0.168	0.661	1.455	0.559
OMF-4S-JS (joint shear)	IDS_0	0.117	0.270	0.772	1.413	0.491
	IDS_1	0.116	0.268	0.773	1.420	0.492
	IDS_2	0.115	0.265	0.754	1.378	0.485
	IDS_3	0.106	0.249	0.730	1.354	0.483
	IDS_4	0.084	0.201	0.604	1.139	0.456
	IDS_5	0.073	0.177	0.540	1.026	0.452
OMF-4S-JB (joint bond)	IDS_0	0.119	0.267	0.741	1.333	0.483
	IDS_3	0.104	0.241	0.696	1.281	0.482
	IDS_4	0.085	0.200	0.589	1.097	0.459
	IDS_5	0.078	0.183	0.534	0.989	0.441
OMF-4S-CS (column shear)	IDS_0	0.108	0.276	0.902	1.784	0.562
	IDS_3	0.103	0.262	0.852	1.680	0.554
	IDS_4	0.081	0.200	0.631	1.220	0.552
	IDS_5	0.066	0.160	0.484	0.915	0.550
OMF-4S-JCS (joint and Column shear)	IDS_0	0.131	0.270	0.673	1.139	0.467
	IDS_3	0.123	0.251	0.618	1.038	0.472
	IDS_4	0.106	0.212	0.505	0.834	0.449
	IDS_5	0.091	0.185	0.452	0.754	0.456

Table 6.8 Aftershock fragilities for non-ductile RC analytical frame models (continued)

Frame model	IDS	Median values (λ_{as})				Dispersion
		Slight	Moderate	Extensive	Complete	(ζ_{as})
OMF-8S-JS (joint shear)	IDS_0	0.121	0.274	0.769	1.394	0.438
	IDS_1	0.120	0.273	0.769	1.395	0.439
	IDS_2	0.116	0.267	0.759	1.385	0.441
	IDS_3	0.114	0.258	0.724	1.311	0.442
	IDS_4	0.100	0.228	0.644	1.170	0.421
	IDS_5	0.085	0.202	0.600	1.124	0.434
OMF-8S-CS (column shear)	IDS_0	0.112	0.266	0.796	1.494	0.533
	IDS_3	0.112	0.259	0.750	1.382	0.505
	IDS_4	0.096	0.218	0.614	1.115	0.468
	IDS_5	0.081	0.186	0.530	0.967	0.481
OMF-8S-JCS (joint and column shear)	IDS_0	0.131	0.273	0.685	1.164	0.433
	IDS_3	0.125	0.259	0.644	1.089	0.437
	IDS_4	0.116	0.233	0.562	0.931	0.406
	IDS_5	0.108	0.215	0.512	0.844	0.405
OMF-4P-JS (joint shear)	IDS_0	0.106	0.219	0.544	0.919	0.424
	IDS_3	0.099	0.202	0.494	0.828	0.416
	IDS_4	0.080	0.167	0.419	0.713	0.391
	IDS_5	0.069	0.146	0.377	0.65	0.402
OMF-8P-JS (joint shear)	IDS_0	0.142	0.285	0.683	1.130	0.385
	IDS_3	0.122	0.251	0.618	1.040	0.376
	IDS_4	0.096	0.205	0.533	0.925	0.379
	IDS_5	0.081	0.178	0.481	0.851	0.394

Table 6.9 Aftershock fragilities for ductile RC analytical frame models

Frame model	IDS	Median values (λ_{as})				Dispersion
		Slight	Moderate	Extensive	Complete	(ζ_{as})
SMF-4P-RO (rigid offset)	IDS_0	0.169	0.378	2.165	3.023	0.580
	IDS_3	0.105	0.258	1.805	2.618	0.555
	IDS_4	0.075	0.200	1.673	2.511	0.595
	IDS_5	0.012	0.044	0.792	1.376	0.967
SMF-4P-JS (joint shear)	IDS_0	0.157	0.345	1.909	2.648	0.547
	IDS_3	0.139	0.291	1.451	1.973	0.479
	IDS_4	0.113	0.246	1.329	1.835	0.494
	IDS_5	0.025	0.073	0.733	1.139	0.758
SMF-8P-RO (rigid offset)	IDS_0	0.269	0.515	2.097	2.743	0.451
	IDS_3	0.128	0.299	1.872	2.658	0.464
	IDS_4	0.108	0.250	1.552	2.202	0.451
	IDS_5	0.023	0.072	0.885	1.430	0.671
SMF-8P-JS (joint shear)	IDS_0	0.260	0.472	1.721	2.205	0.407
	IDS_3	0.174	0.343	1.492	1.977	0.386
	IDS_4	0.141	0.289	1.372	1.849	0.405
	IDS_5	0.039	0.103	0.848	1.268	0.584

6.4.1 Impact of initial damage states

To address the impact of the extent of damage as a result of mainshocks on the aftershock responses of RC frames (different mainshocks and identical aftershocks), the aftershock fragility curves are developed for analytical frame models across different initial damage states and compared in terms of the median values. For this purpose, the OMF-4S frame and SMF-8P-frame selected for non-ductile and ductile frames, respectively, are discussed in this section. Appendix D shows the comparison of aftershock fragility results developed for all the analytical frame models.

6.4.1.1 Non-ductile 4-story space frame (OMF-4S frame)

Aftershock fragility curves are developed for five analytical frame models created for the OMF-4S frame under various mainshock-damaged conditions defined as the initial damage states (IDSs): OMF-4S-RO, OMF-4S-JS, OMF-4S-JB, OMF-4S-CS, and OMF-4S-JCS models. Figure 6.8 illustrates the comparison of aftershock fragility results with different IDSs across all the four limit damage states for OMF-4S-JS model chosen as the reference frame model. As depicted in the figure, as the extent of damage associated with mainshocks is more severe, the probability of being in a damage (limit) state given an intensity measure (PGV_{as}) increases for all limit states over the entire range of PGV_{as} (no crossover fragility), thereby resulting in the increased vulnerability of structures subjected to multiple earthquakes. Additionally, the aftershock fragility curves for IDS_0 through IDS_2 are almost identical, because the members remain elastic under these mainshock ground motions, as indicated in the PADM generation.

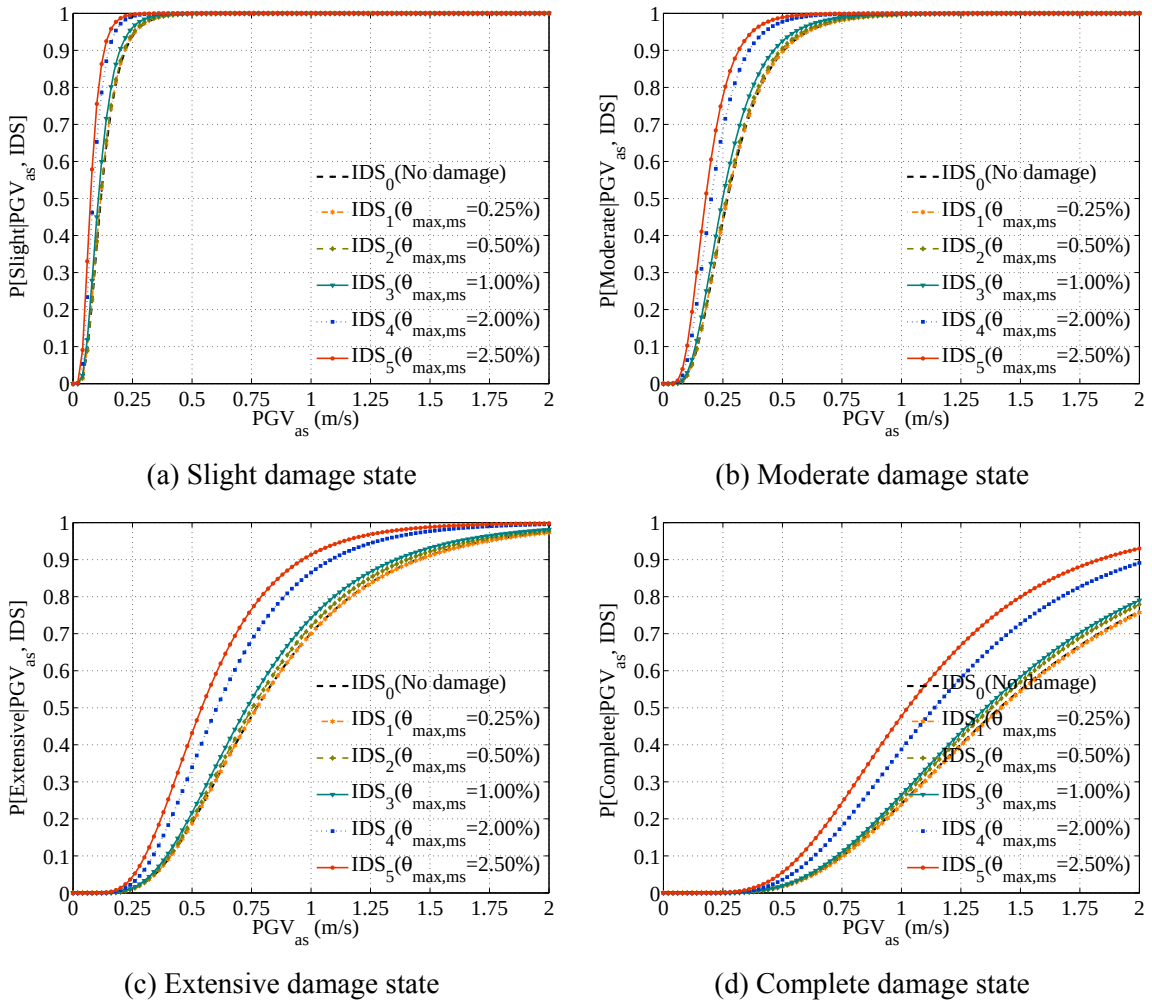

(a) Slight damage state

(b) Moderate damage state

(c) Extensive damage state

(d) Complete damage state

Figure 6.8 Aftershock fragility curves with different IDSs for OMF-4S-JS model

The plot of median values across four limit states is presented in Figure 6.9. As mentioned before, the comparison is performed by evaluating the relative change in the median value of the aftershock fragility curves in Table 6.10. The relative change is computed on the basis of the value for undamaged condition (IDS_0). It can be observed that, for all frame models, there is a pronounced reduction in the median values at the higher levels of initial damage states due to mainshocks. In contrast, there is a slight reduction in the median values at the lower levels. This finding is attributable to the

increased aftershock demand associated with the inelastic behavior of the members subjected to mainshock ground motions.

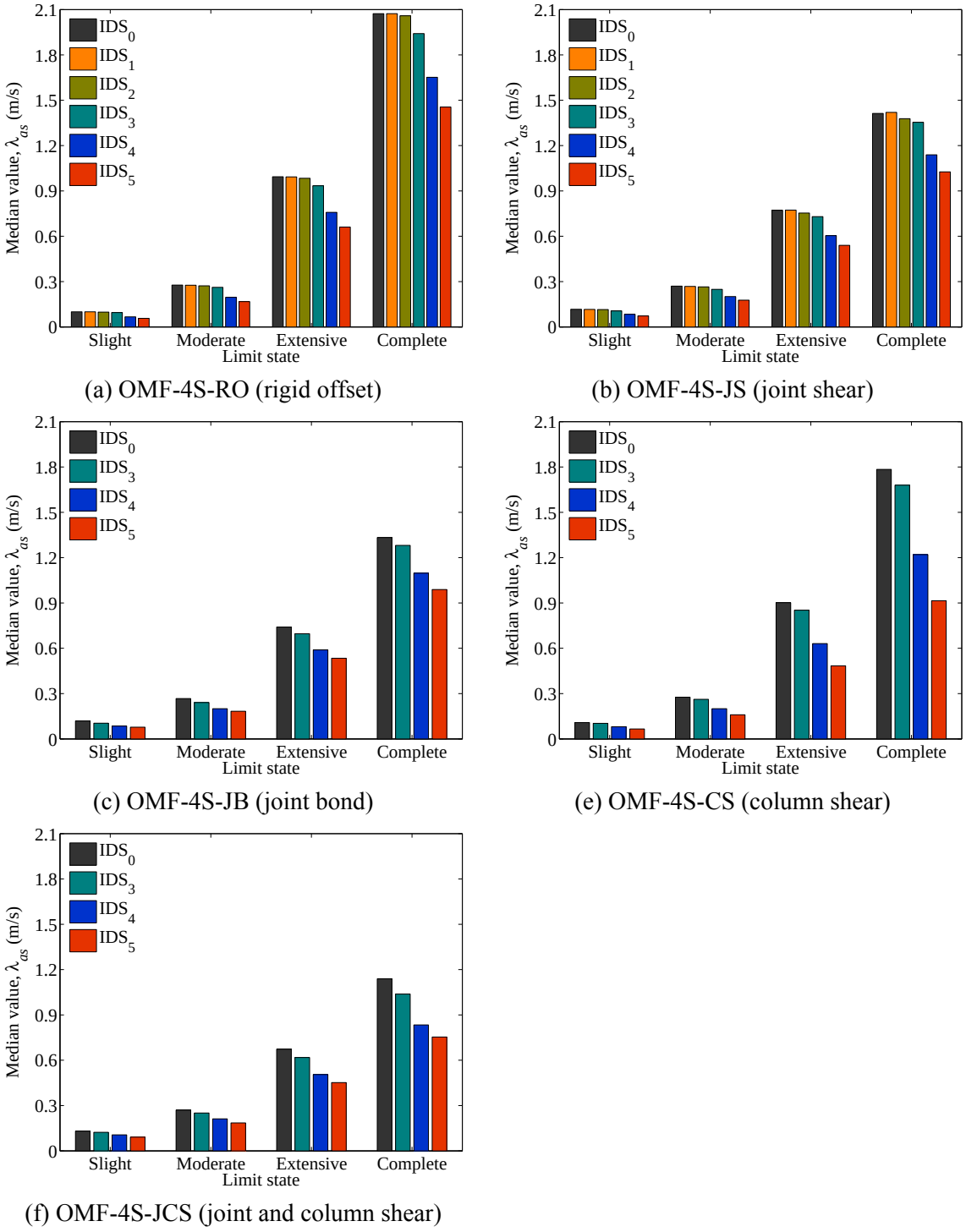

(a) OMF-4S-RO (rigid offset)

(b) OMF-4S-JS (joint shear)

(c) OMF-4S-JB (joint bond)

(e) OMF-4S-CS (column shear)

(f) OMF-4S-JCS (joint and column shear)

Figure 6.9 Median values of aftershock fragility curves with different IDSs for OMF-4S frame

Table 6.10 Difference in median values with different IDSs for OMF-4S frame

Frame model	Damage state transition	Slight	Moderate	Extensive	Complete
OMF-4S-RO	IDS_0 to IDS_1	0	0	0	0
(rigid offset)	IDS_0 to IDS_2	-2	-2	-1	-1
	IDS_0 to IDS_3	-5	-5	-6	-6
	IDS_0 to IDS_4	-33	-29	-24	-20
	IDS_0 to IDS_5	-43	-39	-34	-30
OMF-4S-JS	IDS_0 to IDS_1	-1	-1	0	0
(joint shear)	IDS_0 to IDS_2	-2	-2	-2	-2
	IDS_0 to IDS_3	-9	-8	-5	-4
	IDS_0 to IDS_4	-28	-26	-22	-19
	IDS_0 to IDS_5	-38	-34	-30	-27
OMF-4S-JB	IDS_0 to IDS_3	-13	-10	-6	-4
(joint bond)	IDS_0 to IDS_4	-29	-25	-21	-18
	IDS_0 to IDS_5	-34	-31	-28	-26
OMF-4S-CS	IDS_0 to IDS_3	-5	-5	-6	-6
(column shear)	IDS_0 to IDS_4	-25	-28	-30	-32
	IDS_0 to IDS_5	-39	-42	-46	-49
OMF-4S-JCS	IDS_0 to IDS_3	-6	-7	-8	-9
(joint and	IDS_0 to IDS_4	-19	-21	-25	-27
Column shear)	IDS_0 to IDS_5	-31	-31	-33	-34

§ Difference in median values = $(IDS_i - IDS_0) / IDS_0 \times 100$ (%), where i = 1, 2, 3, 4, 5.

6.4.1.2 Ductile 8-story perimeter frame (SMF-8P frame)

Aftershock fragility curves are generated for two analytical frame models with and without joint shear built for the SMF-8P frame with different mainshock-damaged conditions (IDSs). Figure 6.10 presents the comparison of aftershock fragility curves with different IDSs (except for IDS_1 and IDS_2) across all the four limit damage states for SMF-8P-JS model. As depicted in the figure, as the extent of damage associated with mainshocks increase, the probability of being in a damage (limit) state given an intensity measure (PGV_{as}) increases for all limit states over the entire range of PGV_{as} (no crossover fragility), thereby giving rise to the increased vulnerability of structures under successive earthquakes. Particularly, the mainshock-damaged condition of IDS_5 for all plots has a considerable increase in the probability of being in a damage state. This can be associated with the fact that the structure experiencing the dramatic stiffness and

strength degradation in the mainshock analyses has a significant aftershock demand in the aftershock analyses.

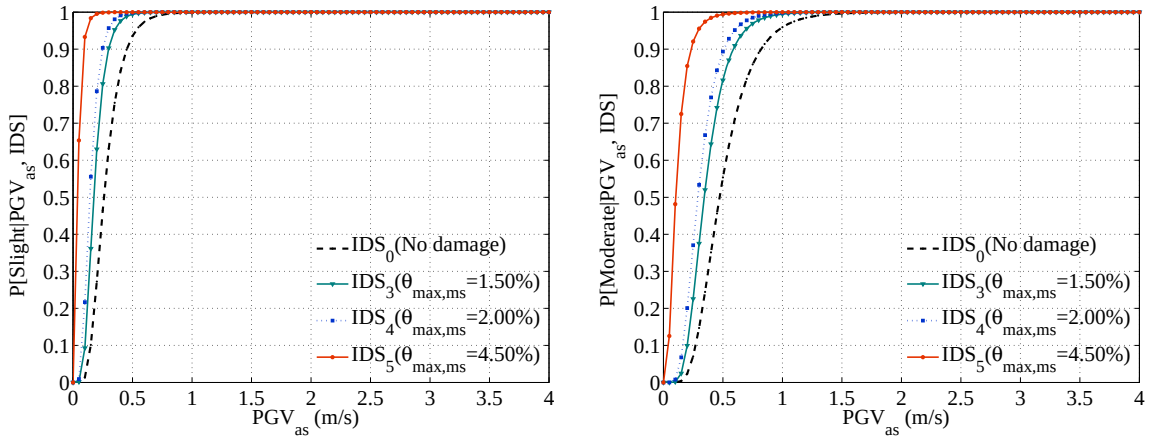

(a) Slight damage state

(b) Moderate damage state

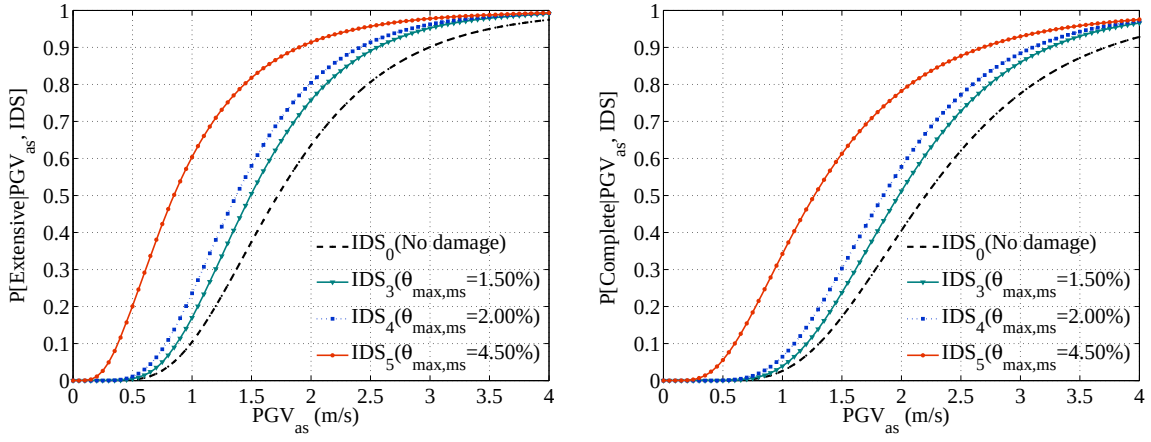

(c) Extensive damage state

(d) Complete damage state

Figure 6.10 Aftershock fragility curves with different IDSs for SMF-8P-JS model

The plot of median values across four limit states is shown in Figure 6.11. As mentioned before, the comparison is performed by evaluating the relative change in the median value of the aftershock fragility curves in Table 6.11. The relative change is computed on the basis of the value for undamaged condition (IDS_0). It can be indicated that, for all frame models, there is a considerable reduction in the median values at the

higher level of initial damage states due to mainshocks. This finding is due to the increased aftershock demand associated with the inelastic behavior of the components subjected to mainshocks.

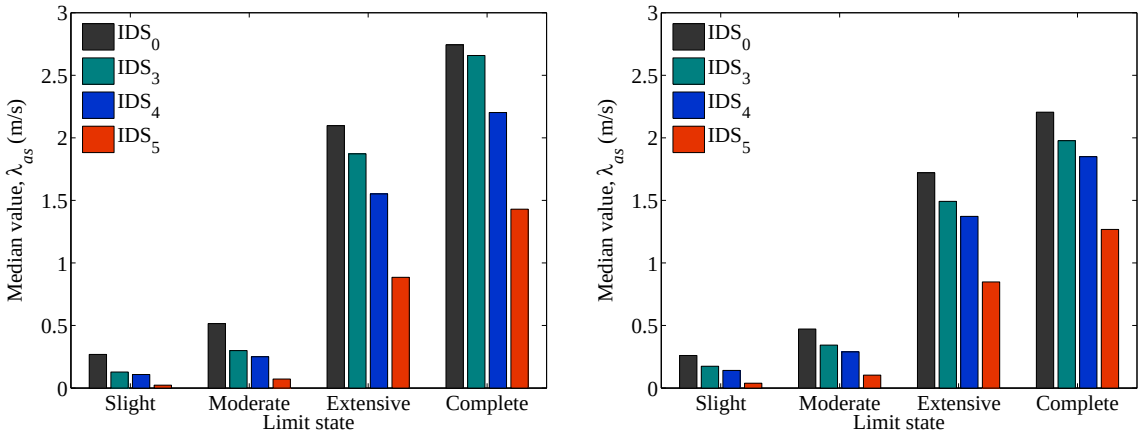

(a) SMF-8P-RO (rigid offset) (b) SMF-8P-JS (joint shear)

Figure 6.11 Median values of aftershock fragility curves with different IDSs for SMF-8P frame

Table 6.11 Difference in median values with different IDSs for SMF-8P frame

Frame model	Damage state transition	Slight	Moderate	Extensive	Complete
SMF-8P-RO (rigid offset)	IDS_0 to IDS_3	-52	-42	-11	-3
	IDS_0 to IDS_4	-60	-51	-26	-20
	IDS_0 to IDS_5	-91	-86	-58	-48
SMF-8P-RO (joint shear)	IDS_0 to IDS_3	-33	-27	-13	-10
	IDS_0 to IDS_4	-46	-39	-20	-16
	IDS_0 to IDS_5	-85	-78	-51	-42

§ Difference in median values = $(IDS_i - IDS_0) / IDS_0 \times 100$ (%), where i = 3, 4, 5.

6.4.2 Impact of modeling characteristics

To investigate the impact of analytical modeling techniques on the seismic performances of RC frames in an aftershock environment, the aftershock fragility curves are compared in terms of the median values of these curves. For this purpose, four RC frames with different modeling variables are chosen in this research: OMF-4S and OMF-8S frames for non-ductile frames and SMF-4P and SMF-8P frames for ductile frames.

6.4.2.1 Non-ductile 4-story space frame (OMF-4S frame)

Figure 6.12 depicts the comparison of the median values with five different modeling characteristics for the OMF-4S frame across the four limit states. The influence of the modeling characteristics on their aftershock demand is investigated by comparing the relative change in the median value of the aftershock fragility curves, as indicated in Table 6.12. In the table, the value of relative change is calculated on the basis of the reference frame model (OMF-4S-JS). As mentioned before, the negative change refers to increased vulnerability. The following bulleted list addresses the effect of the modeling variables in the OMF-4S frame.

- Overall, OMF-4S-JCS model is the most vulnerable when compared to other modeling types associated with the concurrent inelastic action (cyclic deterioration) of joint and column shears. However, for the slight damage state (limit), the positive change can be found (less vulnerable), which is attributed to the difference in the best linear fit (slope and intercept) of the PADMs indicated in Table 6.3 and the usage of identical limit states for all frame models. However, as shown in Figure 6.12, the comparison of the median values with different

analytical frame models demonstrates that the difference in the modeling characteristics is not significant at the slight or moderate damage states.

- The impact of the joint bond model associated with discontinuous beam bottom reinforcement within joints on the aftershock fragility curves is examined by evaluating the relative difference in the median values of two frame models (OMF-4S-JS and OMF-4S-JB models). OMF-4S-JB model has the negative change in the median values within -6% over the entire range of initial damage states, indicating that accounting for the insufficient anchorage results in the slight increase in its vulnerability.
- The column shear model (OMF-4S-CS) is less vulnerable at lower initial damage states (IDS_0 to IDS_4) compared to the joint shear model (OMF-4S-JS). However, the percentage change in the median values between the two frame models is approximately -10% at all four limit damage states under severely mainshock-damaged condition (IDS_5), demonstrating that the column shear model is more vulnerable at this initial damage state. It is associated with the increased aftershock demand as a result of the dramatic loss in stiffness and strength of columns governed by shear failure under mainshock ground motions with IDS_5.
- The joint rigid offset model (OMF-4S-RO) is the least vulnerable structure because it behaves as flexure-dominated structures designed by the modern seismic codes. Particularly, in the table, the relative change in the median values significantly increases with positive values at higher limit states: 22~29% for the extensive damage state and 42~47% for the complete damage state. This observation demonstrates that analytical frame model without crucial components

such as beam-column joints and column shears may result in the underestimation of the aftershock demand.

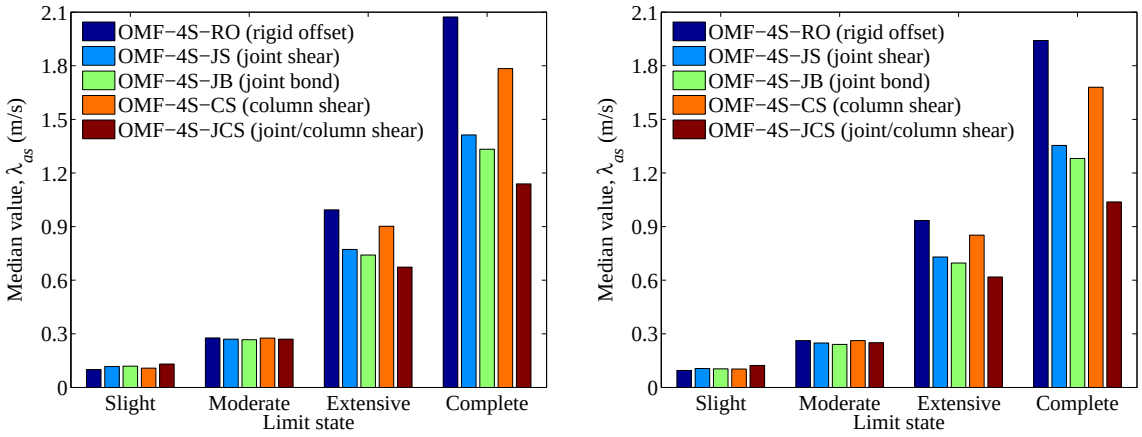

(a) IDS_0 (b) IDS_3

(c) IDS_4 (b) IDS_5

Figure 6.12 Median values of aftershock fragility curves with different modeling characteristics for OMF-4S frame

Table 6.12 Difference in median values with different modeling techniques for OMF-4S frame

IDS	Frame model	Slight	Moderate	Extensive	Complete
IDS_0	OMF-4S-RO (rigid offset)	-15	3	29	47
	OMF-4S-JS (joint shear)	–	–	–	–
	OMF-4S-JB (joint bond)	2	-1	-4	-6
	OMF-4S-CS (column shear)	-8	2	17	26
	OMF-4S-JCS (joint/column shear)	12	0	-13	-19
IDS3	OMF-4S-RO (rigid offset)	-10	5	28	43
	OMF-4S-JS (joint shear)	–	–	–	–
	OMF-4S-JB (joint bond)	-2	-3	-5	-5
	OMF-4S-CS (column shear)	-3	5	17	24
	OMF-4S-JCS (joint/column shear)	16	1	-15	-23
IDS_4	OMF-4S-RO (rigid offset)	-20	-2	25	45
	OMF-4S-JS (joint shear)	–	–	–	–
	OMF-4S-JB (joint bond)	1	0	-2	-4
	OMF-4S-CS (column shear)	-4	0	4	7
	OMF-4S-JCS (joint/column shear)	26	5	-16	-27
IDS_5	OMF-4S-RO (rigid offset)	-22	-5	22	42
	OMF-4S-JS (joint shear)	–	–	–	–
	OMF-4S-JB (joint bond)	7	3	-1	-4
	OMF-4S-CS (column shear)	-10	-10	-10	-11
	OMF-4S-JCS (joint/column shear)	25	5	-16	-27

§ Difference in median values = $(IDS_{i,others} - IDS_{i,jointshear}) / IDS_{i,jointshear} \times 100$ (%), where i = 0, 3, 4, 5.

6.4.2.2 Non-ductile 8-story space frame (OMF-8S frame)

Figure 6.13 shows the comparison of the median values with three different modeling techniques for the OMF-8S frame across the four limit states. The impact of the modeling characteristics on their aftershock fragility curves is examined by comparing the relative change in the median value of the curves, as presented in Table 6.13. As is the case of the OMF-4S frame, the relative change is computed on the basis of the reference frame model (OMF-8S-JS). The following bulleted list describes the effect of the modeling characteristics in the OMF-8S frame. The OMF-8S frame has the same trend as the OMF-4S frame.

- OMF-8S-JCS model is the most vulnerable when compared to other modeling types associated with the combined inelastic behavior of joint and column shears. However, for the slight damage state (limit), the positive change can be found (less vulnerable), which is due to the difference in the slope and intercept of the PADMs indicated in Table 6.4 and the usage of identical limit states for all frame models. However, as shown in Figure 6.13, the comparison of the median values with different analytical frame models indicates that the difference in the modeling characteristics is not significant at the slight or moderate damage states.
- The column shear model (OMF-8S-CS) is less vulnerable at IDS_0 through IDS_3 compared to the joint shear model (OMF-8S-JS). However, the percentage change in the median values between the two frame models is approximately -5% (-5%~-14%) at all four limit damage states under IDS_4 (IDS_5), thereby indicating that the column shear model is more vulnerable at these initial damage states. It can be explained that several columns (by shear failure) experience a considerable loss in stiffness and strength under mainshock ground motions corresponding to IDS_4 and IDS_5.

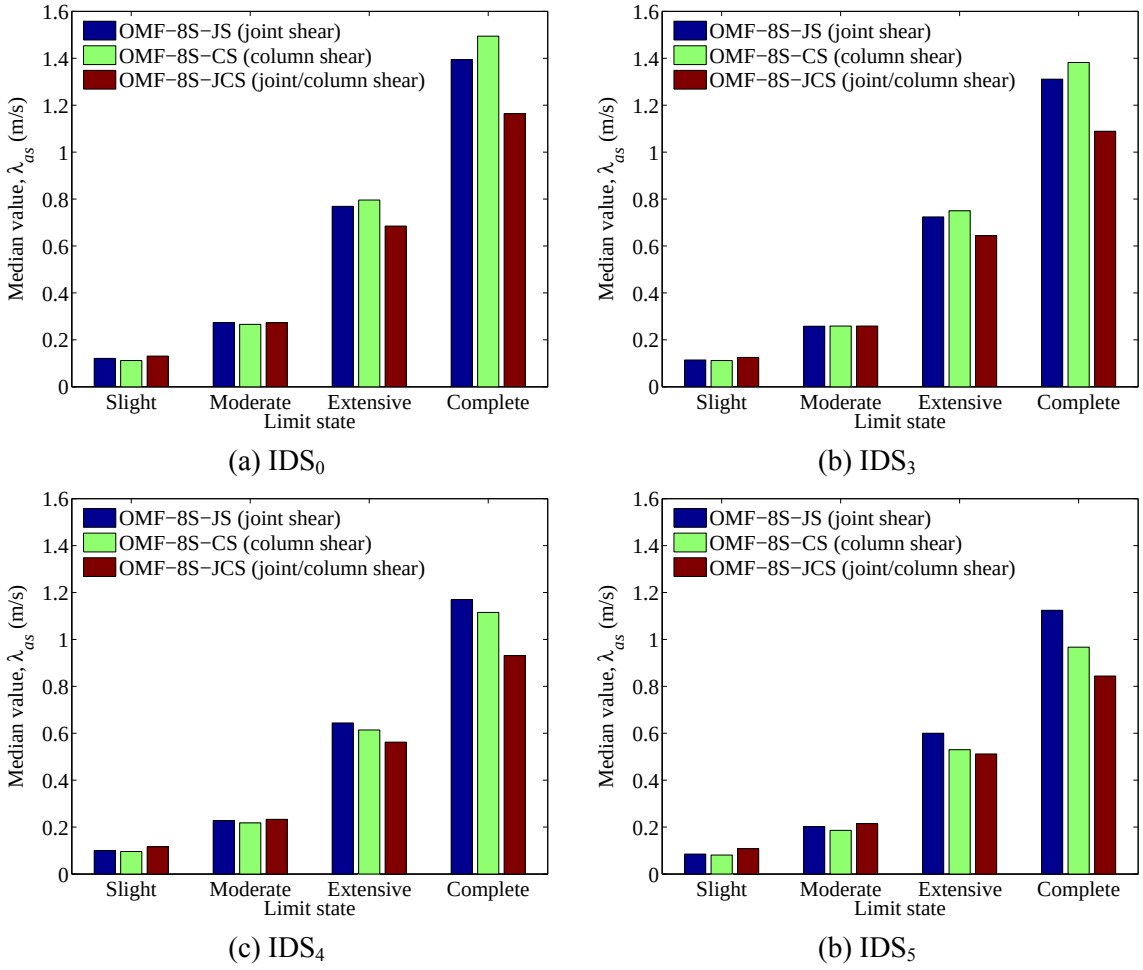

Figure 6.13 Median values of aftershock fragility curves with different modeling characteristics for OMF-8S frame

Table 6.13 Difference in median values with different modeling techniques for OMF-8S frame

IDS	Frame model	Slight	Moderate	Extensive	Complete
IDS$_0$	OMF-8S-JS (joint shear)	–	–	–	–
	OMF-8S-CS (column shear)	-7	-3	4	7
	OMF-8S-JCS (joint/column shear)	8	0	-11	-16
IDS3	OMF-8S-JS (joint shear)	–	–	–	–
	OMF-8S-CS (column shear)	-2	0	4	5
	OMF-8S-JCS (joint/column shear)	10	0	-11	-17
IDS$_4$	OMF-8S-JS (joint shear)	–	–	–	–
	OMF-8S-CS (column shear)	-4	-4	-5	-5
	OMF-8S-JCS (joint/column shear)	16	2	-13	-20
IDS$_5$	OMF-8S-JS (joint shear)	–	–	–	–
	OMF-8S-CS (column shear)	-5	-8	-12	-14
	OMF-8S-JCS (joint/column shear)	27	6	-15	-25

§ Difference in median values = ($IDS_{i,others}$ – $IDS_{i,jointshear}$) / $IDS_{i,jointshear}$ × 100 (%), where i = 0, 3, 4, 5.

6.4.2.3 Ductile 4-story perimeter frame (SMF-4P frame)

Figure 6.14 presents the median values for the SMF-4P frame with and without joint shear across the four limit states. The difference in the median values of the aftershock fragility curves is compared to examine the effect of the joint shear on their aftershock demand, as shown in Table 6.14. Unlike the OMF-4S frame, the relative change in the median value is calculated on the basis of the reference frame model (SMF-4P-RO, rigid offset model). SMF-4P-JS model is more vulnerable when compared to the analytical frame model without joint shear as a result of the increase in the aftershock demand due to joint shear. However, as is the case of the OMF-4S frame, the positive change can be found at the slight or moderate damage state in the table. This is attributable to the fact that the regression coefficient of the PADMs presented in Table 6.6. The effect of joint shear on the aftershock fragility curves is significant at the higher levels of the limit states: -7~-21% for the extensive damage state and -12~-27% for the complete damage state.

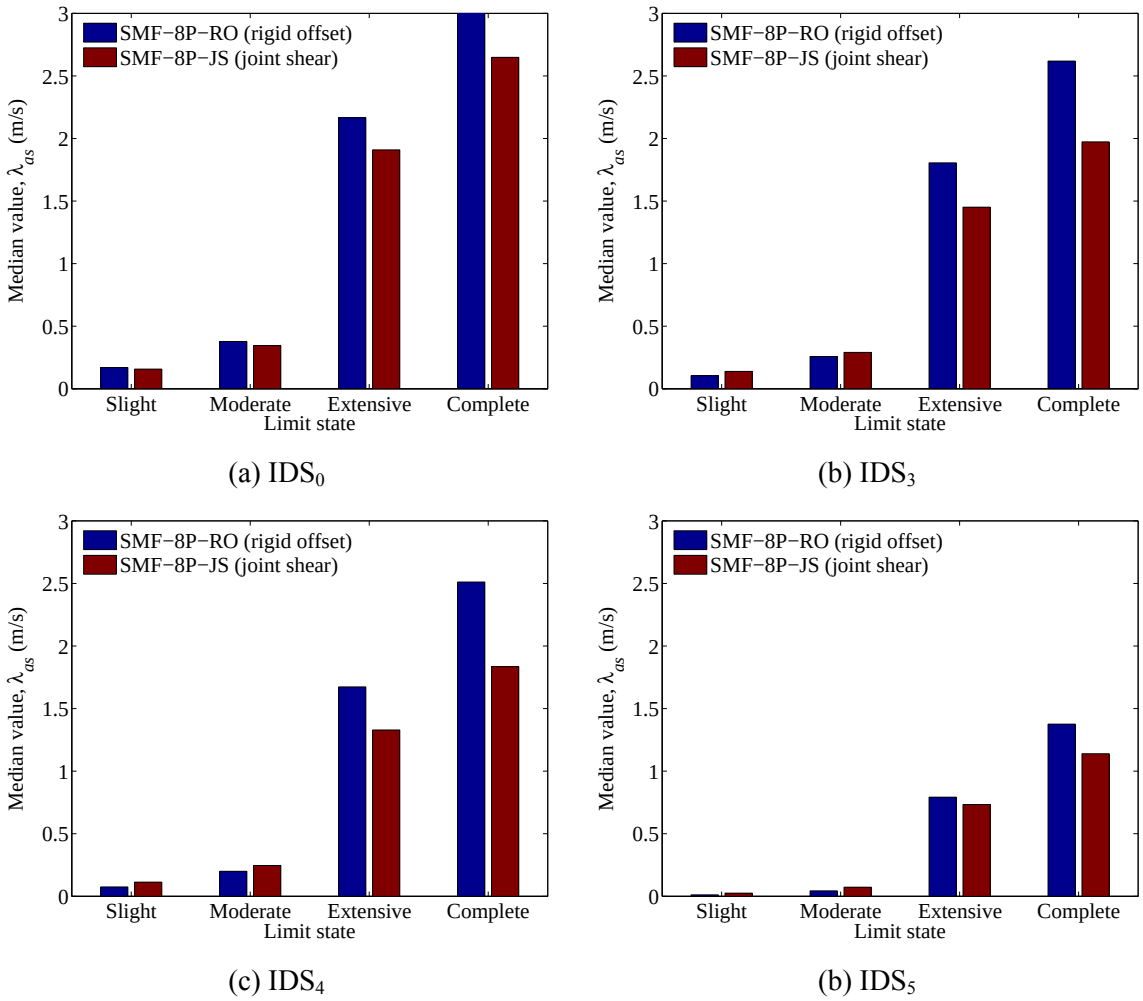

Figure 6.14 Median values of aftershock fragility curves with different modeling characteristics for SMF-4P frame

Table 6.14 Difference in median values with different modeling techniques for SMF-4P frame

IDS	Frame model	Slight	Moderate	Extensive	Complete
IDS$_0$	SMF-4P-RO (rigid offset)	–	–	–	–
	SMF-4P-JS (joint shear)	-7	-9	-12	-12
IDS3	SMF-4P-RO (rigid offset)	–	–	–	–
	SMF-4P-JS (joint shear)	32	13	-20	-25
IDS$_4$	SMF-4P-RO (rigid offset)	–	–	–	–
	SMF-4P-JS (joint shear)	51	23	-21	-27
IDS$_5$	SMF-4P-RO (rigid offset)	–	–	–	–
	SMF-4P-JS (joint shear)	108	66	-7	-17

§ Difference in median values = ($IDS_{i,jointshear}$ – $IDS_{i,rigidoffset}$) / $IDS_{i,rigidoffest}$ × 100 (%), where i = 0, 3, 4, 5.

6.4.2.4 Ductile 8-story perimeter frame (SMF-8P frame)

Figure 6.15 depicts the median values for the SMF-8F frame with and without joint shear across the four limit states. The difference in the median values of the aftershock fragility curves is compared to investigate the effect of the joint shear on their seismic demand, as indicated in Table 6.15. As is the case of the OMF-4S frame, the relative change in the median value is calculated on the basis of the reference frame model (rigid offset model). The joint shear model (SMF-8P-JS) is more vulnerable when compared to the analytical frame model without joint shear as a result of the increase in the aftershock demand due to joint shear. However, as is the case of the OMF-4S frame, the positive change can be found at the slight or moderate damage state in the table, which is owing to the fact that the regression coefficient such as the slope and intercept of PADMs listed in Table 6.7. Nevertheless, as shown in Figure 6.15, the comparison of the median values for the frame models with and without joint shear demonstrates that this difference is negligible at the slight or moderate damage states. On the other hand, the impact of joint shear on the structural performance is considerable at the higher levels of the limit states: -4~-18% and -11~-20% for the extensive and complete damage states, respectively.

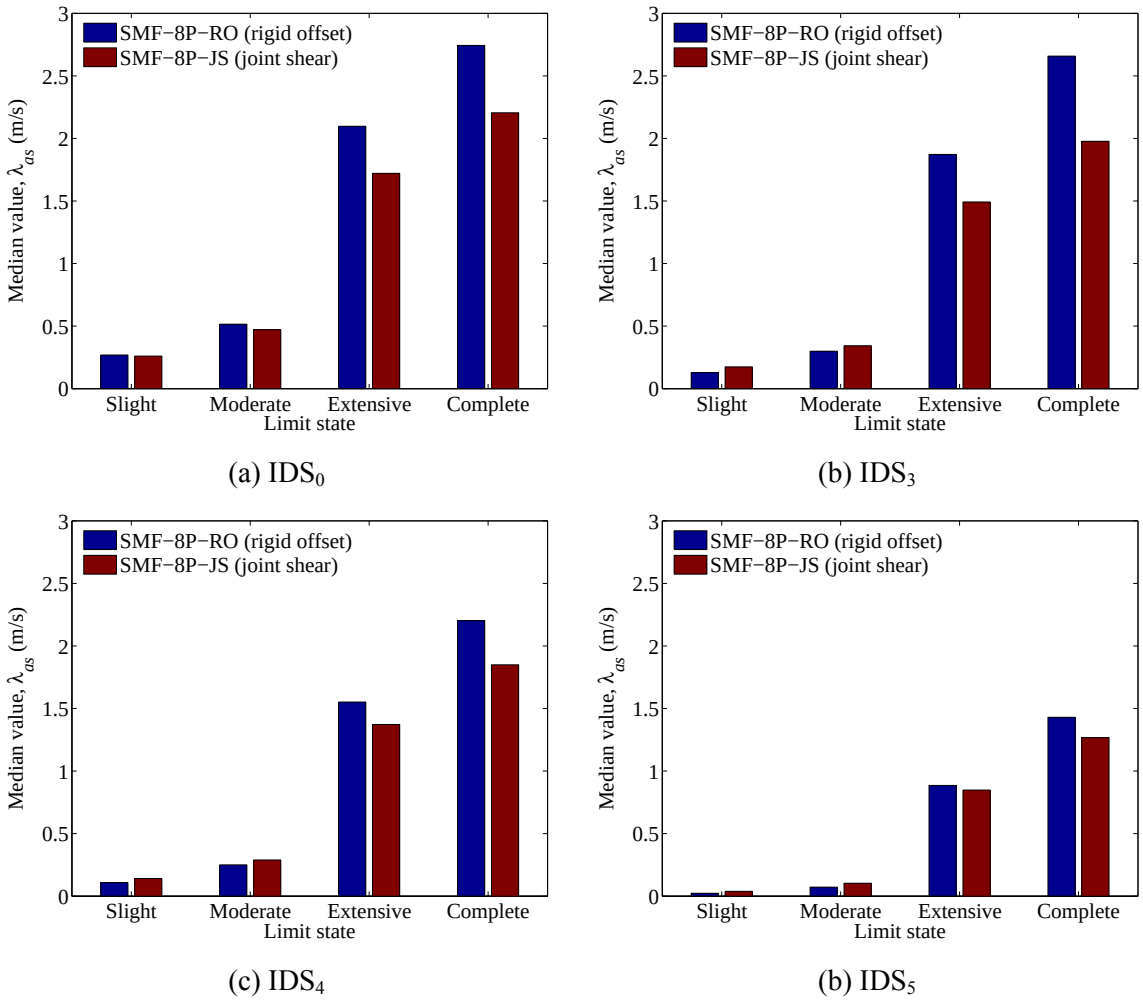

(a) IDS_0 (b) IDS_3

(c) IDS_4 (b) IDS_5

Figure 6.15 Median values of aftershock fragility curves with different modeling characteristics for SMF-8P frame

Table 6.15 Difference in median values with different modeling techniques for SMF-8P frame

IDS	Frame model	Slight	Moderate	Extensive	Complete
IDS_0	SMF-8P-RO (rigid offset)	–	–	–	–
	SMF-8P-JS (joint shear)	-3	-8	-18	-20
IDS3	SMF-8P-RO (rigid offset)	–	–	–	–
	SMF-8P-JS (joint shear)	36	15	-20	-26
IDS_4	SMF-8P-RO (rigid offset)	–	–	–	–
	SMF-8P-JS (joint shear)	31	16	-12	-16
IDS_5	SMF-8P-RO (rigid offset)	–	–	–	–
	SMF-8P-JS (joint shear)	70	43	-4	-11

§ Difference in median values = $(IDS_{i,jointshear} - IDS_{i,rigidoffset}) / IDS_{i,rigidoffest} \times 100$ (%), where i = 0, 3, 4, 5.

6.4.3 Comparison of RC frames

The influence of frame types with an identical modeling technique on the median values of their aftershock fragility curves is investigated in order to evaluate their relative vulnerability under different mainshock-damaged conditions. For this purpose, four types of modeling characteristics are selected in this research: joint shear for all frames, column shear with and without joint model for four frames, and joint rigid offset for three frames.

6.4.3.1 Comparison of RC frames with joint shear

The median values of aftershock fragility curves for six RC frames (OMF-4S, OMF-8S, OMF-4P, OMF-8P, SMF-4P, SMF-8P) with joint shear are plotted in terms of four initial damage states (IDS_0, IDS_3, IDS_4, and IDS_5) and limit states in Figure 6.16. Since non-ductile and ductile RC frames have different maximum drifts corresponding to initial damage states, as mentioned in Chapter 5, the comparison of aftershock fragility curves for these frame types is performed for only undamaged condition (IDS_0). The following bulleted list addresses the difference in the vulnerability of the frames with joint shear.

- For non-ductile frames, the OMF-4P frame is the most vulnerable, followed by OMF-8P, because the median values are the smallest values across the four limit states as well as the four initial damage states. Perimeter frames are more vulnerable than space frames as a result of their inherent characteristic (P-Δ effects) and smaller maximum joint shear strength. Furthermore, there is no or a little difference between the OMF-4S and OMF-4P frames. In this case, the building height does not affect the vulnerability of these structures.

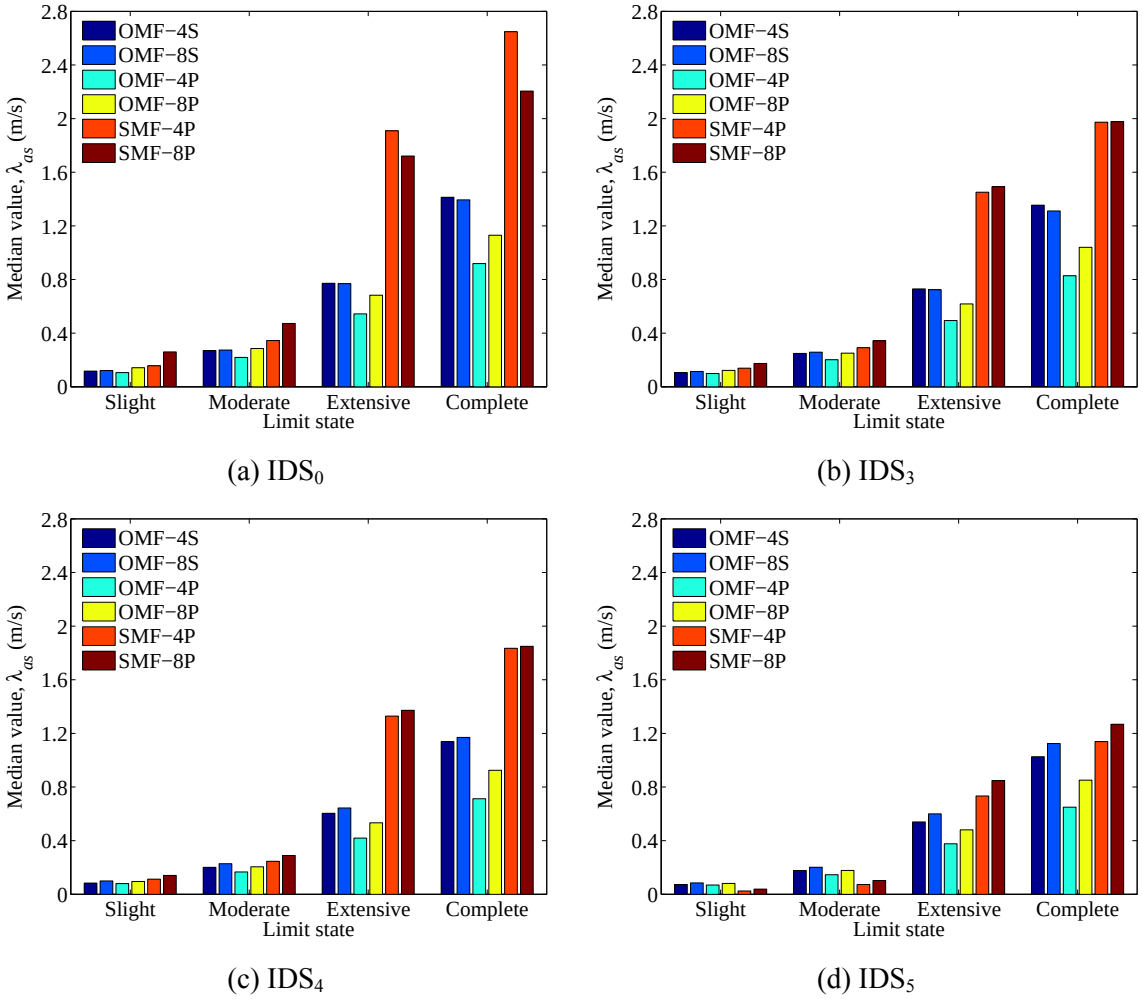

(a) IDS_0 (b) IDS_3

(c) IDS_4 (d) IDS_5

Figure 6.16 Comparison of median values for RC frames with joint shear

- For ductile frames, the SMF-4P frame is more vulnerable for all damaged conditions (IDS_3 to IDS_5), as shown in Figure 6.16(b), 6.16(c), and 6.16(d). On the other hand, in the case of undamaged condition (IDS_0), the SMF-8P frame is more considerably vulnerable at the extensive and complete damage states, as depicted in Figure 6.16(a). This difference can be explained by the fact that the SMF-4P frame actually experiences more damage even if two frames have the same initial damage states corresponding to maximum interstory drifts.

- For frame models with joint shear, as mentioned before, the comparison of median values is conducted for the undamaged condition (IDS_0), as depicted in Figure 6.16(a). The OMF-4P frame is the most vulnerable while the OMF-8P is the least vulnerable. From the figure, the difference in the median values between non-ductile and ductile RC frames is observed, particularly extensive and complete damage states. It is attributed to the fact that the slight difference in the median values of the capacity model for both non-ductile and ductile frames.

6.4.3.2 Comparison of RC frames with column shear and with joint and column shear

The median values of aftershock fragility curves for four non-ductile RC frame models (OMF-4S-CS and OMF-8S-CS for column shear and OMF-4S-JCS and OMF-8S-JCS for combined joint and column shear) are plotted in terms of four initial damage states (IDS_0, IDS_3, IDS_4, and IDS_5) and limit states in Figure 6.17. The following bulleted list describes some important findings for aftershock fragility results of the frames with column shear.

- As mentioned in Section 6.4, the non-ductile RC frames including the combined joint and column shear modeling are more vulnerable when compared to those with only column shear. OMF-4S-JCS model is the most vulnerable structure while OMF-4S-CS model is the least vulnerable.
- For non-ductile frames with column shear, the OMF-4S frame is more vulnerable except for IDS_5. Figure 6.17(d) infers that the OMF-8S frame undergoes more severe damage under mainshock ground motions associated with IDS_5 even if the same initial damage state is imposed for the two frames.

- For non-ductile frames with joint and column shear, the OMF-4S frame is more vulnerable across the four limit states and initial damage states.

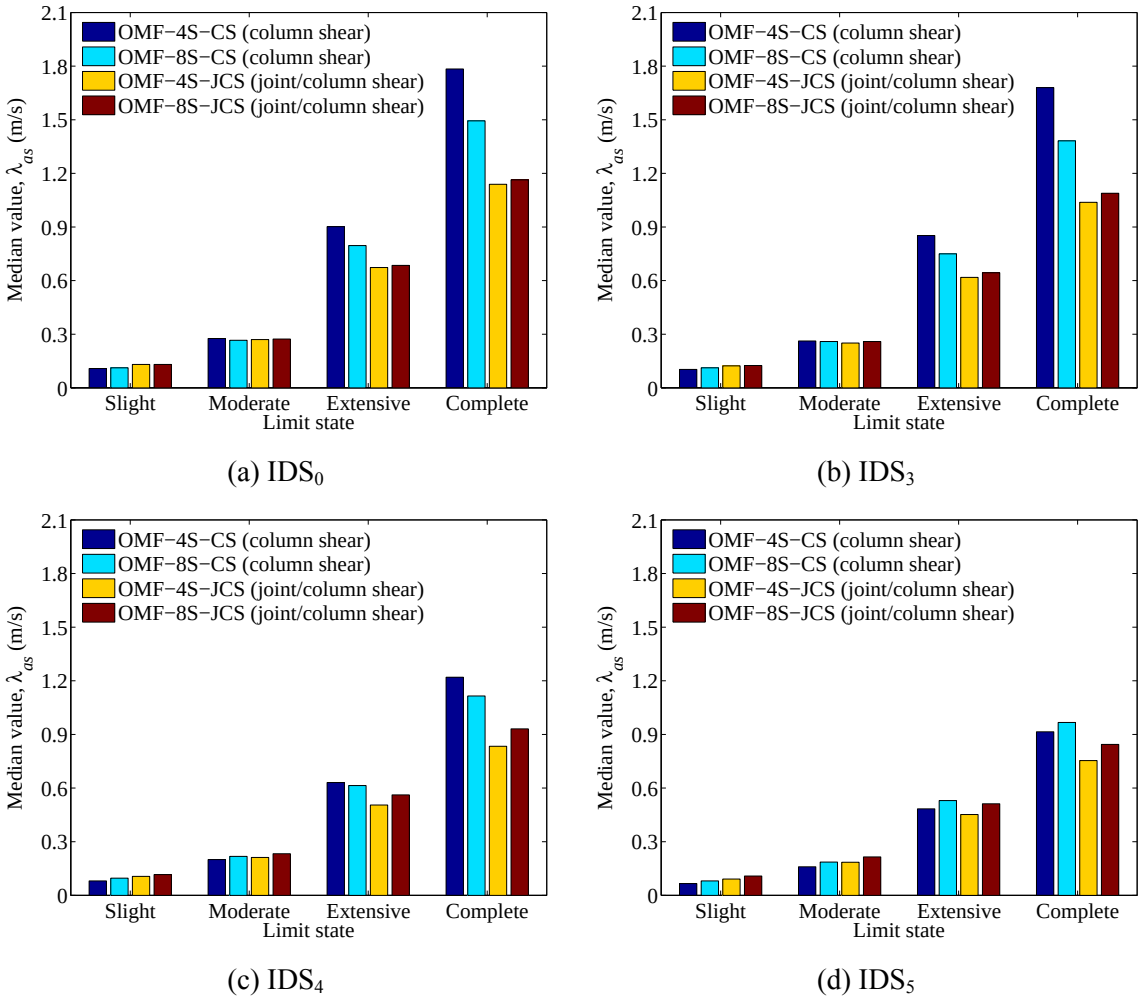

Figure 6.17 Comparison of median values for RC frames with joint shear

6.4.3.3 Comparison of RC frames with joint rigid offset

The median values of aftershock fragility curves for three RC frames (OMF-4S, SMF-4P, SMF-8P with joint rigid offset model are plotted in terms of four initial damage states (IDS$_0$, IDS$_3$, IDS$_4$, and IDS$_5$) and four capacity limit states in Figure 6.18. As mentioned in Section 6.4.2.1, the direct comparison of aftershock fragility curves for non-ductile and

ductile frames is performed for only undamaged condition (IDS_0). The following are some of the significant findings of this chapter.

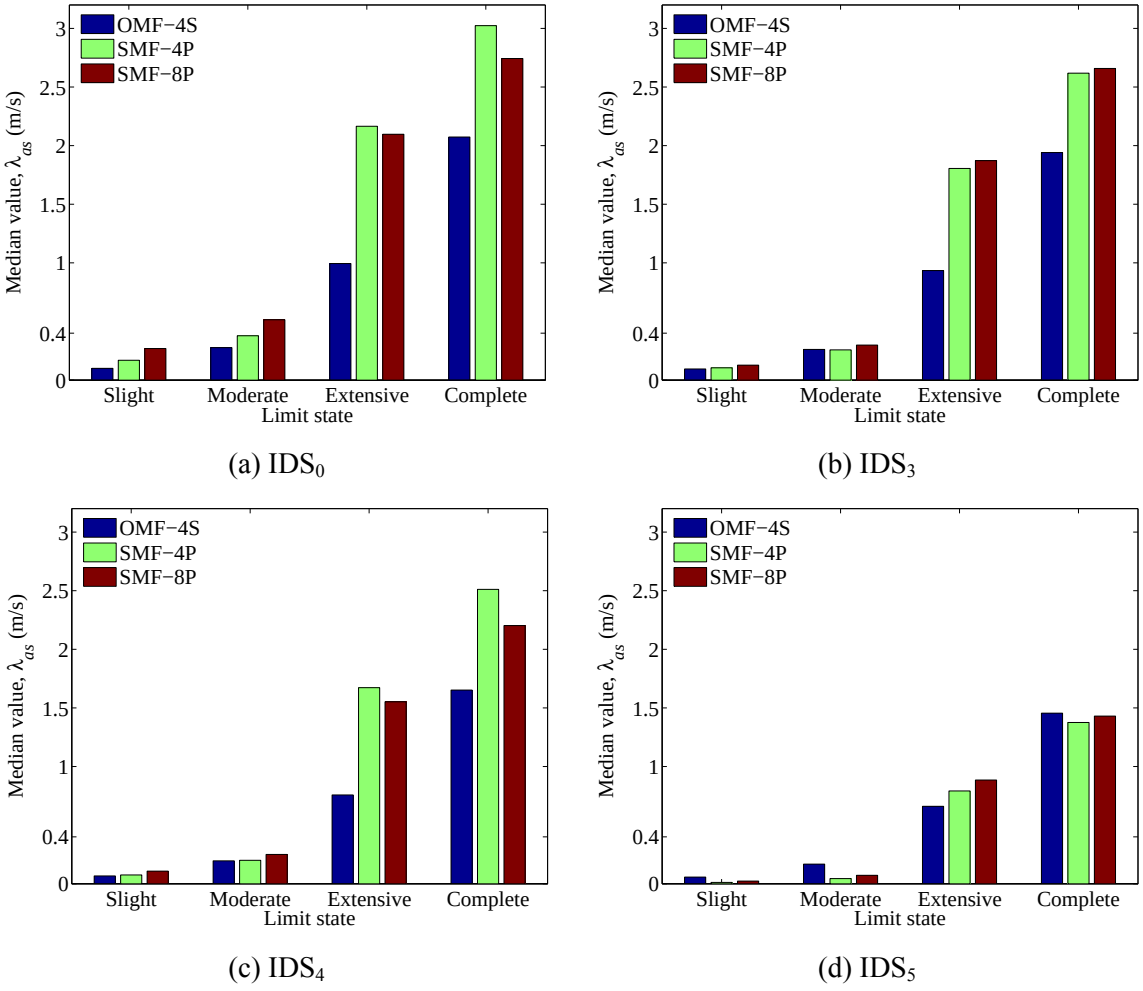

Figure 6.18 Comparison of median values for RC frames with joint rigid offset model

- For ductile frames, the SMF-8P frame is more vulnerable across under IDS_0 and IDS_4 while the SMF-4P frame is more vulnerable under IDS_3 and IDS_5. The relative vulnerability is different for each mainshock-damaged condition
- For non-ductile and ductile frame models, the median values are compared for the undamaged condition (IDS_0), as depicted in Figure 6.18(a). The OMF-4P frame is

still the most vulnerable among all three frame models even if it does not include the analytical modeling of the critical components. It is due to the fact that the column design follows the older design codes such as widely spaced transverse reinforcement and lower concrete strength.

6.4.4 Simulation method of damaging earthquakes

This section presents the applicability of cyclic pushover analysis (CPO) approach generating hypothetical mainshocks to the development of aftershock fragility curves. This is accomplished by comparing these aftershock fragility results with those from IDA approach. In contrast to the IDA approach, the CPO approach can be easily applied and much less computationally intensive. To generate the aftershock fragility curves using the CPO approach, OMF-4S-JS model is selected in this research. In addition to the description in Section 5.5.2, the input drift history is defined as shown in Figure 6.19(a); maximum roof drift is determined where maximum interstory drift reaches the target drift associated with an initial damage state; each drift of total seven drift levels has two cycles to account for the cyclical effect (stiffness and strength deterioration); and residual drifts are assumed to be 0%, 5%, 6%, 7%, 10%, and 13% of maximum drifts for IDS_1, IDS_2, IDS_3, IDS_4, IDS_5, and IDS_6, respectively, which are the median values obtained from the IDA approach. Figure 6.19(b) shows the associated base shear-roof drift relationship for the frame model. The simulated results describe the stiffness and strength deterioration of associated with cyclic loadings.

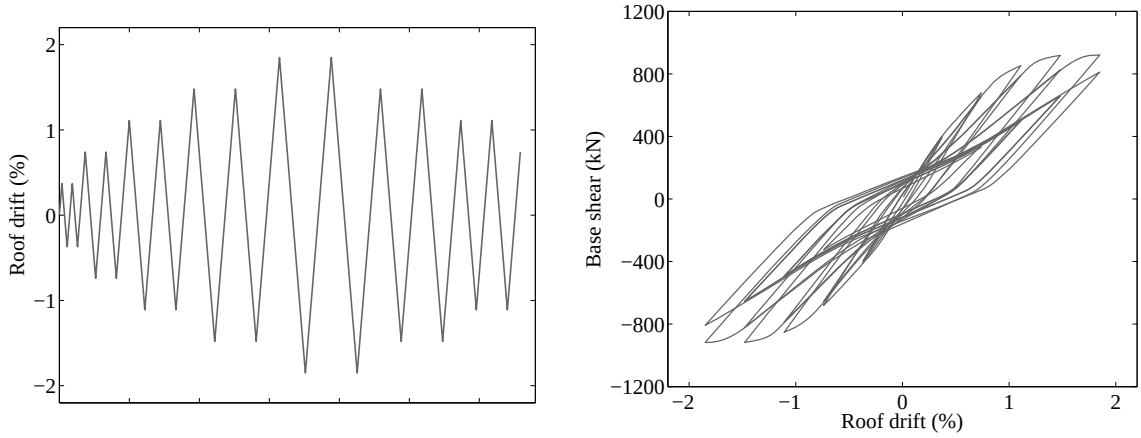

(a) Imposed input drift (b) Cyclic behavior

Figure 6.19 Imposed roof drift history and associated base shear-roof drift hysteresis

Figure 6.20(a) and Figure 6.20(b) depict the comparison plots for the aftershock fragility curves with different IDSs at the extensive and complete limit states, respectively, using the IDA and CPO approaches. The aftershock fragility curves have same trend as the results of IDA approach in that the probability of being in a damage state increases over the entire range of PGV_{as} as the extent of initial damage state is more severe. Moreover, Figure 6.21 shows the comparison of the median values of the aftershock fragility curves for the IDA and CPO approaches with different initial damage states and capacity limit states. The difference in the median values between the IDA and CPO approaches is very small at lower limit states (slight and moderate), but the percentage change in the median values is -10% at the complete limit state of IDS_4 and IDS_5, thereby indicating that, in the case of using the CPO approach, a mainshock-damaged structure is more vulnerable to an aftershock ground motion. Additionally, the CPO approach can provide conservative results within a reasonable margin of 10%, and

therefore it can be easily utilized where the rapid evaluation of aftershock fragility assessment is needed.

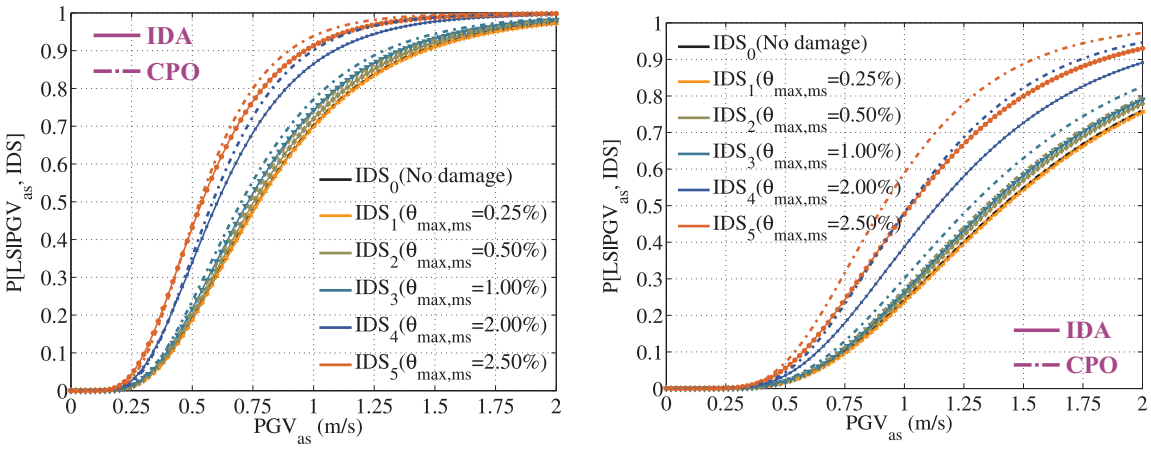

(a) Extensive damage state (b) Complete damage state

Figure 6.20 Comparison of aftershock fragility curves using IDA and CPO approaches

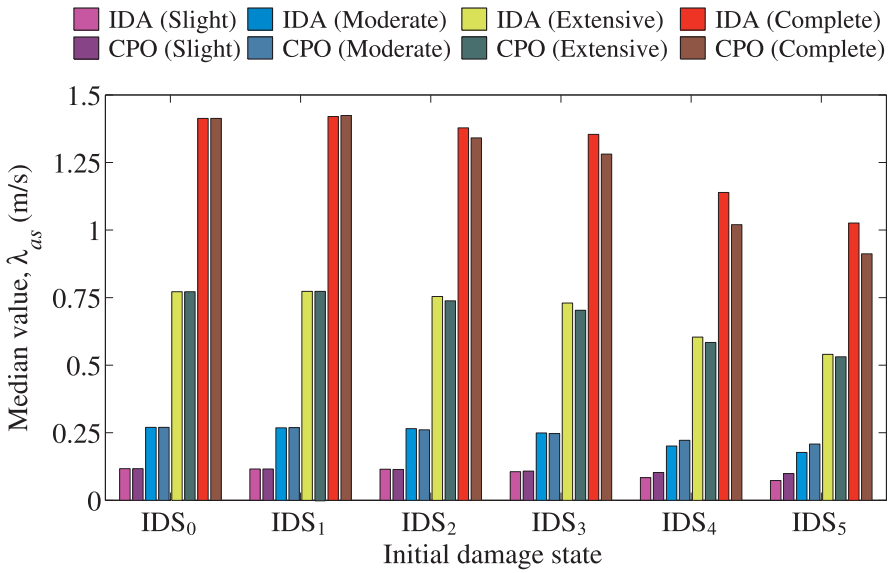

Figure 6.21 Comparison of median values with different IDSs using IDA and CPO approaches

6.4.5 Sensitivity analysis for degrading slope in joint shear model

To investigate the effect of the descending branch in joint shear model on the seismic performance and aftershock fragility curves, two joint shear models with different degrading behavior are described in addition to the original joint shear model: baseline model with original descending slope (K_{deg}), Model 1 ($0.5K_{deg}$), and Model 2 ($1.5K_{deg}$), as shown in Figure 6.22. The original joint shear model (baseline) is constructed using the mean value of the joint modeling parameters obtained through the model validation, listed in Table 3.7 and Table 3.8 for non-ductile beam-column joints or Table 3.11 and Table 3.12 for ductile beam-column joints. For this sensitivity analysis, the OMF-4S-JS model is chosen, and its two models are newly modeled with different degrading behavior for all joints in this section. Then, the aftershock fragility curves for undamaged condition (IDS_0) and damaged condition (IDS_5) are generated across the four limit damage states.

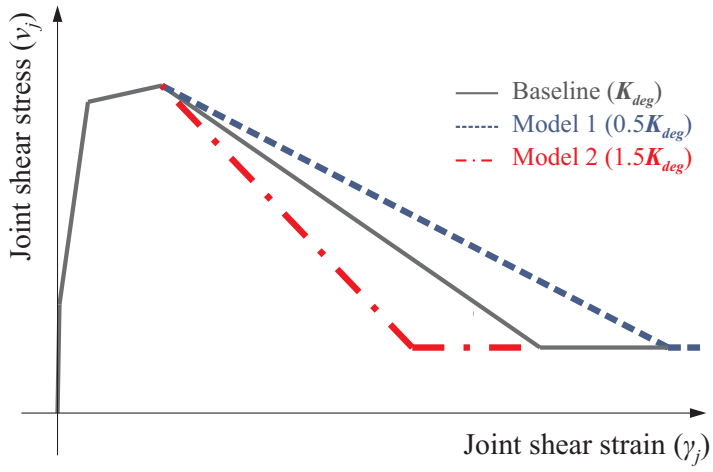

Figure 6.22 Joint shear models with different degrading behaviors

Figure 6.23(a) and Figure 6.23(b) depict the aftershock fragility curves with different joint degrading behavior at the complete limit state under undamaged (IDS_0) and damaged (IDS_5) conditions, respectively. It can be indicated that there is no or little difference in the aftershock fragility curves between the baseline model and Model 1 ($0.5K_{deg}$). Additionally, the relative change in the median values between the baseline model and Model 2 ($1.5K_{deg}$) is approximately -2% and -7% for IDS_0 and IDS_5, respectively. However, the joint degrading behavior does not significantly affect the aftershock fragility curves although the median values are slightly reduced with an increase in the descending slope. It may be attributed to the fact that the suite aftershock ground motions includes a wide range of their intensity (from small to large earthquakes) and many of them are not large enough to produce the joint deformation after maximum joint shear strength.

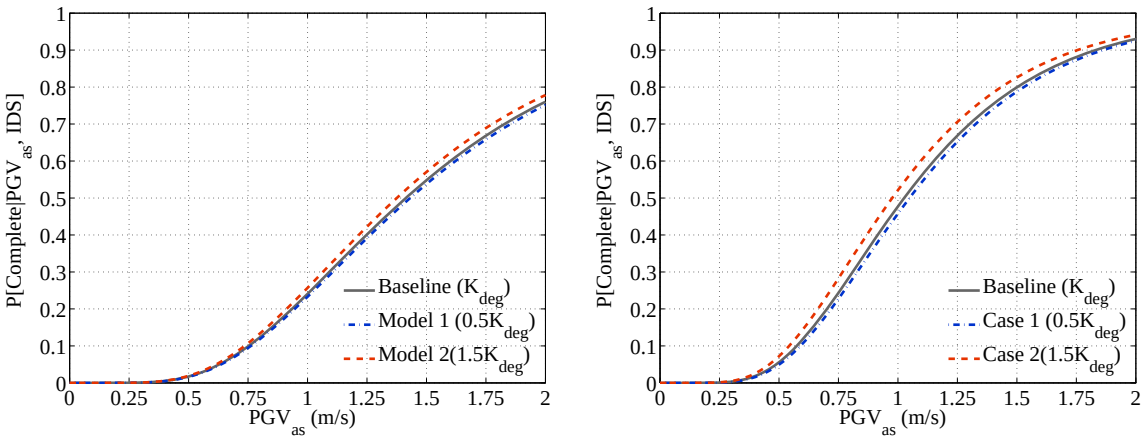

(a) IDS_0 (complete damage) (b) IDS_5 (complete damage)

Figure 6.23 Aftershock fragility curves for joint shear models with different degrading behaviors

6.5 Summary

PADMs and aftershock fragility curves with different initial damage states are generated for non-ductile and ductile RC frames chosen in this research with various modeling characteristics in order to investigate how the extent of existing damage associated with mainshocks affects the additional damage as a result of aftershock ground motions. To probe the increased vulnerability associated with the accumulation of damage, the aftershock fragility curves are compared in terms of the relative change in their median values.

The following are some of the significant findings of this chapter:

- For all RC frame models, as the extent of damage associated with mainshocks is more severe (as the initial damage state increases), the probability of being in a damage (limit) state given a PGV_{as} increases for all four limit states over the entire range of PGV_{as}, thereby resulting in the increased vulnerability of structures subjected to multiple earthquakes. Crossover fragility curves are not observed for all RC frame models, thereby demonstrating the appropriate selection of the identical suite of aftershock ground motions. Additionally, the aftershock fragility curves for IDS_0 through IDS_2 are almost identical, because the components remain elastic under these mainshock ground motions, as explained in the PADM generation.
- For non-ductile RC frames, the joint and column shear model is the most vulnerable when compared to other modeling types associated with the concurrent inelastic action (cyclic deterioration) of joint and column shears. Additionally, as a result of inadequate embedment length in joints, the joint bond model is a more

vulnerable structure compared to the joint shear model. Moreover, the column shear model is more vulnerable when many columns experiences inelastic shear behavior (IDS_5) when compared to the joint shear model. Finally, the joint rigid offset model is the least vulnerable structure since it behaves as a ductile frame.

- For ductile RC frames, the impact of joint shear on the aftershock demand of structures is more vulnerable because the inelastic action in joints reduces the column shear force as well as increases the aftershock demand. Thus, the conventional analytical modeling technique such as the rigid offset method is not appropriate for evaluating the seismic performance for ductile frames experiencing significant joint deformations.
- The cyclic pushover analysis (CPO) approach, an alternative approach for simulating damaging earthquakes, is introduced. The aftershock fragility curves using the CPO approach are compared with those using incremental dynamic analysis (IDA) approach commonly employed in this research. The CPO approach offers reasonable results compared to the IDA approach, and therefore, since it is computationally efficient, it can be easily employed when rapid estimation is required.

CHAPTER 7

CONCLUSIONS AND FUTURE WORK

7.1 Summary and Conclusions

Although the knowledge and technology of seismic analysis and seismic risk assessment tools have rapidly advanced in the past several decades, current seismic design codes and damage estimation methods ignore the effect of successive earthquakes on structures. In light of recent strong seismic events, mainshock-damaged structures are shown to be more vulnerable to severe damage and collapse. The increase in aftershock vulnerability significantly threatens the safety of occupants in these structures. Additionally, a mainshock-damaged structure may increase the risk of major damage or building collapse and the associated loss of life and property. The increased vulnerability estimation associated with the additional damage plays a significant role in assessing potential losses to facilitate crucial decision making such as emergency response mobilization, inspection priority, recovery strategy, and re-occupancy decision. The main objective of this research is to develop a probabilistic framework to account for these increased vulnerabilities in terms of the extent of damage associated with mainshock ground motions. Aftershock fragility curves are developed accounting for both the uncertainty from the seismic hazard and the uncertainty from the structural capacity. This proposed approach also allows for the inherent variability, such as modeling characteristics associated with the design codes, present in non-ductile and ductile RC frames found in California.

For a reliable estimate of seismic risk assessment, the accurate analytical models of RC frame's primary components reflecting the design codes such as their reinforcing details is established. Following a review of existing analytical modeling techniques, the analytical models describing shear behavior in the columns and shear or bond responses in the joints of the RC frames are employed, modified, and developed in this research. To resolve the drawback of an existing model (Elwood 2004), this research substantiates the applicability of the model to experimental older columns subjected to reversed cyclic pushover loadings by comparing the analytical results from experimental results available in the literature. For beam-column joint models, an existing joint shear stress-strain model is utilized with modification to the degrading slope in order to form its backbone curve. Since this model was developed for non-ductile interior joints, this research shows the applicability of the model to other joint types such as non-ductile exterior joints, ductile exterior and interior joints by comparing experimental results with analytical predictions. In addition, reduced joint shear strength associated with insufficient anchorage is accounted for by employing an existing bond strength model for non-ductile joints with discontinuous beam bottom reinforcement. Finally, hysteric rules including the effect of cyclic deterioration are extracted in comparison to experimental results. Application of the proposed column shear model and beam-column joint model for seismic demand analyses of RC frames demonstrates the significance of capturing the inelastic response of the components accurately in assessing their seismic performance.

A major task in the current research is to seek an understanding of the RC building inventory in a region which can reflect the design and detailing aspects of non-ductile and ductile RC frames. For this purpose, non-ductile and ductile RC frames

designed by Liel (2008) and Haselton (2006), respectively, are selected in this research, whose frames are representative of design and construction practices as well as typical of office buildings and industrial facilities in California. Based on the building information and analytical modeling techniques of components, high fidelity analytical frame models accounting for geometric and material nonlinearities are created in OpenSees (McKenna et al. 2010). Moreover, since the joint model presented in the model validation is developed based on experimental joint shear strength, the non-ductile joint shear strength model is proposed in order to ensure the applicability of this joint model to analytical frame models. The joint strength model is obtained through the statistical method based on collected experimental results available in the literature. Finally, the seismic performance for these analytical frame models is evaluated through the pushover analysis and nonlinear time history analysis. Not only do the analytical models with joint shear increase the drift demand, they also reduce the maximum shear force and initial stiffness due to the spread of inelastic action into joints. The analytical frame model with joint shear and column shear is the most vulnerable because it has a sudden drop of lateral load resistance in pushover analysis and the largest maximum and residual deformation in both analyses. However, it is observed that the concentrated inelastic action in joints delays the inelastic shear response in columns compared to the frame model with only column shear.

A framework for the development of analytical aftershock fragility assessment is described in order to develop a quantitative evaluation tool for their accumulated damage and increased vulnerability associated with aftershock ground motions. Aftershock fragility curves relate the probability of meeting or exceeding a particular limit state

given an imposed aftershock intensity demand. Unlike existing aftershock fragility assessment using a stripe approach (IDA), the framework is developed using a cloud method (NTHA) for aftershock analysis to account for realistic ground motions that can occur at the site of interest. Details about various parts of the framework including the stochastic analytical frame models with material uncertainties, assembling a ground motion (mainshock and aftershock) motion suite, simulating damaging earthquakes associated with the characterization of existing mainshock-damaged conditions (initial damage states), performing mainshock-aftershock analyses, computing probabilistic aftershock demand models (PADMs), defining the capacity limit state models, and generating aftershock fragility curves. Particularly, the mainshock-damaged condition of structures can be achieved by linking visible damage with member response based on the observation of existing experimental column tests and by generating mainshock ground motions through IDA or CPO approach. Additionally, the aftershock fragility function is developed by modifying the classical fragility function and by assuming the lognormal distribution of aftershock demand and capacity limit state. Moreover, the ground motions with smaller aftershock intensity do not considerably affect the final responses for mainshock-damaged structures, and therefore, aftershock ground motions that can cause the additional damage to structures should be selected.

PADMs and aftershock fragility curves with different initial damage states are generated for non-ductile and ductile RC frames with various modeling characteristics and frame attributes in order to investigate how the extent of existing damage associated with mainshocks affects the additional damage as a result of aftershock ground motions. To probe the increased vulnerability associated with the accumulation of damage, the

aftershock fragility curves are compared in terms of the relative change in their median values. The following are some of the main findings from the aftershock fragility analysis:

- For all RC frame models, as the extent of damage associated with mainshocks is more severe (as the initial damage state increases), the probability of being in a damage (limit) state given a PGV_{as} increases for all four limit states over the entire range of PGV_{as}, thereby resulting in the increased vulnerability of structures subjected to multiple earthquakes. Crossover fragility curves are not observed for all RC frame models, thereby demonstrating the appropriate selection of the identical suite of aftershock ground motions.
- For non-ductile RC frames, the joint and column shear model is the most vulnerable when compared to other modeling types associated with the concurrent inelastic action (cyclic deterioration) of joint and column shears. Additionally, as a result of inadequate embedment length in joints, the joint bond model is a more vulnerable structure compared to the joint shear model. Moreover, the column shear model is more vulnerable when many columns experiences inelastic shear behavior (IDS_5) when compared to the joint shear model. Finally, the joint rigid offset model is the least vulnerable structure since it behaves as a ductile frame.
- For ductile RC frames, the impact of joint shear on the aftershock demand of structures is more vulnerable because not only does the inelastic action in joints reduce the column shear force but also increases the aftershock demand. Thus, the conventional analytical modeling technique such as the rigid offset method is not appropriate for evaluating the seismic performance for ductile frames experiencing significant joint deformations.

- The cyclic pushover analysis (CPO) approach, an alternative approach for simulating damaging earthquakes, is introduced. The CPO approach provides reasonable results compared to the IDA approach, and therefore, since it is computationally efficient, it can be easily employed when rapid estimation is required.

7.2 Research Impact

This research presents a rigorous probabilistic performance assessment framework in an aftershock environment to develop aftershock fragility curves for common non-ductile and ductile RC frames in California. A primary contribution of this research is the refinement and evaluation of an approach for the generation of aftershock fragility curves that would facilitate a quantitative evaluation of the increased vulnerability and cumulative damage potential of RC frames in terms of their mainshock-damaged conditions. Additional benefits and contributions of this research include the following:

- High fidelity analytical models allowing for an in-depth understanding of the performance and behavior of RC frames common to California.
- A deep understanding of the impact of various modeling considerations on the seismic vulnerability of RC buildings.
- The output in this research will not only be a means to provide a building tagging methodology for making evacuation and re-occupancy decisions, but also a reliable analytical damage estimation tool prior to building visual inspection.

- The aftershock fragility curves can be used in the seismic loss assessment package tool, HAZUS-MH, to provide a better estimate of the vulnerability of RC buildings undergoing repeated earthquake loadings.

7.3 Recommendation for Future Work

The work in the present research should be extended through additional research in the following areas:

- This research looked at the vulnerability assessment of low- and mid-rise RC frames to reduce the computational intensity of the analyses. However, the aftershock fragility curves for high-rise RC frames should be expanded to investigate the effect of building heights on the aftershock demand analyses.
- This research involved the relationship between visible damage and response of columns to define the existing mainshock-damaged conditions of structures. However, damage is unlikely to be only concentrated in columns during earthquakes. Therefore, performance and collapse potential associated with other factors such as beam-column joints should be investigated.
- The link between visible damage and response mechanism is quantified in terms of the maximum drift of columns. However, other engineering demand parameters such as residual drift will serve as a damage indicator to evaluate their residual capacity after earthquakes.
- Provided that the correlation of visible damage with component response is established, this framework can be also extended to bridge structures or steel buildings to investigate the cumulative effect of multiple earthquakes on their

load carrying capacity. Particularly, this framework can be applied to concrete bridge structures without additional efforts.

- Three-dimensional effects including the torsional motions and irregularities as well as the presence of masonry infill walls should be incorporated in the finite element frame models and their influences on the seismic demand response of RC frames should be addressed.
- The modeling parameters of Pinching4 material utilized in the beam-column joint models are employed as the median values of those obtained from the model validation. The automatic formulation that can calculate the values of damage parameters would be required through the statistical method based on material and geometry properties, as is the case of the determination of joint shear strength.

APPEDIX A

ANALYTICL RESULTS OF FRAME'S COMPONENTS

This appendix provides the comparison of experimental results with analytical predictions for RC frame's critical components: shear-dominated columns, non-ductile exterior and interior beam-column joints experiencing the joint shear failure and joint bond failure, and ductile exterior and interior beam-column joints. Figure A.1 presents the comparison of experimental and analytical shear force-drift hysteresis for shear-dominated columns, and Table A.1 indicates the comparison of experimental and analytical maximum column shear force. Figure A.2 and A3 depict the comparison of experimental and analytical lateral force-deformation (drift) hysteresis for non-ductile exterior beam-column joint assemblages exhibiting the joint shear failure and joint bond failure, respectively. Table A.2 presents the comparison of experimental and analytical maximum lateral force for these joints. Figure A.4 shows the comparison of experimental and analytical lateral force-deformation (drift) hysteresis for non-ductile interior beam-column joint subassemblages, and Table A.3 indicates the comparison of experimental and analytical maximum lateral force for these joint. Figure A.5 and Figure A.6 present the comparison of experimental and analytical lateral force-deformation (drift) hysteresis for ductile exterior and interior, respectively, beam-column joint subassemblages. Table A.4 and Table A.5 indicate the comparison of experimental and analytical maximum lateral force for these exterior and interior joints, respectively.

A.1 Simulated Response for Flexure-Shear-Critical Columns

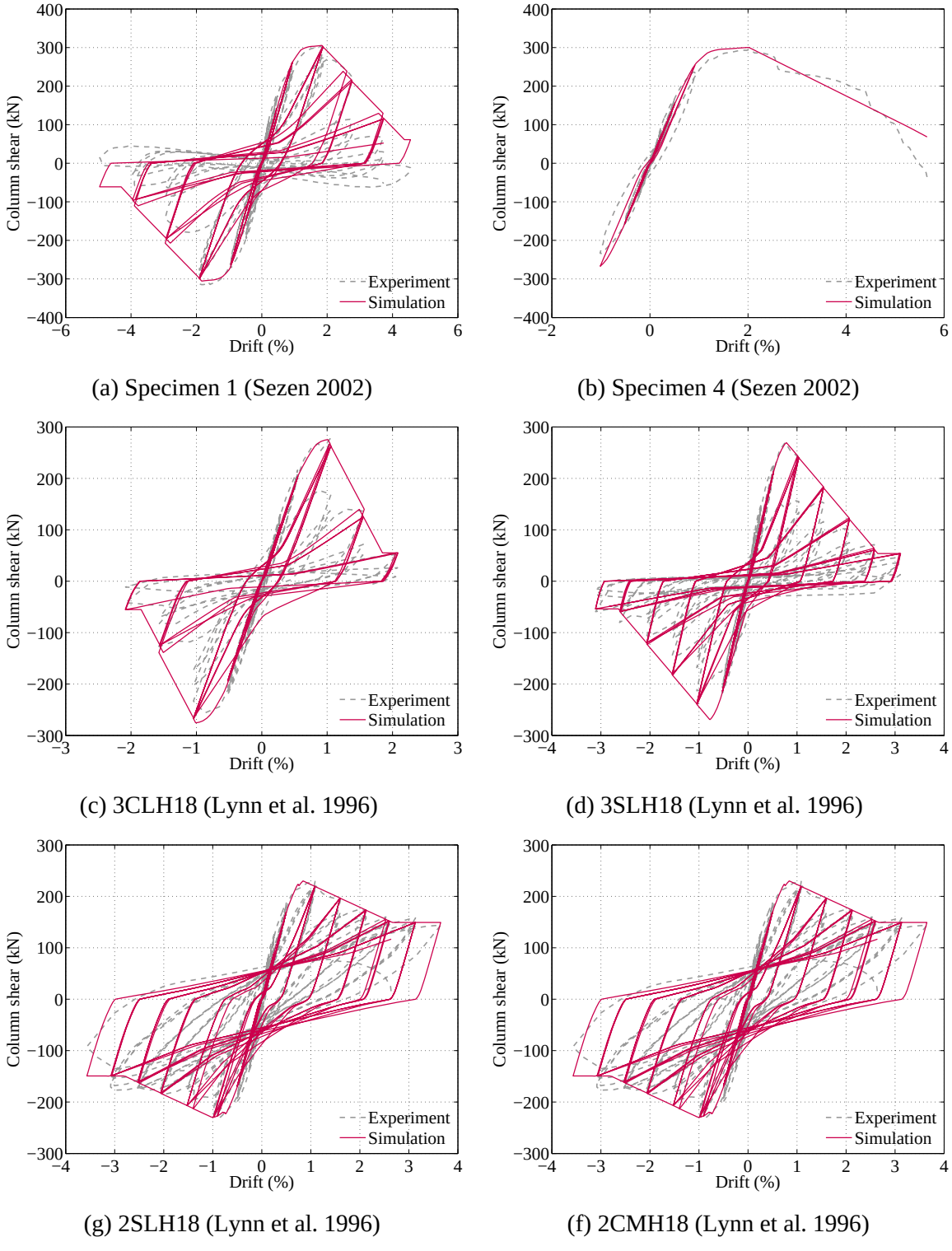

(a) Specimen 1 (Sezen 2002)

(b) Specimen 4 (Sezen 2002)

(c) 3CLH18 (Lynn et al. 1996)

(d) 3SLH18 (Lynn et al. 1996)

(g) 2SLH18 (Lynn et al. 1996)

(f) 2CMH18 (Lynn et al. 1996)

Figure A.1 Comparison between experimental and analytical force-drift hysteresis loops for flexure-shear-critical columns

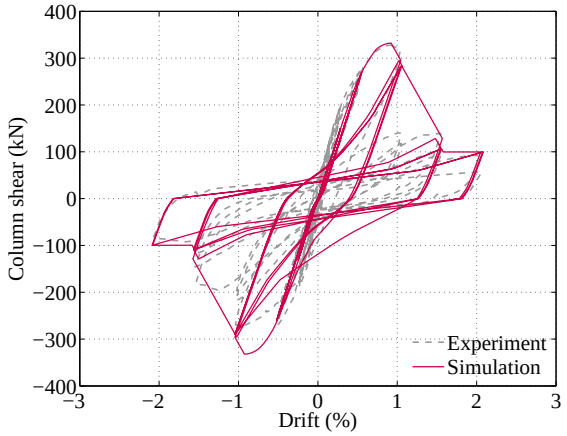

(a) 3CMH18 (Lynn et al. 1996)

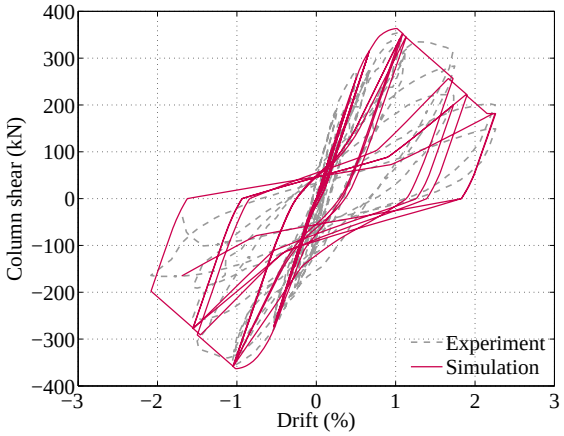

(b) 3CMD12 (Lynn et al. 1996)

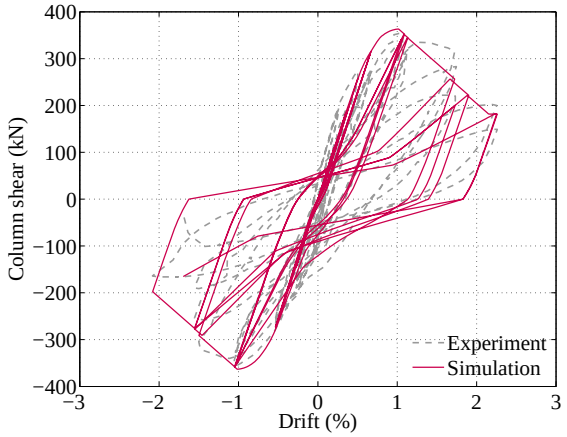

(c) 3SMD12 (Lynn et al. 1996)

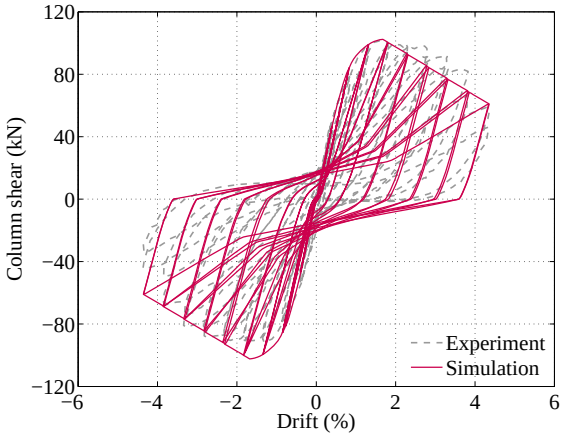

(d) 2D16-R-S (Ohue et al. 1985)

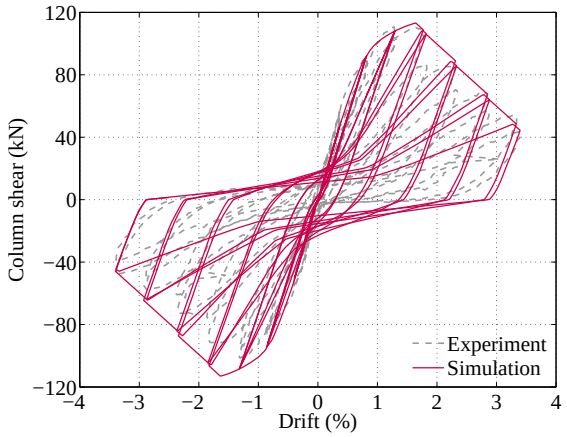

(e) 4D13-R-S (Ohue et al. 1985)

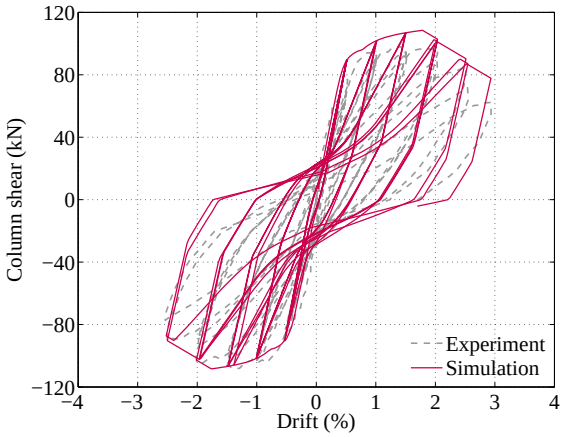

(f) H-2-1/5 (Esaki 1996)

Figure A.1 Comparison between experimental and analytical force-drift hysteresis loops for flexure-shear-critical columns (continued)

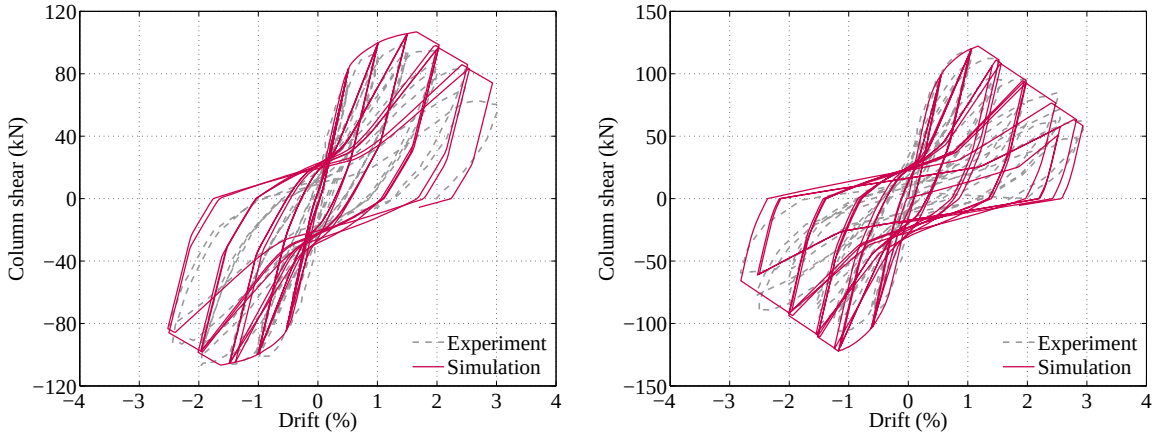

(a) HT-2-1/5 (Esaki 1996)

(b) H-2-1/3 (Esaki 1996)

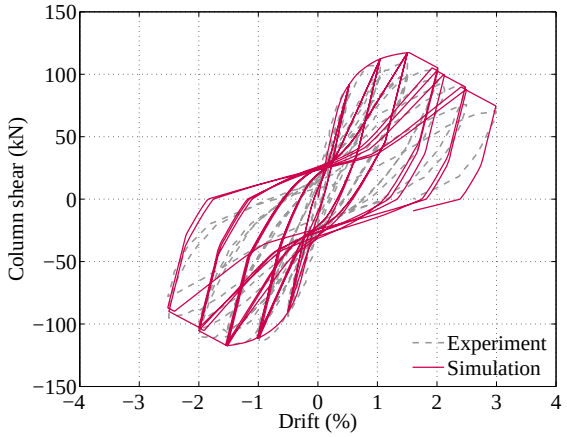

(c) HT-2-1/3 (Esaki 1996)

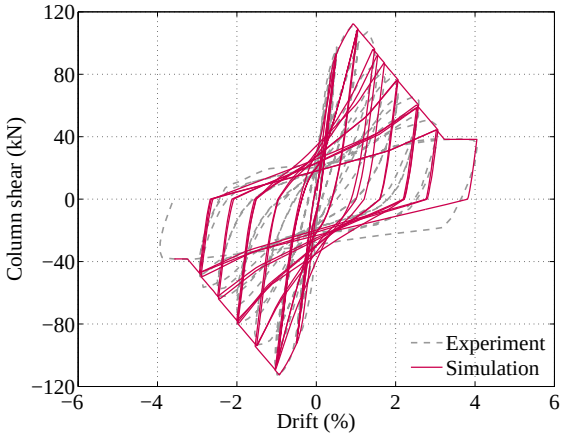

(d) HPRC19-32 (Nagasaka 1982)

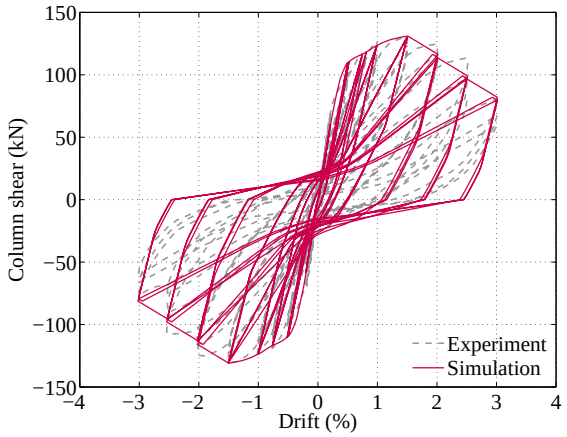

(e) CA025C (Ono et al. 1989)

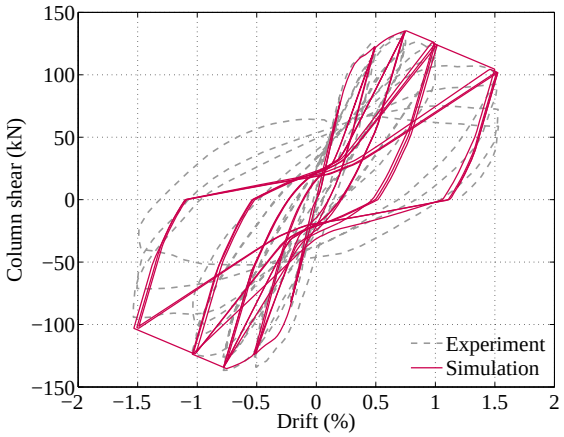

(f) CA060C (Ono et al. 1989)

Figure A.1 Comparison between experimental and analytical force-drift hysteresis loops for flexure-shear-critical columns (continued)

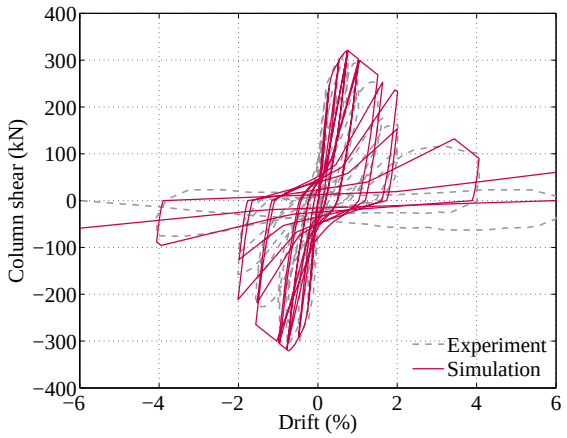

(a) No. 5 (Mostafaei et al. 2009)

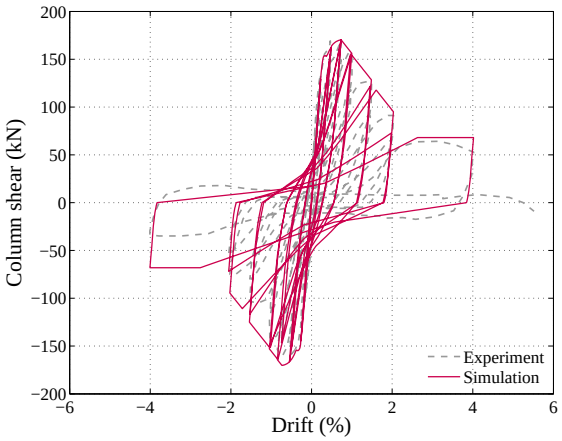

(b) No. 4 (Ousalem et al. 2002)

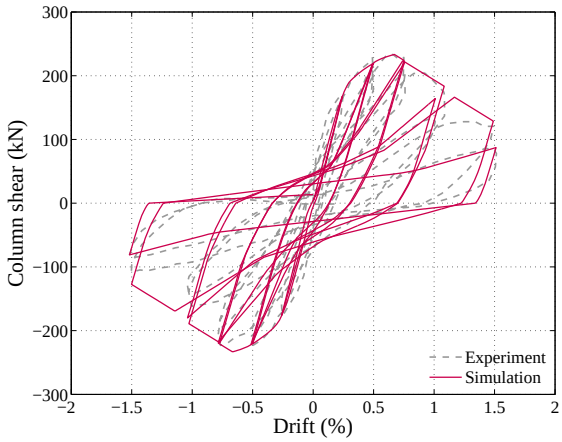

(c) No. 8 (Ousalem et al. 2002)

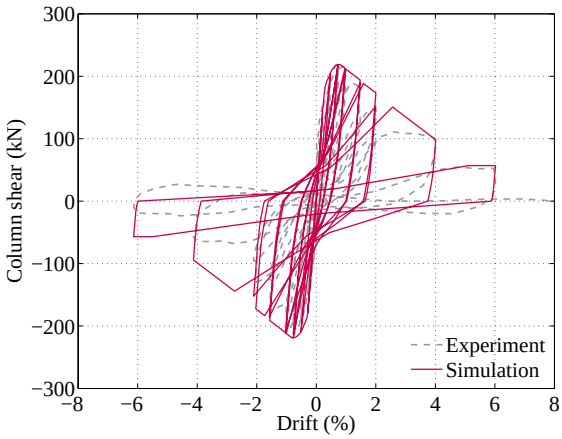

(d) No. 12 (Ousalem et al. 2002)

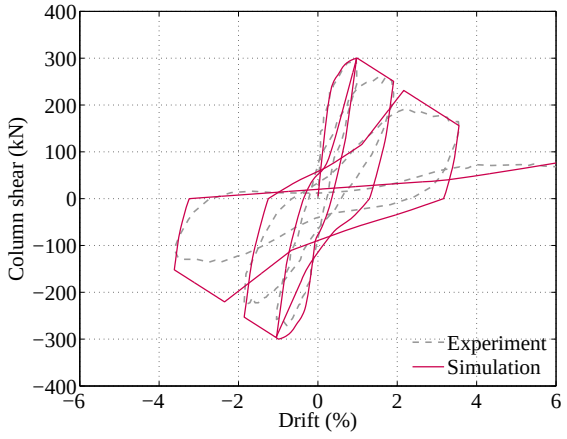

(e) No. 14 (Ousalem et al. 2003)

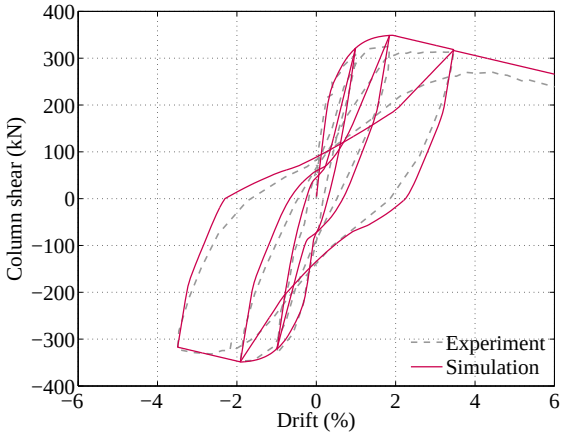

(f) No. 15 (Ousalem et al. 2003)

Figure A.1 Comparison between experimental and analytical force-drift hysteresis loops for flexure-shear-critical columns (continued)

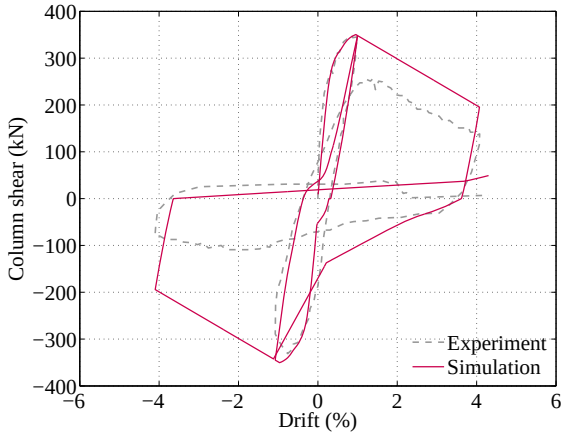

(a) No. 16 (Ousalem et al. 2003)

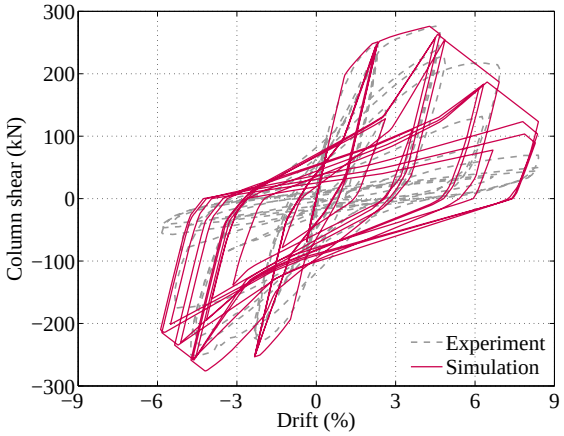

(b) U1 (Saatcioglu and Ozcebe 1989)

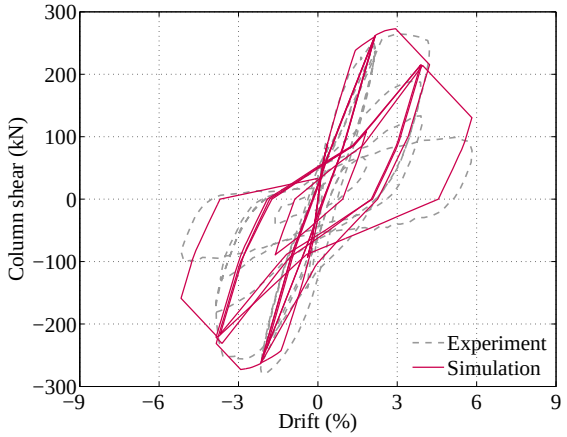

(c) U2 (Saatcioglu and Ozcebe 1989)

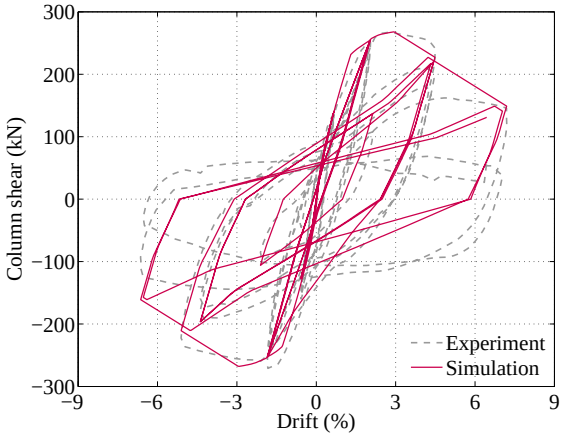

(d) U3 (Saatcioglu and Ozcebe 1989)

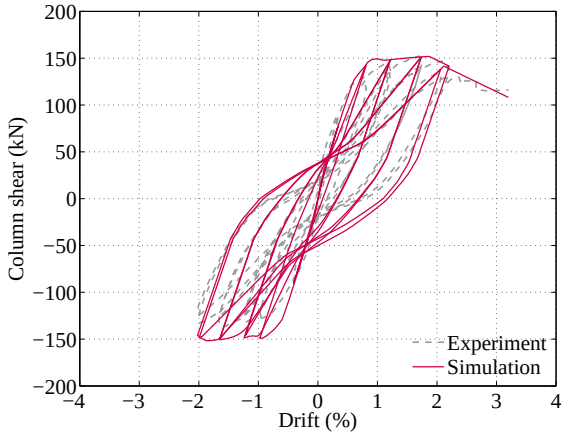

(e) 43-H-3 (Ikeda 1968)

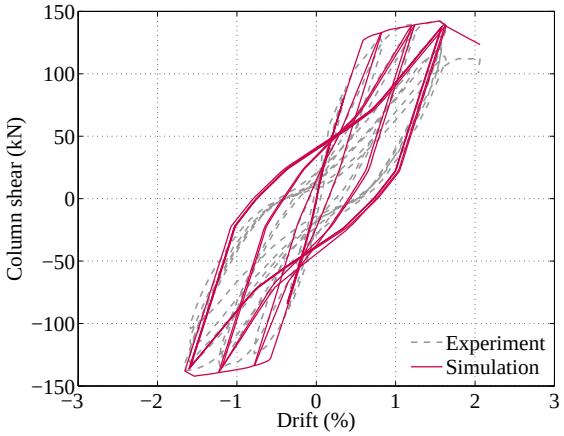

(f) 44-H-4 (Ikeda 1968)

Figure A.1 Comparison between experimental and analytical force-drift hysteresis loops for flexure-shear-critical columns (continued)

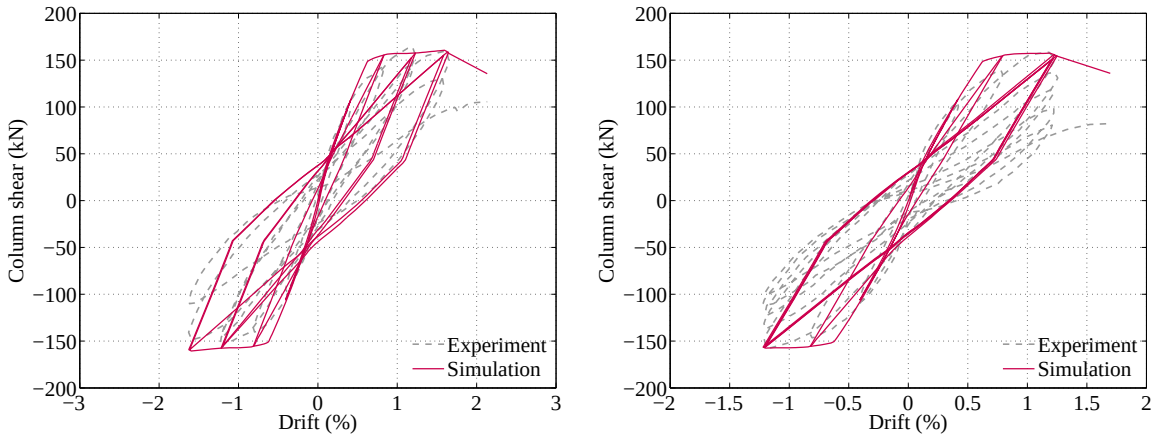

(a) 45-H-5 (Ikeda 1968)

(b) 46-H-6 (Ikeda 1968)

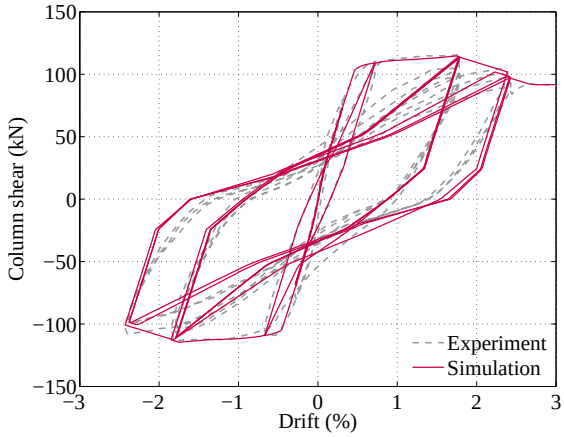

(c) 62-L-4 (Ikeda 1968)

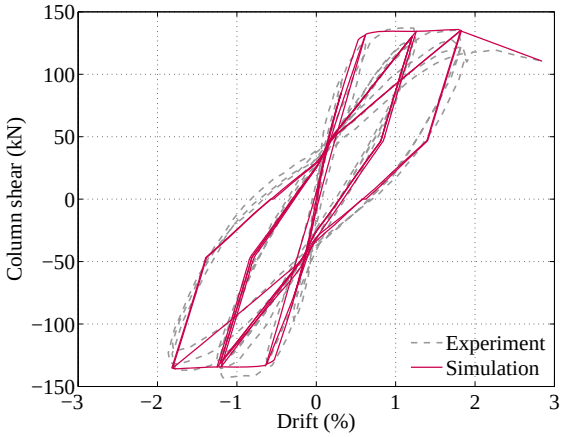

(d) 63-L-5 (Ikeda 1968)

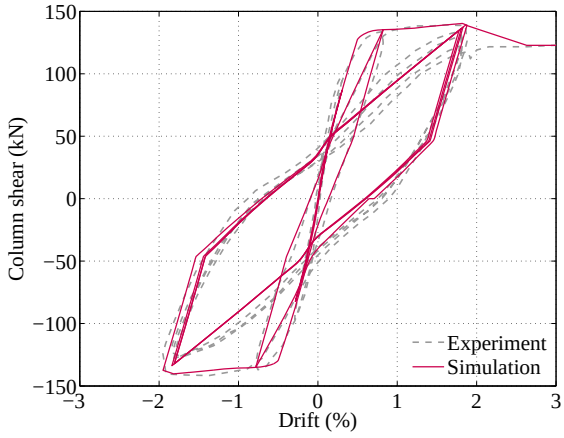

(e) 64-L-6 (Ikeda 1968)

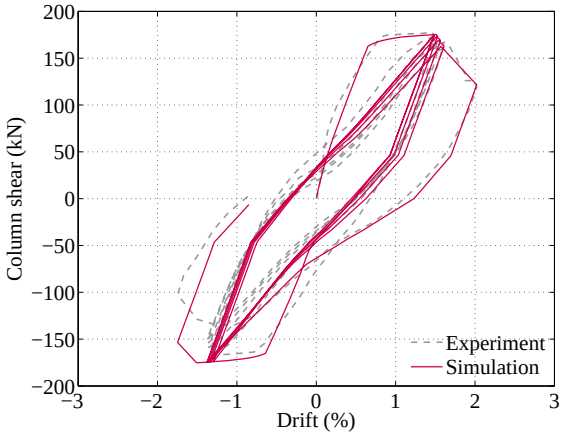

(f) 81-$_1C_{32}$ (Kokusho 1964)

Figure A.1 Comparison between experimental and analytical force-drift hysteresis loops for flexure-shear-critical columns (continued)

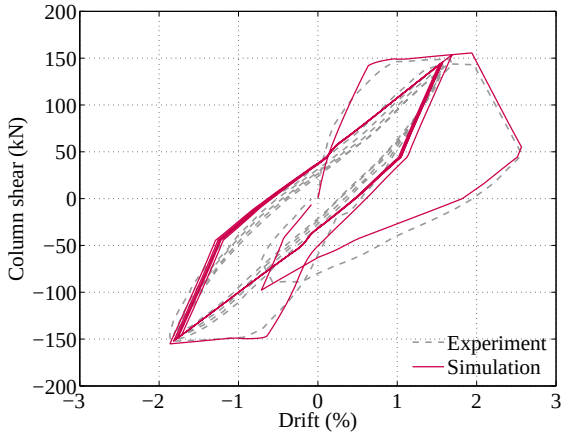

(a) 372-$_2$C$_{12}$ (Kokusho 1964)

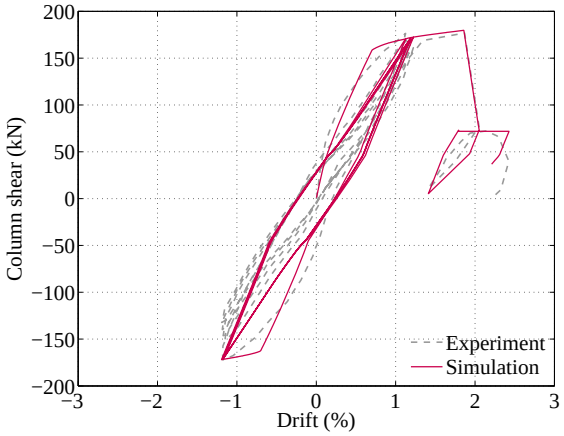

(b) 373-$_2$C$_{22}$ (Kokusho 1964)

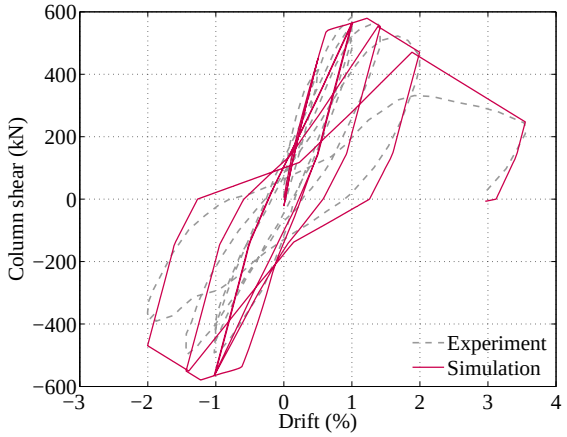

(c) 115-085A56 (Takeda and Yoshioka 1970)

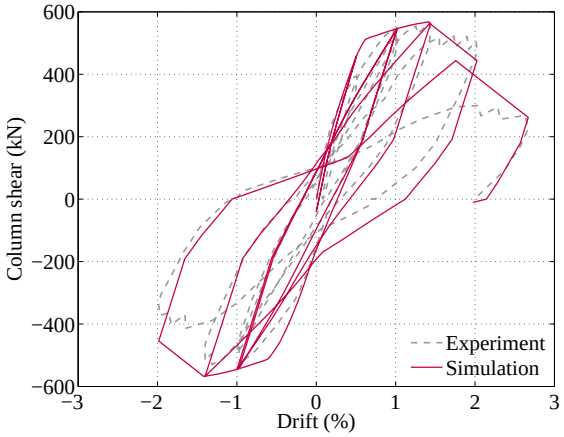

(d) 118-085A80 (Takeda and Yoshioka 1970)

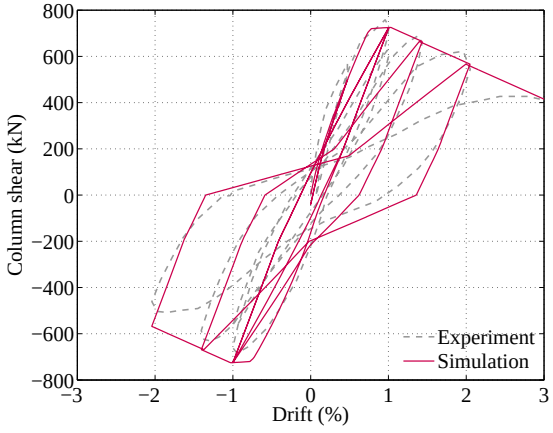

(e) 139-1.2AA56 (Takeda and Yoshioka 1970)

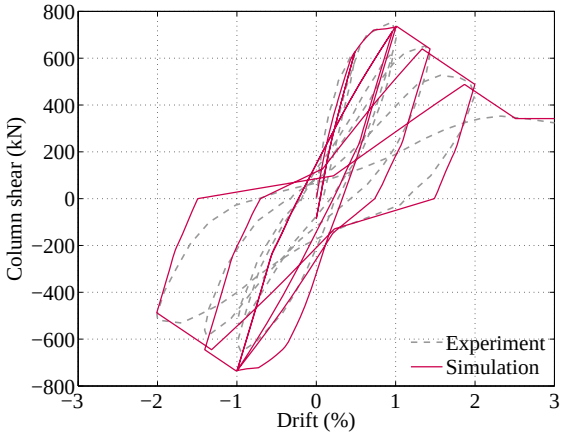

(f) 140-1.2AA80 (Takeda and Yoshioka 1970)

Figure A.1 Comparison between experimental and analytical force-drift hysteresis loops for flexure-shear-critical columns (continued)

Table A.1 Comparison of experimental and analytical maximum shear force for flexure-shear-critical columns

Reference	Specimen	Maximum shear force (kN)		Difference
		Experiment	Analysis	(%)
Sezen (2002)	Specimen 1	315	306	-2.9
	Specimen 4	295	300	+1.9
Lynn et al. (1996)	3CLH18	277	275	-0.6
	3SLH18	270	269	-0.2
	2SLH18	233	230	-1.3
	2CMH18	306	302	-1.2
	3CMH18	328	332	+1.3
	3CMD12	356	363	+2.0
	3SMD12	367	358	-2.6
Ohue et al. (1985)	2D16RS	101	102	+1.0
	4D13RS	111	113	+2.3
Esaki (1996)	H-2-1/5	108	108	+0.2
	HT-2-1/5	107	107	-0.0
	H-2-1/3	118	122	+3.3
	HT-2-1/3	116	117	+1.0
Nagasaka (1982)	HPRC19-32	113	113	+0.0
Ono et al. (1989)	CA025C	130	131	+0.6
	CA060C	137	135	-1.0
Mostafaei et al. (2009)	No. 5	322	321	-0.2
Ousalem et al. (2002)	No. 4	170	170	+0.3
	No. 8	233	233	+0.1
	No. 12	220	219	-0.5
Ousalem et al. (2003)	No. 14	300	300	-0.0
	No. 15	347	349	+0.6
	No. 16	349	350	+0.4
Saatcioglu and Ozcebe (1989)	U1	276	276	-0.1
	U2	279	273	-2.0
	U3	271	268	-1.1
Ikeda (1968)	43-H-3	152	152	-0.2
	44-H-4	142	142	+0.0
	45-H-5	164	161	-2.2
	46-H-6	158	157	-0.6
	62-L-4	115	115	-0.6
	63-L-5	143	136	-5.0
	64-L-6	142	140	-1.0
Kokusho (1964)	81-$_1C_{32}$	178	175	-1.5
	372-$_2C_{12}$	152	156	+2.1
	373-$_2C_{22}$	177	180	+1.7
Takeda and Yoshioka (1970)	115-085A56	584	579	-0.7
	118-085A80	563	568	+0.8
	139-12AA56	758	725	-4.4
	140-12AA80	754	736	-2.4

A.2 Simulated Response for Non-Ductile Exterior Beam-Column Joint Subassemblages–Joint Shear Failure

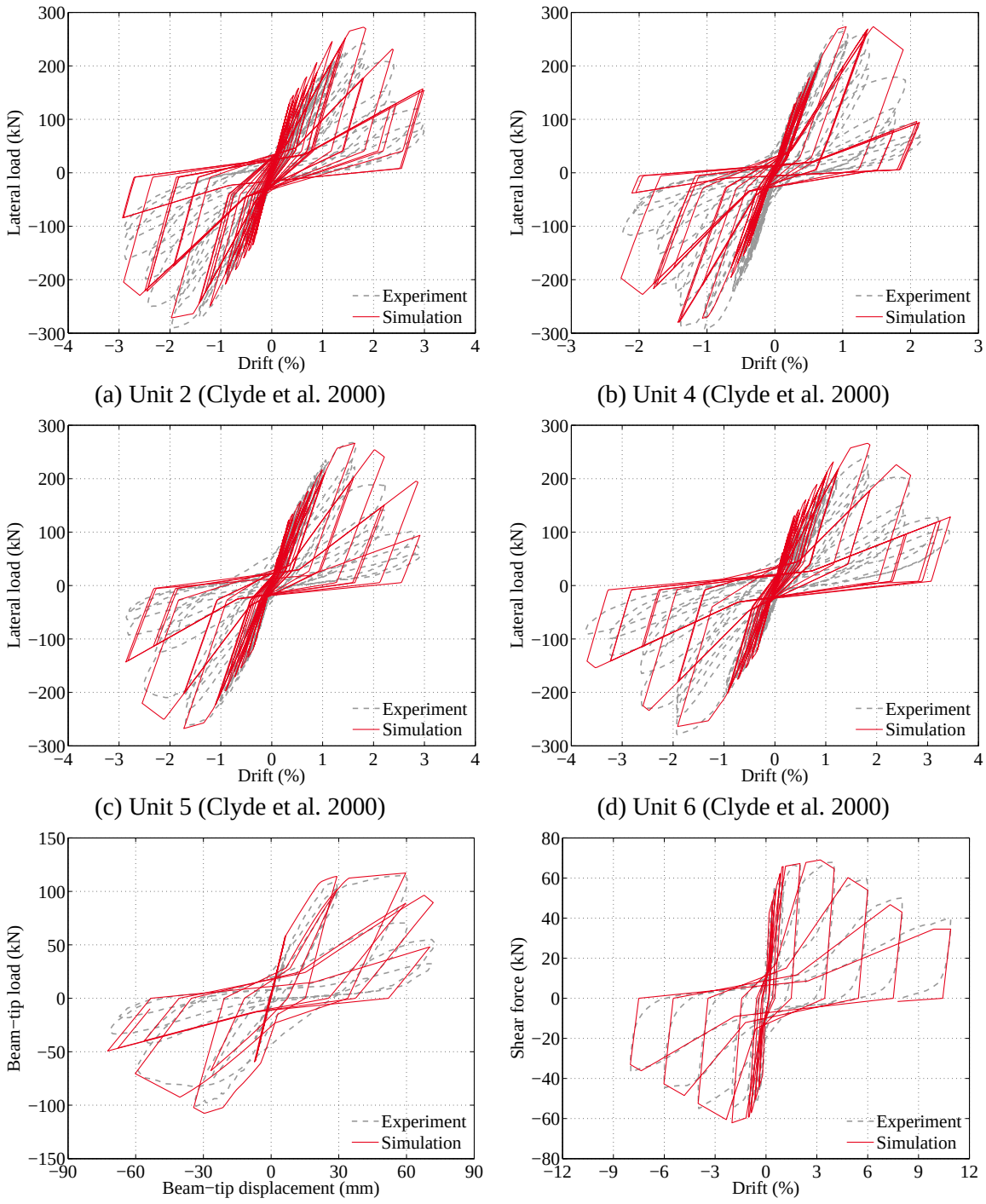

(a) Unit 2 (Clyde et al. 2000)

(b) Unit 4 (Clyde et al. 2000)

(c) Unit 5 (Clyde et al. 2000)

(d) Unit 6 (Clyde et al. 2000)

(e) T1 (Ghobarah and Said 2002)

(f) JO (Ilki et al. 2011)

Figure A.2 Comparison between hysteretic responses of experiment and analysis for non-ductile exterior joints with joint shear failure

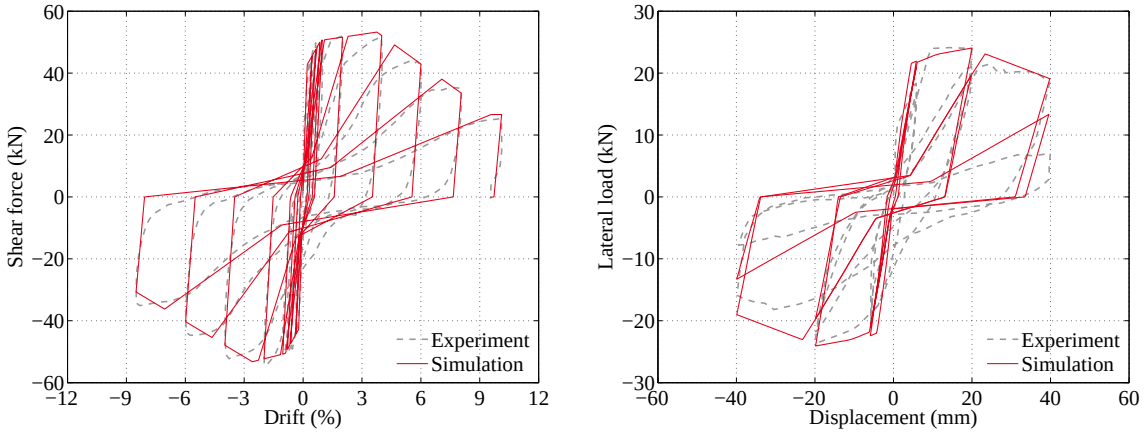

(a) JOP (Ilki et al. 2011)

(b) A0 (Karayannis et al. 2008)

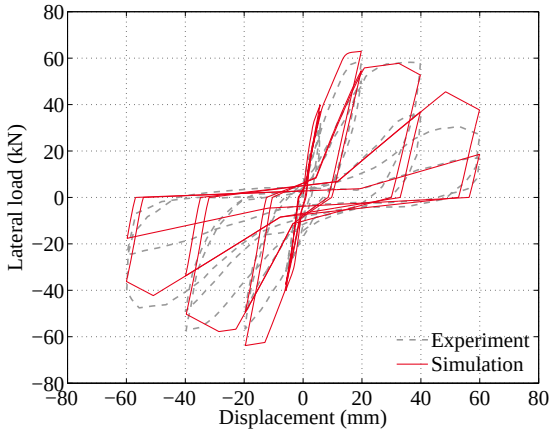

(c) B0 (Karayannis et al. 2008)

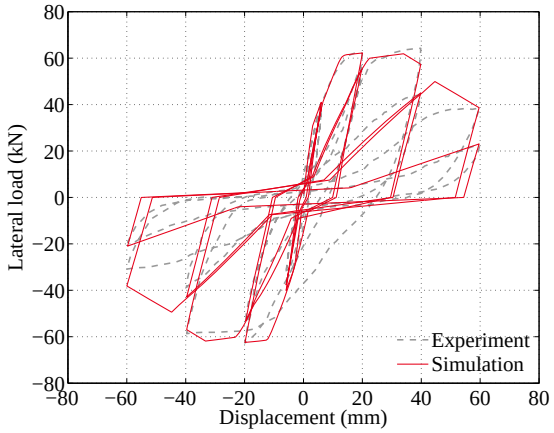

(d) C0 (Karayannis et al. 2008)

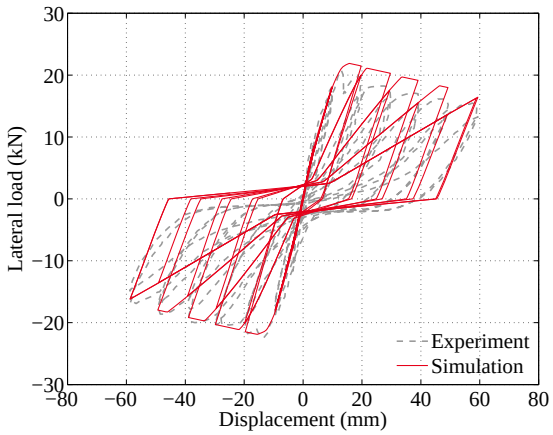

(e) RC-1 (Liu 2006)

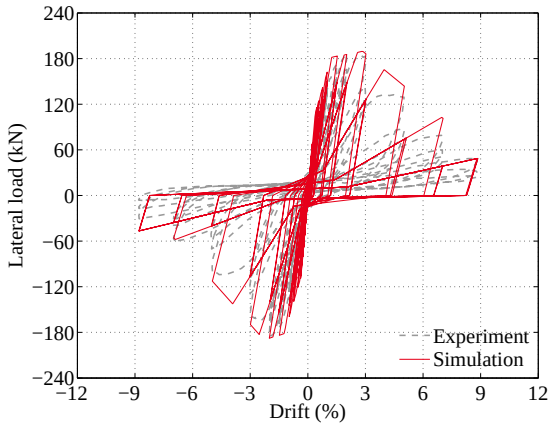

(f) Unit 3 (Pantelides et al. 2002)

Figure A.2 Comparison between hysteretic responses of experiment and analysis for non-ductile exterior joints with joint shear failure (continued)

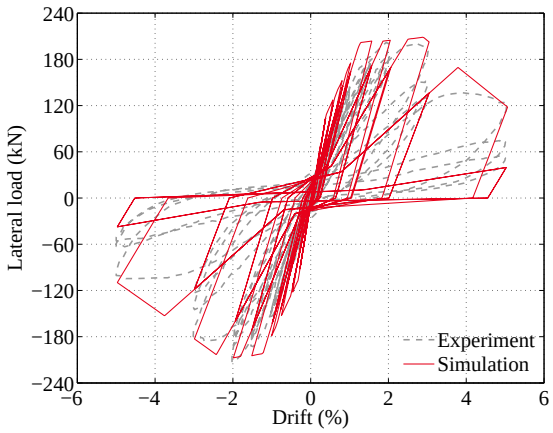

(a) Unit 4 (Pantelides et al. 2002)

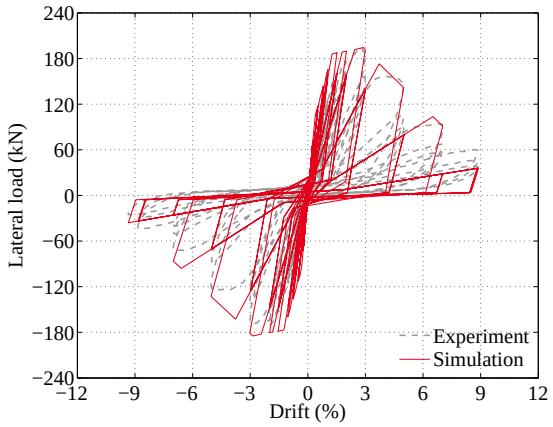

(b) Unit 5 (Pantelides et al. 2002)

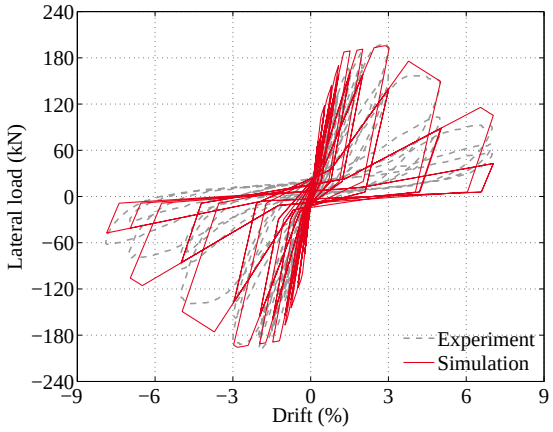

(c) Unit 6 (Pantelides et al. 2002)

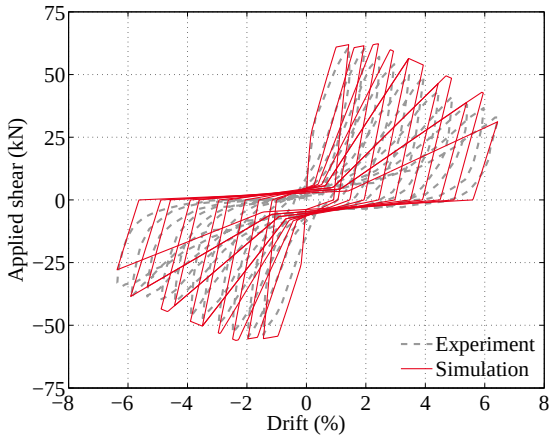

(d) G1 (Tsonos 2007)

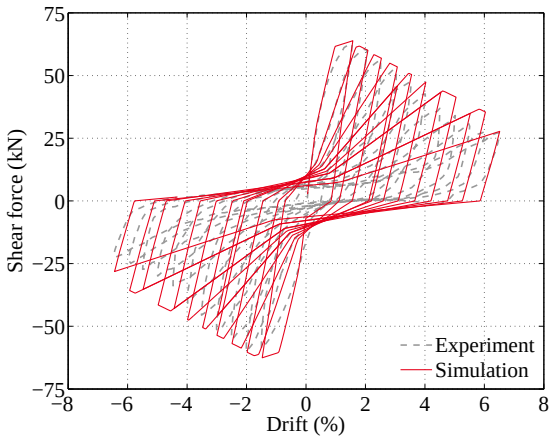

(e) F1 (Tsonos and Papanikolaou 2003)

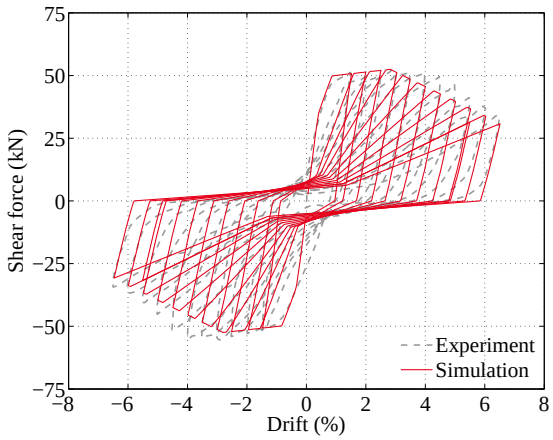

(f) F2 (Tsonos and Papanikolaou 2003)

Figure A.2 Comparison between hysteretic responses of experiment and analysis for non-ductile exterior joints with joint shear failure (continued)

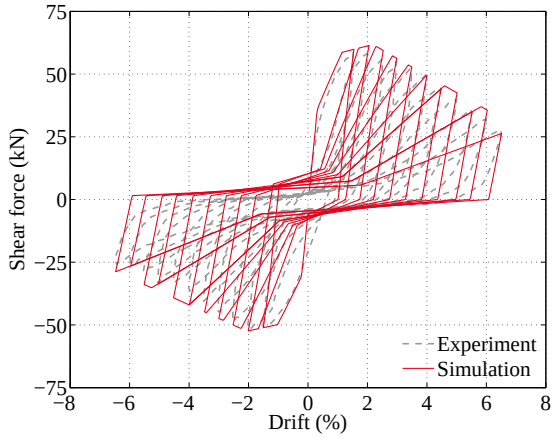

(a) L1 (Tsonos and Papanikolaou 2003)

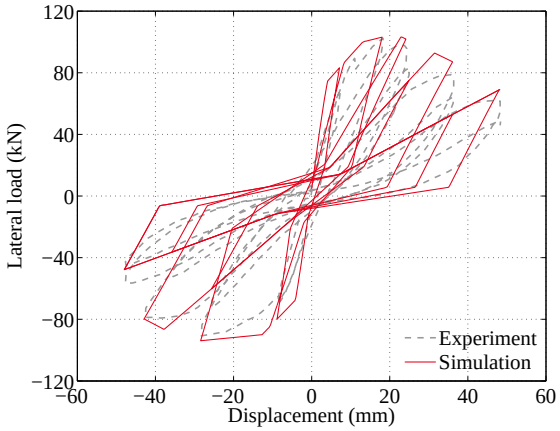

(b) BS-L (Wong 2005)

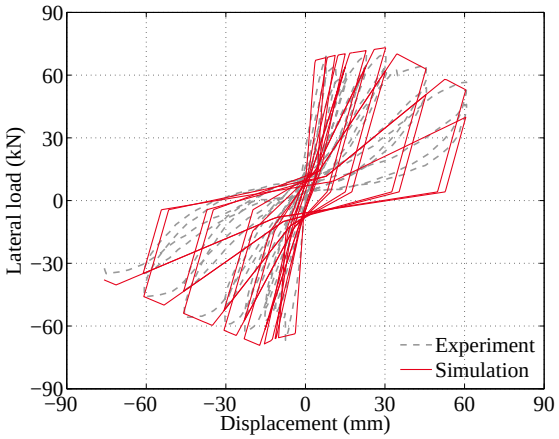

(c) BS-OL (Wong 2005)

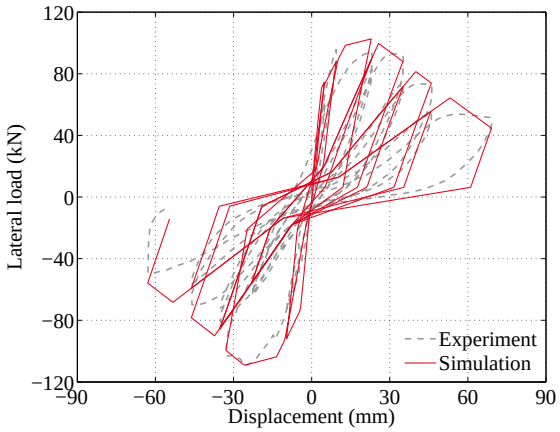

(d) BS-U (Wong 2005)

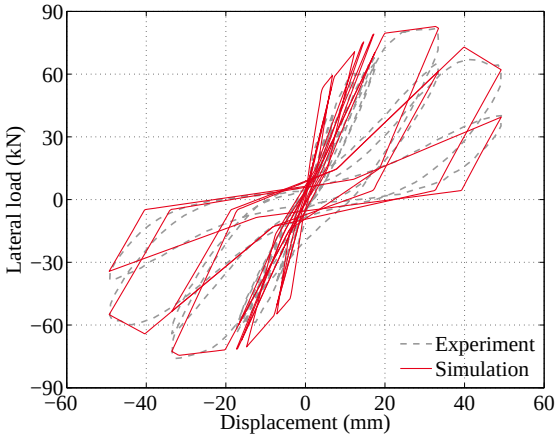

(e) JA-NN03 (Wong 2005)

Figure A.2 Comparison between hysteretic responses of experiment and analysis for non-ductile exterior joints with joint shear failure (continued)

A.3 Simulated Response for Non-Ductile Exterior Beam-Column Joint Subassemblages –Joint Bond Failure

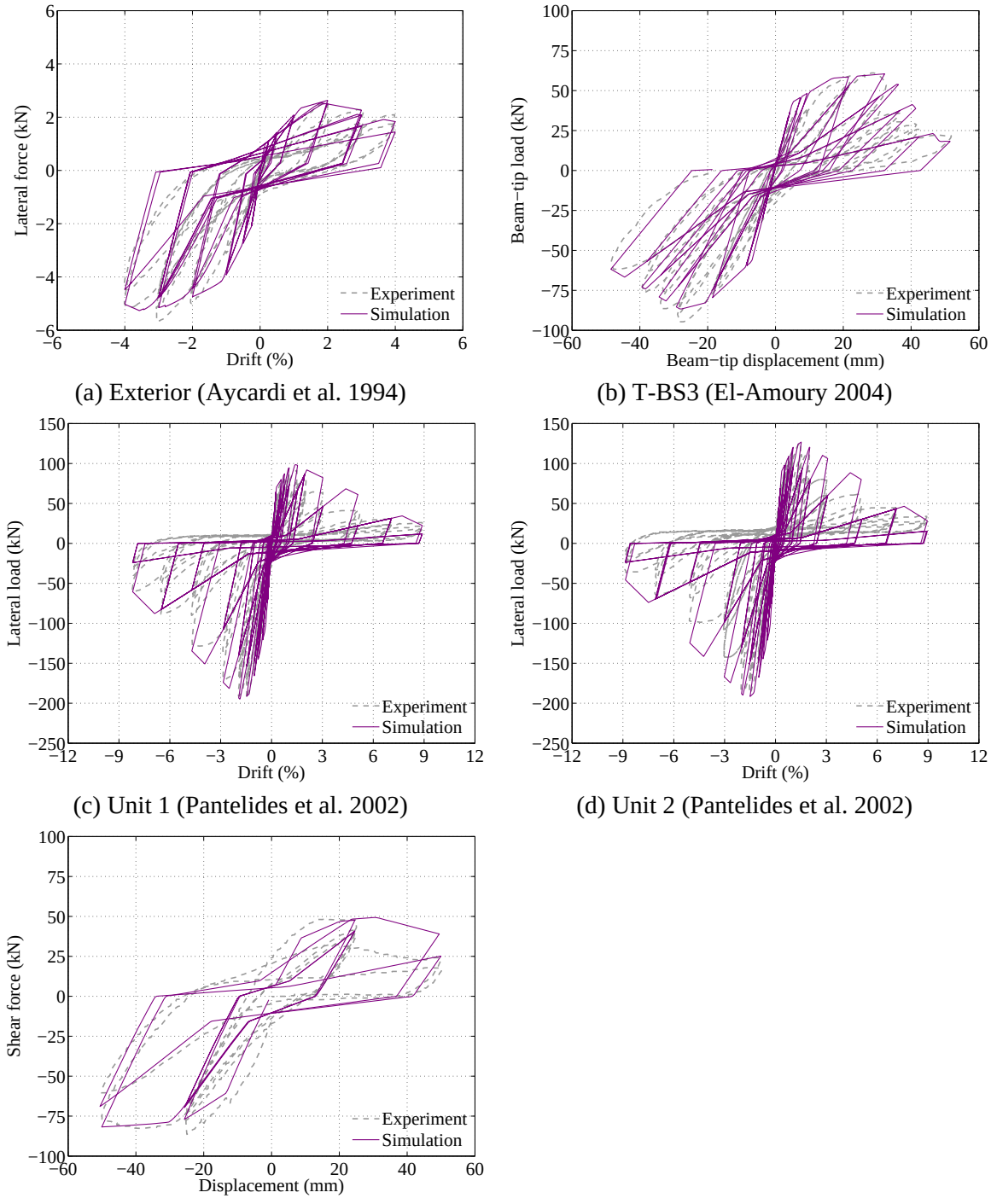

(a) Exterior (Aycardi et al. 1994)

(b) T-BS3 (El-Amoury 2004)

(c) Unit 1 (Pantelides et al. 2002)

(d) Unit 2 (Pantelides et al. 2002)

(e) SP-1 (Sasmal et al. 2011)

Figure A.3 Comparison between hysteretic responses of experiment and analysis for non-ductile exterior joints with joint bond failure

Table A.2 Comparison of experimental and analytical maximum lateral force for non-ductile exterior beam-column joint subassemblages

Reference	Specimen	Maximum lateral force (kN)		Difference (%)
		Experiment	Analysis	
Joint shear failure				
Clyde et al. (2000)	Unit 2	291	272	-6.3
	Unit 4	292	280	-4.1
	Unit 5	267	266	-0.4
	Unit 6	279	266	-4.7
Ghobarah and Said (2002)	T1	115	117	+1.9
Ilki et al. (2011)	JO	68	69	+1.7
	JOP	55	53	-2.3
Karayannis et al. (2008)	A0	24	24	-0.2
	B0	58	63	+7.7
	C0	64	62	-2.8
Liu (2006)	RC-1	23	22	-2.7
Pantelides et al. (2002)	Unit 3	186	190	+1.7
	Unit 4	213	209	-2.1
	Unit 5	194	194	+0.3
	Unit 6	198	196	-1.3
Tsonos and Papanikolaou (2003)	F1	68	64	+1.8
	F2	55	52	-5.4
	L1	59	61	+4.7
Tsonos (2007)	G1	61	62	+1.8
Wong (2005)	BS-L	102	103	+0.9
	BS-OL	70	73	+4.5
	BS-U	110	109	-0.4
	JA-NN03	82	83	+1.2
Joint bond failure				
Aycardi et al. (1994)	Exterior	+2.5 (-5.7)	+2.6 (-5.3)	+4.0 (-6.9)
El-Amoury (2004)	T-SB3	+61 (-95)	+60 (-87)	-0.9 (-8.4)
Pantelides et al. (2002)	Unit 1	+91 (-194)	+99 (-195)	+8.1 (+0.4)
	Unit 2	+126 (-188)	+127 (-192)	+0.4 (+2.1)
Sasmal et al. (2011)	SP-1	+48 (-86)	+49 (-82)	+2.2 (-5.4)

A.4 Simulated Response for Non-Ductile Interior Beam-Column Joint Subassemblages

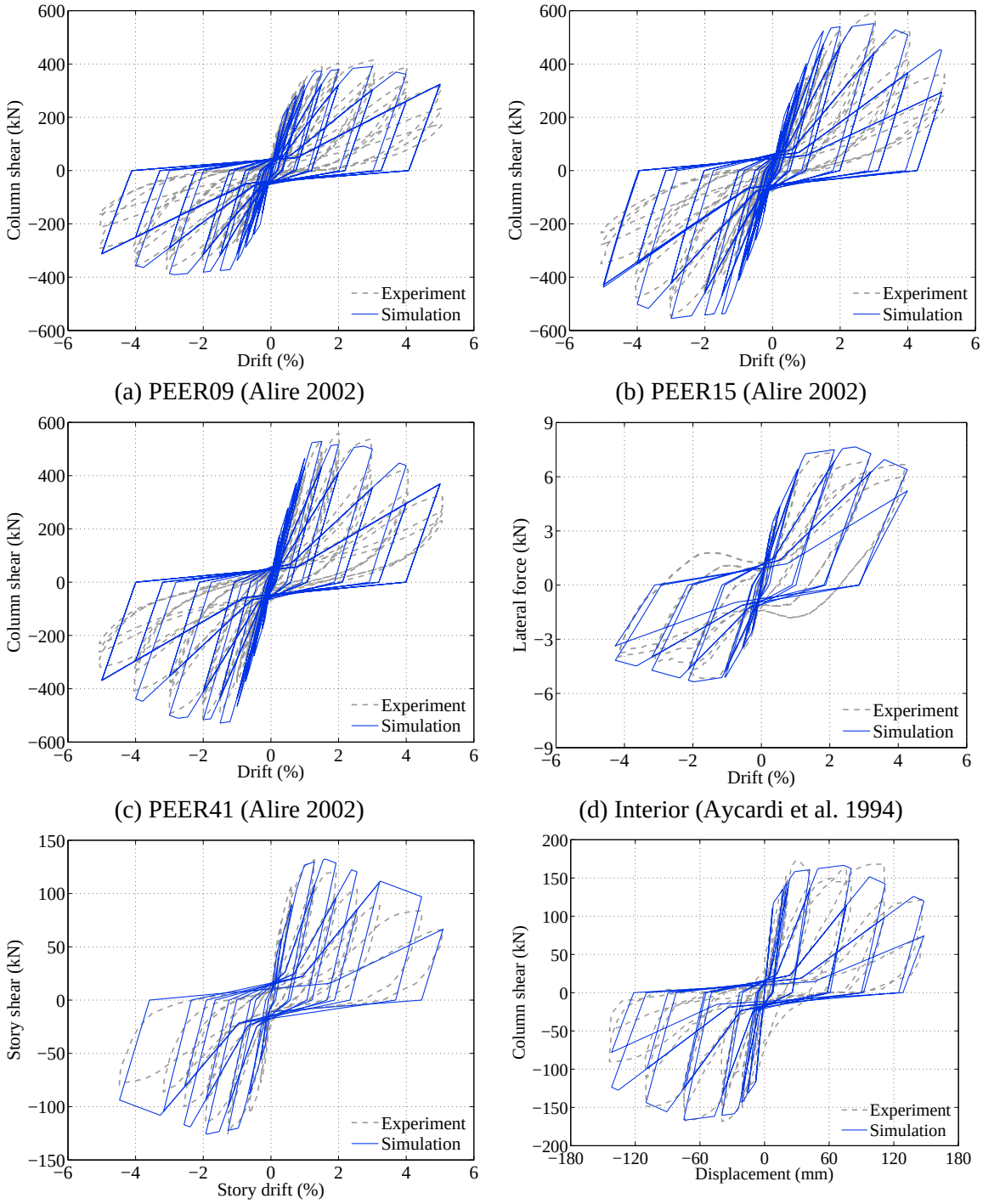

Figure A.4 Comparison between hysteretic responses of experiment and analysis for non-ductile interior joints

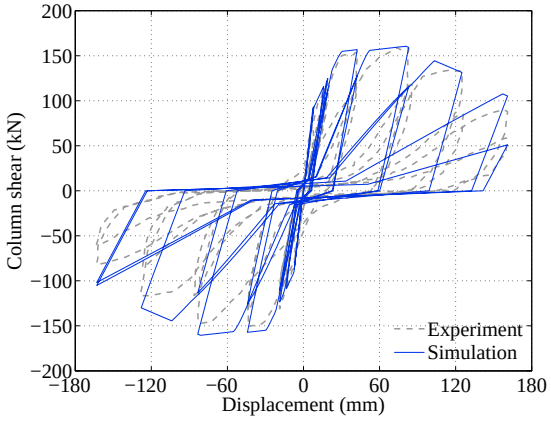

(a) O5 (Hakuto et al. 2000)

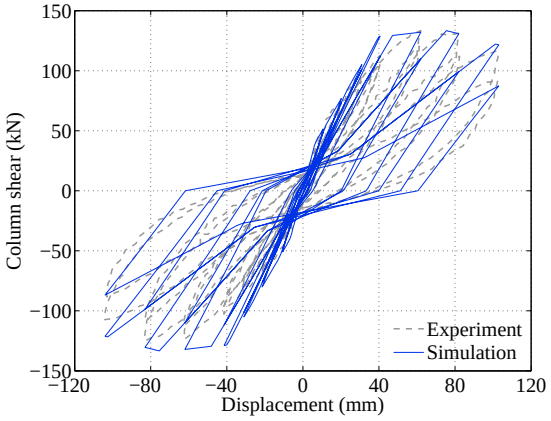

(b) JI0 (Lee et al. 2010)

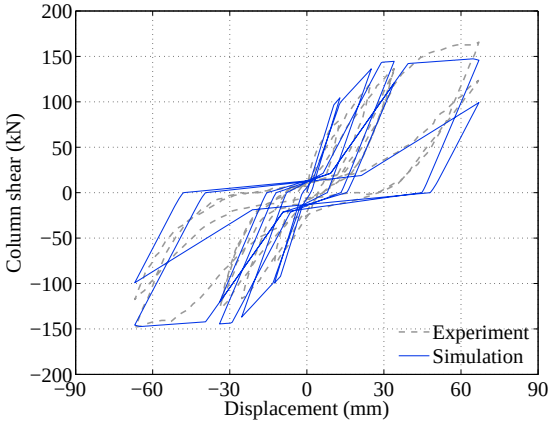

(c) A1 (Li et al. 2002)

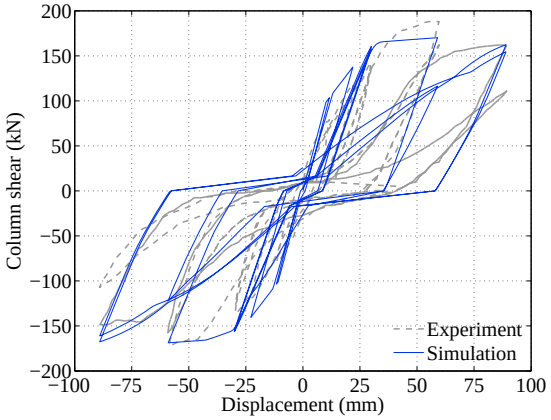

(d) M1 (Li et al. 2002)

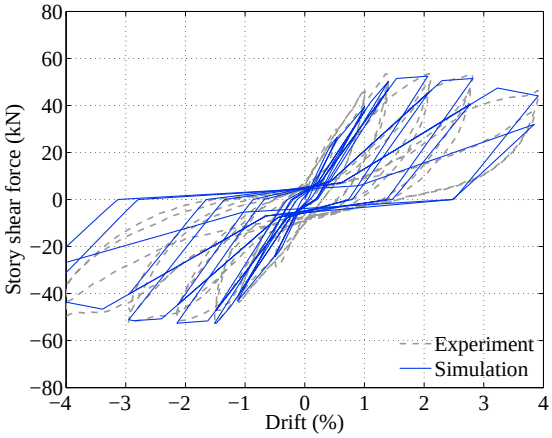

(e) AL1 (Li et al. 2009)

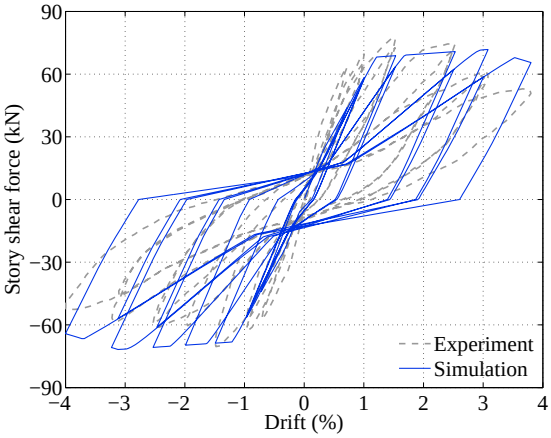

(f) AS1 (Li et al. 2009)

Figure A.4 Comparison between hysteretic responses of experiment and analysis for non-ductile interior joints (continued)

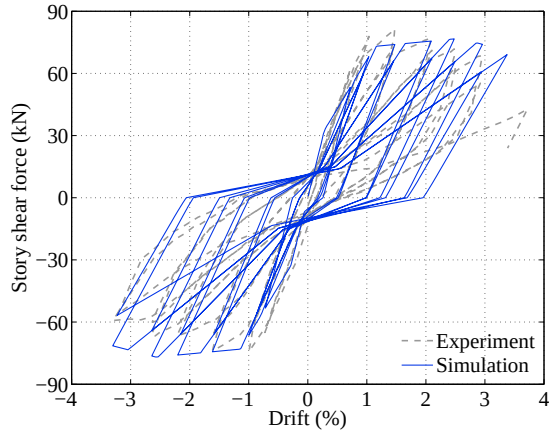

(a) AL2 (Li et al. 2009)

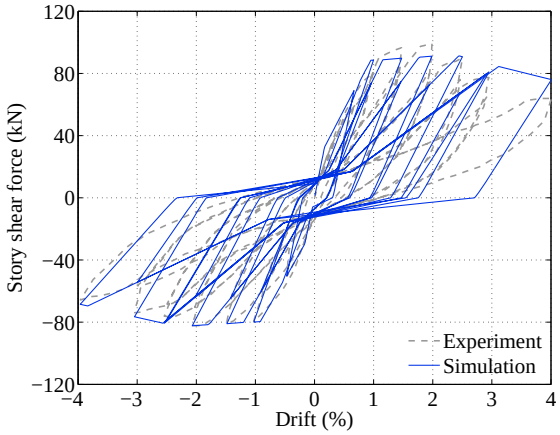

(b) AS2 (Li et al. 2009)

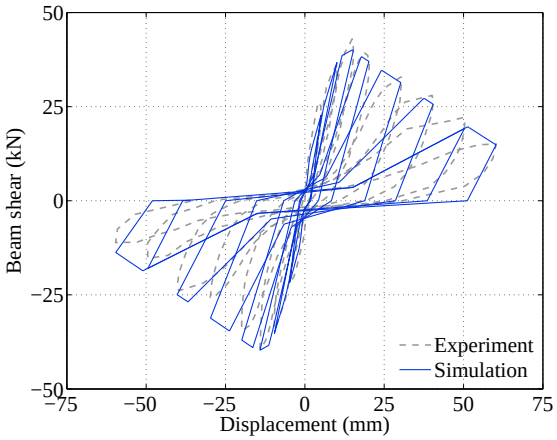

(c) No. 1 (Ohwada 1970)

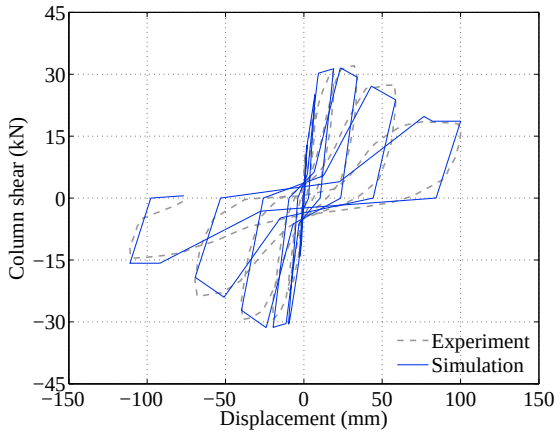

(d) P2 (Ohwada 1973)

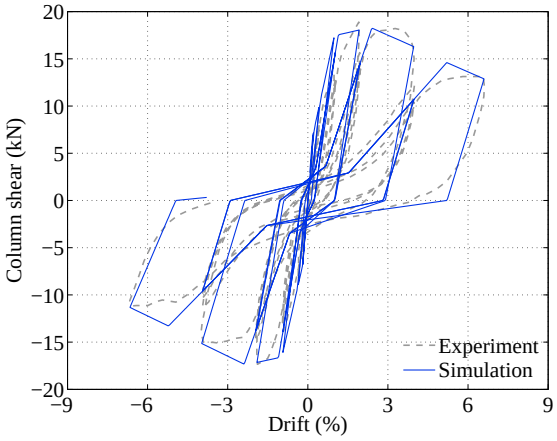

(e) JO-1 (Ohwada 1977)

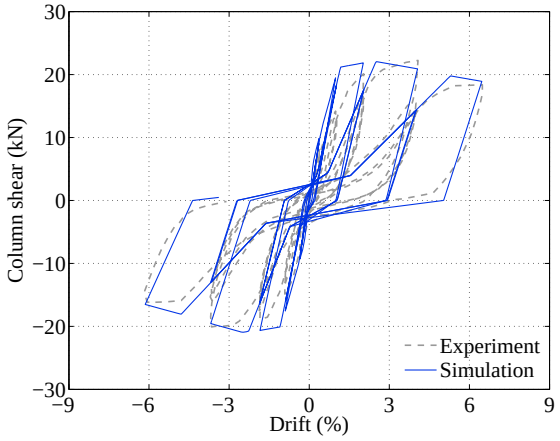

(f) JE-1 (Ohwada 1977)

Figure A.4 Comparison between hysteretic responses of experiment and analysis for non-ductile interior joints (continued)

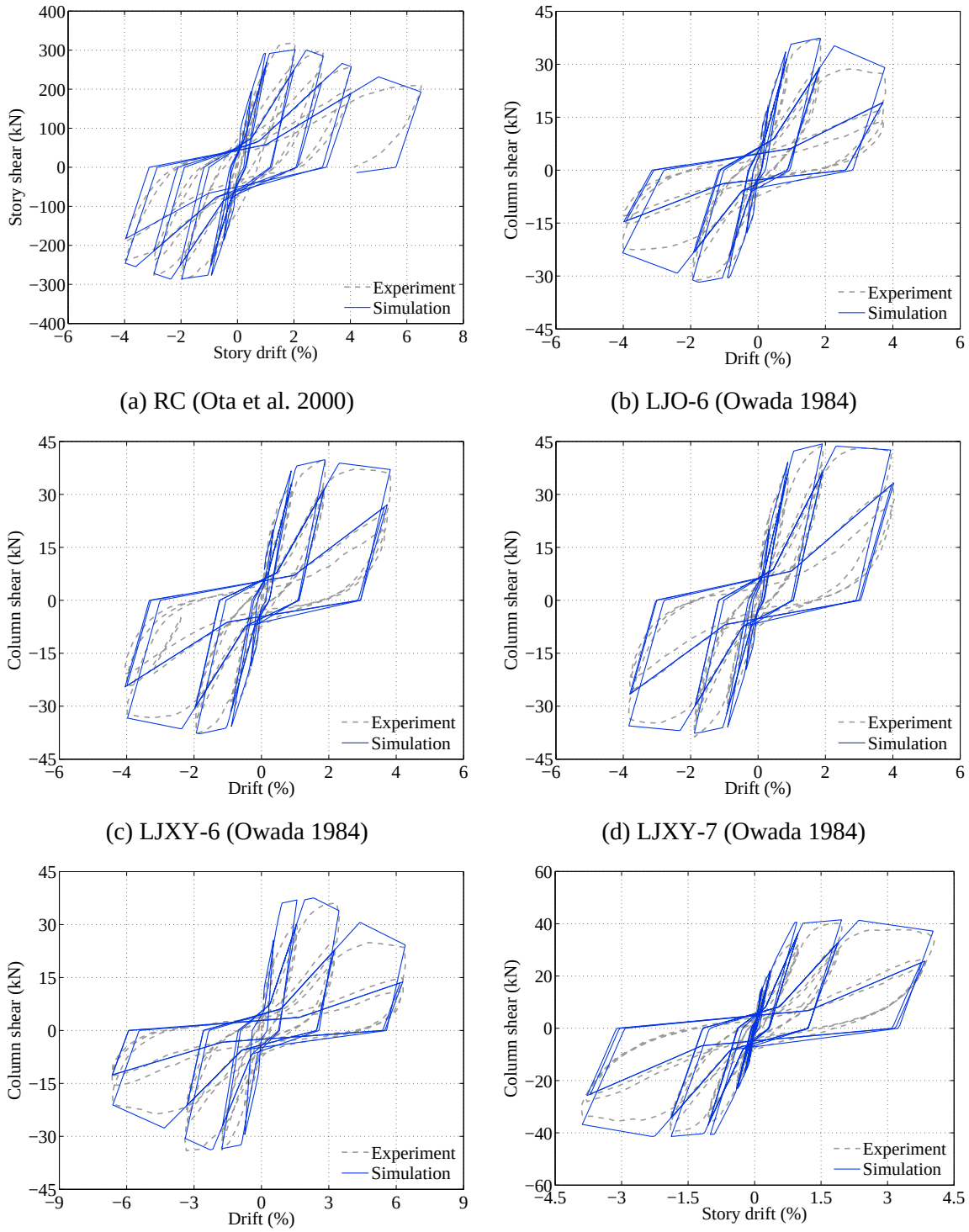

(a) RC (Ota et al. 2000)

(b) LJO-6 (Owada 1984)

(c) LJXY-6 (Owada 1984)

(d) LJXY-7 (Owada 1984)

(e) LJXY-8 (Owada 1984)

(f) JO-5 (Owada 2000)

Figure A.4 Comparison between hysteretic responses of experiment and analysis for non-ductile interior joints (continued)

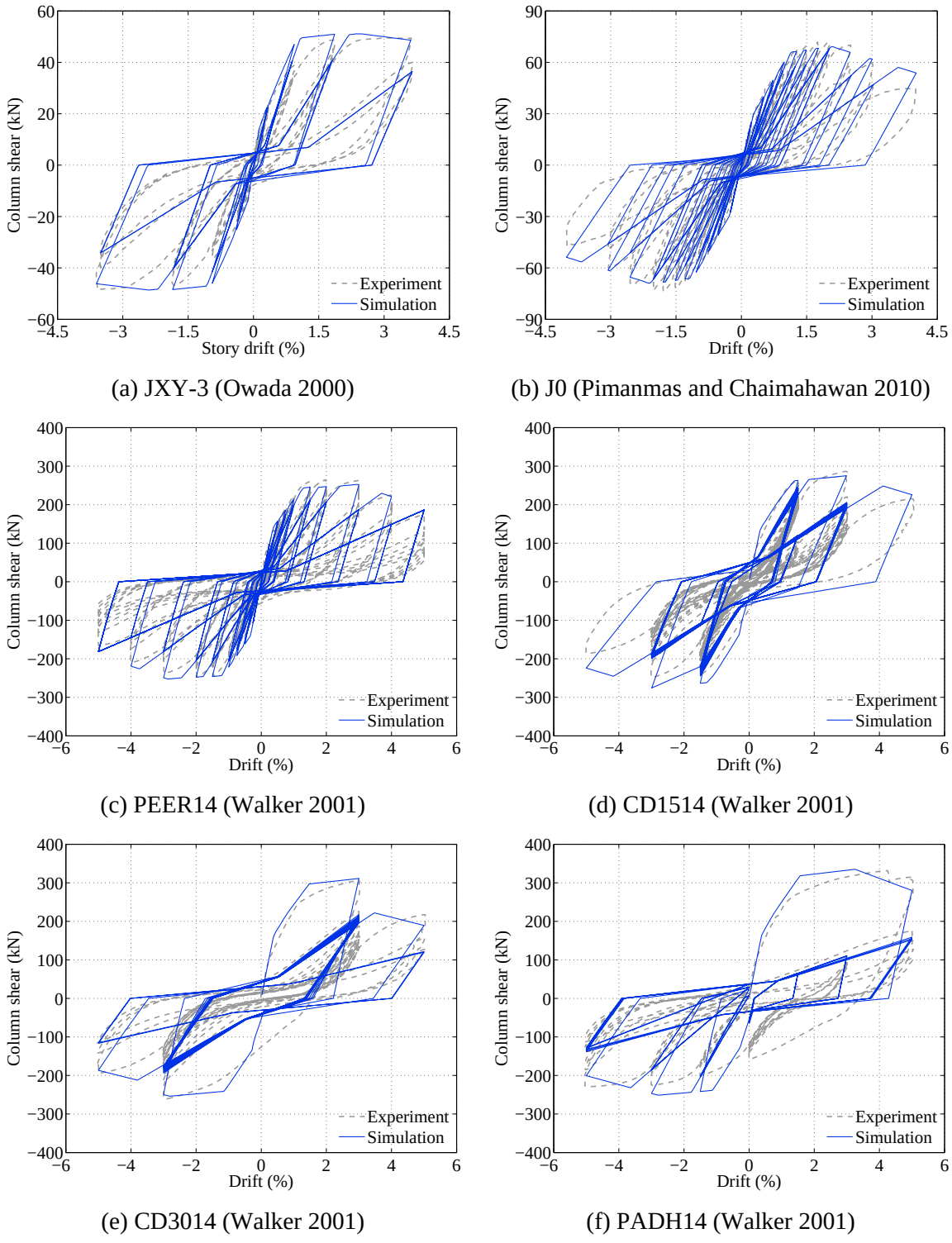

(a) JXY-3 (Owada 2000)

(b) J0 (Pimanmas and Chaimahawan 2010)

(c) PEER14 (Walker 2001)

(d) CD1514 (Walker 2001)

(e) CD3014 (Walker 2001)

(f) PADH14 (Walker 2001)

Figure A.4 Comparison between hysteretic responses of experiment and analysis for non-ductile interior joints (continued)

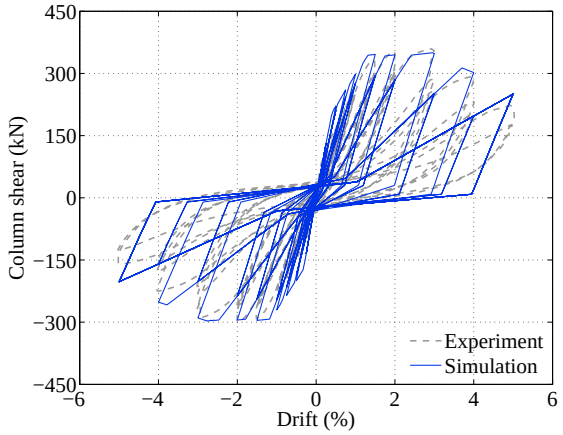

(a) PEER22 (Walker 2001)

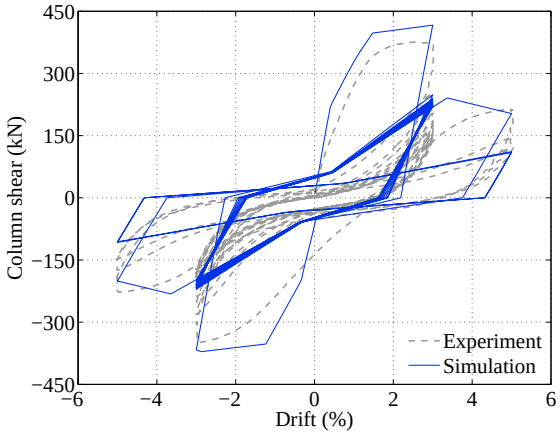

(b) CD3022 (Walker 2001)

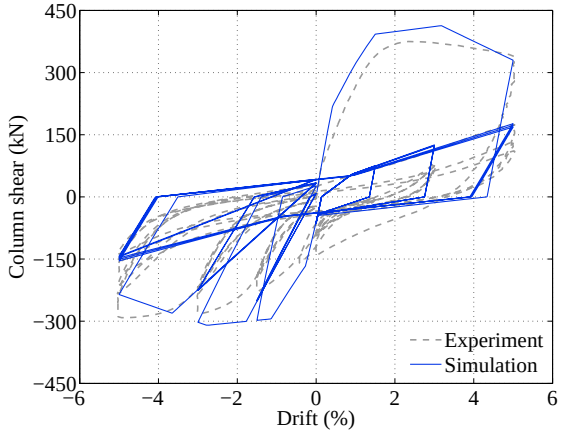

(c) PADH 22 (Walker 2001)

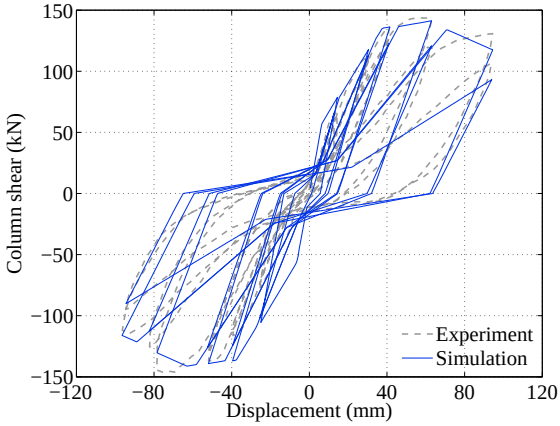

(d) Ho-JI1 (Wang and Hsu 2009)

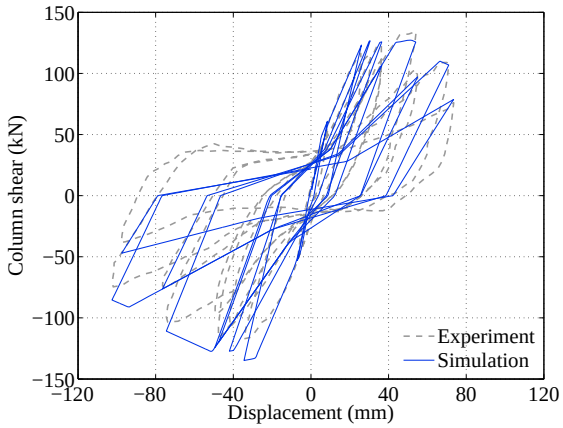

(e) Ko-JI1 (Wang and Hsu 2009)

Figure A.4 Comparison between hysteretic responses of experiment and analysis for non-ductile interior joints (continued)

Table A.3 Comparison of experimental and analytical maximum lateral force for non-ductile interior beam-column joint subassemblages

Reference	Specimen	Maximum lateral force (kN)		Difference (%)
		Experiment	Analysis	
Alire (2002)	PEER0995	416	390	-6.1
	PEER1595	599	555	-7.4
	PEER4150	560	529	-5.7
Aycardi et al. (1994)	Interior	7.3	7.7	+4.6
Hakuto et al. (2000)	O4	173	167	-3.7
	O5	159	161	+1.0
Goto and Joh (1996)	J-OH	132	132	+0.4
Lee et al. (2010)	JI0	133	133	-0.1
Li et al. (2002)	A1	166	147	-11.0
	M1	188	170	-9.5
Li et al. (2009)	AS1	77	72	-7.2
	AL1	53	52	-1.8
	AS2	99	91	-7.9
	AL2	81	77	-5.6
Ohwada (1970)	NO1	43	40	-6.9
Ohwada (1973)	P2	32	32	-1.7
Ohwada (1977)	JO-1	19	18	-3.5
	JE-1	22	22	-0.9
Ota et al. (2004)	RC	318	301	-5.3
Owada (1984)	LJO-6	37	37	+1.1
	LJXY-6	40	40	-0.1
	LJXY-7	44	44	+1.1
	LJXY-8	36	38	+3.9
Owada (2000)	JO-5	40	41	+3.4
	JXY-3	50	51	+3.2
Pimanmas & Chaimahawan (2010)	J0	72	69	-4.0
Walker (2001)	PEER14	265	253	-4.5
	CD1514	286	276	-3.8
	CD3014	306	311	+1.9
	PADH14	332	335	+1.0
	PEER22	359	350	-2.7
	CD3022	376	416	+10.9
	PADH22	375	413	+10.2
Wang and Hsu (2009)	Ko-JI1	134	135	0.4
	Ho-JI1	146	141	-3.3

A.5 Simulated Response for Ductile Exterior Beam-Column Joint Subassemblages

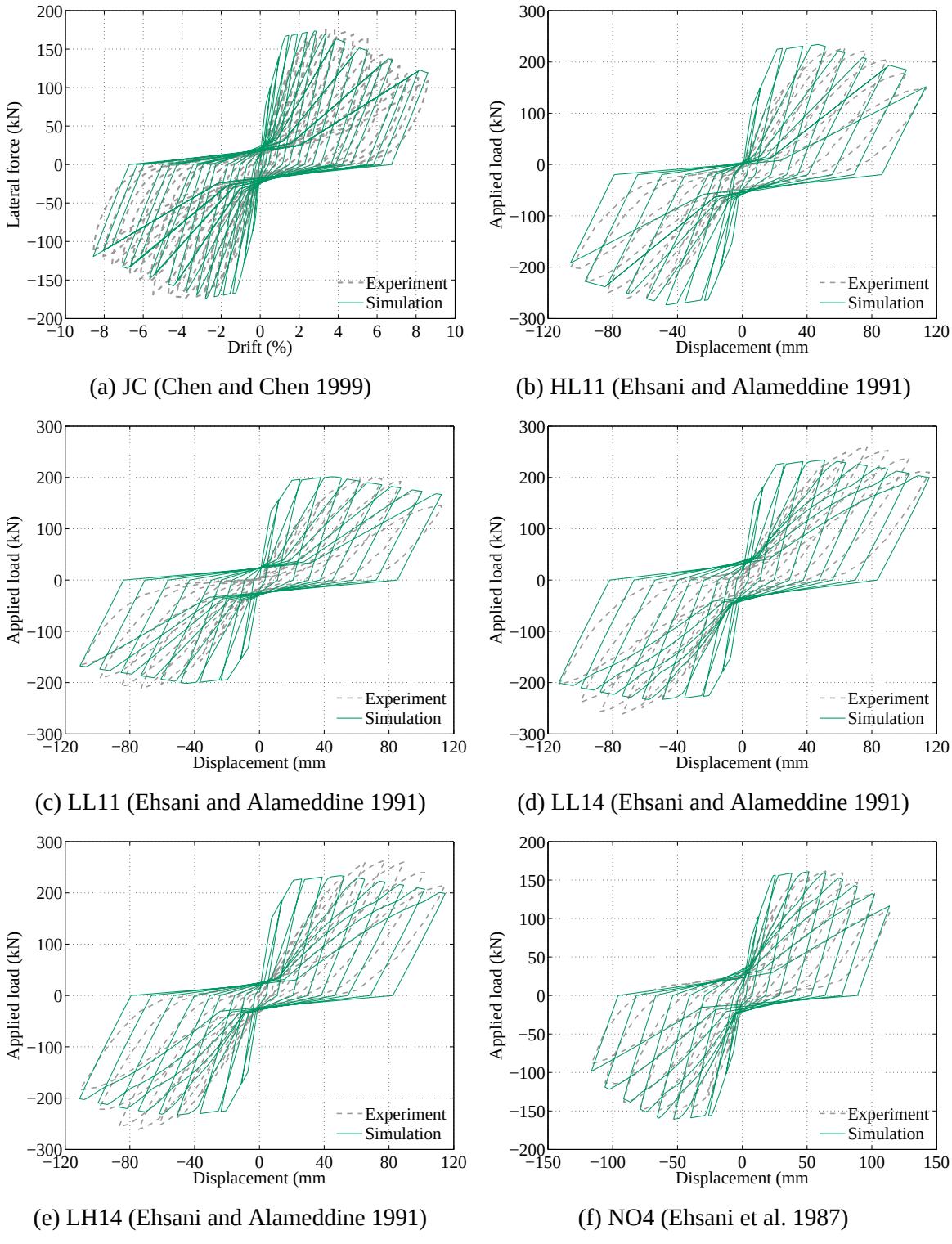

(a) JC (Chen and Chen 1999)

(b) HL11 (Ehsani and Alameddine 1991)

(c) LL11 (Ehsani and Alameddine 1991)

(d) LL14 (Ehsani and Alameddine 1991)

(e) LH14 (Ehsani and Alameddine 1991)

(f) NO4 (Ehsani et al. 1987)

Figure A.5 Comparison between hysteretic responses of experiment and analysis for ductile exterior joints

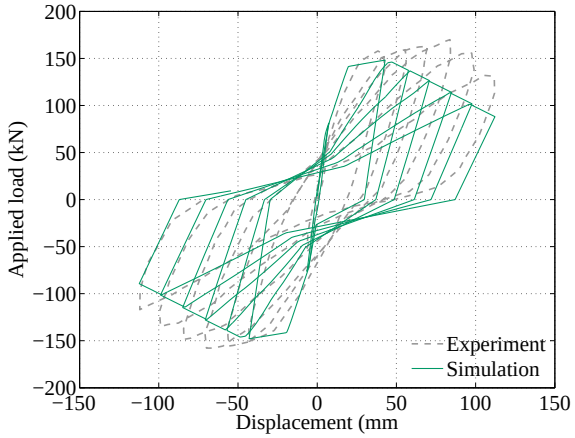

(a) NO5 (Ehsani et al. 1987)

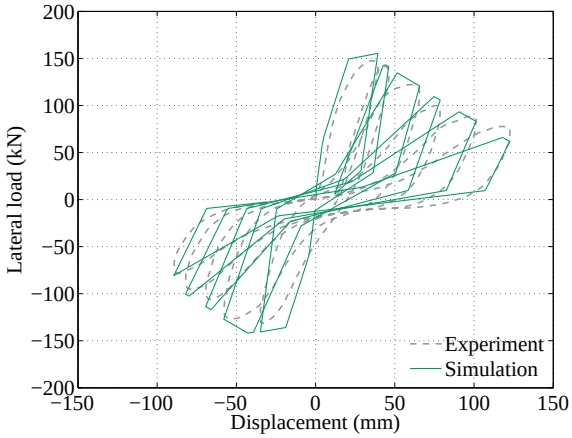

(b) 1B (Ehsani and Wight 1985)

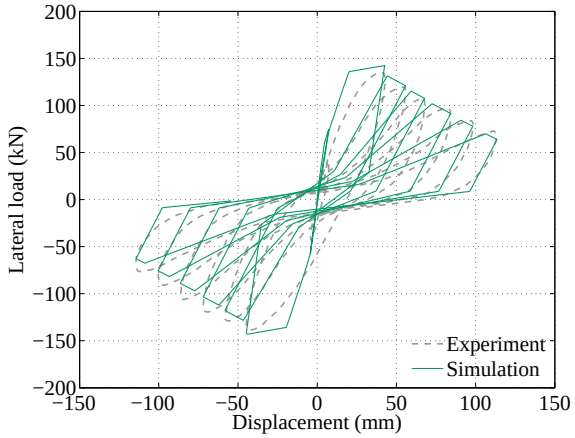

(c) 2B (Ehsani and Wight 1985)

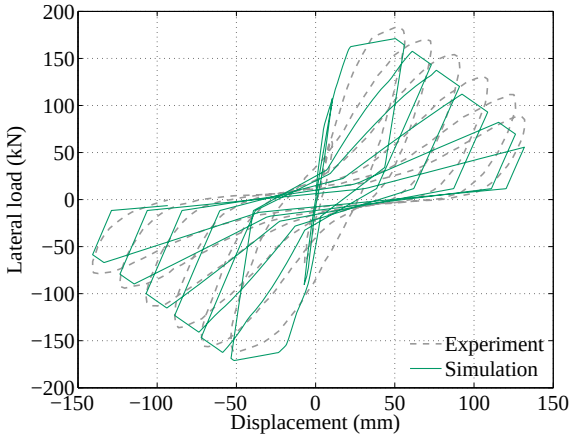

(d) 3B (Ehsani and Wight 1985)

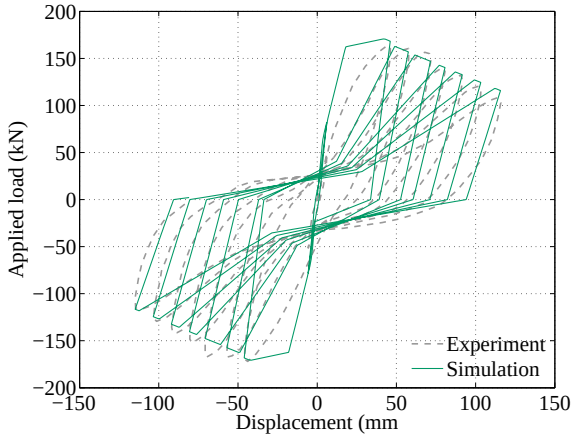

(e) 5B (Ehsani and Wight 1985)

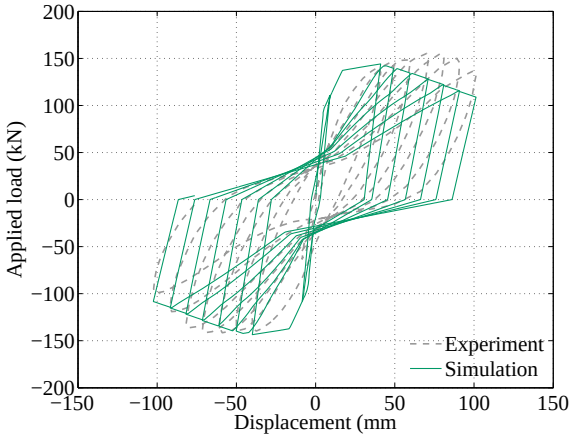

(f) 6B (Ehsani and Wight 1985)

Figure A.5 Comparison between hysteretic responses of experiment and analysis for ductile exterior joints (continued)

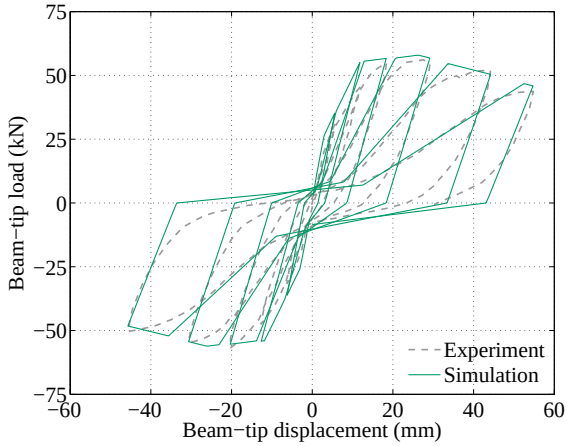

(a) B1 (Fujii and Morita 1991)

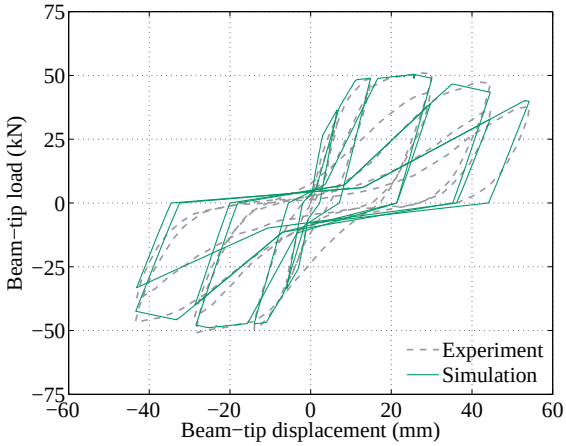

(b) B2 (Fujii and Morita 1991)

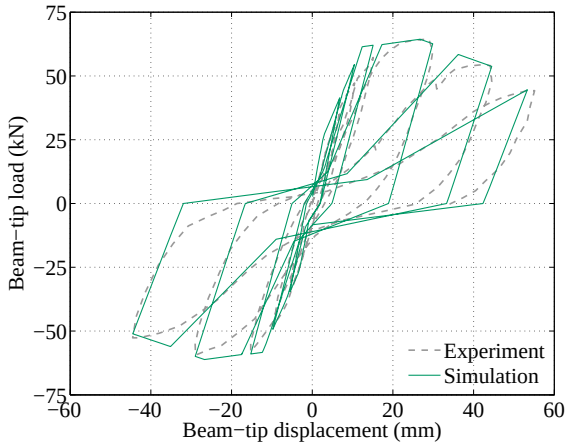

(c) B3 (Fujii and Morita 1991)

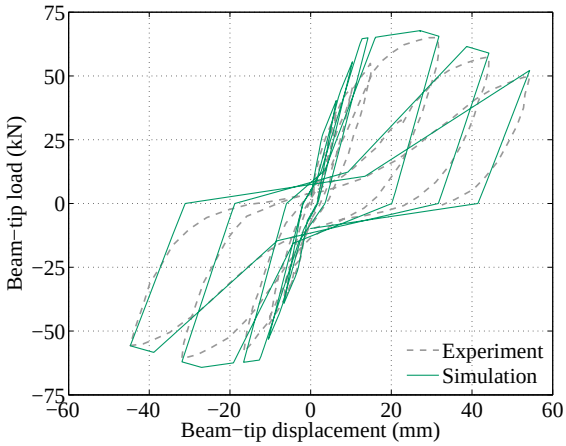

(d) B4 (Fujii and Morita 1991)

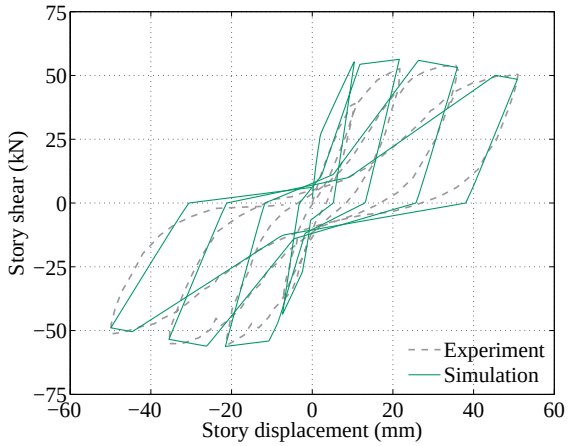

(e) A-0 (Ishida et al. 1996)

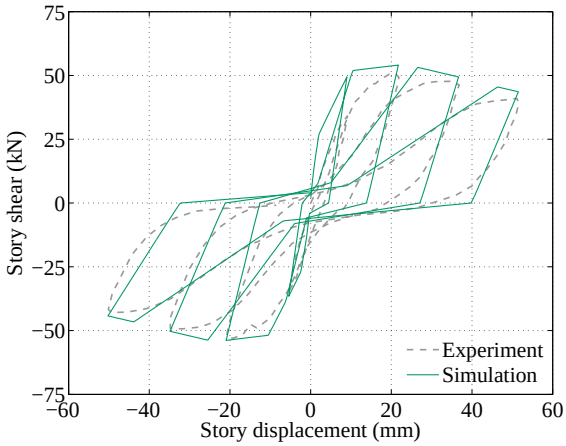

(f) A-0-F (Ishida et al. 1996)

Figure A.5 Comparison between hysteretic responses of experiment and analysis for ductile exterior joints (continued)

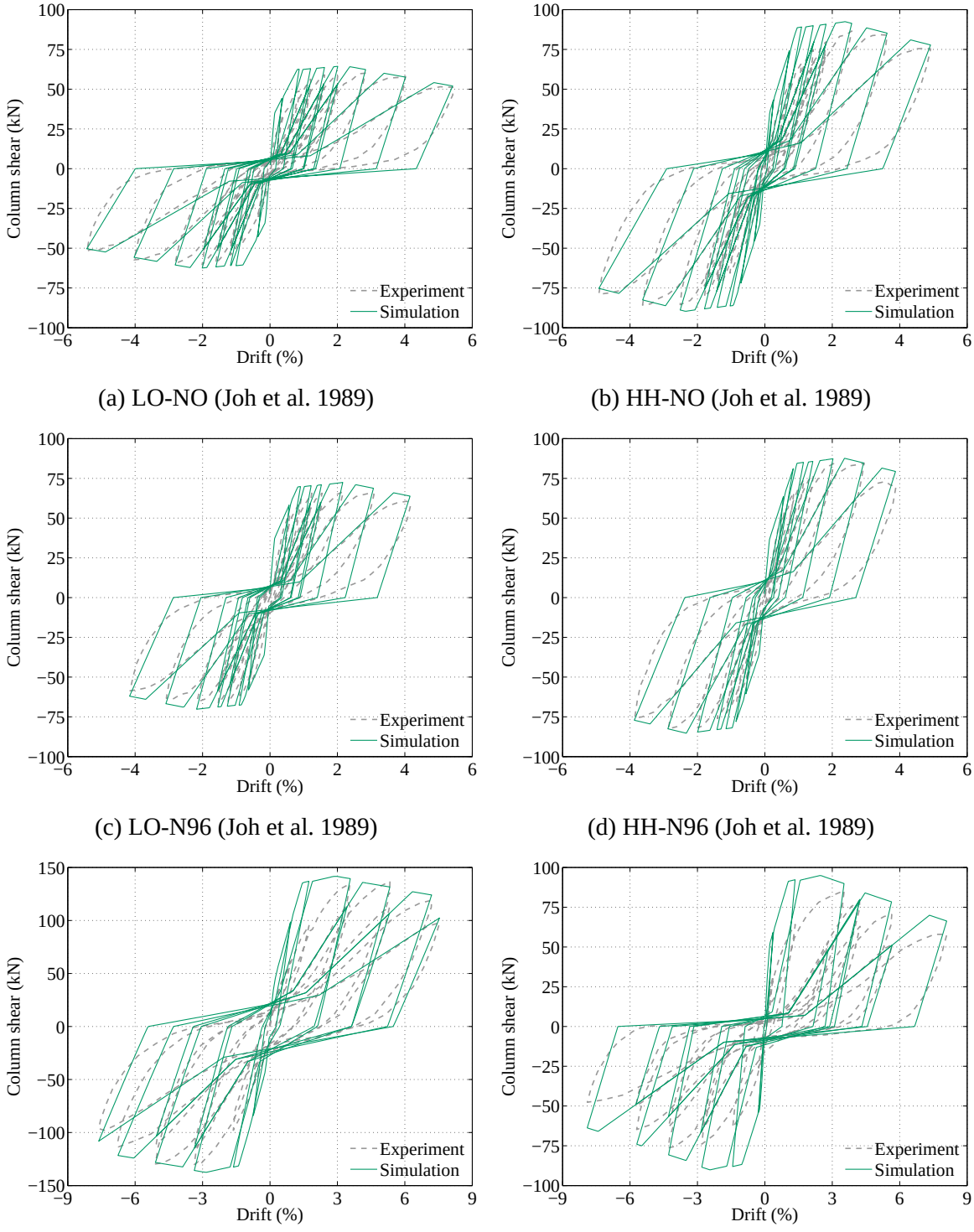

(a) LO-NO (Joh et al. 1989)

(b) HH-NO (Joh et al. 1989)

(c) LO-N96 (Joh et al. 1989)

(d) HH-N96 (Joh et al. 1989)

(e) NRC-J5 (Joh et al. 1992)

(f) NRC-J10 (Joh et al. 1992)

Figure A.5 Comparison between hysteretic responses of experiment and analysis for ductile exterior joints (continued)

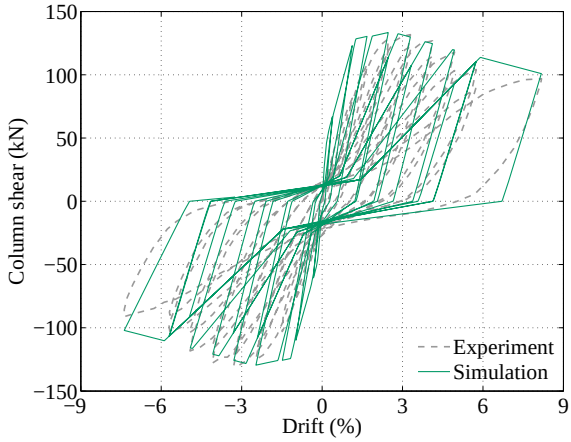

(a) NRC-J13 (Joh et al. 1992)

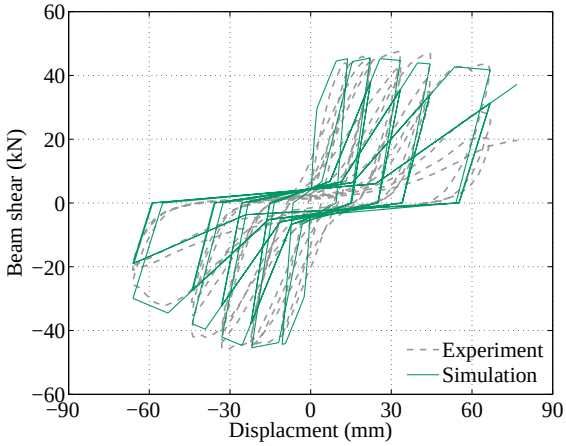

(b) NO03 (Kaku and Asakusa 1991)

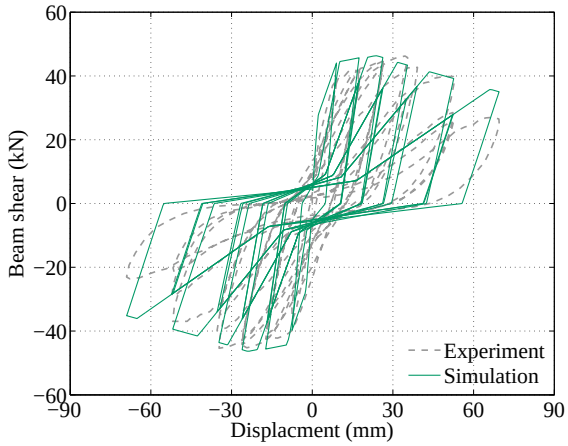

(c) NO05 (Kaku and Asakusa 1991)

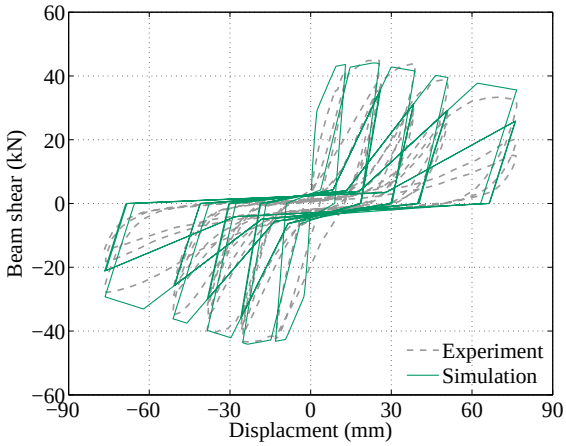

(d) NO06 (Kaku and Asakusa 1991)

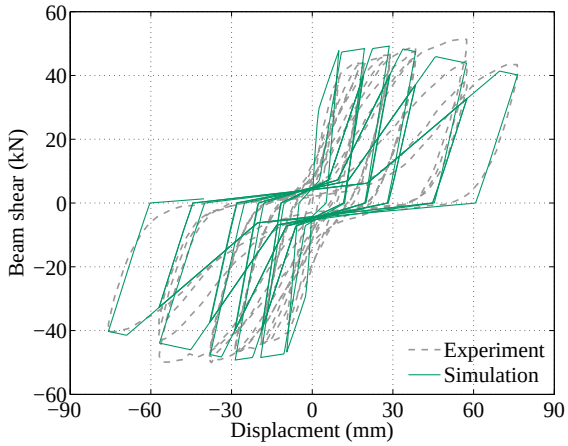

(e) NO09 (Kaku and Asakusa 1991)

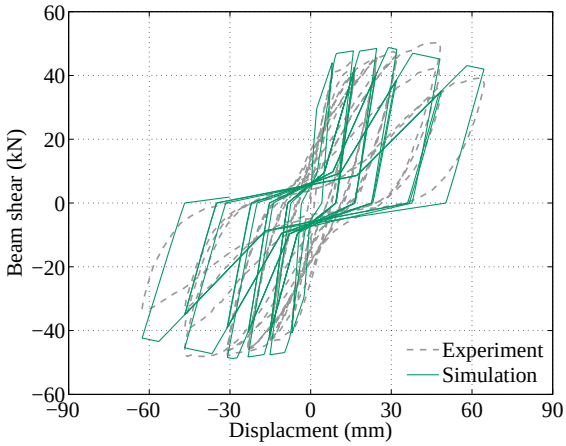

(f) NO11 (Kaku and Asakusa 1991)

Figure A.5 Comparison between hysteretic responses of experiment and analysis for ductile exterior joints (continued)

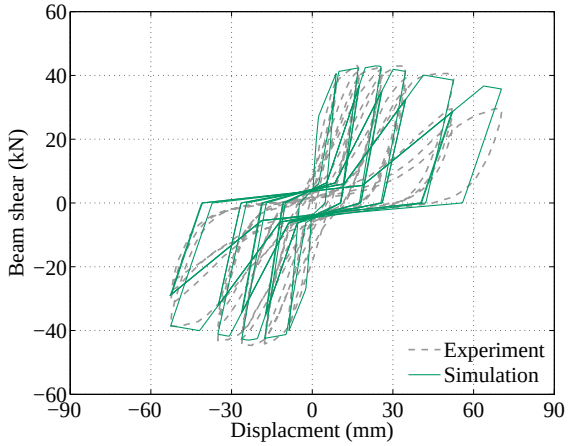

(a) NO12 (Kaku and Asakusa 1991)

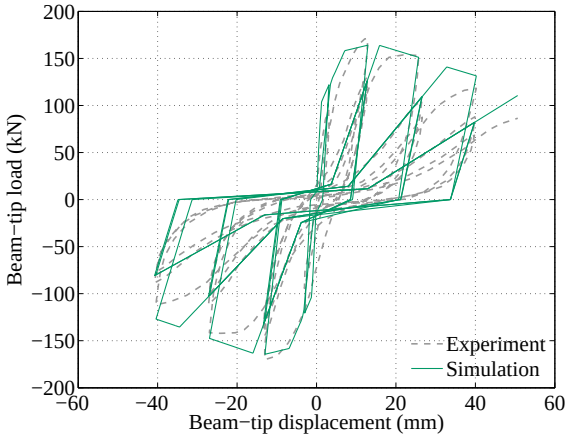

(b) U41L (Kanada et al. 1984)

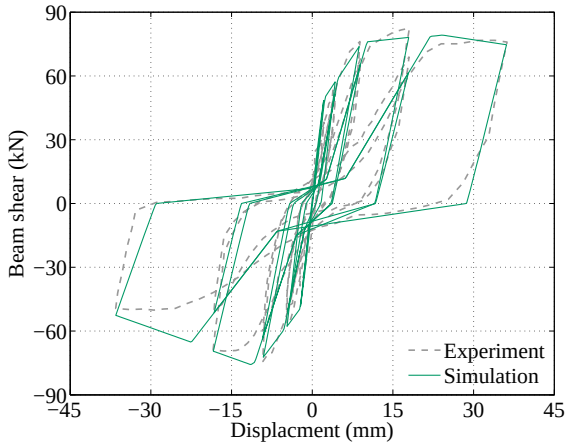

(c) EJ+0.0 (Lee and Lee 2000)

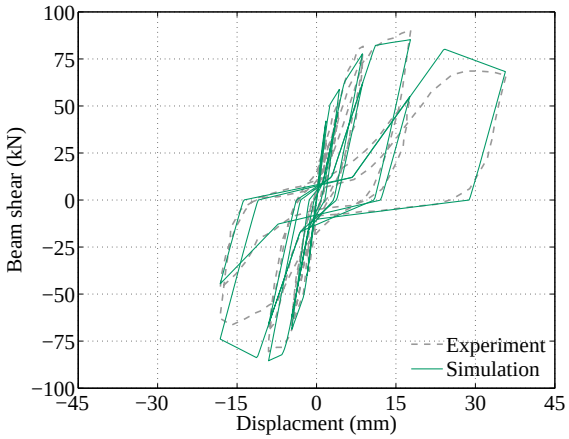

(d) EJ+0.1 (Lee and Lee 2000)

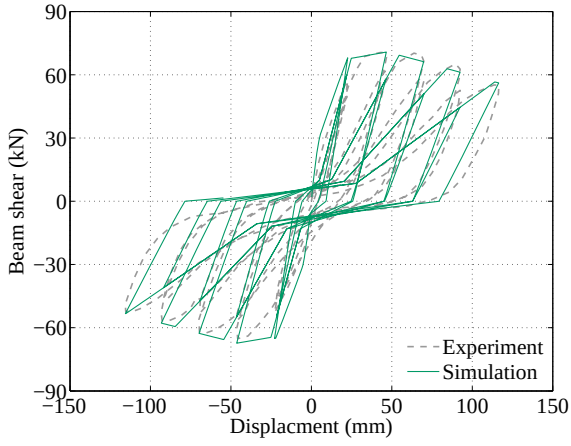

(e) RC-2 (Nishiyama et al. 1989)

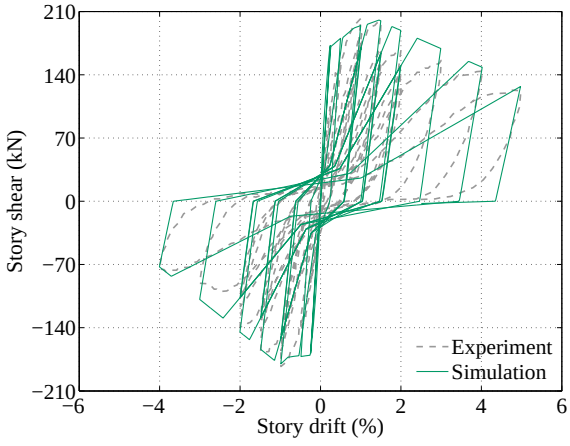

(f) O-5 (Takeuchi et al. 2003)

Figure A.5 Comparison between hysteretic responses of experiment and analysis for ductile exterior joints (continued)

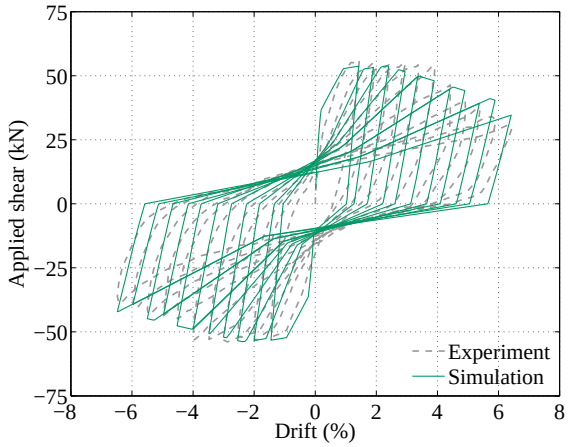

(a) A1 (Tsonos 2007)

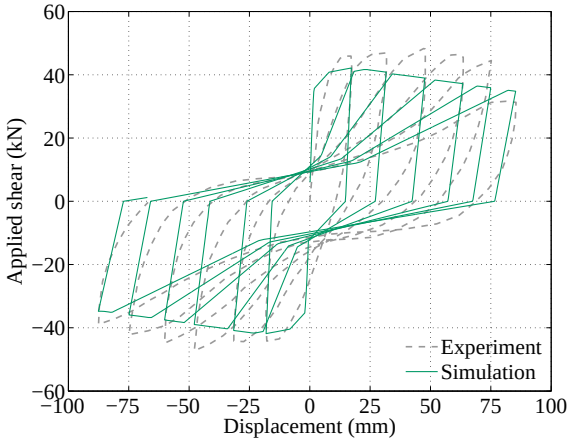

(b) S1 (Tsonos et al. 1992)

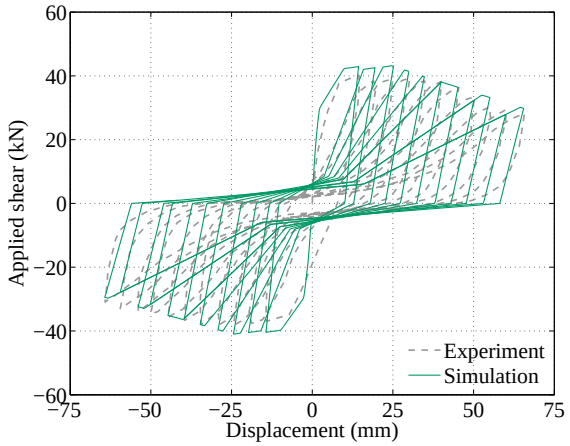

(c) S2 (Tsonos et al. 1992)

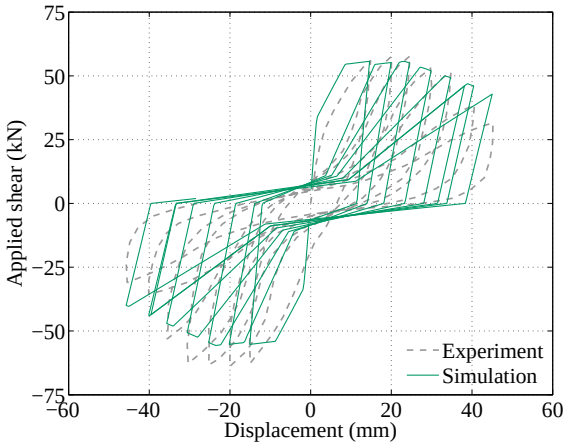

(d) S6 (Tsonos et al. 1992)

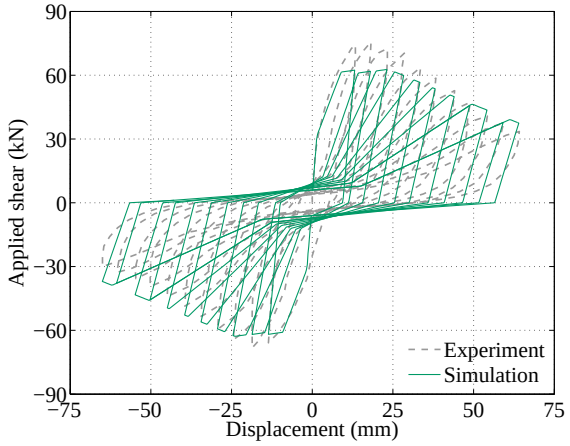

(e) S6’ (Tsonos et al. 1992)

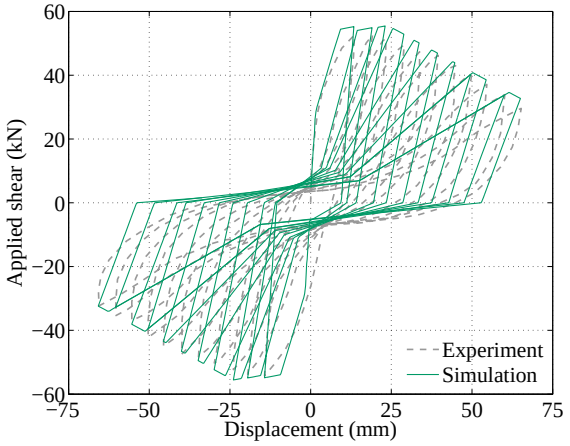

(f) F2 (Tsonos et al. 1992)

Figure A.5 Comparison between hysteretic responses of experiment and analysis for ductile exterior joints (continued)

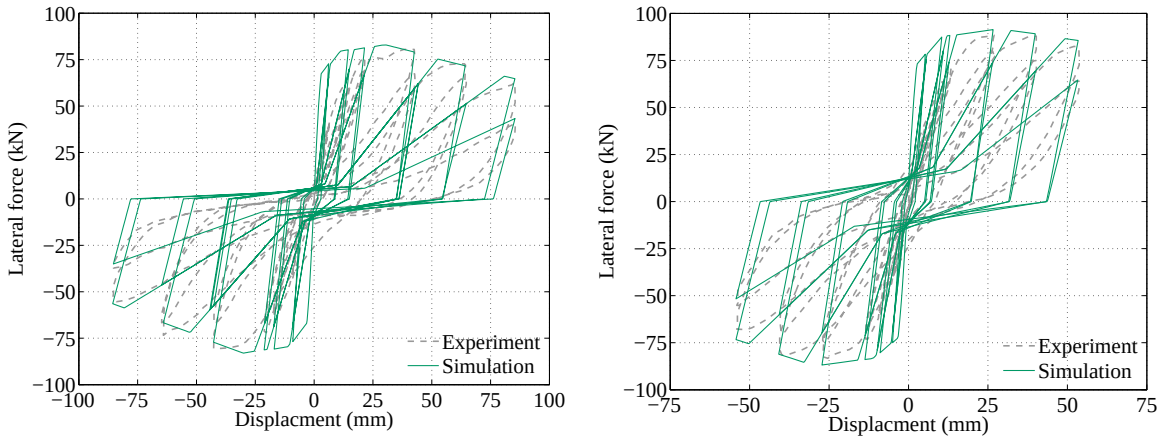

(a) JA-NY03 (Wong 2005)

(b) JA-NY15 (Wong 2005)

Figure A.5 Comparison between hysteretic responses of experiment and analysis for ductile exterior joints (continued)

Table A.4 Comparison of experimental and analytical maximum lateral force for ductile exterior beam-column joint subassemblages

Reference	Specimen	Maximum lateral force (kN)		Difference
		Experiment	Analysis	(%)
Chen and Chen (1999)	JC	175	174	-1.1
Ehsani & Alameddine (1991)	HL11	262	273	+4.6
	LL11	212	202	-5.0
	LL14	261	234	-10.4
	LH14	264	233	-11.5
Ehsani et al. (1987)	NO4	161	161	-0.4
	NO5	170	148	-14.7
Ehsani and Wight (1985)	1B	147	155	+5.1
	2B	139	143	+3.0
	3B	183	171	-6.9
	5B	172	171	-0.7
	6B	155	144	-7.8
Fujii and Morita (1991)	B1	57	58	+1.9
	B2	51	50	-1.2
	B3	64	64	-0.1
	B4	65	68	+4.1
Ishida et al. (1996)	A-0	55	56	+1.5
	A-0-F	53	54	+2.0
Joh et al. (1989)	LO-NO	60	64	+6.2
	HH-NO	87	92	+6.4
	LO-N96	67	72	+7.9
	HH-N96	85	88	+3.4
Joh et al. (1992)	NRC-J5	137	142	+3.5
	NRC-J10	85	95	+10.0
	NRC-J13	132	133	+1.2
Kaku and Asakusa (1991)	NO03	48	45	-4.9
	NO05	46	46	+0.3
	NO06	45	44	-1.6
	NO09	51	49	-4.3
	NO11	50	49	-3.3
	NO12	43	43	-0.2
Kanada et al. (1984)	U41L	171	164	-4.2
Lee and Lee (2000)	EJ+0.0	82	79	-4.1
	EJ+0.1	90	85	-5.7
Nishiyama et al.(1989)	RC-2	71	71	+0.3
Takeuchi et al. (2003)	O-5	203	201	-1.0
Tsonos (2007)	A1	56	54	-3.7
Tsonos et al. (1992)	S1	48	42	-14.5
	S2	40	43	+7.0
	S6	58	56	-3.7
	S6'	76	63	-20.5
	F2	54	56	+2.4
Wong (2005)	JA-NY03	81	83	+3.0
	JA-NY15	88	91	+3.3

A.6 Simulated Response for Ductile Interior Beam-Column Joint Subassemblages

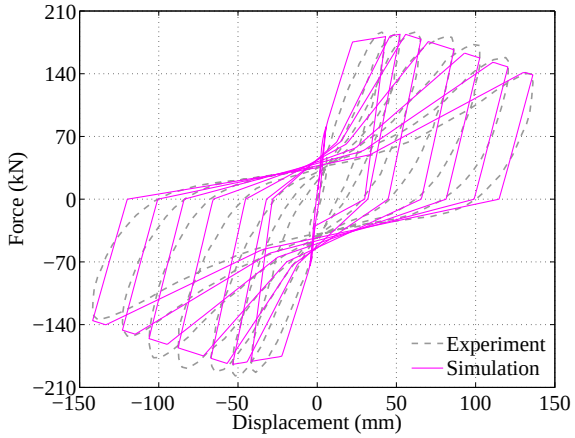

(a) X1 (Durrani and Wight 1985)

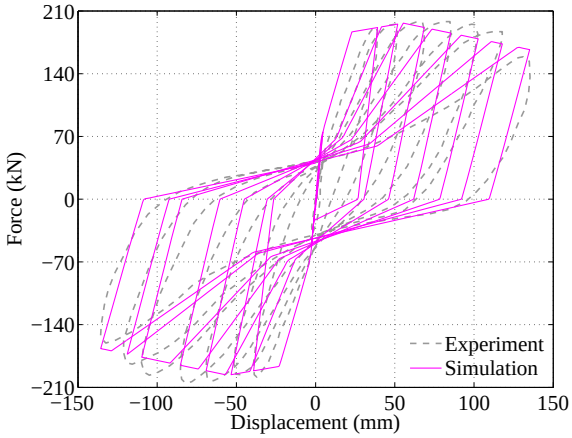

(b) X2 (Durrani and Wight 1985)

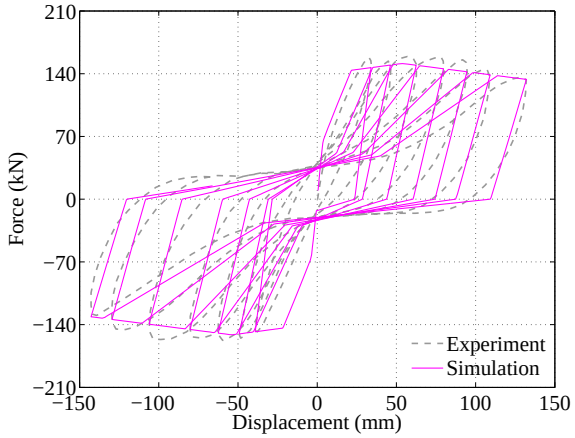

(c) X3 (Durrani and Wight 1985)

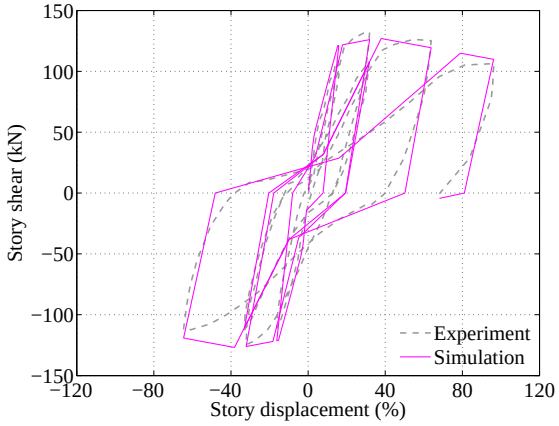

(d) HLC (Endoh et al. 1991)

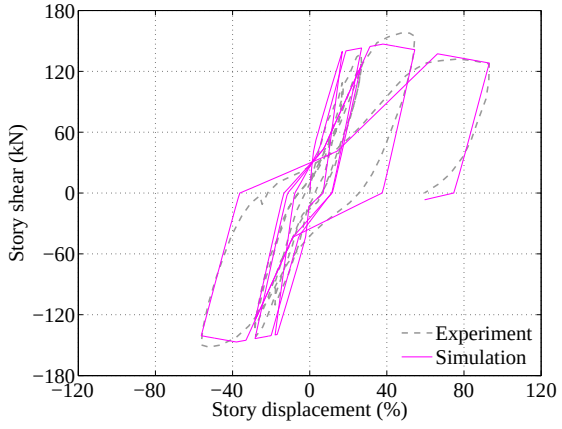

(e) LA1 (Endoh et al. 1991)

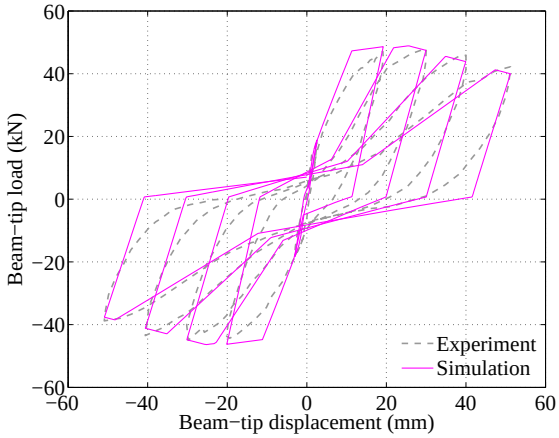

(f) A1 (Fujii and Morita 1991)

Figure A.6 Comparison between hysteretic responses of experiment and analysis for ductile interior joints

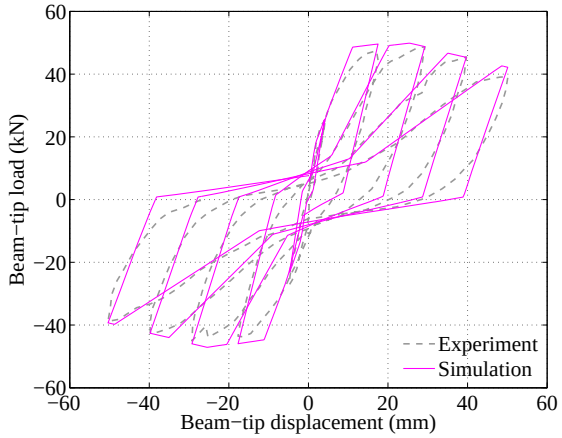

(a) A3 (Fujii and Morita 1991)

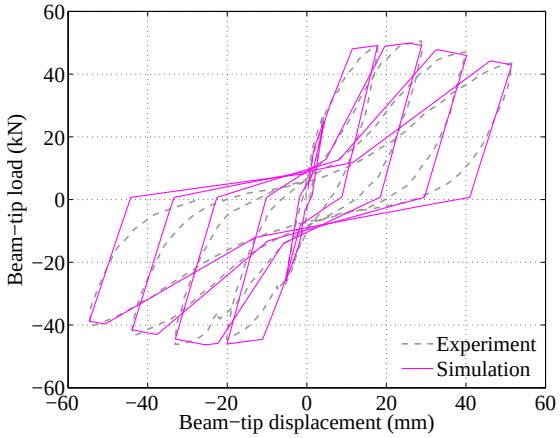

(b) A4 (Fujii and Morita 1991)

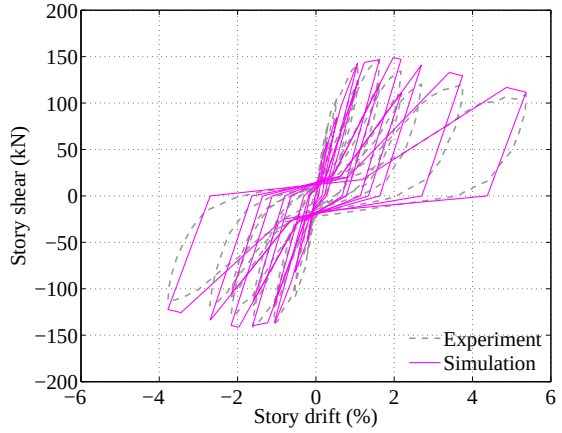

(c) HH (Goto and Joh 1996)

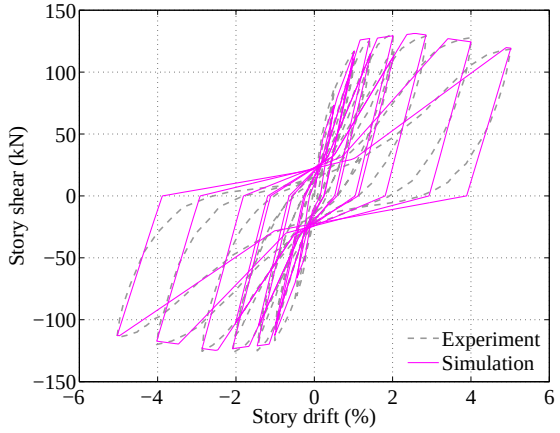

(d) LM-60 (Goto and Joh 2003)

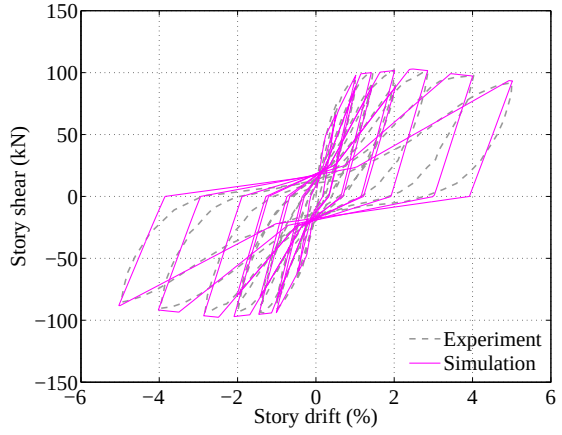

(e) LM-125 (Goto and Joh 2003)

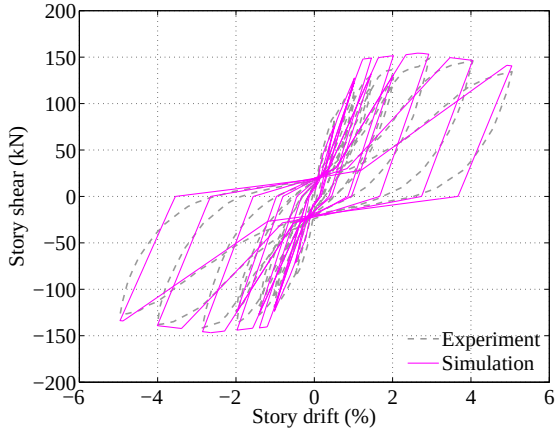

(f) HM-60 (Goto and Joh 2003)

Figure A.6 Comparison between hysteretic responses of experiment and analysis for ductile interior joints (continued)

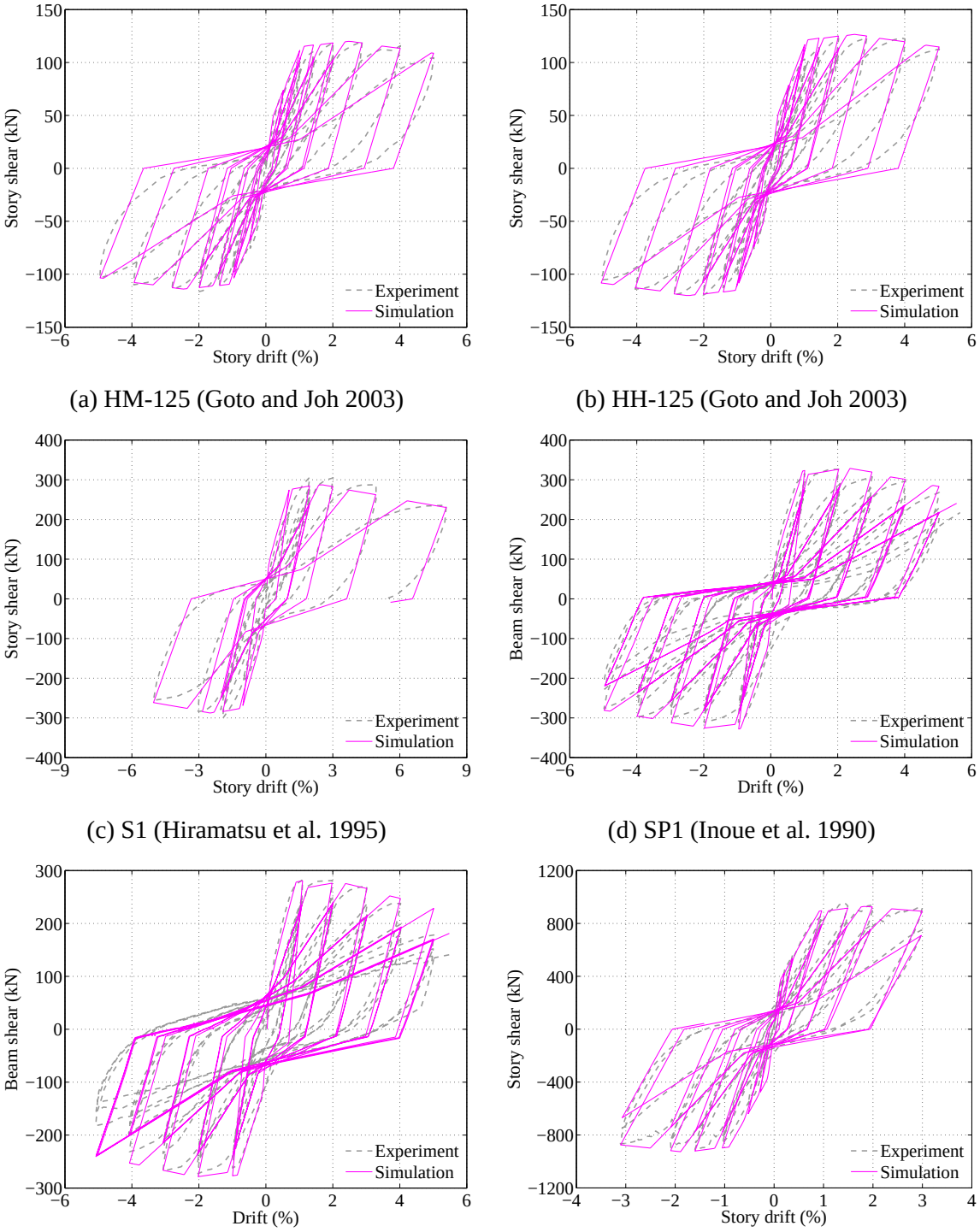

Figure A.6 Comparison between hysteretic responses of experiment and analysis for ductile interior joints (continued)

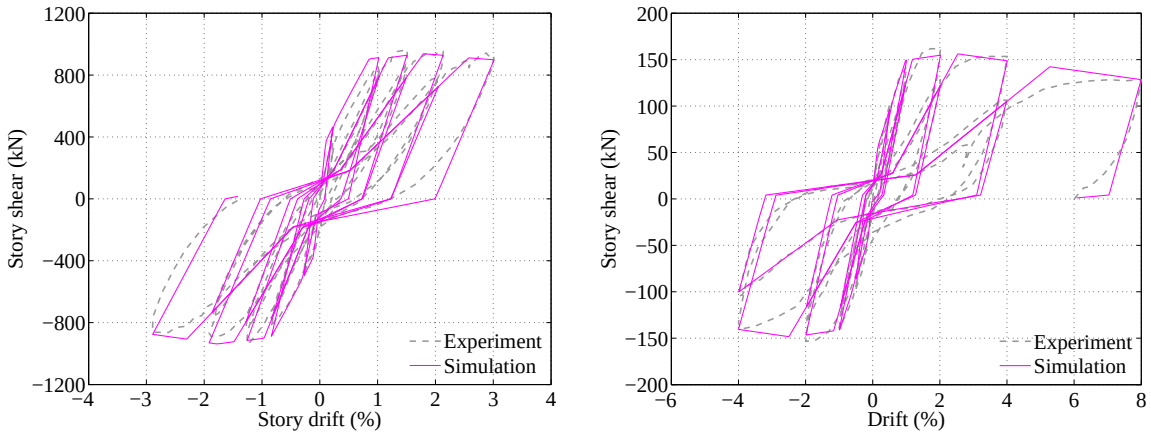

(a) ES (Ishida et al. 1996)

(b) NO1 (Jinno et al. 1991)

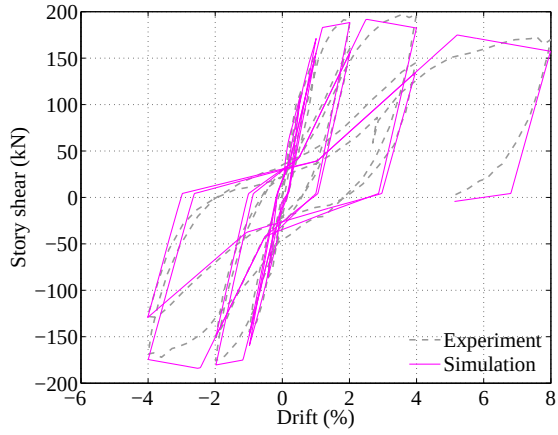

(c) NO2 (Jinno et al. 1991)

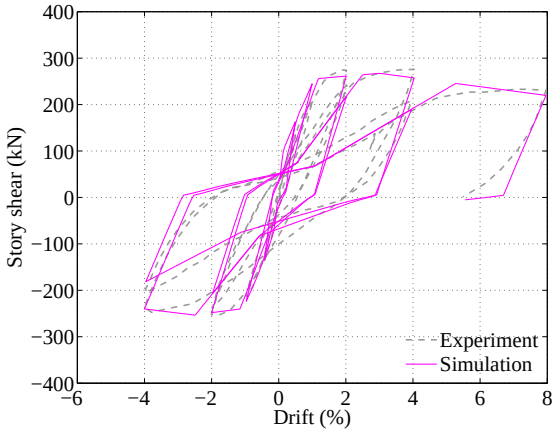

(d) NO3 (Jinno et al. 1991)

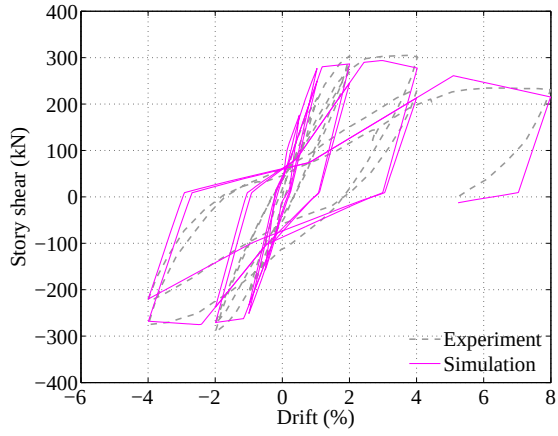

(e) NO4 (Jinno et al. 1991)

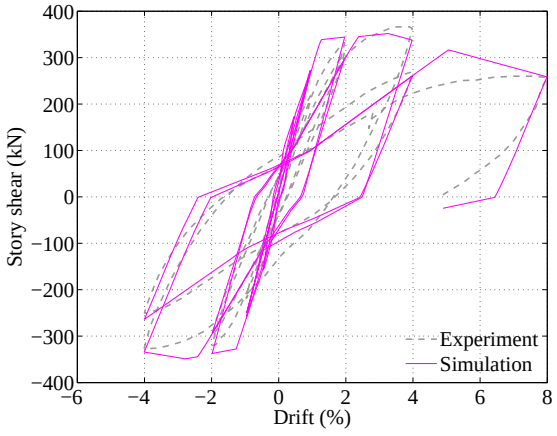

(f) NO5 (Jinno et al. 1991)

Figure A.6 Comparison between hysteretic responses of experiment and analysis for ductile interior joints (continued)

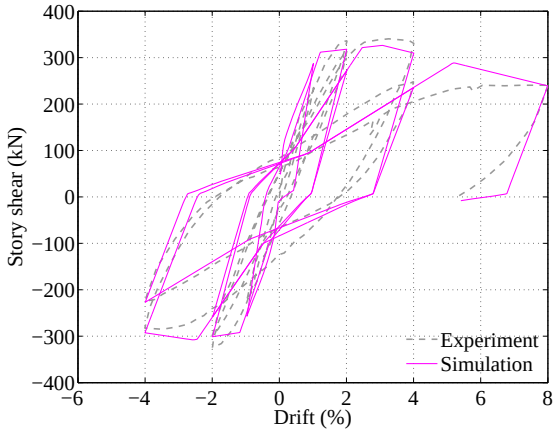

(a) NO6 (Jinno et al. 1991)

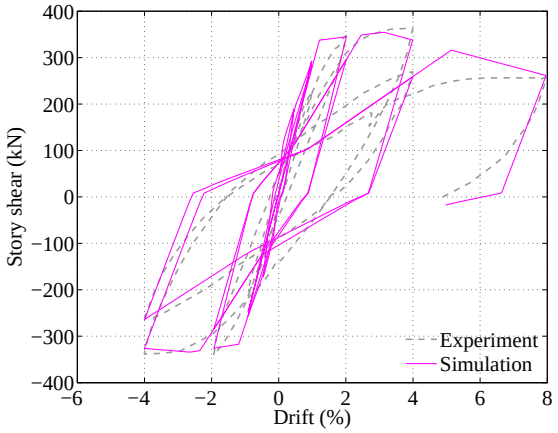

(b) NO7 (Jinno et al. 1991)

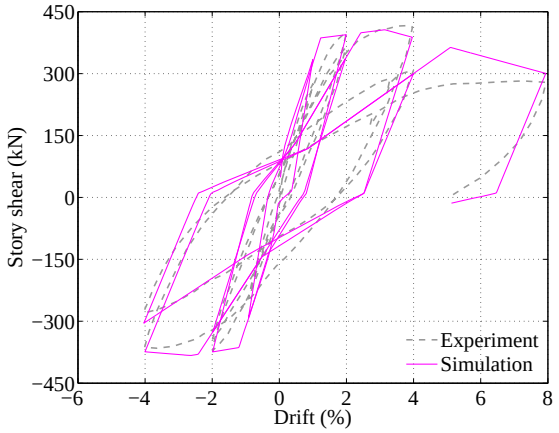

(c) NO8 (Jinno et al. 1991)

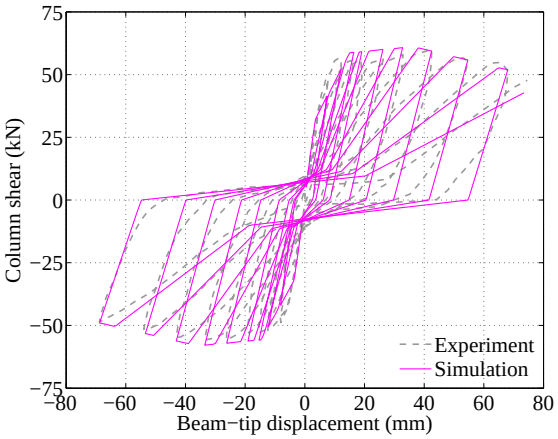

(d) JXO-B1 (Joh et al. 1991a)

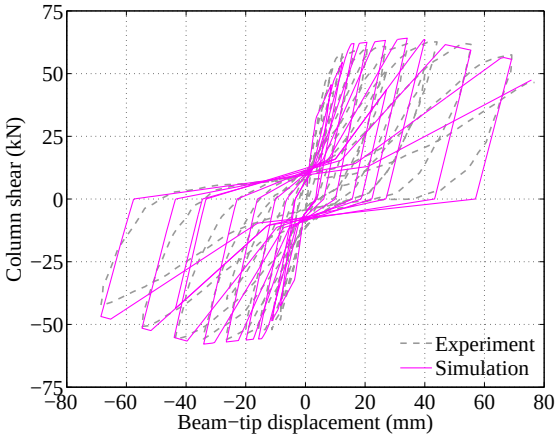

(e) JXO-B5 (Joh et al. 1991a)

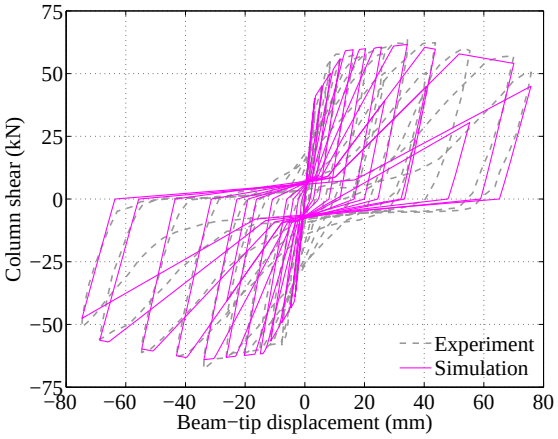

(f) JXO-B8MH (Joh et al. 1991b)

Figure A.6 Comparison between hysteretic responses of experiment and analysis for ductile interior joints (continued)

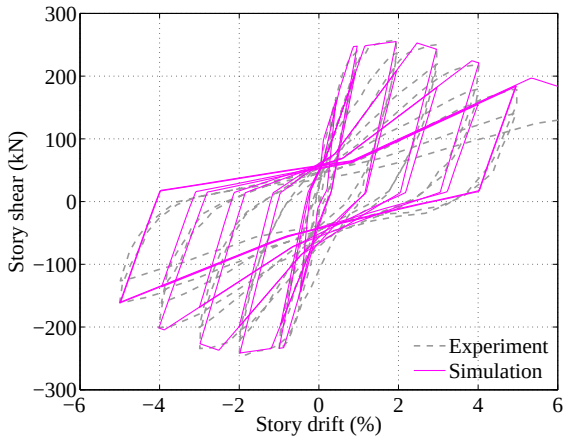

(a) J31A (Kaku et al. 1993)

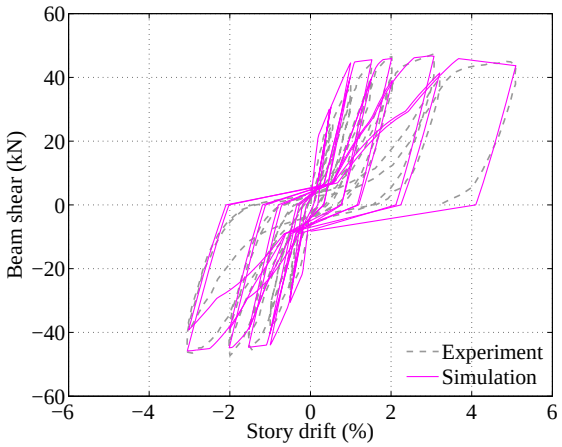

(b) NN.1 (Kamimura et al. 2004)

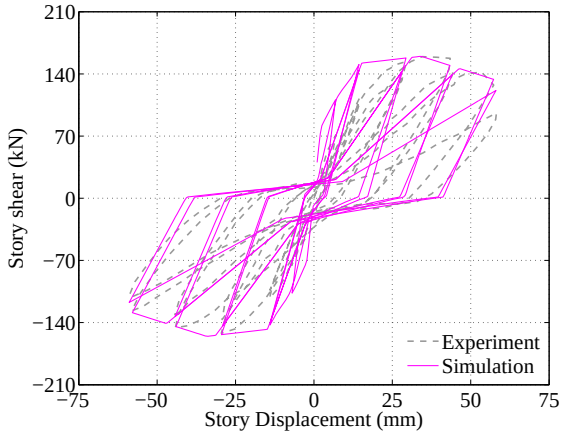

(c) MKJ-1 (Kashiwasazaki et al. 1992)

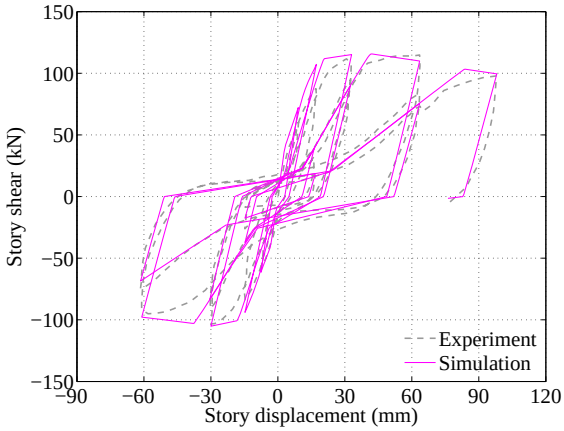

(d) J1 (Kitayama et al. 1991)

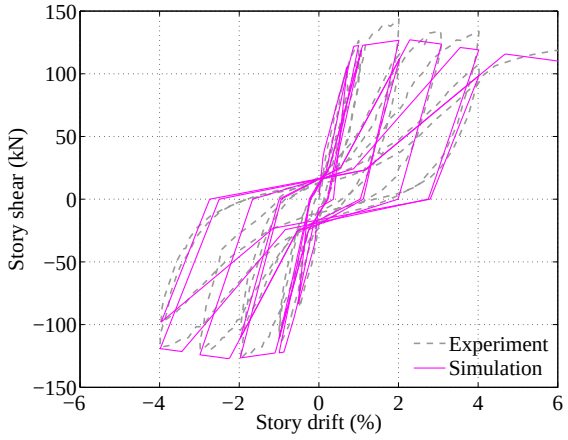

(e) PB1 (Kitayama et al. 2000)

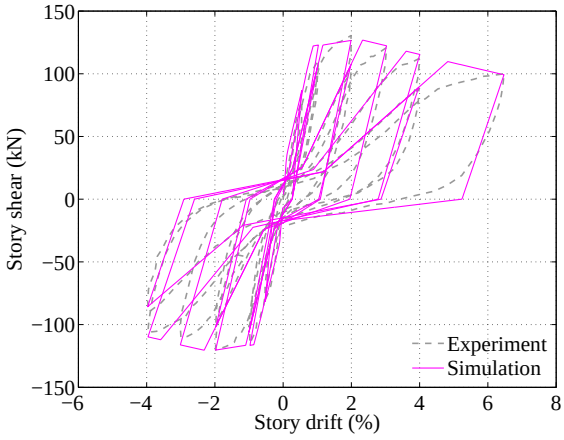

(f) PNB2 (Kitayama et al. 2000)

Figure A.6 Comparison between hysteretic responses of experiment and analysis for ductile interior joints (continued)

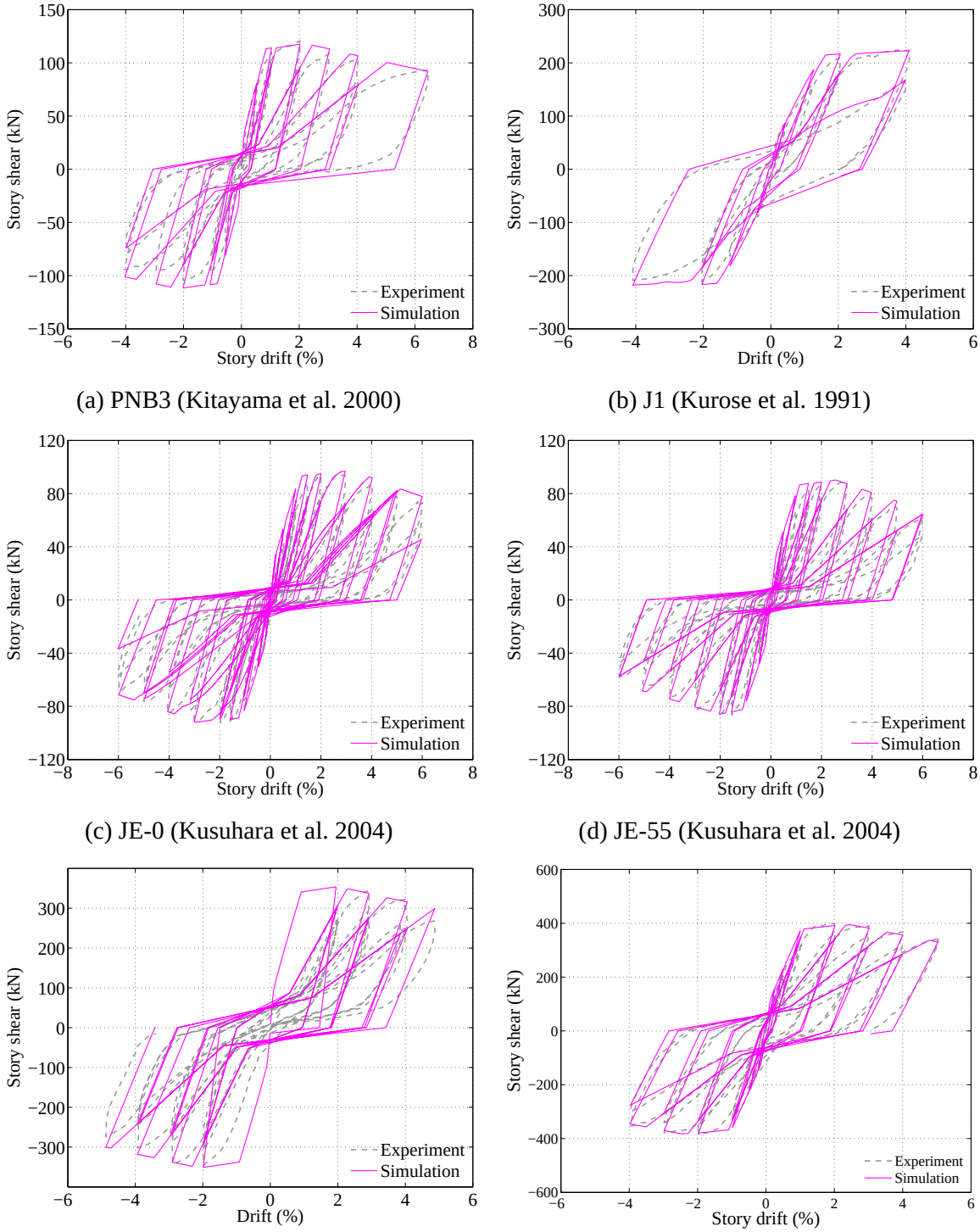

(a) PNB3 (Kitayama et al. 2000)

(b) J1 (Kurose et al. 1991)

(c) JE-0 (Kusuhara et al. 2004)

(d) JE-55 (Kusuhara et al. 2004)

(e) J1 (Lee et al. 2009)

(f) B-0 (Matsumoto et al. 2010)

Figure A.6 Comparison between hysteretic responses of experiment and analysis for ductile interior joints (continued)

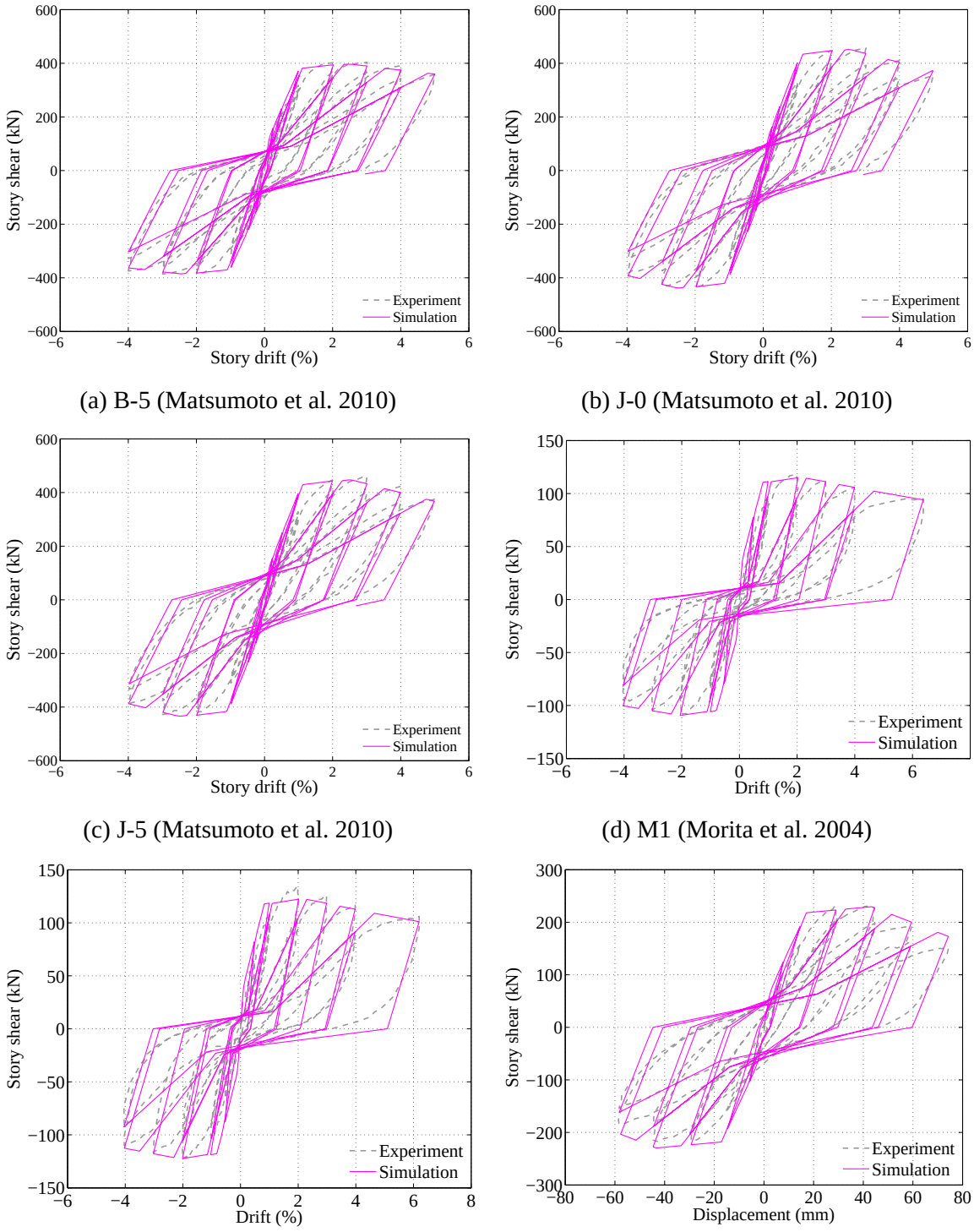

(a) B-5 (Matsumoto et al. 2010)

(b) J-0 (Matsumoto et al. 2010)

(c) J-5 (Matsumoto et al. 2010)

(d) M1 (Morita et al. 2004)

(e) M6 (Morita et al. 2004)

(f) OKJ-1 (Noguchi and Kashiwazaki 1992)

Figure A.6 Comparison between hysteretic responses of experiment and analysis for ductile interior joints (continued)

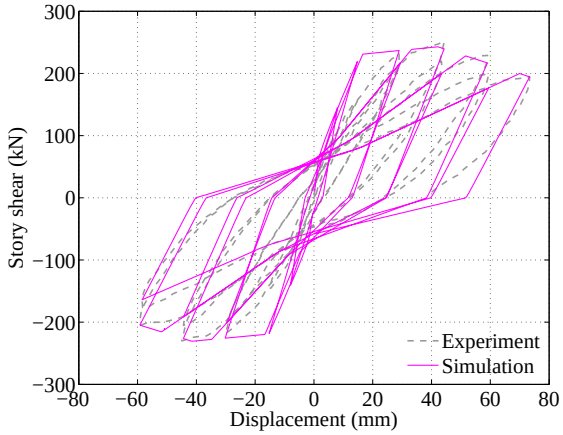

(a) OKJ-4 (Noguchi and Kashiwazaki 1992)

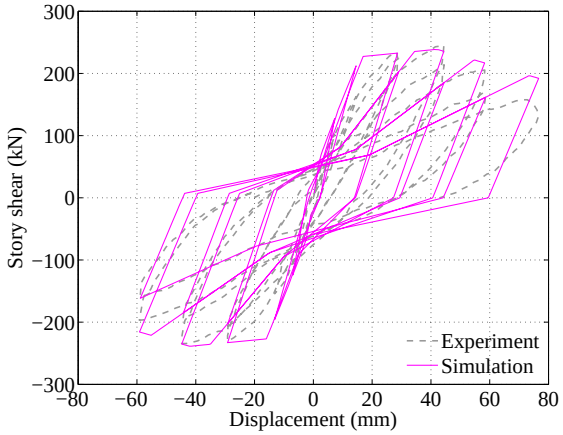

(b) OKJ-5 (Noguchi and Kashiwazaki 1992)

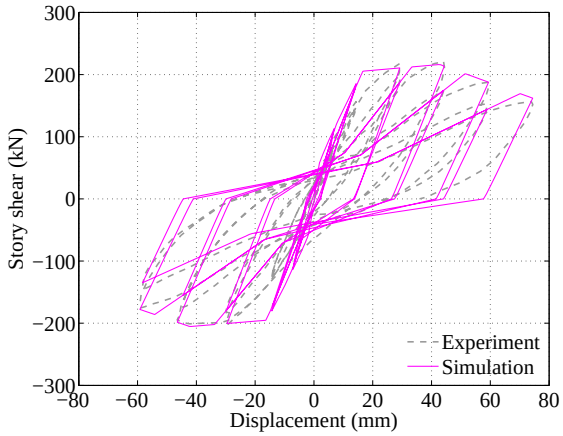

(c) OKJ-6 (Noguchi and Kashiwazaki 1992)

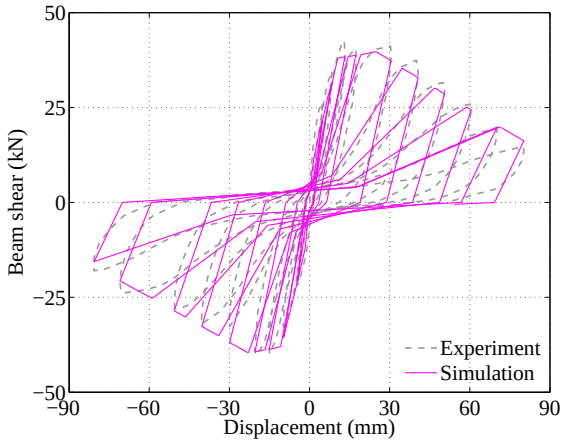

(d) No. 2 (Ohwada 1970)

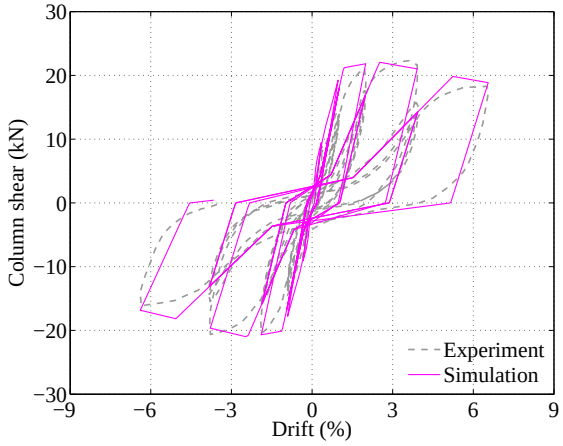

(e) JO-2 (Ohwada 1977)

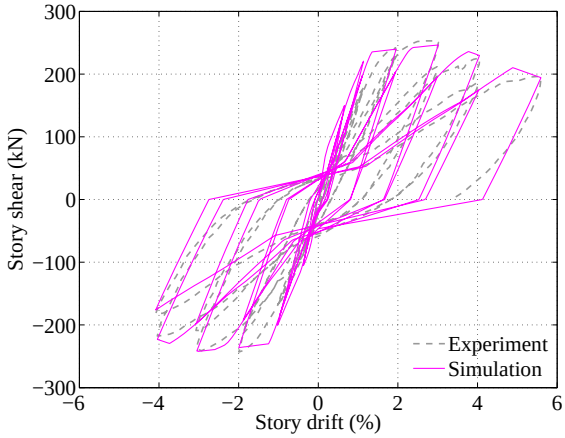

(f) J-1 (Oka and Shiohara 1992)

Figure A.6 Comparison between hysteretic responses of experiment and analysis for ductile interior joints (continued)

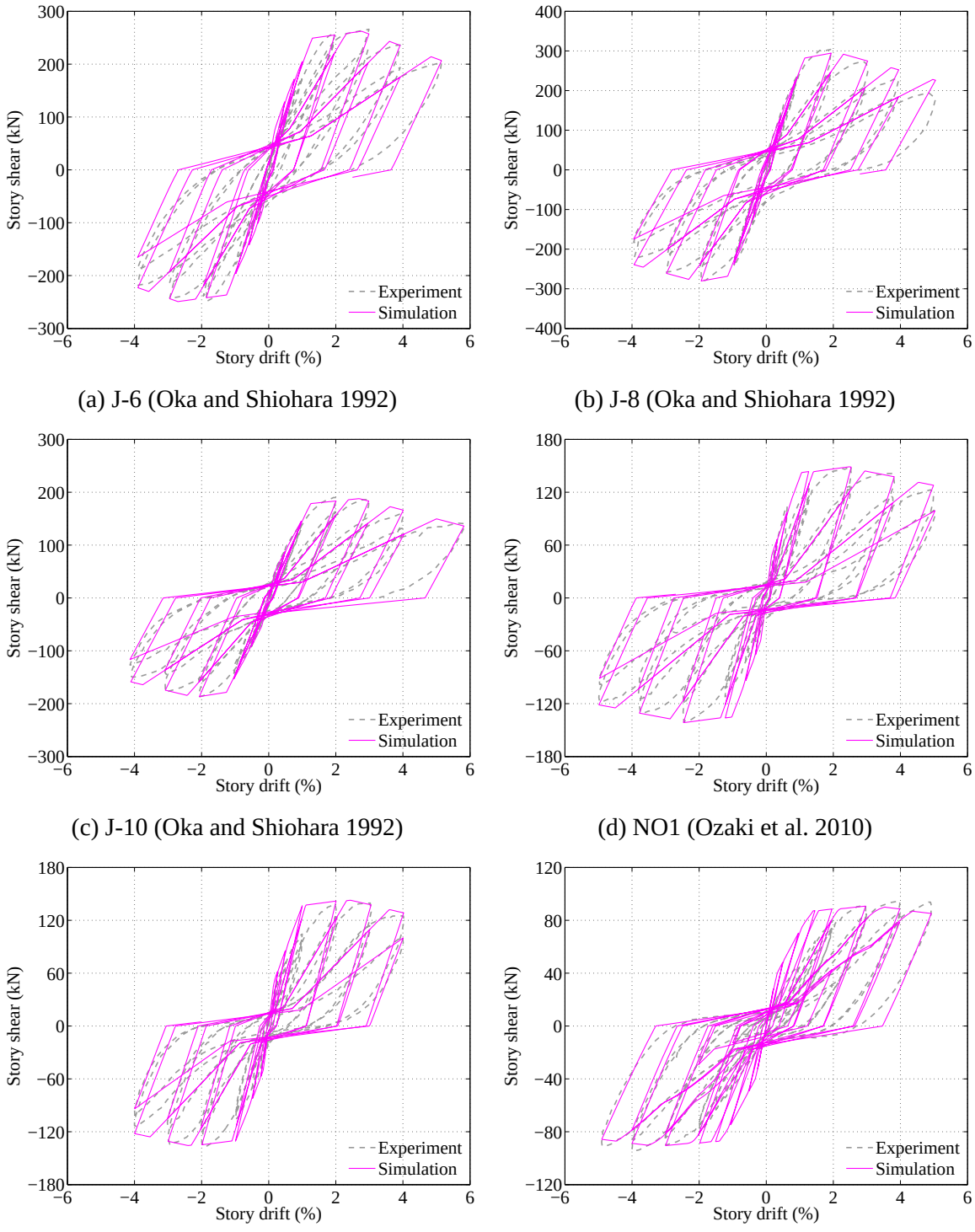

(a) J-6 (Oka and Shiohara 1992)

(b) J-8 (Oka and Shiohara 1992)

(c) J-10 (Oka and Shiohara 1992)

(d) NO1 (Ozaki et al. 2010)

(e) NO2 (Ozaki et al. 2010)

(f) SP1 (Raffaelle and Wight 1995)

Figure A.6 Comparison between hysteretic responses of experiment and analysis for ductile interior joints (continued)

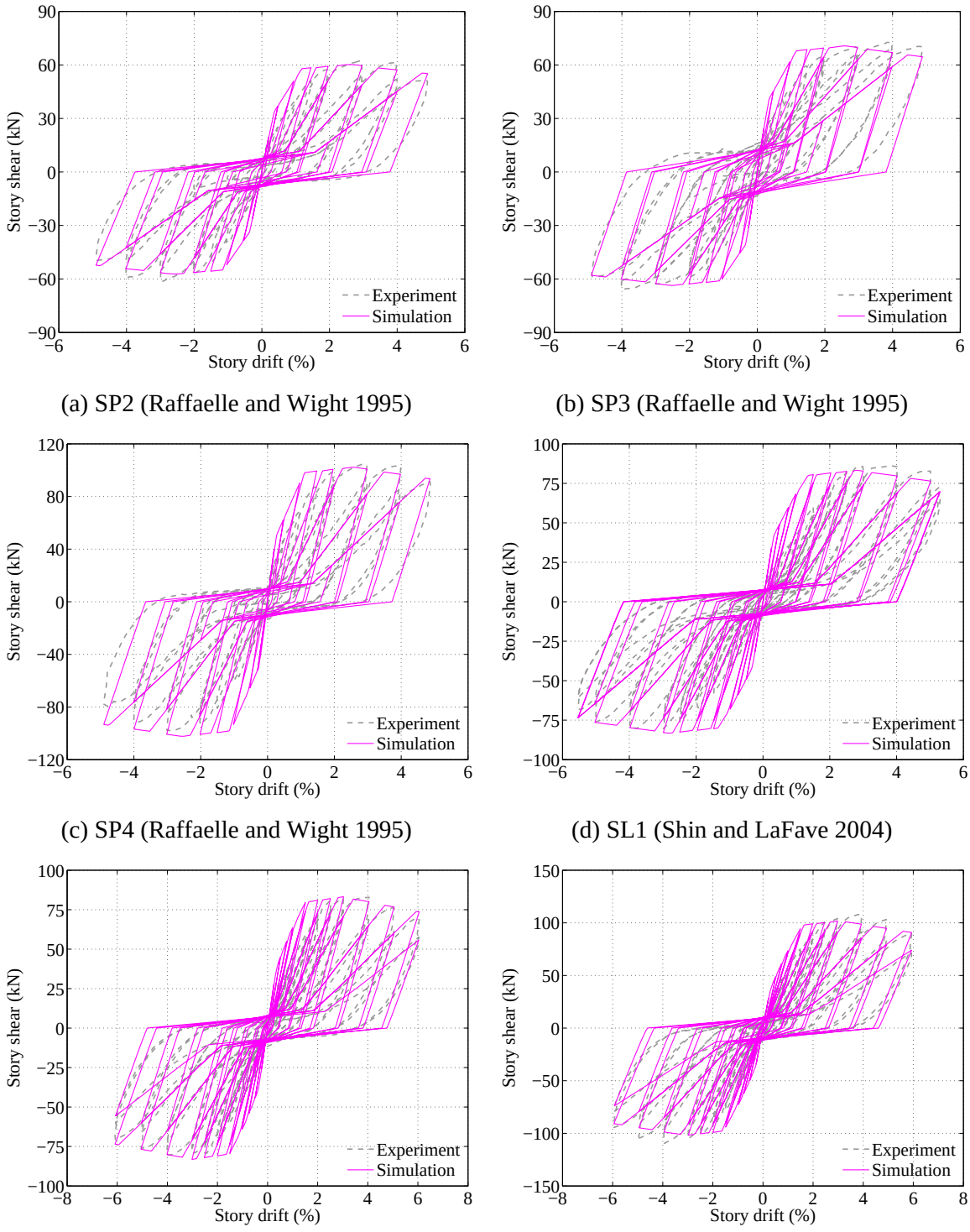

(a) SP2 (Raffaelle and Wight 1995)

(b) SP3 (Raffaelle and Wight 1995)

(c) SP4 (Raffaelle and Wight 1995)

(d) SL1 (Shin and LaFave 2004)

(e) SL2 (Shin and LaFave 2004)

(f) SL4 (Shin and LaFave 2004)

Figure A.6 Comparison between hysteretic responses of experiment and analysis for ductile interior joints (continued)

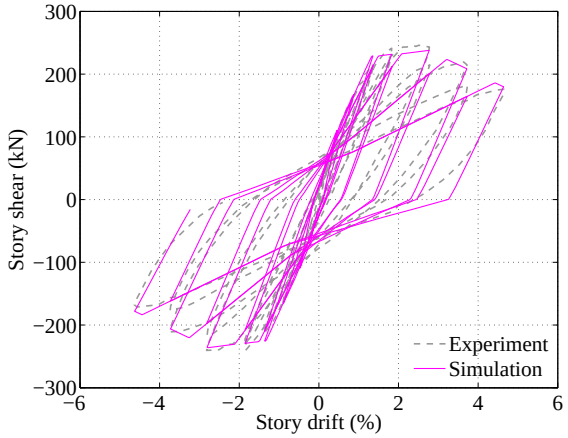

(a) B-1 (Shinjo et al. 2009)

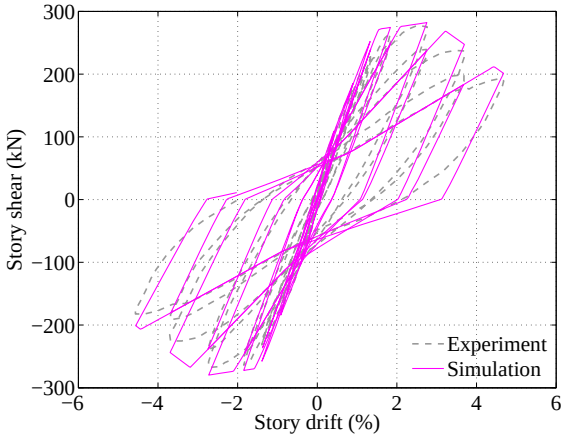

(b) J-1 (Shinjo et al. 2009)

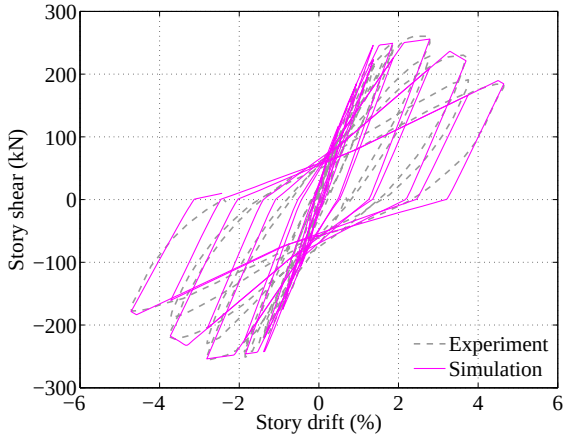

(c) BJ-1 (Shinjo et al. 2009)

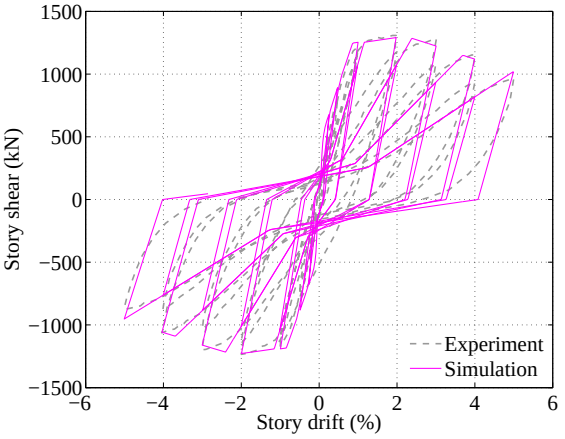

(d) NO1 (Takamori et al. 2006)

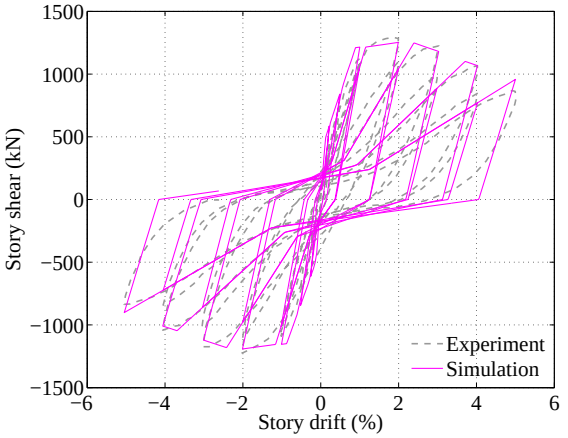

(e) NO2 (Takamori et al. 2006)

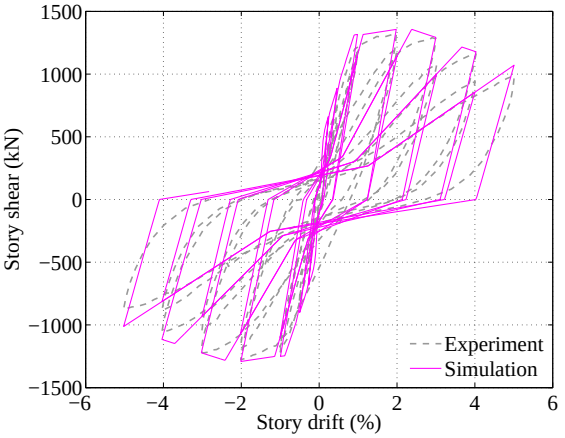

(f) NO3 (Takamori et al. 2006)

Figure A.6 Comparison between hysteretic responses of experiment and analysis for ductile interior joints (continued)

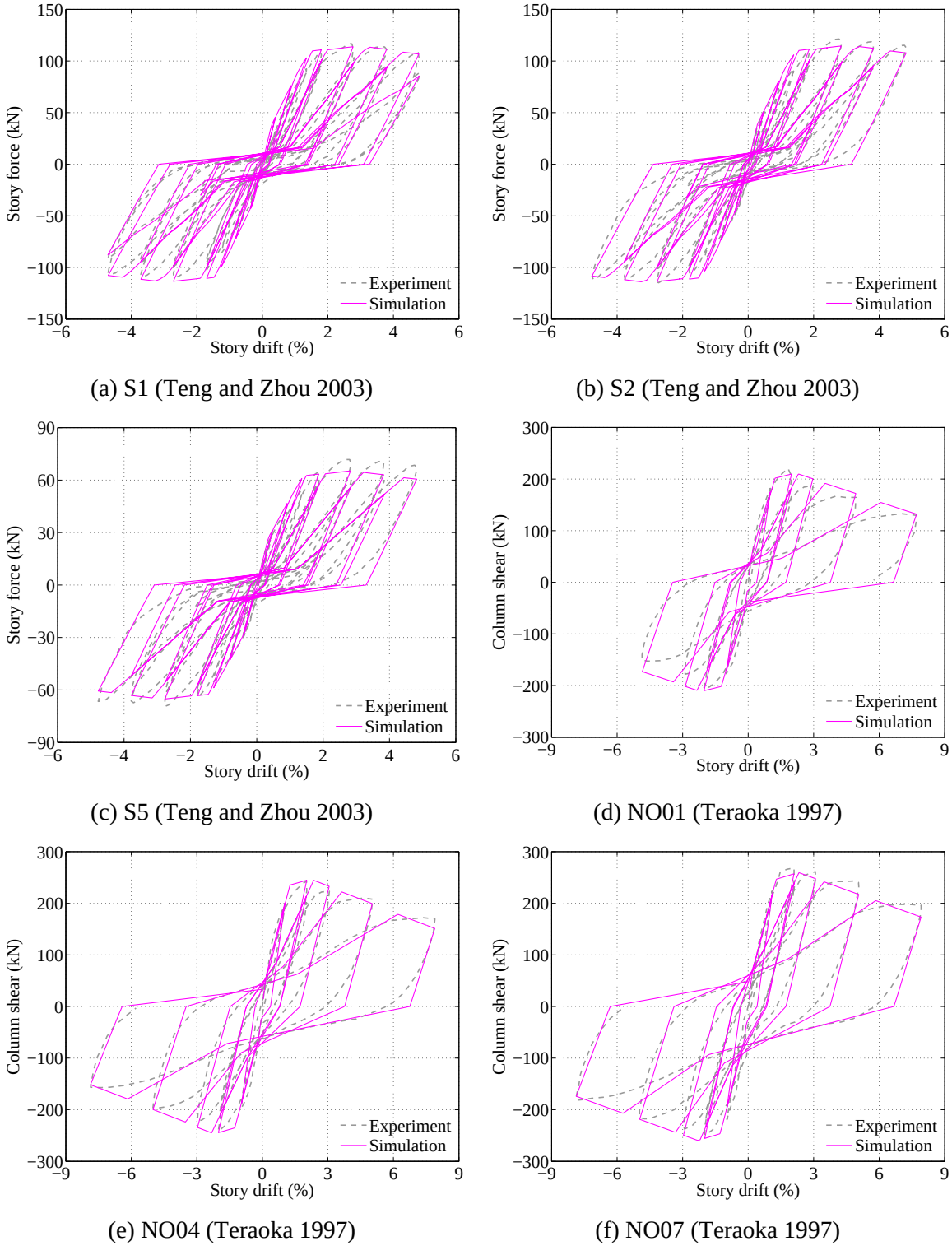

(a) S1 (Teng and Zhou 2003)

(b) S2 (Teng and Zhou 2003)

(c) S5 (Teng and Zhou 2003)

(d) NO01 (Teraoka 1997)

(e) NO04 (Teraoka 1997)

(f) NO07 (Teraoka 1997)

Figure A.6 Comparison between hysteretic responses of experiment and analysis for ductile interior joints (continued)

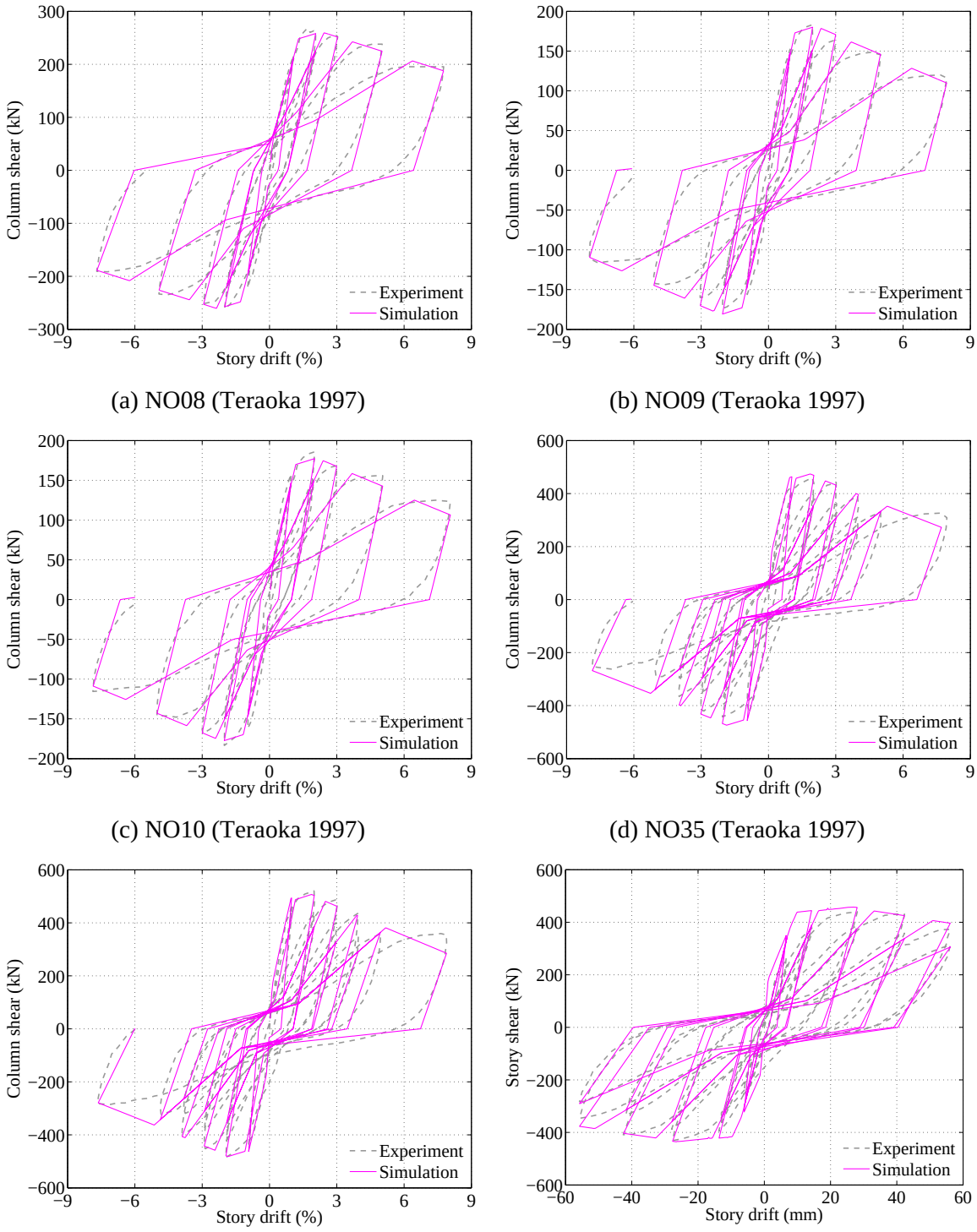

(a) NO08 (Teraoka 1997)

(b) NO09 (Teraoka 1997)

(c) NO10 (Teraoka 1997)

(d) NO35 (Teraoka 1997)

(e) NO36 (Teraoka 1997)

(f) No. 1 (Yashita et al. 1996)

Figure A.6 Comparison between hysteretic responses of experiment and analysis for ductile interior joints (continued)

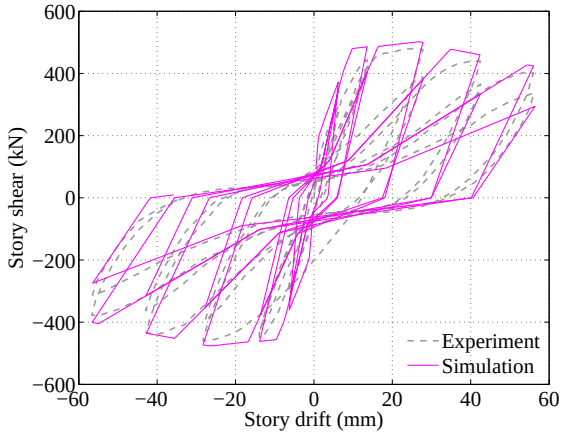

(a) No. 3 (Yashita et al. 1996)

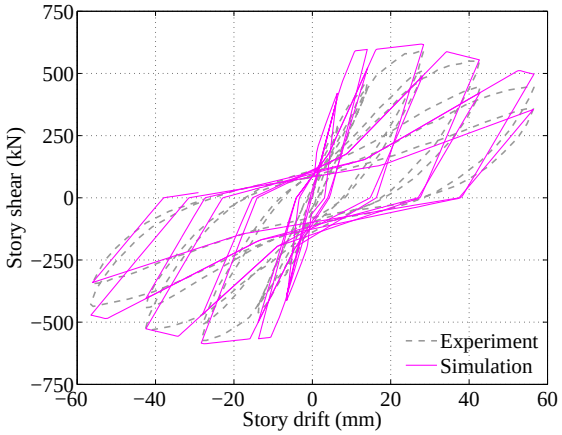

(b) No. 4 (Yashita et al. 1996)

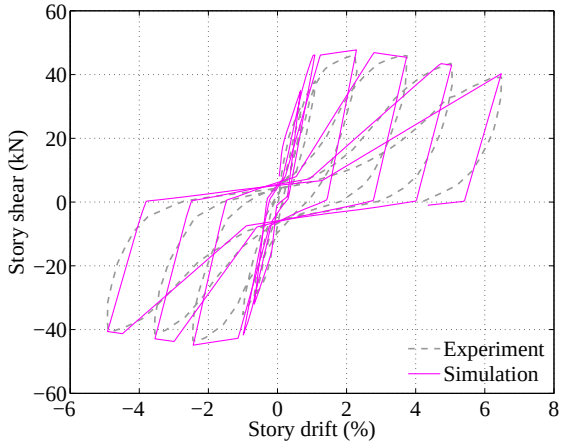

(c) NO1 (Yoshino et al. 1997)

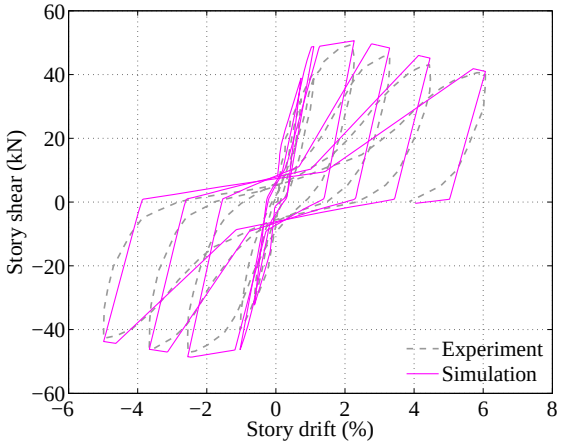

(d) NO3 (Yoshino et al. 1997)

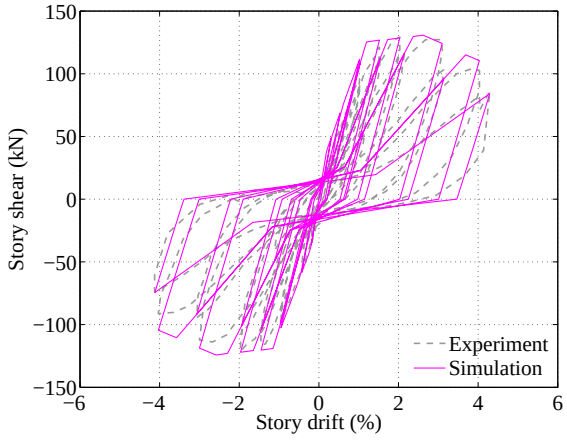

(e) S3 (Zaid et al. 1999)

Figure A.6 Comparison between hysteretic responses of experiment and analysis for ductile interior joints (continued)

Table A.5 Comparison of experimental and analytical maximum lateral force for ductile interior beam-column joint subassemblages

Reference	Specimen	Maximum lateral force (kN)		Difference
		Experiment	Analysis	(%)
Durrani and Wight (1985)	X1	197	184	-7.0
	X2	205	196	-4.6
	X3	159	151	-5.1
Endoh et al. (1991)	HLC	132	127	-4.2
	LA1	158	149	-7.4
Fujii and Morita (1991)	A1	48	49	+1.9
	A3	49	50	+2.3
	A4	51	50	-1.4
Goto and Joh (1996)	HH	146	149	+1.8
Goto and Joh (2003)	LM-60	131	131	+0.2
	LM-125	102	103	+0.6
	HM-60	149	154	+3.6
	HM-125	120	120	+0.0
	HH-125	123	127	+2.7
Hiramatsu et al. (1995)	S1	307	288	-6.7
Inoue et al. (1990)	SP1	326	328	+0.6
	SP2	283	281	-0.8
Ishida et al. (2001)	CN	958	929	-3.1
	ES	964	938	-2.8
Jinno et al. (1991)	NO1	162	156	-3.5
	NO2	197	192	-2.9
	NO3	276	267	-3.2
	NO4	305	294	-3.8
	NO5	366	352	-4.1
	NO6	340	326	-4.3
	NO7	363	355	-2.5
	NO8	416	406	-2.5
Joh et al. (1991a)	JXO-B1	60	61	+1.2
	JXO-B5	63	64	+2.3
Joh et al. (1991b)	JXO-8MH	68	64	-5.9
Kaku et al. (1993)	J31A	257	255	-0.9
Kamimura et al. (2004)	NN.1	47	47	-1.0
Kashiwazaki et al. (1992)	MKJ-1	159	160	+0.2
Kitayama et al. (1991)	J1	115	116	+0.7
Kitayama et al. (2000)	PB1	144	127	-13.1
	PNB2	130	127	-2.9
	PNB3	121	118	-2.8
Kurose et al. (1991)	J1	224	223	-0.6
Kusuhara et al. (2004)	JE-0	94	97	+3.0
	JE-55	89	90	+1.3
Lee et al. (2009)	J1	346	354	+2.3
Matsumoto et al. (2010)	B-0	399	394	-1.1
	B-5	404	397	-1.7
	J-0	457	452	-1.2
	J-5	459	448	-2.6

Table A.5 Comparison of experimental and analytical maximum lateral force for ductile interior beam-column joint subassemblages (continued)

Reference	Specimen	Maximum lateral force (kN)		Difference
		Experiment	Analysis	(%)
Morita et al. (2004)	M1	118	115	-2.8
	M6	135	122	-10.3
Noguchi and Kashiwazaki (1992)	OKJ-1	231	230	-0.6
	OKJ-4	252	243	-3.7
	OKJ-5	245	239	-2.8
	OKJ-6	221	216	-2.4
Ohwada (1970)	No. 2	43	40	-7.3
Ohwada (1977)	JO-2	22	2	-1.2
Oka and Shiohara (1992)	J-1	253	246	-2.6
	J-6	266	262	-1.4
	J-8	304	295	-3.2
	J-10	189	188	-1.0
Ozaki et al. (2010)	NO1	149	149	-0.2
	NO2	140	143	+2.2
Raffaelle and Wight (1992)	SP1	95	91	-4.4
	SP2	62	60	-3.2
	SP3	73	71	-2.7
	SP4	105	102	-2.3
Shin and LaFave (2004)	SL1	86	83	-3.4
	SL2	83	83	+0.4
	SL4	109	102	-7.6
Shinjo et al. (2009)	B-1	246	238	-3.4
	J-1	278	282	+1.6
	BJ-1	260	256	-1.8
Takamori et al. (2006)	NO1	1308	1291	-1.3
	NO2	1293	1252	-3.2
	NO3	1323	1357	+2.4
Teng and Zhou (2003)	S1	117	114	-2.4
	S2	121	115	-5.9
	S5	72	65	-9.9
Teraoka (1997)	NO01	221	210	-5.1
	NO04	243	245	+0.8
	NO07	268	259	-3.4
	NO08	268	259	-3.4
	NO09	183	181	-1.3
	NO10	186	177	-4.8
	NO35	460	474	+3.0
	NO36	520	507	-2.6
Yashito et al. (1996)	No. 1	440	458	+4.0
	No. 3	480	502	+4.4
	No. 4	594	618	+3.8
Yoshino et al. (1997)	NO1	46	48	+3.2
	NO3	49	51	+2.3
Zaid et al. (1999)	S3	129	131	+1.2

APPEDIX B

FRAME DESIGN INFORMATION

This appendix provides the structural design details for each of the RC frames modeled and analyzed in Chapter 4. The ductile and non-ductile RC frames are designed by Haselton (2006) and Liel (2008), respectively, in accordance with the design codes. The design information helps facilitate the fiber-section beam-column elements, compute the beam-column joint shear strength, and model the shear behavior in columns.

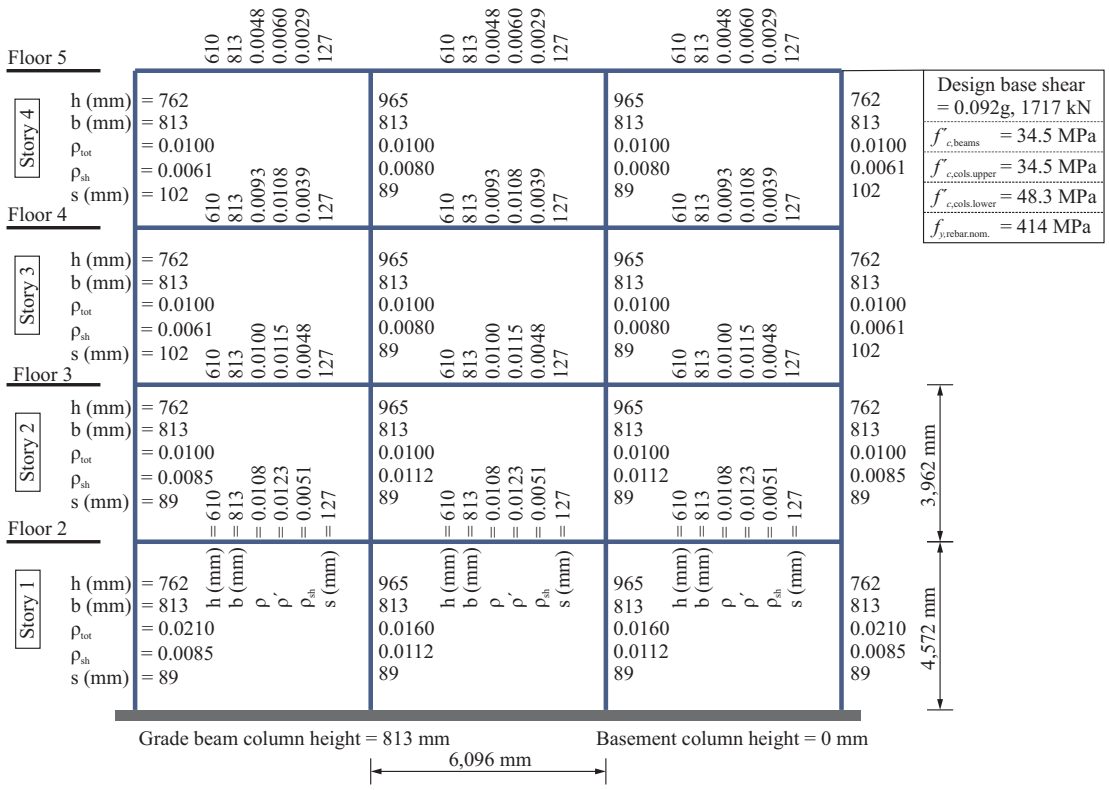

Figure B.1 Design information of 4-story ductile perimeter frame (SMF-4P) (Haselton 2006)

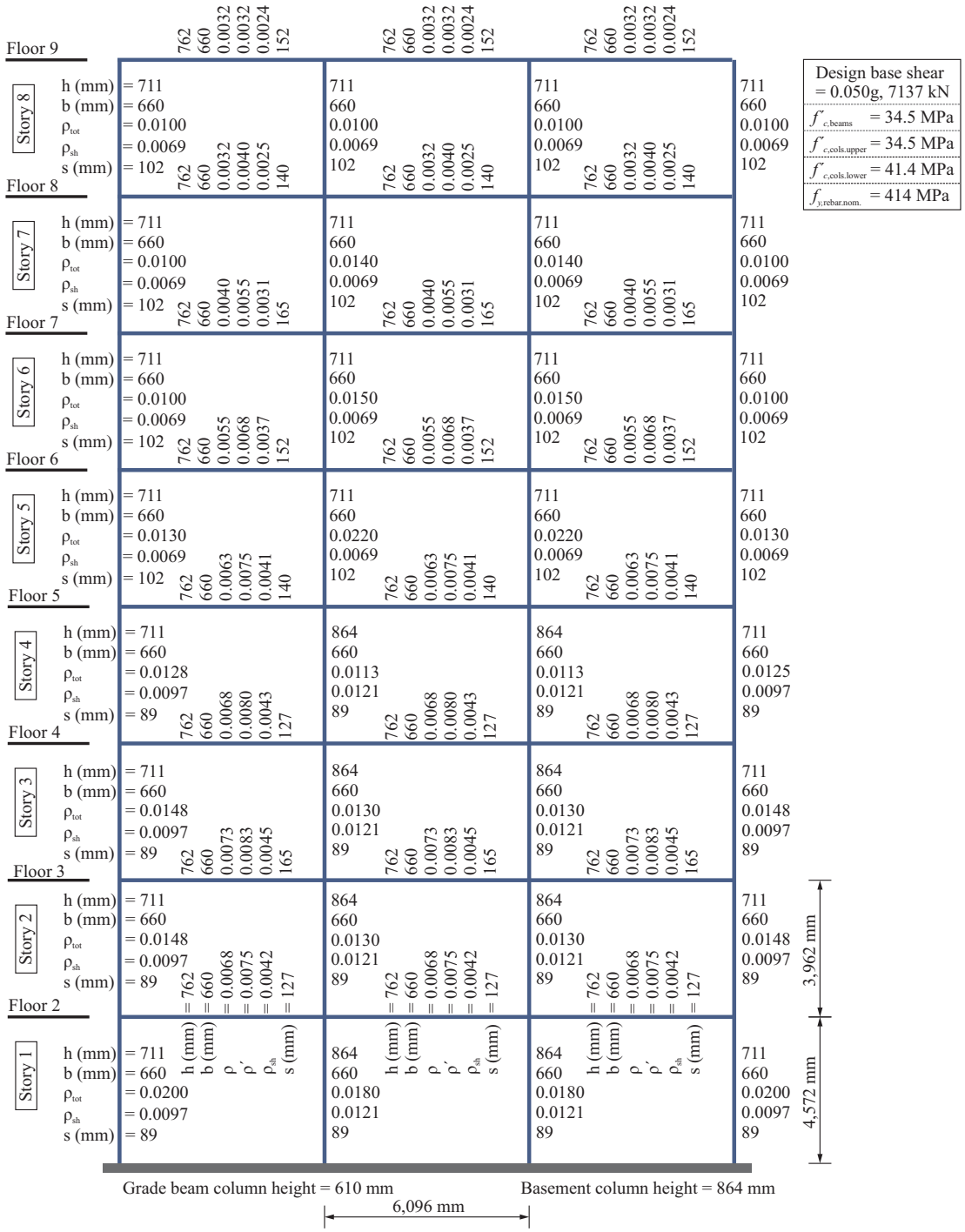

Figure B.2 Design information of 8-story ductile perimeter frame (SMF-8P) (Haselton 2006)

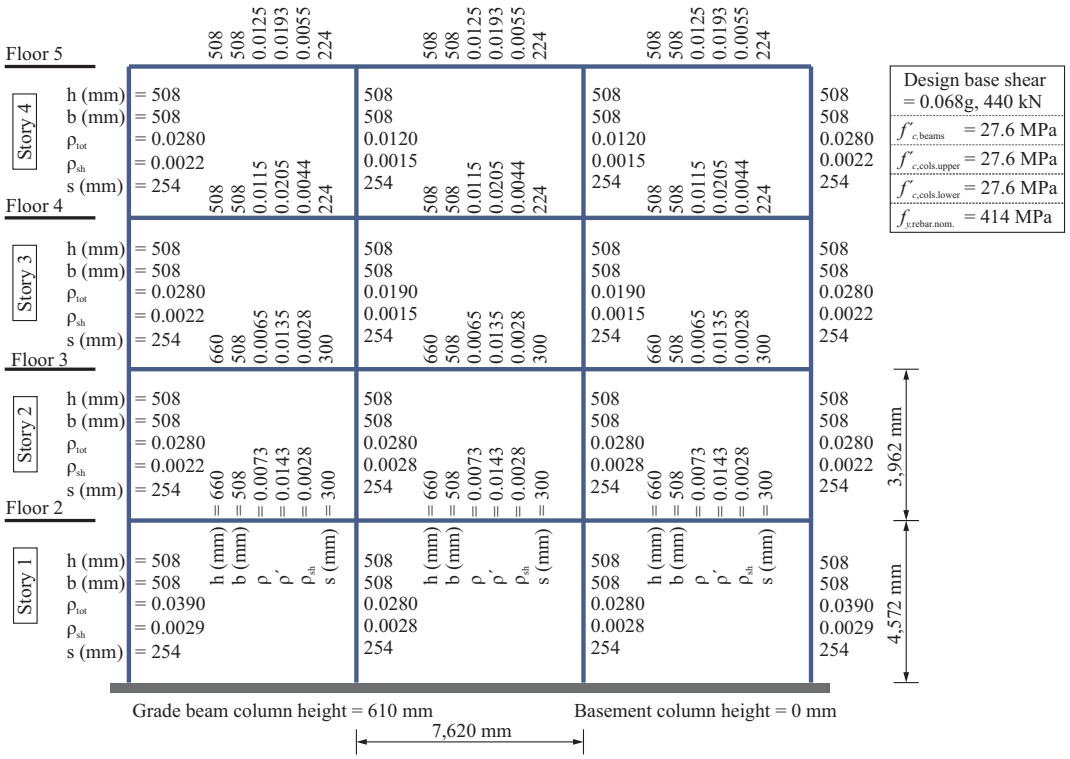

Figure B.3 Design information of 4-story non-ductile space frame (OMF-4S) (Liel 2008)

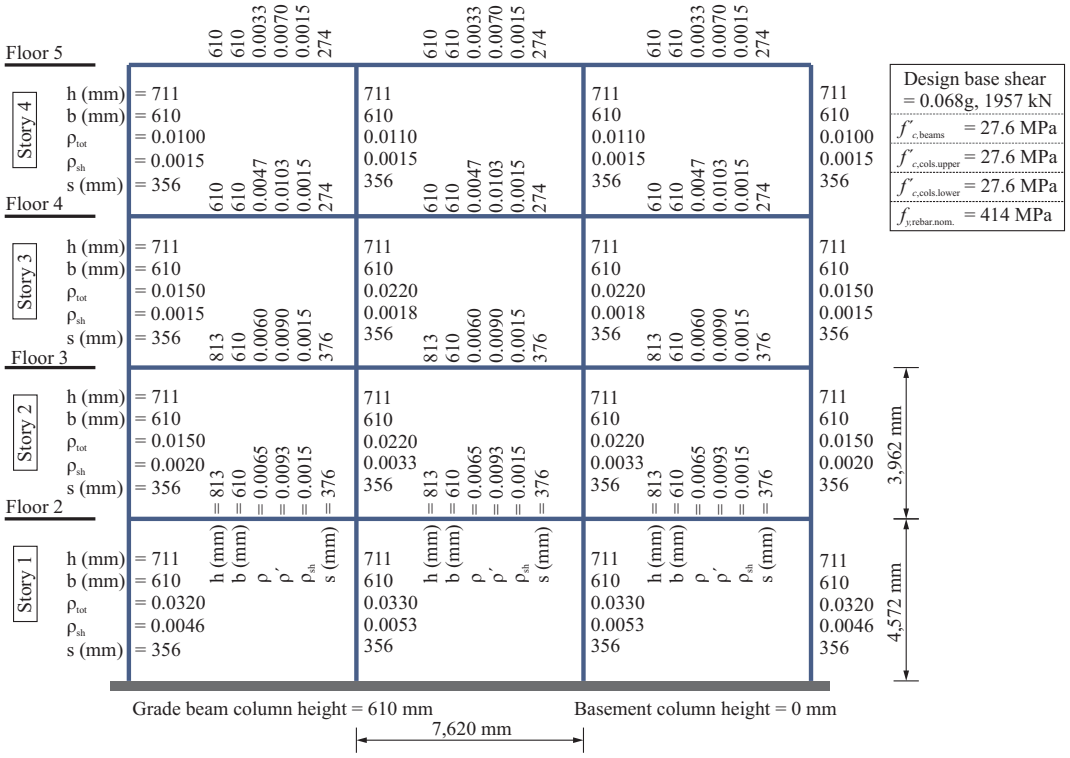

Figure B.4 Design information of 4-story non-ductile perimeter frame (OMF-4P) (Liel 2008)

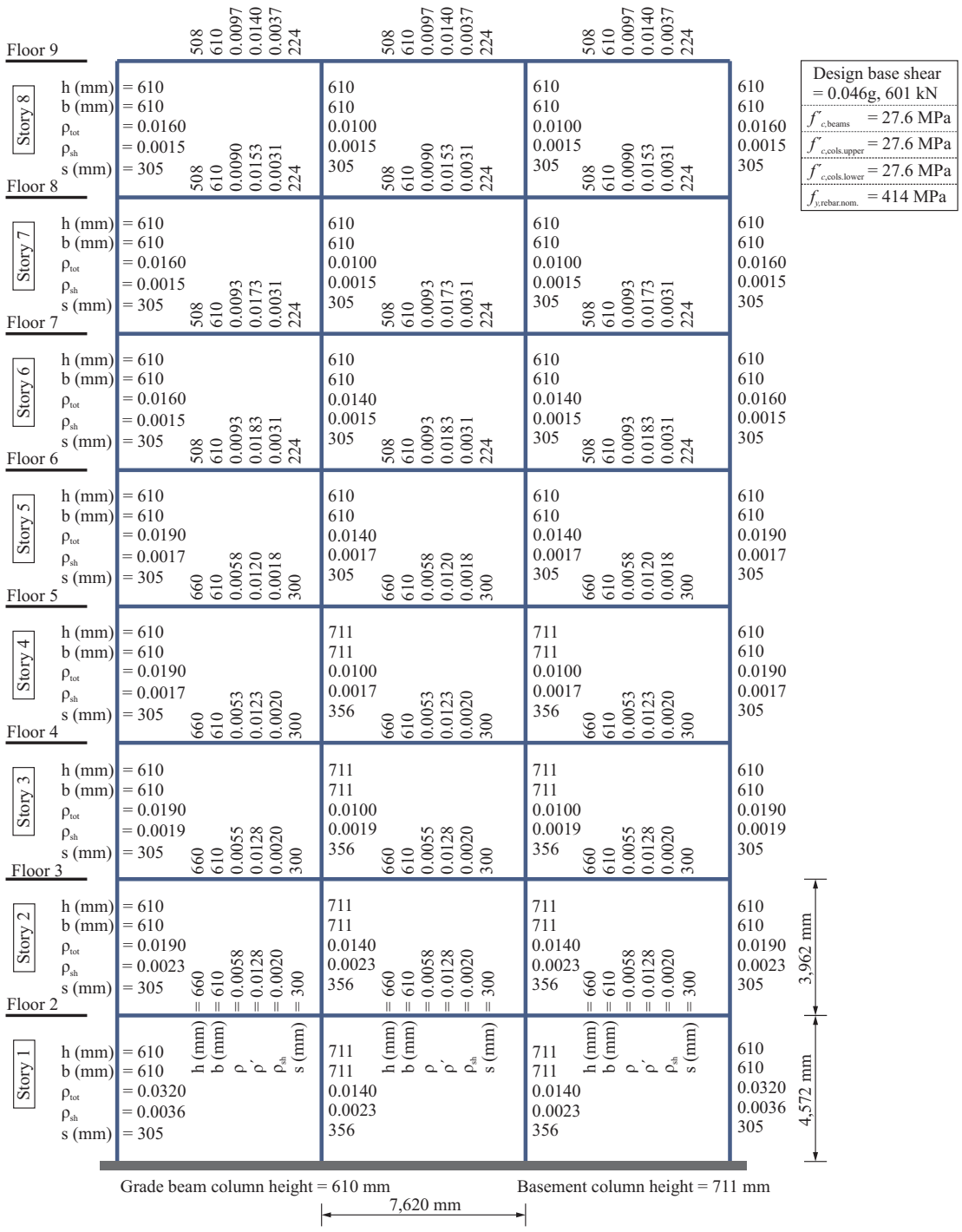

Figure B.5 Design information of 8-story non-ductile space frame (OMF-8S) (Liel 2008)

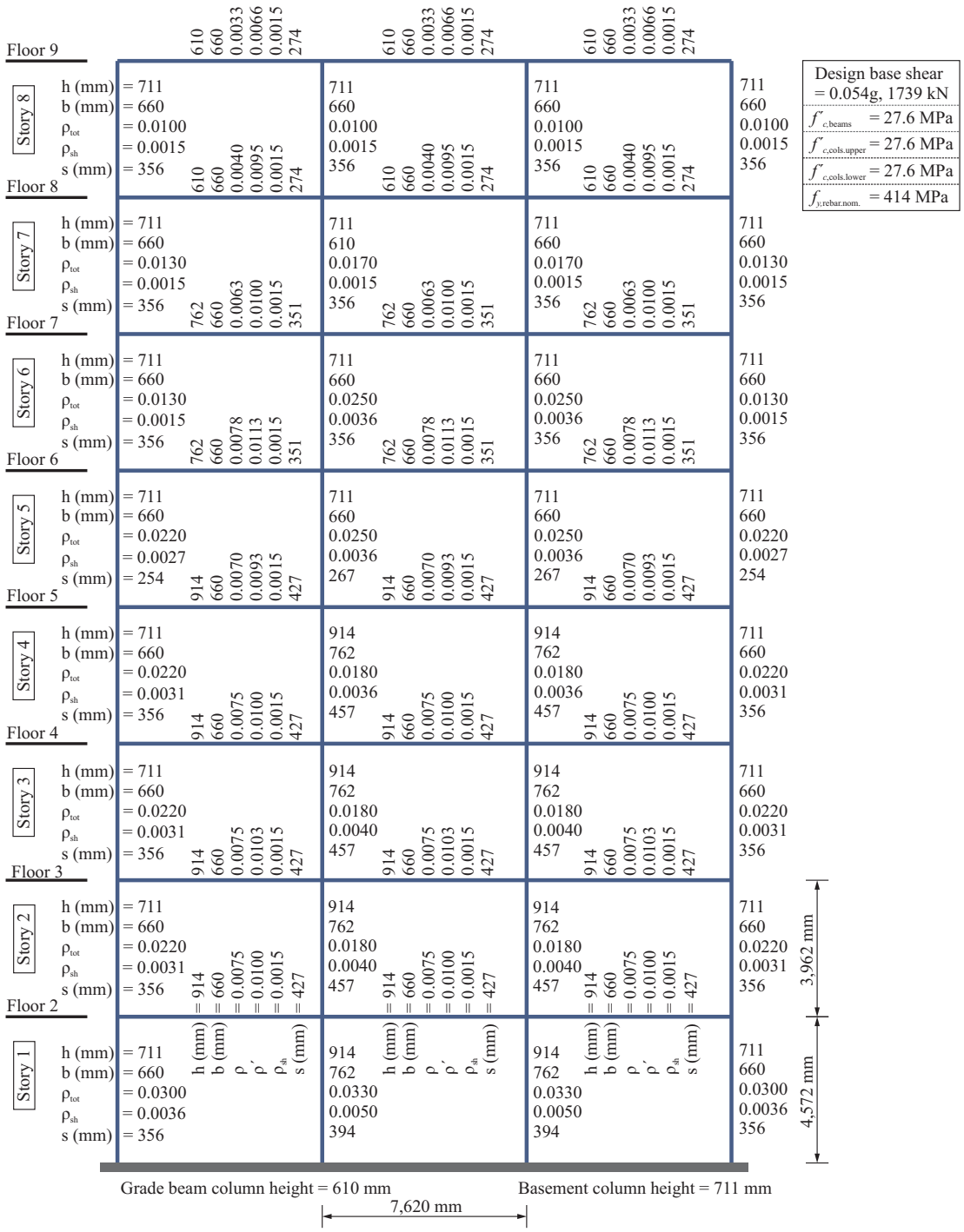

Figure B.6 Design information of 8-story non-ductile perimeter frame (OMF-8P) (Liel 2008)

APPEDIX C

DATABASE OF NON-DUCTILE AND DUCTILE BEAM-COLUMN JOINTS

This appendix presents the list of experimental non-ductile and ductile RC beam-column joint subassemblages available in the literature in order to propose the formulation of non-ductile and ductile joint shear strength. The tables in this appendix indicate the material and cross-sectional properties of beams, columns, and joints, and the governing failure mechanisms for each specimen. Additionally, the tables contain the comparison of experimental and predicted joint shear strength.

C.1 Database of Non-Ductile Beam-Column Joints

Table C.1 Experimental non-ductile beam-column joint database

No.	Reference	Specimen	Joint type	No. of TBs	Joint				Beam								Column							$\frac{v_{j,\max,pred}}{v_{j,\max,\exp}}$	Failure mode[§]
					f_{cj} (MPa)	f_{yj} (MPa)	s_j (mm)	ρ_j	b_j (mm)	f_{cb} (MPa)	f_{yb} (MPa)	ρ_b	h_b (mm)	b_b (mm)	f_{cc} (MPa)	f_{yc} (MPa)	ρ_c	h_c (mm)	b_c (mm)	e (mm)	ALF		
1	Al-Salloum et al.	ECON1	EXT	0	33.4	-	-	-	160	33.4	510	0.009	350	160	33.4	510	0.016	300	160	-	0.20	0.91	J
2	(2011)	ECON2	EXT	0	33.4	-	-	-	160	33.4	510	0.009	350	160	33.4	510	0.016	300	160	-	0.20	0.90	J
3	Alva et al. (2007)	LVP2	EXT	0	44.2	602	150	0.003	200	44.2	594	0.011	400	200	44.2	594	0.033	300	200	-	0.15	0.77	J
4	Alva et al. (2007)	LVP4	EXT	0	24.6	602	150	0.003	200	24.6	594	0.011	400	200	24.6	594	0.033	300	200	-	0.15	0.79	J
5	Antonopoulos and	C1	EXT	0	19.4	-	-	-	200	19.4	585	0.009	300	200	19.4	585	0.015	200	200	-	0.06	1.27	J
6	Triantafillou (2003)	C2	EXT	0	23.7	-	-	-	200	23.7	585	0.009	300	200	23.7	585	0.015	200	200	-	0.05	1.22	J
7	Beres et al. (1991)	E-01	EXT	0	26.1	-	-	-	381	26.1	490	0.008	610	356	20.7	517	0.020	406	406	-	0.13	1.18	BJ, A
8		E-04	EXT	0	24.5	483	203	0.002	381	24.5	490	0.008	610	356	29.6	501	0.020	406	406	-	0.09	0.99	BJ, A
9		E-05	EXT	0	31.5	-	-	-	381	31.5	490	0.008	610	356	39.4	519	0.020	406	406	-	0.24	1.14	BJ, A
10		E-07	EXT	0	29.3	-	-	-	381	29.3	490	0.008	610	356	22.5	519	0.020	406	406	-	0.12	1.29	BJ, A
11		E-10	EXT	0	20.5	-	-	-	381	20.5	490	0.008	610	356	15.9	517	0.020	406	406	-	0.59	1.06	BJ, A
12		E-12	EXT	0	18.9	-	-	-	381	18.9	474	0.008	610	356	19.2	499	0.009	406	406	-	0.14	1.31	BJ, A
13		E-13	EXT	0	17.0	-	-	-	381	17.0	474	0.008	610	356	14.8	499	0.009	406	406	-	0.18	1.22	BJ, A
14	Biddah (1997)	J4	EXT	0	24.0	-	-	-	610	24.0	440	0.004	610	610	24.0	440	0.007	510	610	-	0.07	1.19	BJ, A
15	Chen (2006)	TDP2	EXT	0	23.8	408	165	0.001	215	23.8	333	0.005	330	200	23.8	333	0.009	230	230	-	0.08	1.29	J
16		TDD2	EXT	0	24.0	408	165	0.001	215	24.0	354	0.008	330	200	24.0	354	0.009	230	230	-	0.09	1.13	J
17		TDP1	EXT	0	22.9	424	165	0.001	215	22.9	348	0.005	330	200	22.9	348	0.009	230	230	-	0.09	1.22	BJ
18	Clyde et al. (2000)	Unit 2	EXT	0	46.2	-	-	-	305	46.2	746	0.024	406	305	46.2	742	0.022	457	305	-	0.10	1.26	J
19		Unit 4	EXT	0	41.0	-	-	-	305	41.0	746	0.024	406	305	41.0	742	0.022	457	305	-	0.25	1.26	J
20		Unit 5	EXT	0	37.0	-	-	-	305	37.0	746	0.024	406	305	37.0	742	0.022	457	305	-	0.25	1.26	J
21		Unit 6	EXT	0	40.1	-	-	-	305	40.1	746	0.024	406	305	40.1	742	0.022	457	305	-	0.10	1.21	J
22	El-Amoury (2004)	T-S1	EXT	0	30.8	-	-	-	250	30.8	477	0.013	400	250	30.8	477	0.022	400	250	-	0.19	0.85	BJ
23		T-SB3	EXT	0	30.6	-	-	-	250	30.6	477	0.013	400	250	30.6	477	0.022	400	250	-	0.20	1.16	BJ, A
24	Filiatrault et al. (1994)	Specimen 1	EXT	0	34.0	-	-	-	350	34.0	475	0.010	450	350	34.0	475	0.023	350	350	-	0.08	0.73	J, A
25	Ghobarah and Said	T1	EXT	0	30.8	-	-	-	250	30.8	425	0.013	400	250	30.8	425	0.022	400	250	-	0.19	0.79	BJ
26	(2002)	T2	EXT	0	30.8	-	-	-	250	30.8	425	0.013	400	250	30.8	425	0.022	400	250	-	0.10	0.84	BJ
27	Hamil (2000)	C4ALN0	EXT	0	42.4	-	-	-	130	42.4	500	0.021	210	110	42.4	500	0.036	150	150	-	0.05	0.96	J
28		C6ALH0	EXT	0	100.8	-	-	-	130	100.8	500	0.021	210	110	100.8	500	0.036	150	150	-	0.04	1.08	J
29		C6LN0	EXT	0	51.2	-	-	-	130	51.2	500	0.021	210	110	51.2	500	0.036	150	150	-	0.04	1.18	J
30		C6LN1A	EXT	0	48.8	-	-	-	130	48.8	500	0.021	210	110	48.8	500	0.036	150	150	-	0.05	0.99	J

Table C.1 Experimental non-ductile beam-column joint database (continued)

No.	Reference	Specimen	Joint type	No. of TBs	Joint f_{cj} (MPa)	Joint f_{yj} (MPa)	Joint s_j (mm)	Joint ρ_j	Beam b_j (mm)	Beam f_{cb} (MPa)	Beam f_{yb} (MPa)	Beam ρ_b	Beam h_b (mm)	Beam b_b (mm)	Column f_{cc} (MPa)	Column f_{yc} (MPa)	Column ρ_c	Column h_c (mm)	Column b_c (mm)	e (mm)	ALF	$\frac{v_{j,\max,pred}}{v_{j,\max,exp}}$	Failure mode§
31	Hamil (2000)	C6LN1AE	EXT	0	44.0	-	-	-	130	44.0	500	0.021	210	110	44.0	500	0.036	150	150	-	0.05	0.88	J
32		C7LN0	EXT	0	38.4	-	-	-	130	38.4	500	0.014	300	110	38.4	500	0.036	150	150	-	0.06	0.93	J
33		C9LN0	EXT	0	40.8	-	-	-	130	40.8	500	0.014	300	110	40.8	500	0.036	150	150	-	0.05	1.02	J
34		C4ALN1	EXT	0	45.6	500	105	0.004	130	45.6	500	0.041	210	110	45.6	500	0.036	150	150	-	0.05	1.07	J
35		C6LN1r	EXT	0	48.8	500	105	0.004	130	48.8	500	0.021	210	110	48.8	500	0.036	150	150	-	0.05	0.98	J
36		C7LN1	EXT	0	37.6	500	150	0.003	130	37.6	500	0.014	300	110	37.6	500	0.036	150	150	-	0.06	0.82	J
37		C7LN3	EXT	0	40.0	500	109	0.003	130	40.0	500	0.014	300	110	40.0	500	0.036	150	150	-	0.06	0.78	J
38		C9LN1	EXT	0	38.4	500	150	0.003	130	38.4	500	0.014	300	110	38.4	500	0.036	150	150	-	0.06	1.00	J
39		C9LN3	EXT	0	36.8	500	109	0.003	130	36.8	500	0.014	300	110	36.8	500	0.036	150	150	-	0.06	0.85	J
40	Hanson and Connor (1967)	V	EXT	0	22.8	-	-	-	343	22.8	352	0.019	508	305	37.4	447	0.055	381	381	-	0.52	0.89	J
41	Hoffschild et al. (1995)	RCBC1	EXT	0	26.3	-	-	-	178	26.3	566	0.012	200	165	26.3	566	0.013	190	190	-	0.10	1.01	J
42	Hwang et al. (2005)	0T0	EXT	0	67.3	-	-	-	370	67.3	430	0.016	450	320	67.3	421	0.037	420	420	-	0.02	1.09	BJ
43		1B8	EXT	0	61.8	-	-	-	370	61.8	435	0.016	450	320	61.8	430	0.037	420	420	-	0.02	0.84	BJ
44		1T44	EXT	0	72.8	498	293	0.004	370	72.8	430	0.016	450	320	72.8	421	0.037	420	420	-	0.02	1.08	BJ
45	Ilki et al. (2011)	JOP	EXT	0	8.3	-	-	-	250	8.3	333	0.007	500	250	8.3	333	0.013	500	250	-	0.13	1.34	J
46	Jinno et al. (1985)	NO05	EXT	0	32.0	-	-	-	280	32.0	392	0.013	380	260	32.0	371	0.038	300	300	-	0.00	1.06	J
47	Kanada et al. (1984)	U40L	EXT	0	24.3	-	-	-	280	24.3	387	0.017	380	260	24.3	385	0.026	300	300	-	0.00	1.18	J
48		U20L	EXT	0	26.7	-	-	-	280	26.7	387	0.009	380	260	26.7	387	0.013	300	300	-	0.00	1.19	BJ, A
49	Karayannis et al. (1998)	J0	EXT	0	20.8	-	-	-	100	20.8	580	0.009	200	100	20.8	580	0.016	200	100	-	0.10	0.96	J
50	Karayannis et al.	A0	EXT	0	31.6	-	-	-	200	31.6	580	0.003	300	200	31.6	580	0.005	300	200	-	0.05	0.96	J
51	(2008)	B0	EXT	0	31.6	-	-	-	200	31.6	580	0.008	300	200	31.6	580	0.005	300	200	-	0.05	0.97	J
52		C0	EXT	0	31.6	-	-	-	200	31.6	580	0.008	300	200	31.6	580	0.013	300	200	-	0.05	1.00	J
53	Kordina (1984)	RE4	EXT	0	32.0	250	150	0.003	200	32.0	420	0.011	300	200	32.0	420	0.020	200	200	-	0.04	0.85	J
54	Le-Trung et al. (2010)	NS	EXT	0	33.8	-	-	-	151	33.8	324	0.012	200	134	33.8	324	0.015	167	167	-	0.00	1.17	J
55	Liu (2006)	RC-1	EXT	0	19.4	-	-	-	215	19.4	324	0.008	330	200	19.4	324	0.009	230	230	-	0.07	0.94	BJ
56		RC-6	EXT	0	25.9	384	165	0.001	250	25.9	307	0.006	330	250	25.9	307	0.018	250	250	-	0.06	0.84	BJ
57	Oh et al. (1992)	EJS-200-0	EXT	0	26.8	-	-	-	170	26.8	434	0.025	200	140	26.8	417	0.027	200	200	-	0.00	1.18	J
58		EJS-400-0	EXT	0	41.7	-	-	-	170	41.7	434	0.025	200	140	41.7	417	0.027	200	200	-	0.00	1.12	J
59	Onish et al. (1990)	NO. 1	EXT	0	25.9	-	-	-	250	25.9	389	0.007	250	250	25.9	389	0.012	250	250	-	0.00	0.75	BJ
60		NO. 2	EXT	0	28.1	314	125	0.002	250	28.1	389	0.007	250	250	28.1	389	0.012	250	250	-	0.00	0.72	BJ

Table C.1 Experimental non-ductile beam-column joint database (continued)

No.	Reference	Specimen	Joint type	No. of TBs	Joint				Beam								Column							ALF	$\frac{v_{j,\max,pred}}{v_{j,\max,exp}}$	Failure mode[§]
					f_{cj} (MPa)	f_{yj} (MPa)	s_j (mm)	ρ_j	b_j (mm)	f_{cb} (MPa)	f_{yb} (MPa)	ρ_b	h_b (mm)	b_b (mm)	f_{cc} (MPa)	f_{yc} (MPa)	ρ_c	h_c (mm)	b_c (mm)	e (mm)			
61	Onish et al. (1990)	NO. 4	EXT	0	25.2	-	-	-	250	25.2	389	0.012	250	250	25.2	389	0.012	250	250	-	0.00	0.99	BJ
62	Pantelides et al.	Unit 1	EXT	0	33.1	-	-	-	406	33.1	459	0.018	406	406	33.1	470	0.025	406	406	-	0.10	1.04	BJ, A
63	(2002)	Unit 2	EXT	0	33.1	-	-	-	406	33.1	459	0.018	406	406	33.1	470	0.025	406	406	-	0.25	1.11	BJ, A
64		Unit 3	EXT	0	34.0	-	-	-	406	34.0	459	0.018	406	406	34.0	470	0.025	406	406	-	0.10	1.12	J
65		Unit 4	EXT	0	34.0	-	-	-	406	34.0	459	0.018	406	406	34.0	470	0.025	406	406	-	0.25	0.98	J
66		Unit 5	EXT	0	31.7	-	-	-	406	31.7	459	0.018	406	406	31.7	470	0.025	406	406	-	0.10	1.04	J
67		Unit 6	EXT	0	31.7	-	-	-	406	31.7	459	0.018	406	406	31.7	470	0.025	406	406	-	0.25	1.02	J
68	Parker and Bullman	4b	EXT	0	39.2	-	-	-	275	39.2	570	0.009	500	250	39.2	550	0.009	300	300	-	0.09	1.17	J
69	(1997)	4c	EXT	0	36.8	-	-	-	275	36.8	570	0.009	500	250	36.8	550	0.009	300	300	-	0.17	1.14	J
70		4d	EXT	0	39.2	-	-	-	275	39.2	570	0.009	500	250	39.2	580	0.036	300	300	-	0.00	1.16	J
71		4e	EXT	0	40.0	-	-	-	275	40.0	570	0.009	500	250	40.0	580	0.036	300	300	-	0.10	1.26	J
72		4f	EXT	0	37.6	-	-	-	275	37.6	570	0.009	500	250	37.6	580	0.036	300	300	-	0.18	1.07	J
73		5b	EXT	0	43.2	480	150	0.005	275	43.2	485	0.009	500	250	43.2	485	0.022	300	300	-	0.08	0.83	J
74	Reys de Ortiz (1993)	BC1	EXT	0	33.8	-	-	-	200	33.8	720	0.011	400	200	33.8	461	0.015	300	200	-	0.00	1.02	J
75		BC2	EXT	0	37.8	461	200	0.003	200	37.8	720	0.011	400	200	37.8	461	0.015	300	200	-	0.00	0.96	J
76		BC3	EXT	0	33.0	-	-	-	200	33.0	720	0.011	400	200	33.0	461	0.021	300	200	-	0.00	0.95	J
77		BC5	EXT	0	37.9	-	-	-	200	37.9	720	0.011	400	200	37.9	461	0.024	300	200	-	0.13	1.05	J
78		BC6	EXT	0	35.0	-	-	-	200	35.0	720	0.011	400	200	35.0	461	0.024	300	200	-	0.14	1.01	J
79	Sagbas (2007)	ED1	EXT	0	31.1	-	-	-	343	31.1	349	0.014	508	305	38.5	335	0.028	381	381	-	0.09	0.92	BJ
80	Salim (2007)	S1	EXT	0	30.2	-	-	-	165	30.2	460	0.016	300	150	30.2	460	0.025	180	180	-	0.09	1.28	J
81	Sarsam and Phipps (1985)	EX2	EXT	0	52.5	-	-	-	155	52.5	504	0.010	305	155	52.5	504	0.025	205	155	-	0.18	1.15	J
82	Sasmal et al. (2011)	SP-1	EXT	0	37.2	500	300	0.001	300	37.2	500	0.007	400	300	37.2	500	0.022	300	300	-	0.09	0.99	J, A
83	Scott (2007)	C1AL	EXT	0	33.4	250	105	0.004	130	33.4	540	0.011	210	110	33.4	540	0.036	150	150	-	0.07	0.91	J
84		C2	EXT	0	49.4	250	105	0.004	130	49.4	540	0.011	210	110	49.4	540	0.036	150	150	-	0.25	1.11	J
85		C3L	EXT	0	35.5	250	105	0.004	130	35.5	540	0.011	210	110	35.5	540	0.036	150	150	-	0.06	0.95	J
86		C4	EXT	0	41.4	250	105	0.004	130	41.4	540	0.021	210	110	41.4	540	0.036	150	150	-	0.29	0.92	J
87		C4A	EXT	0	44.3	250	105	0.004	130	44.3	540	0.021	210	110	44.3	540	0.036	150	150	-	0.28	0.88	J
88		C4AL	EXT	0	35.8	250	105	0.004	130	35.8	540	0.021	210	110	35.8	540	0.036	150	150	-	0.06	0.90	J
89		C6	EXT	0	39.8	250	105	0.004	130	39.8	540	0.021	210	110	39.8	540	0.036	150	150	-	0.31	1.23	J
90		C6L	EXT	0	45.8	250	105	0.004	130	45.8	540	0.021	210	110	45.8	540	0.036	150	150	-	0.05	1.09	J

Table C.1 Experimental non-ductile beam-column joint database (continued)

No.	Reference	Specimen	Joint type	No. of TBs	Joint f_{cj} (MPa)	Joint f_{yj} (MPa)	Joint s_j (mm)	Joint ρ_j	Beam b_j (mm)	Beam f_{cb} (MPa)	Beam f_{yb} (MPa)	Beam ρ_b	Beam h_b (mm)	Beam b_b (mm)	Column f_{cc} (MPa)	Column f_{yc} (MPa)	Column ρ_c	Column h_c (mm)	Column b_c (mm)	e (mm)	ALF	$\frac{v_{j,\max,pred}}{v_{j,\max,exp}}$	Failure mode[§]
91	Scott (2007)	C7	EXT	0	35.2	250	150	0.003	130	35.2	540	0.014	300	110	35.2	540	0.036	150	150	-	0.35	1.08	J
92		C9	EXT	0	35.9	250	150	0.003	130	35.9	540	0.014	300	110	35.9	540	0.036	150	150	-	0.34	1.24	J
93	Shin et al. (1992)	HJC0-R0	EXT	0	78.5	-	-	-	135	78.5	392	0.024	200	120	78.5	392	0.025	150	150	-	0.01	0.84	BJ
94		HJC1-R0	EXT	0	78.5	235	100	0.004	135	78.5	392	0.024	200	120	78.5	392	0.025	150	150	-	0.01	0.78	BJ
95	Taylor (1974)	P1/41/24	EXT	0	26.4	250	100	0.004	120	26.4	500	0.024	200	100	26.4	500	0.041	140	140	-	0.46	0.91	J
96		P2/41/24	EXT	0	29.0	250	100	0.004	120	29.0	500	0.024	200	100	29.0	500	0.041	140	140	-	0.42	0.79	J
97		P2/41/24A	EXT	0	37.6	250	100	0.004	120	37.6	500	0.024	200	100	37.6	500	0.041	140	140	-	0.33	0.78	J
98		A3/41/24	EXT	0	21.6	250	100	0.004	120	21.6	500	0.024	200	100	21.6	500	0.041	140	140	-	0.57	0.76	J
99		B3/41/24	EXT	0	17.6	250	100	0.004	120	17.6	500	0.024	200	100	17.6	500	0.041	140	140	-	0.70	0.78	J
100		C3/41/24X	EXT	0	40.0	250	100	0.004	120	40.0	500	0.024	200	100	40.0	500	0.041	140	140	-	0.31	1.17	J
101		C3/41/24BY	EXT	0	25.6	250	60	0.007	120	25.6	500	0.024	200	100	25.6	500	0.041	140	140	-	0.48	1.09	J
102		C3/41/13Y	EXT	0	22.4	250	100	0.004	120	22.4	500	0.013	200	100	22.4	500	0.041	140	140	-	0.55	0.85	J
103		C3/41/24Y	EXT	0	48.0	250	100	0.004	120	48.0	500	0.024	200	100	48.0	500	0.041	140	140	-	0.26	0.95	J
104		D3/41/24	EXT	0	42.4	250	100	0.004	120	42.4	500	0.024	200	100	42.4	500	0.041	140	140	-	0.07	0.77	J
105	Tsonos (2007)	G1	EXT	0	22.0	500	100	0.013	200	22.0	495	0.009	300	200	22.0	495	0.031	200	200	-	0.23	0.77	J
106	Tsonos and	F1	EXT	0	20.0	-	-	-	200	20.0	520	0.006	300	300	20.0	520	0.023	200	200	-	0.39	0.73	J
107	Papanikolaou (2003)	F2	EXT	0	31.0	-	-	-	200	31.0	530	0.005	300	300	31.0	535	0.008	200	200	-	0.29	0.92	BJ
108		L1	EXT	0	34.0	-	-	-	200	34.0	520	0.008	300	300	34.0	535	0.008	200	200	-	0.26	0.80	J
109	Tsonos et al. (1992)	P1	EXT	0	16.0	-	-	-	200	16.0	485	0.011	300	200	16.0	485	0.031	200	200	-	0.18	1.04	J
110		V1	EXT	0	23.0	-	-	-	200	23.0	485	0.011	300	200	23.0	485	0.031	200	200	-	0.18	1.08	J
111		F1	EXT	0	17.0	-	-	-	200	17.0	485	0.011	300	200	17.0	485	0.031	200	200	-	0.18	0.75	J
112	Uzumeri (1977)	2	EXT	0	31.1	-	-	-	343	31.1	349	0.014	508	305	38.5	335	0.028	381	381	-	0.41	0.90	BJ
113	Wang and Lee (2004)	JE1	EXT	0	20.0	-	-	-	350	20.0	520	0.011	400	300	20.0	461	0.025	400	400	-	0.00	1.27	J
114	Wong (2005)	BS-L	EXT	0	30.9	-	-	-	280	30.9	520	0.009	450	260	30.9	520	0.022	300	300	-	0.15	1.08	J
115		BS-L-300	EXT	0	34.1	-	-	-	280	34.1	520	0.014	300	260	34.1	520	0.022	300	300	-	0.15	0.89	J
116		BS-L-600	EXT	0	36.4	-	-	-	280	36.4	520	0.007	600	260	36.4	520	0.022	300	300	-	0.15	1.11	J
117		BS-L-H1T10	EXT	0	33.3	500	160	0.003	280	33.3	520	0.009	450	260	33.3	520	0.022	300	300	-	0.15	0.91	J
118		BS-LL	EXT	0	42.1	-	-	-	280	42.1	520	0.009	450	260	42.1	520	0.022	300	300	-	0.15	0.98	J
119		BS-L-LS	EXT	0	31.6	-	-	-	280	31.6	520	0.009	450	260	31.6	520	0.022	300	300	-	0.15	1.00	J
120		BS-L-V2T10	EXT	0	32.6	-	-	-	280	32.6	520	0.009	450	260	32.6	520	0.022	300	300	-	0.15	0.88	J

Table C.1 Experimental non-ductile beam-column joint database (continued)

No.	Reference	Specimen	Joint type	No. of TBs	Joint				Beam								Column									Failure mode[§]
					f_{cj} (MPa)	f_{yj} (MPa)	s_j (mm)	ρ_j	b_j (mm)	f_{cb} (MPa)	f_{yb} (MPa)	ρ_b	h_b (mm)	b_b (mm)	f_{cc} (MPa)	f_{yc} (MPa)	ρ_c	h_c (mm)	b_c (mm)	e (mm)	ALF	$\frac{v_{j,\max,pred}}{v_{j,\max,exp}}$	
121	Wong (2005)	BS-L-V4T10	EXT	0	28.3	-	-	-	280	28.3	520	0.009	450	260	28.3	520	0.022	300	300	-	0.15	0.82	J
122		BS-U	EXT	0	31.0	-	-	-	280	31.0	520	0.009	450	260	31.0	520	0.022	300	300	-	0.15	1.00	J
123		JA-NN03	EXT	0	44.8	-	-	-	280	44.8	520	0.007	400	260	44.8	520	0.022	300	300	-	0.03	1.16	BJ
124		JA-NN15	EXT	0	46.0	-	-	-	280	46.0	520	0.007	400	260	46.0	520	0.022	300	300	-	0.15	1.10	BJ
125		JB-NN03	EXT	0	47.4	-	-	-	280	47.4	520	0.010	300	260	47.4	520	0.022	300	300	-	0.03	1.17	BJ
126	Akguzel (2011)	3D1-X	EXT	1	17.4	-	-	-	215	17.4	430	0.006	330	200	17.4	430	0.009	230	230	-	0.21	1.12	J
127		3D1-Y	EXT	1	17.4	-	-	-	215	17.4	430	0.006	330	200	17.4	430	0.009	230	230	-	0.19	1.15	J
128	Antonopoulos & Triantafillou (2003)	T-C	EXT	1	24.6	-	-	-	200	24.6	585	0.009	300	200	24.6	585	0.015	200	200	-	0.05	1.22	J
129	Engindeniz (2008)	SP1-NS	EXT	1	25.8	-	-	-	331	25.8	315	0.013	508	305	25.8	352	0.013	356	356	-	0.10	1.16	J
130		SP1-EW	EXT	1	25.8	-	-	-	331	25.8	316	0.013	508	305	25.8	353	0.013	356	356	-	0.10	1.04	J
131		SP2-NS	EXT	1	34.6	-	-	-	331	34.6	317	0.013	508	305	34.6	354	0.013	356	356	-	0.10	1.18	J
132		SP2-NW	EXT	1	34.6	-	-	-	331	34.6	318	0.013	508	305	34.6	355	0.013	356	356	-	0.10	1.11	J
133	Hanson and Connor (1972)	7	EXT	1	39.3	-	-	-	343	39.3	350	0.019	508	305	40.4	564	0.055	381	381	-	0.49	0.82	BJ
134	Hassan (2011)	U-J-1EW	EXT	1	29.6	-		-	432	29.6	470	0.020	457	406	29.6	470	0.031	457	457	-	0.30	0.88	J
135		U-J-1NS	EXT	1	29.6	-		-	432	29.6	470	0.020	457	406	29.6	470	0.031	457	457	-	0.30	1.00	J
136		B-J-1EW	EXT	1	30.4	-		-	432	30.4	502	0.020	457	406	30.4	502	0.031	457	457	-	0.45	1.11	J
137		B-J-1NS	EXT	1	30.4	-		-	432	30.4	502	0.020	457	406	30.4	502	0.031	457	457	-	0.45	1.20	J
138		U-BJ-1EW	EXT	1	30.3	-		-	432	30.3	535	0.007	457	406	30.3	535	0.031	457	457	-	0.45	0.96	BJ
139		U-BJ-1NS	EXT	1	30.3	-		-	432	30.3	535	0.007	457	406	30.3	535	0.031	457	457	-	0.45	1.04	BJ
140		U-J-2EW	EXT	1	30.5	-		-	432	30.5	503	0.009	762	406	30.5	535	0.031	457	457	-	0.45	0.87	J
141		U-J-2NS	EXT	1	30.5	-		-	432	30.5	503	0.009	762	406	30.5	535	0.031	457	457	-	0.45	0.97	J
142	Ilki et al. (2011)	JO	EXT	1	8.3	-	-	-	250	8.3	333	0.007	500	250	8.3	333	0.013	500	250	-	0.13	1.04	J
143	Park and Mosalam	SP1-EW	EXT	1	24.7	-	-	-	432	24.7	542	0.007	457	406	24.7	498	0.019	457	457	-	0.10	0.94	BJ
144	(2013a)	SP1-NS	EXT	1	24.7	-	-	-	432	24.7	542	0.007	457	406	24.7	498	0.019	457	457	-	0.10	0.99	BJ
145		SP2-EW	EXT	1	24.3	-	-	-	432	24.3	498	0.012	457	406	24.3	498	0.019	457	457	-	0.10	0.81	J
146		SP2-NS	EXT	1	24.3	-	-	-	432	24.3	498	0.012	457	406	24.3	498	0.019	457	457	-	0.10	0.81	J
147		SP3-EW	EXT	1	24.8	-	-	-	432	24.8	542	0.004	762	406	24.8	471	0.031	457	457	-	0.10	0.84	BJ
148		SP3-NS	EXT	1	24.8	-	-	-	432	24.8	542	0.004	762	406	24.8	471	0.031	457	457	-	0.10	0.96	BJ
149		SP4-EW	EXT	1	27.3	-	-	-	432	27.3	498	0.007	762	406	27.3	471	0.031	457	457	-	0.10	0.88	J
150		SP4-NS	EXT	1	27.3	-	-	-	432	27.3	498	0.007	762	406	27.3	471	0.031	457	457	-	0.10	1.04	J

Table C.1 Experimental non-ductile beam-column joint database (continued)

No.	Reference	Specimen	Joint type	No. of TBs	Joint				Beam								Column						ALF	$\frac{v_{j,\max,pred}}{v_{j,\max,exp}}$	Failure mode[§]
					f_{cj} (MPa)	f_{yj} (MPa)	s_j (mm)	ρ_j	b_j (mm)	f_{cb} (MPa)	f_{yb} (MPa)	ρ_b	h_b (mm)	b_b (mm)	f_{cc} (MPa)	f_{yc} (MPa)	ρ_c	h_c (mm)	b_c (mm)	e (mm)			
151	Sanchez et al. (2009)	Test 1	EXT	1	33.0	-	-	-	200	33.0	493	0.010	300	200	33.0	493	0.026	200	200	-	0.20	0.73	CJ
152	Tsonos (2008)	F1	EXT	1	22.0	-	-	-	200	22.0	540	0.012	300	200	22.0	540	0.015	200	200	-	0.17	0.98	J
153		O2	EXT	1	16.2	-	-	-	200	16.2	540	0.012	300	200	16.2	540	0.015	200	200	-	0.23	1.07	J
154	Uzumeri (1977)	1	EXT	1	30.8	-	-	-	343	30.8	347	0.014	508	305	38.5	332	0.028	381	381	-	0.41	0.87	BJ
155		5	EXT	1	31.9	-	-	-	343	31.9	347	0.014	508	305	38.5	336	0.028	381	381	-	0.41	0.91	BJ
156	Aycardi et al. (1994)	Exterior	EXT	2	34.5	386	51	0.003	89	34.5	448	0.006	152	76	30.0	448	0.010	102	102	-	0.09	0.75	BJ, A
157	Barnes et al. (2008)	Unit 1	EXT	2	27.8	-		-	200	27.8	483	0.015	300	200	27.8	483	0.026	200	200	-	0.40	0.93	CJ
158		Unit 2	EXT	2	27.8	-		-	200	27.8	483	0.015	300	200	27.8	483	0.026	200	200	-	0.20	0.83	CJ
159	Beres et al. (1991)	E-02	EXT	2	26.8	-	-	-	381	26.8	490	0.008	610	356	20.8	517	0.020	406	406	-	0.13	1.27	BJ, A
160		E-03	EXT	2	22.6	483	203	0.002	381	22.6	483	0.008	610	356	27.4	501	0.020	406	406	-	0.10	1.01	BJ, A
161		E-06	EXT	2	31.0	-		-	381	31.0	490	0.008	610	356	34.7	519	0.020	406	406	-	0.27	1.16	BJ, A
162		E-08	EXT	2	30.1	-		-	381	30.1	490	0.008	610	356	23.2	519	0.020	406	406	-	0.12	1.16	BJ, A
163		E-09	EXT	2	19.9	-		-	381	19.9	490	0.008	610	356	15.9	517	0.020	406	406	-	0.59	1.10	BJ, A
164		E-11	EXT	2	16.4	-		-	381	16.4	474	0.008	610	356	16.9	499	0.009	406	406	-	0.16	1.30	BJ, A
165		E-14	EXT	2	21.0	-		-	381	21.0	474	0.008	610	356	18.6	499	0.009	406	406	-	0.14	1.20	BJ, A
166	Hanson and Connor (1967)	VA	EXT	2	37.4	-	-	-	343	37.4	343	0.019	508	305	36.1	484	0.055	381	381	-	0.54	1.26	BJ
167	Hatamoto and Bessho (1998)	F-5	EXT	2	44.5	-	-	-	350	44.5	392	0.030	400	300	44.5	392	0.036	425	400	-	0.00	1.16	BJ
168	Woo (2003)	Model 5	EXT	2	26.5	-	-	-	151	26.5	385	0.012	200	134	26.5	385	0.015	167	167	-	0.00	0.94	BJ, A
169	Alire (2002)	PEER0995	INT	0	60.4	-	-	-	406	60.4	504	0.011	508	406	60.4	505	0.012	457	406	-	0.11	1.18	BJ
170		PEER1595	INT	0	61.5	-	-	-	406	61.5	841	0.009	508	406	61.5	538	0.035	457	406	-	0.11	0.95	BJ
171		PEER4150	INT	0	33.0	-	-	-	406	33.0	545	0.022	508	406	33.0	545	0.035	457	406	-	0.10	0.84	BJ
172	Almusallam and	IC1	INT	0	30.0	-	-	-	160	30.0	420	0.009	350	160	30.0	420	0.016	300	160	-	0.20	0.80	BJ
173	Al-Salloum (2007)	IC2	INT	0	25.0	-	-	-	160	25.0	420	0.009	350	160	25.0	420	0.016	300	160	-	0.20	1.04	BJ
174	Beres et al. (1991)	I-11	INT	0	29.9	-	-	-	381	29.9	459	0.008	610	356	29.8	487	0.020	406	406	-	0.09	1.23	BJ
175		I-13	INT	0	25.0	-	-	-	381	25.0	341	0.008	610	356	27.0	550	0.020	406	406	-	0.10	0.93	BJ
176		I-15	INT	0	23.4	-	-	-	381	23.4	461	0.008	610	356	16.2	497	0.020	406	406	-	0.58	1.07	BJ
177		I-17	INT	0	21.2	-	-	-	381	21.2	472	0.008	610	356	15.9	472	0.009	406	406	-	0.17	1.25	BJ
178		I-20	INT	0	20.0	-	-	-	381	20.0	461	0.008	610	356	17.7	478	0.009	406	406	-	0.53	1.03	BJ
179	Chang et al. (1997)	BCB1	INT	0	54.7	-	-	-	300	54.7	354	0.013	400	300	54.7	354	0.023	500	300	-	0.18	1.17	BJ
180		BCS1	INT	0	54.7	-	-	-	300	54.7	354	0.013	400	300	54.7	354	0.023	500	300	-	0.18	1.00	BJ

Table C.1 Experimental non-ductile beam-column joint database (continued)

No.	Reference	Specimen	Joint type	No. of TBs	Joint				Beam								Column							$\frac{v_{j,\max,pred}}{v_{j,\max,exp}}$	Failure mode[§]
					f_{cj} (MPa)	f_{yj} (MPa)	s_j (mm)	ρ_j	b_j (mm)	f_{cb} (MPa)	f_{yb} (MPa)	ρ_b	h_b (mm)	b_b (mm)	f_{cc} (MPa)	f_{yc} (MPa)	ρ_c	h_c (mm)	b_c (mm)	e (mm)	ALF		
181	Dhakal et al. (2005)	C1PD	INT	0	31.6	-	-	-	325	31.6	538	0.027	550	300	31.6	538	0.022	500	350	-	0.11	1.33	J
182		C1ND	INT	0	31.6	-	-	-	325	31.6	538	0.027	550	300	31.6	538	0.022	500	350	-	0.11	1.15	J
183		C4ND	INT	0	32.7	-	-	-	350	32.7	538	0.033	550	300	32.7	538	0.025	400	400	-	0.11	1.20	J
184		C1HD	INT	0	31.6	-	-	-	325	31.6	538	0.027	550	300	31.6	538	0.022	500	350	-	0.11	1.18	J
185		C4HD	INT	0	32.7	-	-	-	350	32.7	538	0.033	550	300	32.7	538	0.025	400	400	-	0.11	1.24	J
186	Goto and Joh (1996)	J-OH	INT	0	31.5	-	-	-	250	31.5	426	0.024	350	200	31.5	578	0.038	300	300	-	0.28	1.01	J
187		C5-LO	INT	0	32.7	360	117	0.000	325	32.7	426	0.024	350	200	32.7	578	0.038	200	450	-	0.27	0.84	J
188	Hakuto et al. (2000)	O4	INT	0	52.9	-	-	-	380	52.9	308	0.014	500	300	52.9	321	0.017	460	460	-	0.00	1.30	BJ
189		O5	INT	0	32.8	-	-	-	380	32.8	306	0.012	500	300	32.8	321	0.017	460	460	-	0.00	0.92	BJ
190	Kulkarni and Li (2007)	JA	INT	0	33.7	-	-	-	325	33.7	484	0.011	500	250	33.7	484	0.016	400	400	-	0.30	0.78	BJ
191		JB	INT	0	34.8	-	-	-	325	34.8	484	0.011	500	250	34.8	484	0.016	400	400	-	0.30	0.79	BJ
192	Lee et al. (2010)	JI0	INT	0	27.0	-	-	-	350	27.0	456	0.009	600	300	27.0	456	0.025	400	400	-	0.19	0.83	J
193	Li et al. (2002)	A1	INT	0	32.3	-	-	-	600	32.3	503	0.006	600	300	32.3	460	0.025	300	900	-	0.00	1.01	J
194		M1	INT	0	32.0	499	150	0.001	600	32.0	503	0.006	600	300	32.0	460	0.025	300	900	-	0.00	1.02	BJ
195	Liu and Park (1998)	Unit 2	INT	0	48.9	-	-	-	380	48.9	321	0.010	500	300	48.9	321	0.020	300	460	-	0.12	1.06	CJ
196	Noguchi and	NO2	INT	0	34.1	354	150	0.001	250	34.1	325	0.015	300	200	34.1	388	0.023	300	300	-	0.06	1.12	BJ
197	Kurusu (1988)	NO4	INT	0	34.1	354	150	0.001	250	34.1	388	0.012	300	200	34.1	388	0.023	300	300	-	0.06	0.98	BJ
198	Ohwada (1970)	No. 1	INT	0	21.5	-	-	-	175	21.5	392	0.013	300	150	21.5	392	0.032	200	200	-	0.18	0.84	J
199	Ohwada (1973)	P-1	INT	0	11.6	-	-	-	175	11.6	400	0.015	300	150	11.6	400	0.040	200	200	-	0.34	1.15	J
200		P-2	INT	0	13.3	-	-	-	175	13.3	385	0.013	300	150	13.3	385	0.032	200	200	-	0.29	0.99	J
201		P-3	INT	0	12.8	-	-	-	175	12.8	385	0.010	300	150	12.8	385	0.032	200	200	-	0.31	0.83	J
202	Ohwada (1976)	JO-0	INT	0	20.1	-	-	-	100	20.1	402	0.039	150	100	20.1	402	0.034	150	100	-	0.00	1.15	J
203	Ohwada (1977)	JO-1	INT	0	20.0	-	-	-	150	20.0	432	0.020	150	150	20.0	432	0.034	150	150	-	0.00	1.06	J
204	Ohwada (1980)	JO-3	INT	0	20.6	-	-	-	150	20.6	394	0.020	150	150	20.6	394	0.034	150	150	-	0.00	0.91	J
205		JO-4	INT	0	14.0	-	-	-	150	14.0	360	0.020	150	150	14.0	360	0.068	150	150	-	0.00	0.81	J
206		LJO-1	INT	0	20.0	-	-	-	150	20.0	372	0.020	150	150	20.0	372	0.068	150	150	-	0.00	0.91	J
207		LJO-3	INT	0	20.0	-	-	-	150	20.0	372	0.020	150	150	20.0	372	0.045	150	150	-	0.00	0.99	J
208	Ohwada (1981)	LJO-4	INT	0	17.1	-	-	-	135	17.1	368	0.018	200	120	17.1	368	0.023	150	150	-	0.16	1.07	J
209		LJO-5	INT	0	17.1	-	-	-	135	17.1	368	0.018	200	120	17.1	368	0.023	150	150	-	0.41	1.00	CJ
210	Ota et al. (2004)	RC	INT	0	74.2	944	200	0.002	340	74.2	538	0.022	400	280	55.5	538	0.025	400	400	-	0.08	1.09	BJ

Table C.1 Experimental non-ductile beam-column joint database (continued)

No.	Reference	Specimen	Joint type	No. of TBs	Joint				Beam								Column							ALF	$\frac{v_{j,\max,pred}}{v_{j,\max,exp}}$	Failure mode[§]
					f_{cj} (MPa)	f_{yj} (MPa)	s_j (mm)	ρ_j	b_j (mm)	f_{cb} (MPa)	f_{yb} (MPa)	ρ_b	h_b (mm)	b_b (mm)	f_{cc} (MPa)	f_{yc} (MPa)	ρ_c	h_c (mm)	b_c (mm)	e (mm)			
211	Owada (1984)	LJO-6	INT	0	28.9	-	-	-	135	28.9	357	0.018	200	120	28.9	357	0.023	150	150	-	0.23	0.81	J
212	Owada (2000)	JO-5	INT	0	37.6	-	-	-	135	37.6	349	0.018	200	120	37.6	349	0.023	150	150	-	0.17	0.81	J
213	Pessiki et al. (1990)	I-01	INT	0	32.7	-	-	-	381	32.7	483	0.013	610	356	38.3	456	0.020	406	406	-	0.25	1.09	BJ
214		I-02	INT	0	32.5	-	-	-	381	32.5	483	0.013	610	356	38.7	456	0.020	406	406	-	0.24	1.11	BJ
215		I-03	INT	0	30.4	-	-	-	381	30.4	483	0.013	610	356	30.8	486	0.018	406	406	-	0.31	1.11	BJ
216		I-04	INT	0	31.9	-	-	-	381	31.9	483	0.013	610	356	31.7	518	0.019	406	406	-	0.30	1.15	BJ
217		I-05	INT	0	29.8	427	203	0.002	381	29.8	531	0.013	610	356	28.6	427	0.019	406	406	-	0.33	1.13	BJ
218		I-07	INT	0	26.0	-	-	-	381	26.0	481	0.008	610	356	21.7	461	0.020	406	406	-	0.43	1.04	BJ
219		I-08	INT	0	25.4	-	-	-	381	25.4	481	0.008	610	356	22.0	461	0.020	406	406	-	0.43	1.06	BJ
220		I-09	INT	0	29.1	-	-	-	381	29.1	425	0.008	610	356	28.2	461	0.020	406	406	-	0.10	1.06	BJ
221	Pimanmas and Chaimahawan (2010)	J0	INT	0	27.3	-	-	-	188	27.3	480	0.015	300	175	24.2	480	0.029	350	200	-	0.17	1.16	J
222	Supaviriyakit and Pimanmas (2008)	J1	INT	0	26.3	-	-	-	188	26.3	480	0.016	300	175	23.2	480	0.029	350	200	-	0.13	1.12	J
223	Walker (2001)	PEER14	INT	0	31.8	-	-	-	406	31.8	423	0.009	508	406	31.8	423	0.014	457	406	-	0.11	1.02	BJ
224		CD1514	INT	0	29.8	-	-	-	406	29.8	423	0.009	508	406	29.8	423	0.014	457	406	-	0.12	0.96	BJ
225		CD3014	INT	0	42.5	-	-	-	406	42.5	423	0.009	508	406	42.5	423	0.014	457	406	-	0.08	0.97	BJ
226		PADH14	INT	0	42.9	-	-	-	406	42.9	423	0.009	508	406	42.9	423	0.014	457	406	-	0.08	0.93	BJ
227		PEER22	INT	0	38.4	-	-	-	406	38.4	527	0.013	508	406	38.4	538	0.028	457	406	-	0.09	1.04	BJ
228		CD3022	INT	0	38.1	-	-	-	406	38.1	516	0.013	508	406	38.1	510	0.028	457	406	-	0.09	0.96	BJ
229		PADH22	INT	0	36.3	-	-	-	406	36.3	527	0.013	508	406	36.3	538	0.028	457	406	-	0.10	0.96	BJ
230	Wang and Hsu (2009)	Ko-JI1	INT	0	31.7	-	-	-	300	31.7	533	0.016	500	300	31.7	533	0.034	300	300	-	0.14	0.93	J
231		Ho-JI1	INT	0	26.2	-	-	-	350	26.2	541	0.011	400	300	26.2	541	0.025	400	400	-	0.00	0.97	J
232	Hanson and Connor (1972)	8	INT	1	41.8	-	-	-	343	41.8	306	0.019	508	305	41.2	564	0.055	381	381	-	0.48	0.94	BJ
233	Ohwada (1976)	JE-0	INT	1	20.1	-	-	-	100	20.1	402	0.039	150	100	20.1	402	0.034	150	100	-	0.00	1.17	J
234	Ohwada (1977)	JE-1	INT	1	20.0	-	-	-	150	20.0	432	0.020	150	150	20.0	432	0.034	150	150	-	0.00	0.88	J
235	Aycardi et al. (1994)	Interior	INT	2	34.5	-	-	-	102	34.5	448	0.009	76	152	30.0	448	0.010	102	102	-	0.09	1.06	BJ, A
236	Beres et al. (1991)	I-12	INT	2	30.8	-	-	-	381	30.8	459	0.008	610	356	16.5	487	0.020	406	406	-	0.57	1.18	BJ
237		I-14	INT	2	25.0	-	-	-	381	25.0	341	0.008	610	356	26.5	550	0.020	406	406	-	0.10	1.08	BJ
238		I-16	INT	2	24.8	-	-	-	381	24.8	461	0.008	610	356	17.2	497	0.020	406	406	-	0.55	1.14	BJ
239		I-18	INT	2	21.9	-	-	-	381	21.9	472	0.008	610	356	16.8	472	0.009	406	406	-	0.16	1.31	BJ
240		I-19	INT	2	18.9	-	-	-	381	18.9	461	0.008	610	356	16.7	478	0.009	406	406	-	0.56	1.13	BJ

Table C.1 Experimental non-ductile beam-column joint database (continued)

No.	Reference	Specimen	Joint type	No. of TBs	Joint f_{cj} (MPa)	Joint f_{yj} (MPa)	Joint s_j (mm)	Joint ρ_j	Beam b_j (mm)	Beam f_{cb} (MPa)	Beam f_{yb} (MPa)	Beam ρ_b	Beam h_b (mm)	Beam b_b (mm)	Column f_{cc} (MPa)	Column f_{yc} (MPa)	Column ρ_c	Column h_c (mm)	Column b_c (mm)	e (mm)	ALF	$\frac{v_{j,\max,pred}}{v_{j,\max,exp}}$	Failure mode§
241	Hanson and Connor (1972)	9	INT	2	26.2	-	-	-	343	26.2	306	0.019	508	305	41.3	430	0.055	381	381	-	0.47	0.89	BJ
242	Hatamoto and Bessho	F-3	INT	2	44.5	-	-	-	363	44.5	392	0.028	400	325	44.5	392	0.036	425	400	-	0.23	0.99	BJ
243	(1998)	F-4	INT	2	44.5	-	-	-	363	44.5	392	0.028	400	325	44.5	392	0.036	425	400	-	0.00	1.04	BJ
244	Li et al. (2009)	AS1	INT	2	31.4	-	-	-	300	31.4	473	0.011	400	200	31.4	473	0.031	200	400	-	0.00	0.85	J
245		AL1	INT	2	30.3	-	-	-	300	30.3	473	0.011	400	200	30.3	473	0.031	200	400	-	0.00	0.95	J
246		AS2	INT	2	31.9	-	-	-	200	31.9	473	0.011	400	200	31.9	473	0.031	400	200	-	0.00	1.15	J
247		AL2	INT	2	32.1	-	-	-	200	32.1	473	0.011	400	200	32.1	473	0.031	400	200	-	0.00	1.17	J
248		MAS1	INT	2	31.2	252	135	0.003	300	31.2	473	0.011	400	200	31.2	473	0.031	200	400	-	0.00	0.90	J
249	Ohwada (1977)	JI-1	INT	2	20.0	-	-	-	150	20.0	432	0.020	150	150	20.0	432	0.034	150	150	-	0.00	0.84	J
250	Ohwada (1980)	JI-3	INT	2	20.6	-	-	-	150	20.6	394	0.020	150	150	20.6	394	0.034	150	150	-	0.00	0.79	J
251		JI-4	INT	2	20.6	-	-	-	150	20.6	394	0.020	150	150	20.6	394	0.034	150	150	-	0.00	0.99	J
252		JI-5	INT	2	20.6	-	-	-	150	20.6	394	0.020	150	150	20.6	394	0.034	150	150	-	0.00	0.94	J
253		JXY-1	INT	2	14.0	-	-	-	150	14.0	360	0.020	150	150	14.0	360	0.068	150	150	-	0.00	0.90	J
254		LJXY-1	INT	2	20.0	-	-	-	150	20.0	372	0.020	150	150	20.0	372	0.068	150	150	-	0.00	0.83	BJ
255		LJXY-3	INT	2	20.0	-	-	-	150	20.0	372	0.020	150	150	20.0	372	0.068	150	150	-	0.00	0.81	BJ
256	Ohwada (1981)	LJXY-5	INT	2	17.1	-	-	-	135	17.1	368	0.018	200	120	17.1	368	0.023	150	150	-	0.41	0.96	CJ
257	Owada (1984)	LJXY-6	INT	2	28.9	-	-	-	135	28.9	357	0.018	200	120	28.9	357	0.023	150	150	-	0.23	0.88	CJ
258		LJXY-7	INT	2	28.9	-	-	-	135	28.9	357	0.018	200	120	28.9	357	0.023	150	150	-	0.23	0.79	CJ
259		LJXY-8	INT	2	28.9	-	-	-	135	28.9	357	0.018	200	120	28.9	357	0.023	150	150	-	0.23	0.93	CJ
260	Owada (2000)	JXY-3	INT	2	37.6	-	-	-	135	37.6	349	0.018	200	120	37.6	349	0.023	150	150	-	0.17	0.84	CJ
261	Pessiki et al. (1990)	I-10	INT	2	22.3	-	-	-	381	22.3	425	0.008	610	356	27.7	476	0.020	406	406	-	0.34	1.09	BJ
	Mean																					***1.01***	
	Minimum																					***0.72***	
	Maximum																					***1.34***	
	COV																					***0.15***	

§ J and BJ refer to joint shear failure without and without beam yielding, respectively.

Note that subscripts *j*, *b*, and *c* indicate joint, beam, and column, respectively.

C.2 Database of Ductile Beam-Column Joints

Table C.2 Experimental ductile beam-column joint database

No.	Reference	Specimen	Joint type	No. of TBs	Joint f_{cj} (MPa)	Joint f_{yj} (MPa)	Joint s_j (mm)	Joint ρ_j	Beam b_j (mm)	Beam f_{cb} (MPa)	Beam f_{yb} (MPa)	Beam ρ_b	Beam h_b (mm)	Beam b_b (mm)	Column f_{cc} (MPa)	Column f_{yc} (MPa)	Column ρ_c	Column h_c (mm)	Column b_c (mm)	e (mm)	ALF	$\frac{v_{j,\max,pred}}{v_{j,\max,exp}}$	Failure mode[§]
1	Adachi et al. (1995)	A0	EXT	0	73.9	939	50	0.005	190	73.9	969	0.020	250	160	73.9	969	0.031	220	220	-	0.06	1.05	J
2	Alva et al. (2007)	LVP3	EXT	0	23.9	602	82	0.006	200	23.9	594	0.011	400	200	23.9	594	0.033	300	200	-	0.15	0.82	J
3		LVP5	EXT	0	25.9	602	82	0.006	200	25.9	594	0.011	400	200	25.9	594	0.033	300	200	-	0.15	0.81	J
4	Chen and Chen (1999)	JC	EXT	0	20.0	397	75	0.006	400	20.0	439	0.016	500	300	20.0	457	0.016	500	500	-	0.00	0.83	BJ
5		JE	EXT	0	19.9	397	75	0.006	400	19.9	439	0.016	500	300	19.9	457	0.016	500	500	100	0.00	0.78	BJ
6	Chun and Kim (2004)	JC-2	EXT	0	40.8	384	150	0.003	425	40.8	392	0.020	500	350	40.8	392	0.025	500	500	-	0.05	0.89	BJ
7	Chutarat and Aboutaha (2003)	Specimen 1	EXT	0	27.6	365	102	0.012	381	27.6	483	0.014	457	356	27.6	483	0.028	406	406	-	0.00	0.95	BJ
8	Ehsani and	LL8	EXT	0	55.8	437	102	0.012	337	55.8	437	0.015	508	318	55.8	437	0.028	356	356	-	0.04	0.97	BJ
9	Alameddine (1991)	LH8	EXT	0	55.8	437	61	0.020	337	55.8	437	0.019	508	318	55.8	437	0.028	356	356	-	0.04	1.12	BJ
10		HH8	EXT	0	55.8	437	61	0.020	337	55.8	437	0.019	508	318	55.8	437	0.032	356	356	-	0.07	0.95	BJ
11		LH11	EXT	0	73.8	437	61	0.020	337	73.8	437	0.015	508	318	73.8	437	0.028	356	356	-	0.03	1.03	BJ
12		HH11	EXT	0	73.8	437	61	0.020	337	73.8	437	0.019	508	318	73.8	437	0.032	356	356	-	0.06	1.02	BJ
13		LL14	EXT	0	93.8	437	102	0.012	337	93.8	437	0.015	508	318	93.8	437	0.028	356	356	-	0.02	1.15	BJ
14		LH14	EXT	0	93.8	437	61	0.020	337	93.8	437	0.015	508	318	93.8	437	0.028	356	356	-	0.02	1.18	BJ
15		HH14	EXT	0	93.8	437	61	0.020	337	93.8	437	0.019	508	318	93.8	437	0.032	356	356	-	0.04	1.11	BJ
16		HL8	EXT	0	55.8	437	102	0.012	337	55.8	437	0.019	508	318	55.8	437	0.032	356	356	-	0.07	0.92	J
17		LL11	EXT	0	73.8	437	102	0.012	337	73.8	437	0.015	508	318	73.8	437	0.028	356	356	-	0.03	1.20	J
18		HL11	EXT	0	73.8	437	102	0.012	337	73.8	437	0.019	508	318	73.8	437	0.032	356	356	-	0.06	1.04	J
19		HL14	EXT	0	93.8	437	102	0.012	337	93.8	437	0.019	508	318	93.8	437	0.032	356	356	-	0.04	1.25	J
20	Ehsani and Wight	1B	EXT	0	33.6	437	112	0.013	279	33.6	331	0.018	480	259	33.6	490	0.025	300	300	-	0.06	0.82	J
21	(1985)	2B	EXT	0	35.0	437	99	0.015	279	35.0	331	0.020	439	259	35.0	490	0.032	300	300	-	0.07	0.85	J
22		3B	EXT	0	40.9	437	84	0.017	279	40.9	331	0.018	480	259	40.9	490	0.025	300	300	-	0.06	0.91	BJ
23		5B	EXT	0	24.3	437	109	0.012	320	24.3	331	0.018	480	300	24.3	414	0.044	340	340	-	0.13	0.79	J
24		6B	EXT	0	38.4	437	127	0.010	320	38.4	331	0.016	480	300	38.4	490	0.020	340	340	-	0.07	1.22	BJ
25	Ehsani et al. (1987)	NO3	EXT	0	64.7	437	76	0.019	279	64.7	448	0.012	439	259	64.7	448	0.032	300	300	-	0.07	1.02	BJ
26		NO4	EXT	0	67.3	437	99	0.015	279	67.3	448	0.015	439	259	67.3	448	0.040	300	300	-	0.05	0.88	BJ
27		NO5	EXT	0	44.6	437	99	0.015	279	44.6	448	0.017	439	259	44.6	448	0.025	300	300	-	0.06	0.99	BJ
28	Fujii and Morita (1987)	GOO	EXT	0	45.6	367	70	0.004	198	45.6	369	0.020	250	175	45.6	369	0.031	220	220	-	0.04	1.09	BJ
29	Fujii and Morita	B1	EXT	0	30.0	291	52	0.005	190	30.0	1069	0.017	250	160	30.0	387	0.031	220	220	-	0.07	1.17	J
30	(1991)	B2	EXT	0	30.0	291	52	0.005	190	30.0	409	0.016	250	160	30.0	387	0.031	220	220	-	0.07	0.95	J

Table C.2 Experimental ductile beam-column joint database (continued)

No.	Reference	Specimen	Joint type	No. of TBs	Joint f_{cj} (MPa)	Joint f_{yj} (MPa)	Joint s_j (mm)	Joint ρ_j	Beam b_j (mm)	Beam f_{cb} (MPa)	Beam f_{yb} (MPa)	Beam ρ_b	Beam h_b (mm)	Beam b_b (mm)	Column f_{cc} (MPa)	Column f_{yc} (MPa)	Column ρ_c	Column h_c (mm)	Column b_c (mm)	e (mm)	ALF	$\frac{v_{j,\max,pred}}{v_{j,\max,exp}}$	Failure mode§
31	Fujii and Morita	B3	EXT	0	30.0	291	52	0.005	190	30.0	1069	0.017	250	160	30.0	387	0.031	220	220	-	0.24	1.05	J
32	(1991)	B4	EXT	0	30.0	291	35	0.015	190	30.0	1069	0.017	250	160	30.0	387	0.031	220	220	-	0.24	1.09	J
33	Hamada et al. (1999)	J-10	EXT	0	57.4	950	55	0.005	350	57.4	745	0.018	430	250	34.3	527	0.026	450	450	-	-0.19	0.90	BJ
34	Hamil (2000)	C4ALN3	EXT	0	52.0	500	63	0.006	130	52.0	500	0.041	210	110	52.0	500	0.036	150	150	-	0.04	0.84	J
35		C4ALN5	EXT	0	63.0	500	31	0.012	130	63.0	500	0.041	210	110	63.0	500	0.036	150	150	-	0.04	0.86	J
36		C6LN3	EXT	0	61.0	500	63	0.006	130	61.0	500	0.041	210	110	61.0	500	0.036	150	150	-	0.04	1.14	J
37		C6LN5	EXT	0	46.0	500	31	0.012	130	46.0	500	0.041	210	110	46.0	500	0.036	150	150	-	0.05	0.86	J
38		C6ALH3	EXT	0	121.0	500	63	0.006	130	121.0	500	0.041	210	110	121.0	500	0.036	150	150	-	0.04	1.06	J
39		C7LN5	EXT	0	50.0	500	31	0.012	130	50.0	500	0.027	300	110	50.0	500	0.036	150	150	-	0.04	0.83	J
40		C9LN5	EXT	0	44.0	500	31	0.012	130	44.0	500	0.027	300	110	44.0	500	0.036	150	150	-	0.05	0.93	J
41	Hanson and Connor (1967)	I-A	EXT	0	22.1	364	82	0.005	343	22.1	330	0.019	508	305	36.7	481	0.055	381	381	-	0.54	0.74	BJ
42	Hwang et al. (2005)	3T3	EXT	0	69.0	471	97	0.003	370	69.0	430	0.016	450	320	69.0	421	0.037	420	420	-	0.02	0.95	BJ
43		2T4	EXT	0	71.0	498	146	0.004	370	71.0	430	0.016	450	320	71.0	421	0.037	420	420	-	0.02	1.02	BJ
44	Ishida et al. (1996)	A-0	EXT	0	27.0	271	50	0.005	190	27.0	700	0.015	250	160	27.0	700	0.031	220	220	-	0.15	1.01	J
45		A-0-F	EXT	0	27.0	271	50	0.005	190	27.0	467	0.015	250	160	27.0	467	0.031	220	220	-	0.15	0.92	BJ
46	Iwaoka et al. (2005)	J15-3	EXT	0	180.0	935	80	0.002	295	180.0	682	0.036	400	260	180.0	690	0.027	380	330	-	0.05	1.04	J
47		J10-1	EXT	0	115.0	935	80	0.002	295	115.0	682	0.036	400	260	115.0	690	0.027	380	330	-	0.05	0.96	J
48	Jinno et al. (1985)	NO06	EXT	0	28.9	304	100	0.004	280	28.9	392	0.013	380	260	28.9	371	0.038	300	300	-	0.00	1.06	BJ
49		NO07	EXT	0	28.9	304	100	0.004	280	28.9	392	0.013	380	260	28.9	371	0.038	300	300	-	0.00	1.07	BJ
50		NO08	EXT	0	28.9	304	50	0.008	280	28.9	392	0.013	380	260	28.9	371	0.038	300	300	-	0.00	1.10	BJ
51		NO09	EXT	0	28.9	304	100	0.008	280	28.9	392	0.013	380	260	28.9	371	0.038	300	300	-	0.00	1.08	BJ
52		NO10	EXT	0	28.9	304	100	0.008	280	28.9	392	0.013	380	260	28.9	371	0.038	300	300	-	0.00	1.02	BJ
53	Joh et al. (1989)	LO-NO	EXT	0	27.9	380	110	0.001	275	27.9	606	0.024	350	200	27.9	581	0.025	260	350	-	0.02	1.13	J
54		HO-NO	EXT	0	29.6	380	38	0.004	275	29.6	606	0.024	350	200	29.6	581	0.025	260	350	-	0.02	0.99	J
55		MM-NO	EXT	0	27.8	380	38	0.004	275	27.8	606	0.024	350	200	27.8	581	0.028	260	350	-	0.02	1.00	J
56		HH-NO	EXT	0	29.3	380	38	0.004	275	29.3	606	0.024	350	200	29.3	581	0.025	260	350	-	0.02	0.86	J
57		H'O-NO	EXT	0	31.5	380	38	0.004	275	31.5	606	0.024	350	200	31.5	581	0.025	260	350	-	0.02	1.08	J
58		LO-N96	EXT	0	31.5	380	100	0.002	275	31.5	606	0.024	350	200	31.5	581	0.034	260	350	-	0.30	1.04	J
59		HH-N96	EXT	0	30.5	380	38	0.004	275	30.5	606	0.024	350	200	30.5	581	0.034	260	350	-	0.31	0.92	J
60	Joh et al. (1990)	NRC-J1	EXT	0	51.5	815	36	0.006	225	51.5	1091	0.032	250	200	51.5	1091	0.024	250	250	-	0.02	1.03	J

Table C.2 Experimental ductile beam-column joint database (continued)

No.	Reference	Specimen	Joint type	No. of TBs	Joint				Beam							Column									Failure mode[§]
					f_{cj} (MPa)	f_{yj} (MPa)	s_j (mm)	ρ_j	b_j (mm)	f_{cb} (MPa)	f_{yb} (MPa)	ρ_b	h_b (mm)	b_b (mm)	f_{cc} (MPa)	f_{yc} (MPa)	ρ_c	h_c (mm)	b_c (mm)	e (mm)	ALF	$\frac{v_{j,\max,pred}}{v_{j,\max,exp}}$	
61	Joh et al. (1990)	NRC-J2	EXT	0	81.8	815	36	0.006	225	81.8	1091	0.032	250	200	81.8	1091	0.024	250	250	-	0.02	1.07	J
62		NRC-J3	EXT	0	86.9	840	36	0.003	225	86.9	1091	0.032	250	200	86.9	1091	0.024	250	250	-	0.02	1.02	J
63		NRC-J4	EXT	0	88.9	815	36	0.006	225	88.9	1091	0.032	250	200	88.9	1091	0.024	250	250	-	0.30	1.00	J
64	Joh et al. (1992)	NRC-J5	EXT	0	58.1	762	36	0.006	225	58.1	753	0.024	250	200	58.1	1092	0.024	250	250	-	0.02	0.90	J
65		NRC-J6	EXT	0	32.2	762	36	0.006	225	32.2	753	0.024	250	200	32.2	1092	0.024	250	250	-	0.02	1.09	J
66		NRC-J7	EXT	0	57.7	762	35	0.006	225	57.7	753	0.016	350	200	57.7	1092	0.024	250	250	-	0.02	0.85	J
67		NRC-J8	EXT	0	53.7	717	42	0.002	225	53.7	675	0.025	250	200	53.7	675	0.028	250	250	-	0.02	1.19	J
68		NRC-J9	EXT	0	49.3	770	36	0.006	225	49.3	675	0.017	250	200	49.3	675	0.020	250	250	-	0.02	0.85	J
69		NRC-J10	EXT	0	65.7	760	42	0.002	225	65.7	675	0.017	250	200	65.7	675	0.020	250	250	-	0.02	1.25	BJ
70		NRC-J11	EXT	0	78.7	760	42	0.002	225	78.7	675	0.011	250	200	78.7	675	0.020	250	250	-	0.02	1.26	BJ
71		NRC-J12	EXT	0	83.7	717	42	0.002	225	83.7	698	0.025	250	200	83.7	698	0.024	250	250	-	0.02	0.79	BJ
72		NRC-J13	EXT	0	79.4	770	36	0.006	225	79.4	698	0.025	250	200	79.4	698	0.024	250	250	-	0.02	0.98	BJ
73		NRC-J14	EXT	0	64.9	717	42	0.002	225	64.9	547	0.025	250	200	64.9	698	0.024	250	250	-	0.02	1.09	BJ
74	Kaku and Asakusa	3	EXT	0	41.7	250	52	0.005	190	41.7	381	0.016	220	160	41.7	360	0.016	220	220	-	0.00	0.97	BJ
75	(1991)	4	EXT	0	44.7	281	52	0.001	190	44.7	381	0.016	220	160	44.7	360	0.016	220	220	-	0.17	0.81	BJ
76		5	EXT	0	36.7	281	52	0.001	190	36.7	381	0.016	220	160	36.7	360	0.016	220	220	-	0.09	0.83	BJ
77		6	EXT	0	40.4	281	52	0.001	190	40.4	381	0.016	220	160	40.4	360	0.016	220	220	-	0.00	1.25	BJ
78		9	EXT	0	40.6	250	52	0.005	190	40.6	381	0.016	220	160	40.6	395	0.018	220	220	-	0.00	0.89	BJ
79		11	EXT	0	41.9	281	52	0.001	190	41.9	381	0.016	220	160	41.9	395	0.018	220	220	-	0.08	0.82	BJ
80		12	EXT	0	35.1	281	52	0.001	190	35.1	381	0.016	220	160	35.1	395	0.018	220	220	-	0.00	0.87	BJ
81		13	EXT	0	46.4	250	52	0.005	190	46.4	381	0.016	220	160	46.4	395	0.018	220	220	-	-0.04	1.04	BJ
82		14	EXT	0	41.0	281	52	0.001	190	41.0	381	0.016	220	160	41.0	381	0.016	220	220	-	0.08	0.81	BJ
83		15	EXT	0	39.7	281	52	0.001	190	39.7	381	0.016	220	160	39.7	381	0.016	220	220	-	0.08	0.78	BJ
84		17	EXT	0	39.7	250	52	0.005	190	39.7	381	0.016	220	160	39.7	395	0.011	220	220	-	0.00	1.15	BJ
85	Kanada et al. (1984)	U41L	EXT	0	26.7	387	100	0.004	280	26.7	387	0.017	380	260	26.7	385	0.026	300	300	-	0.00	1.19	BJ
86		U42L	EXT	0	30.1	387	50	0.008	280	30.1	387	0.017	380	260	30.1	385	0.026	300	300	-	0.00	1.33	BJ
87	Kawai et al. (1997)	O8V	EXT	0	88.1	928	65	0.003	400	88.1	522	0.024	450	325	88.1	522	0.027	475	475	-	0.67	0.90	BJ
88	Lee and Lee (2000)	EJ+0.0	EXT	0	19.0	673	75	0.003	250	19.0	451	0.015	300	200	19.0	451	0.027	300	300	-	0.00	1.22	J
89		EJ+0.1	EXT	0	19.0	673	75	0.003	250	19.0	451	0.015	300	200	19.0	451	0.027	300	300	-	0.10	1.13	J
90	Lee and Lee (2001)	HJ2-0.0	EXT	0	38.0	671	96	0.002	250	38.0	540	0.022	300	200	38.0	504	0.027	300	300	-	0.00	1.02	J

Table C.2 Experimental ductile beam-column joint database (continued)

No.	Reference	Specimen	Joint type	No. of TBs	Joint				Beam							Column								$\frac{v_{j,\max,pred}}{v_{j,\max,exp}}$	Failure mode[§]
					f_{cj} (MPa)	f_{yj} (MPa)	s_j (mm)	ρ_j	b_j (mm)	f_{cb} (MPa)	f_{yb} (MPa)	ρ_b	h_b (mm)	b_b (mm)	f_{cc} (MPa)	f_{yc} (MPa)	ρ_c	h_c (mm)	b_c (mm)	e (mm)	ALF		
91	Lee and Lee (2001)	HJ2-0.15	EXT	0	38.0	671	96	0.002	250	38.0	540	0.022	300	200	38.0	504	0.027	300	300	-	0.15	1.00	J
92		HJ2-0.30	EXT	0	38.0	671	96	0.002	250	38.0	540	0.022	300	200	38.0	504	0.027	300	300	-	0.30	1.08	J
93		HJ5-0.0	EXT	0	38.0	671	32	0.006	250	38.0	540	0.022	300	200	38.0	504	0.027	300	300	-	0.00	1.00	J
94		HJ5-0.15	EXT	0	38.0	671	32	0.006	250	38.0	540	0.022	300	200	38.0	504	0.027	300	300	-	0.15	1.15	J
95		HJ5-0.3	EXT	0	38.0	671	32	0.006	250	38.0	540	0.022	300	200	38.0	504	0.027	300	300	-	0.30	1.24	J
96		NJ2-0.0	EXT	0	23.5	671	96	0.002	250	23.5	442	0.016	300	200	23.5	504	0.027	300	300	-	0.00	0.97	J
97		NJ2-0.15	EXT	0	23.5	671	96	0.002	250	23.5	442	0.016	300	200	23.5	504	0.027	300	300	-	0.15	1.01	J
98		NJ2-0.3	EXT	0	23.5	671	96	0.002	250	23.5	442	0.016	300	200	23.5	504	0.027	300	300	-	0.30	1.01	J
99		NJ5-0.0	EXT	0	23.5	671	32	0.006	250	23.5	442	0.016	300	200	23.5	504	0.027	300	300	-	0.00	1.01	J
100		NJ5-0.15	EXT	0	23.5	671	32	0.006	250	23.5	442	0.016	300	200	23.5	504	0.027	300	300	-	0.15	1.08	J
101		NJ5-0.3	EXT	0	23.5	671	32	0.006	250	23.5	442	0.016	300	200	23.5	504	0.027	300	300	-	0.30	1.08	J
102	Megget (1971)	Unit 1	EXT	0	28.3	317	127	0.006	293	28.3	286	0.013	460	255	28.3	305	0.012	380	330	-	0.00	1.03	BJ
103	Megget (1974)	Unit A	EXT	0	22.1	317	50	0.016	293	22.1	374	0.017	460	255	22.1	365	0.025	380	330	-	0.07	0.88	BJ
104	Nishiyama et al. (1989)	RC2	EXT	0	29.8	335	50	0.008	250	29.8	425	0.025	300	200	29.8	425	0.032	300	300	-	0.04	0.95	BJ
105	Ogawa et al. (2003)	BUCS	EXT	0	18.6	402	50	0.004	280	18.6	388	0.010	400	260	18.6	388	0.027	300	300	-	0.20	0.88	J
106		BUVS	EXT	0	18.6	402	50	0.004	280	18.6	389	0.010	400	260	18.6	388	0.027	300	300	-	0.62	1.03	J
107	Oh et al. (1992)	EJS-200-0.3N	EXT	0	26.8	375	64	0.004	170	26.8	434	0.025	200	140	26.8	417	0.027	200	200	-	0.00	1.01	J
108		EJS-200-2-0.6N	EXT	0	24.0	375	32	0.007	170	24.0	434	0.025	200	140	24.0	417	0.027	200	200	-	0.00	0.98	J
109		EJS-200-2-0.6N'	EXT	0	24.0	375	64	0.004	170	24.0	434	0.025	200	140	24.0	417	0.031	200	200	-	0.00	0.95	J
110		EJS-400-0.3N	EXT	0	41.7	375	64	0.004	170	41.7	434	0.025	200	140	41.7	417	0.027	200	200	-	0.00	0.96	J
111		EJS-400-0.6N	EXT	0	44.6	375	32	0.007	170	44.6	434	0.025	200	140	44.6	417	0.027	200	200	-	0.00	1.00	BJ
112		EJS-400-0.6N'	EXT	0	44.6	375	64	0.004	170	44.6	434	0.025	200	140	44.6	417	0.031	200	200	-	0.00	0.96	BJ
113		EJS-400-0.6H	EXT	0	43.1	765	32	0.009	170	43.1	417	0.036	200	140	43.1	417	0.027	200	200	-	0.00	0.99	J
114		EJS-400-1.2H	EXT	0	43.1	765	16	0.018	170	43.1	417	0.036	200	140	43.1	417	0.027	200	200	-	0.00	0.97	BJ
115	Onish et al. (1990)	NO. 5	EXT	0	28.1	314	55	0.005	250	28.1	389	0.012	250	250	28.1	389	0.012	250	250	-	0.00	0.95	BJ
116	Parker and Bullman (1997)	5f	EXT	0	43.2	480	100	0.008	275	43.2	515	0.014	500	250	43.2	485	0.022	300	300	-	0.15	0.80	J
117	Sasmal et al. (2011)	SP-3	EXT	0	35.0	250	140	0.002	300	35.0	500	0.018	400	300	35.0	500	0.022	300	300	-	0.10	1.16	J
118	Smith (1972)	Unit 4	EXT	0	20.5	310	70	0.011	293	20.5	296	0.013	460	255	20.5	274	0.012	380	330	-	0.00	1.30	BJ
119		Unit 5	EXT	0	20.1	310	95	0.005	293	20.1	301	0.013	460	255	20.1	274	0.012	380	330	-	0.00	1.19	BJ
120		Unit 6	EXT	0	17.7	310	76	0.010	293	17.7	299	0.013	460	255	17.7	297	0.012	380	330	-	0.00	1.17	BJ

Table C.2 Experimental ductile beam-column joint database (continued)

No.	Reference	Specimen	Joint type	No. of TBs	Joint				Beam								Column							ALF	$\frac{v_{j,\max,pred}}{v_{j,\max,exp}}$	Failure mode[§]
					f_{cj} (MPa)	f_{yj} (MPa)	s_j (mm)	ρ_j	b_j (mm)	f_{cb} (MPa)	f_{yb} (MPa)	ρ_b	h_b (mm)	b_b (mm)	f_{cc} (MPa)	f_{yc} (MPa)	ρ_c	h_c (mm)	b_c (mm)	e (mm)			
121	Takeuchi et al. (2003)	O-5	EXT	0	42.0	327	100	0.004	375	42.0	445	0.011	450	350	42.0	553	0.029	400	400	-	0.10	1.36	J
122	Teroaka (1997)	NO1	EXT	0	34.8	328	45	0.006	453	32.6	421	0.011	560	365	33.4	421	0.025	540	540	-	0.01	1.17	BJ
123		NO3	EXT	0	38.9	328	47	0.006	453	32.6	434	0.014	560	365	33.4	421	0.025	540	540	-	0.01	1.20	BJ
124		NO4	EXT	0	39.1	328	48	0.005	453	32.6	434	0.014	560	365	33.4	421	0.025	540	540	-	0.01	1.13	BJ
125	Tsonos (1996)	MS4	EXT	0	33.6	495	42	0.012	200	33.6	466	0.006	300	200	33.6	485	0.031	200	200	-	0.29	0.84	BJ
126	Tsonos (2007)	A1	EXT	0	35.0	540	50	0.010	200	35.0	500	0.006	300	200	35.0	500	0.016	200	200	-	0.14	1.04	BJ
127		E1	EXT	0	22.0	540	50	0.010	200	22.0	495	0.009	300	200	22.0	495	0.031	200	200	-	0.23	0.74	J
128		E2	EXT	0	35.0	540	50	0.010	200	35.0	495	0.006	300	200	35.0	495	0.031	200	200	-	0.14	1.09	BJ
129	Tsonos et al. (1992)	S1	EXT	0	37.0	495	70	0.007	200	37.0	485	0.006	300	200	37.0	485	0.023	200	200	-	0.18	1.24	BJ
130		S2	EXT	0	26.0	495	70	0.007	200	26.0	465	0.006	300	200	26.0	465	0.008	200	200	-	0.18	1.03	BJ
131		S3	EXT	0	19.0	495	70	0.007	200	19.0	465	0.006	300	200	19.0	465	0.008	200	200	-	0.18	0.96	BJ
132		S4	EXT	0	21.0	495	70	0.007	200	21.0	485	0.010	300	200	21.0	465	0.012	200	200	-	0.18	1.10	J
133		S5	EXT	0	25.0	495	70	0.007	200	25.0	485	0.011	300	200	25.0	465	0.019	200	200	-	0.18	1.05	J
134		S6	EXT	0	33.0	495	70	0.007	200	33.0	485	0.011	300	200	33.0	485	0.015	200	200	-	0.18	1.13	J
135		S6'	EXT	0	29.0	495	70	0.007	200	29.0	485	0.011	300	200	29.0	485	0.031	200	200	-	0.18	0.95	BJ
136		O1	EXT	0	20.0	495	70	0.011	200	20.0	485	0.011	300	200	20.0	485	0.031	200	200	-	0.18	1.25	J
137		F2	EXT	0	24.0	495	70	0.011	200	24.0	485	0.011	300	200	24.0	485	0.031	200	200	-	0.18	1.04	J
138	Uzumeri (1977)	6	EXT	0	36.2	357	44	0.015	381	36.2	352	0.011	508	381	37.7	340	0.028	381	381	-	0.42	1.02	BJ
139		7	EXT	0	30.8	365	76	0.009	381	30.8	352	0.011	508	381	30.8	340	0.028	381	381	-	0.52	0.96	BJ
140		8	EXT	0	26.3	365	44	0.015	381	26.3	352	0.015	508	381	26.3	390	0.028	381	381	-	0.61	0.87	BJ
141	Wong (2005)	BS-L-H2T10	EXT	0	42.1	500	130	0.004	280	42.1	520	0.009	450	260	42.1	520	0.022	300	300	-	0.15	0.91	J
142		JA-NY03	EXT	0	34.9	500	100	0.005	280	34.9	520	0.007	400	260	34.9	520	0.022	300	300	-	0.03	1.25	BJ
143		JA-NY15	EXT	0	38.5	500	100	0.005	280	38.5	520	0.007	400	260	38.5	520	0.022	300	300	-	0.15	1.21	BJ
144		JB-NY03	EXT	0	34.2	500	100	0.005	280	34.2	520	0.010	300	260	34.2	520	0.022	300	300	-	0.03	1.28	BJ
145	Adachi et al. (1995)	B-1EW	EXT	1	73.9	939	50	0.005	190	73.9	969	0.020	250	160	73.9	969	0.031	220	220	-	0.06	1.03	BJ
146		B-1NS	EXT	1	73.9	939	50	0.005	190	73.9	969	0.020	250	160	73.9	969	0.031	220	220	-	0.06	1.11	BJ
147		B-2EW	EXT	1	73.9	939	50	0.005	190	73.9	969	0.020	250	160	73.9	969	0.031	220	220	-	0.06	1.05	J
148		B-2NS	EXT	1	73.9	939	50	0.005	190	73.9	969	0.020	250	160	73.9	969	0.031	220	220	-	0.06	1.15	J
149	Ishida et al. (1996)	B-1E	EXT	1	27.0	271	50	0.005	190	27.0	700	0.015	250	160	27.0	700	0.031	220	220	-	0.15	0.97	J
150		B-1N	EXT	1	27.0	271	50	0.005	190	27.0	700	0.015	250	160	27.0	700	0.031	220	220	-	0.15	1.01	J

Table C.2 Experimental ductile beam-column joint database (continued)

No.	Reference	Specimen	Joint type	No. of TBs	Joint				Beam								Column									Failure mode[§]
					f_{cj} (MPa)	f_{yj} (MPa)	s_j (mm)	ρ_j	b_j (mm)	f_{cb} (MPa)	f_{yb} (MPa)	ρ_b	h_b (mm)	b_b (mm)	f_{cc} (MPa)	f_{yc} (MPa)	ρ_c	h_c (mm)	b_c (mm)	e (mm)	ALF	$\frac{v_{j,\max,pred}}{v_{j,\max,exp}}$	
151	Ishida et al. (1996)	C-1E	EXT	1	27.0	271	54	0.005	190	27.0	467	0.015	250	160	27.0	467	0.031	220	220	-	0.15	0.96	BJ
152		C-1N	EXT	1	27.0	271	54	0.005	190	27.0	467	0.015	250	160	27.0	467	0.031	220	220	-	0.15	0.99	BJ
153		B-2E	EXT	1	28.4	271	50	0.005	190	28.4	700	0.015	250	160	28.4	700	0.031	220	220	-	0.14	1.16	J
154		B-2N	EXT	1	28.4	271	50	0.005	190	28.4	700	0.015	250	160	28.4	700	0.031	220	220	-	0.14	0.95	J
155		C-2E	EXT	1	28.4	271	54	0.005	190	28.4	467	0.015	250	160	28.4	467	0.031	220	220	-	0.14	0.96	BJ
156		C-2N	EXT	1	28.4	271	54	0.005	190	28.4	467	0.015	250	160	28.4	467	0.031	220	220	-	0.14	0.83	BJ
157	Uzumeri (1977)	3	EXT	1	27.0	427	76	0.005	343	27.0	350	0.014	508	305	39.4	336	0.028	381	381	-	0.40	0.90	BJ
158		4	EXT	1	31.0	379	76	0.009	343	31.0	349	0.014	508	305	38.2	332	0.028	381	381	-	0.42	0.86	BJ
159	Canbolat and Wight (2008)	3-N	EXT	2	29.0	441	95	0.010	394	29.0	450	0.016	457	254	29.0	450	0.012	356	533	-	0.03	0.76	BJ
160	Ehsani et al. (1985)	3S	EXT	2	29.0	437	112	0.013	279	29.0	345	0.008	439	259	29.0	490	0.032	300	300	-	0.09	0.84	BJ
161	Fujii and Morita	GBO,NS	EXT	2	37.0	367	70	0.004	198	37.0	369	0.020	250	175	37.0	369	0.031	220	220	-	0.05	1.28	BJ
162	(1987)	GBS1,NS	EXT	2	38.3	367	70	0.004	198	38.3	369	0.020	250	175	38.3	369	0.031	220	220	-	0.05	0.88	BJ
163		GBS2,NS	EXT	2	28.8	367	70	0.004	198	28.8	369	0.020	250	175	28.8	369	0.031	220	220	-	0.07	1.00	BJ
164		GBS3,NS	EXT	2	38.3	367	70	0.004	198	38.3	369	0.020	250	175	38.3	369	0.031	220	220	-	0.05	0.91	BJ
165		GBS4,NS	EXT	2	38.4	367	70	0.004	198	38.4	369	0.020	250	175	38.4	369	0.031	220	220	-	0.05	0.95	BJ
166		GBSU,NS	EXT	2	34.7	367	35	0.008	198	34.7	369	0.020	250	175	34.7	369	0.031	220	220	-	0.06	0.94	BJ
167	Kurose et al. (1991)	J3E	EXT	2	27.6	409	152	0.008	305	27.6	459	0.029	457	279	27.6	459	0.051	457	330	-	0.00	0.96	BJ
168	Nishi et al. (1992)	JY-2	EXT	2	24.9	448	40	0.004	135	24.9	366	0.018	150	120	24.9	366	0.023	150	150	-	0.70	1.04	BJ
169		JXY-2Y	EXT	2	24.9	448	40	0.004	135	24.9	366	0.018	150	120	24.9	366	0.023	150	150	-	0.70	0.90	BJ
170	Sekine and Ogura	No. 1	EXT	2	26.3	283	76	0.003	215	26.3	345	0.014	280	180	26.3	352	0.013	250	250	-	0.06	1.02	BJ
171	(1979)	No. 2	EXT	2	26.3	283	76	0.003	215	26.3	345	0.014	280	180	26.3	352	0.013	250	250	-	0.06	0.88	BJ
172	Tsubosaki et al. (1993)	J13EW	EXT	2	60.3	800	50	0.004	270	60.3	711	0.019	320	240	60.3	973	0.044	300	300	-	0.29	0.90	BJ
173	Aoyama et al. (1993)	H2	INT	0	45.6	441	56	0.005	250	45.6	544	0.008	300	200	45.6	544	0.027	300	300	-	0.04	1.11	BJ
174		H4	INT	0	64.2	441	58	0.005	250	64.2	544	0.008	300	200	64.2	809	0.027	300	300	-	0.03	0.87	BJ
175	Chang et al. (1997)	BCS2	INT	0	54.7	352	100	0.005	300	54.7	354	0.014	400	300	54.7	354	0.023	500	300	-	0.18	1.11	BJ
176	Durrani and Wight	X1	INT	0	34.3	352	152	0.008	321	34.3	345	0.015	419	279	34.3	414	0.031	362	362	-	0.05	1.07	BJ
177	(1985)	X2	INT	0	33.6	352	102	0.012	321	33.6	345	0.015	419	279	33.6	414	0.031	362	362	-	0.06	1.08	BJ
178	Durrani and Wight	X3	INT	0	31.0	352	152	0.008	321	31.0	345	0.011	419	279	31.0	331	0.020	362	362	-	0.05	1.25	BJ
179	Endoh et al. (1991)	HLC	INT	0	40.6	290	60	0.004	250	40.6	368	0.017	300	200	40.6	360	0.027	300	300	-	0.05	0.96	BJ
180		LA1	INT	0	34.8	286	45	0.007	250	34.8	801	0.020	300	200	34.8	550	0.035	300	300	-	0.06	1.12	J

Table C.2 Experimental ductile beam-column joint database (continued)

No.	Reference	Specimen	Joint type	No. of TBs	Joint f_{cj} (MPa)	Joint f_{yj} (MPa)	Joint s_j (mm)	Joint ρ_j	Beam b_j (mm)	Beam f_{cb} (MPa)	Beam f_{yb} (MPa)	Beam ρ_b	Beam h_b (mm)	Beam b_b (mm)	Column f_{cc} (MPa)	Column f_{yc} (MPa)	Column ρ_c	Column h_c (mm)	Column b_c (mm)	e (mm)	ALF	$\frac{v_{j,\max,pred}}{v_{j,\max,exp}}$	Failure mode§
181	Endoh et al. (1991)	A1	INT	0	30.6	320	45	0.006	250	30.6	780	0.020	300	200	30.6	539	0.035	300	300	-	0.06	1.12	J
182	Fujii and Morita (1987)	OBO	INT	0	43.5	367	70	0.004	190	43.5	369	0.011	250	160	43.5	369	0.031	220	220	-	0.05	1.05	BJ
183	Fujii and Morita	A1	INT	0	40.2	291	52	0.005	190	40.2	1069	0.017	250	160	40.2	643	0.042	220	220	-	0.08	1.20	J
184	(1991)	A2	INT	0	40.2	291	52	0.005	190	40.2	409	0.016	250	160	40.2	387	0.042	220	220	-	0.08	0.92	J
185		A3	INT	0	40.2	291	52	0.005	190	40.2	1069	0.017	250	160	40.2	643	0.042	220	220	-	0.23	1.20	J
186		A4	INT	0	40.2	291	35	0.015	190	40.2	1069	0.017	250	160	40.2	643	0.042	220	220	-	0.23	1.28	J
187	Goto and Joh (1996)	BJ-PL	INT	0	29.7	326	50	0.004	250	29.7	395	0.014	350	200	29.7	640	0.031	300	300	-	0.17	1.06	BJ
188		BJ-PH	INT	0	30.5	326	40	0.009	250	30.5	395	0.014	350	200	30.5	640	0.031	300	300	-	0.17	1.08	BJ
189		J-HH	INT	0	32.8	381	42	0.016	250	32.8	426	0.024	350	200	32.8	578	0.038	300	300	-	0.27	1.04	J
190		J-HO	INT	0	31.4	381	42	0.016	250	31.4	426	0.024	350	200	31.4	578	0.038	300	300	-	0.28	1.06	J
191		J-MM	INT	0	32.4	381	40	0.008	250	32.4	426	0.024	350	200	32.4	578	0.038	300	300	-	0.27	0.97	J
192		J-MO	INT	0	32.7	381	40	0.008	250	32.7	426	0.024	350	200	32.7	578	0.038	300	300	-	0.27	0.95	J
193		J-LO	INT	0	31.7	360	117	0.000	250	31.7	426	0.024	350	200	31.7	578	0.038	300	300	-	0.28	0.87	J
194	Goto and Joh (2003)	LM-60	INT	0	26.4	411	50	0.003	325	26.4	396	0.016	350	200	26.4	379	0.018	300	450	60	0.17	0.90	BJ
195		LM-125	INT	0	26.0	411	50	0.003	325	26.0	396	0.012	350	200	26.0	379	0.018	300	450	125	0.17	0.98	BJ
196		HM-60	INT	0	24.3	411	50	0.003	325	24.3	396	0.020	350	200	24.3	379	0.018	300	450	60	0.17	0.79	BJ
197		HM-125	INT	0	28.9	411	50	0.003	325	28.9	413	0.016	350	200	28.9	379	0.018	300	450	125	0.17	0.97	BJ
198		HH-125	INT	0	31.4	411	32	0.004	325	31.4	413	0.016	350	200	31.4	379	0.018	300	450	125	0.17	0.98	BJ
199	Goto and Joh (2004)	UM-0	INT	0	24.0	355	50	0.003	325	24.0	697	0.018	350	200	24.0	388	0.020	300	450	-	0.17	0.94	J
200		UM-60	INT	0	24.6	355	50	0.003	325	24.6	697	0.018	350	200	24.6	388	0.020	300	450	60	0.17	1.16	J
201		UM-125	INT	0	25.2	355	50	0.003	325	25.2	697	0.018	350	200	25.2	388	0.020	300	450	125	0.17	1.11	J
202		UU-125	INT	0	25.4	355	24	0.005	325	25.4	697	0.018	350	200	25.4	388	0.020	300	450	125	0.17	1.02	BJ
203		HU-125	INT	0	22.2	355	24	0.005	325	22.2	408	0.016	350	200	22.2	388	0.017	300	450	125	0.17	0.90	BJ
204	Hayashi et al. (1993)	NO47	INT	0	54.2	347	50	0.007	350	54.2	382	0.017	400	300	54.3	645	0.022	400	400	-	0.20	1.29	BJ
205		NO48	INT	0	54.2	347	50	0.007	350	54.2	645	0.011	400	300	54.3	645	0.022	400	400	-	0.20	1.19	BJ
206		NO49	INT	0	54.2	347	50	0.007	350	54.2	599	0.019	400	300	54.3	645	0.022	400	400	-	0.20	1.00	BJ
207		NO50	INT	0	54.2	347	50	0.007	350	54.2	858	0.008	400	300	54.3	645	0.022	400	400	-	0.20	1.19	BJ
208	Hiramatsu et al. (1995)	S1	INT	0	52.2	876	40	0.003	255	52.2	836	0.015	300	210	52.2	836	0.023	300	300	-	0.20	1.03	J
209	Inoue et al. (1990)	SP2	INT	0	43.3	1253	52	0.003	371	43.3	473	0.018	417	301	43.3	473	0.018	440	440	-	0.28	0.98	BJ
210	Ishida et al. (2001)	CN	INT	0	33.4	365	130	0.002	625	33.4	462	0.014	750	450	33.4	464	0.016	700	800	-	0.09	1.04	BJ

Table C.2 Experimental ductile beam-column joint database (continued)

No.	Reference	Specimen	Joint type	No. of TBs	Joint				Beam								Column							ALF	$\frac{v_{j,\max,pred}}{v_{j,\max,exp}}$	Failure mode[§]
					f_{cj} (MPa)	f_{yj} (MPa)	s_j (mm)	ρ_j	b_j (mm)	f_{cb} (MPa)	f_{yb} (MPa)	ρ_b	h_b (mm)	b_b (mm)	f_{cc} (MPa)	f_{yc} (MPa)	ρ_c	h_c (mm)	b_c (mm)	e (mm)			
211	Ishida et al. (2001)	EN	INT	0	33.4	365	130	0.002	625	33.4	462	0.014	750	450	33.4	464	0.016	700	800	135	0.09	1.09	BJ
212	Irisawa et al. (1996)	No. 1	INT	0	25.8	354	110	0.008	400	25.8	383	0.013	550	300	25.8	378	0.012	500	500	-	0.11	1.06	BJ
213	Ishida et al. (2004)	HS-HS	INT	0	70.0	1116	50	0.004	250	70.0	707	0.011	300	200	70.0	707	0.018	300	300	-	0.10	0.94	BJ
214	Ishikawa and Kamimura (1990)	No. 3	INT	0	23.3	330	50	0.010	215	23.3	373	0.016	250	180	23.3	373	0.032	250	250	-	0.18	0.97	BJ
215	Iwaoka et al. (2005)	J15-1	INT	0	182.0	935	80	0.002	260	182.0	682	0.037	400	220	182.0	690	0.030	380	300	-	0.25	0.98	J
216	Jinno et al. (1991)	NO1	INT	0	28.3	686	50	0.003	350	28.3	405	0.017	400	300	28.3	405	0.029	400	400	-	0.17	0.99	BJ
217		NO2	INT	0	28.3	686	50	0.003	350	28.3	913	0.017	400	300	28.3	913	0.029	400	400	-	0.17	1.08	J
218		NO3	INT	0	80.2	686	50	0.003	350	80.2	593	0.017	400	300	80.2	593	0.029	400	400	-	0.17	0.99	BJ
219		NO4	INT	0	80.2	686	50	0.003	350	80.2	593	0.017	400	300	80.2	593	0.029	400	400	-	0.17	0.89	BJ
220		NO5	INT	0	80.2	686	50	0.003	350	80.2	913	0.017	400	300	80.2	913	0.029	400	400	-	0.17	0.86	BJ
221		NO6	INT	0	101.9	686	50	0.003	350	101.9	726	0.017	400	300	101.9	726	0.029	400	400	-	0.17	0.96	BJ
222		NO7	INT	0	101.9	686	50	0.003	350	101.9	913	0.017	400	300	101.9	913	0.029	400	400	-	0.17	0.95	BJ
223		NO8	INT	0	101.9	686	50	0.003	350	101.9	913	0.023	400	300	101.9	913	0.029	400	400	-	0.17	0.91	BJ
224	Joh and Goto (2000)	PL-13	INT	0	26.4	366	50	0.004	250	26.4	363	0.010	350	200	26.4	402	0.022	300	300	-	0.09	0.96	BJ
225		PH-16	INT	0	23.6	366	40	0.005	250	23.6	344	0.012	350	200	23.6	402	0.027	300	300	-	0.13	0.93	BJ
226		PH-13	INT	0	26.3	366	40	0.005	250	26.3	363	0.014	350	200	26.3	402	0.027	300	300	-	0.13	0.91	BJ
227		PH-10	INT	0	25.6	366	40	0.005	250	25.6	372	0.012	350	200	25.6	402	0.027	300	300	-	0.11	0.90	BJ
228	Joh et al. (1988)	X0-1	INT	0	21.3	363	88	0.002	225	21.3	363	0.008	350	150	21.3	363	0.011	300	300	-	0.16	1.07	BJ
229	Joh et al. (1991a)	JXO-B1	INT	0	21.3	307	88	0.002	225	21.3	371	0.008	350	150	21.3	371	0.011	300	300	-	0.16	1.04	BJ
230		JXO-B5	INT	0	23.0	307	88	0.002	225	23.0	371	0.008	350	150	23.0	371	0.011	300	300	75	0.15	0.90	BJ
231		JXO-B6	INT	0	22.4	307	88	0.002	225	22.4	371	0.008	350	150	22.4	371	0.011	300	300	75	0.15	0.87	BJ
232	Joh et al. (1991b)	JX0-B8LH	INT	0	26.9	377	88	0.002	250	26.9	404	0.006	350	200	26.9	404	0.020	300	300	-	0.15	1.29	BJ
233		JX0-B8MH	INT	0	28.1	377	45	0.004	250	28.1	404	0.006	350	200	28.1	404	0.020	300	300	-	0.14	1.27	BJ
234	Kaku et al. (1993)	J11A	INT	0	57.6	893	86	0.005	280	57.6	371	0.022	350	260	57.6	371	0.033	400	300	-	0.24	1.19	BJ
235		J12A	INT	0	56.6	893	86	0.005	280	56.6	371	0.030	350	260	56.6	371	0.033	400	300	-	0.25	1.02	BJ
236		J31A	INT	0	55.2	893	85	0.005	280	55.2	363	0.025	350	260	55.2	371	0.033	400	300	-	0.25	1.02	BJ
237		J32A	INT	0	55.2	893	65	0.006	280	55.2	363	0.032	350	260	55.2	371	0.033	400	300	-	0.25	1.09	BJ
238	Kamimura et al.	NN.1	INT	0	36.2	344	50	0.004	265	36.2	345	0.018	250	180	36.2	380	0.018	250	350	-	0.03	1.17	BJ
239	(2004)	NN.2	INT	0	36.2	344	50	0.004	265	36.2	345	0.018	250	180	36.2	380	0.018	250	350	55	0.03	1.13	BJ
240	Kashiwazaki et al. (1992)	MKJ-1	INT	0	84.3	675	50	0.009	250	84.3	771	0.011	300	200	84.3	644	0.009	300	300	-	0.10	1.21	BJ

Table C.2 Experimental ductile beam-column joint database (continued)

No.	Reference	Specimen	Joint type	No. of TBs	Joint				Beam								Column									Failure mode[§]
					f_{cj} (MPa)	f_{yj} (MPa)	s_j (mm)	ρ_j	b_j (mm)	f_{cb} (MPa)	f_{yb} (MPa)	ρ_b	h_b (mm)	b_b (mm)	f_{cc} (MPa)	f_{yc} (MPa)	ρ_c	h_c (mm)	b_c (mm)	e (mm)	ALF	$\frac{v_{j,\max,pred}}{v_{j,\max,exp}}$	
241	Kashiwazaki et al.	MKJ-2	INT	0	84.3	675	50	0.009	250	84.3	771	0.017	300	200	84.3	718	0.027	300	300	-	0.07	1.20	BJ
242	(1992)	MKJ-3	INT	0	98.5	675	50	0.009	250	98.5	742	0.015	300	200	98.5	794	0.017	300	300	-	0.07	1.20	BJ
243		MKJ-4	INT	0	98.5	675	50	0.009	250	98.5	742	0.022	300	200	98.5	771	0.038	300	300	-	0.07	1.22	BJ
244	Kawai et al. (1997)	I8C	INT	0	85.5	928	65	0.003	400	85.5	522	0.027	450	325	85.5	522	0.027	475	475	-	0.20	1.22	BJ
245	Kitayama et al. (1991)	J1	INT	0	25.7	368	75	0.003	250	25.7	401	0.020	300	200	25.7	401	0.023	300	300	-	0.08	1.01	BJ
246		B1	INT	0	24.5	235	70	0.003	250	24.5	371	0.021	300	200	24.5	351	0.035	300	300	-	0.08	0.90	BJ
247		B2	INT	0	24.5	235	54	0.003	250	24.5	371	0.021	300	200	24.5	351	0.035	300	300	-	0.08	0.91	BJ
248		B3	INT	0	24.5	235	32	0.009	250	24.5	311	0.017	300	200	24.5	371	0.023	300	300	-	0.08	0.96	BJ
249		A1	INT	0	30.6	320	45	0.006	250	30.6	780	0.021	300	200	30.6	539	0.035	300	300	-	0.06	1.14	BJ
250		A4	INT	0	30.6	320	45	0.006	250	30.6	780	0.015	300	200	30.6	539	0.035	300	300	-	0.06	0.94	BJ
251	Kitayama et al. (1992)	I1	INT	0	98.8	360	75	0.004	250	98.8	799	0.033	300	200	98.8	747	0.051	300	300	-	0.04	0.76	BJ
252		I3	INT	0	41.4	360	75	0.004	250	41.4	799	0.024	300	200	41.4	361	0.035	300	300	-	0.03	1.02	BJ
253		I5	INT	0	85.4	250	75	0.004	250	85.4	769	0.015	300	200	85.4	534	0.035	300	300	-	0.02	1.21	BJ
254		I6	INT	0	85.4	250	75	0.004	250	85.4	772	0.017	300	200	85.4	534	0.035	300	300	-	0.02	1.01	BJ
255	Kitayama et al. (2000)	PB-1	INT	0	21.0	404	60	0.007	300	21.0	534	0.024	380	250	21.0	517	0.051	350	350	-	0.34	1.03	BJ
256		PNB-2	INT	0	21.0	404	60	0.007	300	21.0	534	0.024	380	250	21.0	517	0.051	350	350	-	0.34	1.06	BJ
257		PNB-3	INT	0	21.9	404	60	0.007	300	21.9	534	0.024	380	250	21.9	517	0.051	350	350	-	0.33	1.14	BJ
258	Kurose et al. (1991)	J1	INT	0	24.1	550	102	0.007	457	24.1	463	0.011	508	406	24.1	463	0.024	508	508	-	0.00	0.81	BJ
259	Kusuhara et al. (2004)	JE-0	INT	0	27.0	364	74	0.003	250	27.0	387	0.016	300	180	27.0	345	0.023	280	320	-	0.00	0.97	BJ
260	Kusuhara et al. (2004)	JE-55	INT	0	27.0	364	74	0.003	250	27.0	387	0.016	300	180	27.0	345	0.023	280	320	55	0.00	0.94	BJ
261		JE-55S	INT	0	27.0	364	37	0.009	250	27.0	387	0.016	300	180	27.0	345	0.023	280	320	55	0.00	1.03	BJ
262	Lee et al. (2009)	J1	INT	0	40.0	510	50	0.008	325	40.0	510	0.021	400	300	40.0	514	0.063	350	350	-	0.00	0.93	J
263		BJ1	INT	0	40.0	510	50	0.008	325	40.0	510	0.012	400	300	40.0	514	0.063	350	350	-	0.00	0.87	BJ
264	Leon (1990)	BCJ2	INT	0	27.6	414	51	0.005	229	27.6	414	0.009	305	203	27.6	414	0.028	254	254	-	0.00	1.04	BJ
265		BCJ3	INT	0	27.6	414	51	0.004	254	27.6	414	0.009	305	203	27.6	414	0.023	254	305	-	0.00	0.90	BJ
266	Matsumoto et al.	B-0	INT	0	54.6	1276	50	0.005	350	54.6	522	0.020	400	250	54.6	746	0.022	400	450	-	0.20	1.01	BJ
267	(2010)	B-5	INT	0	55.4	1276	50	0.005	350	55.4	522	0.020	400	250	55.4	746	0.022	400	450	50	0.20	0.98	BJ
268		B-10	INT	0	57.0	1276	50	0.005	350	57.0	522	0.020	400	250	57.0	746	0.022	400	450	100	0.20	1.00	BJ
269		B-10S	INT	0	58.4	1276	50	0.005	350	58.4	522	0.020	400	250	58.4	746	0.022	400	450	100	0.20	0.95	BJ
270		J-0	INT	0	54.6	1276	50	0.005	350	54.6	710	0.020	400	250	54.6	746	0.022	400	450	-	0.20	0.98	J

Table C.2 Experimental ductile beam-column joint database (continued)

No.	Reference	Specimen	Joint type	No. of TBs	Joint				Beam								Column							ALF	$\frac{v_{j,\max,pred}}{v_{j,\max,exp}}$	Failure mode[§]
					f_{cj} (MPa)	f_{yj} (MPa)	s_j (mm)	ρ_j	b_j (mm)	f_{cb} (MPa)	f_{yb} (MPa)	ρ_b	h_b (mm)	b_b (mm)	f_{cc} (MPa)	f_{yc} (MPa)	ρ_c	h_c (mm)	b_c (mm)	e (mm)			
271	Matsumoto et al.	J-5	INT	0	55.4	1276	50	0.005	350	55.4	710	0.020	400	250	55.4	746	0.022	400	450	50	0.20	0.96	J
272	(2010)	J-10	INT	0	57.0	1276	50	0.005	350	57.0	710	0.020	400	250	57.0	746	0.022	400	450	100	0.20	0.99	J
273		J-10S	INT	0	58.4	1276	50	0.005	350	58.4	710	0.020	400	250	58.4	746	0.022	400	450	100	0.20	0.94	J
274	Meinheit and Jirsa	1	INT	0	26.2	409	152	0.005	305	26.2	449	0.022	457	279	26.2	457	0.021	457	330	-	0.40	1.11	J
275	(1981)	2	INT	0	41.8	409	152	0.005	305	41.8	449	0.022	457	279	41.8	449	0.043	457	330	-	0.25	0.90	J
276		3	INT	0	26.6	409	152	0.005	305	26.6	449	0.022	457	279	26.6	402	0.067	457	330	-	0.39	0.99	J
277		4	INT	0	36.1	409	152	0.004	432	36.1	449	0.015	457	406	36.1	438	0.043	330	457	-	0.30	0.83	J
278		5	INT	0	35.9	409	152	0.005	305	35.9	449	0.022	457	279	35.9	449	0.043	457	330	-	0.04	0.89	J
279		6	INT	0	36.7	409	152	0.005	305	36.7	449	0.022	457	279	36.7	449	0.043	457	330	-	0.48	0.83	BJ
280		7	INT	0	37.2	409	152	0.004	432	37.2	449	0.015	457	406	37.2	438	0.043	330	457	-	0.47	0.83	J
281		12	INT	0	35.2	423	51	0.024	305	35.2	449	0.022	457	279	35.2	449	0.043	457	330	-	0.30	0.78	BJ
282		13	INT	0	41.3	409	51	0.015	305	41.3	449	0.022	457	279	41.3	449	0.043	457	330	-	0.25	1.00	J
283		14	INT	0	33.2	409	51	0.011	432	33.2	449	0.015	457	406	33.2	438	0.043	330	457	-	0.32	0.83	J
284	Morita et al. (2004)	M1	INT	0	17.1	344	80	0.003	300	17.1	520	0.019	400	300	17.1	520	0.059	350	300	-	0.00	1.13	J
285		M2	INT	0	18.2	344	80	0.003	300	18.2	520	0.019	400	300	18.2	520	0.059	350	300	-	0.00	1.06	J
286		M3	INT	0	18.8	344	80	0.003	300	18.8	520	0.019	400	300	18.8	520	0.059	350	300	-	0.00	1.16	J
287		M4	INT	0	20.6	429	40	0.021	300	20.6	520	0.019	400	300	20.6	520	0.059	350	300	-	0.00	1.18	J
288		M6	INT	0	19.4	344	80	0.003	300	19.4	520	0.013	400	300	19.4	520	0.059	350	300	-	0.00	0.99	J
289	Nakamura et al. (1991)	No. 1	INT	0	65.3	880	60	0.004	350	65.3	582	0.017	400	300	65.3	785	0.022	400	400	-	0.09	0.99	BJ
290		No. 2	INT	0	68.4	880	60	0.004	350	68.4	785	0.017	400	300	68.4	785	0.022	400	400	-	0.09	0.92	J
291		No. 4	INT	0	91.9	880	60	0.004	350	91.9	785	0.017	400	300	91.9	785	0.022	400	400	-	0.07	0.92	BJ
292		No. 5	INT	0	64.1	873	60	0.012	350	64.1	785	0.017	400	300	64.1	785	0.022	400	400	-	0.10	0.92	BJ
293		No. 6	INT	0	63.1	873	60	0.012	350	63.1	785	0.017	400	300	63.1	785	0.022	400	400	-	0.10	0.86	BJ
294		No. 7	INT	0	76.0	873	60	0.012	350	76.0	785	0.017	400	300	76.0	785	0.022	400	400	-	0.08	0.95	BJ
295	Nishi et al. (1992)	JO-2	INT	0	24.9	448	40	0.004	135	24.9	366	0.016	150	120	24.9	366	0.023	150	150	-	0.70	1.10	BJ
296	Noguchi and	OKJ-1	INT	0	70.0	955	50	0.009	250	70.0	718	0.023	300	200	70.0	718	0.028	300	300	-	0.12	1.12	BJ
297	Kashiwazaki (1992)	OKJ-4	INT	0	70.0	955	50	0.009	250	70.0	718	0.018	300	200	70.0	718	0.028	300	300	-	0.12	0.98	BJ
298		OKJ-5	INT	0	70.0	955	50	0.009	250	70.0	718	0.025	300	200	70.0	718	0.034	300	300	-	0.12	1.12	J
299		OKJ-6	INT	0	53.5	955	50	0.009	250	53.5	718	0.020	300	200	53.5	718	0.028	300	300	-	0.12	1.05	J
300	Ohwada (1970)	No. 2	INT	0	21.5	245	40	0.003	175	21.5	392	0.013	300	150	21.5	392	0.032	200	200	-	0.18	0.76	J

Table C.2 Experimental ductile beam-column joint database (continued)

No.	Reference	Specimen	Joint type	No. of TBs	Joint				Beam							Column								$\frac{v_{j,\max,pred}}{v_{j,\max,exp}}$	Failure mode[§]
					f_{cj} (MPa)	f_{yj} (MPa)	s_j (mm)	ρ_j	b_j (mm)	f_{cb} (MPa)	f_{yb} (MPa)	ρ_b	h_b (mm)	b_b (mm)	f_{cc} (MPa)	f_{yc} (MPa)	ρ_c	h_c (mm)	b_c (mm)	e (mm)	ALF		
301	Ohwada (1970)	No. 3	INT	0	21.5	245	20	0.007	175	21.5	392	0.013	300	150	21.5	392	0.032	200	200	-	0.18	0.90	J
302	Ohwada (1973)	P-4	INT	0	13.4	245	20	0.007	175	13.4	385	0.013	300	150	13.4	385	0.032	200	200	-	0.29	1.19	BJ
303	Ohwada (1977)	JO-2	INT	0	20.0	450	40	0.004	150	20.0	432	0.020	150	150	20.0	432	0.034	150	150	-	0.00	1.03	J
304	Ohwada (1980)	LJO-2	INT	0	20.0	407	50	0.003	150	20.0	372	0.020	150	150	20.0	372	0.068	150	150	-	0.00	1.06	J
305	Oka and Shiohara	J-1	INT	0	81.2	1374	50	0.004	270	81.2	627	0.019	300	240	81.2	627	0.034	300	300	-	0.11	1.07	BJ
306	(1992)	J-2	INT	0	81.2	1374	50	0.004	270	81.2	1429	0.017	300	240	81.2	627	0.034	300	300	-	0.11	1.26	J
307		J-4	INT	0	72.8	1374	50	0.004	270	72.8	506	0.022	300	240	72.8	492	0.053	300	300	-	0.13	0.97	BJ
308		J-5	INT	0	72.8	1374	50	0.004	270	72.8	824	0.019	300	240	72.8	824	0.034	300	300	-	0.13	0.98	J
309		J-6	INT	0	79.2	775	100	0.002	270	79.2	663	0.019	300	240	79.2	663	0.034	300	300	-	0.12	0.92	BJ
310		J-8	INT	0	79.2	775	50	0.004	270	79.2	364	0.043	300	240	79.2	364	0.077	300	300	-	0.12	0.92	J
311		J-10	INT	0	39.2	598	50	0.004	270	39.2	687	0.019	300	240	39.2	687	0.034	300	300	-	0.12	1.03	J
312		J-11	INT	0	39.2	401	50	0.004	270	39.2	365	0.042	300	240	39.2	365	0.077	300	300	-	0.12	0.90	J
313	Otani et al. (1984)	J1	INT	0	25.7	368	75	0.003	250	25.7	401	0.020	300	200	25.7	401	0.023	300	300	-	0.08	1.01	BJ
314		J2	INT	0	24.0	368	75	0.006	250	24.0	401	0.020	300	200	24.0	401	0.023	300	300	-	0.08	1.01	BJ
315		J3	INT	0	24.0	368	25	0.017	250	24.0	401	0.020	300	200	24.0	401	0.023	300	300	-	0.08	1.03	BJ
316		J4	INT	0	25.7	368	75	0.003	250	25.7	401	0.020	300	200	25.7	401	0.023	300	300	-	0.30	1.04	BJ
317		J5	INT	0	28.7	368	75	0.003	250	28.7	401	0.020	300	200	28.7	401	0.023	300	300	-	0.07	1.07	BJ
318	Owada (1992)	J0C-1	INT	0	31.2	447	40	0.004	135	31.2	340	0.014	150	120	31.2	343	0.023	150	150	-	0.13	1.32	BJ
319		J0T-1	INT	0	31.2	447	40	0.004	135	31.2	340	0.014	150	120	31.2	343	0.023	150	150	-	-0.07	0.90	CJ
320		J0R-1	INT	0	31.2	447	40	0.004	135	31.2	340	0.014	150	120	31.2	343	0.023	150	150	-	0.13	0.85	BJ
321	Ozaki et al. (2010)	1	INT	0	32.8	338	50	0.004	240	32.8	410	0.022	300	180	32.8	410	0.018	300	300	-	0.09	0.98	BJ
322		2	INT	0	32.8	338	50	0.004	249	32.8	410	0.020	300	198	32.8	410	0.018	300	300	42	0.09	0.99	BJ
323	Raffaelle and Wight	SP1	INT	0	28.6	476	89	0.008	305	28.6	441	0.010	381	254	28.6	441	0.018	356	356	51	0.02	1.10	BJ
324	(1995)	SP2	INT	0	26.8	476	89	0.008	267	26.8	441	0.009	381	178	26.8	441	0.018	356	356	89	0.03	1.11	BJ
325		SP3	INT	0	37.7	476	89	0.008	273	37.7	441	0.009	381	191	37.7	441	0.018	356	356	83	0.02	1.14	BJ
326		SP4	INT	0	19.3	476	89	0.008	273	19.3	441	0.006	559	191	19.3	441	0.018	356	356	83	0.04	1.08	BJ
327	Shinjo et al. (2009)	B-1	INT	0	111.0	1452	48	0.004	350	70.0	549	0.028	400	300	111.0	528	0.022	400	400	-	0.10	1.07	BJ
328		J-1	INT	0	110.0	1452	48	0.004	350	71.0	716	0.032	400	300	110.0	528	0.022	400	400	-	0.10	0.99	J
329		BJ-1	INT	0	110.0	1452	48	0.004	350	70.0	549	0.032	400	300	110.0	528	0.022	400	400	-	0.10	1.00	J
330	Suzuki et al. (2002)	E00	INT	0	24.0	358	100	0.004	315	24.0	384	0.018	500	230	24.0	384	0.014	500	400	-	0.25	1.04	J

Table C.2 Experimental ductile beam-column joint database (continued)

No.	Reference	Specimen	Joint type	No. of TBs	Joint				Beam								Column							ALF	$\frac{v_{j,\max,pred}}{v_{j,\max,exp}}$	Failure mode[§]
					f_{cj} (MPa)	f_{yj} (MPa)	s_j (mm)	ρ_j	b_j (mm)	f_{cb} (MPa)	f_{yb} (MPa)	ρ_b	h_b (mm)	b_b (mm)	f_{cc} (MPa)	f_{yc} (MPa)	ρ_c	h_c (mm)	b_c (mm)	e (mm)			
331	Suzuki et al. (2002)	E085	INT	0	23.0	358	100	0.004	315	23.0	384	0.018	500	230	23.0	384	0.014	500	400	85	0.25	1.02	J
332		E135	INT	0	22.7	358	100	0.003	365	22.7	384	0.013	450	230	22.7	384	0.019	300	500	135	0.25	0.96	J
333	Takamori et al. (2006)	NO1	INT	0	48.0	334	60	0.006	575	49.6	435	0.013	900	450	48.0	430	0.024	700	700	85	0.21	1.00	BJ
334		NO2	INT	0	48.0	334	60	0.006	540	43.4	435	0.017	900	380	48.0	430	0.024	700	700	125	0.21	0.99	BJ
335		NO3	INT	0	48.0	334	60	0.006	575	43.4	435	0.013	900	450	48.0	430	0.024	700	700	-	0.21	1.03	BJ
336		NO4	INT	0	48.0	334	60	0.006	575	50.0	436	0.021	900	450	48.0	430	0.024	700	700	-	0.21	0.92	BJ
337	Takatani and Maruta (2003)	N	INT	0	36.3	849	90	0.003	435	36.3	517	0.019	500	370	36.3	534	0.022	500	500	-	0.15	1.04	BJ
338	Teng and Zhou (2003)	S1	INT	0	33.0	440	75	0.008	300	33.0	510	0.014	400	200	33.0	530	0.031	300	400	-	0.11	0.95	BJ
339		S2	INT	0	34.0	440	75	0.008	300	34.0	510	0.014	400	200	34.0	530	0.031	300	400	50	0.11	0.93	BJ
340		S3	INT	0	35.0	440	75	0.008	300	35.0	510	0.014	400	200	35.0	530	0.031	300	400	100	0.11	0.94	BJ
341		S5	INT	0	39.0	440	50	0.012	300	39.0	425	0.009	400	200	39.0	530	0.047	200	400	50	0.11	0.94	BJ
342		S6	INT	0	38.0	440	50	0.012	300	38.0	425	0.009	400	200	38.0	530	0.047	200	400	100	0.11	0.92	BJ
343	Teraoka et al. (1997)	HJ4	INT	0	54.2	338	50	0.007	350	54.2	382	0.017	400	300	54.3	645	0.022	400	400	-	0.18	0.90	BJ
344		HJ5	INT	0	54.2	338	50	0.007	350	54.2	645	0.011	400	300	54.3	645	0.022	400	400	-	0.18	0.85	BJ
345		HJ6	INT	0	54.2	338	50	0.007	350	54.2	858	0.008	400	300	54.3	645	0.022	400	400	-	0.18	0.88	BJ
346		HJ7	INT	0	92.6	681	50	0.009	350	92.6	422	0.023	400	300	83.4	645	0.022	400	400	-	0.21	0.91	BJ
347		HJ8	INT	0	92.6	681	50	0.009	350	92.6	599	0.015	400	300	83.4	645	0.022	400	400	-	0.21	0.90	BJ
348		HJ9	INT	0	92.6	681	50	0.009	350	92.6	858	0.011	400	300	83.4	645	0.022	400	400	-	0.21	0.95	BJ
349	Teroaka (1997)	HNO1	INT	0	88.7	681	50	0.009	350	88.7	611	0.015	400	300	93.9	604	0.027	400	400	-	0.16	0.96	BJ
350		HNO3	INT	0	88.7	681	50	0.009	350	88.7	441	0.029	400	300	93.9	442	0.027	400	400	-	0.16	0.81	BJ
351		HNO4	INT	0	88.7	681	50	0.009	350	88.7	604	0.029	400	300	93.9	442	0.027	400	400	-	0.16	0.77	BJ
352		HNO5	INT	0	116.9	681	50	0.009	350	116.9	634	0.018	400	300	107.6	604	0.027	400	400	-	0.14	0.94	BJ
353		HNO6	INT	0	116.9	681	50	0.009	350	116.9	604	0.029	400	300	107.6	604	0.027	400	400	-	0.14	0.82	BJ
354		NO1	INT	0	33.6	390	57	0.011	270	33.6	406	0.022	300	240	32.2	431	0.027	300	300	-	0.25	0.87	J
355		NO2	INT	0	33.6	390	53	0.015	270	33.6	406	0.022	300	240	32.2	431	0.027	300	300	-	0.25	0.87	J
356		NO19	INT	0	30.8	375	35	0.008	320	36.2	417	0.018	320	260	36.2	436	0.011	380	380	-	0.15	1.09	BJ
357		NO20	INT	0	30.8	375	35	0.008	320	36.2	417	0.021	320	260	36.2	436	0.011	380	380	-	0.15	1.02	BJ
358		NO21	INT	0	25.2	300	35	0.006	300	25.2	426	0.011	300	260	28.4	399	0.021	340	340	-	0.09	1.16	BJ
359		NO22	INT	0	26.7	300	35	0.006	300	26.7	426	0.015	300	260	28.4	399	0.021	340	340	-	0.09	1.00	BJ
360		NO23	INT	0	34.0	300	35	0.006	300	34.0	426	0.015	300	260	30.9	399	0.021	340	340	-	0.19	1.02	BJ

Table C.2 Experimental ductile beam-column joint database (continued)

No.	Reference	Specimen	Joint type	No. of TBs	Joint f_{cj} (MPa)	Joint f_{yj} (MPa)	Joint s_j (mm)	Joint ρ_j	Beam b_j (mm)	Beam f_{cb} (MPa)	Beam f_{yb} (MPa)	Beam ρ_b	Beam h_b (mm)	Beam b_b (mm)	Column f_{cc} (MPa)	Column f_{yc} (MPa)	Column ρ_c	Column h_c (mm)	Column b_c (mm)	e (mm)	ALF	$\frac{v_{j,\max,pred}}{v_{j,\max,exp}}$	Failure mode[§]
361	Teroaka (1997)	NO26	INT	0	35.6	300	35	0.006	300	35.6	399	0.019	300	260	34.3	399	0.021	340	340	-	0.17	0.92	BJ
362		NO28	INT	0	36.2	300	35	0.006	300	36.2	399	0.026	300	260	36.2	399	0.021	340	340	-	0.16	0.84	J
363		NO29	INT	0	44.0	300	35	0.006	300	44.0	399	0.019	300	260	42.7	399	0.021	340	340	-	0.23	0.98	BJ
364		NO30	INT	0	44.0	300	35	0.006	300	44.0	428	0.034	300	260	42.7	399	0.021	340	340	-	0.23	0.86	J
365	Watanabe et al. (1998)	WJ-1	INT	0	29.0	364	36	0.013	250	29.0	326	0.008	300	200	29.0	358	0.026	300	300	-	0.07	0.85	BJ
366		WJ-3	INT	0	29.0	364	36	0.013	250	29.0	364	0.008	300	200	29.0	373	0.026	300	300	-	0.07	0.76	BJ
367		WJ-6	INT	0	29.0	364	36	0.013	250	29.0	358	0.012	300	200	29.0	373	0.040	300	300	-	0.07	0.71	BJ
368	Yashita et al. (1996)	No. 1	INT	0	43.1	823	44	0.004	358	43.1	409	0.023	395	300	43.1	409	0.020	415	415	-	0.10	1.28	BJ
369		No. 3	INT	0	54.3	823	44	0.004	358	54.3	405	0.017	395	300	54.3	405	0.020	415	415	-	0.10	1.08	BJ
370		No. 4	INT	0	53.8	823	44	0.004	358	53.8	702	0.017	395	300	53.8	702	0.020	415	415	-	0.10	1.06	J
371	Yoshino et al. (1997)	No. 1	INT	0	28.6	420	50	0.005	215	28.6	382	0.013	250	180	28.6	379	0.025	250	250	-	0.16	0.96	BJ
372		No. 3	INT	0	28.6	420	50	0.005	215	28.6	379	0.016	250	180	28.6	379	0.025	250	250	-	0.16	0.96	BJ
373		No. 4	INT	0	28.6	420	50	0.005	215	28.6	379	0.011	250	180	28.6	379	0.025	250	250	-	0.16	1.04	BJ
374	Yoshiya et al. (1991)	No. 2	INT	0	39.2	364	32	0.004	338	39.2	388	0.025	450	300	39.2	365	0.021	500	375	-	0.24	0.89	BJ
375		No. 3	INT	0	39.2	810	32	0.007	338	39.2	388	0.025	450	300	39.2	365	0.021	500	375	-	0.24	0.95	BJ
376	Zaid et al. (1999)	S3	INT	0	28.0	390	40	0.005	250	28.0	470	0.019	300	200	28.0	450	0.038	300	300	-	0.04	0.94	BJ
377	Asou (1993)	No.1	INT	1	65.8	931	100	0.006	370	52.6	510	0.018	400	300	65.8	510	0.024	440	440	-	0.18	1.18	BJ
378	Canbolat and Wight (2008)	3-S	INT	1	29.0	441	95	0.010	394	29.0	450	0.011	457	254	32.0	450	0.012	356	533	140	0.04	1.07	BJ
379	Fujii and Morita	GBO,EW	INT	1	37.0	367	70	0.004	190	37.0	369	0.011	250	160	37.0	369	0.031	220	220	-	0.05	0.99	BJ
380	(1987)	GBS1,EW	INT	1	37.0	367	70	0.004	190	37.0	369	0.011	250	160	37.0	369	0.031	220	220	-	0.05	0.90	BJ
381		GBS2,EW	INT	1	37.0	367	70	0.004	190	37.0	369	0.011	250	160	37.0	369	0.031	220	220	-	0.05	0.91	BJ
382		GBS3,EW	INT	1	37.0	367	70	0.004	190	37.0	369	0.011	250	160	37.0	369	0.031	220	220	-	0.05	0.99	BJ
383		GBS4,EW	INT	1	37.0	367	70	0.004	190	37.0	369	0.011	250	160	37.0	369	0.031	220	220	-	0.05	0.97	BJ
384		GBSU,EW	INT	1	34.7	367	35	0.008	190	34.7	369	0.011	250	160	34.7	369	0.031	220	220	-	0.06	1.00	BJ
385	Hanson and Connor (1972)	10	INT	1	39.3	310	104	0.013	343	39.3	303	0.019	508	305	37.7	447	0.055	381	381	-	0.52	0.93	BJ
386	Ishida et al. (2001)	CS	INT	1	33.4	365	130	0.002	625	33.4	462	0.014	750	450	33.4	464	0.016	700	800	-	0.09	0.99	BJ
387		ES	INT	1	33.4	365	130	0.002	625	33.4	462	0.014	750	450	33.4	464	0.016	700	800	135	0.09	0.98	BJ
388		ES-J	INT	1	33.4	365	130	0.002	625	33.4	371	0.013	750	450	33.4	464	0.016	700	800	135	0.09	1.10	BJ
389	Kurose et al. (1991)	J3N	INT	1	27.6	409	152	0.008	305	27.6	463	0.020	457	279	27.6	459	0.051	457	330	-	0.00	1.10	BJ
390	Nishi and Ohwada (1993)	JXY-3X	INT	1	21.5	448	40	0.004	135	21.5	382	0.016	150	120	21.5	382	0.023	150	150	-	0.81	1.05	J

Table C.2 Experimental ductile beam-column joint database (continued)

No.	Reference	Specimen	Joint type	No. of TBs	Joint				Beam								Column									Failure mode[§]
					f_{cj} (MPa)	f_{yj} (MPa)	s_j (mm)	ρ_j	b_j (mm)	f_{cb} (MPa)	f_{yb} (MPa)	ρ_b	h_b (mm)	b_b (mm)	f_{cc} (MPa)	f_{yc} (MPa)	ρ_c	h_c (mm)	b_c (mm)	e (mm)	ALF	$\frac{v_{j,\max,pred}}{v_{j,\max,exp}}$	
391	Nishi et al. (1992)	JX-2	INT	1	24.9	448	40	0.004	135	24.9	366	0.016	150	120	24.9	366	0.023	150	150	-	0.70	1.24	BJ
392		JXY-2X	INT	1	24.9	448	40	0.004	135	24.9	366	0.016	150	120	24.9	366	0.023	150	150	-	0.70	1.07	BJ
393	Ohwada (1977)	JE-2	INT	1	20.0	450	40	0.004	150	20.0	432	0.020	150	150	20.0	432	0.034	150	150	-	0.00	0.99	BJ
394	Owada (1992)	J1T-1	INT	1	31.2	447	40	0.004	135	31.2	340	0.014	150	120	31.2	343	0.023	150	150	-	-0.07	0.86	J
395		J1R-1	INT	1	31.2	447	40	0.004	135	31.2	340	0.014	150	120	31.2	343	0.023	150	150	-	0.13	0.86	BJ
396	Shin and LaFave	SL1	INT	1	29.9	448	79	0.006	368	29.9	503	0.008	406	279	35.8	538	0.015	330	457	89	0.00	1.15	BJ
397	(2004)	SL2	INT	1	36.2	448	79	0.006	318	36.2	503	0.012	406	178	40.7	538	0.015	330	457	140	0.00	1.12	BJ
398		SL4	INT	1	31.2	448	64	0.012	279	31.2	510	0.008	406	279	31.5	503	0.026	368	279	-	0.00	0.97	BJ
399	Sugano et al. (1991)	J4-0	INT	1	30.4	922	50	0.012	370	30.4	385	0.031	400	300	30.4	400	0.024	440	440	-	0.33	0.95	J
400		J6-0	INT	1	60.5	922	50	0.012	370	60.5	385	0.031	400	300	60.5	400	0.024	440	440	-	0.17	1.04	BJ
401		J8-0	INT	1	77.6	922	50	0.012	370	77.6	385	0.031	400	300	77.6	400	0.024	440	440	-	0.13	1.17	BJ
402		J8H-0	INT	1	80.1	922	50	0.012	370	80.1	568	0.031	400	300	80.1	568	0.024	440	440	-	0.13	1.03	BJ
403	Tsubosaki et al. (1993)	J13NS	INT	1	60.3	800	50	0.004	270	60.3	711	0.014	320	240	60.3	973	0.044	300	300	-	0.29	0.75	BJ
404	Goto et al. (1999)	B17-13X	INT	2	22.8	291	50	0.008	250	22.8	389	0.017	350	200	22.8	387	0.035	300	300	-	0.15	1.01	BJ
405		B17-13Y	INT	2	22.8	291	50	0.008	250	22.8	389	0.017	350	200	22.8	387	0.035	300	300	-	0.15	1.00	BJ
406		B17-13LX	INT	2	19.7	291	50	0.008	250	19.7	389	0.017	350	200	19.7	387	0.035	300	300	-	0.17	0.91	BJ
407		B17-13LY	INT	2	19.7	291	50	0.008	250	19.7	389	0.017	350	200	19.7	387	0.035	300	300	-	0.17	1.07	BJ
408		B17-19X	INT	2	20.3	291	50	0.008	250	20.3	384	0.014	350	200	20.3	387	0.035	300	300	-	0.16	0.97	BJ
409		B17-19Y	INT	2	20.3	291	50	0.008	250	20.3	384	0.014	350	200	20.3	387	0.035	300	300	-	0.16	1.03	BJ
410	Gumaraes et al. (1992)	J2	INT	2	27.6	550	102	0.008	457	27.6	463	0.015	508	406	26.1	459	0.040	508	508	-	0.00	0.86	BJ
411		J4	INT	2	31.6	550	102	0.008	457	31.6	463	0.010	508	406	29.1	523	0.040	508	508	-	0.00	0.84	BJ
412		J5	INT	2	77.9	550	102	0.008	457	77.9	561	0.023	508	406	95.1	543	0.063	508	508	-	0.00	1.05	BJ
413		J6	INT	2	92.1	570	64	0.016	457	92.1	523	0.019	508	406	70.3	561	0.063	508	508	-	0.00	0.87	BJ
414	Hiramatsu et al. (1995)	S2	INT	2	52.2	876	40	0.003	255	52.2	836	0.015	300	210	52.2	836	0.023	300	300	-	0.20	1.01	BJ
415	Hosono et al. (2001)	TD-1	INT	2	23.0	404	90	0.005	300	23.0	538	0.026	380	250	23.0	517	0.051	350	350	-	0.31	1.05	BJ
416	Inoue et al. (1990)	SP1	INT	2	43.3	1253	52	0.003	371	43.3	473	0.018	417	301	43.3	473	0.018	440	440	-	0.28	1.12	BJ
417	Joh and Goto (2000)	TH-13	INT	2	22.8	373	25	0.008	250	22.8	334	0.017	350	200	22.8	387	0.035	300	300	-	0.17	0.96	BJ
418		TH-13A	INT	2	19.7	373	25	0.008	250	19.7	334	0.017	350	200	19.7	387	0.035	300	300	-	0.19	0.88	BJ
419		TH-19	INT	2	20.0	373	25	0.008	250	20.0	384	0.014	350	200	20.0	387	0.035	300	300	-	0.18	0.89	BJ
420		TL-13	INT	2	23.2	373	50	0.004	250	23.2	334	0.010	350	200	23.2	387	0.027	300	300	-	0.10	0.94	BJ

Table C.2 Experimental ductile beam-column joint database (continued)

No.	Reference	Specimen	Joint type	No. of TBs	Joint				Beam								Column									Failure mode[§]
					f_{cj} (MPa)	f_{yj} (MPa)	s_j (mm)	ρ_j	b_j (mm)	f_{cb} (MPa)	f_{yb} (MPa)	ρ_b	h_b (mm)	b_b (mm)	f_{cc} (MPa)	f_{yc} (MPa)	ρ_c	h_c (mm)	b_c (mm)	e (mm)	ALF	$\frac{v_{j,\max,pred}}{v_{j,\max,exp}}$	
421	Joh et al. (1988)	X2-1	INT	2	22.5	363	88	0.002	225	22.5	363	0.008	350	150	22.5	363	0.023	300	300	-	0.15	1.07	BJ
422		X2-2	INT	2	22.3	363	88	0.002	225	22.3	363	0.008	350	150	22.3	363	0.023	300	300	-	0.15	0.88	BJ
423		X2-3	INT	2	20.6	1334	30	0.006	225	20.6	363	0.008	350	150	20.6	363	0.023	300	300	-	0.17	0.97	BJ
424		X2-4	INT	2	23.3	363	88	0.002	225	23.3	363	0.005	600	150	23.3	363	0.023	300	300	-	0.15	1.15	BJ
425	Kurose et al. (1991)	J2E	INT	2	27.6	409	152	0.008	305	27.6	463	0.028	457	279	27.6	459	0.068	457	330	-	0.00	1.08	BJ
426		J2N	INT	2	27.6	409	152	0.008	305	27.6	463	0.030	457	279	27.6	459	0.068	457	330	-	0.00	1.10	BJ
427	Meinheit and Jirsa	8	INT	2	33.1	409	152	0.005	305	33.1	449	0.022	457	279	33.1	449	0.043	457	330	-	0.32	0.95	BJ
428	(1981)	9	INT	2	31.0	409	152	0.005	305	31.0	449	0.022	457	279	31.0	449	0.043	457	330	-	0.35	0.99	J
429		10	INT	2	29.6	409	152	0.005	305	29.6	449	0.022	457	279	29.6	449	0.043	457	330	-	0.36	1.05	J
430		11	INT	2	25.6	409	152	0.004	432	25.6	449	0.015	457	406	25.6	438	0.043	330	457	-	0.42	1.01	J
431	Nakamura et al. (1991)	No. 3	INT	2	65.5	880	60	0.004	350	65.5	785	0.017	400	300	65.5	785	0.022	400	400	-	0.09	1.00	BJ
432	Ohwada (1977)	JI-2	INT	2	20.0	450	40	0.004	150	20.0	432	0.020	150	150	20.0	432	0.034	150	150	-	0.00	1.01	BJ
433	Teroaka (1997)	NO3	INT	2	30.4	390	57	0.011	270	30.9	406	0.022	300	240	32.2	431	0.027	300	300	-	0.24	0.97	J
434		NO4	INT	2	36.6	390	57	0.011	270	39.6	411	0.025	300	240	39.6	431	0.027	300	300	-	0.32	0.99	J
435		NO5	INT	2	36.6	390	53	0.015	270	39.6	411	0.025	300	240	39.6	431	0.027	300	300	-	0.32	1.01	J
436		NO6	INT	2	39.6	390	57	0.011	270	39.6	411	0.025	300	240	39.6	431	0.027	300	300	-	0.30	0.98	BJ
437		NO7	INT	2	46.7	390	57	0.011	270	41.5	411	0.025	300	240	41.5	431	0.027	300	300	-	0.25	1.02	BJ
438		NO8	INT	2	46.7	390	53	0.015	270	41.5	411	0.025	300	240	41.5	431	0.027	300	300	-	0.25	1.04	BJ
439		NO9	INT	2	30.5	390	71	0.003	270	28.9	406	0.022	300	240	28.9	431	0.027	300	300	-	0.25	1.05	J
440		NO10	INT	2	30.5	390	57	0.011	270	28.9	406	0.022	300	240	28.9	431	0.027	300	300	-	0.25	1.17	J
441		NO11	INT	2	32.2	390	71	0.003	270	26.0	396	0.025	300	240	26.0	431	0.027	300	300	-	0.33	1.02	J
442		NO12	INT	2	32.2	390	57	0.011	270	26.0	396	0.025	300	240	26.0	431	0.027	300	300	-	0.33	1.08	J
443		NO24	INT	2	39.4	300	35	0.006	300	33.0	601	0.010	300	260	32.1	399	0.021	340	340	-	0.15	1.21	BJ
444		NO27	INT	2	32.2	300	35	0.006	300	33.6	399	0.019	300	260	37.0	399	0.021	340	340	-	0.18	1.10	BJ
445		NO31	INT	2	31.9	328	45	0.006	453	32.6	421	0.016	560	365	33.4	421	0.025	540	540	-	0.11	1.12	BJ
446		NO32	INT	2	33.7	312	40	0.005	453	32.6	421	0.016	560	365	33.4	421	0.025	540	540	-	0.10	1.14	BJ
447		NO33	INT	2	34.7	314	45	0.010	453	32.6	421	0.016	560	365	33.4	421	0.025	540	540	-	0.10	1.18	BJ
448		NO34	INT	2	39.4	390	40	0.007	400	35.5	429	0.015	500	300	33.0	427	0.017	500	500	-	0.20	1.19	BJ
449		NO35	INT	2	39.4	390	40	0.007	400	35.5	429	0.015	500	300	33.0	427	0.017	500	500	75	0.20	1.12	BJ
450		NO36	INT	2	39.4	390	40	0.007	400	35.5	429	0.018	500	300	33.0	427	0.017	500	500	-	0.20	1.24	BJ

Table C.2 Experimental ductile beam-column joint database (continued)

No.	Reference	Specimen	Joint type	No. of TBs	Joint f_{cj} (MPa)	Joint f_{yj} (MPa)	Joint s_j (mm)	Joint ρ_j	Beam b_j (mm)	Beam f_{cb} (MPa)	Beam f_{yb} (MPa)	Beam ρ_b	Beam h_b (mm)	Beam b_b (mm)	Column f_{cc} (MPa)	Column f_{yc} (MPa)	Column ρ_c	Column h_c (mm)	Column b_c (mm)	e (mm)	ALF	$\frac{v_{j,\max,pred}}{v_{j,\max,exp}}$	Failure mode§
451	Teroaka (1997)	NO37	INT	2	39.4	390	40	0.007	400	35.5	429	0.015	500	300	33.0	427	0.017	500	500	-	0.20	1.19	BJ
452		NO38	INT	2	39.4	390	40	0.007	400	35.5	429	0.015	500	300	33.0	427	0.017	500	500	75	0.20	1.12	BJ
453	Tsubosaki et al. (1993)	J12EW	INT	2	60.3	800	50	0.004	270	60.3	711	0.021	320	240	60.3	973	0.044	300	300	-	0.29	0.79	BJ
454		J12NS	INT	2	60.3	800	50	0.004	270	60.3	711	0.020	320	240	60.3	973	0.044	300	300	-	0.29	0.75	BJ
	Mean																					***1.01***	
	Minimum																					***0.71***	
	Maximum																					***1.36***	
	COV																					***0.12***	

§ J, BJ, CJ, and A refer to joint shear failure without member yielding, joint shear failure after beam yielding, and joint shear failure after column yielding, bond failure associated with short embedment length, respectively.

Note that subscripts *j*, *b*, and *c* indicate joint, beam, and column, respectively.

APPEDIX D

AFTERSHOCK FRAGILITY CURVES

Using the framework for the development of aftershock fragility curves proposed in Chapter 5, Chapter 6 present the applicability of the framework to analytical frame models with different modeling characteristics. The aftershock fragility curves are developed in terms of the four limit states and initial damage states associated with mainshock-damaged conditions to evaluate the increased vulnerability and damage accumulation due to mainshock-aftershock sequences. This appendix not only contains the aftershock fragility curves with different initial damage states for the analytical models, but also presents the comparison of the median values of these curves across the four limit states.

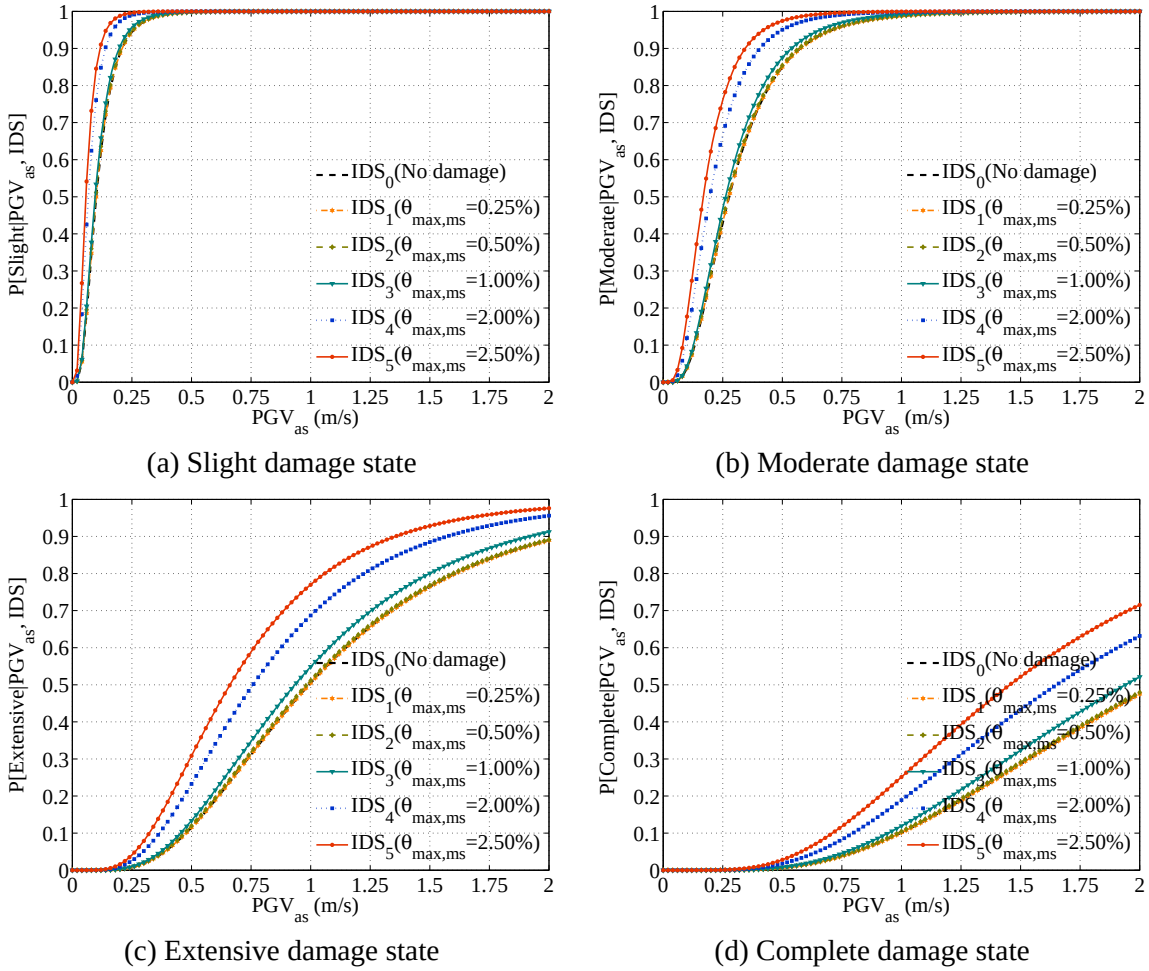

(a) Slight damage state

(b) Moderate damage state

(c) Extensive damage state

(d) Complete damage state

Figure D.1 Aftershock fragility curves with different IDSs for OMF-4S-RO model

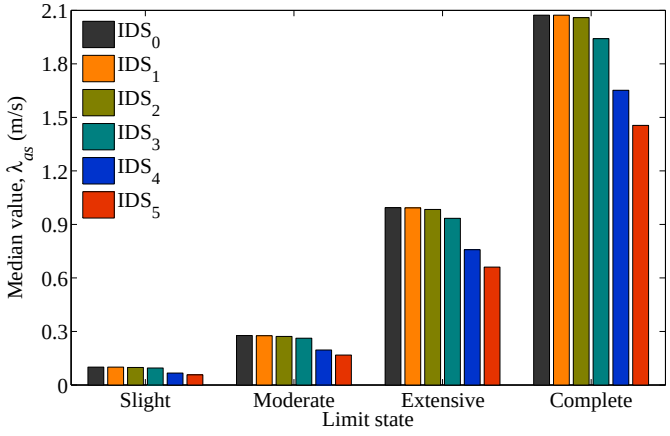

Figure D.2 Median values of aftershock fragility curves for OMF-4S-RO model

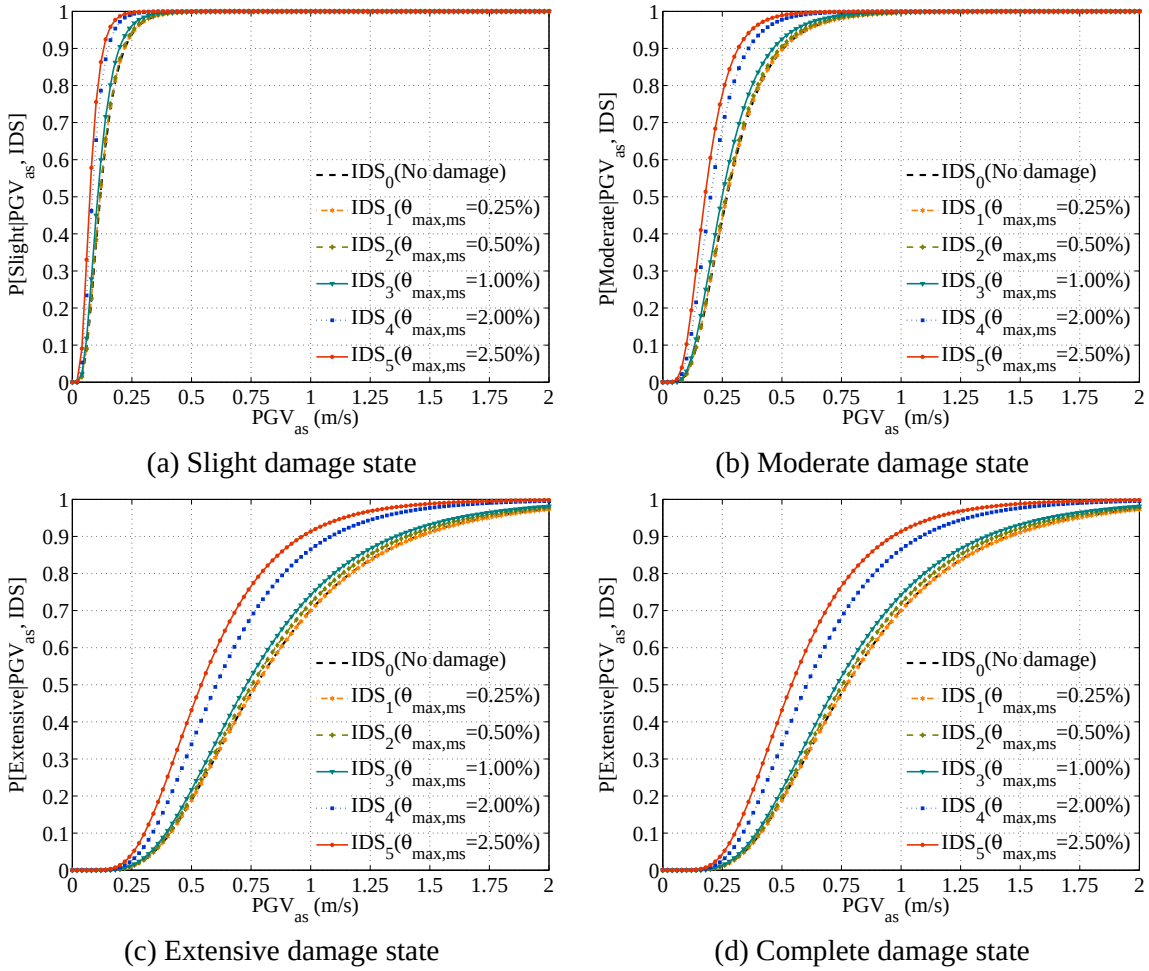

(a) Slight damage state

(b) Moderate damage state

(c) Extensive damage state

(d) Complete damage state

Figure D.3 Aftershock fragility curves with different IDSs for OMF-4S-JS model

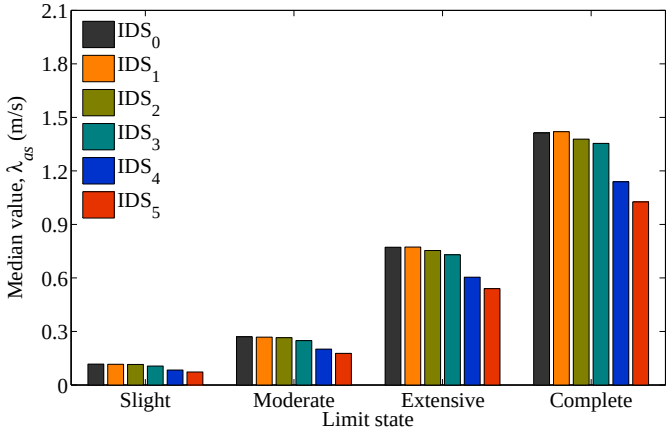

Figure D.4 Median values of aftershock fragility curves for OMF-4S-JS model

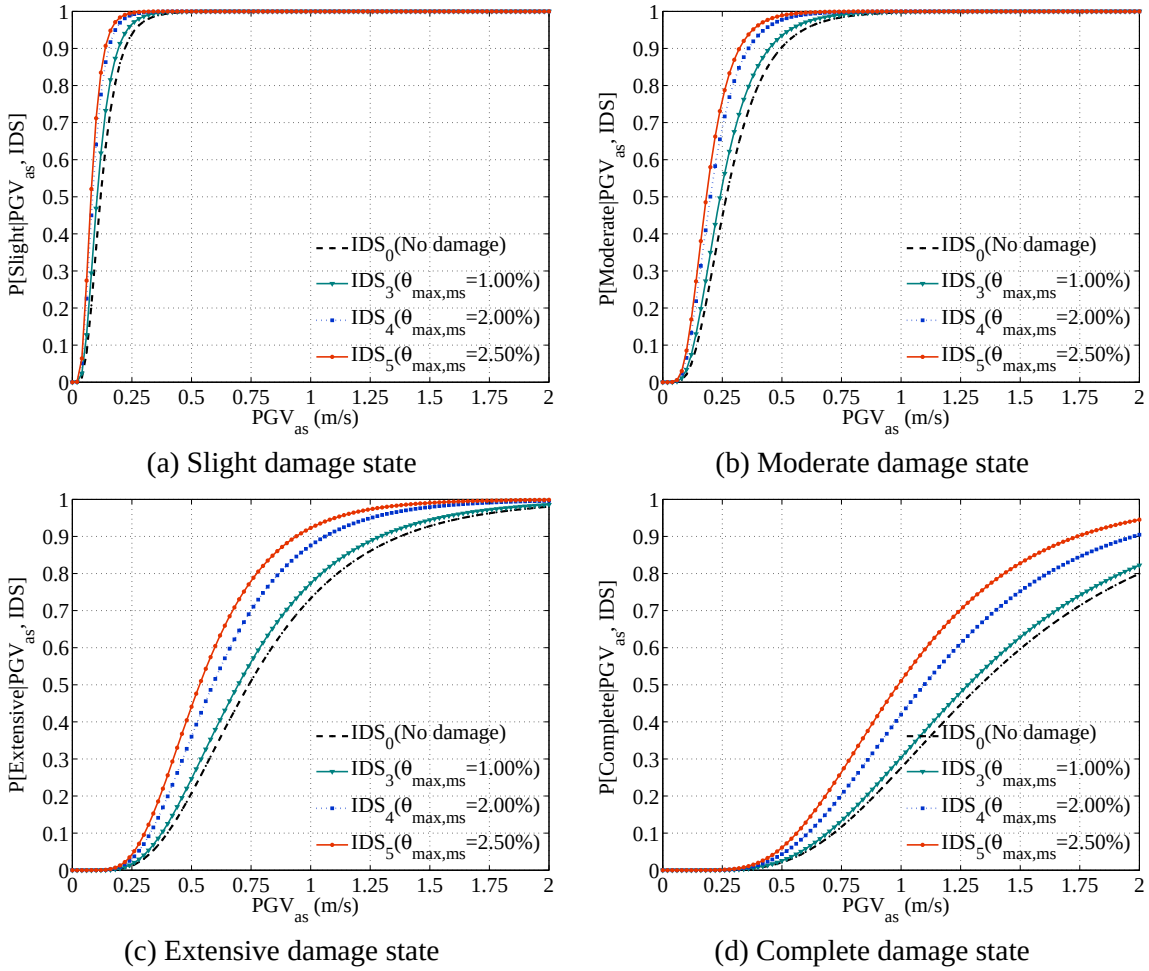

(a) Slight damage state

(b) Moderate damage state

(c) Extensive damage state

(d) Complete damage state

Figure D.5 Aftershock fragility curves with different IDSs for OMF-4S-JB model

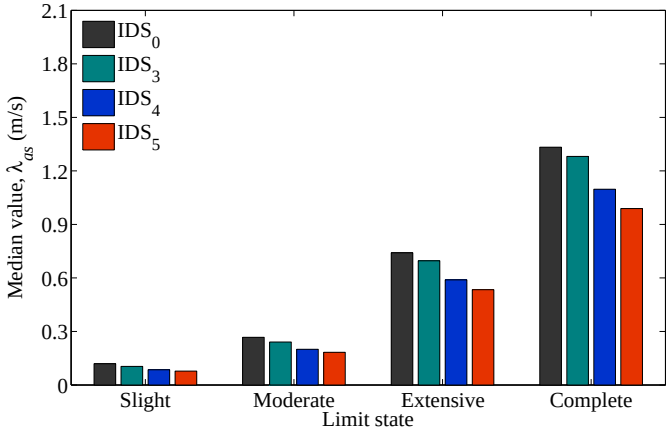

Figure D.6 Median values of aftershock fragility curves for OMF-4S-JB model

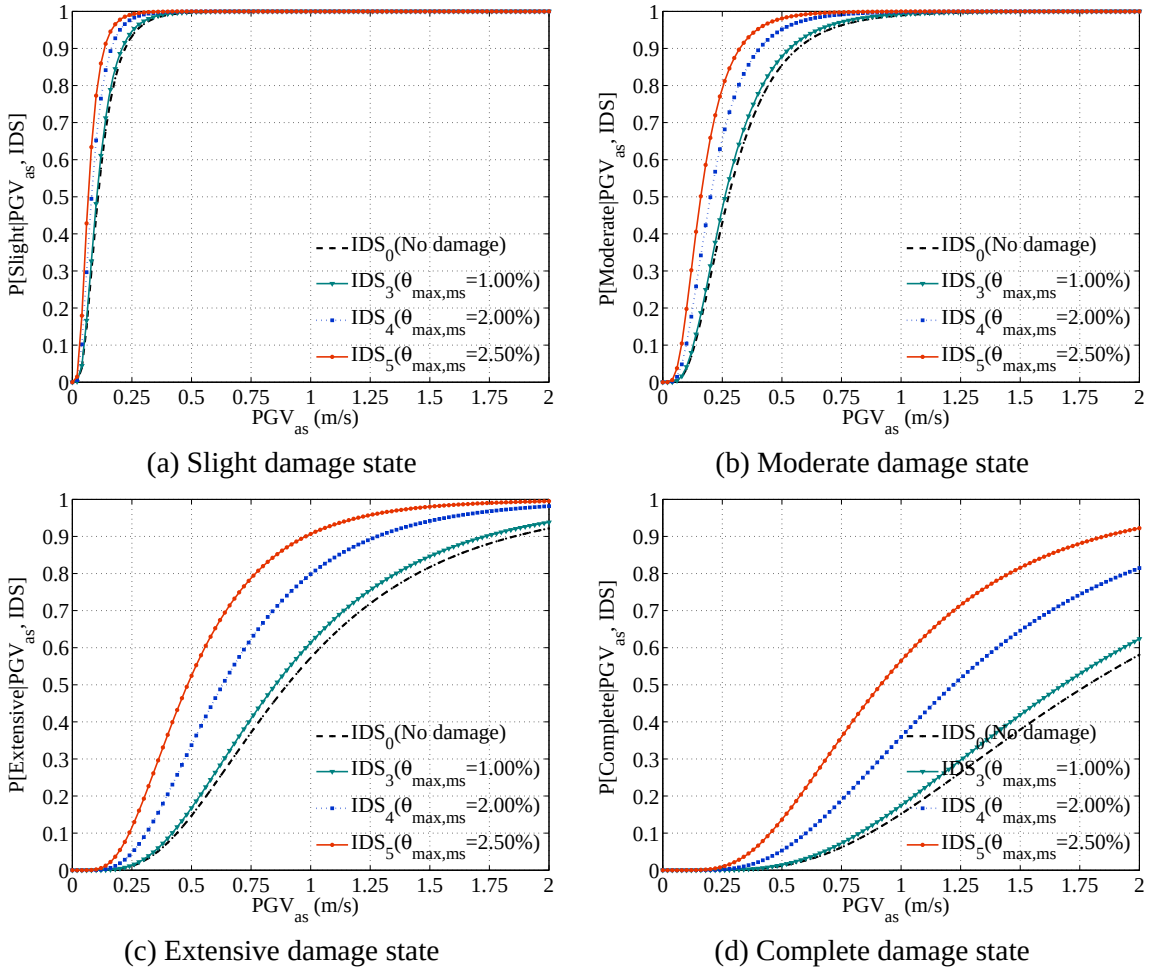

(a) Slight damage state

(b) Moderate damage state

(c) Extensive damage state

(d) Complete damage state

Figure D.7 Aftershock fragility curves with different IDSs for OMF-4S-CS model

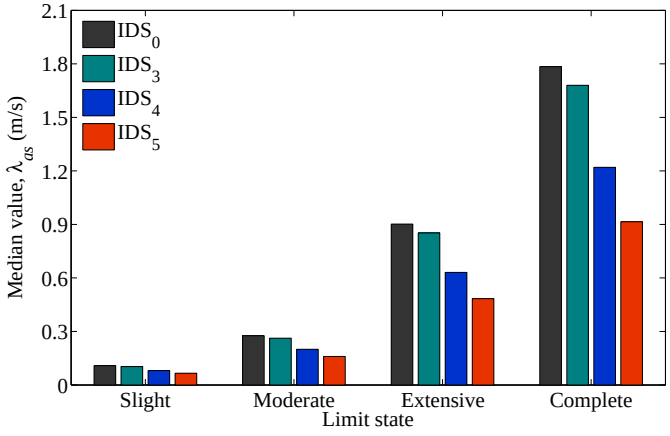

Figure D.8 Median values of aftershock fragility curves for OMF-4S-CS model

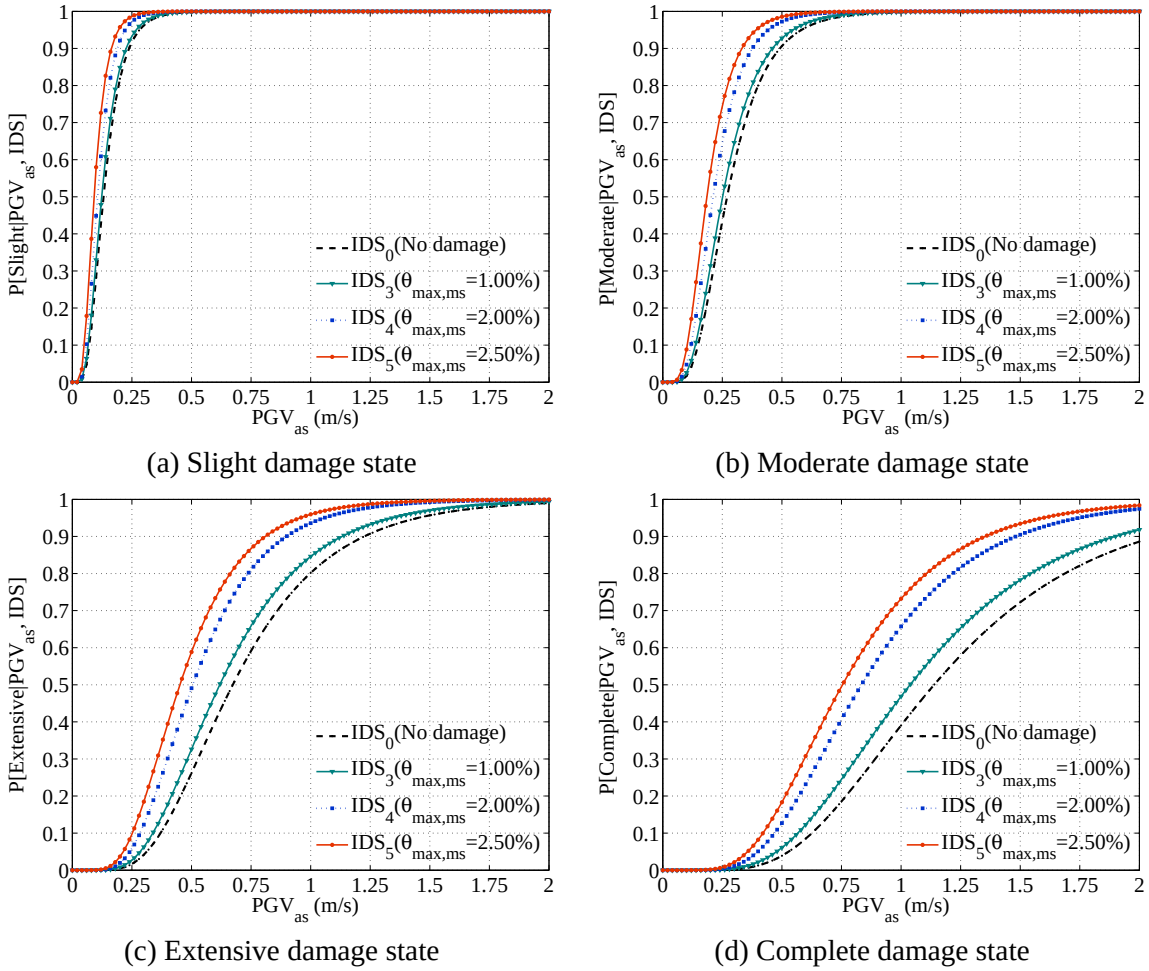

(a) Slight damage state

(b) Moderate damage state

(c) Extensive damage state

(d) Complete damage state

Figure D.9 Aftershock fragility curves with different IDSs for OMF-4S-JCS model

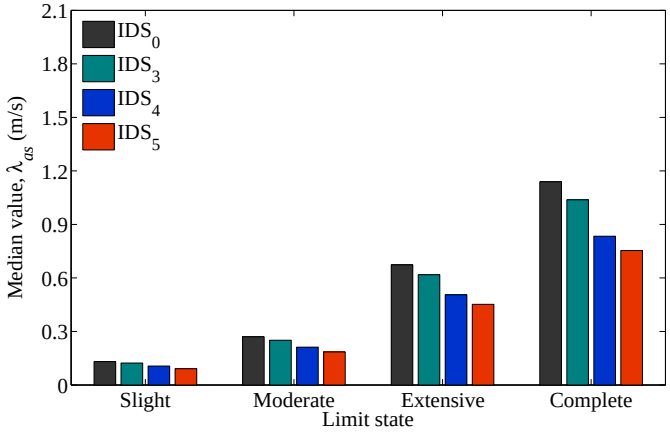

Figure D.10 Median values of aftershock fragility curves for OMF-4S-JCS model

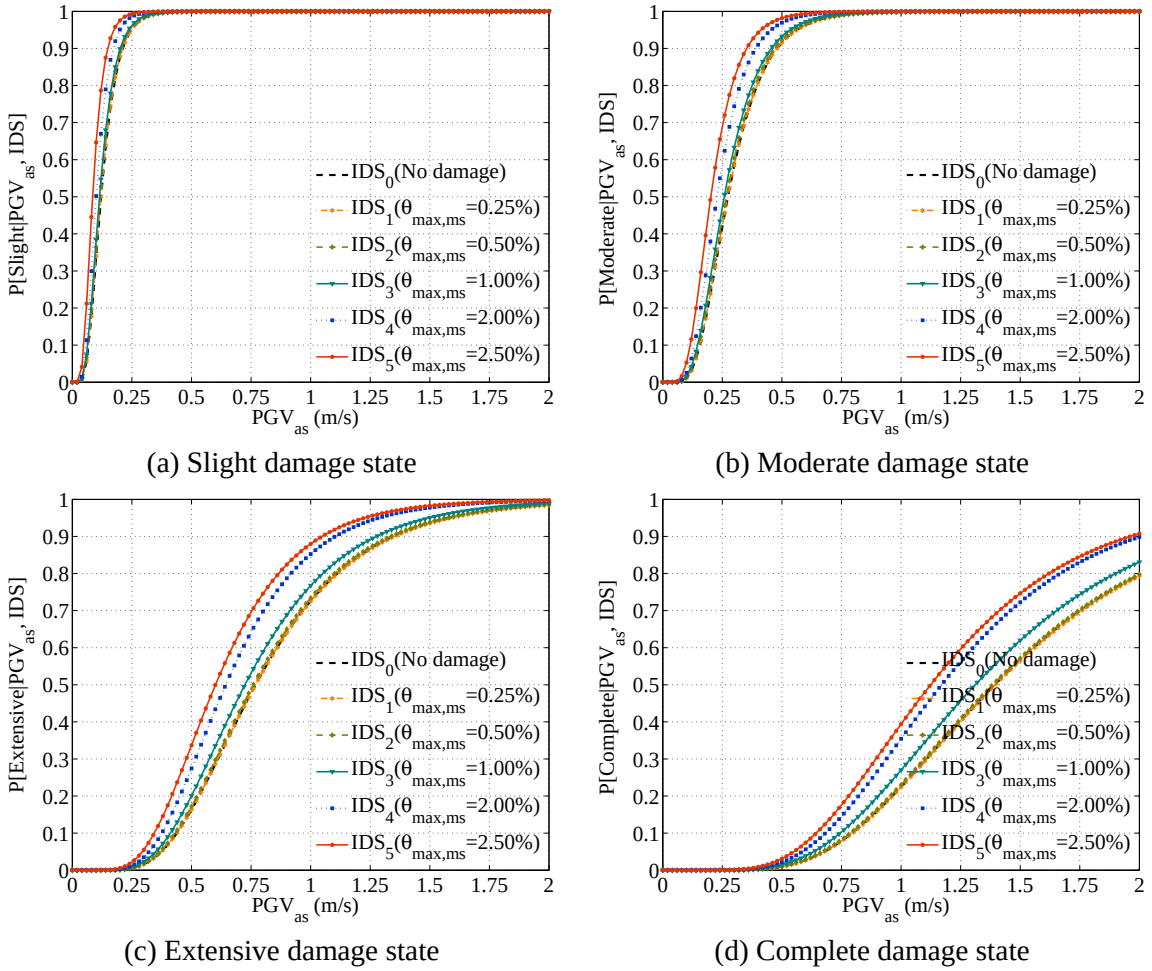

(a) Slight damage state

(b) Moderate damage state

(c) Extensive damage state

(d) Complete damage state

Figure D.11 Aftershock fragility curves with different IDSs for OMF-8S-JS model

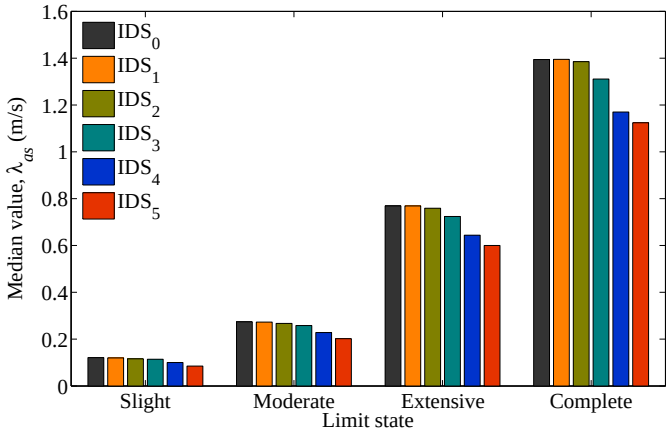

Figure D.12 Median values of aftershock fragility curves for OMF-8S-JS model

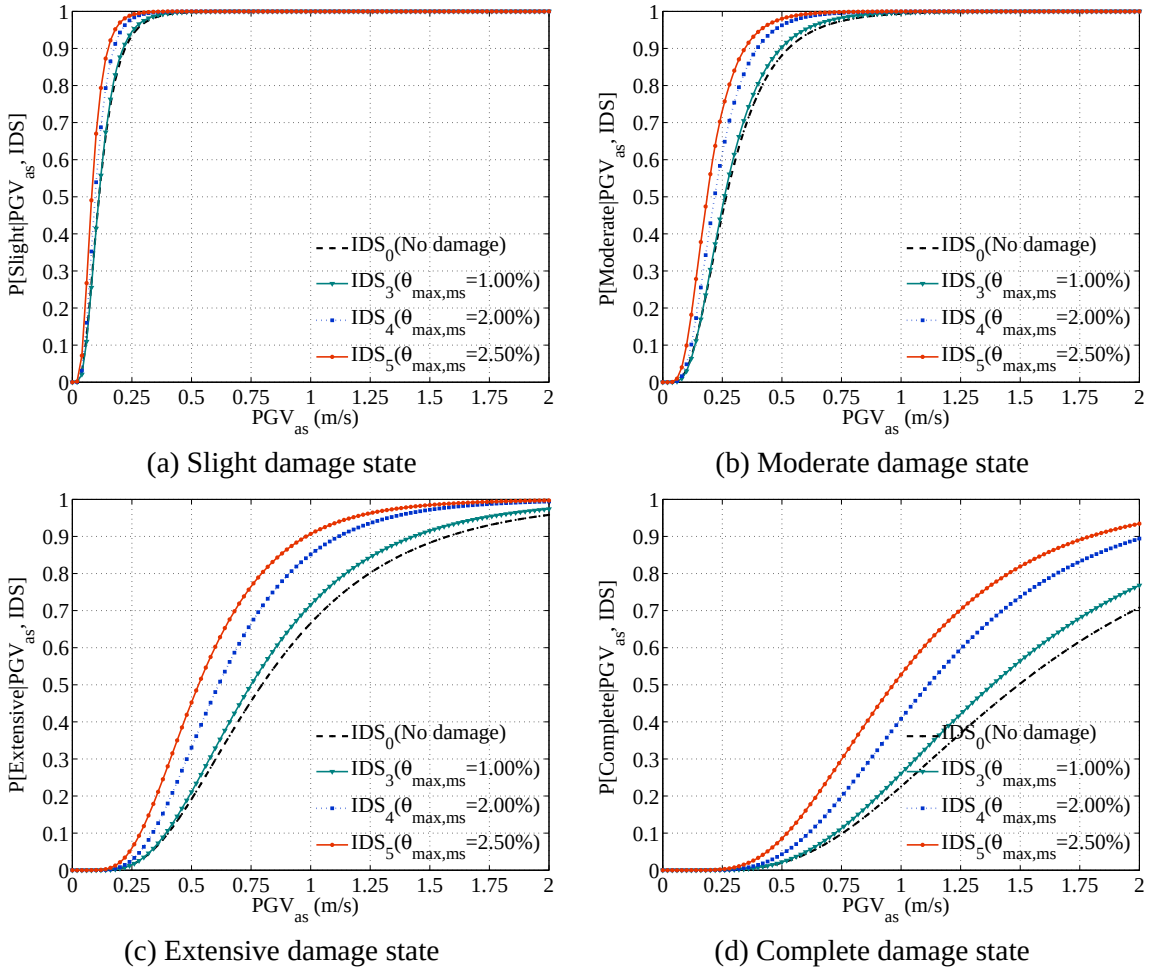

(a) Slight damage state

(b) Moderate damage state

(c) Extensive damage state

(d) Complete damage state

Figure D.13 Aftershock fragility curves with different IDSs for OMF-8S-CS model

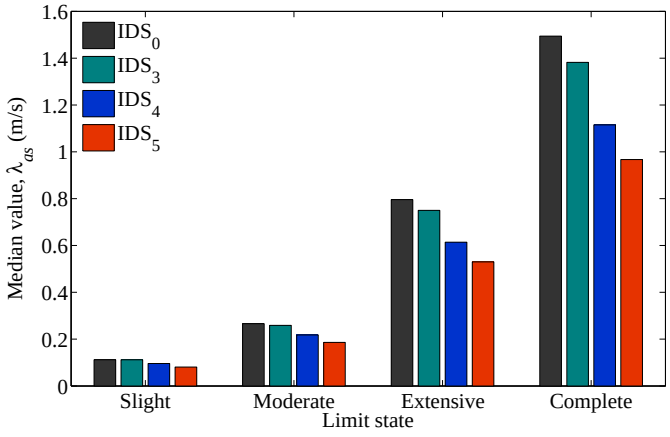

Figure D.14 Median values of aftershock fragility curves for OMF-8S-CS model

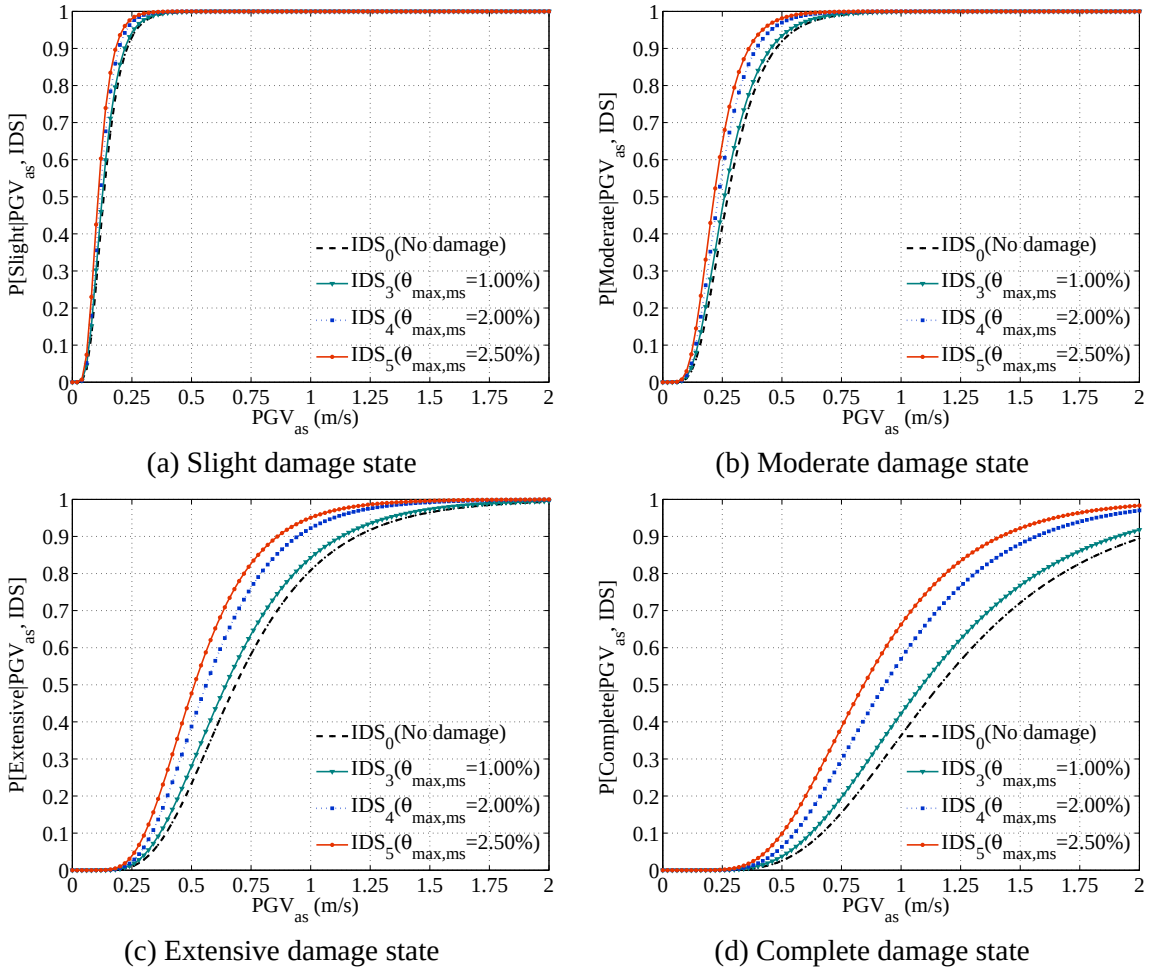

(a) Slight damage state

(b) Moderate damage state

(c) Extensive damage state

(d) Complete damage state

Figure D.15 Aftershock fragility curves with different IDSs for OMF-8S-JCS model

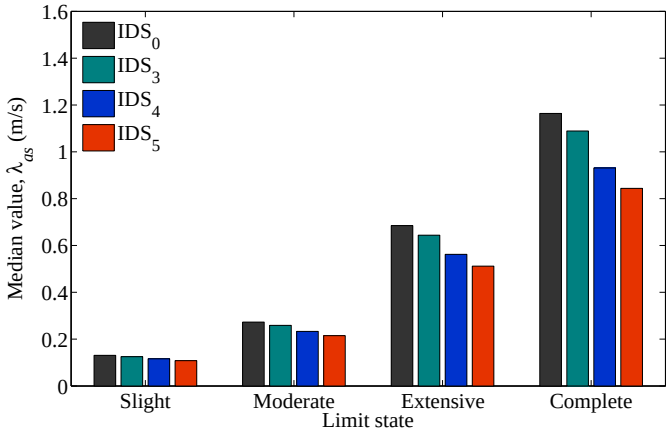

Figure D.16 Median values of aftershock fragility curves for OMF-8S-JCS model

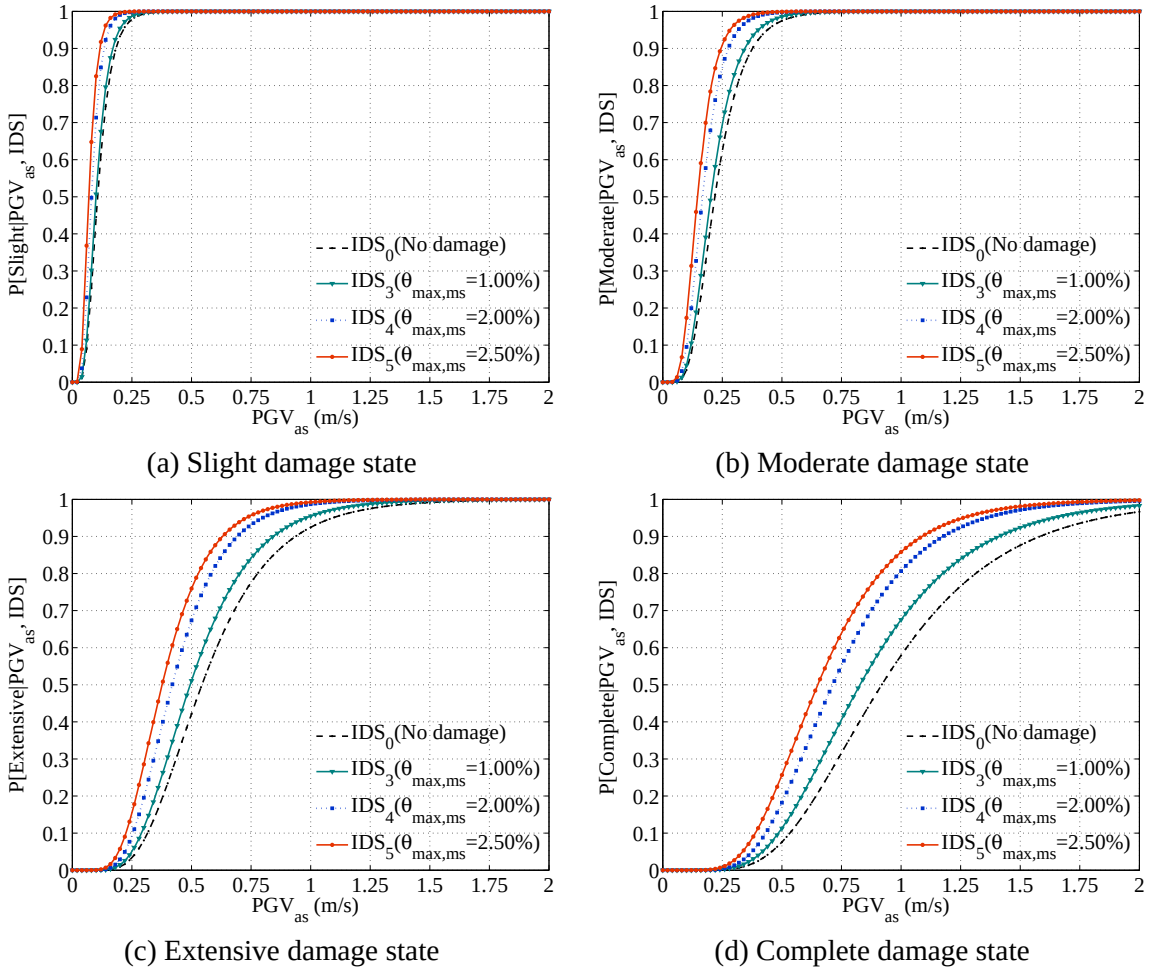

(a) Slight damage state

(b) Moderate damage state

(c) Extensive damage state

(d) Complete damage state

Figure D.17 Aftershock fragility curves with different IDSs for OMF-4P-JS model

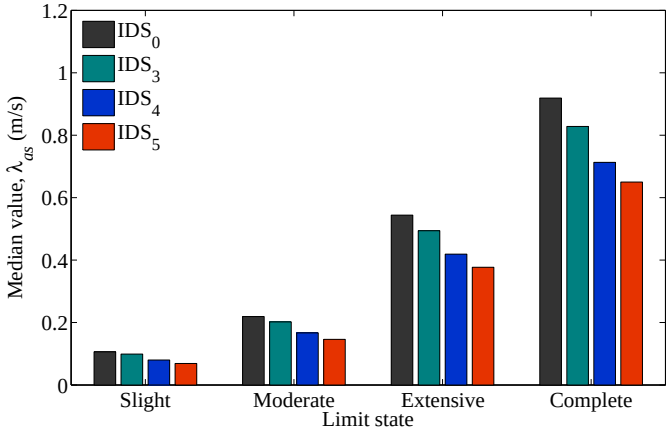

Figure D.18 Median values of aftershock fragility curves for OMF-4P-JS model

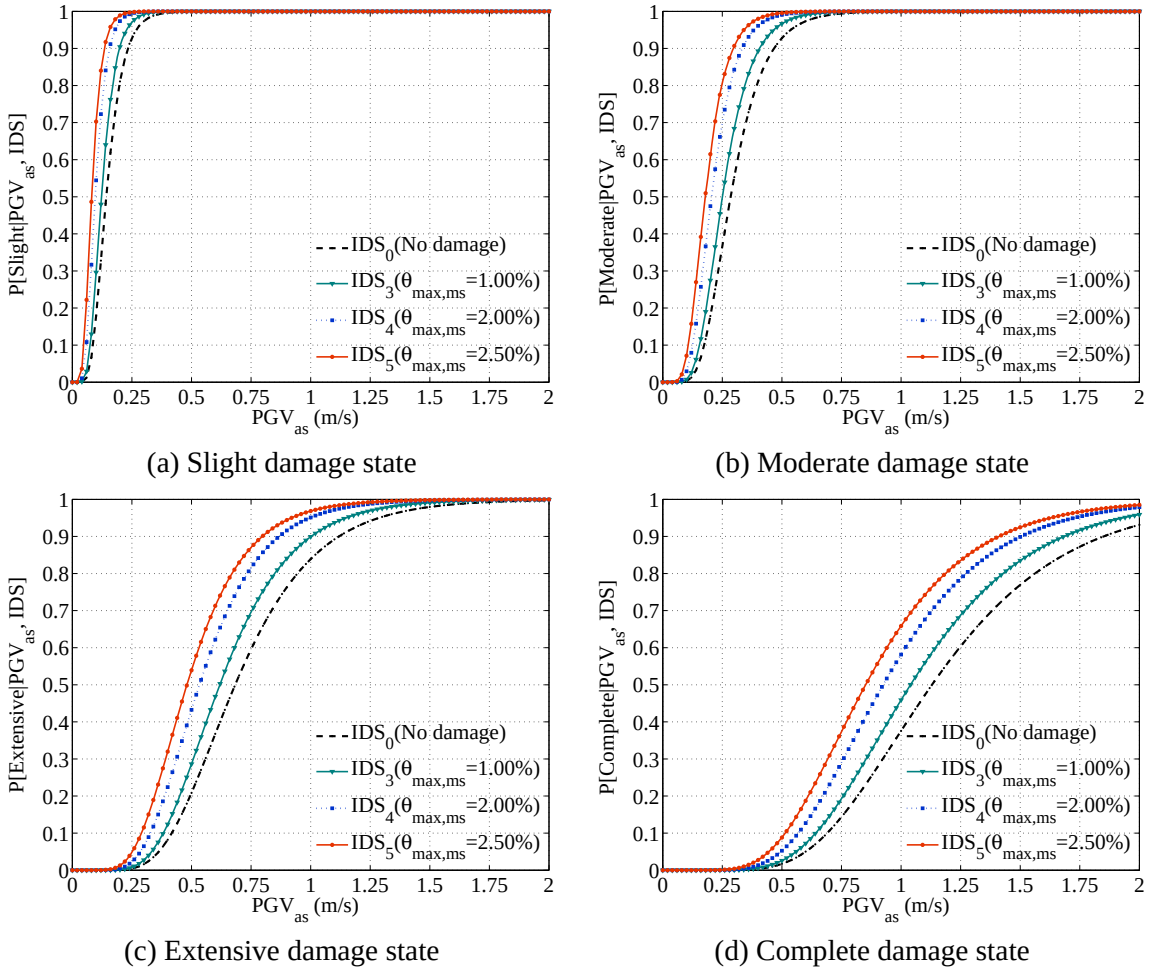

(a) Slight damage state

(b) Moderate damage state

(c) Extensive damage state

(d) Complete damage state

Figure D.19 Aftershock fragility curves with different IDSs for OMF-8P-JS model

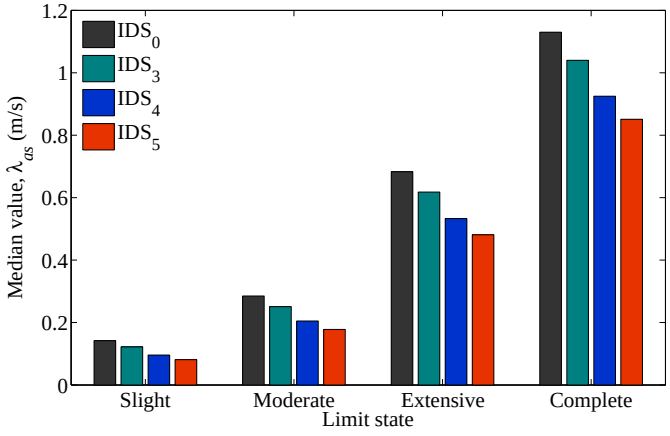

Figure D.20 Median values of aftershock fragility curves for OMF-8P-JS model

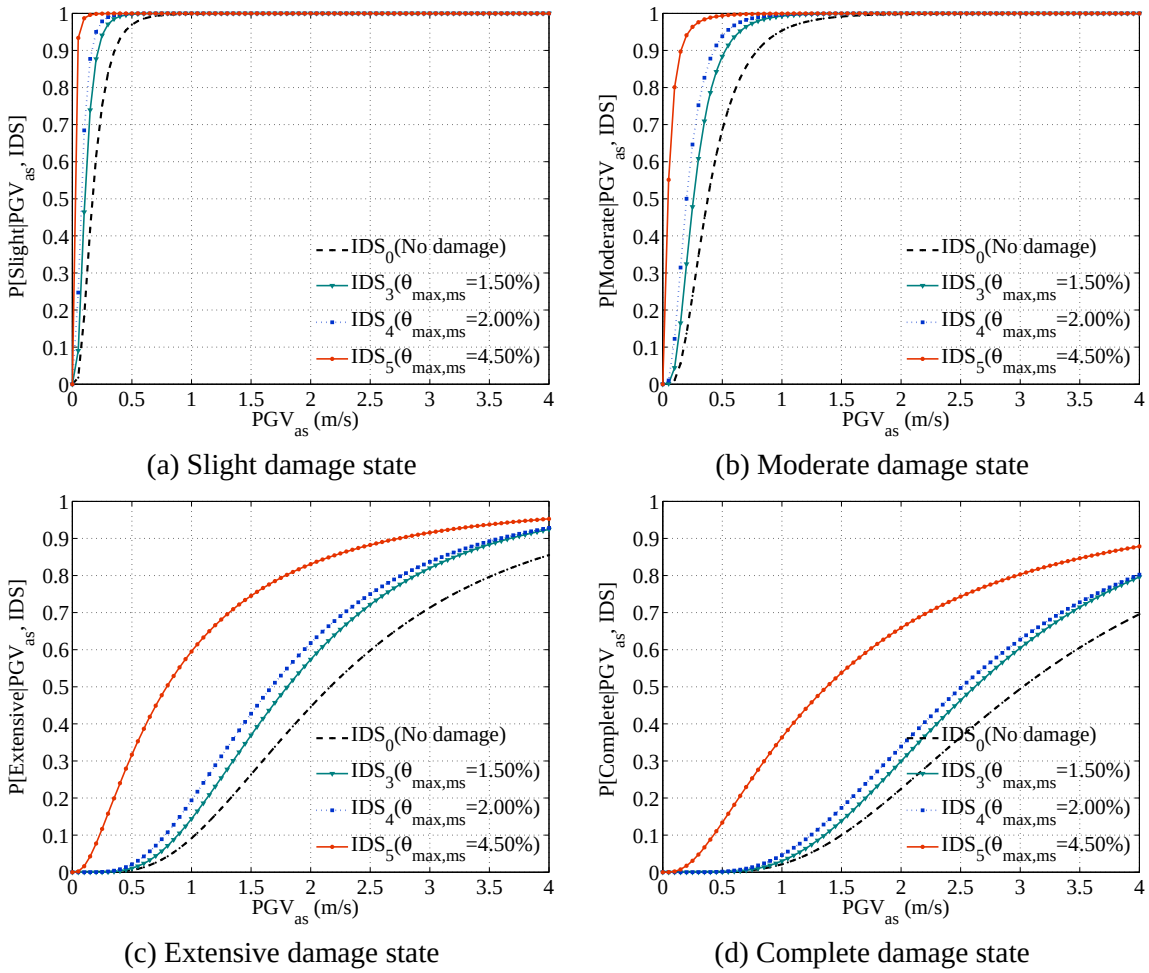

(a) Slight damage state

(b) Moderate damage state

(c) Extensive damage state

(d) Complete damage state

Figure D.21 Aftershock fragility curves with different IDSs for SMF-4P-RO model

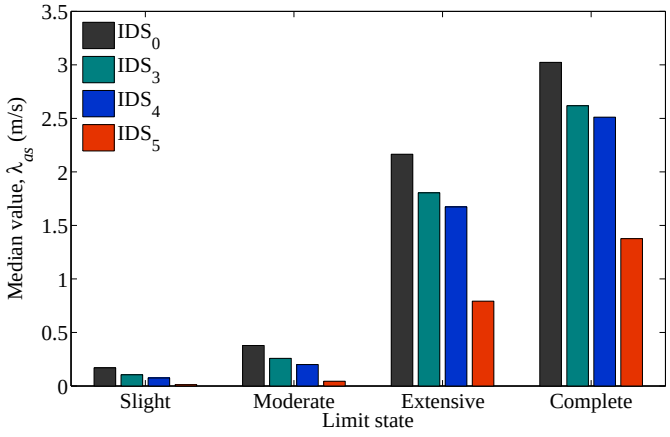

Figure D.22 Median values of aftershock fragility curves for SMF-4P-RO model

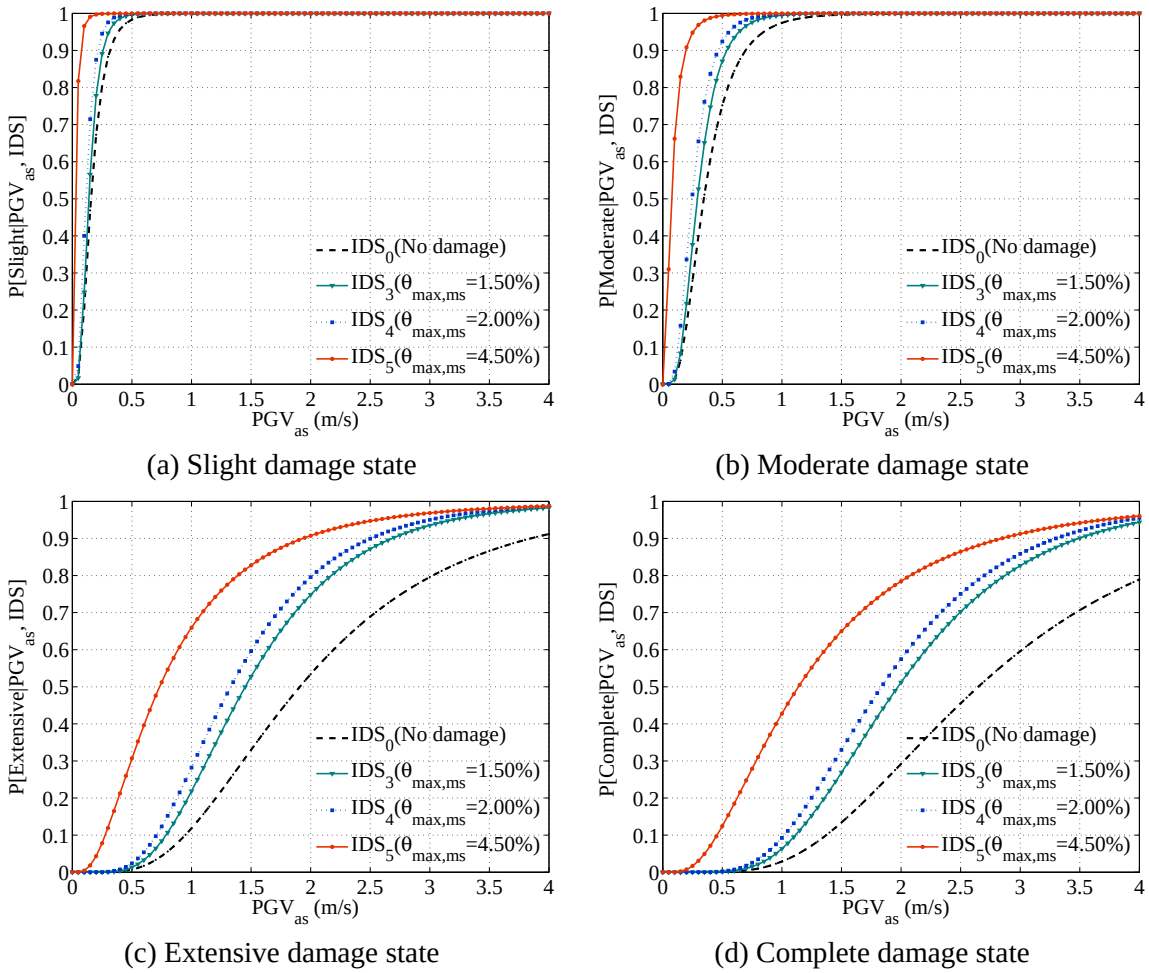

(a) Slight damage state

(b) Moderate damage state

(c) Extensive damage state

(d) Complete damage state

Figure D.23 Aftershock fragility curves with different IDSs for SMF-4P-JS model

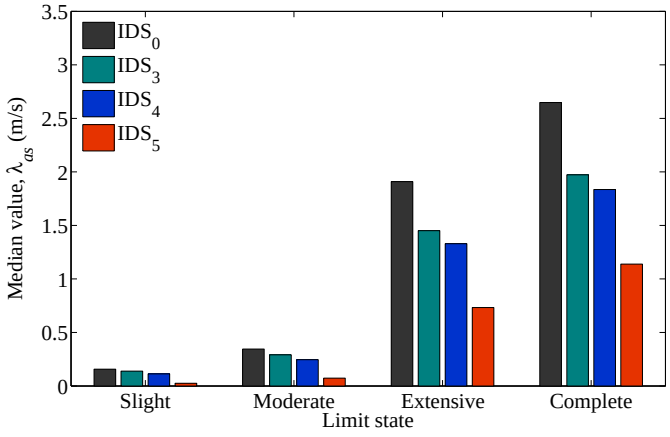

Figure D.24 Median values of aftershock fragility curves for SMF-4P-JS model

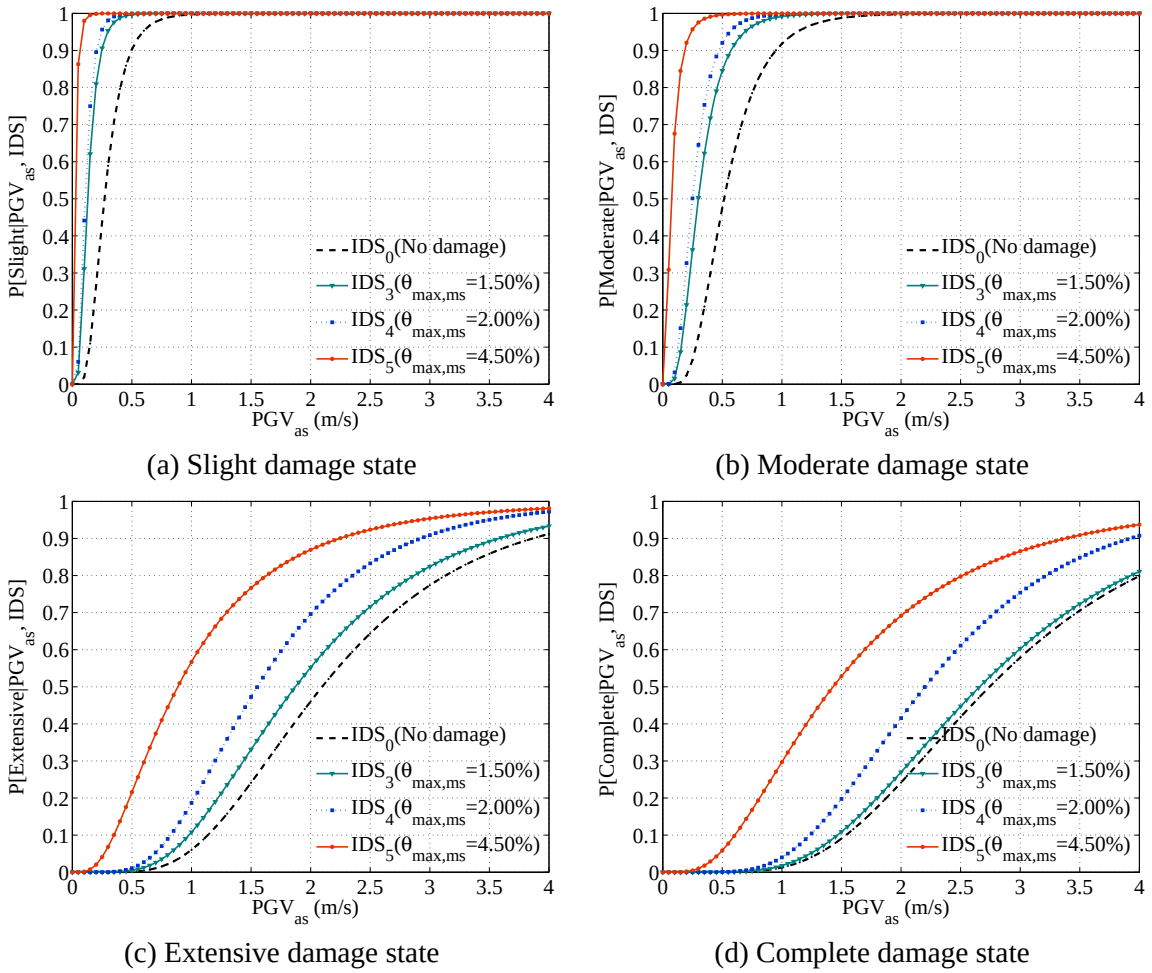

(a) Slight damage state

(b) Moderate damage state

(c) Extensive damage state

(d) Complete damage state

Figure D.25 Aftershock fragility curves with different IDSs for SMF-8P-RO model

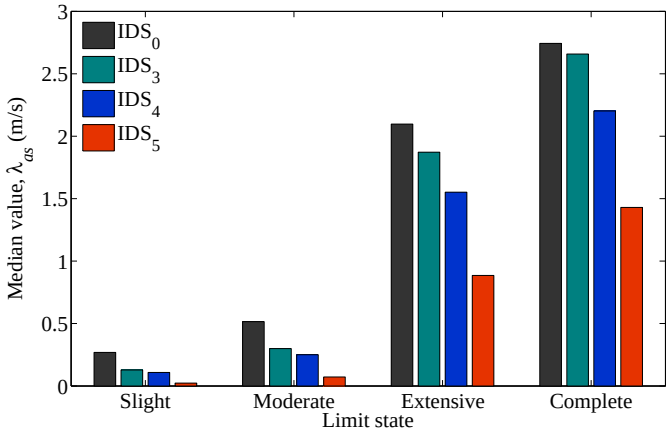

Figure D.26 Median values of aftershock fragility curves for SMF-8P-RO model

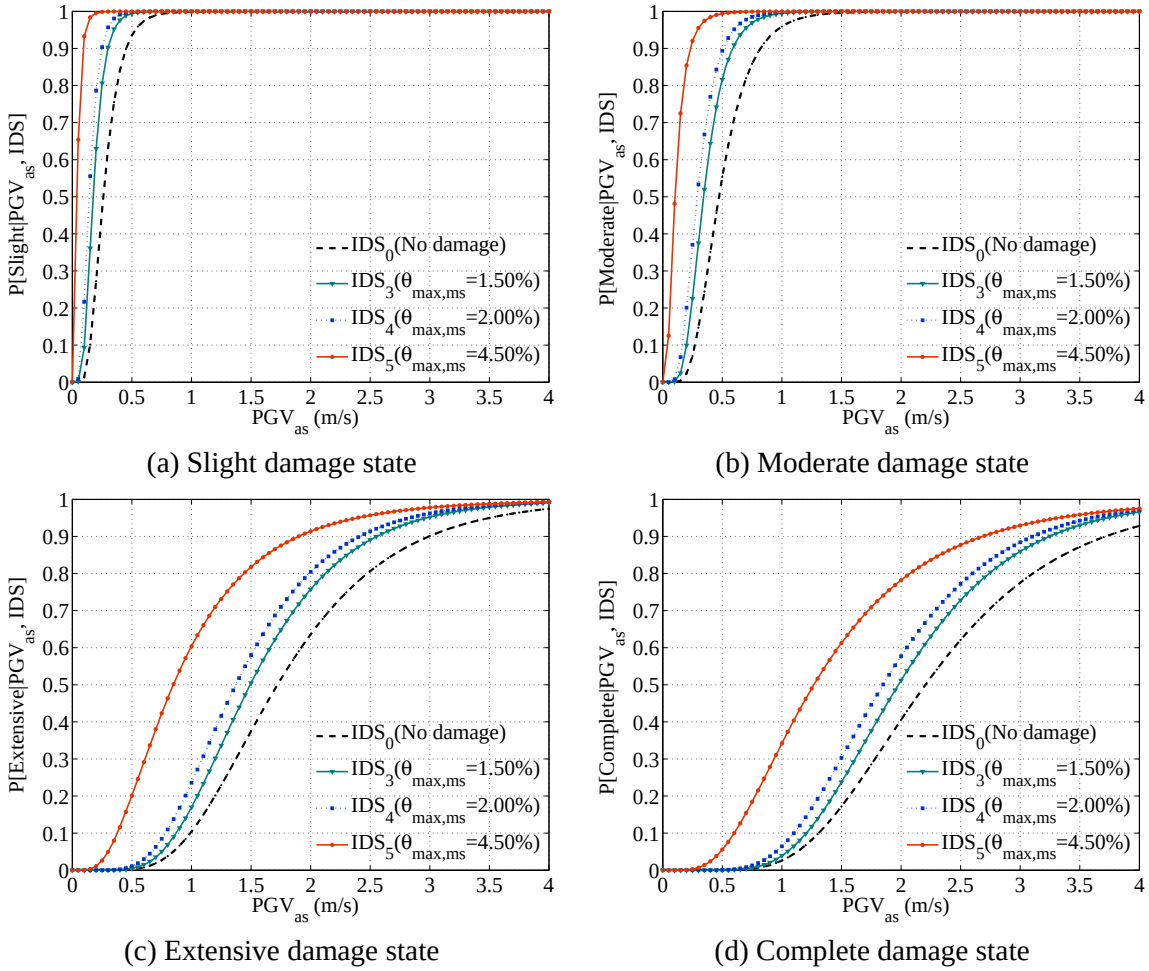

(a) Slight damage state

(b) Moderate damage state

(c) Extensive damage state

(d) Complete damage state

Figure D.27 Aftershock fragility curves with different IDSs for SMF-8P-JS model

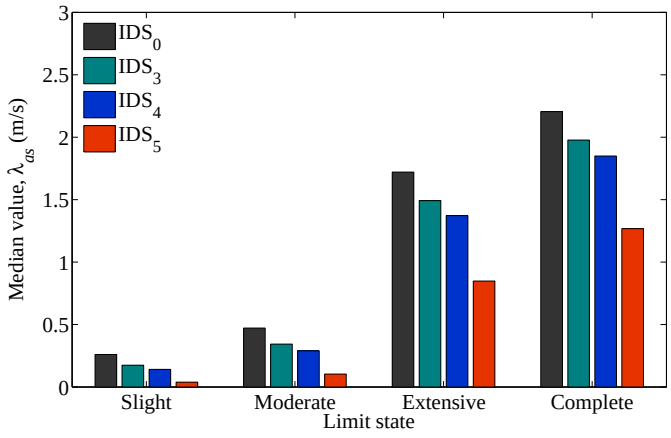

Figure D.28 Median values of aftershock fragility curves for SMF-8P-JS model

REFERENCES

ACI Committee 318 (1963) *Building code requirements for reinforced concrete (ACI 318-71) and commentary (ACI 318R-63)*, American Concrete Institute, Detroit, MI.

ACI Committee 318 (1971) *Building code requirements for reinforced concrete (ACI 318-71) and commentary (ACI 318R-71)*, American Concrete Institute, Farmington Hills, MI.

ACI Committee 318 (1989) *Building code requirements for reinforced concrete (ACI 318-89) and commentary (ACI 318R-89)*, American Concrete Institute, Detroit, MI.

ACI Committee 318 (2002) *Building code requirements for reinforced concrete (ACI 318-02) and commentary (ACI 318R-02)*, American Concrete Institute, Farmington Hills, MI.

ACI-ASCE Committee 352 (2002) *Recommendations for design of beam-column connections in monolithic reinforced concrete structures*, American Concrete Institute, Farmington Hills, MI.

Adachi, M., Ishida K., Fujii S., Watanabe, F., and Morita, S. (1995) *Bi-directional seismic loading tests of high-strength R/C corner column-beam subassemblage (1) (in Japanese)*, Summaries of Technical Papers of Annual Meeting Architectural Institute of Japan, pp. 91–92.

Akguzel, U. (2011) *Seismic performance of FRP retrofitted exterior RC beam-column joints under varying axial and bidirectional loading*, Ph.D. Thesis, Department of Civil and Natural Resources Engineering, University of Canterbury, Christchurch, New Zealand.

Alath, S. and Kunnath, S.K. (1995) *Modeling inelastic shear deformations in RC beam-column joints*, Engineering Mechanics: Proceedings of 10th Conference, University of Colorado at Boulder, Boulder, CO, May 21–24, ASCE, New York, Vol. 2, pp. 822–825.

Alire, D.A. (2002) *Seismic evaluation of existing unconfined reinforced concrete beam-column joints*, M.S. Thesis, Department of Civil and Environmental Engineering, University of Washington, Seattle, WA.

Almusallam, T.H., and Al-Salloum, Y.A. (2007) *Seismic response of interior RC beam-column joints upgraded with FRP sheets. II: Analysis and parametric study*, ASCE Journal of Composites for Construction, Vol. 11, No. 6, pp. 590–600.

Al-Salloum, Y.A., Siddiqui, N.A., Elsanadedy, H.M., Abadel, A.A., and Aqel, M.A. (2011) *Textile-reinforced mortar versus FRP as strengthening material for seismically deficient RC beam-column joints*, ASCE Journal of Composites for Construction, Vol. 15, No. 6, pp. 920–933.

Altoontash, A. (2004) *Simulation and damage models for performance assessment of reinforced concrete beam-column joints*, Ph.D. Thesis, Department of Civil and Environmental Engineering, Stanford University, CA.

Alva, G.M.S., de Cresce El Debs, A.L.H., and El Debs, M.K. (2007) *An experimental study on cyclic behaviour of reinforced concrete connection*s, Canadian Journal of Civil Engineering, Vol. 34, No. 4, pp. 565–575.

Amadio, C., Fragiacomo, M., and Rajgelj, S. (2003) *The effects of repeated earthquake ground motions on the non-linear response of SDOF systems*, Earthquake Engineering and Structural Dynamics, Vol. 32, No. 2, pp. 291–308.

American Society of Civil Engineers (ASCE) (2000) *Prestandard and commentary for the seismic rehabilitation of buildings*, FEMA-356, Federal Emergency Management Agency, Washington DC.

American Society of Civil Engineers (ASCE) (2005) *ASCE 7-05: Minimum design loads for buildings and other structures*, Reston, VA.

Anderson, M., Lehman, D., and Stanton, J. (2008) *A cyclic shear stress-strain model for joints without transverse reinforcement,* Engineering Structures, Vol. 30, No. 4, pp. 941–954.

Ang, G.B., Priestley, M.J.N., and Park, R. (1981) *Ductility of reinforced bridge piers under seismic loading*, Report 81-3, Department of Civil Engineering, University of Canterbury, Christchurch, New Zealand.

Antonopulos, C.P. and Triantafillou, T.C. (2003) *Experimental investigation of FRP-strengthened RC beam-column joints,* ACSE Journal of Composites for Construction, Vol. 7, No. 1, pp. 39–49.

Aoyama, H., Lee, S., Tasai, A., and Otani, S. (1993) *Bond characteristics of beam bars passing through reinforced concrete interior beam-column joints using high-strength concrete–Part 1: Outline of experiment (in Japanese)*, Summaries of Technical Papers of Annual Meeting Architectural Institute of Japan, pp. 837–838.

Applied Technology Council (ATC) (1985) *Earthquake damage evaluation data for California*, Report No. ATC-13, Applied Technology Council, Redwood City, CA.

Applied Technology Council (ATC) (1996) *Seismic evaluation and retrofit of concrete buildings*, Report No. ATC-40, California Seismic Safety Commission (SSC 96-01), Sacramento, CA.

Aschheim, M. and Black, E. (1999) *Effects of prior earthquake damage on response of simple stiffness-degrading structures,* Earthquake Spectra, Vol. 15, No. 1, pp. 1–24.

Aschheim, M. and Moehle, J.P. (1992) *Shear strength and deformability of RC bridge columns subjected to inelastic displacements*, UCB/EERC 92/04, University of California, Berkeley, CA.

Asou, N., Nagashima, T., and Sugano, S. (1993) *Force characteristic of beam column connection using high strength concrete (Fc600) and reinforcement (SD490) (in*

Japanese), Proceedings of the Japan Concrete Institute, Vol. 15, No. 2, pp. 553–558.

Attaalla, S.A. (2004) *General analytical model for normal shear stress of type 2 normal and high strength concrete beam-column joints*, ACI Structural Journal, Vol. 101, No. 1, pp. 65–75.

Aycardi, L.E., Mander, J.B., and Reinhorn, A.M. (1994) *Seismic resistance of reinforced concrete frame structures designed only for gravity loads: Experimental performance of subassemblages*, ACI Structural Journal, Vol. 91, No. 5, pp. 552–563.

Azizinamini, A., Johal, L.S., Hanson, N.W., Musser, D.W., and Corley, W.G. (1988) *Effects of transverse reinforcement on seismic performance of columns–A partial parametric investigation*, Project No. CR-96 17, Construction Technology Laboratories, Skokie, Illinois.

Bae, S. (2005) *Seismic performance of full-scale reinforced concrete columns*, Ph.D. Thesis, Department of Civil, Architectural and Environmental Engineering, The University of Texas at Austin, TX.

Baker, J.W. and Cornell, C.A. (2006) *Vector-valued ground motion intensity measures for probabilistic seismic demand analysis*, PEER Report 2006/08, Pacific Earthquake Engineering Research Center, University of California, Berkeley, CA.

Baker, J.W., Shahi, S.K., and Jayaram, N. (2011) *New ground motion selection procedures and selected motions for the PEER Transportation Research Program*, PEER Report 2011/03, Pacific Earthquake Engineering Research Center, University of California, Berkeley, CA.

Barkhordary, M. and Tariverdilo, S. (2011) *Vulnerability of ordinary moment resistant concrete frames*, Earthquake Engineering and Engineering Vibration, Vol. 10, No. 4, pp. 519–533.

Bartlett, F.M. and MacGregor, J.G. (1996) *Statistical analysis of the compressive strength of concrete in structures*, ACI Material Journal, Vol. 93, No. 2, pp. 158–168.

Barnes, M., Jigoral, S., Park, S., and Moehle, J. (2008) *Evaluation of exterior non-ductile reinforced concrete building joints experiencing early column failure*, Pacific Earthquake Engineering Center, University of California, Berkeley, CA.

Bazzurro, P., Cornell, C.A., Menun, C., Motahari, M., and Luco, N. (2006) *Advanced seismic assessment guidelines*, PEER Report 2006/05, Pacific Earthquake Engineering Research Center, University of California, Berkeley, CA.

Bearman, C.F. (2012) *Post-earthquake assessment of reinforced concrete frames*, M.S. Thesis, Department of Civil and Environmental Engineering, University of Washington, Seattle, WA.

Beres, A., White, R.N., and Gergely, P. (1992) *Seismic performance of interior and exterior beam-to-column joints related to lightly reinforced concrete frame*

buildings: Detailed experimental results, Report No. 92-7, School of Civil and Environmental Engineering, Cornell University, Ithaca, NY.

Berry, M., Parrish, M., and Eberhard, M. (2004) *PEER structural performance database user's manual*, Pacific Earthquake Engineering Research Center, University of California, Berkeley, CA.

Biddah, A.M.S. (1997) *Seismic behaviour of existing and rehabilitated reinforced concrete frame connections*, Ph.D. Thesis, McMaster University, Ontario, Canada.

Bonacci, J. and Pantazopoulou, S. (1993) *Parametric investigation of joint mechanics*, ACI Structural Journal, Vol. 90, No. 1, pp. 61-70.

Bracci, J.M., Reinhorn, A.M., and Mander, J.B. (1992) *Seismic resistance of reinforced concrete frame structures designed only for gravity loads: Part I–Design and properties of a 1/3 scale model structure*, Technical Report NCEER–92–0027, National Center of Earthquake Engineering Research, State University of New York at Buffalo, NY.

Canbolat, B.B. and Wight, J.K. (2008) *Experimental investigation on seismic behavior of eccentric reinforced concrete beam-column-slab connections*, ACI Structural Journal, Vol. 105, No. 2, pp. 154–162.

Celik, O.C. and Ellingwood, B.R. (2008) *Modeling beam-column joints in fragility assessment of gravity load designed reinforced concrete frames*, Journal of Earthquake Engineering, Vol. 12, No. 3, pp. 357–381.

Celik, O.C. and Ellingwood, B.R. (2010) Seismic fragilities for non-ductile reinforced concrete frames–Role of aleatoric and epistemic uncertainties, Structural Safety, 32(1), pp. 1-12.

Chang, K.W., Kim, Y.I., and Oh, Y.H. (1997) *Slab effect on inelastic behavior of high strength RC beam-column joints (in Korean)*, Journal of the Korean Concrete Institute, Vol. 9, No. 2, pp. 167–177.

Chen, C.C. and Chen, G-K. (1999) *Cyclic behavior of reinforced concrete eccentric beam-column corner joints connecting spread-ended beams*, ACI Structural Journal, Vol. 96, No. 3, pp. 443–450.

Chen, T.-H. (2006) *Retrofit strategy of non-seismically designed frame systems based on a metallic haunch system*, M.S. Thesis, Department of Civil Engineering, University of Canterbury, Christchurch, New Zealand.

Chun, S.-C. and Kim, D.-Y. (2004) *Evaluation of mechanical anchorage of reinforcement by exterior beam-column joint experiments*, 13th World Conference on Earthquake Engineering, Paper No. 0326, Vancouver, BC, Canada.

Chutarat, N. and Aboutaha, R.S. (2003) *Cyclic response of exterior reinforced concrete beam-column joints reinforced with headed bars–experimental investigation*, ACI Structural Journal, Vol. 100, No. 2, pp. 259–264.

Clyde, C., Pantelides, C.P., and Reaveley, L.D. (2000) *Performance-based evaluation of exterior reinforced concrete building joints for seismic excitation*, PEER Report

2000/05, Pacific Earthquake Engineering Center, University of California, Berkeley, CA.

Cornell, A.C., Jayaler, F., Hamburger, R.O., and Foutch, A.D. (2002) *Probabilistic basis for 2000 SAC Federal Emergency Management Agency steel moment frame guidelines*, ASCE Journal of Structural Engineering, Vol. 128, No. 4, pp. 526–533.

Decanini, L., Gavarini, C., and Mollaioli, F. (2000) *Some remarks on the Umbria-Marche earthquakes of 1997*, European Earthquake Engineering, Vol. 3, pp. 18– 48.

Decanini L.D., Liberatore, D., Liberatore, L., and Sorrentino, L. (2012) *Preliminary report on the 2012, May 20, Emilia earthquake*, Vol. 1, http://www.eqclearinghouse.org/2012-05-20-italy-it/.

DesRoches, R., Comerio, M., Eberhard, M., Moony, W., and Rix, G.J. (2011) *Overview of the 2010 Haiti earthquake*, Earthquake Spectra, Vol. 27, No. S1, pp. S1–S21.

Dhakal, R.P., Pan, T.-C., Irawan, P., Tsai, K.-C., Lin, K.-C., and Chen, C.-H. (2005) *Experimental study on the dynamic response of gravity-designed reinforced concrete connections*, Engineering Structures, Vol. 27, No. 1, pp. 75–87.

Durrani, A.J. and Wight, J.K. (1985) *Behavior of interior beam-to-column connections under earthquake-type loading*, ACI Journal, Vol. 82, No. 3, pp. 343–349.

Eberhard, M.O., Baldridge, S., Marshall, J., Mooney, W., and Rix, G.J. (2010) *The M_w 7.0 Haiti Earthquake of January 12, 2010*, USGS/EERI Advance Reconnaissance Team Report, US Geological Survey Open-File Report.

Ehsani, M.R. and Alameddine, F. (1991) *Design recommendations for type 2 high strength reinforced concrete connections*, ACI Structural Journal, Vol. 88, No. 3, pp. 277–291.

Ehsani, M.R. and Wight, J.K. (1985) *Exterior reinforced concrete beam-to-column connections subjected to earthquake-type loading*, ACI Journal, Vol. 82, No. 4, pp. 492–499.

Ehsani, M.R., Moussa, A.E., and Vallenilla, C.R. (1987) *Comparison of inelastic behavior of reinforced ordinary-and high strength concrete frames*, ACI Structural Journal, Vol. 84, No. 2, pp. 161–169.

El-Amoury, T.A. (2004) *Seismic rehabilitation of concrete frame beam-column joints*, Ph.D. Thesis, McMaster University, Ontario, Canada.

Ellingwood, B.R., Celik, O.C., and Kinali, K. (2007) *Fragility assessment of building structural systems in Mid-America*, Earthquake Engineering and Structural Dynamics, Vol. 36, No. 13, pp. 1935–1952.

Ellingwood, B.R., Taftali, B., and DesRoches, R. (2010) *Seismic performance assessment of steel frames with shape memory alloy connections, Part II – Probabilistic seismic demand assessment*, Journal of Earthquake Engineering, Vol. 14, No. 5, pp. 631–645.

Ellingwood, B.R. and Wen, Y.-K. (2005) *Risk-benefit-based design decisions for low-probability/high consequence earthquake events in Mid-America*, Progress on Structural Engineering and Materials, Vol. 7, No. 2, pp. 56–70.

Elwood, K.J., Matamoros, A.B., Wallace, J.W., Lehman, D., Heintz, J.A., Mitchell, A.D., Moore, M.A., Valley, M.T., Lowes, L.N., Comartin, C.D., and Moehle, J.P. (2007) *Update to ASCE/SEI 41 concrete provisions*, Earthquake Spectra, Vol. 23, No. 3, pp. 493–523.

Elwood, K.J. and Moehle, J.P. (2003) *Shake table tests and analytical studies on the gravity load collapse of reinforced concrete frames*, PEER Report 2005/13, Pacific Earthquake Engineering Research Center, University of California, Berkeley, CA.

Elwood, K.J. and Moehle, J.P. (2005) *Drift capacity of reinforced concrete columns with light transverse reinforcement*, Earthquake Spectra, Vol. 12, No. 1, pp. 71–89.

Endoh, Y., Kamura, T., Otani, S., and Aoyama, H. (1991) *Behavior of RC beam-column connections using light-weight concrete*, Transactions of the Japan Concrete Institute, Vol. 13, pp. 319–326.

Engindeniz, M. (2008) *Repair and strengthening of pre-1970 RC corner beam-column joints using CFRP composites*, Ph.D. Thesis, School of Civil and Environmental Engineering, Georgia Institute of Technology, GA.

Esaki, F. (1996) *Reinforcing effect of steel plate hoops on ductility of R/C square column*, 11th World Conference on Earthquake Engineering, Paper No. 199, Acapulco, Mexico.

Faisal, A., Majid, T.A., and Hatzigeorgiou, G.D. (2013) *Investigation of story ductility demands of inelastic concrete frames subjected to repeated earthquakes*, Soil Dynamics and Earthquake Engineering, Vol. 44, pp. 42–53.

FEMA (2003) *HAZUS-MH MR4 technical manual, earthquake model*, Federal Emergency Management Agency, Washington, DC.

FEMA 306 (1998) *Evaluation of earthquake damaged concrete and masonry wall buildings: Basic procedures manual*, Federal Emergency Management Agency, Redwood City, CA.

Filiatrault, A., Ladicani, K., and Massicotte, B. (1994) *Seismic performance of code designed fiber reinforced concrete joints*, ACI Structural Journal, Vol. 91, No.5, pp. 564–571.

Fujii, S. and Morita, S. (1987) *Behavior of exterior reinforced concrete beam-column-slab subassemblages under bi-directional loading*, Pacific Conference on Earthquake Engineering, Wairakei, New Zealand, Vol. 1, pp. 339-350.

Fujii, S. and Morita, S. (1991) *Comparison between interior and exterior RC beam-column joint behavior*, Design of Beam-Column Joints for Seismic Resistance (SP123), American Concrete Institute, Detroit, MI, pp. 145–165.

German, S.A. (2013) *Automated damage assessment of reinforced concrete columns for post-earthquake evaluations*, Ph.D. Thesis, School of Civil and Environmental Engineering, Georgia Institute of Technology, GA.

Ghobarah, A. and Said, A. (2002) *Shear strengthening of beam-column joints*, Engineering Structures, Vol. 24, No. 7, pp. 881–888.

Goto, Y. and Joh, O. (1996) *An experimental study on shear failure mechanism of RC interior beam-column joints*, 11th World Conference on Earthquake Engineering, Paper No. 1194, Acapulco, Mexico.

Goto, Y. and Joh, O. (2003) *Experimental study on shear resistance of RC interior eccentric beam-column joints*, 9th East Asia-Pacific Conference on Structural Engineering and Construction, Bali, Indonesia, RSC-170.

Goto, Y. and Joh, O. (2004) *Shear resistance of RC interior eccentric beam-column joints*, 13th World Conference on Earthquake Engineering, Paper No. 649, Vancouver, BC, Canada.

Goto, Y., Joh, O., and Yoshida, H. (1999) *Characteristic of beam reinforcement bond and failure after beam reinforcement yielding in RC interior beam column connection (in Japanese)*, Proceedings of the Japan Concrete Institute, Vol. 21, No. 3, pp. 655–660.

Guimaraes, G.N., Kreger, M.E., and Jirsa, J.O. (1992) *Evaluation of joint-shear provisions for interior beam-column-slab connections using high-strength materials*, ACI Structural Journal, Vol. 89, No. 1, pp. 89–98.

Gulkan, P. and Sozen, M. (1999) *Procedure for determining seismic vulnerability of building structures*, ACI Structural Journal, Vol. 96, No. 3, pp. 336–342.

Hakuto, S., Park, R., and Tanaka, H. (2000) *Seismic load tests on interior and exterior beam-column joints with substandard reinforcing details*, ACI Structural Journal, Vol. 97, No. 1, pp. 11–25.

Hamada, M., Ishibashi, H., and Horie, A. (1999) *Experimental study about RC exterior beam connection subjected to tensile axial force (in Japanese)*, Proceedings of the Japan Concrete Institute, Vol. 21, No. 3, pp. 667–672.

Hamil, S.J. (2000) *Reinforced concrete beam-column connection behavior*, Ph.D. Thesis, Durham University, UK.

Hanson, N.W. and Conner, H.W. (1967) *Seismic resistance of RC beam-column joints*, ACSE Journal of Structural Division, Vol. 93, No. ST5, pp. 533–560.

Hanson, N.W. and Conner, H.W. (1972) *Tests of RC beam-column joints under simulated seismic loading*, Portland Cement Association Research and Development Bulletin.

Haselton, C.B. (2006) *Assessing seismic collapse safety of modern reinforced concrete moment frame buildings*, Ph.D. Thesis, Department of Civil and Environmental Engineering, Stanford University, CA.

Haselton, C.B., Liel, A.B., Deierlein, G., Dean, B.S., and Chou, J.H. (2011) *Seismic collapse safety of reinforced concrete buildings. I: Assessment of ductile moment frames*, ASCE Journal of Structural Engineering, Vol. 137, No. 4, pp. 481–491.

Hassan, W.M. (2011) *Analytical and experimental assessment of seismic vulnerability of beam-column joints without transverse reinforcement in concrete buildings*, Ph.D. Thesis, Department of Civil and Environmental Engineering, University of California, Berkeley, CA.

Hatamoto, H. and Bessho, S. (1988) *Structural Behavior of columns and beam-column assemblages in a 30 storey reinforced concrete building*, 9th World Conference on Earthquake Engineering, Tokyo-Kyoto, Japan, Vol. IV, pp. 627–632.

Hatzigeorgiou, G.D. and Liolios, A.A. (2010) *Nonlinear behaviour of RC frames under repeated strong ground motions*, Soil Dynamics and Earthquake Engineering, Vol. 30, No. 10, pp. 1010–1025.

Hauksson, E. and Jones, L.M. (1995) *The 1994 Northridge earthquake sequence in California: Seismological and tectonic aspects*, Journal of Geophysical Research, Vol. 100, No. B7, pp. 12335–12355.

Hayashi, K., Teraoka, M., Mollick, A.A., and Kanoh, Y. (1993) *Bond characteristic of RC interior beam-column connections using high strength materials (in Japanese)*, Proceedings of the Japan Concrete Institute, Vol.15, No. 2, pp. 583–588.

Healy, J.J., Wu, S.T., and Murga, M. (1980) *Structural building response review*, UREG/CR–1423, 1, US Nuclear Regulatory Commission, Washington, DC.

Hiramatsu, K., Suzuki, M., Saito, K., and Tokota, K. (1995) *Experimental study on high-strength RC interior beam-column Joints with slabs and transverse beams (in Japanese)*, Summaries of Technical Papers of Annual Meeting Architectural Institute of Japan, pp. 75–76.

Hoffman, G.W., Kunnath, S.K., Mander, J.B., and Reinhorn, A.M. (1992) *Gravity-load-designed reinforced concrete buildings: Seismic evaluation strategies for Improved Seismic Resistance*, Technical Report NCEER-92-0016, National Center of Earthquake Engineering Research, State University of New York at Buffalo, NY.

Hoffschild, T.E., Prion, H.G.L., and Chery, S. (1995) *Seismic retrofit of beam-to-column joints with grouted steel tubes*, Recent Developments in Lateral Force Transfer in Buildings (SP157), American Concrete Institute, Detroit, MI, pp. 397–426.

Hosono, T., Kitayama, K., K., Tajima, H., and Kishida, J. (2001) *Failure characteristic of RC interior beam-column connection subjected to bi-directional loading (in Japanese)*, Proceedings of the Japan Concrete Institute, Vol. 23, No. 3, pp. 379–384.

Hwang, S. and Lee, H. (1999) *Analytical model for predicting shear strengths of exterior reinforced concrete beam-column joints for seismic resistance*, ACI Structural Journal, Vol. 96, No. 5, pp. 846–857.

Hwang, S. and Lee, H. (2000) *Analytical model for predicting shear strengths of interior reinforced concrete beam-column joints for seismic resistance*, ACI Structural Journal, Vol. 97, No. 1, pp. 35–44.

Hwang, S.J., Lee, H.J., Liao, T.F., Wang, K.C., and Tsai, H.H. (2005) *Role of hoops on shear strength of RC beam-column joints*, ACI Structural Journal, Vol. 102, No. 3, pp. 445–453.

Ikeda, A. (1968) *Report of the training institute for engineering teachers*, Yokohama National University, Japan. Also in A list of past experimental results of reinforced concrete columns by Hirosawa, M. (1973) Building Research Institute, Ministry of Construction, Japan.

Ilki, A., Bedirhanoglu, I., and Kumbasar, N. (2011) *Behavior of FRP-retrofitted joints built with plain bars and low-strength concrete*, ASCE Journal of Composites for Construction, Vol. 15, No. 3, pp. 312–326.

Inoue, H., Higashi, K., and Ohta, K. (1990) *Experimental study on effect of transverse beam and slab of reinforced cross type beam-column joints (in Japanese)*, Summaries of Technical Papers of Annual Meeting Architectural Institute of Japan, pp. 379–380.

International Code Council (2003) 2003 *International Building Code*, Falls Church, VA.

International Conference of Building Officials (1961) *Uniform Building Code*, Whittier, CA.

Irisawa, I. Yoshino, T., and Sasaya, T. (1996) *Mechanical properties of precast beam-column connections (in Japanese)*, Proceedings of the Japan Concrete Institute, Vol. 18, No. 2, pp. 1265–1 270.

Ishida, K., Akiyuma, K., Pareek, S., and Kuroda, K. (2004), *Experimental study of beam-column joints of RC structures using high-strength concrete and steel (2) (in Japanese)*, Proceedings of Tohoku Branch Research, Architectural Institute of Japan, Vol. 67, pp. 77–80.

Ishida, K., Fujii, S., Morita, S., and Choi, G. (1996) *Shear strength of exterior beam column connection under bi-axial earthquake loading (in Japanese)*, Proceedings of the Japan Concrete Institute, Vol. 18, No. 2, pp. 953–958.

Ishida, K., Shima, K., Higashi, K., and Fujii, S. (2001) *Real scale test of RC interior beam-column connections (in Japanese)*, Proceedings of the Japan Concrete Institute, Vol. 23, No. 3, pp. 343–348.

Ishikawa, Y. and Kamimura, T. (1990), *Experimental study on shear resistance of RC interior beam-column connections (in Japanese)*, Proceedings of the Japan Concrete Institute, Vol. 12, No. 2, pp. 669-674.

Iwaoka, S., Hori, S., Naruse, T., Watanabe, T., Yamamoto, K., and Konno, S. (2005) *Experimental study on the beam-column joints of ultra-high-strength reinforced concrete structures (in Japanese)*, Summaries of Technical Papers of Annual Meeting Architectural Institute of Japan, pp. 245–246.

Jeong, S.-H., Mwafy, A.M., and Elnashai, A.S. (2012) *Probabilistic seismic performance assessment of code-compliant multi-story RC buildings*, Engineering Structures, Vol. 34, pp. 527–537.

Jinno, Y., Kanada, K., Fujii, S., and Morita, S. (1985) *On design concepts of exterior beam-column joints of reinforced concrete structures (in Japanese)*, Research Report Collection of Kinki Branch, Architectural Institute of Japan, Vol. 25, pp. 117–120.

Jinno, Y., Kawachi, T., Kadoriku, J., and Kumagai, H. (1991) *An experimental study on behaviour of reinforced concrete interior beam-column joints using high-strength materials: Part1 Test program and results (in Japanese)*, Summaries of Technical Papers of Annual Meeting Architectural Institute of Japan, pp. 591–592.

Joh, O. and Goto, Y. (2000) *Beam-column joint behavior after beam yielding in RC ductile frames*, 12th World Conference on Earthquake Engineering, Paper No. 2196, Auckland, New Zealand.

Joh, O., Goto, Y., and Shibata, T. (1988) *Behavior of three-dimensional reinforced concrete beam-column subassemblages with slabs*, 9th World Conference on Earthquake Engineering, Tokyo-Kyoto, Japan, Vol. VIII, pp. 587–592.

Joh, O., Goto, Y, and Shibata, T. (1989) *Influence of joint reinforcement to shear resistance characteristic in RC exterior beam column connection (in Japanese)*, Proceedings of the Japan Concrete Institute, Vol. 11, No. 2, pp. 537–542.

Joh, O., Goto, Y., and Shibata, T. (1991a) *Behavior of reinforced concrete beam-column joints with eccentricity*, Design of Beam-Column Joints for Seismic Resistance (SP 123), American Concrete Institute, Detroit, MI, pp. 317–357.

Joh, O., Goto, Y., and Shibata, T. (1991b) *Influence of transverse joint and beam reinforcement and relocation of plastic hinge region on beam-column joint stiffness deterioration*, Design of Beam-Column Joints for Seismic Resistance (SP 123), American Concrete Institute, Detroit, MI, pp. 187–223.

Joh, O., Goto, Y., and Shibata, T. (1992) *Shear resistance performance in RC exterior beam column connection using high strength materials (in Japanese)*, Proceedings of the Japan Concrete Institute, Vol. 14, No. 2, pp. 391–395.

Kaku, A., Masou, K., Kutoka, T., and Muguruma, T. (1993) *Experimental study on deformation characteristic of beam column connection in RC structure (in Japanese)*, Proceedings of the Japan Concrete Institute, Vol. 15, No. 2, pp. 559–564.

Kaku, T. and Asakusa, H. (1991) *Ductility estimation of exterior beam-column subassemblies in reinforced concrete frames*, Design of Beam-Column Joints for Seismic Resistance (SP123), American Concrete Institute, Detroit, MI, pp. 167–185.

Kamimura, T., Takimoto, H., and Tanaka, S. (2004) *Mechanical behavior of reinforced concrete beam-column assemblages with eccentricity*, 13th World Conference on Earthquake Engineering, Paper No. 4, Vancouver, BC, Canada.

Kanada, K., Kondo, G., Fujii, S., and Morita, S. (1984) *Relation between shear failure and anchorage failure in exterior beam-column joints (in Japanese)*, Proceedings of the Japan Concrete Institute, Vol. 6, pp. 433–440.

Kaneko, Y., Mihashi, H., and Ishihara, S. (2001) *Entire load-displacement characteristics for direct shear failure of concrete, Modeling of inelastic behavior of RC structures under seismic load*, American Society of Civil Engineers, Reston, Virginia, pp. 175–192.

Karayannis, C.G., Chalioris, C.E., and Sideris, K.K. (1998) *Effectiveness of RC beam-column connection repair using epoxy resin injections*, Journal of Earthquake Engineering, Vol. 2, No. 2, pp. 217–240.

Karayannis, C.G., Chalioris, C.E., and Sirkelis, G.M. (2008) *Local retrofit of exterior RC beam-column joints using thin RC jackets–An experimental study*, Earthquake Engineering and Structural Dynamics, Vol. 37, No. 5, pp. 727–746.

Kashiwasazaki, T., Kitayama, K., and Noguchi, H. (1992) *Bond characteristic of reinforced concrete beam-column connections using ultra high strength materials (in Japanese)*, Proceedings of the Japan Concrete Institute, Vol. 14, No. 2, pp. 397–400.

Kawai, T., Kimura, H., Iwata, M., and Watai, T. (1997) *Experimental study of resistance mechanism of RC beam-column connections using high strength materials (in Japanese)*, Proceedings of the Japan Concrete Institute, Vol. 19, No. 2, pp. 1011–1016.

Kim, J. and LaFave, J.M. (2009) *Joint shear behavior of reinforced concrete beam-column connections subjected to seismic lateral loading*, Report No. NSEL–020, Department of Civil and Environmental Engineering, University of Illinois at Urbana-Champaign, IL.

Kirçil, M.S. and Polat, Z. (2006) *Fragility analysis of mid-rise R/C frame buildings*, Engineering Structures, Vol. 28, No. 9, pp. 1335–1345.

Kitayama, K., Otani, S., and Aoyama, H. (1987) *Earthquake resistant design criteria for reinforced concrete interior beam-column joints*, Pacific Conference on Earthquake Engineering, Wairakei, New Zealand, Vol. 1, pp. 315–326.

Kitayama, K., Otani, S., and Aoyama, H. (1991) *Development of design criteria for RC interior beam-column joints*, Design of Beam-Column Joints for Seismic Resistance (SP123), American Concrete Institute, Detroit, MI, pp. 97–123.

Kitayama, K., Lee, S., Otani, S., and Aoyama, H. (1992) *Behavior of high-strength R/C beam-column joints*, 10th World Conference on Earthquake Engineering, Madrid, Spain, pp. 3151–3156.

Kitayama, K., Tajima, Y., Okuda, M., and Kishida, S. (2000) *Influences of beam and column bar bond on failure mechanism in reinforced concrete interior beam-column joints*, The 2nd U.S.-Japan Workshop on Performance-Based Earthquake Engineering Methodology for Reinforced Concrete Building Structures, Sapporo, Hokkaido, Japan.

Kokusho, S. (1964) *Report by Building Research Institute*, Tsukuba, Japan. Also in A list of past experimental results of reinforced concrete columns by Hirosawa, M. (1973) Building Research Institute, Ministry of Construction, Japan.

Kordina K. (1984) *Bewehrungsfiihrung in ecken und rahmenendknoten*, Deutscher Ausschuss fur Stahlbeton, Heft 354.

Kulkarni, S.A. and Li, B. (2007) *Experimental investigations on reinforced concrete beam-column joints with vertically distributed layers*, 8th Pacific Conference on Earthquake Engineering, Paper No. 555, Nanyang Technological University, Singapore.

Kunnath, S.K., Hoffmann, G., Reinhorn, A.M., and Mander, J.B. (1995) *Gravity-load-designed reinforced concrete buildings–Part 1: Seismic evaluation of existing construction*, ACI Structural Journal, Vol. 92, No. 3, pp. 343–354.

Kurose, Y., Guimaraes, G.N., Zuhua, L., Kreger, M.E., and Jirsa, J.O. (1991) *Evaluation of slab-beam-column connections subjected to bi-directional loading*, Design of Beam-Column Joints for Seismic Resistance (SP123), American Concrete Institute, Detroit, MI, pp. 39–67.

Kusuhara, F., Azukawa, K., Shiohara, H., and Otani, S. (2004) *Tests of reinforced concrete interior beam-column joint subassemblage with eccentric beams*, 13th World Conference on Earthquake Engineering, Paper No. 185, Vancouver, BC, Canada.

Kwon, O.S. and Elnashai, A. (2006) *The effect of material and ground motion uncertainty on the seismic vulnerability of RC structure*, Engineering Structures, Vol. 28, No. 2, 289–303.

LaFave, J.M. and Shin, M. (2005) *Discussion of "Modeling reinforced-concrete beam-column joints Subjected to cyclic loading" by Lowes, L.N. and Altoontash, A.*, ASCE Journal of Structural Engineering, Vol. 131, No. 6, pp. 992–993.

LeBorgne, M.R. (2012) *Modeling the post shear failure behavior of reinforced concrete columns*, Ph.D. Thesis, The University of Texas at Austin, Austin, TX.

Lee, D.H. and Elnashai, A.S. (2001) *Seismic analysis of RC bridge columns with flexure-shear interaction*, ASCE Journal of Structural Engineering, Vol. 127, No. 5, pp. 546–553.

Lee, C.-J. and Lee, S.-H. (2000) *A study on the shear strength of reinforced concrete exterior beam-column joints (in Korean)*, Journal of Architectural Institute of Korea, Vol. 16, No. 6, pp. 21–28.

Lee, J.-Y., Kim, J.-Y., and Oh, G.-J. (2009) *Strength deterioration of reinforced concrete beam-column joints subjected to cyclic loading*, Engineering Structures, Vol. 31, No. 9, pp. 2070–2085.

Lee K. and Foutch, D.A. (2004) *Performance evaluation of damaged steel frame buildings subjected to seismic loads*, ASCE Journal of Structural Engineering, Vol. 130, No. 4, pp. 588–599.

Lee, S.H. and Lee, D.H. (2001) *A study on the shear characteristic of exterior-type reinforced concrete joints under cyclic loading (in Korean)*, Journal of the Earthquake Engineering Society of Korea, Vol. 5, No. 2, pp. 73–82.

Lee, W.T., Chiou, Y.J., and Shih, M.H. (2010) *Reinforced concrete beam-column joint strengthened with carbon fiber reinforced polymer*, Composite Structures, Vol. 92, No. 1, pp. 48–60.

Leon, R.T. (1989) *Interior joints with variable anchorage lengths*, ASCE Journal of Structural Engineering, Vol. 115, No. 9, pp. 2261–2275.

Leon, R.T. (1990) *Shear strength and hysteretic behavior of interior beam-column joints*, ACI Structural Journal, Vol. 87, No. 1, pp. 3–11.

Le-Trung, K., Lee, K., Lee, J., Lee, D.H., and Woo, S. (2010) *Experimental study of RC beam–column joints strengthened using CFRP composites*, Composites Part B: Engineering, Vol. 41, No. 1, pp. 76–85.

Li, Q. and Ellingwood, B.R. (2007) *Performance evaluation and damage assessment of steel frame buildings under main shock-aftershock earthquake sequences*, Earthquake Engineering and Structural Dynamics, Vol. 36, No. 3, pp. 405–427.

Li, B., Tran, C.T.N., and Pan, T.-C. (2009) *Experimental and numerical investigations on the seismic behavior of lightly reinforced concrete beam-column joints*, ASCE Journal of Structural Engineering, Vol. 135, No. 9, pp. 1007–1018.

Li, B., Wu, Y., and Pan, T.-C. (2002) *Seismic behavior of nonseismically designed interior beam-wide column joints–Part I: Experimental results and observed behavior*, ACI Structural Journal, Vol. 99, No. 6, pp. 791–802.

Liel, A.B. (2008) *Assessing the collapse risk of California's existing reinforced concrete frame structures: Metrics for seismic safety decisions*, Ph.D. Thesis, Department of Civil and Environmental Engineering, Stanford University, CA.

Liel, A.B., Haselton, C.B., and Deierlein, G.G. (2011) *Seismic collapse safety of reinforced concrete buildings. II: Comparative assessment of nonductile and ductile moment frames*, ASCE Journal of Structural Engineering, Vol. 137, No. 4, pp. 492–502.

Liu, C. (2006) *Seismic behavior of beam-column joint assemblies reinforced with steel fibers*, M.S. Thesis, Department of Civil Engineering, University of Canterbury, Christchurch, New Zealand.

Liu, A. and Park, R. (1998) *Seismic load tests on two concrete interior beam-column joints reinforced by plain round bars designed to pre-1970s codes*, Bulletin of the New Zealand Society for Earthquake Engineering, Vol. 31, No. 3, pp. 164–176.

Lowes, L.N. and Altoontash, A. (2003) *Modeling reinforced-concrete beam-column joints subjected to cyclic loading*, ASCE Journal of Structural Engineering, Vol. 129, No. 12, pp. 1686–1697.

Luco, N., Bazzurro, P., and Cornell, C.A. (2004) *Dynamic versus static computation of the residual capacity of a mainshock-damaged building to withstand an*

aftershock, 13th World Conference on Earthquake Engineering, Paper No. 2405, Vancouver, Canada.

Lynn, A.C., Moehle, J.P., Mahin, S.A., and Holmes, W.T. (1996) *Seismic evaluation of existing reinforced concrete building columns*, Earthquake Spectra, Vol. 12, No. 4, pp. 715–739.

MacGregor, J.G., Mirza, S.A., and Ellingwood, B.R. (1983) *Statistical analysis of resistance of reinforced and prestressed concrete members*, Journal of the American Concrete Institute, Vol. 80, No. 3, pp. 165–276.

Maffei, J., Tellen, K., and Nakayama, Y. (2008) *Probability-based seismic assessment of buildings, considering post-earthquake safety*, Earthquake Spectra, Vol. 24, No. 3, pp. 667–699.

Mahin, S.A. (1980) *Effects of duration and aftershocks on inelastic design earthquakes*, 7th World Conference on Earthquake Engineering, Istanbul, Turkey, pp. 677–680.

Mander, J.B., Priestley, M.J.N., and Park, R. (1988) *Theoretical stress-strain model for confined concrete*, ASCE Journal of Structural Engineering, Vol. 114, No. 8, pp. 1804–1826.

Matsumoto, T., Nishihara, H., Nakao, M., and Castro, J.J. (2010) *Performance on shear strength of reinforced concrete eccentric beam-column joints subjected to seismic loading*, Proceedings of the 9th U.S. National and 10th Canadian Conference on Earthquake Engineering, Paper No. 1457, Toronto, Canada.

Mckay, M.D., Conover, W.J., and Beckman, R.J. (1979) *A comparison of three methods for selecting values of input variables in the analysis of output from a computer code*, Technometrics, Vol. 21, No. 2, pp. 239–245.

McKenna, F., Scott, M.H., and Fenves, G.L. (2010) *Nonlinear finite-element analysis software architecture using object composition*, ASCE Journal of Computing in Civil Engineering, Vol. 24, No. 1, pp. 95–107.

Megget, L.M. (1971) *Anchorage of beam reinforcement in seismic resistant reinforced concrete frames*, M.S. Thesis, University of Canterbury, Christchurch, New Zealand.

Megget, L.M. (1974) *Cyclic behavior of exterior reinforced concrete beam-column joints*, Bulletin of New Zealand National Society for Earthquake Engineering, Vol. 7, No. 1, pp. 22–47.

Meinheit, D.F. and Jirsa, J.O. (1977) *The shear strength of reinforced concrete beam-column joints*, Technical Report CESRL Report No. 77-1, University of Texas at Austin, TX.

Meinheit, D.F. and Jirsa, J. (1981) *Shear strength of R/C beam-column connections*, ASCE Journal of Structural Engineering, Vol. 107, No. 11, pp. 2227–2243.

Menegotto, M. and Pinto, P.E. (1973) *Method of analysis for cyclically loaded reinforced concrete plane frames including changes in geometry and non-elastic behavior of elements under combined normal force and bending*, Proceedings of the IABSE

Symposium on Resistance and Ultimate Deformability of Structures Acted on by Well-Defined Repeated Loads, Lisbon, Portugal, pp. 15–22.

Mitra, N. (2007) *An analytical study of reinforced concrete beam-column joint behavior under seismic loading*, Ph.D. Thesis, Department of Civil and Environmental Engineering, University of Washington, Seattle, WA.

Mitra, N. and Lowes, L.N. (2007) *Evaluation, calibration, verification of a reinforced concrete beam-column joint model*, ASCE Journal of Structural Engineering, Vol. 133, No. 1, pp. 105–120.

Moiser, W.G. (2000) *Seismic assessment of reinforced concrete beam-column joints*, M.S. Thesis, Department of Civil and Environmental Engineering, University of Washington, Seattle, WA.

Morita, S. and Kaku, T. (1984) *Slippage of reinforcement in beam-column joint of reinforced concrete frame*, 8th World Conference on Earthquake Engineering, San Francisco, CA, pp. 477–484.

Morita, S., Kitayama, K., Kishida, S., and Nishikawa, T. (2004) *Shear force and capacity in reinforced concrete beam-column joints with good bond along beam and column bars*, 13th World Conference on Earthquake Engineering, Paper No. 1761, Vancouver, BC, Canada.

Mosalam, K.M., Ayala, G., White, R.W., and Roth, C. (1997) *Seismic fragility of LRC frames with and without masonry infill walls*, Journal of Earthquake Engineering, Vol. 1, No. 4, pp. 693–720.

Mostafaei, H., Vecchio, F.J., and Kabeyasawa, T. (2009) *Deformation capacity of reinforced concrete columns*, ACI Structural Journal, Vol. 106, No. 2, pp. 187–195.

Nagasaka, T. (1982) *Effectiveness of steel fiber as web reinforcement in reinforced concrete columns*, Transactions of the Japan Concrete Institute Vol. 4, pp. 493–500.

Nakamura, M., Bessho, S., Usami, S., and Kato, T. (1991) *Experimental study on interior beam-column joint using high strength concrete and rebars (1) (in Japanese)*, Summaries of Technical Papers of Annual Meeting Architectural Institute of Japan, pp. 583–584.

Neter, J., Kutner, M.H., Nachtsheim, C.J., and Wasserman, W. (1996) *Applied linear statistical models*, 4th edition, WCB/McGraw-Hill, Burr Ridge, IL.

Nishi, K. and Ohwada, Y. (1993) *An experimental study on reinforced concrete beam-column joint of exterior frame under biaxial seismic load (3) (in Japanese)*, Summaries of Technical Papers of Annual Meeting Architectural Institute of Japan, pp. 859–860.

Nishi, K., Ota, K., and Ohwada, Y. (1992) *An experimental study on beam-column joint of exterior frame under biaxial seismic load (1) (in Japanese)*, Summaries of Technical Papers of Annual Meeting Architectural Institute of Japan, pp. 207–208.

Nishiyama, M., Nishizaki, T., Muguruma, H., and Watanabe, F. (1989) *Seismic design of prestressed concrete beam–exterior column joints*, Transactions of the Japan Concrete Institute, Vol. 11, pp. 439–446.

Noguchi, H. and Kashiwazaki, T. (1992) *Experimental studies on shear performances of RC interior column-beam joints with high-strength materials*, 10th World Conference on Earthquake Engineering, Madrid, Spain, pp. 3163–3168.

Noguchi, H. and Kurusu, K. (1988) *Correlation of bond and shear in RC beam-column connections subjected to seismic forces*, 9th World Concrete Earthquake Engineering, Tokyo-Kyoto, Japan, Vol. IV, pp. 597–602.

Ogawa, T., Sawada, S., Adachi, H., and Nakanishi, M. (2003) *Study on mechanical properties of R/C exterior beam-column joint under dynamic loading (1) (in Japanese)*, Summaries of Technical Papers of Annual Meeting Architectural Institute of Japan, pp. 539–540.

Oh, B.G., Park, K.C., Hwang, H.S., and Chung, H.S. (1992) *An experimental study on shear capacity of reinforced concrete exterior beam-column joint with high strength concrete (in Korean)*, Proceedings of the Architecture Institute of Korea, Vol. 12, pp. 363–366.

Ohue, M., Morimoto, H., Fujii, S., and Morita, S. (1985) *The behavior of R.C. short columns failing in splitting bond-shear under dynamic lateral loading*, Transactions of the Japan Concrete Institute, Vol. 7, pp. 293–300.

Ohwada, Y. (1970) *A study on RC beam-column connection subjected to lateral load (8) (in Japanese)*, Summaries of Technical Papers of Annual Meeting Architectural Institute of Japan, Vol. 45, pp. 737–738.

Ohwada, Y. (1973) *A study on RC beam-column connection subjected to lateral load (9) (in Japanese)*, Summaries of Technical Papers of Annual Meeting Architectural Institute of Japan, Vol. 48, pp. 1297–1298.

Ohwada, Y. (1976) *A study on effect of lateral beams on RC beam-column joints (1) (in Japanese)*, Summaries of Technical Papers of Annual Meeting Architectural Institute of Japan, pp.1455–1456.

Ohwada, Y. (1977) *A study on effect of lateral beams on RC beam-column joints (2) (in Japanese)*, Proceedings of the Architectural Institute of Japan, Vol. 61, pp. 241–244.

Ohwada, Y. (1980) *A study on effect of lateral beams on RC beam-column joints (4) (in Japanese)*, Summaries of Technical Papers of Annual Meeting Architectural Institute of Japan, pp. 1511–1512.

Ohwada, Y. (1981) *A study on effect of lateral beams on RC beam-column joints (5) (in Japanese)*, Summaries of Technical Papers of Annual Meeting Architectural Institute of Japan, pp. 1437–1438.

Oka, K. and Shiohara, H. (1992) *Tests of high-strength concrete interior beam-column-joint subassemblages*, 10th World Conference on Earthquake Engineering, Madrid, Spain, pp. 3211–3217.

Onish, S., Sugawara, M., and Takibuchi, Y. (1990) *Experimental study on the seismic performance of beam-column connections (in Japanese)*, Proceedings of the Japan Concrete Institute, Vol. 12, No. 2, pp. 681–684.

Ono, A., Nobuaki, S., Adachi, H., and Sakamaki, Y. (1989) *Elasto-plastic behavior of reinforced concrete column with fluctuating axial force*, Transactions of the Japan Concrete Institute Vol. 11, pp. 239–246.

Ota, T., Hatato, T., Nezu, S., Sugimoto, H., Masuda, Y., Sugimoto, K., and Eto, H. (2004) *Experimental study on pre-cast RC beam-column joint (1) (in Japanese)*, Summaries of Technical Papers of Annual Meeting Architectural Institute of Japan, pp. 849–850.

Otani, S., Kobayashi, Y., and Aoyama, H. (1984) *Reinforced concrete interior beam-column joints under simulated earthquake loading*, US-New Zealand-Japan Seminar on Design of Reinforced Concrete Beam-Column joints, Monterey, CA.

Otani, S. and Sozen, M.A. (1972) *Behavior of multistory reinforced concrete frames during earthquakes*, Structural Research Series No. 392, University of Illinois at Urbana-Champaign, IL.

Ousalem, H., Kabeyasawa, T., Tasai, A., and Ohsugi, Y. (2002) *Experimental study on seismic behavior of reinforced concrete columns under constant and variable*, Proceedings of Japan Concrete Institute, Vol. 24, No. 2, pp. 229–234.

Ousalem, H., Kabeyasawa, T., Tasai, A., and Iwamoto, J. (2003) *Effect of hysteretic reversals on lateral and axial capacities of reinforced concrete columns*, Proceedings of Japan Concrete Institute, Vol. 25, No. 2, pp. 367–372.

Owada, Y. (1984) *Studies on reinforced concrete beam-column joints under biaxial seismic load (2) (in Japanese)*, Summaries of Technical Papers of Annual Meeting Architectural Institute of Japan, pp. 1869–1870.

Owada, Y. (1992) *Seismic behaviors of beam-column joint of reinforced concrete exterior frame under varying axial load*, 10th World Conference on Earthquake Engineering, Madrid, Spain, pp. 3181–3184.

Owada, Y. (2000) *Three-dimensional behaviors of reinforced concrete beam-column joint under seismic load*, 12th World Conference on Earthquake Engineering, Paper No. 0707, Auckland, New Zealand.

Ozaki, E., Nishio, A., Tajima, K., and Shirai, N. (2010) *Damage evaluation of RC beam column joints based on the image measurement (in Japanese)*, Proceedings of the Japan Concrete Institute, Vol. 32, No. 2, pp. 301–306.

Ozbolt, J., Mayer, U., and Vocke, H. (2001) *Smeared fracture FE-analysis of reinforced concrete structures–Theory and examples*, Modeling of inelastic behavior of RC structures under seismic load, American Society of Civil Engineers, Reston, Virginia, pp. 234-256.

Pantelides, C.P., Hansen, J., Nadauld, J., and Reaveley, L.D. (2002) *Assessment of reinforced concrete building exterior joints with substandard details*, PEER

Report 2002/18, Pacific Earthquake Engineering Center, University of California, Berkeley, CA.

Park, S. and Mosalam, K.M. (2012) *Analytical model for predicting shear strength of unreinforced exterior beam-column joints,* ACI Structural Journal, Vol. 109, No. 2, pp. 149–160.

Park, S. and Mosalam, K.M. (2013a) *Experimental investigation of nonductile RC corner beam-column joints with floor slabs*, ASCE Journal of Structural Engineering, Vol. 139, No. 1, pp. 1–14.

Park, S. and Mosalam, K.M. (2013b) *Simulation of reinforced concrete frames with nonductile beam-column joints*, Earthquake Spectra, Vol. 29, No. 1, pp. 233–257.

Park, R. and Paulay, T. (1990) *Use of interlocking spirals for transverse reinforcement in bridge columns*, Strength and Ductility of Concrete Substructures of Bridges, RRU (Road Research Unit) Bulletin 84, Vol. 1, pp. 77–92.

Parker, D.E. and Bullman, P.J.M. (1997) *Shear strength within RC beam-column joints*, The Structural Engineer, Vol. 75, No. 4, pp. 53–57.

Paulay, T. (1989) *Equilibrium criteria for reinforced concrete beam-column joints*, ACI Structural Journal, Vol. 86, No. 6, pp. 635–643.

PEER (2011) *NISEE earthquake engineering online archive*, Pacific Earthquake Engineering Research Center, University of California, Berkeley, CA, http://nisee.berkeley.edu/elibrary/.

Pessiki, S.P., Conley, C.H., Gergely, P., and White, R.N. (1990) *Seismic behavior of lightly-reinforced concrete column and beam-column joint details*, Report No. NCEER-90-0014, National Center for Earthquake Engineering Research, State University of New York at Buffalo, NY.

Pimanmas, A. and Chaimahawan, P. (2010) *Shear strength of beam-column joint with enlarged joint area*, Engineering Structures, Vol. 32, No. 9, pp. 2529–2545.

Pincheira, J.A., Dotwiala, F.S., and D'Souza J.T. (1999) *Seismic analysis of older reinforced concrete columns*, Earthquake Spectra, Vol. 15, No. 2, pp. 245–272.

Priestley, M.J.N. (1997) *Displacement based seismic assessment of reinforced concrete buildings*, Journal of Earthquake Engineering, Vol. 1, No. 1, pp. 157–92.

Popov, E.P. (1994) *Development of US seismic codes*, Journal of Constructional Steel Research, Vol. 29, No. 1–3, pp. 191–207.

Pujol, S., Ramirez, J.A., and Sozen, M.A. (1999) *Drift capacity of reinforced concrete columns subjected to cyclic shear reversals,* Seismic Response of Concrete Bridges, SP-187, American Concrete Institute, Farmington Hills, MI, pp. 255–274.

Raffaelle, G.S. and Wight, J.K. (1995) *Reinforced concrete eccentric beam-column connections subjected to earthquake-type loading*, ACI Structural Journal, Vol. 92, No. 1, pp. 45–55.

Raghunandan, M, Liel, A.B., Ryu, H., Luco, N., and UMA, S.R. (2012) *Aftershock fragility curves and tagging assessments for a mainshock-damaged building*, 15th World Conference on Earthquake Engineering, Paper No. 4124, Lisbon, Portugal.

Ramamoorthy, S.K., Gardoni, P., and Bracci, J.M. (2006) *Probabilistic demand models and fragility curves for reinforced concrete frames*, ASCE Journal of Structural Engineering, Vol. 132, No. 10, pp. 1563–1572.

Ranf, R.T., Eberhard, M.O., and Malone, S. (2007) *Post-earthquake prioritization of bridge inspections*, Earthquake Spectra, Vol. 131, No. 1, pp. 131–146.

Reys de Ortiz, I. (1993) *Strut-and-tie modeling of reinforced concrete short beams and beam-column joints*, Ph.D. Thesis, University of Westminster, UK.

Rossetto, T. and Elnashai, A.S. (2003) *Derivation of vulnerability functions for European-type RC structures based on observational data*, Engineering Structures, Vol. 25, No. 10, pp. 1241–1263.

Ruiz-García, J. and Negrete-Manriquez, J.C. (2011) *Evaluation of drift demands in existing steel frames under as-recorded far-field and near-fault mainshock-aftershock seismic sequences*, Engineering Structures, Vol. 33, No. 2, pp. 621–634.

Ryu, H., Luco, N., Uma, S.R., and Liel, A.B. (2011) *Developing fragilities for mainshock-damaged structures through incremental dynamic analysis*, Proceedings of the 9th Pacific Conference on Earthquake Engineering, Paper No. 225, Auckland, New Zealand.

Saatcioglu, M. and Grira, M. (1999) *Confinement of reinforced concrete columns with welded reinforcement grids*, ACI Structural Journal, Vol. 96, No. 1, pp. 29–39.

Saatcioglu, M. and Ozcebe, G. (1989) *Response of reinforced concrete columns to simulated seismic loading*, ACI Structural Journal, Vol. 86, No. 1, pp. 3–12.

Sagbas, G. (2007) *Nonlinear finite element analysis of beam-column subassemblies*, M.S. Thesis, Department of Civil Engineering, University of Toronto, Canada.

Salim, I.B. (2007) *The influence of concrete strengths of the behavior of the external beam-column joints*, M.S. Thesis, Universiti Teknologi Malaysia.

Sanchez, V.M., Lloyd, B., Hassan, W.M., and Moehle J.P. (2009) *Evaluation of non-ductile reinforced concrete building corner joint experiencing early column failure*, Pacific Earthquake Engineering Center, University of California, Berkeley, CA.

Sarsam, K.F. and Phipps, M.E. (1985) *The shear design of in-situ reinforced beam-column joints subjected to monotonic loading*, Magazine of Concrete Research, Vol. 37, No. 130, pp. 16–28.

Sasmal, S., Lakshmanan, N., Ramanjaneyulu, K., Iyer, N.R., Novák, B., Srinivas, V., Kumar, K.S., and Roehm, C. (2011) *Development of upgradation schemes for gravity load designed beam–column sub-assemblage under cyclic loading*, Construction and Building Materials, Vol. 25, No. 8, pp. 3625–3638.

Scott, R.H. (1992) *The effects of detailing on RC beam/column connection behavior*, The Structural Engineer, Vol. 70, No. 18, pp. 318–324.

Scott, M.H. and Fenves, G.L. (2006) *Plastic hinge integration methods for force-based beam-column elements*, ASCE Journal of Structural Engineering, Vol. 132, No. 2, pp. 244–252.

Seckin, M. and Ogura, K. (1979) *Experimental studies on reinforced concrete beam-column joints (exterior)*, Transactions of the Japan Concrete Institute, Extra, No. 2443.

Sedra, N., Eberhard, M., Irfanoglu, A., Matamoros, A., Pujol, S., Haraldsson, O.S., Lattanzi, D.A., Lauer, S.L., Lyon, B., Messmer, J., Nasi, K., Rautenberg, J., Symithe, S., and Douilly, R. (2010) *The Haiti Earthquake Database*, http://nees.org/resources/1797.

Sezen, H. (2002) *Seismic behavior and modeling of reinforced concrete building columns*, Ph.D. Thesis, Department of Civil and Environmental Engineering, University of California at Berkeley, CA.

Sezen, H. and Chowdhury, T. (2009) *Hysteretic model for the lateral behavior of reinforced concrete columns including shear deformation*, ASCE Journal of Structural Engineering, Vol. 135, No. 2, pp. 139–146.

Sezen, H. and Moehle J.P. (2003) *Bond-slip behavior of reinforced concrete members,* Proceedings of Fib Symposium on Concrete Structures in Seismic Regions, Athens, Greece.

Shafieezadeh, A. (2011) *Seismic vulnerability assessment of wharf structures*, Ph.D. Thesis, School of Civil and Environmental Engineering, Georgia Institute of Technology, GA.

Shafieezadeh, A., Ramanathan, K., Padgett, J.E., and DesRoches, R. (2012) *Fractional order intensity measures for probabilistic seismic demand modeling applied to highway bridges*, Earthquake Engineering and Structural Dynamics, Vol. 41, No. 3, pp. 391–409.

Sharma, A., Eligehausen, E., and Reddy, G.R. (2011) *A new model to simulate joint shear behavior of poorly detailed beam-column connections in RC structures under seismic loads, Part I: Exterior joints*, Engineering Structures, Vol. 33, No. 3, pp. 1034–1051.

Shin, M. and LaFave, J.M. (2004) *Modeling of cyclic joint shear deformation contributions in RC beam-column connections to overall frame behavior,* Structural Engineering and Mechanics, Vol. 18, No. 5, pp. 645–669.

Shin, S.W., Lee, K.S., and Ghosh, S.K. (1992) *High-strength concrete beam-column joints*, 10th World Conference on Earthquake Engineering, Madrid, Spain, pp. 3145–3150.

Shing, P.B. and Spencer, B. (2001) *Modeling of shear behavior of RC bridge structures, Modeling of inelastic behavior of RC structures under seismic load,* American Society of Civil Engineers, Reston, Virginia, pp. 315-333.

Shinjo, H., Matsunaga, K., Kawakami, H., and Kosaka, H. (2009) *Loading tests of RC beam-column joint using high-strength concrete*, Reports of Technical Research and Development Center of Sumitomo Mitsui Construction Co., Ltd., No. 9, pp. 93–99.

Shinozuka, M., Feng, M.Q., Lee, J., and Naganuma, T. (2000) *Statistical analysis of fragility curves*, ASCE Journal of Engineering Mechanics, Vol. 126, No. 12, pp. 1224–1231.

Shiohara, H. (2004) *Quadruple flexural resistance in R/C beam-column joints*, 13th world Conference on Earthquake Engineering, Paper No. 491, Vancouver, Canada.

Singhal, A. and Kiremidjian, A.S. (1996) *Method for probabilistic evaluation of seismic structural damage*, ASCE Journal of Structural Engineering, Vol. 122, No. 12, pp. 1459–1467.

Smith, B.J. (1972) *Exterior reinforced concrete joints with low axial load under seismic loading*, M.S. Thesis, Department of Civil Engineering, University of Canterbury, Christchurch, New Zealand.

Smyrou, E., Tasiopoulou, P., Bal, I.E., Gazetas, G., and Vintzileou, E. (2011) *Structural and geotechnical aspects of the Christchurch (2011) and Darfield (2010) earthquakes in N.Zealand*, 7th National Conference on Earthquake Engineering, Istanbul, Turkey.

Spacone, E., Filippou, F.C., and Taucer, F.F. (1996) *Fibre beam-column model for nonlinear analysis of R/C frames: Part I Formulation*, Earthquake Engineering and Structural Dynamics, Vol. 25, No. 7, pp. 711–725.

Stevens, N.J., Uzumeri, S.M., and Collins, M.P. (1991) *Reinforced concrete subjected to reversed cyclic shear–Experiments and constitutive model*, ACI Structural Journal, Vol. 88, No. 2, pp. 135–146.

Sugano, K., Nagashima, T., Kimura, H., and Ichikawa, A. (1991) *Behavior of beam-column joints using high-strength materials*, Design of Beam-Column Joints for Seismic Resistance (SP123), American Concrete Institute, Detroit, MI, pp. 359–377.

Sunasaka, Y. and Kiremidjian, A.S. (1993) *A method for structural safety evaluation under mainshock-aftershock earthquake sequences*, Report No. 105, The Jone A. Blume Earthquake Engineering Center, Department of Civil and Environmental Engineering, Stanford University, CA.

Supaviriyakit, T. and Pimanmas, A. (2008) *Comparative performance of sub-standard interior reinforced concrete beam-column connection with various joint reinforcing details*, Materials and Structures, Vol. 41, No. 3, pp. 543–557.

Suzuki, K., Kondo, T., Kudo, Y., Sato, M., Kurosawa, R., and Hirosawa, M. (2002) *Experimental study on seismic performance of RC eccentricity beam-column joint–Part 1: Experiment result and scale-effect (in Japanese)*, Summaries of Technical Papers of Annual Meeting Architectural Institute of Japan, pp. 623–624.

Takamori, N., Hayashi, K., Sasaki, S., and Teraoka, M. (2006) *Experimental study on full-scale R/C interior beam-column joints (in Japanese)*, Proceedings of the Japan Concrete Institute, Vol. 28, No. 2, pp. 283–288.

Takatani, S. and Maruta, M. (2003) *Experimental study on bond behavior of mechanical anchorage in beam column connections (in Japanese)*, Proceedings of the Japan Concrete Institute, Vol. 25, No. 2, pp. 463–468.

Takeda, T. and Yoshioka, K. (1970) *Report of the Engineering Research Laboratory*, Ohbayashi-Gumi, Ltd., Japan. Also in A list of past experimental results of reinforced concrete columns by Hirosawa, M. (1973) Building Research Institute, Ministry of Construction, Japan.

Takeuchi, H., Nakamura, K., Hayakawa, K., and Ichikawa, M. (2003) *An experimental study on exterior beam joints with mechanical anchorage used circular anchor plate*, Proceedings of the Japan Concrete Institute, Vol. 25, No. 2, pp. 913–918.

Tanaka, H. and Park, R. (1990) *Effect of lateral confining reinforcement on the ductile behavior of reinforced concrete columns*, Report 90-2, Department of Civil Engineering, University of Canterbury , Christchurch, New Zealand.

Taylor, H.P.J. (1974) *The behavior of in situ concrete beam-column joints*, Technical Report 42.492, Cement and Concrete Association.

Teng, S. and Zhou, H. (2003) *Eccentric reinforced concrete beam-column joints subjected to cyclic loading*, ACI Structural Journal, Vol. 100, No. 2, pp. 139–148.

Teraoka, M. (1997) *A study on seismic design of R/C beam-column joint in high rise frame structure (in Japanese)*, Research Report, Extra Issue No. 5, Fujita Institute of Technology, Tokyo, Japan.

Tsai, K.C., Loh, C.H., Lin, K.C., and Chen, C.H. (2000) *Cyclic load tests of 0.7 scale 2-story RC frames retrofitted with steel jackets*, National Center for Research on Earthquake Engineering, Taiwan.

Tsonos A.G. (1996) *Influence of P-Δ effect and axial force variations on seismic performance of R/C beam-column joints*, 11th World Conference on Earthquake Engineering, Paper No. 679, Acapulco, Mexico.

Tsonos, A.G. (2007) *Cyclic load behavior of reinforced concrete beam-column subassemblages of modern structures*, ACI Structural Journal, Vol. 104, No. 4, pp. 468–478.

Tsonos, A.G. (2008) *Effectiveness of CFRP-jackets and RC-jackets in post-earthquake and pre-earthquake retrofitting of beam–column subassemblages*, Engineering Structures, Vol. 30, No. 3, pp. 777–793.

Tsonos, A.G. and Papanikolaou, K.V. (2003) *Post-earthquake repair and strengthening of reinforced concrete beam-column connections (theoretical & experimental investigation)*, Bulletin of the New Zealand Society for Earthquake Engineering, Vol. 36, No. 2, pp. 73–93.

Tsonos, A.G., Tegos, I.A., and Penelis, G.Gr. (1992) *Seismic resistance of type 2 exterior beam-column joints reinforced with inclined bars*, ACI Structural Journal, Vol. 89, No. 1, pp. 3–12.

Tsubosaki, H., Shiohara, H., Oka, K., and Furukawa J. (1993) *Evaluation of slab-beam-column joints subjected to bidirectional loading (1) (in Japanese)*, Summaries of Technical Papers of Annual Meeting Architectural Institute of Japan, pp. 877–878.

Uma, S.R., Ryu, H., Luco, N., Liel, A.B., and Raghunandan, M. (2011) *Comparison of main-shock and aftershock fragility curves developed for New Zealand and US buildings*, Proceedings of the 9th Pacific Conference on Earthquake Engineering, Paper No. 227, Auckland, New Zealand.

USGS (2000) *Implications for earthquake risk reduction in the United States from the Kocaeli, Turkey, Earthquake of August 17, 1999*, U.S. Geological Survey Circular 1193.

Uzumeri, S.M. (1977) *Strength and ductility of cast-in-place beam-column joints*, Reinforced Concrete Structures in Seismic Zones (SP53), American Concrete Institute, Detroit, MI, pp. 293–350.

Vamvatsikos, D. and Cornell, A.C. (2002) *Incremental Dynamic Analysis*, Earthquake Engineering and Structural Dynamics, Vol. 31, No. 3, pp. 491–514.

Vamvatsikos, D. and Cornell, C.A. (2006) *Direct estimation of the seismic demand and capacity of oscillators with multi-linear static pushovers through IDA*, Earthquake Engineering and Structural Dynamics, Vol. 35, No. 9, pp. 1097–1117.

Vecchio, F.J. and Collins, M.P. (1986) *The modified compression field theory for reinforced concrete elements subjected to shear*, ACI Structural Journal, Vol. 83, No. 2, pp. 219–231.

Walker, S.G. (2001) *Seismic performance of existing reinforced concrete beam-column joints*, M.S. Thesis, Department of Civil and Environmental Engineering, University of Washington, Seattle, WA.

Wang, Y.-C. and Hsu, K. (2009) *Shear strength of RC jacketed interior beam-column joints without horizontal shear reinforcement*, ACI Structural Journal, Vol. 106, No. 2, pp. 222–232.

Wang, Y.-C. and Lee M.-G. (2004) *Rehabilitation of nonductile beam-column joint using concrete jacketing*, 13th World Conference on Earthquake Engineering, Paper No. 3159, Vancouver, BC, Canada.

Watanabe, K., Abe, K., Murakawa, J., and Noguchi, H. (1988) *Strength and deformation of reinforced concrete interior beam-column joints*, Transactions of the Japan Concrete Institute, Vol. 10, pp. 183–188.

Watanabe, F. and Ichinose, T. (1992) *Strength and ductility of RC members subjected to combined bending and shear*, Concrete Shear in Earthquake, Elsevier Applied Science, New York, pp. 429–438.

Wong, H.F. (2005) *Shear strength and seismic performance of non-seismically designed RC beam-column joints*, Ph.D. Thesis, Department of Civil Engineering, The Hong Kong University of Science and Technology.

Woo, S.W. (2003) *Seismic performance of RC frames in a low to moderate seismicity region*, Ph.D. Thesis, Department of Civil Engineering, Korea University, Korea.

Yashita, N., Ishiwata, Y., Ichikawa, M., Furukawa, J. Morimoto, H., and Matsuzaki, Y. (1996) *Experimental study on reinforced concrete interior beam-column joint with high rise R/C structure (1) (in Japanese)*, Summaries of Technical Papers of Annual Meeting Architectural Institute of Japan, pp. 841–842.

Yeo, G.L. and Cornell, C.A. (2005) *Stochastic characterization and decision bases under time-dependent aftershock risk in performance-based earthquake engineering*, PEER Report 2005/13, Pacific Earthquake Engineering Research Center, University of California, Berkeley, CA.

Yoshino, M., Takeda, S., and Kamimura, T. (1997) *Behavior of interior RC beam column connections after yielding of longitudinal beam reinforcement (in Japanese)*, Proceedings of the Japan Concrete Institute, Vol. 19, No. 2, pp. 987–992.

Yoshiya, H., Sumi, A., Masuo, K., Segawa, T., and Hisatoku, T. (1991) *Experimental study on behaviour of reinforced concrete interior beam-column joints (in Japanese)*, Summaries of Technical Papers of Annual Meeting Architectural Institute of Japan, pp. 627–628.

Youssef, M. and Ghobarah, A. (2001) *Modelling of RC beam-column joints and structural walls*, Journal of Earthquake Engineering, Vol. 5, No. 1, pp. 93–111.

Yucemen, M.S., Ozcebe, G., and Pay, A.C. (2004) *Prediction of potential damage due to severe earthquakes*, Structural Safety, Vol. 26, No. 3, pp. 349–366.

Zaid, S., Shiohara, H., and Otani, S. (1999) *Test of a joint reinforcing detail improving joint capacity of R/C interior beam-column joint*, The 1st Japan-Korea Joint Seminar on Earthquake Engineering for Building Structures, Seoul National University, Seoul, Korea.

Zhu, Z. (2011) *Column recognition and defects/damage properties retrieval for rapid infrastructure assessment and rehabilitation using machine vision*, Ph.D. Thesis, School of Civil and Environmental Engineering, Georgia Institute of Technology, GA.

VITA

JONG-SU JEON

Jong-Su Jeon was born on November 5 in Geochang, Korea. Upon graduating High School in 1997, he entered Hanyang University in Seoul. He obtained his Bachelor of Engineering degree in Civil Engineering in 2002. Upon completion of his Bachelor's degree, he continued to graduate school at the same university pursuing a Master's degree in Civil Engineering with emphasis in Structural Engineering and Mechanics. Having obtained in his Master's degree in Fall 2004, he joined the Structural Division at Sambo Engineering Co, LTD. In 2009, he entered the Georgia Institute of Technology to pursue his Doctoral studies in Civil Engineering with a special emphasis in Earthquake Engineering and minor in Probability and Statistics. He obtained another Master's degree in Civil Engineering en route his Doctoral degree in Summer 2011.